THE JOURNAL
OF
CHEMICAL PHYSICS

Volume 22 Number 11

NOVEMBER, 1954

Published by the
AMERICAN INSTITUTE OF PHYSICS
Lancaster, Pa. and New York, N. Y.

THE JOURNAL
OF
CHEMICAL PHYSICS

VOLUME 22, NUMBER 11 NOVEMBER, 1954

Mass Spectrometric Study of the Evaporation Products of Strontium Oxide on Platinum*

P. W. BICKEL AND L. V. HOLROYD
Department of Physics, University of Missouri, Columbia, Missouri
(Received February 18, 1954)

The vapor above the SrO-Pt system was bombarded with electrons and the ion fragments analyzed by a mass spectrometer. Evaporator temperatures ranged from 1600°K to 1800°K. Log Sr^+ *vs* 1/T plots were found to be time dependent initially. Eventually the plots became stable, and could be represented by two straight lines having a slope of 60 kcal/mole at the higher temperatures and of 138 kcal/mole at the lower temperatures. The appearance potential for Sr^+ was approximately 5 volts. The ratio of Sr^+ to SrO^+ was between 10 and 100. These results indicate that thermal dissociation of SrO took place. An explanation based on a diffusion-limited mechanism is offered for the smaller slope of the upper part of the log Sr^+ *vs* 1/T plot. The behavior of the SrO-Pt system is compared with that of the BaO-Pt system. The latter system does not appear to exhibit thermal dissociation.

INTRODUCTION

THE commercial value of the oxide-coated cathode has led to many investigations of the behavior of the cathode system with regard to such phenomena as diffusion, conductivity, or electron emission.[1,2] There has been less work on the physical properties of the constituents of the cathode—BaO, SrO, and CaO. Mass spectrometer studies of the evaporation products from BaO and SrO systems have been carried out by Plumlee and Smith[3], and by Aldrich.[4] The latter made an extensive investigation of such systems as BaO-Ta, BaO-Mo, BaO-Pt, and also made some preliminary measurements on SrO-Pt. His results indicated that there was a considerable difference in the behavior of the two systems BaO-Pt and SrO-Pt. The SrO appeared to dissociate upon evaporation while the BaO did not. A more thorough study of SrO-Pt was undertaken to resolve this question. The results are presented below.

EXPERIMENTAL METHODS

The experimental arrangement was essentially the same as that previously described in reference 4, and as shown in Fig. 1. A modified Nier type 60° spectrometer was employed with an evaporator mounted at the base of its ion gun assembly. Since the temperatures involved in the case of BaO were moderate (1000°C), a platinum-faced cathode could be used. This type of cathode is similar in construction to that used in cathode-ray guns. The temperature of the platinum button was determined by means of a Pt-PtRh thermocouple. In case of SrO, the conventional button cathode proved unusable since the temperature was relatively high (1500°C). The metallic vapors from the incandescent structure of the cathode diffused throughout the ion gun, and for this and other reasons it was found necessary to revert to the less satisfactory but simpler platinum ribbon heater. This platinum ribbon was heated by ac, and its temperature recorded by a Pt-PtRh thermocouple on the back of the strip. When checked with an optical pyrometer, the temperature was found to be uniform in the central part of the strip for a length of approximately 3 mm. Only this central region of the strip was coated with $SrCO_3$.

The $BaCO_3$ and $SrCO_3$ were sprayed onto the evaporators which had previously been fired at 1500°C for several hours, or until no evaporation products other than platinum were observed. The sprayed cathode was mounted in the ion gun assembly, the apparatus pumped out and baked for four hours, and the carbonate was then converted. With all filaments and cathodes at the highest operating temperatures the

* Supported in part by the U. S. Office of Naval Research.
[1] I. G. Hermann and P. S. Wagener, *The Oxide Coated Cathode* (Chapman and Hall, London, 1951), Vols. I and II.
[2] A. S. Eisenstein, *Advances in Electronics* (Academic Press Inc., New York, 1948), Vol. I. Part 1.
[3] R. H. Plumlee and L. P. Smith, J. Appl. Phys. **21**, 811 (1950).
[4] L. T. Aldrich, J. Appl. Phys. **21**, 1168 (1951).

pressure in the spectrometer was no greater than 3×10^{-7} mm Hg.

EXPERIMENTAL RESULTS

Barium Oxide

Both Ba^+ and BaO^+ as well as other complexes of Ba and O were observed when the vapor above the BaO was bombarded by 70-ev electrons. Nothing of interest beyond what was previously reported[4] was observed. The following data are presented so as to allow a comparison with SrO-Pt. The Ba^+ and BaO^+ ion currents were equal in magnitude and plots of reciprocal of absolute temperature *vs* log Ba^+ and log BaO^+ yielded straight lines of slope corresponding to a latent heat of 87 kcal/mole. No high mass combinations of Ba, O, and Pt were observed and there was no observable ion emission from the sample surface.

Strontium Oxide

The system SrO-Pt proved much more difficult to study than BaO-Pt. The temperature dependence of the Sr^+ ion current (derived from electron bombardment of the vapor) was at first seemingly irreproducible. Systematic study showed, however, that the sample actually passed through a series of changes as the temperature was cycled, and eventually equilibrium conditions were reached where reproducible data could be obtained. The results are shown in Fig. 2 which represents the data obtained on one of the three samples. The data on the different samples were essentially identical. Curve A in Fig. 2 represents the initial run on the sample. The slope of this plot is 164 kcal/mole, but other and less steep slopes could be obtained depending on how long the sample was outgassed at 1500°C. When the sample was left at 1500°C for approximately an hour the ion current gradually decreased. Cycling the temperature led to curves intermediate between A and B. Further cycling or maintaining the temperature at 1500°C eventually led to curve B. All subsequent cycles yield plots parallel to B, but displaced downward to lower currents as time increases. Over an average cycle the displacement would amount to a few percent. The sample of SrO was observed to have been reduced to about 75 percent of the original by the time curves of type B were being obtained. The sample was initially of a flocculent nature, but became a compact cluster of smooth particles after the high temperature treatment. Curve B can be fairly well represented by two straight lines, the upper part having a slope corresponding to 60 kcal/mole and the lower part having a slope corresponding to 138 kcal/mole.

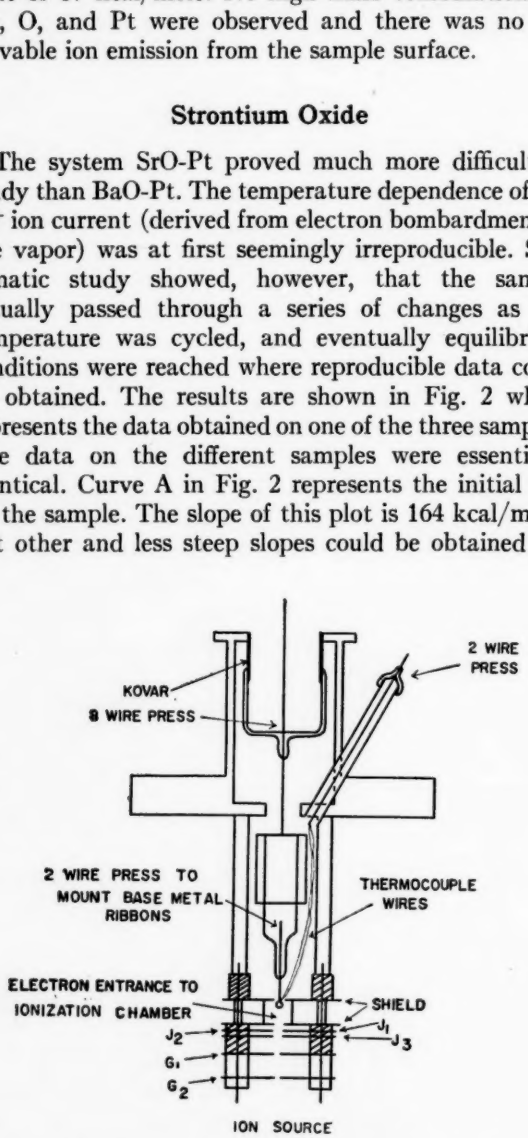

FIG. 1. Ion source for evaporation studies. Spacing between J_1 and J_2 is 1 mm. Slit in J_2 is 3 mm×14 mm. Slits in G_1 and G_2 are 0.25×14 mm. Base metal ribbons are 1.0×0.01 mm 25 mm long.

Points could be obtained on the lower part of curve B as rapidly as the temperature could be raised or lowered. The upper part of curve B was characterized by a tendency to overshoot or undershoot the curve from one point to the next, depending on whether the temperature was being raised or lowered. The ion current would then decrease or increase in a few minutes to a stationary value given by curve B. At the start of the run the SrO^+ current was an order of magnitude less than that for Sr^+, and as time progressed became relatively still smaller. In the absence of an electron current there was an appreciable Sr^+ ion emission from the sample at first, but this emission disappeared as cycling progressed. No definite temperature dependence could be determined for this initial Sr^+ emission.

An appearance potential type of measurement was attempted on the Sr^+ ion current. Sr^+ appeared at about 5 volts of accelerating potential on the ionizing electrons. This voltage has been corrected for contact potential differences. The appearance potential curve exhibited nothing that could be interpreted as an onset of Sr^+ from SrO. Finally, no high mass compounds of Sr, O and Pt were observed, although some Pt^+ ions were observed (not as emission) at the highest temperatures.

DISCUSSION

The results on BaO are interesting, for this study at least, in the manner in which they differ from those obtained for SrO. The Ba^+ to BaO^+ ratio of unity, the general stability of the BaO-Pt system, and the appearance potential of the order of 10 volts[4] for Ba^+ indicate that little dissociation occurs in the case of BaO. This is in contrast with the Sr^+ to SrO^+ ratio of between 10 and 100, the initial instability of the SrO-Pt system, and the appearance potential for Sr^+ of the order of 5 volts. The high Sr^+ to SrO^+ ratio, and the low appearance potential for Sr^+ (first ionization potential of Sr

is 5.67 volts) indicate the presence of uncombined Sr in the atmosphere above the sample. Dissociation is further made plausible by the results of White.[5] His calculations show that the dissociation pressure of Sr above SrO should be relatively large in this temperature range.

The initial high temperature treatment probably serves to remove adsorbed contaminants which might cause the large slope of curve A. However, since the points on curve A actually correspond to a series of transient states of the sample, it is perhaps not proper to attach much significance to its slope. The curve B, which is obtained after lengthy treatment, has a slope at the lower part of the curve of 138 kcal/mole which can be compared with that found by Moore *et al.*[6] using tracer techniques of 116 kcal/mole, and that found by Claassen and Veenemans[7] using gravimetric techniques of 141 kcal/mole. The upper part of curve B has a smaller slope which could be due to a diffusion limited mechanism. For example, the rate of evaporation of free strontium from the surface could be limited by the diffusion of strontium through a strontium-depleted surface layer. This surface layer would be enriched in oxygen from the oxygen atmosphere surrounding the sample. Such a mechanism would also explain the observed time dependent behavior of the Sr^+ ion current as one proceeds from point to point on the upper part of curve B. The subsequent curves which are parallel to B, but displaced downward, result from the depletion of the sample material.

There is also the possibility that the platinum takes an active part in this phenomenon. The reaction of Pt with SrO has been studied by Moore *et al.*[6] Their results indicate that Pt and SrO do not react in such a manner as to form free Sr and at the same time retain the oxygen in the Pt-SrO system. The platinum could still act as a dissociating agent, in which case either surface or volume diffusion in or on the platinum would be the limiting mechanism. In this event one might expect that considerable amounts of strontium would be stored either in or on the platinum. On several occasions when the sample had fallen off the ribbon, it was found that the Sr^+ disappeared in a time less than the response time of the detector. Further, no Sr^+ could be found even if the then bare ribbon was quickly raised to the highest possible temperature.

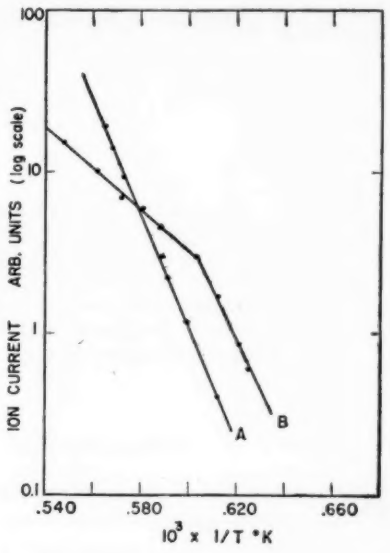

FIG. 2. Log·Sr^+ ion current *vs* 1/T for SrO on Pt. Curve A corresponds to the initial state of the sample and curve B to the final state.

ACKNOWLEDGMENTS

Financial support by the Research Corporation, and by the University of Missouri Research Council, is gratefully acknowledged. The authors also wish to acknowledge their indebtedness to B. Goodman and the late A. S. Eisenstein for their encouragement and helpful criticism.

[5] A. H. White, J. Appl. Phys. **20**, 856 (1949).
[6] Moore, Allison, and Struthers, J. Chem. Phys. **18**, 1572 (1950).
[7] A. Claassen and G. F. Veenemans, Z. Physik **80**, 342 (1933).

Infrared Spectra of CH_3COONa and CD_3COONa and Assignments of Vibrational Frequencies*

LLEWELLYN H. JONES AND EUGENE MCLAREN
Los Alamos Scientific Laboratory, University of California, Los Alamos, New Mexico
(Received March 18, 1954)

The absorption spectra of solid CH_3COONa and CD_3COONa have been observed from 350–5000 cm^{-1}. All of the fundamental frequencies of the acetate ion have been observed and assigned with the exception of that of the torsional oscillation. The assignments for CH_3NO_2 and CD_3NO_2 [2,3] were used as an aid in assigning the $CH_3CO_2^-$ and $CD_3CO_2^-$ frequencies. An approximate force constant, 9.3×10^5 dynes/cm, is given for the C–O bond of $CH_3CO_2^-$ in solid sodium acetate. The spectra of the partially deuterated species were observed and assignments were made with the aid of the Decius-Wilson sum rule and the Teller-Redlich product rule.

INTRODUCTION

FOR the study of the infrared spectra and structure of certain acetate complexes, it was desired to know the fundamental frequencies of the normal modes of vibration of the acetate ion in solid sodium acetate.

The Raman and infrared spectra of sodium acetate have been studied in the past, particularly by Duval, Lecomte, and Douville.[1] No conclusive assignments have been made for the frequencies of the various fundamental vibrations of the acetate ion. Duval *et al.*[1] noted the similarity of the acetate ion to the nitromethane molecule. The infrared and Raman spectra of nitromethane and deuteronitromethane have been studied by Wells and Wilson[2] and T. P. Wilson.[3] The latter author gave fairly conclusive assignments and calculated force constants for the nitromethane molecule.

We have observed the infrared spectra of solid sodium acetate and of the partially and completely deuterated species. By a comparison of their spectra with those of nitromethane and deuteronitromethane, assignments of the fundamental vibrational frequencies have been made.

EXPERIMENTAL

Deuterated sodium acetate was prepared by two methods. In the first method *D* was exchanged for *H* in a solution of malonic acid in D_2O followed by decarboxylation of the deuterated malonic acid[4] and neutralization with NaOH to the calculated pH of neutral sodium acetate. In the second method *D* was exchanged for *H* by heating a solution of sodium acetate in D_2O at 150°C in a sealed tube.[5] This method was also used to prepare the partially deuterated species.

Samples of deuterated sodium acetate prepared by each method gave identical infrared spectra.

Mass analysis of an early sample prepared by the first method indicated the presence of 94 ± 2 percent of the CD_3 species. The sample used for the infrared spectrum, shown in Fig. 1, was further deuterated and believed to be >99 percent CD_3COONa.

The infrared spectra were taken of the solid residue left from evaporation of an aqueous solution of CD_3COONa on silver chloride, sodium chloride, potassium bromide, and KRS-5 windows. Evaporation was performed in a desiccator over magnesium perchlorate to favor anhydrous salt formation. The window material had no specific effect on the observed spectra.

A Perkin-Elmer Model 12-C spectrometer, converted to double-pass operation, was used to record the spectra. Interchangeable cesium bromide, sodium chloride, and lithium fluoride prisms were used to cover the range 270–5000 cm^{-1}. For calibration the absorption bands of H_2O, NH_3, CO_2, HCl, HBr, CH_4, and CO vapors were used.

Results and Discussion

In Fig. 1 are shown the absorption spectra of solid anhydrous CH_3COONa and CD_3COONa in the region 290 cm^{-1} to 3200 cm^{-1}, at room temperature and at 80°K. No absorption band other than that due to atmospheric water vapor appeared in the O–H stretching region, 3100–3800 cm^{-1}, thus showing that the salts were indeed anhydrous.

As discussed by Crawford and Wilson,[6] the nitromethane molecule (and thus the acetate ion) in a rigid configuration can at most have a plane of symmetry. However, they have shown that if the force constants for cross terms such as those involving N–C–H and C–N–O angles are treated as constants independent of the angle of twist about the C–N bond, or restricted to certain functions of this angle, the secular equation can be factored as if the molecule possessed the symmetry C_{2v}. This factoring simplifies the normal coordi-

* This work was sponsored by the U. S. Atomic Energy Commission.

[1] Duval, Lecomte, and Douville, Ann. phys. **17**, 5–71 (1942).
[2] A. J. Wells and E. B. Wilson, J. Chem. Phys. **9**, 314 (1941).
[3] T. P. Wilson, J. Chem. Phys. **11**, 361 (1943).
[4] J. O. Halford and Leigh C. Anderson, J. Am. Chem. Soc. **58**, 736 (1936).
[5] L. D. C. Bok and K. H. Geib, Z. physik. Chem. **A183**, 353 (1939).
[6] B. L. Crawford and E. B. Wilson, J. Chem. Phys. **9**, 323 (1941).

nate treatment, and Wells and Wilson[2] and T. P. Wilson[3] have made their frequency assignments for nitromethane on the basis of a C_{2v} model. To be consistent, we have assigned the vibrations in $CH_3CO_2^-$ similarly, even though we have not made a complete normal coordinate treatment.

In Table I, all the fundamental frequencies are given, except the torsional vibration, for $CH_3CO_2^-$ and $CD_3CO_2^-$. The CH_3NO_2 and CD_3NO_2 frequency assignments of Wilson[3] are given also to illustrate the great similarity of the acetate ion to the nitromethane molecule.

Assignments of Fundamentals

All of the fundamentals can be assigned by comparison with nitromethane. In the case of nitromethane, both Raman and infrared data were available. Furthermore, polarization of the Raman bands and envelopes of the infrared bands gave valuable information on the symmetry type of the vibrations. Therefore, the frequencies reported by Wilson[3] for nitromethane are certainly reliable.

The C—H stretching frequencies are obvious, and as with nitromethane, the lower and less intense frequency must belong to representation A_1. As with nitromethane, the B_1 and B_2 C—H stretching vibrations have the same frequency; apparently, the degeneracy remains even at low temperature as no splitting was observed at 80°K.

The unsymmetrical C—O stretching frequency is obviously the very strong band at 1578 cm^{-1} shifted to 1563 in $CD_3CO_2^-$. The symmetrical C—O stretching frequency of $CD_3CO_2^-$ is at 1406 cm^{-1}. Some confusion arises in trying to assign the symmetrical C—O stretching of $CH_3CO_2^-$, as there are three CH_3 deformation frequencies in the same region. It was necessary to use a thin path and cool to 80°K in order to resolve these frequencies. The B_1 and B_2 CH_3 deformation frequencies are assigned as 1440 and 1488 cm^{-1}, shifting to 1045 and 1030 cm^{-1}, resepectively, by analogy with nitromethane and in order to satisfy the Teller-Redlich product rule.[7] The other two frequencies in this region, 1408 and 1425 cm^{-1}, then arise from the symmetrical CO stretching and the symmetrical CH_3 deformation. Probably they interact, and it is arbitrary to make a choice. However, in nitromethane the symmetrical N—O stretching frequency is unshifted in CD_3NO_2; thus, it seems probable that the band at 1408 cm^{-1} is the C—O symmetrical stretching frequency of $CH_3CO_2^-$.

The C—C stretching frequencies of $CH_3CO_2^-$ and $CD_3CO_2^-$ are remarkably similar to the C—N stretching frequencies of CH_3NO_2 and CD_3NO_2 respectively, thus aiding in the frequency assignments. Furthermore, the C—C frequency of $CH_3CO_2^-$, at 924 cm^{-1}, is split at low temperatures, perhaps due to coupling with a

[7] G. Herzberg, *Infrared and Raman Spectra* (D. Van Nostrand Company, Inc., New York, 1947), p. 232.

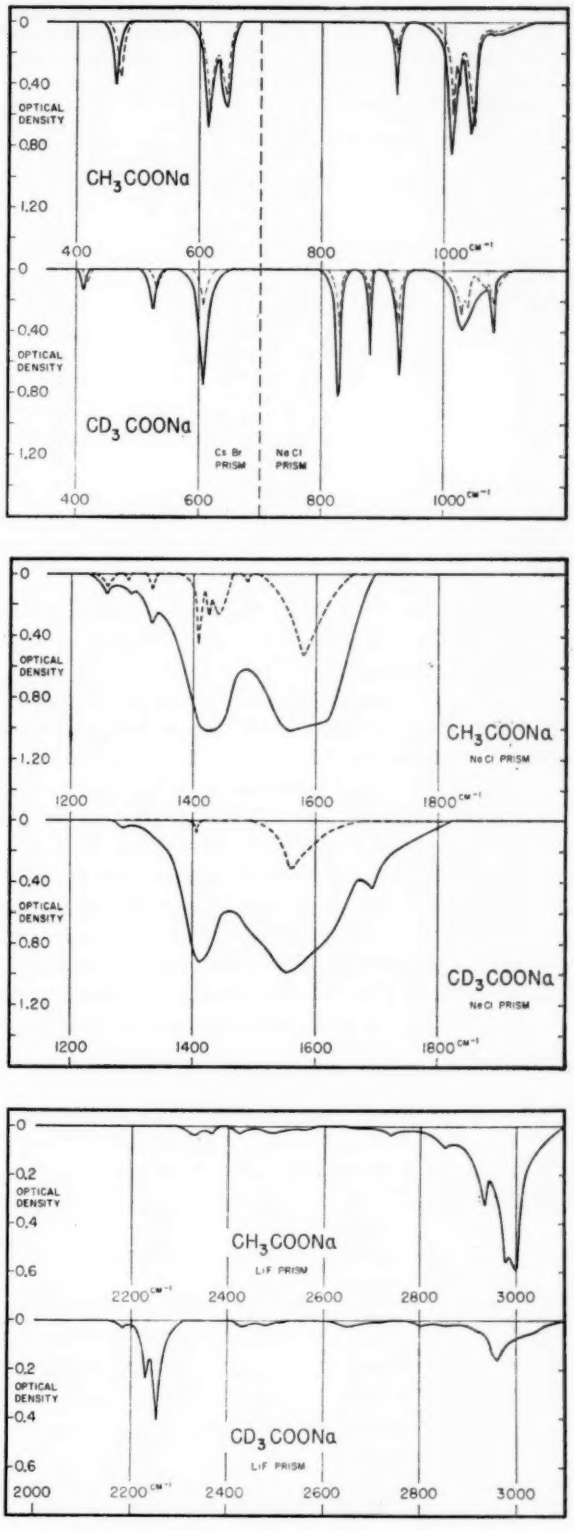

FIG. 1. Absorption spectra of CH_3COONa and CD_3COONa from 350 cm^{-1} to 3100 cm^{-1}.

Solid lines represent absorption spectra at room temperature. For each compound the same sample was used throughout.

Broken lines represent absorption spectra at 80° Kelvin. In the region 1200–1800 cm^{-1} a thinner sample was used at this low temperature in order to gain resolution.

TABLE I. Fundamental frequencies of $CH_3CO_2^-$, $CD_3CO_2^-$, CH_3NO_2, and CD_3NO_2 in solid sodium acetate and gaseous nitromethane.

Representation (C_{2v})		Type of vibration	Assigned frequency, cm^{-1} CH_3COO^-	CD_3COO^-	Product ratio[a] Theor.	Obs.	Analogous Nitromethane[b] frequencies cm^{-1} CH_3NO_2	CD_3NO_2
A_1	ν_1	C−H stretching	2933	2230			2965	2160
	ν_2	CH_3 deformation	1425	1081			1413	1090
	ν_3	C−O stretching	1408	1406	1.95	1.92	1384	1384
	ν_4	C−C stretching	924	880			921	879
	ν_5	CO_2 deformation	645	609			647	632
A_2	ν_6	Torsion about C−C bond	...	...			...	...
B_1	ν_7	C−H stretching	2999	2254			3048	2290
	ν_8	C−O stretching	1578	1563			1582	1571
	ν_9	CH_3 deformation	1440	1045	2.58	2.56	1449	1051
	ν_{10}	CH_3 rocking	1012	828			1097	*ca.* 879
	ν_{11}	CO_2 rocking	465	411			476	424
B_2	ν_{12}	C−H stretching	2999	2254			3048	2290
	ν_{13}	CH_3 deformation	1488	1030	2.53	2.535	1488	1051
	ν_{14}	CH_3 rocking	1045	928			1153	944
	ν_{15}	CO_2 rocking	615	525			599	560

[a] See reference 7.
[b] See reference 3.

lattice frequency. A similar splitting occurs for the peak at 880 cm^{-1} in $CD_3CO_2^-$, thus further substantiating the assignments.

The CO_2 deformation and CH_3 rocking frequencies are assigned by analogy with nitromethane. There might be a question as to the choice between 615 and 645 cm^{-1} for the CO_2 deformation frequency. However, the regular decrease of this frequency in progressing through the partially deuterated species indicates that 645 cm^{-1} is the correct choice (see Table II).

The B_1 and B_2 CO_2 rocking motions are assigned as 465 and 615 cm^{-1}, respectively, under the same argument used in assigning the two NO_2 rocking frequencies of nitromethane. That is, the moment of inertia of the CO_2 group about an axis perpendicular to its plane is very much larger than that about an axis lying in its plane and perpendicular to the symmetry axis, both axes passing through the center of gravity of the CO_2 group. This implies that the CO_2 rocking motion in the CCO_2 plane should have a considerably lower frequency than the CO_2 rocking motion perpendicular to this plane (Class B_2).

In order to check the validity of these assignments, the Teller-Redlich product rule[7] was applied. The structure of the acetate ion has not been given, so the dimensions used in calculating moments of inertia are subject to correction, but also these dimensions are not very critical. They are listed below:

C−H	1.08A
C−C	1.50A
C−O	1.27A
O−C−O angle	125°
HCH angle	109°28′.

The C−H distance and tetrahedral structure of the CH_3 group cannot be far off. The C−O distance and O−C−O angle were assumed similar to those of sodium formate.[8] The C−C distance was chosen as 1.50, slightly shorter than the normal C−C distance of hydrocarbons (1.54A), because the C−C frequency is somewhat higher than usual. The general agreement of the experimental and theoretical product ratio lends confidence to the assignments.

TABLE II. Fundamental frequencies of $CH_3CO_2^-$, $CH_2DCO_2^-$, $CHD_2CO_2^-$, and $CD_3CO_2^-$.

Type of motion	Frequency, cm^{-1} $CH_3CO_2^-$	$CH_2DCO_2^-$	$CHD_2CO_2^-$	$CD_3CO_2^-$
C−H stretching	2933	2218	2228	2230
	2999	2942	2254	2254
	2999	[3000][a]	[3000][a]	2254
CH_3 deformation	1425	1440	1256	1081
	1440	[1420][a]	1246	1045
	1488	1236	1067	1030
CO_2 stretching	1408	[1407][a]	[1407][a]	1406
	1578	[1572][a]	1566	1563
C−C stretching	924	(894)?	(892)?	880
CH_3 rocking	1012	938	860	828
	1045	957	936	928
CO_2 deformation	645	638	628	609
CO_2 rocking	465	442	426	411
	615	576	550	525

[a] Values in brackets were not resolved as distinct absorption bands. They were chosen for compatibility of spectra and to satisfy the Decius-Wilson sum rule and the Teller-Redlich product rule.

Partially Deuterated Species

Some of the frequencies for the partially deuterated species were also observed. The assignments are given in Table II along with those of $CH_3CO_2^-$ and $CD_3CO_2^-$.

Because of the complexity of the spectra of these mixed species, some of the frequencies are uncertain. Values were chosen for reasonable agreement with the

[8] W. H. Zachariasen, Phys. Rev. **53**, 917 (1938).

observed spectra, with the Decius-Wilson sum rule[9] and with the Teller-Redlich product rule.[7]

According to the Decius-Wilson sum rule, the following relations should be approximately satisfied by the fundamental frequencies:

$$2(\sum\nu^2)H_3+(\sum\nu^2)D_3=3(\sum\nu^2)H_2D$$
$$(\sum\nu^2)H_3+2(\sum\nu^2)D_3=3(\sum\nu^2)HD_2.$$

For brevity, H_3 is used for $CH_3CO_2^-$, H_2D for $CH_2DCO_2^-$, etc. These relations should hold for all the fundamental frequencies, as well as for all the fundamental frequencies within a given symmetry class. Since the torsional vibration (class A_2) was not observed, it must be factored out. Using all of the other fourteen frequencies of each species (from Table II), good agreement is obtained as shown below.

$$2(\sum\nu^2)H_3+(\sum\nu^2)D_3=108.74\times10^6,$$
$$3(\sum\nu^2)H_2D=108.54\times10^6,$$
$$(\sum\nu^2)H_3+2(\sum\nu^2)D_3=93.39\times10^6,$$
$$3(\sum\nu^2)HD_2=92.53\times10^6.$$

When the frequencies involving hydrogens for the partially deuterated species are assigned to the various symmetry classes of C_{2v} (as A_1, B_1, and B_2), the sum rule agreement is poor, for the individual symmetry classes, regardless of how these frequencies are assigned. However, fair agreement can be obtained by assigning average values of the squares of the C—H stretching, CH_3 deformation, and CH_3 rocking frequencies to the appropriate symmetry classes. When this is done, the Sum Rule equations are in reasonable agreement for the individual symmetry classes (A_1, B_1, and B_2). This averaging process appears reasonable in that the symmetry of the methyl group is destroyed.

In applying the Teller-Redlich product rule[7] to the partially deuterated species, it is again necessary to factor out the torsional vibration. Now we wish to compare the observed and calculated product ratios, using all frequencies except those of the torsional vibration, for two cases: $CH_3CO_2^-/CHD_2CO_2^-$ and $CH_2DCO_2^-/CD_3CO_2^-$. In each case, two hydrogens are being replaced with deuteriums. These two hydrogens contribute to six vibrations of all symmetry types. There is only one vibration of class A_2 to which three hydrogens contribute. Therefore, two hydrogens contribute 2/3 of a vibration to this symmetry class. Thus the six vibrations from these two hydrogens are distributed as

Class A_1	4/3 vibrations
A_2	2/3 vibrations
B_1	2 vibrations
B_2	2 vibrations.

Using these numbers for the number of vibrations involving the two replaced hydrogen atoms, and the structure listed earlier in this paper, we arrive at satisfactory agreement with the Teller-Redlich product rule, as seen in Table III. As with the sum rule, assignments among the individual symmetry classes for the partially deuterated species do not give satisfactory agreement with the product rule. However, if appropriate averages are taken of the hydrogen frequencies, and these averages are used in the appropriate symmetry classes, reasonable agreement with the product rule is obtained for the individual symmetry classes.

TABLE III. Product ratios[a] for $CH_3CO_2^-$ and deuterated species.

	Observed	Calculated
P_{H_3}/P_{HD_2}	5.510	5.449
P_{H_2D}/P_{D_3}	5.559	5.498

[a] See reference 7.

TABLE IV. Combination frequencies for CH_3COO^- and CD_3COO^-.

CH_3COO^-, cm^{-1} Observed	Calculated	Assignment	CD_3COO^- Observed	Calculated
1082	1110	$\nu_5+\nu_{11}$	···	1020
1258	1260	$\nu_5+\nu_{15}$	···	1134
1292	1290	$2\nu_5$	···	1218
1332	1389	$\nu_4+\nu_{11}$	1288	1291
2332	2332	$\nu_3+\nu_4$	···	2286
2367	2364	$\nu_4+\nu_9$	···	1925
2420	2412	$\nu_4+\nu_{13}$	1903	1910
2490	2500	$\nu_{10}+\nu_{13}$	···	1858
2530	2533	$\nu_{13}+\nu_{14}$	···	1958
2560	2590	$\nu_8+\nu_{10}$	···	2391
2738	2816	$2\nu_3$	2800	2812
2830	2833	$\nu_2+\nu_3$	2479	2487
2854	2850	$2\nu_2$	2167	2162
2976	2986	$\nu_3+\nu_8$	2961	2969
4295	4341	$\nu_1+\nu_3$	···	3636
4382	4407	$\nu_3+\nu_7$	···	3660
···	1936	$\nu_4+\nu_{10}$	1695	1708
···	2223	$\nu_5+\nu_8$	2183	2172
···	2896	$\nu_3+\nu_{13}$	2431	2436
···	3018	$\nu_8+\nu_9$	2615	2608
···	3003	$\nu_2+\nu_8$	2650	2644
···	3644	$\nu_5+\nu_{12}$	2852	2863

Combination Frequencies

One strong combination band was observed for each of $CH_3CO_2^-$ and $CD_3CO_2^-$ at 2976 and 2961 cm^{-1}, respectively. These must be combinations of the symmetric and asymmetric C—O stretching frequencies, calculated as 2986 and 2969 cm^{-1}. Several other weaker combination bands have been observed and are listed in Table IV with probable assignments.

Force Constants

The similarity in their spectra indicates that $CH_3CO_2^-$ and CH_3NO_2 have similar force constants. It was not deemed worthwhile to carry out a normal coordinate treatment of the complete acetate ion. However, it

[9] J. C. Decius and E. B. Wilson, J. Chem. Phys. **19**, 1409–1412 (1951).

TABLE V. Values of k_1 and k_{12} for NO_2 group of nitromethane and CO_2 group of the acetate ion.

	$k_1 \times 10^{-5}$ dynes/cm	$k_{12} \times 10^{-5}$ dynes/cm
CH_3NO_2, accurate value of Wilson[a]	9.72	2.54
CH_3NO_2, by simplified treatment	9.87	1.54
$CH_3CO_2^-$, by simplified treatment	9.27	1.70

[a] See reference 3.

would be useful to be able to determine the effect of complexing on the C−O force constant.

For this purpose, the NO_2 group of nitromethane was treated as a separate triatomic molecule using the two N−O stretching frequencies, and the NO_2 bending frequency assigned by Wilson[3] (see Table I). The potential function used was:

$$2V = k_1[(\Delta R_1)^2 + (\Delta R_2)^2] + k_{12}(\Delta R_1)(\Delta R_2) + k_\alpha(\Delta\alpha)^2.$$

Values of k_1 and k_{12} were calculated to compare with the accurate values calculated by T. P. Wilson.[3] The agreement is good, and such a simplified treatment should be satisfactory to determine approximately the relative change of C−O force constant in $CH_3CO_2^-$ when the group complexes with other ions.

In Table V are given the values of k_1 and k_{12} calculated by this simplified method, along with those of T. P. Wilson. Also given are values of k_1 and k_{12} calculated by this simplified method for the CO_2 group of sodium acetate using $R_{C-O} = 1.27$A and O−C−O angle = 125°, as above.

THE JOURNAL OF CHEMICAL PHYSICS VOLUME 22, NUMBER 11 NOVEMBER, 1954

Charge-Transfer-No-Bond Adsorption

F. A. MATSEN, A. C. MAKRIDES, AND N. HACKERMAN
Departments of Chemistry and Physics, The University of Texas, Austin
(Received November 24, 1953)

The theory of charge-transfer complex is applied to adsorption on metals and semiconductors. The heat of adsorption at zero coverage is given in terms of the ionization energy of the adsorbate, the electronic work function of the adsorbent, an image energy, and an interaction energy. For metals a linear relationship between heat (at zero coverage) and extent of adsorption is deduced from two of the simpler forms of theoretical isotherms. The functional dependence of the extent of adsorption on the ionization energy of the adsorbate is thus obtained.

The treatment for semiconductors is modified to take into account the space charge generated in the semiconductor on adsorption.

This treatment is shown to be consistent with reported experimental data for adsorption on iron powder of long chain nitriles, esters, alcohols, amines, and thiols.

INTRODUCTION

A DESCRIPTION of the adsorption of certain molecules on metals by the charge-transfer complex has been suggested by Mulliken.[1] The concept has been further developed by Mignolet[2] who cited as support the positive surface potentials obtained from noble gases and simple hydrocarbons adsorbed on various metals. Recently charge-transfer adsorption on semiconductors has been treated by Boudart[3] and by Weisz.[4] In this paper, the theory of the charge-transfer complex has been applied to adsorption on both metals and semiconductors.

METALS

Ionization energies of common adsorbates are from 9 to 12 ev, while work functions are from 2 to 5 ev. Therefore, transfer of an electron from the adsorbed molecule to the metal will be an endothermic process. Complex theory provides surface acceptor levels which lie far enough below the Fermi level of the metal to make the process exothermic.

In charge-transfer complex theory, the ground state of the complex is described by a linear combination of the wave function for a no-bond state and that for a dative state in which an electron has been transferred from a Lewis base to a Lewis acid. For adsorption on a metal, the metal is the acid, the electron affinity of the acid is set equal to the work function, and the coulomb energy to the image energy. The heat of adsorption at zero coverage is then given by

$$X_0 = \{-(W_D - W_{NB}) + [(W_D - W_{NB})^2 + 4\beta^2]^{\frac{1}{2}}\}/2. \quad (1)$$

Here W_{NB} and W_D are the energies of the zero order no-bond, and dative states, respectively, and β the interaction integral. The difference in energy between the dative and no-bond form[1,5] is given approxi-

[1] R. S. Mulliken, J. Am. Chem. Soc. **74**, 811 (1952).
[2] J. C. P. Mignolet, J. Chem. Phys. **21**, 1298 (1953).
[3] M. Boudart, J. Am. Chem. Soc. **74**, 1531 (1952).
[4] P. B. Weisz, J. Chem. Phys. **21**, 1531 (1953).
[5] Hastings, Franklin, Schiller, and Matsen, J. Am. Chem. Soc. **75**, 2900 (1953).

mately by

$$W_D - W_{NB} = I_B - \Phi - e^2/4R, \qquad (2)$$

where I_B is the ionization energy of the base, Φ the work function of the metal, and $e^2/4R$ the image energy. In the last term, R is the separation of the charge on the base from the surface of the metal.[6]

The interaction integral β almost certainly varies with the base, but it is believed that the effect of its variation is small compared to the variation in I_B.[7] It is expected that its value is less than the 2.5–3 ev usually given for the β of neighboring π orbitals.[8] A spectroscopic value of 1.3 ev was obtained for iodine complexes and is used here. In Fig. 1, X_0 is plotted against I_B with $\Phi = 4.7$ ev and $R = 1$ A.

It is to be expected that the quasi ions generated in the adsorbed molecules will repel each other. This repulsion can account for the decrease in heat of adsorption with coverage which has been frequently observed.[9]

SEMICONDUCTORS

Semiconductors of the *p* type may also be regarded as Lewis acids and one may again associate the electron affinity with the work function. Experimental values[10] of the latter fall in the same range as for metals so that electron transfer from adsorbate to semiconductor without complex formation would again be an endothermic process. The formation of a charge-complex will generate new acceptor levels localized near the surface of the solid and lying below the Fermi level. At zero coverage the treatment resembles formally that given for metals except that the image force $e^2/4R$ is replaced by e^2/KR. The dielectric constant of many semiconductors is about five;[4] consequently, this term is numerically not much different from that for metals. Therefore, the heat of adsorption at zero coverage should show the same dependence on the ionization energy of the base as exhibited by metals and may be of about the same order of magnitude. However, since the Fermi level of the semiconductor is raised on adsorption, one might expect a more rapid drop in the heat of adsorption with coverage than one obtains from the quasi-ion repulsion alone for adsorption on metals. In fact, the increase in the Fermi level may be rapid enough to limit the coverage as suggested by both Boudart and Weisz (see below).

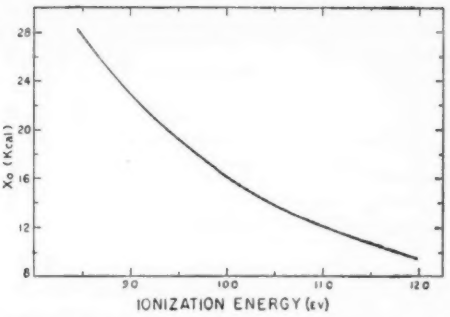

FIG. 1. The heat of adsorption at zero coverage as a function of ionization energy according to

$$X_0 = \{-(W_D - W_{NB}) + [(W_D - W_{NB})^2 + 4\beta^2]^{\frac{1}{2}}\}/2$$

with $\Phi = 4.7$ ev, $R = 1.0$ A, $\beta = 1.3$ ev.

RELATIONSHIP BETWEEN HEAT AND EXTENT OF ADSORPTION

The relationship between heat and extent of adsorption can be obtained from a theoretical isotherm. There are a wide variety of such isotherms in the literature differing in basic assumptions and approximations made. Only two of the simpler forms are considered here. The first is that obtained by Fowler[11] who, to the Bragg-Williams approximation, allowed for the interaction between adsorbed molecules. For charge-transfer adsorption on metals the interaction would mainly be electrostatic repulsion between quasi ions of the base. The Fowler expression may be written in the form

$$-X_1\theta/kT + \ln(\theta/1-\theta) = X_0/kT + \ln PQ_a/Q_g. \qquad (3)$$

Here Q_a/Q_g is the ratio of the partition functions for the adsorbed and gaseous molecules and is assumed constant;[12] θ is the fraction of the surface covered; X_0 is the heat of adsorption at zero coverage, and X_1 is the molecular interaction constant. For repulsive interaction X_1 is negative.

The second isotherm is that due to Halsey and Taylor[13] who assume a heterogeneous surface. The following is their isotherm if the distribution function $N(E)$ is constant over the range X_0 to $X_0 + \Delta X$. The quantity ΔX is taken as negative so X_0 is again the heat of adsorption at zero coverage

$$\ln[\exp(-\Delta X/kT) - \exp(\Delta X[\theta-1]/kT)]/[\exp(\Delta X[\theta-1]/kT) - 1] = X_0/kT + \ln PQ_a/Q_g. \qquad (4)$$

[6] A rough estimate of R is 1 A. The effective radius of the atom is given by $(\sigma/2) - r_{\text{covalent}}$. For N_2 and O_2 the kinetic diameter, σ, is 3.7 A, while the triple-bond covalent radius of N, and the double-bond covalent radius of O is 0.55 A yielding 1.30 A for the radius of the atom. Ionization decreases this somewhat.

[7] Treatments based on this type of assumption have been moderately successful. See for example G. W. Wheland, J. Am. Chem. Soc. **64**, 900 (1942); F. A. Matsen, J. Am. Chem. Soc. **72**, 5243 (1950), and reference 5 above. See, however, C. A. Coulson and J. de Heer, J. Chem. Soc. **1952**, 483.

[8] Since transition metals in general adsorb most strongly, it appears that β is large only for metals with vacant *d* orbitals.

[9] See for example O. Beeck, *Advances in Catalysis* (Academic Press, Inc., New York, 1950), Vol. II, p. 151; E. K. Rideal and B. M. W. Trapnell, Proc. Roy. Soc. (London) **A205**, 409 (1951).

[10] Few experimental values of Φ for semiconductors are available. For NiO a value of 4.5 ev is reported [H. B. Michaelson, J. Franklin Inst. **249**, 455 (1950)]. Reported values for other semiconductors range from 1 to 7 ev. Values of $\Phi \simeq 10$ ev, required to make $\Phi - I$ a positive quantity, are not common.

[11] R. H. Fowler, *Statistical Mechanics* (University Press, Cambridge, England, 1936).

[12] Q_a contains the partition function for the vibration of the adsorbed molecule against the metal. The classical form may be taken to be proportional to $\sqrt{X_0}$. The variation in this term is small compared to the variation in the $\exp(X_0/kT)$.

[13] G. Halsey and H. S. Taylor, J. Chem. Phys. **15**, 624 (1947).

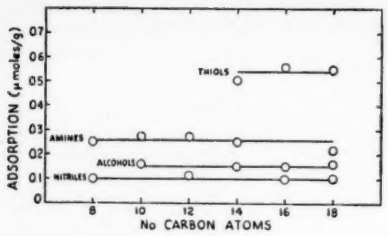

FIG. 2.

These isotherms reach saturation only for $P\rightarrow\infty$ and $\theta=1$. For systems to which these isotherms apply, comparisons of adsorbability must be made at finite, equal pressures. Plots of θ, at fixed values of PQ_a/Q_g, against the left side of Eqs. (3) and (4) show that for θ in the range 0.1 to 0.7, for a wide range of ΔX (or X_1), and to within 300 calories at room temperature, θ (saturation value) is a linear function of X_0. Figure 1 then gives the functional dependence of the saturation value of θ on the ionization energy of the base at constant pressure. It is believed that this is the situation which obtains in adsorption on metals although confirming data are lacking.

The dependence of θ upon the heat of adsorption, X_0, for semiconductors should be different from that found for metals. Weisz[4] has shown that adsorption by charge-transfer on a semiconductor can be limited by the space charge in the semiconductor. He derives the following expression for the saturation value of θ

$$\theta_s=A(KEB)^{\frac{1}{2}}. \tag{5}$$

Here E is the potential at the surface of the semiconductor, K the dielectric constant, B the relative concentration of acceptors, and

$$A=\left(\frac{1}{2\pi e}\cdot\frac{1}{a\cdot 10^{23}}\right)^{\frac{1}{2}},$$

where e is the electronic charge and a the surface area per surface molecule of solid.

In the Weisz scheme the electron is held to the solid by the potential E, numerically equal to $\Phi-I$, and electron transfer (i.e., adsorption) continues until the field is reduced to zero by the space charge of the electrons. However, the quantity $\Phi-I$ appears to be negative in most cases of interest. If one assumes complex formation, the electron will be held to the surface by an amount of energy X_0 and electron transfer will continue until the space charge provides an electron repulsion equal to X_0. This statement implies that the space charge does not affect X_0 in the first order. With this interpretation, the Weisz formula can be modified

$$\theta_s=A(KX_0B)^{\frac{1}{2}}. \tag{6}$$

For alcohols, thiols, and amines, which are discussed below, the cross sectional area is about 22 A^2; assuming, with Weisz, $a=4.6$ A^2, we have

$$\theta_s=0.75(KB)^{\frac{1}{2}}\sqrt{X_0}. \tag{7}$$

According to Eq. (7), the saturation value of θ for adsorption on semiconductors should vary as the square root of X_0. For a reasonable value of $X_0=1$ ev and with $B=10^{-2}$, $\theta_s=0.2$. The values of θ_s calculated with the aid of (7) appear in general to be smaller than those found experimentally.

EXPERIMENTAL

In this laboratory, the adsorption from benzene solution of a number of Lewis bases on iron powder has been determined.[14] This adsorption was found to consist of two types. In the first, the material adsorbed was easily removed, while in the second it was removed with some difficulty (repeated washings with pure solvent at higher temperatures). The amount firmly adsorbed was a reproducible quantity and independent of concentration once a certain small concentration ($\sim$0.001M) was exceeded. The extent of adsorption was also very nearly independent of chain length (see Fig. 2), which suggests orientation of the adsorbed molecules with base end toward the metal. The total surface area of the adsorbent was measured by adsorption of krypton and the BET method. Using cross sectional areas for adsorbate molecules obtained by extrapolation to zero compression with surface films on water of these molecules,[15] the fraction of the true surface area covered was from 0.1 to 0.6. It is believed that the second type of adsorption is no-bond-charge transfer adsorption with binding energy considerably in excess of the first type which appears to be ordinary van der Waals adsorption.

The iron powder was prepared in a reducing atmosphere. The samples were exposed, however, to air at room temperature during the adsorption experiments. From the data available,[16] it appears that such exposure results in a surface covered by one or more layers of chemisorbed oxygen and/or oxide.

If this surface can be treated as a metal, a plot of θ determined at equal pressures (concentrations) against I_B should be similar to that of Fig. 1 (calculated with $\Phi=4.7$ ev and $R=1$ A).[17] If, on the other hand, the surface is to be treated as a semiconductor, as seems more reasonable, a plot of θ_s against the square root of I_B should now give a curve similar to that of Fig. 1. Such a treatment assumes that Φ for the surface oxide is not greatly different from 4.7 ev. As noted above

[14] E. L. Cook and N. Hackerman, J. Phys. and Colloid Chem. **55**, 549 (1951); N. Hackerman and A. H. Roebuck, Ind. Eng. Chem. **46**, 1481 (1954).

[15] N. K. Adam, *The Physics and Chemistry of Surfaces* (Oxford University Press, London, 1949), p. 50.

[16] See S. Brunauer and P. H. Emmett, J. Am. Chem. Soc. **62**, 1732 (1940); M. H. Armbruster and J. B. Austin, J. Am. Chem. Soc. **68**, 1347 (1946); E. K. Rideal and B. M. W. Trapnell, Proc. Roy. Soc. (London) **A205**, 409 (1951).

[17] Values of the work function of iron range from 3.9 to 4.8 ev. Some values are 4.47 ev [G. Siljeholm, Ann. Physik. **10**, 178 (1931)], 4.48 ev [H. B. Wahlin, Phys. Rev. **61**, 509 (1942)], and 4.31 ev [S. C. Jain and K. S. Krishnan, Proc. Roy. Soc. (London) **A215**, 431 (1952)].

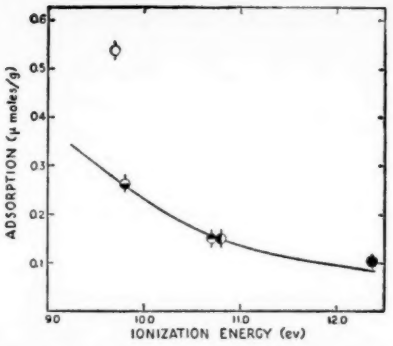

FIG. 3. The ionization energies are for the ethyl substituted derivatives [see W. C. Price, Chem. Rev. **41**, 257 (1947)]. The ionization energy of the acid is used for the ester [see J. D. Morrison and A. J. C. Nicholson, J. Chem. Phys. **20**, 1021 (1952)]. ● Nitriles; ◐ Alcohols; ◓ Esters; ◒ Amines; ○ Thiols.

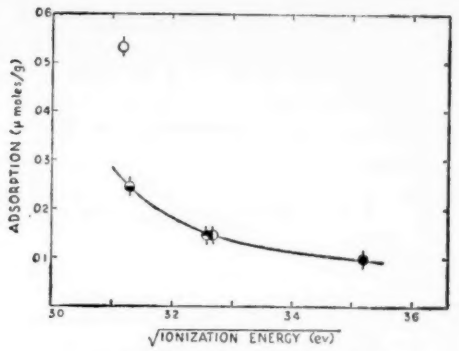

FIG. 4. See caption for Fig. 3.

values of Φ for oxides are in the same range as those for metals.

The resulting curves (see Figs. 3, 4) are both similar to the curve of Fig. 1. The data for thiols do not fall on the curve.[18]

Benzene with an ionization energy of 9.24 ev is also a good base as is shown by the existence of a benzene-iodine complex, even though it lacks an unshared electron pair. In the experiments reported here, benzene was not strongly adsorbed. This can be attributed to a larger surface-charge separation or a smaller β.[19]

HOMOGENEITY OF SURFACE

The fact that θ_s is experimentally observed to be a smooth function of the ionization energy gives some indirect evidence on the homogeneity of the surface. When θ_s is less than one it is usual to assume that only certain sites are available and/or have the binding energy necessary for adsorption. The slow variation discussed above of θ_s with I_B, a factor external to the surface, shows that the sites are gradually being brought into service as the ionization energy of the base is lowered. Thus the distribution in energy of the surface sites cannot be a stepped function as one might expect of a heterogeneous surface. The site distribution has at most a small smooth dependence on energy and may in fact be independent of energy. In the latter case, the surface would be regarded as homogeneous.

This argument is independent of the theories formulated above and has a fundamental importance of its own. It forms, however, the necessary basis for the development already given.

[18] Since R for sulfur is larger than for N and O, it should not fit on the same curve. Furthermore, one expects variation in going to the next row in the periodic table. It is interesting that sulfur is also slightly anomalous in the position of the spectrum of its complex with iodine. In both the adsorption and the frequency *versus* I_B curves, a decrease of 1 volt in the ionization energy of sulfur would place it on the curve (see reference 5). This suggests that complex theory in its present crude form is not equipped to handle such large interactions. It is clear, however, that the ionization energy must be regarded as a fundamental variable.

[19] Mulliken (see reference 1) believes the iodine molecule to be at right angles to the benzene ring and directed toward and slightly penetrating its center. The metal cannot assume such a position. For the unshared pair bases the geometry of the iodine and of the metal complexes should be approximately the same.

Dielectric Polarization in Polar Substances. Remark on a Paper by F. E. Harris and B. J. Alder

H. FRÖHLICH
Department of Theoretical Physics, University of Liverpool, Liverpool, England
(Received August 14, 1953)

A correction of a formula for the static dielectric constant derived by Harris and Alder is given in this paper.

THE purpose of the present paper is to correct some of the mistakes occurring in a recent paper by Harris and Alder[1] (quoted as H.A.) on dielectric polarization in polar substances. In this paper a general formula for the static dielectric constant ϵ was derived (H.A. Eqs. (13), (13 a–c)) which differs from formulas by Onsager,[2] Kirkwood[3] and myself,[4] quoted as O., K., and F. Thus from F. (8.5)

$$\epsilon-\epsilon_\infty=\frac{3\epsilon}{2\epsilon+\epsilon_\infty}\frac{4\pi N_0}{3kT}\mathfrak{y}_F\mathfrak{y}_F^*=\frac{2\epsilon+\epsilon_\infty}{2\epsilon+1}\frac{3\epsilon}{2\epsilon+1}\frac{4\pi N_0}{3kT}\mathfrak{y}_{0K}\mathfrak{y}_{0K}^*, \quad (1)$$

where ϵ_∞ is the high-frequency dielectric constant and N_0 is the number of dipolar molecules per unit volume. The dipole moments $\mathfrak{y}_F$ and $\mathfrak{y}_{0K}$ are defined by

$$\mathfrak{y}_F=\frac{2\epsilon+\epsilon_\infty}{2\epsilon+1}\mathfrak{y}_{0K}=\frac{\epsilon_\infty+2}{3}\mathfrak{y}_V \quad (2)$$

in terms of the vacuum moment $\mathfrak{y}_V$ of a molecule. $\mathfrak{y}_F^*$ (or $\mathfrak{y}_{0K}^*$) differs from $\mathfrak{y}_F$ (or $\mathfrak{y}_{0K}$) owing to short-range interaction between dipoles. In the absence of such interaction $\mathfrak{y}_F=\mathfrak{y}_F^*(\mathfrak{y}_{0K}=\mathfrak{y}_{0K}^*)$. In this case Eq. (1) becomes identical with Onsager's Eqs. (O. 26 and 18). The derivation of (1) and (2) is based on a model in which the high frequency contribution ϵ_∞ is not derived from properties of the structure but is treated in a macroscopic way as a temperature-independent quantity. Otherwise the very general formula (F. 7.33) has to be used. Furthermore a free molecule is treated as a sphere of dielectric constant ϵ_∞ containing a dipole $\mathfrak{y}_F$ at its center so that the total moment $\mathfrak{y}_V$ is given by Eq. (2). Kirkwood is interested in the case only in which $\epsilon\gg\epsilon_\infty$ and then finds approximately (K. 13 and 14)

$$\epsilon\simeq\frac{3}{2}\frac{4\pi N_0}{3kT}\mathfrak{y}_{0K}\mathfrak{y}_{0K}^*, \quad (3)$$

where ϵ_∞ has been neglected against ϵ. Clearly in this limit (3), too, becomes identical with (1). Harris and Alder on the other hand present a formula (H.A. 13, 13 a–c) in which expression (1) for $\epsilon-\epsilon_\infty$ is multiplied by a factor f,

$$f=\frac{\epsilon_\infty+2}{3}\frac{2\epsilon+1}{2\epsilon+\epsilon_\infty}. \quad (4)$$

Since the factor f contains the macroscopic constants ϵ and ϵ_∞ only, it would seem that one of the two formulas must be wrong on a simple point, independent of possible refinements of the model. Harris and Alder, however, propose reasons involving specific properties of the model; also they propose three different reasons in the three cases as they did not notice that the quantity denoted by μ in Onsager's and Kirkwood's papers (O. 19 and K. 17a) differs from the quantity so denoted in my book (F. 8.1) (i.e., μ_{0K} and μ_F respectively) so that Onsager's and Kirkwood's formulas follow from (1) in certain limits.

The main error in Harris and Alder's treatment can easily be traced. These authors use as model a homogeneous medium in the shape of a macroscopic sphere in vacuum whose dipole moment for any given microscopic configuration is considered as composed of two contributions: (i) the displacement moment $\mathbf{M}_d$ due to elastic displacement of charge under the direct influence of the applied field; (ii) the orientational moment $\mathbf{M}_0$ due to a specified dipolar configuration including the displacement moment induced thereby in the sphere. The contribution $\mathbf{M}_d$ is then treated on a macroscopic basis in terms of ϵ_∞, and in a straightforward way (see H.A. 8) one finds (V = total volume)

$$\epsilon-1=\frac{3\epsilon}{2\epsilon+1}\frac{4\pi}{3kTV}[\mathbf{M}_0^2]+\frac{(\epsilon+2)(\epsilon_\infty-1)}{\epsilon_\infty+2}, \quad (5)$$

where the symbol $[\cdots]$ denotes formation of the statistical average over all configurational coordinates $(1,2,\cdots j\cdots)$ of the dipoles (j denotes the configurational coordinates of the jth dipole). Now in order to evaluate $[\mathbf{M}_0^2]$, the moment $\mathbf{M}_0=\mathbf{M}_0(1,2,\cdots j\cdots)$ in a specified configuration is written as a sum of contributions of individual molecules,

$$\mathbf{M}_0(1,2,\cdots j\cdots)=\sum_{j=1}^{N_0V}\mathfrak{y}_{sj}, \quad (6)$$

where $\mathfrak{y}_{sj}$ denotes the contribution of the jth molecule. This decomposition of $\mathbf{M}_0$ can be carried through in

[1] F. E. Harris and B. J. Alder, J. Chem. Phys. **21**, 1031 (1953).
[2] L. Onsager, J. Am. Chem. Soc. **58**, 1486 (1936).
[3] J. G. Kirkwood, J. Chem. Phys. **7**, 911 (1939).
[4] H. Fröhlich, *Theory of Dielectrics* (Clarendon Press, Oxford, 1949).

several ways depending on what part of the induced polarization is included in $\mathfrak{y}_{sj}$. Firstly, choose $\mathfrak{y}_{sj}$ such that it becomes independent of all configurational coordinates, except those of the jth dipole; $\mathfrak{y}_{sj}$ in this case will be denoted as $\mathfrak{y}_{sj}'(j)$, and hence

$$\mathbf{M}_0(1,2,\cdots j\cdots)=\sum_j \mathfrak{y}_{sj}'(j). \tag{7}$$

This decomposition is possible only if the polarizability of individual molecules is a scalar (not a tensor). This assumption, however, is implicit in the model used here. The moment $\mathfrak{y}_{sj}'$ is defined as the moment of the jth dipole, including the moment it induces (by displacement polarization) in all the molecules of the sphere, but excluding contributions—either direct or through induction—of all other dipoles. All contributions $\mathfrak{y}_{sj}'(j)$ superpose linearly and add up to form $\mathbf{M}_0$ as required. The value of $\mathfrak{y}_{sj}'(j)$ is obtained by simple electrostatics if the simple molecular model mentioned above is employed; $\mathfrak{y}_{sj}'$ is then the moment of a large sphere of dielectric constant ϵ_∞ containing a rigid dipole $\mathfrak{y}_F(j)$ in its interior. This moment is independent of the size of the sphere and hence is equal to the vacuum moment $\mathfrak{y}_V$. Thus

$$\mathfrak{y}_{sj}'(j)=\mathfrak{y}_V(j). \tag{8}$$

Using (7), clearly

$$[\mathbf{M}_0^2(1,2,\cdots j\cdots)]=\sum_j[\mathfrak{y}_{sj}'(j)\mathbf{M}_0(1,2,\cdots j\cdots)]. \tag{9}$$

Also if $[\cdots]_j$ denotes formation of the statistical average over all configurational coordinates except those of the jth dipole,

$$[\mathfrak{y}_{sj}'(j)\mathbf{M}_0(1,2,\cdots j\cdots)]_j = \mathfrak{y}_{sj}'(j)[\mathbf{M}_0(1,2,\cdots j\cdots)]_j. \tag{10}$$

Here $[\mathbf{M}_0(1,2,\cdots j\cdots)]_j$ depends on the jth configurational coordinate only (denoted by $\langle\mathfrak{y}_\mu\rangle$ by Harris and Alder). It represents the total equilibrium moment of the spherical specimen when the jth dipole has specified coordinates. This quantity has been calculated by Kirkwood; it is equal to $\mathfrak{y}_{0K}(j)$ (see (2)) in the absence of short-range forces. In the presence of such forces, this value is modified and will be denoted by $\mathfrak{y}_{0K}{}^*(j)$. Thus

$$[\mathbf{M}_0(1,2,\cdots j\cdots)]_j=\mathfrak{y}_{0K}{}^*(j). \tag{11}$$

In an isotropic substance the magnitudes $\mu_{0K}{}^*(j)=\mu_{0K}$ and $\mu_{sj}'(j)=\mu_s'$ and the product $\mathfrak{y}_{sj}'(j)\mathfrak{y}_{0K}{}^*(j)=\mathfrak{y}_s'\mathfrak{y}_{0K}{}^*$ are independent of j. Hence Eqs. (5), (8), (9), and (11) yield

$$\epsilon-1=\frac{3\epsilon}{2\epsilon+1}\frac{4\pi N_0}{3kT}\mathfrak{y}_s'\mathfrak{y}_{0K}{}^*+\frac{(\epsilon+2)(\epsilon_\infty-1)}{\epsilon_\infty+2}. \tag{12}$$

Using $\mathfrak{y}_s'=\mathfrak{y}_V$ according to (8) and (2), Eq. (12) is seen to be identical with (1). In the absence of short range forces when $\mathfrak{y}_{0K}{}^*=\mathfrak{y}_{0K}$ it thus reduces to Onsager's formula.

Now to demonstrate Harris and Alder's procedure a second type of decomposition of $\mathbf{M}_0$ different from (7) must first be introduced. In this second case $\mathbf{M}_0$ is divided into contributions from spacially separated regions denoted by $\mathfrak{y}_{sj}''$. Thus let $\mathfrak{y}_{sj}''(1,2,\cdots j\cdots)$ be the moment contained in a molecular volume around the jth dipole and including the moment induced in it by all the other dipoles. Clearly this induced moment depends on the configuration $(1,2,\cdots j\cdots)$ of all the other dipoles. Thus in this case

$$\mathbf{M}_0(1,2,\cdots j\cdots)=\sum_j \mathfrak{y}_{sj}''(1,2,\cdots j\cdots), \tag{13}$$

and hence

$$[\mathbf{M}_0^2(1,2,\cdots j\cdots)] =\sum_j[\mathfrak{y}_{sj}''(1,2,\cdots j\cdots)\mathbf{M}_0(1,2,\cdots j\cdots)], \tag{14}$$

corresponding to Eq. (9) of the first case. The further development leading through Eqs. (10) to (12) is not possible, however, because $\mathfrak{y}_{sj}''$ depends on all configurational coordinates. Harris and Alder think that they can overcome this difficulty by defining in (H.A. 17) their $\mathfrak{y}_{sj}$ denoted here as $\mathfrak{y}_{sjHA}$, as the statistical average of $\mathfrak{y}_{sj}''$ over all configurational coordinates except those of the jth dipole as

$$\mathfrak{y}_{sjHA}(j)=[\mathfrak{y}_{sj}''(1,2,\cdots j\cdots)]_j \tag{15}$$

and assuming $[\mathfrak{y}_{sj}''\mathbf{M}_0]_j=\mathfrak{y}_{sjHA}(j)[\mathbf{M}_0]_j$ (cf. H.A., following the equation subsequent to (H.A. 8), written as $[\mathbf{M}_0^2]=N(\mathfrak{y}_s\langle\mathbf{M}_0\rangle_{\mu_s})$). This latter formula is equivalent with the statement that

$$[\mathfrak{y}_{sj}''(1,2,\cdots j\cdots)\mathbf{M}_0(1,2,\cdots j\cdots)]_j =[\mathfrak{y}_{sj}''(1,2,\cdots j\cdots)]_j \times[\mathbf{M}_0(1,2,\cdots j\cdots)]_j, \text{ incorrect}; \tag{16}$$

and it is wrong because the operation $[\ ]_j$ involves integrations over all but the jth coordinates, and the integral of the product of two functions is not equal to the product of their integrals. However, using the incorrect formula (16), the right-hand side is equal to $\mathfrak{y}_{sjHA}(j)\mathfrak{y}_{0K}{}^*(j)$ and can be written as $\mathfrak{y}_{sHA}\mathfrak{y}_{0K}{}^*$ because the magnitudes $\mu_{sjHA}(j)$ and $\mu_{0K}{}^*(j)$ are independent of j. Thus instead of (12) a formula is obtained in which μ_s' is replaced by μ_{sHA}. Thus using (12)

$$\epsilon-\epsilon_\infty=\frac{\epsilon_\infty+2}{3}\frac{3\epsilon}{2\epsilon+1}\frac{4\pi N_0}{3kT}\mathfrak{y}_{0K}{}^*\begin{cases}\mathfrak{y}_s' & \text{correct}\\ \mathfrak{y}_{SHA} & \text{H.A.}\end{cases} \tag{17}$$

Harris and Alder have evaluated their $\mathfrak{y}_{sHA}$ for the case in which short-range forces are absent and find (H.A. 18)

$$\mathfrak{y}_{sHA}=f\mathfrak{y}_V, \tag{18}$$

where f is given by (4). Thus the correct $\mathfrak{y}_s'=\mathfrak{y}_V$ [see Eq. (8)] yields the correct formula (1) whereas the incorrect replacement of $\mathfrak{y}_s'$ by $\mathfrak{y}_{sHA}$ together with (18) yields the further factor f on the right hand side, i.e., it leads to the incorrect formula (H.A. 13, 13 a–c).

Harris and Alder in private correspondence express

the opinion that wrong ways of averaging, like that in (16), are often used in statistical mechanics. In fact they seem to think that their factor f appears through an improvement of their model over those yielding formula (1). It is of importance, therefore, to notice that Harris and Alder's incorrect method can be applied to a very simple and clearly defined model (rigid point dipoles in a continuum of dielectric constant ϵ_∞; absence of short range forces) and then leads to the incorrect factor f through the incorrect averaging process (16).

It is evident that any conclusions drawn in Harris and Alder's paper are subject to revision.

THE JOURNAL OF CHEMICAL PHYSICS VOLUME 22, NUMBER 11 NOVEMBER, 1954

Statistical Mechanical Derivation of Onsager's Equation for Dielectric Polarization

FRANK E. HARRIS* AND BERNI J. ALDER
Department of Chemistry and Chemical Engineering, University of California, Berkeley, California
(Received October 12, 1953)

The assumptions necessary in deriving the equation for the dielectric polarization in the absence of short-range interactions between the molecules, as represented by the Onsager equation, are made explicit. The equation derived by Harris and Alder for the general case of dielectric polarization of polar liquids is seen to involve an approximation not previously stated. The latter equation, when reduced to the limit represented by the Onsager equation, becomes identical to it when a further simplification is introduced.

THE purpose of the present paper is to make clear the assumptions involved in the derivation of the Onsager[1] equation for dielectric polarization. This is desirable in view of the different equation obtained by Harris and Alder[2] in their formulation of the theory. Their equation in the absence of short-range forces agrees with an equation previously postulated by Piekara,[3] while Fröhlich's[4] and Kirkwood's[5] theories agree with Onsager's.

The general formula for the static dielectric constant ϵ derived by Onsager,[1] Kirkwood,[5] and Fröhlich[4] quoted as O, K, and F is (see F 8.5):

$$\epsilon-\epsilon_\infty=\frac{3\epsilon}{2\epsilon+\epsilon_\infty}\frac{4\pi N_0}{3kT}\boldsymbol{\mu}_F\boldsymbol{\mu}_F^*=\frac{2\epsilon+\epsilon_\infty}{2\epsilon+1}\frac{3\epsilon}{2\epsilon+1}\frac{4\pi N_0}{3kT}\boldsymbol{\mu}_{OK}\boldsymbol{\mu}_{OK}^*, \quad (1)$$

where ϵ_∞ is the high-frequency dielectric constant and N_0 is the number of dipolar molecules per unit volume. The dipole moments $\boldsymbol{\mu}_F$ and $\boldsymbol{\mu}_{OK}$ are defined by

$$\boldsymbol{\mu}_F=\frac{2\epsilon+\epsilon_\infty}{2\epsilon+1}\boldsymbol{\mu}_{OK}=\frac{\epsilon_\infty+2}{3}\boldsymbol{\mu}_V \quad (2)$$

in terms of the vacuum moment $\boldsymbol{\mu}_V$ of a molecule. $\boldsymbol{\mu}_F^*$ (or $\boldsymbol{\mu}_{OK}^*$) differs from $\boldsymbol{\mu}_F$ (or $\boldsymbol{\mu}_{OK}$) owing to short-range interaction between dipoles. In the absence of such interaction $\boldsymbol{\mu}_F=\boldsymbol{\mu}_F^*$ ($\boldsymbol{\mu}_{OK}=\boldsymbol{\mu}_{OK}^*$). In this case Eq. (1) becomes identical with Onsager's equation (O 26 and 18). The derivation of (1) and (2) is based on a model in which the high-frequency contribution ϵ_∞ is not derived from properties of the structure but is treated in a macroscopic way as a temperature independent quantity. Otherwise the very general formula (F 7.33) has to be used. Furthermore, a free molecule is treated as a sphere of dielectric constant ϵ_∞ containing a dipole $\boldsymbol{\mu}_F$ at its center so that the total moment $\boldsymbol{\mu}_V$ is given by Eq. (2). Kirkwood is only interested in the case in which $\epsilon\gg\epsilon_\infty$, that is nonpolarizable molecules and then finds approximately (K 13 and 14)

$$\epsilon\simeq\frac{3}{2}\frac{4\pi N_0}{3kT}\boldsymbol{\mu}_{OK}\boldsymbol{\mu}_{OK}^*, \quad (3)$$

where ϵ_∞ has been neglected against ϵ. Clearly in this limit, (3) becomes identical with (1). Harris and Alder on the other hand present a formula (HA 13, 13a–c) in which expression (1) for $\epsilon-\epsilon_\infty$ is multiplied by a factor f,

$$f=\frac{\epsilon_\infty+2}{3}\frac{2\epsilon+1}{2\epsilon+\epsilon_\infty}. \quad (4)$$

In their derivation no particular model for the representation of a molecule has to be adopted.

In comparing the theories, Harris and Alder did not notice that the quantity denoted by $\boldsymbol{\mu}$ in Onsager's and Kirkwood's paper (O 19 and K 17a) differs from the quantity so denoted in Fröhlich's book (F 8.1) (i.e., $\boldsymbol{\mu}_{OK}$ and $\boldsymbol{\mu}_F$, respectively) so that in their paper Fröhlich's theory is treated incorrectly. In the approxi-

*Present address: Chemistry Department, Harvard University, Cambridge, Massachusetts.

[1] L. Onsager, J. Am. Chem. Soc. **58**, 1486 (1936).
[2] F. E. Harris and B. J. Alder, J. Chem. Phys. **21**, 1031 (1953).
[3] A. Piekara and K. Zakrzewski, Nature **144**, 250 (1939).
[4] H. Fröhlich, *Theory of Dielectrics* (Clarendon Press, Oxford, 1949).
[5] J. G. Kirkwood, J. Chem. Phys. **7**, 911 (1939).

mation treated by Kirkwood of unpolarizable molecules, that is $\epsilon_\infty=1$, the factor f of Eq. (4) becomes unity. Thus the disagreement that remains to be resolved is between Onsager's equation to which Fröhlich's equation reduces and the result of Piekara to which Harris and Alder reduce and which differs by the factor f. It should be emphasized at the outset that we do not imply that Onsager has committed an error in treating his model as Piekara tries to show, but rather that his model is not as general as the statistical-mechanical treatment.

In Harris and Alder's treatment a homogeneous medium in the shape of a macroscopic sphere in vacuum is considered, and the moment of this system for any given microscopic configuration is thought of as composed of two contributions: (i) the displacement moment $\mathbf{M}_d$ due to elastic displacement of charge under the direct influence of the applied field; (ii) the orientational moment $\mathbf{M}_0$ due to the specified dipolar configuration including the displacement moment induced thereby in the sphere. The contribution $\mathbf{M}_d$ is then treated on a macroscopic basis in terms of ϵ_∞, and one finds (see *HA* 8) (V = total volume)

$$\epsilon-1=\frac{3\epsilon}{2\epsilon+1}\frac{4\pi}{3kTV}[\mathbf{M}_0^2]+\frac{(\epsilon+2)(\epsilon_\infty-1)}{(\epsilon_\infty+2)}, \quad (5)$$

where the symbol [ ] denotes formation of the statistical average over all the configurational coordinates $(1,2,\ldots j,\ldots)$ of the dipoles (j denotes the configurational coordinates of the jth dipole). Now in order to evaluate $[\mathbf{M}_0^2]$, the moment $\mathbf{M}_0=\mathbf{M}_0(1,2,\ldots j,\ldots)$ in a specified configuration is written as a sum of contributions of individual molecules,

$$\mathbf{M}_0(1,2,\cdots j,\cdots)=\sum_{j=0}^{N}\boldsymbol{\mu}_{s,j}', \quad (6)$$

where $\boldsymbol{\mu}_{s,j}'$ denotes the contribution of the jth molecule. Staying as general as possible, the actual dipole moment of molecule j in the spherical sample will depend on the moment induced by the other molecules surrounding j and therefore on the configuration of these dipoles. Thus

$$[\mathbf{M}_0^2(1,2,\cdots j,\cdots)]$$

$$=\sum_{j=1}^{N}[\boldsymbol{\mu}_{s,j}'(1,2,\cdots j,\cdots)\cdot\mathbf{M}_0(1,2,\cdots j,\cdots)] \quad (7)$$

and

$$\boldsymbol{\mu}_{s,j}'=\boldsymbol{\mu}_{V,j}+\alpha\sum_i\mathbf{T}_{ij}\cdot\boldsymbol{\mu}_i, \quad (8)$$

where $\mathbf{T}_{ij}=-\nabla_j(\mathbf{R}_{ij}/R_{ij}^3)$ is the dipole field at molecule j due to molecule i at a distance R_{ij} away and α is the polarizability of the molecule assumed to be spherically symmetric in this formulation.

Harris and Alder now proceed by replacing the dipole moment of molecule j by its average value, that is

$$[\mathbf{M}_0^2]=\sum_{j=1}^{N}\boldsymbol{\mu}_{sj}[\mathbf{M}_0(1,2,\cdots j,\cdots)]_j=N\boldsymbol{\mu}_s\cdot\langle\mathbf{M}\rangle_{\mu_s}, \quad (9)$$

where

$$\boldsymbol{\mu}_s=\boldsymbol{\mu}_V+\alpha[\sum_i\mathbf{T}_{ij}\cdot\boldsymbol{\mu}_i]_j \quad (\text{see } HA \text{ 17}), \quad (10)$$

and where [ ]$_j$ denotes formation of the statistical average over all configurational coordinates except those of the jth dipole. The sum has been replaced by N since all the molecules are equivalent in an isotropic substance and $\langle\mathbf{M}\rangle_{\mu_s}$ stands for the moment of the spherical specimen when any dipole in it has specified coordinates.

The approximation involved in Eq. (9) is replacement of the mean of a product of two quantities by the product of their averages. In other words the fluctuations in the dipole moment of a molecule have been omitted and replaced by their average value. Such a procedure tends to become more valid in any real situation when the short range forces are either quite weak or quite strong. In the former case the surroundings of a molecule can be treated in the limit as a continuum and then the instantaneous dipole moment of a given molecule does not depend on the position of the other dipoles in the system. When the structure of the fluid is rigid then thermal motion of the molecules becomes energetically unfavorable and the effective dipole moment does not vary greatly. In most cases the induced moment is about 10 percent of the permanent and any fluctuation in that 10 percent is likely to make a small contribution to the total polarization.

As has been shown, Eq. (9) involves no approximation in so far as you can treat the surroundings of a molecule as a continuum. Yet, when Eq. (9) is substituted into Eq. (5) and the proper conversions made from the spherical sample to an infinite sample, the equation differs by the factor f from Onsager's equation in the situation where short range forces are absent. The above conversion involves replacing $\boldsymbol{\mu}_s$ by $\boldsymbol{\mu}$, the dipole moment of a molecule in an infinite medium. In order to justify this replacement the effect of the surface at macroscopic distance has been shown to be negligible on the dipole moment of a molecule (see *HA* App. I). The additional simplification that has to be introduced to recover Onsager's equation is to set $\boldsymbol{\mu}_s$ equal to $\boldsymbol{\mu}_V$, that is the effect of the induced dipole moment is neglected altogether.

Thus the model which yields Onsager's equation as a limit is one in which $\boldsymbol{\mu}_{s,j}'$ is the moment of the jth dipole, including the moment it induces (by displacement polarization) in all the molecules of the sphere, but excluding contribution—either direct or through induction—of all other dipoles. All contributions $\boldsymbol{\mu}_{s,j}'$ superimpose linearly and add up to form $\mathbf{M}_0$ as required.

The value of $\mu_{s,j}'$ is obtained by simple electrostatics if the simple model of a molecule mentioned at the beginning is employed: $\mu_{s,j}'$ is then the moment of a large sphere of dielectric constant ϵ_∞ containing a rigid dipole μ_F in its interior. This moment is independent of the size of the sphere and hence is equal to the vacuum moment μ_V as required. The rest of the treatment is as before with this model.

The foregoing description then, regards all induced polarization of a molecule even in the case of strong short range forces as interpretable in terms of a polarization of a continuous dielectric of constant ϵ_∞ and cannot therefore adequately deal with problems where a large part of the induced polarization is determined by the local structure. Even in the instance where the surrounding of a molecule can be represented as a continuum a difference in the evaluation of the induced polarization can occur as can be seen from Eq. (10). The second term on the right hand is in general not zero as in the foregoing model. Harris and Alder approximate this term by Onsager's model where a polarizable dipole in a spherical cavity is surrounded by the macroscopic dielectric constant of ϵ rather than ϵ_∞. This must also be done to be consistent with Onsager's general picture. When it comes to the calculation for an actual system with an assumed model, the induced dipole moment is calculated by them from the structure and the use of Eq. (10).

THE JOURNAL OF CHEMICAL PHYSICS VOLUME 22, NUMBER 11 NOVEMBER, 1954

Raman and Infrared Spectra of CF_3Br and CF_3I†

WALTER F. EDGELL AND CHARLES E. MAY
Department of Chemistry, Purdue University, Lafayette, Indiana
(Received April 27, 1953)

The Raman spectra of CF_3Br and CF_3I have been obtained at -100°C and -40°C, respectively. The infrared spectra of both compounds have been obtained at 30°C, and some measurements have been made at 160°C. The observed frequencies were assigned to the fundamental modes of vibration, their combinations and differences. The frequencies were interpreted in correlation with other CF_3X molecules in terms of the pertinent "natural" frequencies of vibration.

INTRODUCTION

A GROWING interest in organic fluorine compounds has suggested a need for detailed spectroscopic investigation of this class of compounds. Such data are of utility not only for semi-empirical use in identification and analysis, but also for the determination of the intramolecular forces. While a substantial amount of work has been done, it is evident that its fullest utilization is dependent upon new theoretical contributions. In connection with such studies, this laboratory has been engaged for some time in spectroscopic investigations of a number of molecules containing the trifluoromethyl group. This paper deals with the Raman and infrared spectra of CF_3I and CF_3Br, a preliminary report of which has already appeared.[1]

Considerable interest has been shown in the infrared spectra[2–5] of these molecules, and some differences in interpretation have been expressed.

SAMPLE PREPARATION

The CF_3Br used for the spectroscopic investigation was a commercial sample. It was distilled through a 50-plate, low-temperature, Podbielniak column at a constant boiling point of -59°C at 760 mm. Only the middle fraction was used for the determination of the spectra. Since the infrared spectra were identical before and after distillation, no major amount of impurity should have been present in the distilled product.

The CF_3I was prepared according to the method of Hazeldine[6] by the following series of reactions:

$$2CF_3COOH+Ag_2O \rightarrow 2CF_3COOAg+H_2O,$$

$$CF_3COOAg+I_2 \xrightarrow{\Delta} CF_3I+AgI+CO_2.$$

Carbon dioxide was removed by passing the gas through a three-foot glass column containing ascarite. CF_3I was then distilled in a similar manner to the CF_3Br and had a constant boiling point of -21°C at 760 mm. Again only the middle fraction was used for spectroscopic work. This sample gave an identical infrared spectrum as a sample distilled through an ordinary 15-plate column. Newly fractionated CF_3I would remain completely colorless for a week if protected from direct light. The sample of CF_3I, when used for the study of

† Portions of this paper were presented before 122nd meeting of the American Chemical Society, Atlantic City, New Jersey, September, 1952 and the 123rd meeting, Los Angeles, March, 1953.

[1] Walter F. Edgell and C. E. May, J. Chem. Phys. **20**, 1822 (1952).

[2] E. K. Plyler and N. Acquista, J. Research Natl. Bur. Standards **48**, 92 (1952).

[3] McGee, Cleveland, and Miller, J. Chem. Phys. **20**, 1044 (1952).

[4] S. R. Polo and M. K. Wilson, J. Chem. Phys. **20**, 1183 (1952).

[5] McGee, Cleveland, Meister, Decker and Miller, J. Chem. Phys. (to be published).

[6] R. N. Hazeldine, J. Chem. Soc. **1951**, 584.

TABLE I. Raman bands.

CF_3Br Frequency cm^{-1}	CF_3Br Intensity (relative)	CF_3Br Depolarization factor	CF_3I Frequency cm^{-1}	CF_3I Intensity (relative)	CF_3I Depolarization factor	Assignment
305	2	0.86	265	2	0.86	E Rock
350	8	0.2	284	20	0.2	A_1 CX stretch
548	1	0.86	537	1	0.86	E CF_3 def.
760	7	0.2	741	9	0.3	A_1 CF_3 def.
1067	4	0.2	1056	4	0.3	A_1 CF_3 stretch
1109	0	p[a]	1018	1	0.2	A_1 {350+760; CF_3Br / 284+741; CF_3I
1188	2	0.86	1168	2	0.86	E CF_3 stretch

[a] Polarized, but not measurable on microdensitometer tracing.

the Raman effect, had to be purified frequently due to the decomposition caused by the mercury arc.

EXPERIMENTAL DETAILS

A three-prism Applied Research Laboratories spectrograph having a camera aperature ratio of $F/3.5$ and a dispersion of 15 A/mm at 4358 A was used for the study of Raman effect. The source was a low-pressure, spiral mercury arc of the type used at the University of Toronto.[7] A current of 18 amperes was used, and the intensity of the arc was enhanced by a cylindrical reflector coated with a silicone resin pigmented with TiO_2.[8]

In general, no filters were required to reduce the background, and Raman bands excited by 4358 A, 4047 A, etc., were measured. However the CF_3I sample was decomposed slowly into iodine and unknown materials by the mercury arc. It was found convenient to reduce this process through the use of a Wratten 2B filter. A sample would remain essentially colorless for 12 hours under such conditions. The presence of the filter eliminated bands caused by the 4047 A Hg line while the free iodine formed by decomposition would lessen the intensity of the bands caused by the 4358 A line.

The Raman effect was studied in the liquid state for both compounds using a sample size of 15 ml. In order to keep the samples of CF_3Br and CF_3I below their normal boiling points, a special cryogenic unit was constructed for use within the Raman arc. It consisted of a water-jacketed unsilvered Dewar with plane glass windows at the bottom. The cryostat was cooled by a stream of air, first dried by passing through silica gel and through glass beads coated with P_2O_5, followed by passing through a copper coil submerged in a dry ice-trichloroethylene mixture and then through a glass coil submerged in liquid nitrogen. All "cold" connections were made with silvered, vacuum jacketed tubes. The temperature was kept at -100 ± 5°C for CF_3Br. By removal of the liquid nitrogen cooler, the sample of CF_3I was kept at -40 ± 5°C. The sample was vacuum transferred into the Raman tube through a commercial, medium, sintered glass disk. Attention was given to cleaning the Raman tube. The fact that the sample was nearly free of dust was shown by the absence of excessive background on the films.

The Raman spectra were recorded on Eastman Tri X Pan film. Slit widths of 150 to 300 microns were used, with exposures varying from 3 to 24 hours. A reference spectrum of argon was employed, and frequencies were calculated by means of the Hartmann dispersion formula and a graphical method. The two methods check within 0.3 cm^{-1}. Values from various films deviate ±1 cm^{-1} from the mean values. Semiquantitative intensity measurements were made from microdensitometer tracings of the films.

Polarization measurements were made by a method similar to that of Glockler and Baker.[9] Opposite panels on the Raman tubes were painted with flat black paint, so that light from the arc could enter the tube only from the two sides perpendicular to the painted ones. The light coming from the Raman tube was analyzed by placing one piece of polaroid film with the proper orientation across the upper half of the slit of the spectrograph and another piece of polaroid film with an orientation perpendicular to the first across the lower half. The depolarization factors were calculated from microdensitometer tracings of the films. Corrections were made for (1) the nonlinearity of peak height with band intensity, (2) the background on the films, (3) the polarization of the spectrograph, and (4) the nonparallel nature of the light from the arc. The intensity measurements assume a uniformity of film response between 4358 A and 4800 A.

Table I contains a summary of the data for the Raman effect, while densitometer tracings of the spectra obtained with unpolarized light are found in Figs. 1 and 2.

The infrared spectra of the gases were observed in the region from 2 to 25 microns. Ten centimeter gas cells were used with pressures from 0.5 mm to 760 mm Hg. Runs were made at 30°C and 160°C. A CaF_2 prism was used from 2 to 8μ and a NaCl prism from 8 to 15μ

[7] Thanks are due to Professor Walsh, who sent us details of his arcs.

[8] This material was kindly furnished to us by the Linde Air Products Laboratory, Tonawanda, New York.

[9] G. Glockler and G. Baker, J. Chem. Phys. **10**, 305 (1942); **10**, 404 (1942).

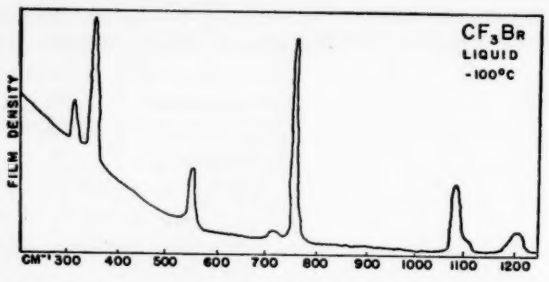

FIG. 1. The Raman spectrum of liquid CF_3Br at $-100°C$.

with the appropriate linear wavelength and constant energy slit cams in a Perkin-Elmer, Model 21, double-beam spectrometer. Two types of runs were made: survey spectra, taken with moderate resolution (slit schedule 4) at 2 minutes per micron, and "high resolution" spectra, taken with narrow slits (schedule 6) at 30 to 60 minutes per micron. The spectrometer was calibrated with acetylene, ammonia and water vapor as primary standards.[10] It was found that the corrections to be applied were dependent upon the warm-up time for the spectrometer and the conditions of operation, in particular the response time and the scanning rate. The spectrometer and its electronic components were warmed up for one-half hour for survey runs and for four hours for "high resolution" runs. Most of the wavelengths reported here, including all fundamentals, were measured from the latter type of run and the uncertainty is believed to be $\pm 0.005\mu$ or less over the whole region. The accuracy is greatest at the longer wavelengths and for the sharper bands.

A KBr prism was used with the NaCl cams in the Model 21 spectrometer to cover the region between 15 and 25μ. Calibration of the nonlinear wavelength scale was effected through the observation of the bands of a number of organic compounds reported in the literature. It is believed the accuracy here is at least ± 2 cm^{-1}.

Figures 3 and 4 are drawings of the infrared spectra under survey conditions. Table II gives the wavelengths of the bands at 30°C. When the resolution was great enough to show the *PQR* branches, they are listed individually in the table. Several additional, extremely weak bands were found at wavelengths less than 4μ for each molecule when one atmosphere pressure was

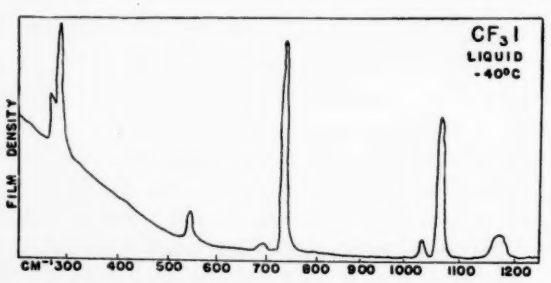

FIG. 2. The Raman spectrum of liquid CF_3I at $-40°C$.

[10] Oetjen, LanKav, and Randall, Rev. Sci. Instr. 13, 515 (1942).

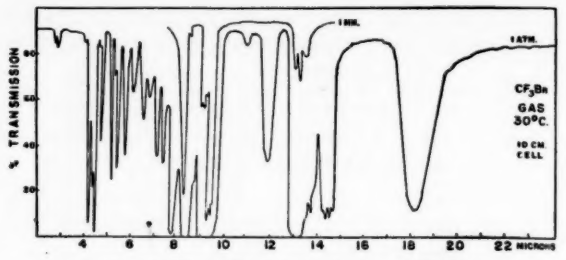

FIG. 3. The infrared spectrum of CF_3Br.

used in the cell. They are not listed in Table II because they could not be measured with accuracy. However, they include the three bands for each molecule tabulated by Polo and Wilson[4] in this region.

The infrared spectral data reported earlier[2–5] are in essential harmony with this work. The wavelength of the bands agrees as well as might be expected, i.e., rather well on the whole. The data of McGee, *et al.*[3,5] do not extend beyond about 2100 cm^{-1}, while several of the very weakest bands generally observed do not appear in their tabulation. We do not find the band of moderate intensity at 830 cm^{-1} and the questionable band at 470 cm^{-1} reported[2] for CF_3Br nor that[4] at 649 cm^{-1}. The same is true for the weak band reported[2,3,5] at 949 cm^{-1}. It has been suggested[3,5] that the band of moderate intensity centering at 730 cm^{-1} is due to CO_2. Because this band has been observed by all the laboratories and has a typical type *A* structure, it is believed to result from CF_3Br. On the other hand, while we observe the complex band centering at about 696 cm^{-1} in the same form shown by Plyler and Acquista,[2] the 689 cm^{-1} branch has been challenged by Polo and Wilson[4] as an impurity. This is likely, since the band shape is not explainable in a simple fashion.

The infrared spectrum of the CF_3I samples, after passing through the ascarite column but before distillation, showed weak bands at about 711, 1111, and 1121 cm^{-1}, a band of moderate intensity at 697 cm^{-1} and a rather strong band at 1250 cm^{-1}. These disappeared upon rectification and presumably are the same as those reported earlier[2] at 711, 1114 and 1246 cm^{-1}. The bands reported at 518,[3,8] 949,[4] and 1173 cm^{-1},[4] also have not been observed. On the other hand, this study reports very weak bands at 1148, 1855, and 1961 cm^{-1} plus a slight shoulder at 1193 cm^{-1} which have not been observed earlier.

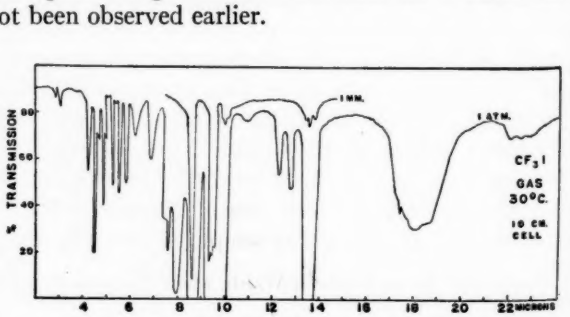

FIG. 4. The infrared spectrum of CF_3I.

DISCUSSION

The microwave spectra[11] of these molecules confirm the expected C_{3v} symmetry. Three fundamentals are of type A_1, and three of type E. All fundamentals, as well as the overtones and combinations, are permitted in both the Raman and infrared spectrum. The type A_1 vibrations are polarized in the Raman effect and have a parallel type band in the infrared spectrum. The moments of inertia may be calculated from the microwave data[11] together with the assumptions of tetrahedral angles and a C−F distance of 1.326 A. With these, the theory of Gerhard and Dennison[12] predicts P, Q, and R branches with a PR separation of 14 cm^{-1} for CF_3Br and 11 cm^{-1} for CF_3I. The type E vibrations are depolarized in the Raman effect and give rise to perpendicular bands in the infrared spectrum. Theory suggests that the dominant feature of these bands would be a prominent Q "branch." The A_1 fundamental modes can be described roughly as a symmetrical CF_3 stretching vibration, a symmetrical CF_3 deformation vibration and a symmetrical C−Br or C−I stretching vibration. The E modes are roughly characterized as an antisymmetrical CF_3 stretching vibration, an antisymmetrical CF_3 deformation vibration and the rocking vibration.

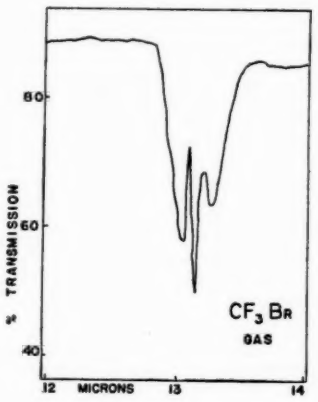

FIG. 5. The parallel band at 13.1μ in CF_3Br.

The Raman and infrared spectra give good evidence of the C_{3v} structure of these molecules. Thus six "strong" lines are observed in the Raman effect, three of which are polarized. In the region of common observation the strong infrared bands correspond to the Raman lines. Of greater importance is the nature of the band envelopes, which are typical of the symmetric top. Examples are the parallel bands at 13.2μ in CF_3Br and 9.3μ and 13.5μ in CF_3I shown in Figs. 5, 6, and 7 under conditions of "high" resolution. The PR separations are in agreement with the theory as can be seen from Table II. This is shown more precisely in the comparison between theory and measurement made at

[11] J. Sheridan and W. Gordy, Phys. Rev. **77**, 292 (1950).
[12] S. L. Gerhard and D. M. Dennison, Phys. Rev. **43**, 197 (1932).

TABLE II. The infrared bands of CF_3Br and CF_3I.

CF_3Br Obs.	CF_3Br Calc. cm^{-1}	CF_3I Obs.	CF_3I Calc. cm^{-1}	Strength	Assignment
	297[a]		265[a]		ν_6, E
	350[a]		286[a]		ν_3, A_1
		449			
		456	455	W−	$\nu_2-\nu_3, A_1$
		461			
550		540		M	ν_5, E
689					Impurity?
693		562			
699	700	572	572	M	$2\nu_3$,[b] A_1
703		576			
723					
730	735	777	787	W	$\nu_1-\nu_3, A_1$
738					
753		735			
761		741		S	ν_2, A_1
766		747			
845	847	808	805	W	$\nu_5+\nu_6, A_1+A_2+E$
907	909	918	920	W−	$\nu_4-\nu_6, A_1+A_2+E$
1077[c]		1067			
1085		1073		S+	ν_1, A_1
1090		1078			
1109		1019			
1116	1111	1026	1027	S	$\nu_2+\nu_3, A_1$
1122		1030			
		1149			Impurity?
1172[d]	1179	1193[c]	1196	W−	$2\nu_2-\nu_3, A_1$
1206		1185		S+	ν_4, E
1303	1311	1269	1281	M	$\nu_2+\nu_5, E$
1382	1382	1332	1338	W	$\nu_1+\nu_6, E$
1426	1435	1359[c]	1359	W	$\nu_1+\nu_3, A_1$
1470	1461			W−	$\nu_2+2\nu_3, A_1$
1503	1503	1443	1450	W	$\nu_4+\nu_6, A_1+A_2+E$
1625	1635	1605	1613	W	$\nu_1+\nu_5, E$
1750	1756	1724	1725	W	$\nu_4+\nu_5, A_1+A_2+E$
1847	1846	1818	1813	W	$\nu_1+\nu_2, A_1$
1889	1879	1768	1768	W−	$2\nu_2+\nu_3, A_1$
		1855	1860	W=	$2\nu_1-\nu_3, A_1$
1963	1967	1916	1926	W	$\nu_4+\nu_2, E$
		1961	1972	W=	$\nu_4+\nu_1-\nu_3, E$
2162	2170	2137	2146	W	$2\nu_1, A_1$
2173	2185				$\nu_1+2\nu_5, A_1+E$
2195	2196	2096	2099	W−	$\nu_1+\nu_2+\nu_3, A_1$
2281	2291	2242	2258	W	$\nu_4+\nu_1, E$
2312	2317	2203	2211	W−	$\nu_4+\nu_2+\nu_3, E$
2389	2412	2331	2370	W	$2\nu_4, A_1+E$
2497	2490	2433	2432	W=	$2\nu_1+\nu_3, A_1$
~3480	3497	~3401	3443	W−	$2\nu_4+\nu_1, A_1+E$
~3570	3618	~3496	3555	W−	$3\nu_4, A_1+A_2+E$

[a] Calculated from the combination bands.
[b] See text for alternate assignment.
[c] Shoulder.
[d] May be an impurity.

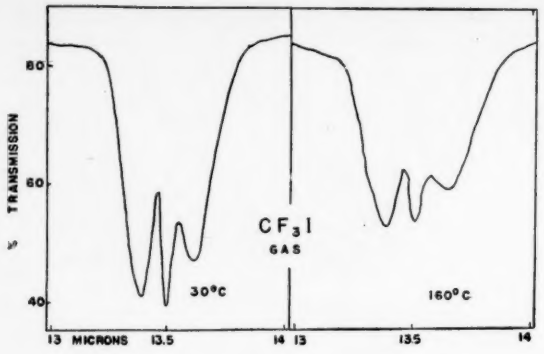

FIG. 6. The effect of temperature on the parallel band at 13.5μ in CF_3I.

about 30°C and about 160°C on the 13.2μ band for CF_3Br and the 13.5μ bands for CF_3I given in Table III and Fig. 6.

The assignment of the fundamentals may be made in a straightforward manner. The frequencies at about 1100 and 1200 cm^{-1} are the CF_3 stretching vibrations. An examination of the band envelopes, see Fig. 7 for example, shows that the lower frequency is the A_1 vibration. This is confirmed in each case by the fact that the corresponding Raman line is polarized. The characteristic liquid-vapor shifts[13] are evident. The remaining strong Raman lines are found at about 550, 750, and a pair between 275 and 350 cm^{-1} for each molecule. The first two are characterized as CF_3 deformation vibrations. Since the higher frequency is polarized in the Raman effect and corresponds to a parallel band in the infrared spectrum (see Table I and Figs. 5 and 6), it arises from the A_1 mode.

Two fundamental modes are yet to be assigned. Two strong Raman lines remain: 350 and 305 cm^{-1} for CF_3Br; 284 and 265 cm^{-1} for CF_3I. On the basis of the polarization data (Table I), the lines at 350 and 284 cm^{-1}, respectively, are assigned to the A_1 vibrational mode, and those at 305 and 265 cm^{-1}, respectively, the E vibrational mode. As discussed below these are substantially C—Br or C—I stretching vibrations and the rocking motion of the CF_3 group against the C—Br or C—I bond. Plyler and Acquista[2] succeeded in finding a weak band at 348 and 284 cm^{-1}, respectively, in CF_3Br and CF_3I, using a long path cell and a spectrometer with KRS-5 optics. No other infrared bands have as yet been observed in this region. Several investigators[2–5] have attempted to arrive at frequencies for these fundamentals from the combination and overtone bands. Their results have not been in agreement. Polo and Wilson[4] were the first to obtain, by this method, the values found in the Raman effect.

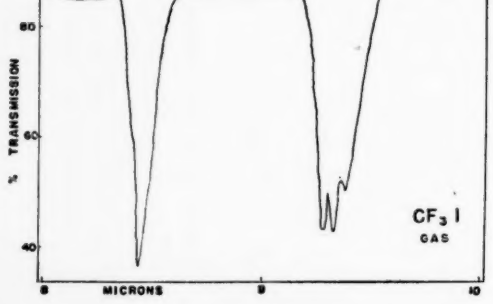

FIG. 7. The perpendicular and parallel bands associated with the "CF_3 stretching" vibrations.

[13] Walter F. Edgell and Willis E. Byrd, J. Chem. Phys. 18, 892 (1950).

TABLE III. *PR* separations for the A_1 CF_3 deformation bands.

Temp. °C	CF_3Br Exp.	CF_3Br Calc.	CF_3I Exp.	CF_3I Calc.
30°	13.3 cm^{-1}	13.7 cm^{-1}	11.6 cm^{-1}	11.4 cm^{-1}
160°	16.1	16.3	13.8	13.6

An examination of Figs. 1 and 2 shows two weak Raman lines not yet discussed for each molecule. The lines found at about 703 and 684 cm^{-1} when they are assumed to be excited by 4358 A are, in reality, the strong Raman lines at 760 and 741 cm^{-1} excited by the satellite mercury line at 4348 A. The weak, polarized lines at 1109 cm^{-1} for CF_3Br and 1018 cm^{-1} for CF_3I are assigned to the type A_1 combination 350+760 =1110 cm^{-1} and 284+741=1025 cm^{-1}, respectively. It is quite possible that they owe a portion of their intensity to resonance with the A_1 CF_3 stretching vibration.

The bands remaining in the infrared are easily interpreted as combinations and differences of the assigned fundamentals. Most binary combinations are observable but weak. The ternary combinations which are observable are all very weak. All bands with the *PQR* structure are assigned to A_1 type vibrations.

The Nature of the Vibrations

It is interesting to compare the fundamental frequencies of CF_3Br and CF_3I with those of other molecules of the type CF_3X. The vibrational spectra of

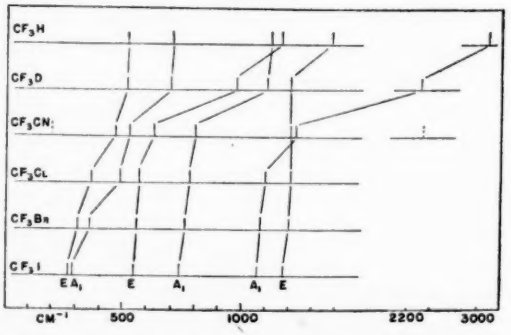

FIG. 8. The trends in the vibrational frequencies of the CF_3X molecules.

CF_3H,[14–16] CF_3D,[17] CF_3CN,[18] and CF_3Cl[19,20] have been studied. The pertinent fundamentals are listed in Table IV and shown in Fig. 8.

The CF_3X molecule is regarded as a CF_3 group (itself possessing four (hypothetical) "natural" vibrations) bonded to the X atom, which gives rise to two "natural" vibrations of the X atom against the (rigid) CF_3 group. The "natural" vibrations of the CF_3 group might be described roughly as the symmetrical CF_3 stretching and deformation vibrations and the antisymmetrical (degenerate) CF_3 stretching and deformation vibrations. The two "natural" vibrations of the X atom against the CF_3 group are the symmetrical $X-CF_3$ stretching vibration and the antisymmetrical (degenerate) rocking motion of the X atom against the CF_3 group. The observed frequencies of vibration of the CF_3X molecule are the result of coupling between these two groups of "natural" frequencies.

As the mass of the X atom approaches zero on the one hand or infinity on the other, the four "natural" frequencies of the CF_3 group should emerge, modified by the variation in the forces active on the atoms of this group. An examination of Fig. 8 reveals that the type A_1 "natural" vibrations of the CF_3 group occur at about 700 cm^{-1} and 1100 cm^{-1} and the type E at about 520 cm^{-1} and 1180 cm^{-1}. The implication is present that the forces acting on the CF_3 atoms are similar in the molecules with X=H, D, Cl, Br, and I.

The actual vibrations are found in the frequency range expected from the coupling of the "natural" vibrations involved in each molecule. Thus, for example the CF_3 group frequencies in general appear at frequencies less than those of the "natural" vibrations in CF_3H and CF_3D and at higher frequencies in CF_3Cl, CF_3Br, and CF_3I. The interaction between the two types of "natural" vibrations in these five molecules is small and increases as the weight of the halogen atom decreases. It is seen that the vibrations found at 284, 350, and 478 cm^{-1} in CF_3I, CF_3Br, and CF_3Cl, respectively, are to be regarded as substantially the stretching vibration of the X atom against the (rigid) CF_3 group, contrary to the earlier assignment.[2] That the coupling is much more pronounced in the CF_3CN molecule is evident from Fig. 8.

That the interaction between the CF_3 and $X-CF_3$ "natural" frequencies is small implies not only that the observed frequencies should contain values not greatly different from the "pure" CF_3 "natural" vibrations but also that the remaining two vibrations should involve a nearly rigid CF_3 group. If this is so and the broad implications of the above are accepted, then it should be possible, for example, to calculate the C–X stretching frequency in CF_3X from the "corresponding" frequency in CH_3X when X=Cl, Br, I and from that of CCl_3X when X=H, D using the modified ratio rule[21] based upon an approximate normal coordinate with a rigid CY_3 group (Y=H, F, Cl). Table V contains a comparison between the calculated and the experimental values. The agreement found there suggests that the above point of view forms a satisfactory basis for interpreting the spectra of the CF_3X molecules.

TABLE IV. The fundamentals of certain CF_3X molecules.

Type	CF_3H[16]	CF_3D[17]	CF_3CN[18]	CF_3Cl[20]
A_1	3031 cm^{-1}	2273	522	478
A_1	1117	1109	1228	1102
A_1	700	693	801	783
E	507	504	464	356
E	1152	1207	1215	1210
E	1372	974	625	560

TABLE V. The ratio rule calculation of the CF_3-X vibrations.

CX stretch frequencies in CF_3X	Calculated cm^{-1}	Experimental cm^{-1}
C–I	292	286
C–Br	357	352
C–Cl	491	478
C–D	2267	2273
C=H	3028	3030

ACKNOWLEDGMENT

Financial support of this research by the Atomic Energy Commission and the Purdue Research Foundation is gratefully acknowledged. One of us (C.M.) wishes to thank the Atomic Energy Commission for a fellowship for the years 1951–1952 and 1952–1953.

[14] G. Glockler and W. F. Edgell, J. Chem. Phys. **9**, 224 (1941).
[15] Rank, Shull, and Pace, J. Chem. Phys. **18**, 885 (1950).
[16] E. K. Plyler and W. S. Benedict, J. Research Natl. Bur. Standards **47**, 202–220 (1951).
[17] W. F. Edgell and C. E. May (to be published).
[18] W. F. Edgell and R. M. Potter (to be published).
[19] L. Kahovec and J. Wagner, Z. physik. Chem. **B48**, 188–92 (1941).
[20] H. W. Thompson and R. B. Temple, J. Chem. Soc. **1948**, 1422–8.
[21] Walter F. Edgell, J. Chem. Phys. **13**, 539 (1945).

Magnitudes of Barriers in Intramolecular Rotation

N. W. LUFT
52, Ladybridge Road, Cheadle Hulme, Cheshire, England
(Received April 8, 1954)

By applying symmetry considerations to intramolecular torsional barriers the over-all barriers are resolved into contributions from the interactions of individual change distributions (i and k). This makes it possible to classify internal potential barriers and calculate their heights and shapes if the Fourier coefficients $C_v{}^{ik}$ are known. Some figures, mainly $C_3{}^{ik}$ values, were obtained from experimental barriers others can be estimated by theoretical methods. The Lennard-Jones potential with $n=12$ and $m=6$ appears to be altogether unsuitable for describing barriers of internal rotation, but a simple repulsive potential $V=a_nR^{-n}$ with $n\sim5$ furnishes a reasonable approximation.

INTRODUCTION

ALTHOUGH a large body of experimental data on torsional frequencies and intramolecular barrier heights have been accumulated over recent years[1–5] only little progress has been made towards systematic correlation. To some extent all available theories[6–10] account for the rapid falling-off in barrier height with increasing distance of rotating groups and for the symmetry properties of composite torsional potentials. The theoretical methods are, however, of rather a preliminary character and were usually applied to only few molecules with simple symmetrical structures.

In spite of this it seems possible, by a suitable combination of certain empirical data with symmetry considerations and theoretical conclusions, to estimate hitherto unknown barrier heights and shapes of a large number of molecules and thus assist interpretation of vibrational spectra and calculation of thermodynamic properties.

SYMMETRY RELATIONS

If at least one of the two rotating groups of the molecule possesses a plane of symmetry, σ_v, which contains the axis of internal rotation and is a symmetry plane for the whole molecule, then

$$V(\phi)=\sum_{k=1} C_k(1-\cos k\phi), \tag{1}$$

where ϕ denotes the angle of twist. Since axially symmetric single and triple bonds ($i,k\cdots$) and lone electron pairs (p) as well as double bonds (π) satisfy the symmetry condition σ_v it is possible to resolve intramolecular torsional barriers into contributions from individual charge distributions as long as this procedure possesses physical significance. Thus[10] we obtain

$$C_k=\tfrac{1}{2}\sum_{1,r} C_k{}^{1r}\cos k\phi_0{}^{1r}, \tag{2}$$

where $C_k{}^{1r}$ is the kth Fourier coefficient for the interaction between the charge clouds 1 and r on opposite sides of the rotation axis and $\phi_0{}^{1r}$ their initial azimuthal angle (for $\phi=0$). For electrons in closed shells and those which do not alter their relative orientation during internal rotation all $C_k{}^{1r}$'s vanish.

Equation (2) has been found useful[11,12] in correlating and estimating various barriers of high and low symmetry. Although coefficients from $k=1$ to $k=12$ are of practical interest, for any one barrier no more than four Fourier coefficients need be retained even in a detailed and accurate representation of low symmetry barriers, whereas C_3 alone is sufficient for ethane and similar cases.

The coefficients $C_k{}^{1r}$ are determined by the separation of the two interacting charge clouds and by their properties, i.e., electronic configuration. The central atoms at the end points of the rotation axis have either tetrahedal or trigonal configurations, the available sites being occupied by bonds or lone pairs. As substitution usually does not alter the bond angles appreciably and since lone pair electrons for first-row elements are very similar in structure, the rotating groups may be classified according to their number of equal and symmetrically placed charge distributions and characterized by indicial symbols, e.g. i^3 denoting $-CH_3$, $-SiX_3$(X=H, F, CH_3, $\cdots$); $-ClO_3$; $ip^2=-OH$, $ik=-CO\cdot X$, $=CXH$, $ip=-NCO$ etc. Then the additivity rules[11] for some simple barriers may be stated as follows:

$$\left.\begin{array}{ll} i^3-klm: & C_{3n}=3(C_{3n}{}^{il}+C_{3n}{}^{il}+C_{3n}{}^{im}) \\ i^3-kl: & C_{3n}=3(C_{3n}{}^{ik}+[-1]^nC_3{}^{il}) \\ i^2-k^2: & C_{2n}=4C_n{}^{ik} \end{array}\right\} \begin{array}{l} n=1,2\cdots; \\ \text{else } C_k=0. \end{array} \tag{3}$$

These and similar symmetry conditions are satisfied automatically in any theory of torsional barriers which makes use of a sufficient number of parameters and can-

[1] G. Herzberg, *Infrared and Raman Spectra of Polyatomic Molecules* (D. Van Nostrand Company, New York, 1945).
[2] K. S. Pitzer, Faraday Soc. Disc. **10**, 66 (1951).
[3] J. G. Aston, Faraday Soc. Disc. **10**, 73 (1951).
[4] A. Eucken and Franck, Z. Elektrochem. **52**, 195 (1948).
[5] Mizushina, Morino, and Shimanouchi, J. Phys. Chem. **56**, 324 (1952).
[6] H. J. Bernstein, J. Chem. Phys. **17**, 262 (1949).
[7] E. N. Lasettre and L. B. Dean, J. Chem. Phys. **17**, 317 (1949).
[8] Au-Chin Tang, J. Chinese Chem. Soc. **18**, 1 (1951).
[9] R. G. Parr and B. L. Crawford, J. Chem. Phys. **16**, 526 (1948).
[10] N. W. Luft, Trans. Faraday Soc. **49**, 118 (1953).
[11] N. W. Luft, Faraday Soc. Disc. **10**, 117 (1951).
[12] N. W. Luft, J. Chem. Phys. **21**, 179 (1953).

not be taken as evidence in favour of a particular theory[8]. From this point of view a consideration of torsional Fourier coefficients for individual charge distributions seems to be preferable to a discussion of overall barrier heights. Apart from being more systematic it is often also simpler than a point-wise calculation of changes in the hindering potential with angle of torsion. A number of Fourier coefficients can be readily obtained from available experimental data on barriers, but on other occasions certain theoretical results to be discussed next may provide a useful guide.

ORDERS OF MAGNITUDE OF TORSIONAL BARRIERS AND THEIR FOURIER COEFFICIENTS

The interactions responsible for the usual types of torsional barriers about single bonds are of a net repulsive nature, as appears from the well-known stability of the staggered or *trans*-configuration of many molecules, and are therefore identical with those repulsive forces which cause a weakening[10,13] of bonds in polyatomic molecules. This implies that for single bond interaction the leading coefficients C_k in Eq. (1) are

TABLE I. Methyl barriers in substituted propanes, $H_3C-CH_2-C\epsilon$.

Molecule	V_0 (kcal/mole)	Ref.
$H_3C-CH_2CH_3$	3.40	2
$H_3C-CH_2C_2H_5$	3.6	1
$H_3C-CH_2C_3H_7$	3.6	1
$H_3C-CH_2CH{:}CH_2$	3.4	17
$H_3C-CH_2C{:}CH$	(~3.0)	3
$H_3C-CH_2CH_2NH_2$	3.4	a

[a] Calculated from the observed Raman shift (see reference 16) at 239 cm^{-1}.

essentially positive and rapidly converging. Although sometimes obscured in symmetrical molecules by the operation of symmetry conditions, this tendency may be demonstrated by reference to rotating groups of low symmetry. Barriers of the type i^2k-ki^2 for instance are known[12] to be adequately described by the first four Fourier coefficients and, for halogenated and methyl substituted ethanes, $c_1 \sim c_3 > c_2$.

The Fourier coefficients C_{3n} $(n=1, 2\cdots)$, however, are sums of bond increments $C_k{}^{1r}$, *viz.* $C_{3n}=4C_{3n}{}^{ii}+C_{3n}{}^{kk}+4C_{3n}{}^{ik}$, whereas the others are differences $C_k=C_k{}^{ii}+C_k{}^{kk}-2C_k{}^{ik}(C\neq 3n)$, so that $C_1{}^{1r}>C_3{}^{1r}$.

Furthermore, for $F_3C-SF_4\cdot F$ the 12-fold barrier was recently[14] determined as $V_0=0.62\pm0.2$ kcal/mole, i.e. $C_{12}(FC-SF)=0.026\pm0.008$ kcal/mole. Although no $C_n(FC-SF)$ with $n<12$ is available, this figure for $C_{12}(FC-SF)$ is considerably smaller than any known $C_3{}^{ik}$, e.g., $C_3(FC-CF)=0.23$ kcal/mole.

The decrease of barrier height with distance is gradual enough to permit of some influence of more distant bonds, e.g. the torsional barriers in propane are not only

[13] N. W. Luft, J. Chem. Phys. **22**, 155 (1954).
[14] P. Kisliuk and G. A. Silvey, J. Chem. Phys. **20**, 517 (1952).

TABLE II. Methyl barriers in molecules $H_3C-R-CH_3$.

$H_3C-R-CH_3$ R=	C–C distance A	Barrier height V_0 kcal/mole	Ref.
...	1.54	2.9±0.15	2, 3, 16
C:C	4.14	≲0.02	see 1, 7
Zn	4.1	0	a
Cd	4.3	0	b
Hg	4.46	0	a
C:C–C:C	6.65	0	...

[a] Boyd, Thompson, and Williams, Faraday Soc. Disc. **9**, 154 (1950).
[b] R. L. Williams and H. W. Thompson, Nature **167**, 766 (1951).

due to repulsion between CH_3 groups and directly opposite CH and CC bonds but interaction between the two methyl groups makes some contribution as suggested by a recent theoretical treatment.[7] A number of experimental results, however, indicate that such influences are usually but slight. Thus in propane derivatives the variation of substituents remote from the rotation axis leaves barriers almost unaffected (Table I) whereas an increase of CC distance from 1.54 to ≳4 A reduces the methyl barriers from 2.9 kcal/mole in ethane to practically zero (Table II). For this reason it seems justified to neglect more distant charge clouds whenever magnitudes, shapes, and Fourier coefficients of barriers between closer substituents are considered.

In order to demonstrate the influence of interaction distance upon the Fourier coefficients one may transform the Fourier expansion, Eq. (1), of the torsional barrier V into a series in negative powers of distance, $R=R_{1r}$, between the origins of individual charge clouds on the two sides of the central bond d (Fig. 1). Thus

$$V=\sum_n a_n R^{-n} \tag{4}$$

and

$$C_k=\frac{2}{\pi}\sum_n \int_0^\pi (a_n/R^n)\cos k\phi d\phi. \tag{5}$$

In general both R and a_n will vary with the angle of torsion ϕ but, at least in principle, either of them may be taken as constant, assuming the a_n's as independent of ϕ and putting

$$R_0=R(\phi=0);\quad R_\pi=R(\phi=\pi),$$
$$C=(R_\pi/R_0)^2=1+(4r_1r_2/R_0^2)\sin\beta_1\sin\beta_2, \tag{6}$$

and

$$\gamma=(C-1)/(C+1),$$

one has

$$R^2=R_0^2(1-\gamma\cos\phi)/(1-\gamma); \tag{7}$$

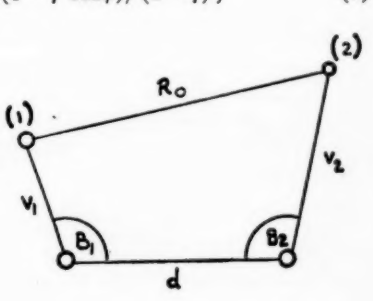

FIG. 1. Internal rotation of two bonds r_1 and r_2.

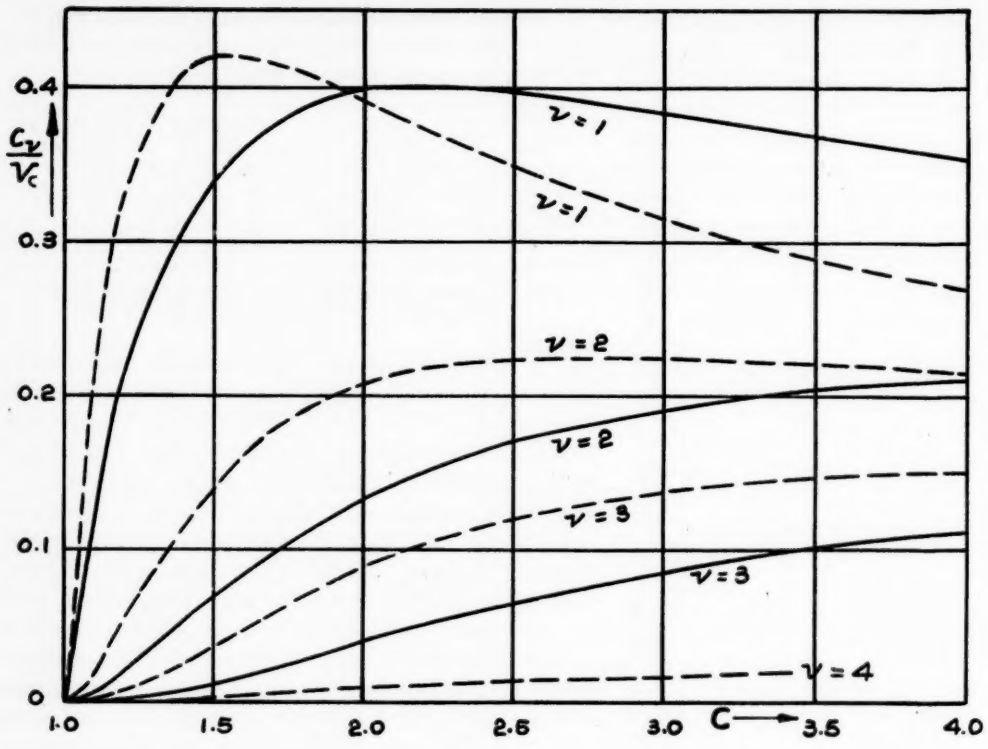

FIG. 2. Fourier coefficients for repulsive potential $V=a_nR^{-n}$; - - - $n=12$; —— $n=6$.

and for small values of γ Eq. (5) may now be integrated by series expansion of R^{-n} in ascending powers of γ. Neglecting terms in γ^3 and higher, the first four coefficients are

$$\left.\begin{aligned} C_1 &\sim \tfrac{1}{2}\gamma \textstyle\sum_n n(1-\gamma)^{n/2}a_n/R_0{}^n \\ C_2 &\sim (1/16)\gamma^2 \textstyle\sum_n n(n+2)(1-\gamma)^{n/2}a_n/R_0{}^n \\ C_3 &\sim (1/192)\gamma^3 \textstyle\sum_n n(n+2)(n+4) \times(1-\gamma)^{n/2}a_n/R_0{}^n \\ C_4 &\sim (1/3072)\gamma^4 \textstyle\sum_n n(n+2)(n+4) \times(n+6)(1-\gamma)^{n/2}a_n/R_0{}^n \end{aligned}\right\} \gamma \ll 1. \quad (8)$$

The polynominals in n ensure that the higher coefficients $C_k{}^{1r}$ fall off with distance more rapidly than the lower ones. On the other hand it follows that the proportionate contributions to $C_k{}^{1r}$ from regions near the rotation axis are larger for small k's than for big ones.

REPULSION THEORY

A much simplified form of the repulsive potential, Eq. (4), with constant coefficients is the function

$$V=a_nR^{-n}-a_mR^{-m}=[\epsilon m/(n-m)] \times[(R_e/R)^n-(n/m)(R_e/R)^m]. \quad (9)$$

Here R_e, the equilibrium distance at which $V=-\epsilon$, is related to the kinetic low velocity collision diameter R_* where $V=0$, by

$$R_e=R_*(n/m)^{1/(n-m)}. \quad (10)$$

For convenience V may be referred to its value, V_C, with the two end atoms in *cis* position ($\phi=0$) at the distance R_0, i.e.

$$V=[V_c/(1-\alpha)][(R_0/R)^n-\alpha(R_0/R)^m], \quad (11)$$

where

$$=(R_0/R_*)^{n-m}. \quad (12)$$

If R_0 and R_π are both smaller than R_*, Eq. (11) can be approximated by the repulsive term alone

$$V=V_c(R_0/R)^n=V_c[(1-\gamma)/(1-\gamma\cos\phi)]^{n/2}. \quad (13)$$

The Fourier coefficients of this potential barrier are given by

$$C_v=(2V_c/\pi)\sum_{i=0}^{v}\sum_{k=0}^{i}(-1)^{i+k} \times\binom{v}{2i}\binom{i}{k}F(v+2k-2i;m), \quad (14)$$

where

$$F(p;2q)=\int_0^\infty \frac{(1-Z)^p(1+Z)^{q-p-1}dZ}{(1+CZ)^q(Z)^{\frac{1}{2}}}. \quad (15)$$

For the usual exponents $n=12$ and 6 this integral can be evaluated in terms of gamma functions and the corresponding values of (C_v/V_c) are plotted in Figs. 2 and 3. With $n=12$ the following expressions obtain

$$C_v/V_0=f_v(C)/128(C)^{\frac{1}{2}} \quad (16)$$

where f_v are polynominals of the 5th degree in C^{-1} *viz.*

$$\left.\begin{aligned} f_1(C) &= 63+21/C+6/C^2 \\ &\quad -6/C^3-21/C^4-63/C^5 \\ f_2(C) &= 63-21/C-42/C^2 \\ &\quad -42/C^3-21/C^4+63/C^5 \\ f_3(C) &= 63-91/C-42/C^2 \\ &\quad +42/C^3+91/C^4-63/C^5 \\ f_4(C) &= 63-189/C+126/C \\ &\quad +126/C^3-189/C^4+63/C^5 \end{aligned}\right\}. \quad (17)$$

In general, the ratios (C_{k+1}/C_k) vary considerably with C and at any given C these ratios are smaller for $n=6$ than for $n=12$.

The simple repulsion barrier Eq. (13), has been used by several authors[3,6,8] for correlation of torsional barriers and exponents $n=5$ to 7 were found to reproduce satisfactorily the barrier heights of a number of components with methyl rotation. On the other hand it was also proposed[15] to apply the Lennard-Jones potential, i.e. Eq. (9) with $n=12$ and $m=6$, which is important in the kinetic theory of gases, to internal torsional barriers. Hereby the positions of charge origins are taken, not without some ambiguity, to be either in the free end atoms or half-way between the end atoms of a bond, making r_i equal or half the length of the rotating bond. These assumptions may now be checked by comparing Fourier coefficients C_3^{ik} obtained from experimental threefold barrier heights[1–10,16,17] with those resulting from the previous formula by using gas kinetic values[18–20] of ϵ. The data adopted are given in Table III.

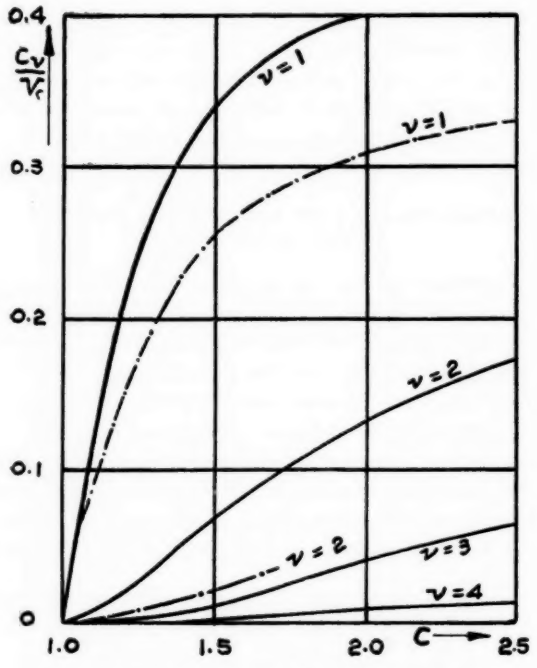

FIG. 3. Fourier coefficients for repulsive potential $V=a_nR^{-n}$; —— $n=6$; -·-·- $n=4$.

TABLE III. Threefold barriers about single bonds.

Bonds $i-k$	C	γ	Diameter R_0 (A)	C_3^{ik} (kcal/mole)
HC−CH	1.82	0.291	2.27	0.16
HC−CF	1.94	0.319	2.37	0.20[a]
FC−CF	2.10	0.352	2.45	0.23
HC−CCl	2.03	0.340	2.57	0.16[b]
ClC−CCl	2.47	0.424	2.74	0.67[c]
HC−CMe	1.99	0.331	2.46	0.25
MeC−CMe	2.26	0.393	2.59	0.36
FC−CCl	2.25	0.374	2.61	0.66[d]
HC−OH	1.84	0.296	2.12	0.18[e]
HC−NH	1.83	0.293	2.19	0.22
HC−OMe	2.07	0.349	2.29	0.45
HC−NMe	2.03	0.340	2.37	0.36
HC−C·OR	1.99	0.331	2.38	0.18
HC−C·NR	1.98	0.330	2.43	0.20
HC−C:O	1.89	0.308	2.32	0.33[f]
HC−C:CH_2	1.93	0.317	2.36	0.49
HC−N·NH_2	2.03	0.339	2.36	0.30[g]
HC−SH	1.74	0.274	2.64	0.24
HC−SMe	1.85	0.298	2.88	0.33

[a] From $V_0(H_3C-CF_3)=3.66$ kcal/mole [Smith, Brown, Nielsen, Smith, and Liang, J. Chem. Phys. **20**, 473 (1952)].
[b] Recently [Smith, Brown, Nielsen, Smith, and Liang, J. Chem. Phys. **20**, 473 (1952)] $\omega_t=205$ cm^{-1} and $V_0=3.045$ kcal/mole were assigned to H_3C-CCl_3 torsion, in good agreement with data by K. S. Pitzer and J. L. Hollenberg, J. Am. Chem Soc. **75**, 2219 (1953).
[c] Cf. $V_0(Cl_3C-CCl_3)\sim12$ kcal/mole from electron diffraction by Mizushima et al, J. Chem. Phys. **17**, 838 (1949).
[d] From $V_0(F_3C-CCl_3)=11.9$ kcal/mole, see N. W. Luft, J. Chem. Phys. **22**, 155 (1954).
[e] From $V_0(H_3C-OH)=1.07$ kcal/mole by E. V. Ivash and D. M. Dennison, J. Chem. Phys. **21**, 1804 (1953).
[f] From $V_0(H_3C-CHO)=1.0$ kcal/mole by K. S. Pitzer and Wm. Weltner, J. Chem. Phys. **71**, 2942 (1949).
[g] Average of $V_0(H_3C-NH\cdot NH_2)=3.2$ kcal/mole and $V_0(H_3C-NH\cdot NH\cdot CH_3)=3.0$ kcal/mole by J. G. Aston et al., J. Am. Chem. Soc. **73**, 1937 (1951).

For charge origins placed midway between the end atoms of the bonds r_i the parameter C has to be replaced by $C'=(C+3)/4$ and γ by $\gamma'=\gamma/(5\gamma-4)$. With this provision, however, and $n=4$, 6, 12 known C_3^{ik}'s resulted in repulsive energies V_c between pairs of single bonds in ethane derivatives which are much too high ($\gg10$ kcal/mole) in comparison with C−C bond energies. For this reason r_i was set equal to the bond length in all subsequent calculations. Although this fails to take proper account of regions close to the rotation axis, in particular lone electron pairs in H_3C-OH, H_3C-NH_2 etc., it probably does not involve serious errors for C_3 and higher Fourier coefficients. The values of repulsive energies ϵ calculated from C_3's are found to be not in agreement with gas kinetic ϵ's. The results are particularly disappointing for $n=12$, where they may differ by a factor of ten or more, and such discrepancy cannot be removed by inclusion of the attraction term since, for the range of distances R considered, it does not exceed ten percent of repulsive interaction.

On the whole, $n=4$ to 6 is much better though not altogether a satisfactory approximation, and it may,

[15] J. van Dranen, J. Chem. Phys. **17**, 262 (1949).
[16] Landolt-Börnstein, *Zahlenwerte und Funktionen* (Springer, Berlin, 1951), vol. I, 2, I.
[17] Smith, Saunders, Nielsen, and Ferguson, J. Chem. Phys. **20**, 847 (1950).
[18] Hirschfelder, Bird, and Spotz, Trans. Am. Soc. Mining Met. Engrs. 921 (1949).
[19] J. W. Linnett and D. F. Heath, Trans. Faraday Soc. **48**, 592 (1952).
[20] Hamann, McManamey, and Pearse, Trans. Faraday Soc. **49**, 351 (1953).

TABLE IV Barriers i^3-rs with small C_3 terms.

Molecular	V_0 (kcal/mole)	Harmonic oscillator ω_t (cm^{-1})	v^*
$H_3C-CH:CH_2$	(1.95)	200	2
H_3C-CHO	(1.0)	140	2
$H_3C-C(CH_3):CH_2$	1.5	160	2
$H_3C-CO\cdot CH_3$	0.5	100	1
$H_3C-CO\cdot OH$	0.9	125	2
$H_3C-CO\cdot F$	0.75	115	2
$H_3C-CO\cdot Cl$	0.6	100	2
$H_3C-CO\cdot OCH_3$	0.9	125	2

therefore, be used for extrapolation to neighboring conditions. Moreover, the ratios $C_3{}^{ik}/C_1{}^{ik}$ corresponding to $n=12$ are larger than those for $n\sim5$ and less compatible with values of $C_1{}^{ik}$ derived from experimentally investigated barriers of low symmetry, e.g. in $H_2ClC-CClH_2$.[6]

ELECTROSTATIC THEORY

According to the electrostatic theory of internal potential barrier the coefficients a_n of Eq. (4) are made up of products of electrical moments,[7,8,10] $\mu_i{}^{(n)}$, *viz.* for a neutral molecule

$$V^{ik}=\sum_{n=3}^{\infty}\sum_{p=1}^{n-1}\{\mu_i{}^{(p)}\mu_k{}^{(n-p-1)}f_{np}{}^{ik}+\mu_k{}^{(p)}\mu_i{}^{(n-p-1)}f_{np}{}^{ki}\}d^{-n}. \quad (18)$$

If moments are expressed in esu and d is measured in A, multiply by $Ne^2/A=329.7$ to convert into kcal/mole. The $f_{np}{}^{ik}$ are functions of d, r_i, r_k, β_i, β_k and ϕ. By placing the origins of the charge distributions in the end points of the rotation axis,[8] $r_i=r_k=0$, $R=d$, the $f_{np}{}^{ik}$ are functions of ϕ and bond angles β_i and β_k only, and the Fourier coefficients assume a particularly simple form

$$C_v{}^{ik}=\sum_{r=0}d^{-(2v+1+r)}\sum_{s=0}\{\mu_i{}^{(v+r-s)}\mu_k{}^{(v+s)}F^{ik}{}_{2v+r+1;v+r-s}+\mu_k{}^{(v+r-s)}\mu_i{}^{(v+s)}F^{ki}{}_{2v+r+1;v+r-s}\}, \quad (19)$$

where the F's are the Fourier transforms of the f's. It is to be seen that for $v=1, 2, 3$ this series starts with terms in d^{-3}, d^{-5} and d^{-7} respectively, and this supports our previous choice of a repulsive exponent $n\sim5$ and the earlier conclusion that the higher C_v's fall off with distance more rapidly than the lower ones. At present, however, the use of Eq. (19) is severely limited since only bond dipole moments $\mu^{(3)}$ are known apart from a few quadrupole and octupole moments which were obtained indirectly, by applying the theory to torsional barriers of known height, and exhibit considerable discrepancy with various authors.[7,8,10]

FOURIER COEFFICIENTS $C_3{}^{ik}$

Unfortunately a rigorous method of theoretical evaluation of Fourier coefficients $C_3{}^{ik}$ is not yet available although the simple repulsion theory, with $n\sim5$ and charge origins in the free end atoms gives the right order of magnitudes from gas-kinetic data. Thus for similar bonds this, or also a plot of $C_3{}^{ik}$ *vs* r_ir_k, may be used for rough interpolation. According to the electrostatic theory, with charge origins placed at the end points of the central bond d, one has up to and including octupole terms $\mu_i{}^{(3)}$ (see reference 8)

$$C_3{}^{ik}=-(5/8)\mu_i{}^{(3)}\mu_k{}^{(3)}\cos^3\beta_i\cos^3\beta_k/d^7, \quad (20)$$

i.e.

$$C_3{}^{ik}\approx(C_3{}^{ii}C_3{}^{kk})^{\frac{1}{2}}, \quad (21)$$

and similarly for the heights V_0 of threefold barriers i^3-k^3. In a few cases where experimental data are available Eq. (21) is satisfied approximately. It also follows that lone pair electrons in the end atoms on the rotation axis, e.g. on the oxygen atom in H_3C-OH, make no contributions to threefold barriers if they possess s, p or hybridized wave functions, i.e. $C_3{}^{pk}=0$. This has been postulated before[7] but then the expansion was only carried up to quadrupole terms and no hybridization of wavefunctions was considered.

In the preceding Table III a number of Fourier coefficients $C_3{}^{ik}$ are given from a review of experimental threefold barrier heights. These figures may be used for calculating unknown and more composite threefold barriers. A particularly interesting case is that of barriers i^3-rs which possess small overall C_3 terms. Some estimated heights of barriers of this type, $V_0=6(C_3{}^{ir}-C_3{}^{is})$, are given in Table IV, where $v^*\sim[V_0/\omega_t]$ is the total number of excited torsional levels, to the harmonic oscillator approximation. The estimated barrier of $H_3C-CO\cdot Cl$ is so low that C_6 terms might be important enough to give rise to a threefold double minimum barrier. Since v^* is so small the actual torsional fundamental is expected to be less than ω_t according to the harmonic oscillator approximation.

BARRIERS OF LOW SYMMETRY, FOURIER COEFFICIENTS $C_1{}^{ik}$

The general Fourier coefficients of several important barriers of low symmetry are listed in Table V. It is to be seen that, apart from cases of internal rotation of two trigonal groups (il,i^2) about a central bond, the overall coefficients C_2 and C_4 represent differences of individual Fourier coefficients and are therefore small. For this reason C_4 and, to a first approximation, also C_2 might be neglected. This is rather gratifying in view of the fact that so far only a few twofold barriers, e.g., in $HO-NO_2$, O_2N-NO_2, have been investigated, from which values

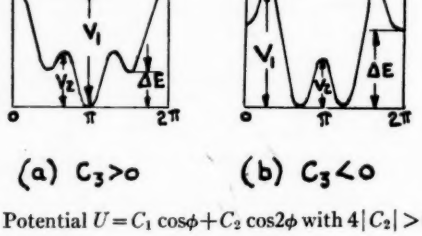

FIG. 4. Potential $U=C_1\cos\phi+C_2\cos2\phi$ with $4|C_2|>C_1>0$.

TABLE V. Fourier coefficients of low symmetry barriers.

Barrier	Example	C_1	C_2	C_3	C_4	Leading coefficients
$il-il$	OHC−CHO	$C_1^{ii}+C_1^{ll}-2C_1^{il}$	$C_2^{ii}+C_2^{ll}+2C_2^{il}$	$C_3^{ii}+C_3^{ll}-2C_3^{il}$	$C_4^{ii}+C_4^{ll}+2C_4^{il}$	C_1; C_2
$iik-iik$	$H_2ClC-CH_2Cl$	$C_1^{ii}+C_1^{kk}-2C_1^{ik}$	$C_2^{ii}+C_2^{kk}-2C_2^{ik}$	$4C_3^{ii}+C_3^{kk}+4C_3^{ik}$	$C_4^{ii}+C_4^{kk}-2C_4^{ik}$	C_1; C_3
$ikk-iik$	HCl_2-CH_2Cl	$C_1^{ii}+C_1^{kk}-2C_1^{ik}$	$-(C_2^{ii}+C_2^{kk}-2C_2^{ik})$	$-(2C_3^{ii}+2C_3^{kk}+5C_3^{ik})$	$C_4^{ii}+C_4^{kk}-2C_4^{ik}$	C_1; C_3
$ikk-ikk$	$HCl_2C-CHCl_2$	$C_1^{ii}+C_1^{kk}-2C_1^{ik}$	$C_2^{ii}+C_2^{kk}-2C_2^{ik}$	$C_3^{ii}+4C_3^{kk}+4C_3^{ik}$	$C_4^{ii}+C_4^{kk}-2C_4^{ik}$	C_1; C_3
i^2k-il	$H_2ClC-CHO$	$C_1^{ii}+C_1^{kl}-C_1^{ik}-C_1^{il}$	$-(C_2^{ii}-C_2^{kl}-C_2^{ik}+C_2^{il})$	$-2C_3^{ii}+C_3^{kl}-C_3^{ik}+2C_3^{il}$	$-C_4^{ii}+C_4^{kl}+C_4^{ik}-C_4^{il}$	C_1; (C_2)
ik^2-il	HCl_2C-CHO	$C_1^{ii}+C_1^{kl}-C_1^{ik}-C_1^{il}$	$C_2^{ii}-C_2^{kl}-C_2^{ik}+C_2^{il}$	$C_3^{ii}-2C_3^{kl}+2C_3^{ik}-C_3^{il}$	$C_4^{ii}-C_4^{kl}-C_4^{ik}+C_4^{il}$	C_1; (C_2)
i^2k-kl	$H_2ClC-CClO$	$C_1^{kk}-C_1^{kl}-C_1^{ik}+C_1^{il}$	$C_2^{kk}+C_2^{kl}-C_2^{ik}-C_2^{il}$	$C_3^{kk}-C_3^{kl}+2C_3^{ik}-2C_3^{il}$	$C_4^{kk}+C_4^{kl}-C_4^{ik}-C_4^{il}$	C_1; (C_2)
ik^2-kl	$HCl_2C-CClO$	$C_1^{kk}-C_1^{kl}-C_1^{ik}+C_1^{il}$	$-(C_2^{kk}+C_2^{kl}-C_2^{ik}-C_2^{il})$	$-2C_3^{kk}+2C_3^{kl}-C_3^{ik}+C_3^{il}$	$-C_4^{kk}-C_4^{kl}+C_4^{ik}+C_4^{il}$	C_1; (C_2)
$iip-iip$	(H_2N-NH_2)	$C_1^{ii}+C_1^{pp}-2C_1^{ip}$	$C_2^{ii}+C_2^{pp}-2C_2^{ip}$	$4C_3^{ip}$	C_4^{ip}	C_1; C_2
$ipp-iip$	$(HO-NH_2)$	$C_1^{ip}+C_1^{pp}-2C_1^{ip}$	$-(C_2^{ip}+C_2^{pp}-2C_2^{ip})$	$-2C_3^{ip}$	C_4^{ip}	C_1; C_2
$ipp-ipp$	$(HO-OH)$	$C_1^{ip}+C_1^{pp}-2C_1^{ip}$	$C_2^{ip}+C_2^{pp}-2C_2^{ip}$	C_3^{ip}	C_4^{ip}	C_1; C_2

of C_2^{ik} could be evaluated. Moreover, resonance of the two unsaturated rotating groups in $il-il$ seems to confer some double bond character upon the central bond and thus add a term $-C_2^{\pi}$ to the over-all C_2. Without this the C_1 and C_2 terms, being positive, would result in a double-minimum potential (Fig. 4a) for barriers $il-il$, etc., whereas the known planarity of molecules, e.g. O_2N-NO_2, $\phi-NO_2$, $H_2C:CH-CH:CH_2$ indicates that $-C_2^{\pi}$ is appreciable. With butadiene it may be estimated from the "true resonance energy" R.E. ~ 7 cal/mole $\sim 2C_2^{\pi}$. On the other hand, known[3] experimental data for the *gauche*-maximum $V_m \sim C_1 - 2C_2[1+(C_1/4C_2)^2] \approx 5.0$ kcal/mole and the energy difference between *cis-trans* isomers $\Delta E \sim 2C_1 = 2.4$ kcal/mole give the over-all $\bar{C}_2 \sim -1.8$ kcal/mole, and thus $C_2 = \bar{C}_2 + C_2^{\pi}$ 1.7 kcal/mole. This is reasonable but probably not very accurate since $C_3 \sim 0.7$ from Table III and Eq. (21), has been neglected.

In a similar way it can be shown that the barriers in HO−OH and H_2N-NH_2 are double minima (Fig. 4a) and that in $HO-NH_2$ leads to *cis-trans* isomerism (Fig. 4b). By using the known torsional fundamental for H_2N-OH, $\omega_t \sim 430$ cm^{-1}, and the equilibrium torsional angle in HO−OH, $\phi_m \sim 110°$, the approximate assumption that in the three compounds OH and NH bonds, exclusive of lone pairs, are equivalent leads to the results given in Table VI.

If C_1 and C_3 are the predominant coefficients then again two barrier types may occur depending on whether $C_3 \gtrless 0$. Thus usually the types $(iik)^2$ and $(ikk)^2$ have stable *trans*-configurations and secondary minima in *gauche*-positions, whereas $(ikk)(kii)$ should attain an energy minimum when the single substituents on either side include a dihedral angle of about 60° (*g* forms), and a less stable minimum at 180° (*g'* form). This is exemplified in Table VII by using results of recent[10] calculations on methyl substituted ethanes. The case of the corresponding chlorine compounds is analogous. In agreement with experiment[6,21] $ClCH_2-CH_2Cl$, and $Cl_2CH-CHCl_2$ are found to have similar shapes, the maximum V_1 for the latter compound is expected to be about 3 kcal/mole higher than for the former one. Bernstein's[6] data for $ClCH_2-CH_2Cl$, however, result in coefficients C_v for Cl_2CH-CH_2Cl which yield a low-energy minimum in *g'* position. This is at variance with dipole moment determinations[21,22] which seem to suggest that $\Delta E(g \to g')$ is sufficiently high to have escaped observation, i.e. $\gtrsim 3$ kcal/mole. For this reason Bernstein's figures, $\Delta E = 1.1$ and $V_1 = 4.5$ kcal/mole for CH_2Cl-CH_2Cl, are supposedly too low as also indicated by recent[23] electron diffraction results.

The important Fourier coefficients C_1^{ik} for individual bonds are hard to obtain from experimental data since low-symmetry barriers have yet been little investigated

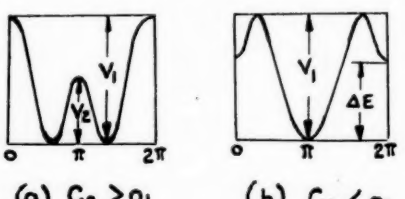

FIG. 5. Potential $U = C_1 \cos\phi + C_3 \cos 3\phi$ with $3|C_3| > C_1 > 0$.

TABLE VI. C_1, C_2 barriers.

Molecule	C_2(est.) kcal/mole	$I_r \times 10^{40}$ g cm^2	C_1 kcal/mole	C_2	V_1 kcal/mole	V_2	ΔE kcal/mole	ω_t(est.) cm^{-1}	ω_t(exp) cm^{-1}
H_2N-OH	−0.5	0.95	2.7	−2.0	6.6	—	4.4	(430)	430[a]
HO−OH	0.25	0.75	2.7	+2.0	6.9	1.8	—	480	~470[b]
H_2N-NH_2	1.0	1.52	2.7	+2.0	7.9	2.8	—	270	360[c]

[a] P. A. Giguere and I. D. Liu, Can. J. Research **30**, 948 (1952).
[b] P. A. Giguere (private communication).
[c] D. W. Scott et al, J. Am. Chem. Soc. **71**, 2293 (1949).

TABLE VII. Low symmetry barriers with predominant C_1 and C_2 terms.

Molecule	$\Delta E(t \to g$ or $g \to g')$ kcal/mole	V_1 kcal/mole
$H_2ClC-CClH_2$	1.3	~6
HCl_2C-CH_2Cl	~3	>7.5
$HCl_2C-CHCl_2$	~2	~9
$MeCH_2-CH_2Me$	1.5	9.1
$MeCH-CH_2Me$	3.8	8.5
$Me_2CH-CHMe_2$	2.1	10.3

[21] J. R. Thomas and W. G. Gwinn, J. Am. Chem. Soc. **71**, 2785 (1949).
[22] A. Turkevich and J. Y. Beach, J. Am. Chem. Soc. **61**, 3127 (1939).
[23] J. Ainsworth and J. Karle, J. Chem. Soc. **20**, 425 (1952).

and also because the few known C_1's represent always differences. To some approximation $C_1{}^{ik}$ seems to be about 10 to 15 times $C_3{}^{ik}$ for CH, CF, CCl and CC bonds, and this seems to be in agreement with what may be expected by applying the simple repulsive barrier $V=a_nR^{-n}$ with $n\sim5$. For double bonds, however, this rule does not appear to be valid.

CONCLUSIONS

The consideration of Fourier coefficients C_v is regarded as the basis of a more systematic and general treatment of intra-molecular torsional barriers. Coefficients C_3 are evaluated from known heights of threefold barriers and provide a useful means of checking consistency of observed barrier heights and predicting magnitudes of unknown barriers of threefold symmetry. They are also essential in certain barriers of low symmetry, whereas coefficients C_2 are usually small and unimportant except for barriers $il-il$. At the present, sufficient knowledge of coefficients $C_1{}^{ik}$ is lacking and their experimental determination from suitably selected barriers of low symmetry appears to be of prime importance. In some cases $C_1{}^{ik}$ was found to be 10 to 15 times the value of $C_3{}^{ik}$ for the same bond in good agreement with deductions from the simple repulsive potential $V=a_nR^{-n}$ and $n\sim5$.

ACKNOWLEDGMENT

The author acknowledges helpful correspondence with Professor P. A. Giguère of the Laval University, Quebec, Canada.

THE JOURNAL OF CHEMICAL PHYSICS VOLUME 22, NUMBER 11 NOVEMBER, 1954

Configurational Interaction in Simple Molecular Orbital Theory

W. MOFFITT
Mallinckrodt Chemical Laboratory, Harvard University, Cambridge, Massachusetts

(Received February 26, 1954)

The application of simple MO theory in the interpretation of electronic spectra is investigated. Certain simple theorems are derived and their applications, particularly with respect to configurational interaction in the polyacene series, are discussed. The potentialities and difficulties of this approach are enumerated, and it is concluded that the theory should only be used with caution.

INTRODUCTION

IT has recently been shown how the perimeter model of the catacondensed hydrocarbons enables their electronic spectra to be classified[1] and the principal characteristics of these band systems to be rationalized.[2] Whereas it is not difficult to understand why this method of handling the unsaturation electrons should be successful, it is less obvious to see how it should be applied more generally, and in particular to peri-condensed systems. It is therefore natural to ask whether the now standard procedures of molecular orbital theory,[3] which are apparently equally well suited to the treatment of all alternant hydrocarbons,[4] cannot be applied in this context.

But the very reasons which contributed to the success of the perimeter model are those which have limited the use of molecular orbital theory. The perimeters were chosen deliberately for four reasons. In the first place, recent calculations[5] had indicated that the cyclic polyenes could be represented by particularly simple wave functions, both in their ground and lower excited states. Secondly, the effects of configurational interaction (CI) could be understood clearly, at least in qualitative terms: the nightmare of "second-order" CI[2,6] was dispelled by viewing the orbital theories from an atomic viewpoint.[5,7] Thirdly, although it was evident that exceedingly painstaking calculations must be undertaken before even the simplest of these systems could be handled accurately on a nonempirical basis, the qualitative insight gained was sufficient to enable one to make fruitful use of the known benzene spectrum: it was possible to construct a reasonably well-founded semiempirical theory.[2] Lastly, and perhaps no less importantly, Platt's use of the perimeter model in the classification of spectra[1] was so successful that its quantitative formulation was a matter of some urgency. For these reasons, the perimeter theory was adopted in favor of the conventional MO theory. As will appear, it is not yet obvious how similar considerations may be advanced to justify the use of the latter method.

In this note, the potentialities, limitations and difficulties associated with the molecular orbital method will be discussed. Closely analogous arguments will, of

[1] J. R. Platt, J. Chem. Phys. **17**, 484 (1949).
[2] W. Moffitt, J. Chem. Phys. **22**, 320 (1954).
[3] J. E. Lennard-Jones and C. A. Coulson, Trans. Faraday Soc. **35**, 811 (1939).
[4] C. A. Coulson, and G. S. Rushbrooke, Proc. Cambridge Phil. Soc. **36**, 193 (1940).
[5] W. Moffitt and J. Scanlan, Proc. Roy. Soc. (London) **A218**, 464 (1953); **A220**, 530 (1953).
[6] Coulson, Craig, and Jacobs, Proc. Roy. Soc. (London) **A206**, 297 (1951).
[7] W. Moffitt, Proc. Roy. Soc. (London) **A210**, 245 (1951); **A218**, 486 (1953); Repts. Progr. Phys. Vol. XVII, p. 173 (1954).

necessity, apply also to the free-electron treatment, which has recently been shown to resemble closely the former method. For our starting point we take the orbitals and their energies as these are prescribed by the simplest MO theory (see Sec. 1). We then discuss the properties of certain electron assignments to these orbitals, namely of the ground and lower excited configurations. For alternant hydrocarbons, certain simple results are immediately apparent (See Sec. 2). In the subsequent two sections, these results are applied to the polyacenes, to benzene, triphenylene and coronene, and compared with the observed spectra of these molecules. Finally, in Sec. 5, the performance of the method is critically reviewed and compared with the perimeter theory.

1. MOLECULAR ORBITALS

As is customary in dealing with conjugated hydrocarbons,[3] electrons are assigned to molecular orbitals ψ_ξ which are linear combinations of supposedly orthogonal atomic $2p\pi$ orbitals ϕ_m:

$$\psi_\xi=\sum_m \phi_m c_\xi{}^m, \tag{1}$$

where the expansion coefficients $c_\xi{}^m$ may be determined when the roots of the appropriate secular equation have been found. These roots give the orbital energies ϵ_ξ in the form

$$\epsilon_\xi=\alpha+k_\xi\beta, \tag{2}$$

where α, β are the usual Coulomb and resonance integrals, respectively. For a system of $2N$ conjugated atoms, $2N$ linearly independent molecular orbitals are obtained, and with each of these a given value of ϵ_ξ, and therefore also of k_ξ is associated.

An important class of such hydrocarbons has been called alternant.[4,8] A conjugated molecule of this type is said to be alternant if its unsaturated atoms may all be assigned to one of two groups, such that no two members of the same group are nearest neighbors. The members of a particular group are called "starred" atoms, when those of the other group are called "unstarred." The properties of alternant hydrocarbons, which account, inter alia, for all condensed systems containing only even-membered rings, are peculiarly symmetrical and show certain unique features.

For example, the antibonding orbitals, for which $k<0$, may be constructed immediately whenever the bonding orbitals with $k>0$ are known. For simplicity, it will be supposed that the known orbitals have been chosen as real. Then, corresponding to each ψ_ξ with $k_\xi>0$, namely,

$$\psi_\xi=\sum_m{}^\dagger \phi_m c_\xi{}^m+\sum_m{}^0 \phi_m c_\xi{}^m, \tag{3}$$

we may construct another,

$$\psi_{\xi'}=\sum_m{}^\dagger \phi_m c_\xi{}^m-\sum_m{}^0 \phi_m c_\xi{}^m, \tag{4}$$

for which $k_{\xi'}=-k_\xi<0$. In both these formulas, the summation $\sum^\dagger$ is taken only over the starred atoms and $\sum^0$ only over the unstarred atoms. Thus, if N bonding orbitals are known, the N antibonding orbitals are easily determined. Moreover, the orbital energies are symmetrically disposed about the value $\epsilon=\alpha$, corresponding to a non-bonding orbital, which is generally absent.

Now consider two particular bonding orbitals ξ, η and the antibonding orbitals ξ', η' which may be constructed from these, respectively. Then it is evident that

$$\epsilon_{\xi'}-\epsilon_\eta=-\beta(k_\xi+k_\eta)=\epsilon_{\eta'}-\epsilon_\xi, \tag{5}$$

and therefore that the energies of excitation corresponding to the processes $(\eta)^{-1}(\xi')$ and $(\xi)^{-1}(\eta')$ are equal. In this approximation, where overlap is neglected, it may also be shown that the concomitant dipole vectors $\mathbf{q}$ are equal. It is only necessary to separate the summation over atoms into a summation first over starred and then over unstarred atoms:

$$\begin{aligned}\mathbf{q}_{\xi'\eta}&=\int \psi_{\xi'}\mathbf{r}\psi_\eta dv=\sum_m\sum_n c_{\xi'}{}^m c_\eta{}^n\int \phi_m\mathbf{r}\phi_n dv\\&=(\sum_m{}^\dagger+\sum_m{}^0)(\sum_n{}^\dagger+\sum_n{}^0)c_{\xi'}{}^m c_\eta{}^n\mathbf{r}_m\delta_{mn}\\&=\sum_m{}^\dagger c_{\xi'}{}^m c_\eta{}^m\mathbf{r}_m+\sum_m{}^0 c_{\xi'}{}^m c_\eta{}^m\mathbf{r}_m\\&=\sum_m{}^\dagger c_\xi{}^m c_\eta{}^m\mathbf{r}_m-\sum_m{}^0 c_\xi{}^m c_\eta{}^m\mathbf{r}_m=\mathbf{q}_{\eta'\xi},\end{aligned} \tag{6}$$

where $\mathbf{r}_m$ is the position vector of the mth atom. Again, the charge density associated with an electron in either ξ or ξ' is the same; on the mth atom, both are equal to $(c_\xi{}^m)^2$ when, as we suppose to be the case, ψ_ξ is normalized.[4]

[It may be anticipated that the degeneracy of the excitation processes $(\eta)^{-1}(\xi')$ and $(\xi)^{-1}(\eta')$, symbolized by Eq. (5), will form an important part of the ensuing discussion. In order to forestall the objection that the use of Eq. (2) neglects overlap, and therefore invalidates Eq. (5), it should be mentioned that a defence of our present procedure is given in an appendix.]

2. CONFIGURATIONS

Let us now consider the assignment of electrons to orbitals in those cases where there is no orbital degeneracy, and the ψ_ξ are all real. In general, for an alternant hydrocarbon of $2N$ atoms there will be N bonding and N antibonding orbitals. The ground state is therefore described by putting all $2N$ unsaturation electrons, pairwise, into the N available bonding

[8] H. C. Longuet-Higgins, J. Chem. Phys. **18**, 265 (1950).

orbitals. Excited states arise from assignments in which one or more of the electrons occupy antibonding orbitals. It seems reasonable to consider only those configurations in which one electron is excited. Such excited configurations have certain interesting properties for alternant hydrocarbons which will now be considered.

We first recall the theorem[4] that in the ground state the electrons are uniformly distributed among the carbon atoms, so that the total π-electronic charge density is unity at each of these. It follows from the preceding section that the same holds for all excited configurations obtained by taking an electron from any bonding orbital ξ and putting it into the corresponding antibonding orbital ξ', where $k_{\xi'}=-k_\xi$. However, if the excited electron is allotted to any other orbital η', say, where ξ, η' do not bear this special relation one to the other, the associated configuration will in general have a nonuniform charge distribution, for now $(c_{\xi^m})^2$ is only accidentally equal to $(c_{\eta'^m})^2$. For these latter configurations, therefore, the molecular orbital method apparently fails to achieve that measure of self-consistency which it automatically attains for ground state problems: the assumption of equal Coulomb integrals α at all carbon atoms does not lead to charge densities of unity everywhere.

On the other hand, such excited configurations $(\xi)^{-1}(\eta')$ have a special property which is not shared by the $(\xi)^{-1}(\xi')$. Namely, there is always a second excited configuration $(\eta)^{-1}(\xi')$ with the same energy—at least to this approximation. Before any premature conclusions are drawn as to the charge distribution in the corresponding excited states, the interactions of at least these two degenerate configurations must be taken into account. And in order correctly to consider this point, antisymmetrized functions must be constructed to represent more precisely our electron assignments.

[It may be remarked that in the simple case of no orbital degeneracy, the two degenerate configurations have the same symmetry with respect to the molecule's point group: the orbitals ξ, η, ξ', and η' will all span irreducible representations of this group; if not, they would be degenerate. Now let a particular symmetry operator $\mathfrak{R}$, say, interchange atoms m and n. If both are starred or unstarred, let $\lambda=+1$; otherwise, let $\lambda=-1$. Under $\mathfrak{R}$, all four orbitals acquire a factor ±1, which we shall call ι_ξ for ξ, and so on. Then, as a result of this symmetry operation, the product $\xi\eta'$ is multiplied by $\iota_\xi\iota_{\eta'}$, and $\eta\xi'$ by $\iota_\eta\iota_{\xi'}$. But from Eqs. (3) and (4) it is immediately apparent that both factors are equal to $\lambda\iota_\xi\iota_\eta$. It follows that the two configurations have the same symmetry. By exactly similar reasoning, it may be seen that configurations $(\xi)^{-1}(\xi')$ and $(\eta)^{-1}(\eta')$ also transform together under the elements of the point group. For the case of degenerate representations (vide infra), a more careful but no more difficult analysis must be undertaken.]

The correct ground state function is, of course, a single determinant of the usual closed shell type, namely,

$$\Theta_N=\{(2N)!\}^{-\frac{1}{2}}\times det\{\cdots,\psi_\xi(2N-1)\alpha(2N-1),\psi_\xi(2N)\beta(2N)\}=|\cdots\eta\bar{\eta}\cdots\xi\bar{\xi}|, \quad (7)$$

say, where we have only explicitly displayed orbital ξ in the first form, and introduced a convenient abbreviation in the second. The unspecified electrons here, as in what follows, are assumed to be in completed shells. If it is supposed that the molecular orbitals are orthogonal, the function (7) is normalized to unity. Corresponding to any one-electron excitation, we may always form a singlet and a triplet function. We shall restrict ourselves to the singlets, since we are primarily interested in transitions whose oscillator strengths are considerably greater than those associated with spin-forbidden processes. A typical example is the configuration $(\xi)^{-1}(\eta')$, whose antisymmetrized representative is

$$\Theta_A=\frac{1}{\sqrt{2}}\{|\cdots\eta\bar{\eta}\xi\bar{\eta}'|+|\cdots\eta\bar{\eta}\eta'\bar{\xi}|\}. \quad (8_1)$$

Similarly,

$$\Theta_B=\frac{1}{\sqrt{2}}\{|\cdots\eta\bar{\xi}'\xi\bar{\xi}|+|\cdots\xi'\bar{\eta}\xi\bar{\xi}|\}, \quad (8_2)$$

$$\Theta_C=\frac{1}{\sqrt{2}}\{|\cdots\eta\bar{\eta}\xi\bar{\xi}'|+|\cdots\eta\bar{\eta}\xi'\bar{\xi}|\}, \quad (8_3)$$

$$\Theta_D=\frac{1}{\sqrt{2}}\{|\cdots\eta\bar{\eta}'\xi\bar{\xi}|+|\cdots\eta'\bar{\eta}\xi\bar{\xi}|\}, \quad (8_4)$$

represent the configurations $(\eta)^{-1}(\xi')$, $(\xi)^{-1}(\xi')$, and $(\eta)^{-1}(\eta')$, respectively.

Now, as we have seen, Θ_A and Θ_B will have the same symmetry, as well as the same energy in the first approximation. These configurations will therefore "interact" in the sense that the matrix element

$$\int\Theta_A\mathfrak{IC}\Theta_B dV=2(\eta\eta'|\xi'\xi)-(\eta\eta'|\xi\xi'), \quad (9)$$

where, for example,[9]

$$(\eta\eta'|\xi'\xi)=\int\int\psi_\eta(1)\psi_{\eta'}(2)\frac{1}{r_{12}}\psi_{\xi'}(1)\psi_\xi(2)dv_1dv_2, \quad (10)$$

will not in general vanish. If the interaction of these two configurations alone is considered, it is easily seen that the degenerate pair splits to form functions

$$\Theta_{J,K}=\frac{1}{\sqrt{2}}(\Theta_A\pm\Theta_B), \quad (11)$$

[9] This specific form of the interaction elements holds for the usual method of antisymmetrized molecular orbitals, which is known to contain serious errors. These errors may be remedied, at least in part, by the procedures given in references 5 and 7.

respectively. The degeneracy of Θ_A, Θ_B will not always be perfect in higher approximations; nevertheless, it may be expected that their separation is sufficiently small for Eq. (11) to hold quite accurately. For reasons which have been discussed elsewhere,[5] it is unfortunately very difficult to assess this splitting quantitatively. However, despite the fact that we are not in a position to give a sound estimate of the energy separating Θ_J and Θ_K, we can obtain some insight into the properties of these functions on the basis of Eq. (11).

For simplicity, let us temporarily assume, as is consistent with simple MO theory, that the configurational interaction considered so far (first-order CI) is the only kind that need be taken into account. Θ_J and Θ_K will then represent excited states of the molecule, as will Θ_C and Θ_D. Indeed, all states arising from one-electron excitations will be represented by such functions. Now, it has already been noted that the charge distribution in states Θ_C and Θ_D is uniform, just as in the ground state Θ_N of any alternant hydrocarbon. It is easily verified using Eq. (11) that, although this is patently not true for the configurations Θ_A and Θ_B, the charge distribution in the states that arise from these functions, namely Θ_J and Θ_K, is also uniform. The charge density associated with the mth atom is

$$1-\tfrac{1}{2}(c_\xi{}^m)^2+\tfrac{1}{2}(c_{\eta'}{}^m)^2-\tfrac{1}{2}(c_\eta{}^m)^2+\tfrac{1}{2}(c_{\xi'}{}^m)^2; \qquad (12)$$

by use of Eqs. (3) and (4), the quantity (12) reduces to unity. This point is more fully discussed in an appendix. (Many-electron excitations may, of course, be handled by analogous methods to give the same result.) By considering only first-order CI, it is clear that the simple molecular orbital theory achieves the same measure of self consistency for excited states that it does for ground states. This is an important result, since it means that the method is formally as well suited to the treatment of both excited and ground states of alternant hydrocarbons.

A second result, which is particularly significant in the interpretation of spectra, may be obtained concerning the intensity of transitions from the ground state Θ_N to states Θ_J and Θ_K. Since we have shown in Eq. (6) that the dipole vectors associated with processes $\Theta_N \rightarrow \Theta_A$, Θ_B are equal, it follows immediately that these vectors combine to give, in general, strong dipole strengths for transitions $\Theta_N \rightarrow \Theta_J$. But the purely electronic dipole strengths of transitions $\Theta_N \rightarrow \Theta_K$ vanish, the component vectors cancelling in this case. This is very relevant in the analysis of the weak α bands that occur in so many condensed hydrocarbon spectra (vide infra). Again, first-order CI plays a role that must not be neglected. Instead of two overlapping bands of equal intensity ($\Theta_N \rightarrow \Theta_A, \Theta_B$), we anticipate two distinct, noncoincident band systems, one of which is strong and the other very weak ($\Theta_N \rightarrow \Theta_J, \Theta_K$, respectively).

In the following two sections, these considerations will be applied to the polyacenes and to certain other molecules. The simplest molecular orbital theory will be employed and attention will be paid to the qualitative conclusions which may be drawn from first-order configurational interaction.

3. POLYACENES

The molecular orbitals for the polyacenes have been discussed systematically by Coulson.[10] Since molecules of this type (e.g., naphthalene, anthracene, and so on) belong to the point group $\mathbf{D}_{2h}$, the orbitals may be given systematic names according to their symmetries. Following Coulson, we adopt the following simplified notation: the orbitals are called P, Q, R, and S; all change sign under a reflection in the plane σ_h say, of the molecule. Q and S change sign, whereas P and R are left invariant under a reflection in a plane perpendicular to σ_h and containing the shorter axis of the molecule. R and S change sign, whereas P and Q are left invariant under a reflection in a plane perpendicular to σ_h and containing the longer axis of the molecule. Thus, excitations $P^{\pm 1}R^{\mp 1}$ and $Q^{\pm 1}S^{\mp 1}$ are polarized ($\perp$) along the shorter axis of the molecule, and excitations $P^{\pm 1}Q^{\mp 1}$ and $R^{\pm 1}S^{\mp 1}$ are polarized ($\|$) along the longer axis of the molecule. Excitations $P^{\pm 1}S^{\mp 1}$ and $Q^{\pm 1}R^{\mp 1}$ are forbidden in dipole radiation fields. In order to distinguish orbitals of the same symmetry but of different energy, these are assigned subscripts so that, for example, R_j is always lower in energy than R_{j+1}, and R_1 is the lowest orbital of symmetry R. (The orbitals P, Q, R, and S, respectively, span irreducible representations B_{3u}, B_{2g}, B_{1g}, and A_{1u} of $\mathbf{D}_{2h}$.)

These molecules all contain $2N=4\nu+2$ carbon atoms, where ν is a positive integer. The energies ϵ_ξ of the molecular orbitals are given by Eq. (2) where the k_ξ have the following values:[10]

$$k=+1, \quad k=\tfrac{1}{2}\left\{1\pm\sqrt{\left(9+8\cos\frac{m\pi}{\nu+1}\right)}\right\},$$

$$(m=1, \cdots, \nu),$$

of which the highest value of k, corresponding to the most stable of these orbitals, belongs to the orbital P_1 and, thereafter, the associated orbitals are alternately Q and P, in order of increasing energy. Also,

$$k=-1, \quad k=\tfrac{1}{2}\left\{-1\pm\sqrt{\left(9+8\cos\frac{m\pi}{\nu+1}\right)}\right\},$$

$$(m=1, \cdots, \nu),$$

of which the highest value of k, corresponding to the most stable of these orbitals, belongs to the orbital R_1 and, thereafter, the associated orbitals are alternately S and R, in order of increasing energy.

It is easily verified that bonding orbitals P, Q, R, S, have as their antibonding counterparts orbitals of

[10] C. A. Coulson, Proc. Phys. Soc. (London) **60**, 257 (1948).

symmetry R, S, P, Q, respectively, where this correspondence is made on the basis of Eqs. (3) and (4). That is, whenever there is an orbital of symmetry P with a given energy $\epsilon=\alpha+k\beta$, then there is always an orbital of symmetry R with energy $\epsilon=\alpha-k\beta$, and so on.

It is convenient to discuss the excited states of the polyacenes according to their various symmetries. Consider first those excited states which transform like translations along the longer axis of the molecule ($^1B_{1u}$). If, as we suppose to be the case, they arise from one-electron excitations, they can only be associated with the processes $P^{\pm 1}Q^{\mp 1}$, $R^{\pm 1}S^{\mp 1}$. Now neither of the orbital pairs P and Q nor R and S are related in the sense of Eqs. (3) and (4). Thus, for every configuration $P^{\pm 1}Q^{\mp 1}$ (or $\xi^{-1}\eta'$), there is another of equal energy, namely $S^{\pm 1}R^{\mp 1}$ (or $\eta^{-1}\xi'$), and these are represented, respectively, by functions like (8_1) and (8_2). They therefore split to form states like Θ_J and Θ_K of Eq. (11). Thus, if only first-order CI is considered, all excited states of symmetry $^1B_{1u}$—the upper states of the parallel bands in the polyacenes—occur in pairs. A transition from the ground state (Θ_N) to one of these (Θ_J) is associated with an appreciable oscillator strength, whereas bands corresponding to a transition to the other (Θ_K) should be very weak indeed. These conclusions follow immediately from the considerations of the preceding section.

It is very tempting, on this basis, to make an immediate identification of certain band systems in the polyacene series. Prominent in the spectra of these molecules are two transitions, one very strong and the other very weak. (The latter are only seen when not overlapped by a stronger system to be described later.) The former are Clar's β bands[11] which Platt calls $^1A\rightarrow{}^1B_b$,[1,12] and the latter are Clar's α bands, which Platt calls $^1A\rightarrow{}^1L_b$. The β bands occur at the shorter wavelengths and increase in intensity as one goes from naphthalene to the higher polyacenes. The α bands, which are seen in naphthalene, but obscured in anthracene and naphthacene, reappear in pentacene; their presence is also inferred, as may their location be estimated, from their appearance in isomers of anthracene and naphthacene.[1,2,11] These α bands are uniformly very weak. Both Platt[1] and the present author[2] have attributed these transitions to parallel polarizations.

Let us, therefore, make the provisional assumption that the lowest Θ_J, Θ_K pair of appropriate symmetry is to be identified with the upper states of the β and α bands, respectively. Failing an accurate means of assessing the separation of these two states, we may apply the formula (2) to calculate the mean excitation energy of these two states, namely (5). This may then be compared with the observed mean of the α- and β-band absorption energies.

Such a comparison is made in Fig. 1. It will easily be seen that the specific excitation processes are $S_{\nu/2}{}^{-1}R_{(\nu+2)/2}$ and $P_{(\nu+2)/2}{}^{-1}Q_{(\nu+2)/2}$ for even values of ν and $R_{(\nu+1)/2}{}^{-1}S_{(\nu+1)/2}$, and $Q_{(\nu+1)/2}{}^{-1}P_{(\nu+3)/2}$ for odd values of ν; the associated energies are given by

$$\tfrac{1}{2}|\beta|\left\{\sqrt{\left(9-8\cos\frac{\pi}{\nu+1}\right)}+1\right\}.$$

The resonance integral (β) is set equal to $-24\,000$ cm^{-1}; this value is derived from the known benzene spectrum (vide infra). The full line represents the behavior of the observed mean, and the broken line that predicted on the above assumption. Additional pairs of levels with this symmetry are fairly far removed from the ones which are shown (e.g., some 15 000 cm^{-1} above the indicated pentacene pair, and farther removed for the others). The agreement between the calculated and observed curves is amazingly good, indeed well nigh perfect.

But the method, without elaborate extensions, does not enable us to predict the magnitude of the splitting of these degenerate configurations—that is, the energy separating the upper state of the α from the upper state of the β bands. For naphthalene this splitting (or rather the observed separation of the α and β bands) amounts to some 13 000 cm^{-1}, and for pentacene it is about 9000 cm^{-1}.[12] Matrix elements of the type (9) are easy to write down, but there is little assurance that they may be estimated with sufficient accuracy to merit the effort. The few calculations of this sort which have been made[13] are not encouraging, particularly in view of the indifferent results they achieve for simpler systems like ethylene and oxygen. Those methods that are

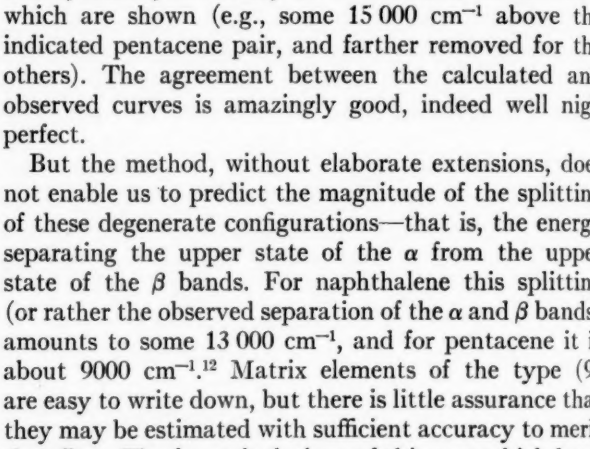

FIG. 1.

[11] E. Clar, *Aromatische Kohlenwasserstoffe* (Julius Springer, Berlin, first edition 1941, second eidtion 1952).
[12] H. B. Klevens and J. R. Platt, J. Chem. Phys. **17**, 470 (1949).
[13] J. Jacobs, Proc. Phys. Soc. (London) **62**, 710 (1949).

most reliable for the simple molecules[5,7] cannot be applied here without a great deal of labor or some drastic approximations. We must be content with the quantitative correlation of Fig. 1, and the qualitative description of the very different α- and β-band systems offered by the simple molecular orbital theory.

It is in this connection particularly that the perimeter theory[2] is more powerful. The polarization attributed to the α- and β-band systems is the same, and their mean excitation energy is estimated with comparable accuracy. However, since the matrix elements representing the splitting of these two levels were of a much higher symmetry (for the ψ_ξ's employed, each c_ξ^m had the same modulus of $(4\nu+2)^{-\frac{1}{2}}$), it was possible to recognize the drift in these as the number of rings was increased. In this way it was possible to exploit a simple but adequate proportionality assumption in conjunction with the known benzene spectrum. It would be possible in the MO theory used in this note to suppose also that the splitting of the two configurations was proportional to their separation from the ground state. And excellent agreement would be obtained with the experimental results in this way. But unless this supposition were to be supported by an elaborate, and probably not very trustworthy analysis of the relevant MO's and matrix elements, it would lack any theoretical justification.

We proceed to consider excited states of symmetry $^1B_{2u}$, transitions to which from the ground state are perpendicularly polarized. These may arise from one-electron excitations of the type $P^{\pm 1}R^{\mp 1}$ or $Q^{\pm 1}S^{\mp 1}$. Let us first consider the process requiring the least energy, in which an electron is removed from the bonding orbital of greatest energy and assigned to the antibonding orbital of least energy. The former orbital is easily seen to be $S_{\nu/2}$ when ν is even and $R_{(\nu+1)/2}$ when ν is odd; the latter is either $Q_{(\nu+2)/2}$ or $P_{(\nu+3)/2}$ under these circumstances, respectively. It is clear that the resultant excited configurations, of least energy, are of the type $\xi^{-1}\xi'$ in both events. When ν is even, $Q_{(\nu+2)/2}$ is the antibonding counterpart of $S_{\nu/2}$, and when ν is odd, $P_{(\nu+3)/2}$ is the antibonding counterpart of $R_{(\nu+1)/2}$, both correspondences being in the sense of Eqs. (3) and (4). In general, therefore, the configurations associated with the upper states of the "longest wavelength" absorptions are nondegenerate configurations like Θ_C of Eq. (8_3). Their energies of excitation are given in terms of the resonance integral by the quantity

$$|\beta|\left\{\sqrt{\left(9-8\cos\frac{\pi}{\nu+1}\right)}-1\right\}.$$

Again, there is an obvious series of bands in the polyacene spectra with which these predicted, perpendicular transitions may be associated.

In addition to the α and β bands, another series of bands is observed in these molecules. Whereas the α bands are very weak, and the β bands are very strong,

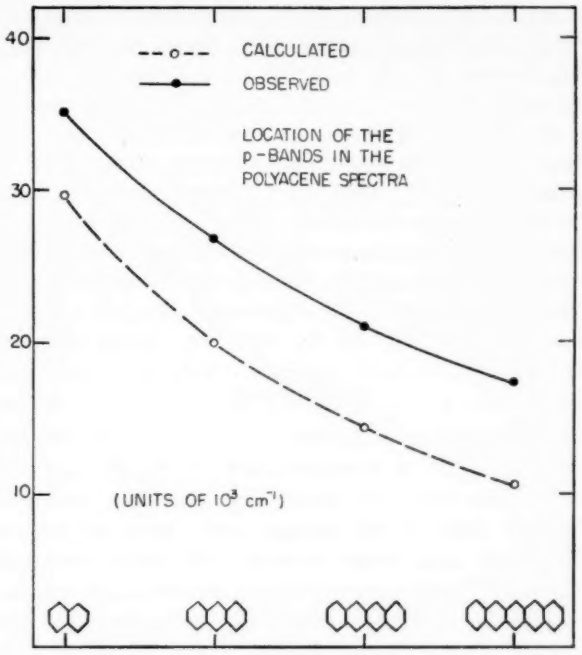

FIG. 2.

these other bands are of only moderate intensity, and are called p bands.[11] (Platt[1,12] calls them $^1A\rightarrow{}^1L_a$.) Apart from naphthalene, where these lie slightly above the α bands,[14] the p bands constitute the longest wavelength systems in the polyacene series. (This is not true for isomers of the polyacenes. In these, the α and β bands are insensitive to the isomerism, whereas the p bands move sharply, and characteristically, to shorter wavelengths.[2]) Coulson[10] first identified these systems in terms of a perpendicular transition $^1A_{1g}\rightarrow{}^1B_{2u}$, ascribing to them exactly the same excitation mechanism that we have given above. Since his method of calculating excitation energies was slightly different from ours (see appendix), we compare the predicted with the observed location of the p bands in Fig. 2; as before, β was set equal to $-24\,000$ cm^{-1}.

The agreement is by no means as good as for the mean of the α and β bands. Also, as Coulson has shown, the predicted intensities are too high by a factor of 10. Moreover, the oscillator strengths of these p bands are observed to remain sensibly constant for all four molecules, but they are predicted to decrease by a factor of 2 on going from naphthalene to pentacene. Now, although it is known that MO intensities are always too high, the results for benzene and ethylene are only too large by a factor of 3 or so. The magnitude of the discrepancy in the case of the p bands is therefore considered to be significant, even within an MO framework; its possible implications are discussed later. The perimeter theory[2] is a definite improvement on the MO theory in this case also.

There is another disturbing feature of the MO

[14] M. Kasha and R. V. Nauman, J. Chem. Phys. **17**, 516 (1949).

theory in these instances. In pentacene, for example, one would expect three excited states of symmetry $^1B_{2u}$ (namely, $R_3{}^{-1}P_5$, $S_2{}^{-1}Q_4$, $R_2{}^{-1}P_4$), which are located just where the mean of the upper states of the α and β bands lie. The intrusion of these levels receives no support from the observed spectrum of pentacene.[12] Admittedly they would interact, perhaps even quite strongly, among themselves. But one would expect to observe at very least one of them to longer wavelengths than the α bands. Again, the interpretation of the very weak α bands is not unambiguous in the MO method. Some of these could also be explained, though not very satisfactorily, as due to symmetry forbidden transitions ($^1A_{1g}\rightarrow{}^1B_{3g}$ or $^1A_{1g}$). Already in anthracene, for example, the mean of the α and β bands coincides with the degenerate pair of configurations $S_1{}^{-1}P_5$, $R_2{}^{-1}Q_3$. (No such difficulties are encountered in the perimeter theory.) Under isomerization, and consquent loss of symmetry, assignments become even more equivocal. Moreover, it becomes difficult to establish generic relations among the band systems, despite the fact that such correspondences are perhaps the most striking features of the spectra of cata-condensed molecules.[12]

4. BENZENE

Now the configurational degeneracy which has been discussed in the preceding sections is really only "accidental." That is, it is a peculiar property of alternant hydrocarbons when treated by means of a simple approximation. And although it may be anticipated that its effects are qualitatively correct in higher approximations, the degeneracy is in no sense dictated by the symmetry of the molecules. However, the analysis of configurational interaction is sufficiently important in the interpretation of spectra,[15] that it is as well to consider also the case of essential degeneracy, which arises so clearly in the benzene molecule.

This particular system has been studied quantitatively by many authors,[2,5,16,17] most of whom use complex molecular orbitals. The most stable, and the most highly excited MO's are nondegenerate and have energy $\alpha\pm2\beta$, respectively; they do not concern us here. In addition to these, there are two pairs of degenerate orbitals of energy $\alpha\pm\beta$. The bonding pair are generally written as complex conjugates one of the other:

$$\psi_{+1}=\frac{1}{\sqrt{6}}(\phi_0+\omega\phi_1+\omega^2\phi_2+\omega^3\phi_3+\omega^4\phi_4+\omega^5\phi_5),$$

$$\psi_{-1}=\psi_{+1}{}^*,\quad \omega=\exp(2\pi i/6).$$

The antibonding pair are similarly expressed:

$$\psi_{+2}=\frac{1}{\sqrt{6}}(\phi_0+\omega^2\phi_1+\omega^4\phi_2+\phi_3+\omega^2\phi_4+\omega^4\phi_5),$$

$$\psi_{-2}=\frac{1}{\sqrt{6}}(\phi_0+\omega^4\phi_1+\omega^2\phi_2+\phi_3+\omega^4\phi_4+\omega^2\phi_5).$$

In this form, the orbitals are eigenfunctions of the operator representing a rotation of $\pi/3$ about the sixfold axis; they span irreducible representations E_{1g}, E_{2u}, respectively, of the appropriate point group $\mathbf{D}_{6h}$. In order to facilitate the comparison with our previous analysis, it is convenient linearly to combine these to form real orbitals with the same energies.

$$R=\sqrt{2}Re\psi_{+1}=\frac{1}{2\sqrt{3}}(2\phi_0+\phi_1-\phi_2-2\phi_3-\phi_4+\phi_5),$$

$$Q=\sqrt{2}Im\psi_{+1}=\tfrac{1}{2}(\phi_1+\phi_2-\phi_4-\phi_5),$$

$$P=\sqrt{2}Re\psi_{+2}=\frac{1}{2\sqrt{3}}(2\phi_0-\phi_1-\phi_2+2\phi_3-\phi_4-\phi_5),$$

$$S=-\sqrt{2}Im\psi_{+2}=\tfrac{1}{2}(-\phi_1+\phi_2-\phi_4+\phi_5).$$

R, Q have energy $\alpha+\beta$, and P, S have energy $\alpha-\beta$. The notation has been chosen (vide infra) with respect to the lower group $\mathbf{D}_{2h}$, under which the polyacenes transform; thus only R and S change sign under a reflection in the plane perpendicular to that of the molecule and bisecting bonds 1–2 and 4–5, whereas only Q and S change sign under a reflection in the plane perpendicular to that of the molecule and containing atoms labelled 0 and 3.

In the ground state, the last four electrons are assigned to orbitals R and Q. However, there are four possible ways of exciting one electron from a highest bonding to a lowest antibonding orbital: $R^{-1}P$, $Q^{-1}S$, both of which are of the type $\xi^{-1}\xi'$, and $R^{-1}S$, $Q^{-1}P$, which form a degenerate $\xi^{-1}\eta'$, $\eta^{-1}\xi'$ pair. We see that they correspond to the configurational functions Θ_C, Θ_D and Θ_A, Θ_B, respectively. As was seen in Sec. 2, the latter pair split to form functions

$$\Theta_Y=\frac{1}{\sqrt{2}}(\Theta_A+\Theta_B),\quad \Theta_V=\frac{1}{\sqrt{2}}(\Theta_A-\Theta_B).$$

(In this particular connection, it is convenient to replace Θ_J, Θ_K of Eq. (11) by Θ_Y, Θ_V.) However, owing to the additional degeneracy of Θ_C and Θ_D, which was not encountered before, these two configurations also split to form functions

$$\Theta_X=\frac{1}{\sqrt{2}}(\Theta_C+\Theta_D),\quad \Theta_U=\frac{1}{\sqrt{2}}(\Theta_C-\Theta_D).$$

(With respect to the lower group, $\mathbf{D}_{2h}$, both Θ_C and Θ_D

[15] See J. R. Platt, J. Chem. Phys. **18**, 1168 (1950), where this importance is stressed for "round-field" spectra.
[16] M. Goeppert-Mayer and A. L. Sklar, J. Chem. Phys. **6**, 645 (1938).
[17] Parr, Craig, and Ross, J. Chem. Phys. **18**, 1561 (1950).

have the same symmetry which is different from that of the Θ_A, Θ_B pair.) Moreover, it is easy to show in this case that $\mathbf{q}_{\xi'\xi}=\mathbf{q}_{\eta'\eta}$, so that the dipole vector associated with an excitation $\Theta_N\rightarrow\Theta_U$ vanishes, whereas these component vectors add to give a considerable resultant for an excitation $\Theta_N\rightarrow\Theta_X$. Without appealing to the full symmetry of the molecule, or going to a higher approximation, the benzene spectrum would be described qualitatively as follows: two intense band systems, $\Theta_N\rightarrow\Theta_X$ and $\Theta_N\rightarrow\Theta_Y$, of excitation energies $2|\beta|+\gamma$ and $2|\beta|+\delta$, respectively, polarized in two mutually perpendicular directions, accompanied by two very weak systems, $\Theta_N\rightarrow\Theta_U$ and $\Theta_N\rightarrow\Theta_V$, with excitation energies $2|\beta|-\gamma$ and $2|\beta|-\delta$ and the same respective polarizations as the strong systems.

This result is, of course, incorrect.[16] Functions Θ_X and Θ_Y span the irreducible, two-dimensional representation ${}^1E_{1u}$ of the full group $\mathbf{D}_{6h}$, whereas Θ_U and Θ_V are of symmetries ${}^1B_{1u}$ and ${}^1B_{2u}$ respectively. The spectrum consists of an intense absorption ${}^1A_{1g}\rightarrow{}^1E_{1u}$, together with successively weaker systems at successively longer wavelengths, ${}^1A_{1g}\rightarrow{}^1B_{1u}$ and ${}^1A_{1g}\rightarrow{}^1B_{2u}$; the latter transitions are electronically forbidden. The mean of the excitation energies for these processes is around 48 000 cm^{-1}, which is the reason for adopting the value $\beta=-24\,000$ cm^{-1} in the preceding section.

Some of the weaknesses of our considerations in earlier paragraphs are nicely brought out by this analysis. Just because two configurations have the same energy in a simple approximation, they may have considerably different energies in a high approximation. Or, equivalently, if two configurations are assigned the same energy by simple MO theory, their splitting is not always symmetrical. For if this were not the case, the separation $|\delta-\gamma|$ between the ${}^1B_{1u}$ and ${}^1B_{2u}$ states in benzene (some 10 000 cm^{-1}) would dictate this same separation between the two essentially degenerate components of the ${}^1E_{1u}$ state. We can see that the good agreement attained for the mean of the α- and β-band locations of the polyacenes (Fig. 1) is in part illusory. Again, the magnitude of the splitting due to configurational interaction is quite large. In molecules of low symmetry, therefore, where configurations of the same symmetry are not widely separated in energy, the interaction pattern may well be complicated and disturb considerably the results of a simple orbital method, such as that used above to describe the polyacenes. The distinction between first-order CI, that is, between configurations of the same energy, and second-order CI, which occurs between configurations of considerably different energies, is broken down. The advantages of the perimeter approach are once more clearly apparent; maximum use of symmetry is made, so that this distinction never fails.

Other molecules exhibiting configurational interaction owing to the presence of doubly degenerate orbitals, analogous to those in benzene, are triphenylene and coronene.[18] Utilizing their full symmetry, it is easy to show that also in each of these molecules there should be one intense system of absorption, with a doubly degenerate upper state, together with two weak systems, associated with electronically forbidden transitions. And their observed spectra do indeed show the expected characteristics.[1,15] On the basis of $\beta=-24\,000$ cm^{-1}, the calculated means of these levels are $\sim$33 000 cm^{-1} for triphenylene and $\sim$26 000 cm^{-1} for coronene, which are in reasonably good agreement with the empirically determined figures of $\sim$35 000 cm^{-1} and $\sim$29 000 cm^{-1}, respectively.

5. DISCUSSION

It was shown in the first two sections that the simple MO theory attains the same degree of self-consistency for the excited states of alternant hydrocarbons that it does for their ground states. This result has significant implications in the interpretation of spectra which were investigated in the ensuring sections. In conclusion, we shall attempt to summarize what we consider to be the more important weaknesses inherent in the method.

As was pointed out some years ago,[19,20] perhaps the most obvious shortcoming of the conventional MO theory lies in the inflexibility of its secular equations. These determine the individual molecular orbitals with no reference to the manner in which they are subsequently to be occupied. In hydrocarbons, such as azulene, charge is allowed to accumulate at particular atoms, no provision is made for the consequent modification of the assumed (uniform) Hartree-Fock field, and as a result dipole moments of unreasonable size are predicted. Even for alternant hydrocarbons, the measure of self-consistency the method automatically assumes, is by no means a guarantee that the best MO's are determined. These are only to be obtained by the use of considerably more elaborate techniques.[21,22] Certain disagreements in the predicted and observed intensities of transitions (e.g., the p bands of Sec. 3) may well be ascribed to bad MO's. For this reason, also, the significance to be attached to the parameters α and β of the simple theory is in considerable doubt. (Pople[23] has just published a paper in which this point is nicely illustrated by means of certain drastic but illuminating approximations.) It may be noticed, however, that the molecular orbitals for the cyclic polyenes, which form the basis of the perimeter theory, are determined by symmetry alone, and therefore do not suffer from this drawback.

---

[18] W. Moffitt and C. A. Coulson, Proc. Phys. Soc. (London) **60**, 309 (1948).
[19] W. Moffitt, Proc. Roy. Soc. (London) **A196**, 510 (1949).
[20] G. W. Wheland and D. E. Mann, J. Chem. Phys. **17**, 264 (1949).
[21] J. E. Lennard-Jones, Proc. Roy. Soc. (London) **A198**, 1, 14 (1949).
[22] C. C. J. Roothaan, Revs. Modern Phys., **23**, 61 (1951).
[23] J. A. Pople, Trans. Faraday Soc. **49**, 1375 (1953).

In order to analyze the importance of configurational interaction, it is advisable to work with good molecular orbitals. Consider, for example, a two-electron system described by means of a single, rather poor molecular orbital ξ. In general, it is possible to represent the best molecular orbital for this purpose, ζ say, in the form

$$\zeta=\xi\cos\theta+\eta\sin\theta,$$

where θ is a parameter of mixing and η another orbital. Then the best single configuration representing the state of the two electrons is

$$\Theta=|\zeta\bar{\zeta}|=\cos^2\theta|\xi\bar{\xi}|+\tfrac{1}{2}\sin 2\theta\{|\xi\bar{\eta}|+|\eta\bar{\xi}|\}+\sin^2\theta|\eta\bar{\eta}|.$$

The original configurational function $|\xi\bar{\xi}|$ may be improved by combining it linearly with other configurations. That is, configurational interaction may simply effect a transformation to best MO's. By starting with ζ, instead of ξ and η, however, this type of CI is seen to be redundant.

But, quite apart from this trivial form, configurational interaction can be important in various other ways. For example, if one adheres strictly to the ASMO program, it stabilizes even the ground state of a molecule as simple as ethylene to the extent of some 10 000 cm^{-1}. This arises from the "second-order" interaction between the ground and most highly excited configurations, $(b_{3u})^2$ and $(b_{2g})^2$, respectively.[5] It is sufficiently drastic to jeopardize the whole utility of the molecular orbital approach. Fortunately this adherence is not necessary. For by referring the underlying physical theory not to a specifically orbital approximation, but to the method of atoms in molecules,[5,7] it can be shown that second-order CI is negligible at least for certain simple systems, including ethylene, the allyl radical and benzene. And there is every reason to suppose that this would also be the case for the cyclic polyenes. However, this has not yet been established for other molecules such as the polyenes and the polyacenes. With the best choice for the orbitals, it is probable that the ground states may be well represented by a single configuration. But our experience of the preceding sections shows that configurational interaction will be of first importance in the excited states. Whether it will turn out that it is possible reasonably to differentiate first-order CI, between no more than two or so configurations of much the same energy, from second-order CI, due to "high-frequency" terms, is also not clear. It certainly seems possible to do this for the cyclic polyenes.

What is most urgently needed is an approximate, though reliable, method of determining the best molecular orbitals, and of assessing configurational interaction quantitatively for relatively large systems. And it appears that this must stem from the fundamental equations of the method of atoms in molecules,[7] rather than from those of antisymmetrized molecular orbital theory.[21,22] A set of simplifications must be chosen judiciously so as to render these equations more tractable—and in this connection the work of Pople[23] may provide valuable clues. The work of Pariser and Parr[24] is an important step in this direction. It grafts certain features of Kimball's hard sphere approximation onto the conventional ASMO formalism. The solution of problems is thereby greatly facilitated. Unfortunately, it was found necessary to replace some terms by semi-empirical parameters, and this serves to obscure somewhat the underlying physical basis of their approach.

Until such a time, however, the use of standard molecular orbital theory in the interpretation of spectra must not be undertaken uncritically. Indeed, it seems more profitable to construct theories, such as the perimeter theory, which are based on simple systems that are fairly well understood, in conjunction with suitably selected perturbation techniques.

APPENDIX

There are two points which it is as well to consider in further detail. One concerns the neglect of overlap in the assessment of orbital energies and the other relates to the charge densities associated with carbon atoms in molecular states that cannot be represented by a single determinant.

Wheland[25] has shown that it is possible to include overlap in the simple MO theory without in any way complicating the calculations demanded by the usual secular equations.[3] For the orbital energies he obtained the formula

$$\epsilon_\xi=\alpha+m_\xi\gamma,\quad \gamma=\alpha-S\beta,$$

which certain authors[10,15] use in preference to the formula (2). The parameter m_ξ is related to the parameter k_ξ, which is determined by the secular equations with neglect of overlap, by

$$m_\xi=k_\xi/(1+k_\xi S),$$

where S is the overlap integral $(=1/4)$. In view of the uncertain interpretation of the parameters α, β and therefore also γ, it seems preferable to use that prescription for the orbital energies which most nearly reflects the results of more accurate calculations. (Unfortunately, it is impossible to amass sufficient experimental data which have a direct bearing on this question.) Such a comparison is made in the accompanying table using the most recent calculations on the allyl radical,[7] the hypothetical planar molecule cyclobutadiene and the benzene molecule;[5] the designation of transitions is taken from the relevant articles. Only one-electron excitations from the ground configurations are considered and in those cases where the upper configurations are degenerate, a suitable mean is listed. After a description of the transitions, the calculated excitation energies are given in electron volts, followed by the predictions of the simpler formulas which are

[24] R. Pariser and R. Parr, J. Chem. Phys. **21**, 466, 767 (1953).
[25] G. W. Wheland, J. Am. Chem. Soc. **63**, 2025 (1941).

TABLE I. One-electron excitation energies.

Allyl radical	eV	Δk	Δm
$\kappa^2\iota \rightarrow \kappa^2\lambda$	4.6	1.41	2.19
$\kappa\iota^2$	4.7	1.41	1.04
$\kappa\iota\lambda$	7.8	2.83	3.23
Cyclobutadiene			
$O^2 1^2 \rightarrow O\ 1^3$	6.3	2.00	1.33
$O^2 1\ 2$	5.8	2.00	4.00
$O\ 1^2 2$	11.1	4.00	5.33
Benzene			
$O^2 1^4 \rightarrow O^2 1^2 2$	5.9	2.00	2.13
$O^2 1^3 3$	10.2	3.00	4.80
$O\ 1^4 2$	7.9	3.00	2.66
$O\ 1^4 3$	13.9	4.00	5.33

shown as multiples of β and of γ, respectively. (See Table I.) It will be noticed that by far the better correspondence is attained with the more accurate calculations by the simple formula (2). Apparently, it is better to neglect overlap than to include it in such simple calculations. It may also be remarked that the average value of β (weighted in such a manner as to recognize the respective degeneracies of the excitations) given on the basis of these calculations is 2.9 for the allyl radical and also for cyclobutadiene, whereas it is 3.1 ev for benzene. (In the calculations, the carbon-carbon distances were all taken to be 1.39A.) These are very close to each other and to the value of just under 3.0 ev which was taken for β in Sec. 3 on the basis of the observed benzene spectrum.

Finally, we consider the electron distribution in a state which is represented by a superposition

$$\Omega_K = \sum_X \Theta_X \Upsilon_{XK}$$

of configurational functions Θ_X, each of which is a single determinant of the type

$$\Theta_X = det\{x_1(1), \cdots, x_i(i), \cdots, x_n(n)\}.$$

The symbol $x_i(j)$, for example, is taken to represent the product of an orbital ψ_ξ and of a spin function whose arguments are the space and spin coordinates of electron j. Another configuration Θ_Y is represented by a similar determinantal array of functions $y_i(j)$ in this notation, where x_i and y_i may or may not be identical. It will be supposed that the orbitals are all orthonormal. The probability of finding an electron in the "volume" element $d\tau_1$, another in $d\tau_2$ and so on, is given by

$$\rho_K d\tau_1 d\tau_2 \cdots d\tau_n,$$

where $d\tau$ contains both space and spin coordinates and

$$\rho_K = \sum_X \sum_Y \Upsilon_{XK}^* \Upsilon_{YK} \Theta_X^* \Theta_Y.$$

Now the probability of finding just one electron in any prescribed volume element, irrespective of the other $(n-1)$ electrons, is found by integrating over the space and spin coordinates of the latter and by remembering that these are all identical. The appropriate probability density is therefore

$$\{(n-1)!\}^{-1} \int_2 \cdots \int_n \rho_K d\tau_2 \cdots d\tau_n$$
$$= \{(n-1)!\}^{-1} \sum_X \sum_Y \Upsilon_{XK}^* \Upsilon_{YK} \times \int_2 \cdots \int_n \Theta_X^* \Theta_Y d\tau_2 \cdots d\tau_n.$$

Now let us consider the coefficient D_{XY} say, of $\Upsilon_{XK}^* \Upsilon_{YK}$ in this expression. We may distinguish three cases. First, if for more than one y_i an identical counterpart cannot be found from among the x_j—that is, the relevant configurations differ in the spin and orbital assignment of more than one electron—it is easy to show that D_{XY} vanishes identically. Next, and this is of course a well-known result for closed shell structures,

$$D_{XX} = \sum_i x_i^*(1) x_i(1).$$

And finally, let Θ_X, Θ_Y differ in the assignment of only one electron. Then if x_r is that function in Θ_X which has no counterpart among the y_i and if y_s is that function in Θ_Y which has no counterpart among the x_j,

$$D_{XY} = p x_r^*(1) y_s(1),$$

where $p = \pm 1$: $p = +1$ if the sequence $\{y_1, \cdots, y_n\}$ can be rearranged by means of an even permutation so as to duplicate the sequence $\{x_1, \cdots, x_n\}$, with y_s in place of x_r, and $p = -1$ if this is accomplished by means of an odd permutation. We see immediately that the result of superposing two configurations which differ in the assignment of more than one electron leads simply to a superposition of their respective electron densities. (These were the only cases explicitly considered above. A verification of the statements made in Sec. 2 is now obvious.) If, however, configurations differ in the assignment of only one electron, we notice that an interference effect may occur. We had occasion to consider this case for an excited state of the azulene molecule, as described by the perimeter method.[2]

Partial Molal Volumes of Hydrocarbons in Water Solution

W. L. MASTERTON*
Department of Chemistry and Chemical Engineering, University of Illinois, Urbana, Illinois
(Received April 12, 1954)

The partial molal volumes of benzene, methane, ethane and propane in water solution have been determined at temperatures ranging from 10–40°C. All the volumes measured were less than those of the same hydrocarbons in nonpolar solvents. This decrease in volume is explained in terms of the abnormally high internal pressure of water, which decreases the free volume available to the hydrocarbon molecules. The temperature dependence of the partial molal volumes of the aliphatic hydrocarbons differs sharply from that of benzene. It is suggested that this is caused by a difference in solution structure in the two cases.

INTRODUCTION

THE thermodynamics of aqueous solutions of hydrocarbons have been investigated in this laboratory during the past several years. Claussen and Polglase[1] determined the solubilities, heats of solution, and entropies of solution of methane, ethane, propane and butane in water. Bohon and Claussen[2] carried out a similar study for the aromatic hydrocarbons.

It has long been known that the lower aliphatic hydrocarbons form solid hydrates. Structures of the clathrate type have been proposed for these hydrates,[3] and verified by x-ray diffraction studies,[4,5] (see urea clathrates).[6] These ice-like structures contain voids large enough to accommodate hydrocarbon molecules. Such structures must exist in solution as well as in the solid phase. One may then picture hydrocarbon molecules in solution as being surrounded by oriented cages of water molecules. Claussen and Polglase[1] used this concept to explain the negative enthalpies and entropies of solution of the aliphatic hydrocarbons.

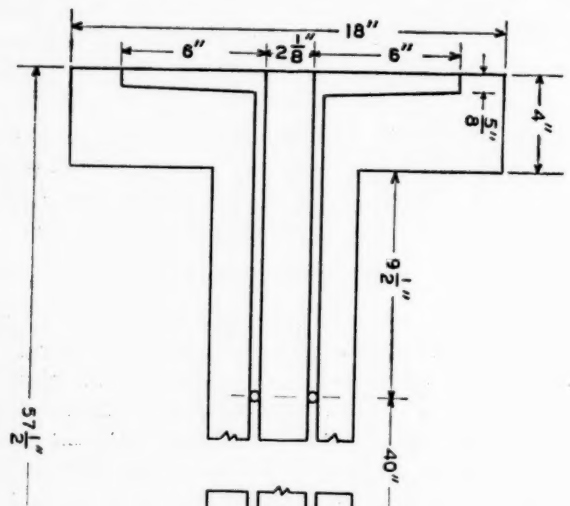

FIG. 1. Copper block (vertical section).

No hydrates of the aromatic hydrocarbons have ever been reported, presumably because these molecules are too large to fit into the voids in the hydrate structures. It has been found possible to explain the thermodynamics of aqueous solutions of the aromatic hydrocarbons without assuming the presence of structures of the type described above.

It is of interest to determine whether the partial molal volumes of hydrocarbons in water solution agree with this model of their solution structures. The partial molal volume $\bar{V}$ in these extremely dilute solutions was found to be identical with the apparent molal volume ψ. The latter can be determined from the specific gravities and concentrations of the hydrocarbon solutions by the following equation:

$$\psi=(1-d/d_0-y/d_0)M_2/y, \tag{1}$$

where M_2=molecular weight of hydrocarbon, y=concentration of hydrocarbon in g/cc, and d, d_0=densities of solution and pure water, respectively, at the temperature at which y is measured.

Since the solubilities of the hydrocarbons are extremely small (benzene, 1.70×10^{-3} g/cc; methane, 2.30×10^{-5} g/cc), an extremely sensitive method must be chosen for the determination of the specific gravities. Such a method should give results accurate to about seven decimal places.

Several methods are available for the determination of specific gravities of extremely dilute solutions. Various modifications of the float method have been described in the literature. They suffer from the common problem of temperature control. A procedure in which the solution and reference liquid were compared simultaneously would obviously reduce this difficulty. Such

* This paper is based on a thesis presented by the author in partial fulfillment of the requirements for the Ph.D. degree at the University of Illinois, June, 1952.
[1] W. F. Claussen and M. F. Polglase, J. Am. Chem. Soc. **74**, 4817 (1952).
[2] R. L. Bohon and W. F. Claussen, J. Am. Chem. Soc. **73**, 1571 (1951).
[3] W. F. Claussen, J. Chem. Phys. **19**, 259, 662, 1425 (1951).
[4] R. Cole, Ph.D. thesis, University of Illinois (1951).
[5] M. V. Stackelberg, Naturwiss. **36**, 327, 359 (1949).
[6] F. Cramer, Angew. Chem. **64**, 437 (1952).

a method is that of Frivold[7] which utilizes the principle of communicating tubes.

In this method, solution and reference liquid (air-free conductivity water) are placed in two vertical tubes connected at the bottom and near the top by valves. Upon first allowing the upper valves to be opened for equilibration and then opening the lower valves, flow will occur if the solution differs from the reference liquid in specific gravity. Wirth, Thompson, and Utterback[8] measured indirectly the drop of the liquid level in one of the tubes as a result of this flow. An alternative procedure is to measure the volume of liquid which must be withdrawn from one side of the apparatus to prevent flow. This volume is simply related to the specific gravity of the solution by the equation

$$V/ah = 1 - d/d_0, \qquad (2)$$

where V = volume of water withdrawn to achieve equilibrium, a = cross sectional area of the liquid surfaces in the tubes, h = distance between the upper and lower valves, and d/d_0 = specific gravity of the solution.

EXPERIMENTAL

A. The Copper Block Specific Gravity Apparatus

It was found necessary to construct the apparatus out of copper so as to allow for the rapid equilibration of any temperature difference between the two tubes. An accuracy of one part in ten million in specific gravity requires temperature control accurate to ±0.0001°C, which is difficult to achieve in a glass apparatus. The dimensions of the apparatus are indicated in Fig. 1.

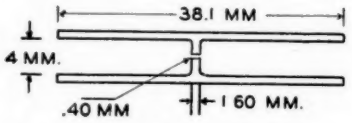

FIG. 2. Glass capillary.

The copper block was enclosed in a wooden insulating chamber which formed an air bath. Attached to the inside of each of the walls of the chamber was a hollow steel tank one inch thick. By circulating water from a refrigeration bath through these tanks, experiments could be made at temperatures as low as 5°C. A resistance coil inserted inside the chamber permitted operating temperatures up to 50°C. The temperature of the air bath could be maintained to within ±0.01°C while the high thermal conductivity of the copper block itself insured that the temperatures of the two columns of liquid would be equal within ±0.00001°C. The copper surfaces of the block were lined with tin to prevent corrosion.

In order to detect flow of liquid through the lower valves, a glass capillary was inserted into the lower connecting tube and a dye was injected at one edge of the capillary. The flow of dye through the capillary was observed through an optical system with the eyepiece outside the apparatus. The dimensions of the capillary are quite critical; if it is too large, a significant amount of flow will occur before it can be detected, leading to low values of V in Eq. (2). On the other hand, too fine a capillary would greatly reduce the rate of flow of the dye and seriously affect the sensitivity of the instrument. The capillary chosen was 1.6 mm in length and 0.4 mm in diameter. Its design is shown in Fig. 2.

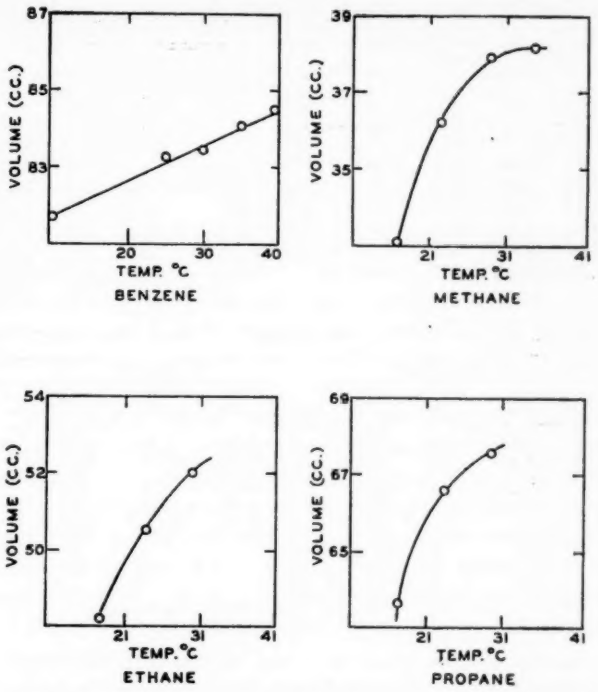

FIG. 3. Change of partial molal volume with temperature.

The glass tube was sealed into the lower horizontal tube with sealing wax. It was found that the dye would move across the capillary by diffusion and mixing in about ten minutes while a difference of one part in ten million in specific gravity would cause the dye to flow across the capillary in three minutes.

The volume of liquid withdrawn to achieve equilibrium was accurately measured in a capillary burette. This consisted of a piece of calibrated capillary tubing fastened to a meter stick.

Frequent blank runs were made in the course of the experimental determinations. These consisted of filling both sides of the apparatus with conductivity water and measuring the difference in specific gravities of the two columns of water. In no case was a difference detected greater than one part in ten million, the limit of accuracy of the experiments.

B. Preparation and Analysis of Solutions

Special precautions were taken to insure that the only factor producing a difference in specific gravity between

[7] O. E. Frivold, Physik. Z. **21**, 529 (1920).
[8] Wirth, Thompson, and Utterback, J. Am. Chem. Soc. **57**, 400 (1935).

TABLE I. Apparent molal volumes of benzene in water solution.

$T=10.1°C$			$T=25.2°C$			$T=30.0°C$		
$y\times10^4$	$1-d/d_0\times10^5$	ψ cc	$y\times10^4$	$1-d/d_0\times10^5$	ψ cc	$y\times10^4$	$1-d/d_0\times10^5$	ψ cc
1.62	0.78	81.9	1.24	0.90	83.7	1.81	1.29	83.6
1.96	0.82	81.4	3.07	1.95	83.0	2.13	1.42	83.2
2.48	1.09	81.5	3.75	2.41	83.1	2.44	1.54	83.0
3.79	1.84	81.8	4.00	2.68	83.4	3.47	2.26	83.2
3.99	1.92	81.8	5.87	3.53	82.8	4.72	3.07	83.2
4.57	2.26	81.8				5.02	3.30	83.3
6.04	2.80	81.7				5.88	3.78	83.2
						6.52	4.36	83.4
Av.=81.7			Av.=83.2			Av.=83.3		

$T=34.9°C$			$T=39.9°C$		
$y\times10^4$	$1-d/d_0\times10^5$	ψ cc	$y\times10^4$	$1-d/d_0\times10^5$	ψ cc
2.50	1.85	83.9	1.76	1.50	84.7
4.69	3.59	84.1	2.57	2.16	84.8
6.67	4.85	83.9	4.01	3.16	84.4
			4.58	3.49	84.0
			4.79	3.89	84.6
Av.=84.0			Av.=84.5		

solution and standard was the presence of the solute being investigated. A difference in concentration of dissolved air or of isotopic composition would cause spurious specific gravity differences. To avoid this a sample of conductivity water was rendered air-free by boiling under vacuum. It was then split into two portions, one of which served as the solvent for the hydrocarbon solution and the other as reference liquid.

1. *Benzene solutions*

The benzene used to prepare the solutions was purified by the method of Mair *et al.*[9] The solutions were prepared by placing one portion of the air-free conductivity water in contact with benzene vapor arising from a tube connected to the solution flask. The solution process was hastened by stirring the water in the solution flask with a magnetic stirrer. Solution was carried out under vacuum.

The concentrations of the benzene solutions could be adjusted by varying the time of exposure of the solution flask to benzene vapor. Stirring was continued for several minutes after the solution was shut off from contact with the benzene vapor. This insured uniform concentration of the solution. Solution and standard were then successively admitted to the block. About fifteen minutes were allowed for the liquids to come to the temperature of the block. The specific gravity of the solution was then determined. In each experiment measurements were taken until three successive determinations agreed within one part in the seventh decimal place.

Portions of the solution were then withdrawn from the block and analyzed by means of an ultraviolet spectrophotometer. It was found that the absorption peak at 2537 A obeyed Beer's law within ½ of 1 percent at optical densities up to 1.0. Portions of the solution withdrawn from various sections of the block showed uniform concentrations within at least 1 percent. Evaporation of benzene apparently occurred only from the trays above the vertical tubes provided the solutions were analyzed within two to three hours after admission to the block.

From the concentrations of the solutions and their specific gravities the apparent molal volumes could be calculated by means of Eq. (1). The data on benzene solutions is given in Table I.

2. *Aliphatic Hydrocarbon Solutions*

The aliphatic hydrocarbons studied were methane, ethane, and propane. The hydrocarbons used were all of research grade (99 mole percent pure). They were

TABLE II. Apparent molal volumes of aliphatic hydrocarbons in water solution.

Methane

$T=16.8°C$			$T=23.0°C$			$T=29.1°C$		
$y\times10^5$	$1-d/d_0\times10^5$	ψ cc	$y\times10^5$	$1-d/d_0\times10^5$	ψ cc	$y\times10^5$	$1-d/d_0\times10^5$	ψ cc
2.30	2.48	33.3	1.04	1.35	36.8	1.63	2.23	38.0
2.31	2.58	33.8	1.53	1.92	36.2	1.75	2.44	38.4
2.34	2.48	33.0	1.95	2.47	36.5	1.83	2.48	37.8
2.35	2.95	36.2[a]	1.95	2.38	35.5			
2.41	2.54	33.0	1.96	2.50	36.5			
2.43	2.57	33.0	2.25	2.81	36.0			
			2.63	3.42	36.9			
Av.=33.2			Av.=36.3			Av.=38.0		

$T=35.1°C$		
$y\times10^5$	$1-d/d_0\times10^5$	ψ cc
1.43	1.95	37.9
1.44	1.93	37.6
1.49	2.10	38.7
1.55	1.92	35.9[a]
1.58	2.19	38.3
	Av.=38.2	

Ethane

$T=16.9°C$			$T=23.0°C$			$T=29.1°C$		
$y\times10^5$	$1-d/d_0\times10^5$	ψ cc	$y\times10^5$	$1-d/d_0\times10^5$	ψ cc	$y\times10^5$	$1-d/d_0\times10^5$	ψ cc
3.61	2.17	48.2	3.68	2.52	50.7	3.35	2.49	52.3
			4.70	3.20	50.5	4.59	3.34	51.9
			5.14	3.44	50.2			
			5.61	3.82	50.5			
			Av.=50.5			Av.=52.1		

Propane

$T=16.9°C$			$T=23.0°C$			$T=29.1°C$		
$y\times10^5$	$1-d/d_0\times10^5$	ψ cc	$y\times10^5$	$1-d/d_0\times10^5$	ψ cc	$y\times10^5$	$1-d/d_0\times10^5$	ψ cc
6.48	2.96	64.1	4.88	2.52	66.8	3.91	2.10	67.8
6.53	2.83	63.2	5.30	2.64	66.8	4.45	2.34	67.3
7.79	3.45	63.5	5.63	2.93	67.0	4.66	2.45	67.3
			6.31	3.13	65.9			
Av.=63.6			Av.=66.6			Av.=67.5		

[a] Value omitted in obtaining average.

[9] Mair, Termini, Willingham, and Rossini, J. Research Natl. Bur. Standards 37, 229 (1946).

freed of traces of carbon dioxide by passing over ascarite. The purified gases were brought into contact with samples of air-free water stirred by means of a magnetic stirrer in an apparatus similar to that used for benzene.

Experiments were run to determine the time necessary for saturation. It was found that four hours were sufficient to achieve saturation with the technique used. Samples saturated for periods up to twelve hours gave partial molal volumes identical with those obtained after four hours contact.

Before admitting the hydrocarbon gas to the saturation apparatus all the air was removed from the system. The initial pressure read on the manometer was then the vapor pressure of water at the temperature of the solution. Gas was admitted to the solution flask until the desired pressure, as read on the manometer, was reached. The final pressure of the gas after saturation was reached was recorded. The difference between final and initial pressures gave the partial pressure of the hydrocarbon gas. From this pressure and the temperature of the solution, it was possible to calculate the concentration of the solution. Henry's law was used to calculate the effect of pressure on the solubility; data in the literature indicates that it holds within one-half of one percent for such extremely dilute solutions. The data of Claussen and Polglase[1] was used to calculate the solubilities of the gases at one atmosphere pressure at the temperature of the solution.

The specific gravities of the solutions were measured in the same manner as those of the benzene solutions. Once again it was found that the apparent molal volumes were independent of concentration.

The data on solutions of methane, ethane, and propane is given in Table II. It will be noted that the precision is considerably less than for the benzene solutions, probably because the concentration data was less accurate.

DISCUSSION OF RESULTS

It is instructive to compare the partial molal volumes of the hydrocarbons in water solution to their volumes in nonaqueous solvents. The molal volume of pure benzene at 25°C is 89.5 cc; the partial molal volume in water is 83.1 cc. This is a decrease in water solution of 6.4 cc.

The simplest explanation of this decrease in volume involves the large internal pressure of water as compared to that of benzene itself. Gjaldbaek and Hildebrand[10] found that the partial molal volume of methane, ethane, and nitrogen decreased sharply as the internal pressure of the solvent increased. The fact that the decrease in volume for benzene is relatively small is probably due to the rather small compressibility of benzene at high pressure.[11] The coefficient of expansion α of benzene in water solution is independent of temperature and slightly smaller than that of pure benzene, as would be expected in a solvent of high internal pressure.

[10] J. C. Gjaldbaek and J. H. Hildebrand, J. Am. Chem. Soc. **72**, 1077 (1950).

TABLE III. Partial molal volumes of methane and ethane at 25°C.

Solvent	P (int.)	Methane	Ethane
Per-fluoro n-heptane	1430 atmos	68.4 cc	82.9 cc
n-hexane	2190	60.0	69.3
Carbon tetrachloride	3050	51.7	66.0
Water	12 000	37.3	51.2

The partial molal volumes of the aliphatic hydrocarbons in water solution are considerably less than the corresponding values in nonaqueous solvents. Table III gives the partial molal volumes of methane and ethane at 25°C in various solvents. The values for carbon tetrachloride are taken from Horiuti;[12] those for the other organic liquids are from Gjaldbaek and Hildebrand.[10] Values of the internal pressures are taken from Hildebrand and Scott.[13]

It will be noted from the curves that the change of partial molal volume with temperature for the aliphatic hydrocarbons is of a quite different nature than that of benzene. The linear increase observed with benzene does not occur with the aliphatics; instead the rate of increase of the partial molal volume with temperature (the coefficient of expansion α) decreases with increasing temperature. This leads one to believe that there are two competing processes going on in the case of the aliphatic hydrocarbons. The normal thermal expansion, which increases $\bar{V}$, would be expected to give a nearly linear slope as it does with benzene. The other process is apparently a breaking down of the cage-like structure of water molecules around the aliphatic hydrocarbon molecules. This produces a decrease in the partial molal volume analogous to that observed when ice melts. The above curves thus represent the net result of these two processes.

ACKNOWLEDGMENT

The author is greatly indebted to W. H. Rodebush, who suggested this problem and under whose advice and guidance the work was performed. W. F. Claussen designed the apparatus and supervised its construction, installation and testing.

The research was aided by funds supplied by the Office of Naval Research and by a predoctoral fellowship provided by the U. S. Atomic Energy Commission.

[11] P. W. Bridgman, J. Chem. Phys. **9**, 794 (1941).

[12] J. Horiuti, Sci. Papers Inst. Phys. Chem. Research (Tokyo) **17**, 125 (1931).

[13] J. H. Hildebrand and R. L. Scott, *The Solubility of Non-Electrolytes* (Reinhold Publishing Corporation, New York, 1950).

An Infrared Band of a Molecular Complex Between Hydrogen Fluoride and Chlorine Trifluoride*†

J. PAUL PEMSLER, *Goodyear Atomic Corporation, Portsmouth, Ohio*

AND

D. F. SMITH, *Technical Division, K-25 Plant, Carbide and Carbon Chemicals Company, Oak Ridge, Tennessee*

(Received April 8, 1954)

A band at 2.57μ wavelength has an absorbance which depends upon the product of the partial pressures of hydrogen fluoride and chlorine trifluoride and is hence attributable to a molecular complex $HF \cdot ClF_3$. This complex is present only in low concentration. The temperature variation per unit product of the pressures indicates a heat of reaction of 3.9 kcal per mole for the reaction $HF + ClF_3 \rightleftarrows HF \cdot ClF_3$. The band is a hydrogen-fluorine stretching vibration. The complex probably does not contain a hydrogen bond.

A PECULIAR distortion of the hydrogen fluoride fundamental absorption band at 2.47μ has been observed in mixtures of HF and ClF_3. This band has been studied in some detail with different mixtures and pressures of HF and ClF_3. It has been found that the distortion is caused by an infrared band which is coincident with the P branch of the HF, and procedures have been devised to measure the absorbance of this band. Correlation of the absorbance with the partial pressures of the HF and ClF_3 demonstrated that this band must be ascribed to a molecular complex formed by one molecule of HF combining with one molecule of ClF_3.

In Fig. 1, the spectrum of HF is shown as it occurs either alone or in the presence of most gases, together with the spectrum of a mixture of HF and ClF_3. The enhanced absorbance d_4 at 2.53μ is caused by the complex. It is evaluated from the records as the measured absorbance d_2 at 2.53μ, less the absorbance d_1 measured at 2.42μ, less the absorbance d_3, the normal difference between the absorbance at 2.53μ and 2.42μ for HF in the absence of ClF_3, that is, $d_4 = d_2 - d_1 - d_3$. The absorbance d_3 is a function of d_1. This function was determined from other records of the HF spectrum. Such an elaborate procedure is required because of the observed behavior of the HF monomer spectrum. With the resolution of the Perkin-Elmer model 21 infrared spectrophotometer with an NaCl prism as used in these experiments, the individual rotation lines were not resolved in spite of their wide spacings. With such low resolution the observed spectrum of hydrogen fluoride appears to be enhanced, without serious distortion, when foreign gases are present to broaden the individual lines. Since the complex, on the other hand, should have large moments of inertia, the spectrum should consist of closely spaced rotational lines and, even at low resolution, the absorbance d_4 should be proportional to the molecular density of the complex.

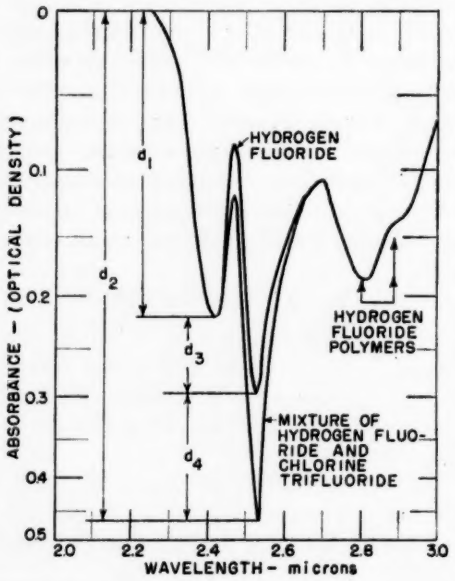

FIG. 1. Spectra of hydrogen fluoride and complex.

The absorbance d_4 has been measured in various mixtures of ClF_3 and HF. These mixtures were prepared by filling an infrared cell to a measured pressure p_0 of HF, evacuating the sample handling system with the cell closed, building up the pressure in the manifold with ClF_3, opening the cell, measuring the pressure of the mixture in the cell, closing the cell, and recording the spectrum. Successive increments of ClF_3 were then added to the cell to obtain additional records. The partial pressure of HF was taken to be the initial pressure p_0 of HF, corrected for the small HF impurity (about 1.5 percent mole percent) in the ClF_3. The partial pressure of the complex was negligible compared with the total pressure. The ClF_3 partial pressure is taken as the measured pressure less the partial pressure of HF. In one case, after the total pressure in the cell had been built up to a maximum pressure near 1 atmos, the cell was opened and portions of this mixture were removed from the system. Spectral records were made at measured pressures after the removal of

* This document is based on work performed for the U. S. Atomic Energy Commission by Carbide and Carbon Chemicals Company, a Division of Union Carbide and Carbon Corporation, at Oak Ridge, Tennessee.

† Presented at the Symposium on Molecular Structure and Spectroscopy, The Ohio State University, Columbus, Ohio, in June, 1954.

each portion. The partial pressure ratio for HF and ClF_3 was taken as invariant.

The absorbance d_4 of the complex should be proportional to the partial pressure p_c of the complex so that

$$d_4 = bp_c,$$

where b is a constant of proportionality. If the complex is in equilibrium with HF and ClF_3,

$$d_4 = bKp^{n_1}(HF)p^{n_2}(ClF_3),$$

where K is the equilibrium constant of the reaction,

$$n_1HF + n_2ClF_3 \rightleftarrows n_1HF \cdot n_2ClF_3.$$

$p(HF)$ is the partial pressure of HF, and $p(ClF_3)$ is the partial pressure of ClF_3.

The measured values of d_4 are plotted *versus* the product of the HF and ClF_3 partial pressures in Figs. 2 and 3. The fact that the points fall so nearly on a single

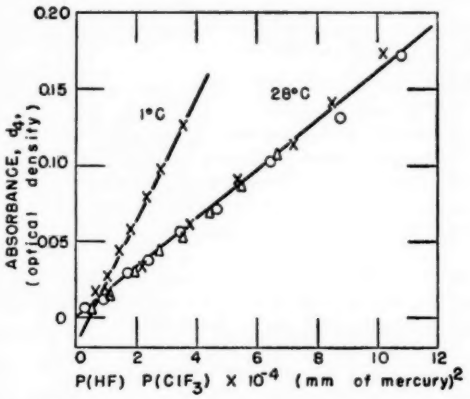

FIG. 2. Variation of absorbance of complex band with product of partial pressures of hydrogen fluoride and chlorine trifluoride at 1°C and 28°C. X at 1°C $p_0(HF)=73.0$ mm Hg; X at 28°C $p_0=202.4$ mm Hg; Δ at 28°C $p_0=103.8$ mm Hg; 0 at 28°C $p(HF)/p(ClF_3)=0.420$.

straight line, even though nearby points correspond to different ratios of the partial pressures of HF and ClF_3, is proof that the absorption is due to a complex $HF \cdot ClF_3$ with $n_1=n_2=1$. The failure of the line drawn for the 1°C measurements to pass through the origin is probably due to a small shift in the background.

These measurements were made in a 100 mm long Monel infrared cell with fluorothene windows. The cell could be thermostated by passing water at constant temperature through a 5-turn coil of $\frac{1}{4}$-in. Monel tubing contained within the cell and wound close to the outer wall. Measurements were made at 1, 21, and 52°C, as well as at ambient temperature, 28°C. Satisfactory measurements could not be made with steam blown through the coils because of the rapid formation of window bands in the region of absorption of the $HF \cdot ClF_3$ at this higher temperature.

The slopes m of the lines in Figs. 2 and 3 are the product of b and the equilibrium constant. As b should

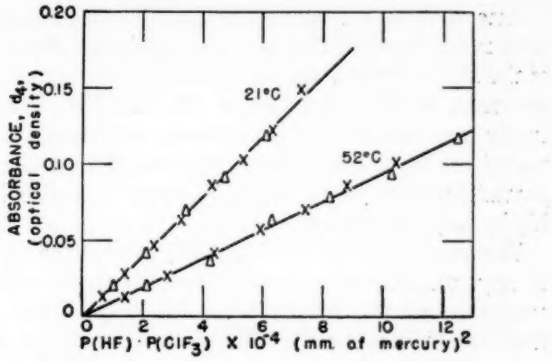

FIG. 3. Variation of absorbance of complex band with product of partial pressures of hydrogen fluoride and chlorine trifluoride at 21°C and 52°C. X at 21°C $p_0(HF)=112$ mm Hg; Δ at 21°C $p_0(HF)=168$ mm Hg; X at 52°C $p_0(HF)=180$ mm Hg; Δ at 52°C $p_0(HF)=272$ mm Hg.

depend on the temperature in the same way as the molecular density, the variation of the factor mT/T_0 where T is the absolute temperature and T_0 is arbitrarily taken as 273°K, should be the same as the temperature variation of the equilibrium constant, so that from the integrated form of the van't Hoff equation

$$\ln\left(\frac{mT}{T_0}\right) = -\frac{\Delta H}{RT} + B,$$

where ΔH is the heat of reaction, R is the gas constant per mole, and B is a constant. As ΔH varies only slightly with temperature, a plot of $\log(mT/T_0)$ *versus* $1/T$ should be a nearly straight line over the temperature range at which measurements have been made, and the slope should be $\Delta H/2.303R$ per degree. Figure 4 is a plot of $\log mT/T_0$ *versus* $1/T$. The line drawn corresponds to a value of $\Delta H=-3.92$ kcal per mole. The approximations which have been employed in the interpretation of these experiments probably give rise to more serious uncertainty in the value of ΔH than do the experimental errors.

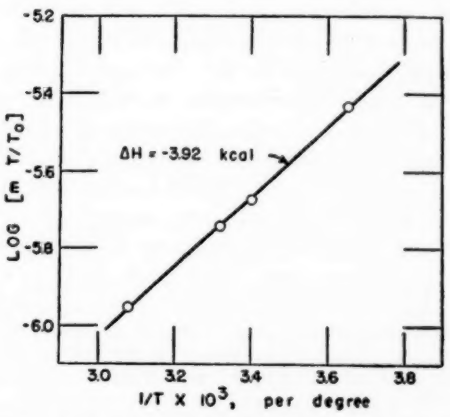

FIG. 4. Evaluation of the heat of the reaction $ClF_3+HF \rightleftarrows HF \cdot ClF_3$.

Attempts to determine the equilibrium constant K were made by observing the decrease in the absorbance of the HF polymer band because of the depletion of HF monomer in the formation of the $HF \cdot ClF_3$. The decrease was small. The equilibrium constant was estimated to be about 1×10^{-5}/mm at 21°, so that the partial pressure of the $HF \cdot ClF_3$ never exceeded 1 mm Hg by any large amount.

The wavelength of this $HF \cdot ClF_3$ band is the shortest of any fundamental vibration ever observed, with the exception of the fundamental HF vibrational band itself, so that without doubt the vibration is a H—F stretching vibration. Its displacement from the HF fundamental is much smaller than the separation between the HF monomer and polymer absorption. This suggests that this complex involves a bonding of the F of the HF to the ClF_3, rather than a hydrogen bond. Rogers and Katz,[1] in interpreting F^{18} exchange rates between HF and ClF_3, postulated a complex.

The 3.51μ band of $DF \cdot ClF_3$ has also been observed as coincident with the long wavelength branch of the DF band in mixtures of DF and ClF_3.

[1] M. T. Rogers and J. J. Katz, J. Am. Chem. Soc. **74**, 1375 (1952).

THE JOURNAL OF CHEMICAL PHYSICS VOLUME 22, NUMBER 11 NOVEMBER, 1954

Ionization and Dissociation by Electron Impact; Methylene, Methyl, and Methane

A. LANGER, *Westinghouse Research Laboratories, East Pittsburgh, Pennsylvania,*
J. A. HIPPLE, *Pennsylvania State College, State College, Pennsylvania,*
AND
D. P. STEVENSON, *Shell Development Company, Emeryville, California*

(Received April 19, 1954)

The appearance potentials of C^+, CH^+, and CH_2^+ in the mass spectra of methylene, methyl, and methane are found to be mutually consistent and when combined with the spectroscopic value of the ionization potential of the carbon atom (11.26 ev) lead to 15.5±0.5 ev/molecule for the heat of atomization of methane. This value (15.5) when further combined with the heat of formation of methane (−0.78 ev/molecule) and the dissociation energy of H_2 (4.48 ev/molecule) yields 5.7$_6$ ev/atmos or 133 kcal/mole for the heat of sublimation of graphite.

The set of appearance potentials confirmed the spectroscopic value for the heat of dissociation of CH^+ (3.6 ev/molecule) and yield the following additional energetic quantities: $D(CH_2-H)=3.7_5\pm0.3$ ev/molecule, $D(CH-H)=3.9_9\pm0.3$ ev/molecule, $D(CH_3^+-H)=1.3_4\pm0.1$ ev/molecule, $D(CH_2^+-H)=5.5_4\pm0.2$ ev/molecule, and $D(CH^+-H)=3.3_7\pm0.2$ ev/molecule. Earlier determinations of $I^a(CH_4)$, $I^a(CH_3)$ and $D(CH_3-H)$ are confirmed (within the experimental error) and the ionization potential of the methylene radical, $I^a(CH_2)$, is found to be 11.7$_5$±0.1 ev/molecule.

Combination of the appearance potentials of CH_2^+ in the methane and diazomethane mass spectra gives 46±6 kcal/mole for the heat of formation of diazomethane.

INTRODUCTION

THE spacing of the energy levels of the various states of combination of four hydrogen atoms with one carbon atom has been a subject of speculation and experimentation[1–3] for many years. Although the dissociation energies, $D(CH_3-H)$[4–6] and $D(C-H)$[7] appear to be well established,[8] such is not the case for $D(CH_2-H)$ and $D(CH-H)$. Furthermore the sum of these four dissociation energies, the heat of atomization of methane, $A_t(CH_4)$, is intimately related to that continuing subject of debate, the heat of sublimation of graphite, through the accurately known heat of formation of methane and dissociation energy of hydrogen.

With the objective of obtaining information on the unknown quantities mentioned above there was undertaken a mass spectrometric study of the ionization and dissociation by electron impact of methane, methyl, and methylene.[9] Although methane has been the subject of several previous such studies[10] it was deemed desirable to include its study in order to assure self-consistency of the measurements on the various molecules that were to be intercombined to derive the quantities of interest.

EXPERIMENTAL METHODS AND RESULTS

A special ion source for this study was constructed for a 90° sector analyzer mass spectrometer.[11,12] The features of the source were the following:

[1] J. H. Van Vleck, J. Chem. Phys. **2**, 20, 297 (1934).
[2] H. H. Voge, J. Chem. Phys. **4**, 581 (1936); **16**, 984 (1948).
[3] Glockler, Discussions Faraday Soc., Hydrocarbon **10**, 26 (1951).
[4] D. P. Stevenson, J. Chem. Phys. **10**, 291 (1942).
[5] Anderson, Kistiakowsky, and Van Artsdalen, J. Chem. Phys. **10**, 305 (1942).
[6] Butler and Polanyi, Trans. Faraday Soc. **39**, 19 (1943).
[7] Douglas and Clark, Can. J. Research **A20**, 71 (1942).
[8] See reference 3 for contrary opinion re $D(C-H)$.
[9] A preliminary report of the measurement of the ionization potential of methylene was made several years ago. Langer and Hipple, Phys. Rev. **69**, 691 (1946).
[10] (a) L. G. Smith, Phys. Rev. **51**, 263 (1937); (b) M. B. Koffel and R. A. Lad, J. Chem. Phys. **16**, 420 (1948); (c) J. J. Mitchell and F. F. Coleman, *ibid.* **17**, 44 (1949); (d) R. E. Honig, *ibid.* **16**, 105 (1948); (e) Geerk and Neuert, Z. Naturforsch. **5A**, 502 (1950); (f) McDowell and Warren, Discussions Faraday Soc., Hydrocarbons **10**, 53 (1951).
[11] J. A. Hipple, J. Appl. Phys. **13**, 551 (1942).
[12] Hipple, Grove, and Hickam, Rev. Sci. Instr. **16**, 69 (1945).

(1) the use of double slits for entries to and exits from the ionization chamber of both electrons and positive ions in order to minimize external field penetration;

(2) the use of an indirectly heated oxide-coated platinum cathode, and

(3) the use of a hemicylindrical ion repeller that was considerably longer than the positive ion exit slit from the ionization chamber. The cathode heater consisted of a tubular ceramic with imbedded tungsten heater wires. The electron trap was always maintained 6 volts positive with respect to the ionization chamber in order to trap secondary electrons emitted from the platinum collector plate.

The gases for study were admitted to the ionization chamber through a 1-mm i.d. quartz tube that ended at a suitable hole in the top center of the ion repeller. The quartz tube could be heated over the 4-cm length immediately preceding its end by means of a close winding of tungsten wire surrounded by a radiation shield. The temperature of the quartz tube was determined by means of a "platinum" thermocouple inserted through a hole in the radiation shield and placed in contact with the quartz *ca* 1 cm from its end.

TABLE I. Mass spectrum of diazomethane ~75°C, 75 ev.

M/q	Relative intensity	
42	0.010	
29	0.024	
28	1.00	
27	0.50	
26	0.44	
25	0.062	C_2H_2 ??
24	0.020	
14	0.020	$A(CH_2^+)=12.7\pm0.3$ ev
13	0.007	
12	0.002	

The gases, methane, lead tetramethyl, or diazomethane admixed with argon, entered the quartz tube through a pinhole leak in a platinum foil from a light shielded reservoir. Ohio Chemical Company methane was used without treatment. The lead tetramethyl was from the generous gift of the Ethyl Corporation.[13] Linde Company spectroscopically pure argon was employed.

Diazomethane was prepared by the reaction of hydrazine and chloroform in absolute alcohol in the presence of potassium hydroxide. A stream of argon was employed to sweep the diazomethane from the reaction vessel as it was formed and carry it over potassium hydroxide pellets at −30°C to remove entrained alcohol. The diazomethane was condensed from the argon stream by passage through a trap chilled with liquid air and stored in this trap maintained at this low temperature. As vaporized from the trap into the gas reservoir of the mass spectrometer no evidence of either ethanol or chloroform could be found in the mass spectrum of the diazomethane.

[13] J. A. Hipple and D. P. Stevenson, Phys. Rev. **63**, 121 (1943).

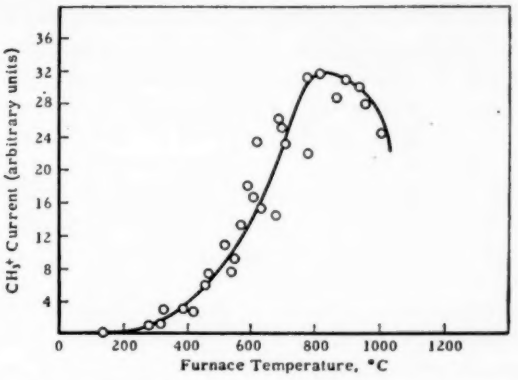

FIG. 1. CH_3^+ from $Pb(CH_3)_4$ as a function of furnace temperature —electron energy ~11 volts (corrected).

The mass spectrum of diazomethane characteristic of 75 volt ionizing electrons at 75°C is given in Table I.

The appropriate furnace temperature for measurements on methyl and methylene radicals were chosen as the temperatures at which the methyl and methylene ion currents from lead tetramethyl and diazomethane, respectively, had approximately their maximum values. There is shown in Fig. 1 the dependence of methyl ion current in the mass spectrometer on furnace temperature for constant lead tetramethyl flow. The data in Fig. 1 confirm the previously reported observation[12] and fix the temperature (indeterminant in the earlier work) of maximum methyl yield at 850±50°C. Similarly 780°C was chosen as an appropriate furnace temperature for methylene formation from diazomethane. The variation of CH_2^+ with furnace temperature for constant CH_2N_2 flow is shown in Fig. 2.

In the appendix to this paper further experimental results on the pyrolysis of other substances are summarized.

The appearance potentials of the various ions in the mass spectra were determined from the ion yield—ionizing electron energy curves by means of the vanishing current method.[10(a),14] The additive constant in the voltage scale was determined by association of the

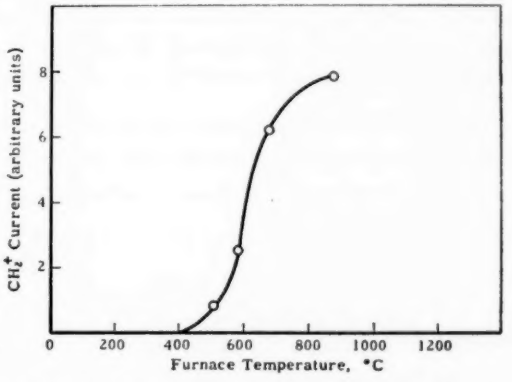

FIG. 2. CH_2^+ from CH_2N_2 as a function of furnace temperature—electron energy ~11 volts (corrected).

[14] T. Mariner and W. Bleakney, Phys. Rev. **72**, 807 (1947).

TABLE II. Appearance potentials of ions CH_j^+ in the mass spectra of CH_4, CH_3, and CH_2.

Ion	CH_4	CH_3	CH_2
	ev		
CH_4^+	13.10±0.1		
CH_3^+	14.30±0.1	9.85±0.1	
CH_2^+	15.5 ±0.2	15.30±0.1	11.90±0.1
CH^+	23.4 ±0.2	16.2 ±0.2	17.1 ±0.2
C^+	27.0 ±0.2	17.8 ±0.2	18.0 ±0.2

appearance potential of A^+ in the mass spectrum of the simultaneously admitted argon with the spectroscopically determined ionization potential of argon, 15.76 ev.[15]

The appearance potentials determined from five or six series of measurements on each ion are summarized in Table II. The repeatability of determination varied from ±0.05 ev in the cases of ions of high probability of formation, CH_4^+ and CH_3^+ from CH_4, CH_3^+ from CH_3, and CH_2^+ from CH_2 to ±0.2 ev in the cases of ions of low probability of formation as C^+ from CH_4. No search was made for "higher" appearance potentials such as have been found[10(a),(f)] for CH_2^+ in the methane mass spectrum.

DISCUSSION

The discussion of the appearance potentials summarized in Table II will be divided into two parts. In the first part the data will be examined ion by ion for mutual compatability and assignment of state to the ions, and the nature of the accompanying neutral products. Only differences between appearance potentials are used in this section, and thus the quality of the absolute calibration of the ionizing electron energy scale will not affect the arguments other than in the comparison of our results with those of previous investigations. For the purposes of this first section it will be presumed that the dissociation energies, $D(CH_3-H)=4.42\pm0.04$ ev, $D(C^+-H)=3.61$ ev, and $D(C-H)=3.47$ ev are reliable. The conclusions reached in the first part of the discussion are summarized in Table III.

In the second part of the discussion the appearance potentials (Table II) are combined with data from other sources by means of conclusions of the first part (Table III) to derive a self-consistent set of dissociation energies, $D(CH_m-H)$ and $D(CH_m^+-H)$ $(0\leq m\leq 3)$ and the heats of atomization of CH_{m+1} and C^+H_{m+1} where the heat of atomization, $A_t(CH_j)$, of CH_j is the energy required for the reaction,

$$CH_j^{(gas)}=C^{(gas)}+j\cdot H.$$

Part I

CH_4^+

The appearance potential of CH_4^+, $A(CH_4^+)=13.1\pm0.1$, in the methane mass spectrum is in excellent agreement with all previously reported determinations of this quantity, *viz.* 13.2 ± 0.4,[10(a)] 13.0 ± 0.2,[10(b)] 13.04 ± 0.02,[10(c)] $13.0_4\pm0.03$,[10(d)] 13.3 ± 0.3,[10(e)] and $13.1_2\pm0.03$.[10(f)] This agreement lends confidence to the reliability of the calibration of our voltage scale and thus to the significance of the results of calculations in which our data are combined with data from other sources. This appearance potential is to be associated with the vertical ionization potential of methane, and it will be assumed that the difference between the vertical and adiabatic ionization potentials is no larger than the uncertainty of the determinations.

CH_3^+

The appearance potential, $A_1(CH_3^+)=14.3\pm0.1$, in the methane mass spectrum is in essential agreement with the literature values, namely, 14.5 ± 0.4,[10(a)] 14.4 ± 0.3,[10(b)] $14.5_2\pm0.05$,[10(c)] 14.5 ± 0.3,[10(e)] and $14.3_9\pm0.02$.[10(f)] The appearance potential of this ion in the methyl mass spectrum, $A_2(CH_3^+)=9.8_5\pm0.1$ is 0.22 ev lower than the previous measurement by the mass spectrometric method, $10.0_7\pm0.1$.[13] This difference is coincident, with the difference between the present determination of $A_1(CH_3^+)=14.3\pm0.1$ and the value found in the earlier study of the methyl radical, $A_1(CH_3^+)=14.5_0\pm0.1$.[10(a),13] Thus this research leads to the same value for $D(CH_3-H)$ as the earlier one[13] when this dissociation energy is associated with the difference $A_1(CH_3^+)-A_2(CH_3^+)=4.4_5\pm0.1$ ev.

In order for the association of $A_1(CH_3^+)-A_2(CH_3^+)$ with $D(CH_3-H)$ to be valid, it is necessary that the methyl ion in both processes of formation be in the same electronic state and that in the case of methane the

TABLE III. Energetic quantities to be associated with the appearance potentials, $A(CH_m^+)$, $0\geq m\leq 4$ listed in Table II.

	CH_4	CH_3	CH_2
CH_4^+	$I_v^z(CH_4)\geq I_{ad}^z(CH_4)$		
CH_3^+	$I^z(CH_3)+D(CH_3-H)$	$I_v^z(CH_3)\cong I_{ad}^z(CH_3)$	
CH_2^+	$I^z(CH_2)+D(CH_3-H)$ $+D(CH_2-H)-D(H-H)$	$I^z(CH_2)+D(CH_2-H)$	$I_v^z(CH_2)\cong I_{ad}^z(CH_2)$
CH^+	$I^z(CH)+A_t(CH_4)-D(C-H)$ $=I^z(CH)+D(CH_3-H)$ $+D(CH_2-H)+D(CH-H)$	$I^z(CH)+E_{CH}+(A^1\Pi)+D(CH_2-H)$ $+D(CH-H)-D(H-H)$ $=I^z(CH)+E_{CH}+(A^1\Pi)+A_t(CH_3)$ $-D(C-H)-D(H-H)$	$I^z(CH)+E_{CH}+(A^1\Pi)+D(CH-H)$ $=I^z(CH)+E_{CH}+(A^1\Pi)$ $+A_t(CH_2)-D(C-H)$
C^+	$I^z(C)+A_t(CH_4)$	$I^z(C)+A_t(CH_3)-D(H-H)$	$I^z(C)+A_t(CH_2)$

[15] Moore, Natl. Bur. Standards. Circ. No. 467, U. S. Government Printing Office, Washington, D. C. (1949).

formation of CH_3^+ proceed through transitions to levels of CH_4^+ above the dissociation limit of the attractive state. If we associate the appearance potential of CH_3^+ in the methyl mass spectrum with the vertical ionization potential of methyl and assume negligible difference between vertical and adiabatic ionization potential, it follows that the difference between $A(CH_4^+)$ and $A_1(CH_3^+)$, $A_1(CH_3^+)-A(CH_4^+)=1.2\pm0.1$ is to be associated with the dissociation energy, $D(CH_3^+-H)$. This is a consequence of our assumption that identical CH_3^+ ions are formed from CH_4 and CH_3. Justification for the validity of this assumption is to be found in the consistency of direct and indirect electron impact determinations of $D(CH_3-H)$[16] and the agreement with the values found by entirely independent methods.[5,6]

The value found for $D(CH_3^+-H)$, 1.2 ev is but one-fourth that of $D(CH_3-H)$. This appears to be a remarkably larger weakening of a bond to be associated with a change from a one electron-pair bond to a three-fourths electron-pair bond, when it is noted that in the cases of H_2 and H_2^+ the change from an electron-pair bond to a one-electron bond reduces the dissociation energy by less than a factor of 2, *visa* 4.48 to 2.65 ev. This qualitative reasonlng suggests that there may be a significant difference between the vertical and adiabatic ionization potentials of methane.

CH_2^+

The appearance potentials of this ion in the methane mass spectrum $A_1(CH_2^+)=15.5\pm0.2$, lies between two of the previously reported values of this quantity, i.e., 15.8 ± 0.5[10(a)] and $15.3_0\pm0.05$.[10(f)] A third much higher value 16.5 ± 0.3 has also been reported.[10(e)] There have been no previously reported values for the appearance potential of this ion in the mass spectra of methyl, $A_2(CH_2^+)=15.3\pm0.1$; methylene, $A_3(CH_2^+)=11.9\pm0.2$; or diazomethane, $A_4(CH_2^+)=12.7\pm0.3$.

If it is assumed that the same state of CH_2^+ obtains for its formation from the three species, CH_4, CH_3, and CH_2; then values may be calculated for the dissociation energy, $D(CH_2-H)$, if the formation of CH_2^+ is associated with the reactions;

$$CH_3+\epsilon^-\rightarrow CH_2^++H+2\epsilon^- \quad A_2(CH_2^+), \qquad (1)$$

$$CH_4+\epsilon^-\rightarrow CH_2^++H_2+2\epsilon^- \quad A_1(CH_2^+). \qquad (2)$$

From $A_2(CH_2^+)-A_3(CH_2^+)$ there is found

$$D(CH_2-H)=3.4\pm0.2$$

while,

$$A_1(CH_2^+)-A_3(CH_2^+)=3.6=D(CH_2-H)+D(CH-H)-D(H-H).$$

Taking $D(CH_3-H)=4.42$ and $D(H-H)=4.48$ one obtains the second value, $D(CH_2-H)=3.7\pm0.2$. The essential agreement between these semi-independent determinations of $D(CH_2-H)$ shows the consistency of the assumptions made in the derivation of the values, namely the identity of the state of CH_2^+ in the three modes of formation and the accompanying formation of H_2 molecules in the case of methane.

The appearance potential in the methylene mass spectrum, $A_3(CH_2^+)$, is naturally associated with the vertical ionization potential of the free radical that should be very little different from the adiabatic ionization potential in the species with unshared electrons. The consistency of $A_1(CH_2^+)$ and $A_2(CH_2^+)$ with $A_3(CH_2^+)$ found above, leads us to believe that the CH_2^+ formed from both methane and methyl are in their ground state.

The differences between the appearance potentials of CH_2^+ and CH_3^+ in the mass spectra of methane and methyl are related to the difference $D(CH_2^+-H)-D(H-H)$ and $D(CH_2^+-H)$, respectively. Thus from $A_1(CH_2^+)-A_1(CH_3^+)=+1.2$, $D(CH_2^+-H)=5.7$, while $A_2(CH_2^+)-A_2(CH_3^+)=5.45=D(CH_2^+-H)$.

It should be noted that Voge[2] and Field[17] have both used the difference $A_1(CH_2^+)-A_3(CH_2^+)$ to estimate the energy of formation of CH_2 from methane.

If the heat of formation of diazomethane from its elements were known, the appearance potential of CH_2^+ in the diazomethane mass spectrum, $A_4(CH_2^+)=12.7\pm0.3$ would provide another datum relative to the energy of CH_2^+ with respect to methane. Since this heat of formation is not known, it is of interest to calculate a value for this quantity by combination of the appearance potential of CH_2^+ in the mass spectrum of methane, $A_1(CH_2^+)$, with that in the diazomethane mass spectrum, $A_4(CH_2^+)$, the heat of formation of methane (-0.78 ev/molecule) and the plausible assumption that the process of formation of CH_2^+ from diazomethane by electron impact is,

$$CH_2N_2\rightarrow CH_2^++N_2+\epsilon^-, \quad A_4(CH_2^+)=12.7.$$

Then, since

$$CH_4\rightarrow CH_2^++H_2+\epsilon^-, \quad A_1(CH_2^+)=15.5;$$

$$C_{gr}+2H_2=CH_4 \quad \Delta H_f=-0.78;$$

$$C_{gr}+H_2+N_2=CH_2N_2 \quad \Delta H_f=-0.78+15.5-12.7=2.0 \text{ ev/molecule}=46 \text{ kcal/mole}.$$

That this is a reasonable value may be seen from the following argument. Following Pauling:[18]

$$\Delta H_f(CH_2N_2)=-2H_{C-H}-2H_{C-N}+\tfrac{1}{3}H_N\equiv N+H_{H-H}+L_c+\text{strain energy}$$
$$=-2(87.3)-2(48.6)+\tfrac{1}{3}(170)+103.4+124.3+\text{strain energy}$$
$$=12.5+\text{strain energy. kcal/mole.}$$

[16] Stevenson, Discussions Faraday Soc. Hydrocarbons **10**, 35 (1951).

[17] F. H. Field, J. Chem. Phys. **19**, 793 (1951).

[18] Pauling, *The Nature of the Chemical Bond* (Cornell University Press, Ithaca, 1939), pp. 53 *et seq.*

The strain energy of cyclopropane is 34.2 kcal[19] and it would be expected to be greater in diazomethane in view of the nitrogen-nitrogen double bond in the ring. Thus it would be expected that,

$$\Delta H_f(CH_2N_2 \text{ gas}) \geq 47 \text{ kcal},$$

and we see that the estimate from the appearance potentials of CH_2^+ in the methane and diazomethane mass spectra is quite acceptable.

CH^+

The present determination of the appearance potential of CH^+ in the methane mass spectrum, $A_1(CH^+) = 23.4 \pm 0.2$ is in excellent agreement with the earlier value due to Smith[10(a)] (23.4±0.6) and approximately one electron volt higher than the determinations by Geerk and Neuert[10(e)] (22.5±0.5) and MacDowell and Warren[10(f)] (22.4±0.1). The last named authors[10(e),(f)] employed a different technique in determining the appearance potential from the ion yield-ionizing electron energy curve than that employed by Smith and ourselves and this may be the source of the discrepancy noted. No previous values have been reported for the appearance potentials of CH^+ in the mass spectra of methyl, $A_2(CH^+) = 16.2 \pm 0.2$ and methylene, $A_3(CH^+) = 17.1 \pm 0.2$.

If it is assumed that the CH^+ ions formed from methylene and methyl are in the same electronic state, the lower value of $A_2(CH^+)$ than of $A_3(CH^+)$ requires in the case of methyl the process

$$CH_3 + \epsilon^- \rightarrow CH^+ + H_2 + 2\epsilon^-, \quad (3)$$

since in the case of methylene the process must be

$$CH_2 + \epsilon^- \rightarrow CH^+ + H + 2\epsilon^-. \quad (4)$$

With assumption of identical states for the CH^+, the difference

$$A_2(CH^+) - A_3(CH^+) = -0.9 = D(CH_2-H) - D(H-H),$$

or since $D(H-H) = 4.48$, $D(CH_2-H) = 3.6$, in excellent agreement with the values deduced from appearance potentials of CH_2^+. This agreement may be taken as confirmation of the validity of the assumption of identity of state of CH^+ from CH_3 and CH_2.

The appearance potential of CH^+ in the methane mass spectrum, $A_1(CH^+) = 23.4$, is to be associated with either the process

$$CH_4 + \epsilon^- \rightarrow CH^+ + 3H + 2\epsilon^-, \quad (5)$$

or

$$CH_4 + \epsilon^- \rightarrow CH^+ + H_2 + H + 2\epsilon^-. \quad (6)$$

If the state of CH^+ from methane is identical with that formed from methyl then if (5) obtains,

$$A_1(CH^+) - A_2(CH^+) = 7.2 = D(CH_3-H) + D(H-H),$$

or

$$D(CH_3-H) = 2.7,$$

while if (6) obtains

$$A_1(CH^+) - A_2(CH^+) = 7.2 = D(CH_3-H).$$

Neither of these alternatives leads to a value of $D(CH_3-H)$ that is compatible with the accepted value of this quantity 4.42.

If it were assumed that the process of formation of CH^+ in the methane mass spectrum is represented by (6) with the ion in the first excited state $A^1\Pi$, with $E_{CH^+}(A^1\Pi) = 2.99$,[20] while the common identical state for this ion in the cases of methyl and methylene is the ground state, $X^1\Sigma$; then

$$A_1(CH^+) - A_2(CH^+) = 7.2 = D(CH_3-H) + E(A^1\Pi),$$

or

$$D(CH_3-H) = 4.2,$$

that is equal, within experimental uncertainty to the accepted 4.42.

An alternate assumption might be that (5) represents the formation of CH^+ in its ground state from methane while the common state of CH^+ formed from CH_3 and CH_2 is the $A^1\Pi$. If this is taken, then

$$A_1(CH^+) - A_2(CH^+) = 7.2 = D(CH_3-H) + D(H-H) - E(A^1\Pi),$$

$$D(CH_3-H) = 5.7,$$

a value that is in poor agreement with the accepted value. However, as will be shown later, there is strong evidence that (5) represents CH^+ formation from methane and that the excited state of CH^+ is the one common to this ion in its formation from CH_3 and CH_2.

C^+

The present determination of the appearance potential of C^+ is the methane mass spectrum, $A_1(C^+) = 27.0 \pm 0.2$ agrees quite well with the Smith[10(a)] value, 26.8±0.8, and is greater than the value due to McDowell and Warren,[10(f)] 26.2±0.2, by an amount about equal to the difference in the case of $A_1(CH^+)$. The value of $A_1(C^+)$ due to Geerk and Neuert,[10(e)] 21.5±1 ev, appears to be in error. No previous determinations have been reported for the appearance potentials of this ion in the mass spectra of methyl, $A_2(C^+) = 17.8 \pm 0.2$, or methylene, $A_3(C^+) = 18.0 \pm 0.2$.

If it is assumed that the C^+ formed from each of the three molecules, CH_4, CH_3, and CH_2 are in the same state and that the processes are representable by the expressions

$$CH_4 + \epsilon^- \rightarrow C^+ + 4H + 2\epsilon^-, \quad (7)$$

$$CH_3 + \epsilon^- \rightarrow C^+ + H_2 + H + 2\epsilon^-, \quad (8)$$

$$CH_2 + \epsilon^- \rightarrow C^+ + 2H + 2\epsilon^-; \quad (9)$$

[19] Golmov, J. Gen. Chem. (U.S.S.R.) 11, No. 5-6, 405 (1940).

[20] Herzberg, *Molecular Spectra and Molecular Structure*. I. (D. Van Nostrand Company, Inc., New York, 1950), second edition.

we find from (8) and (9),

$$A_2(C^+)-A_3(C^+)=0.2=D(CH_2-H)-D(H_2),$$
$$D(CH_2-H)=4.3,$$

and from (7) and (8),

$$A_1(C^+)-A_2(C^+)=9.2 \text{ ev}=D(CH_3-H)+D(H_2),$$
$$D(CH_3-H)=4.7.$$

The value of $D(CH_2-H)$, 4.3, from the combination of Eqs. (8) and (9) is not incompatible with the value deduced above that ranged from 3.4 to 3.7, and similarly the value of $D(CH_3-H)$, 4.7, from Eqs. (7) and (8) is in reasonable agreement with the accepted value, 4.42. Thus Eqs. (7), (8), and (9) are self-consistent with the assumption of the identity of the states of the C^+ in the three processes.

If we assume in addition that the C^+ is in its ground state, then from Eqs. (3) and (8),

$$A_2(C^+)-A_2(CH^+)=1.6=D(C^+-H),$$

while from (4) and (9)

$$A_3(C^+)-A_3(CH^+)=0.9=D(C^+-H)$$

values that are incompatible with the spectroscopic value of Douglas and Clark,[7] $D(C^+-H)=3.6$.

On the other hand, from Eqs. (5) and (7):

$$A_1(C^+)-A_1(CH^+)=3.6=D(C^+-H)$$

if the CH^+ formed from methane is in its ground $X^1\Sigma$ state. Similarly, if it is assumed that the CH^+ formed from CH_3 and CH_2 by processes (3) and (4), respectively, are in the $A^1\Pi$ state, then,

$$A_2(C^+)-A_2(CH^+)=1.6=D(C^+-H)-E(^1\Pi),$$

or

$$D(C^+-H)=4.6,$$

and

$$A_3(C^+)-A_3(CH^+)=0.9=D(C^+-H)-E(^1\Pi),$$

or

$$D(C^+-H)=3.9.$$

These assumptions lead to reasonable agreement between the spectroscopic value of $D(C^+-H)$ and that from $A_3(C^+)-A_3(CH^+)$, and even better (within possible experimental error) agreement in the case of $A_2(C^+)-A_2(CH^+)$. Thus we believe Eq. (5) represents the formation of CH^+ in its ground state from CH_4 and that the common state of formation of CH^+ from CH_3 and CH_2 is $A^1\Pi$ with the processes represented by Eqs. (3) and (4).

The conclusions with respect to the formal energetic significance of the appearance potentials of the ions CH_m^+ in the mass spectra of methane, methyl, and methylene summarized in Table II are given in Table III.

Part II

The ionization potential of the carbon atom is $I^e(C)=11.264$ ev[15] for the formation of C^+ in its ground state, $2P_{\frac{1}{2}}^0$. If it is assumed that the C^+ ions formed from CH_4, CH_3, and CH_2 are in the ground state, then from the appearance potentials $A_i(C^+)$ one calculates by means of the expressions of Table III:

$$A_t(CH_4)=A_1(C^+)-I^e(C)=15.7,$$
$$A_t(CH_3)=A_2(C^+)-I^e(C)+D(H-H)=11.0,$$
$$A_t(CH_2)=A_3(C^+)-I^e(C)=6.7.$$

Taking $I^e(CH)=11.13$ and $D(C-H)=3.47$ from Douglas and Clark[7] and the assignments of Table III:

$$A_t(CH_4)=A_1(CH^+)-I^e(CH)+D(C-H)=15.7,$$
$$A_t(CH_3)=A_2(CH^+)-I^e(CH)-E_{CH^+}(A^1\Pi)+D(C-H)+D(H-H)=10.0,$$
$$A_t(CH_2)=A_3(CH^+)-I^e(CH)-E_{CH^+}(A^1\Pi)+D(C-H)=6.5.$$

Since $D(CH_3-H)=4.42$, these values so found for $A_t(CH_3)$ correspond to $A_t(CH_4)=15.4$ from $A_2(C^+)$ and 14.4 from $A_2(CH^+)$. Either value of $A_t(CH_2)$ leads to $A_t(CH_4)=11.0+D(CH_2-H)$.

The dissociation energy of carbon monoxide found by Hagstrum[21] from electron impact measurements on carbon monoxide, oxygen, nitric oxide and nitrogen, $D(CO)=9.6$ ev., when combined with the heats of formation of methane, carbon monoxide and the dissociation energies of oxygen and hydrogen give for the heat of atomization of methane,

$$A_t(CH_4)=-\Delta H_f(CH_4)+\Delta H_f^0(CO)+D(CO)-1/2D(O_2)+2D(H-H)$$
$$=0.775-1.147+9.60-2.56+8.96$$
$$=15.63 \text{ ev}.$$

The values of $A_t(CH_4)$ from $A_1(C^+)$, $A_1(CH^+)$, and $A_2(C^+)$, 15.7, 15.7, and 15.4, respectively, are in excellent agreement with this value of Hagstrum's, as well as the earlier deduction of Smith[10(a)] based on the appearance potentials of H^+ and C^- in the methane mass spectrum. The values of $A_t(CH_4)$ deducible from $A_2(CH^+)$ as well as $A_3(C^+)$ and $A_3(CH^+)$ are all less than or equal to 15.6 ev. Thus all the present electron impact data that may be interpreted in terms of the heat of atomization of methane and thus the heat of sublimation of graphite are only consistent with the so-called low value 136 kcal/mole.

The recent work of Goldfinger and co-workers[22] that indicates the accommodation coefficient of carbon atoms in graphite to be very small ($<10^{-3}$) makes it possible to reconcile the electron impact values of the heat of atomization of methane and dissociation energy of

[21] H. D. Hagstrum, Revs. Modern Phys. **23**, 185 (1951).
[22] Doehaerd, Goldfinger, and Walbroeck, J. Chem. Phys. **20**, 757 (1952).

carbon monoxide with the apparent heat of sublimation of graphite found from the effusion or evaporation experiments of Brewer, *et al.*[23] and of Marshall and Norton.[24] Thus it is reasonable to take the Hagstrum value for the heat of atomization of methane, 15.63 ev, along with the presumably reliable $D(CH_3-H)=4.42$ and $D(C-H)=3.47$ to fix the sum of $D(CH_2-H)$ and $D(CH-H)$ as

$$D(CH_2-H)+D(CH-H)=15.63-4.42-3.47=7.74 \text{ ev.}$$

It was found above (Part I) that the three appearance potentials of CH_2^+ lead to the two semi-independent determinations of $D(CH_2-H)$, 3.4 and 3.7 ev. The appearance potentials of CH^+ in the methyl and methylene mass spectra give $D(CH_2-H)=3.6$, while those of C^+ in the same radicals give 4.3 and thus the unweighted mean of the values is $D(CH_2-H)=3.7_5\pm0.3$. From the sum, $D(CH_2-H)++D(CH-H)=7.74$, we then have, $D(CH-H)=3.9_9\pm0.3$. With methane, CH_4, as the ground state, the energy levels of $CH_j+(4-j)H(0\leq j\leq 4)$ and the heats of atomization $A_t(CH_j)$ are:

$CH_j+(4-j)H$	Energy−ev/molecule	$A_t(CH_j)$,
CH_4	0.00	15.6_3,
CH_3+H	4.42 ± 0.03	11.2_1,
CH_2+2H	$8.1_7\pm0.3$	7.4_6,
$H+3H$	$12.1_6\pm0.3$	3.4_7,
$C+4H$	$15.6_3\pm0.1$	···.

It may be noted that the energy level of CH_2+2H with respect to methane $8.1_7\pm0.3$ ev/molecule corresponds to 3.6_9 ev/molecule for the endothermicity of the reaction,

$$CH_4=CH_2+H_2.$$

The value 3.6_9, for the heat of this reaction lies at the extreme of the range, 3.0 ± 0.7 ev/molecule, deduced by Long[25] from consideration of the activation energy of the homogeneous pyrolysis of methane, the long wavelength limit of the photodecomposition of ketene and other kinetic considerations.

It may be further noted that the suggestion of Long that an estimate of the heat of formation of diazomethane (2.0 ev/molecule, see foregoing) in combination with the long wavelength limit of the first continuum of the diazomethane absorption spectrum 4710 A according to Kirkbridge and Norrish[26] does not provide useful confirmation of the energy level of CH_2+H_2 with respect to methane. This method of calculation gives for

$$CH_4\rightarrow CH_2+H_2, \quad \Delta H<5.4 \text{ ev.}$$

The inequality contains an unknown and at present unestimatable electronic excitation of CH_2, *visa*

$$CH_2N_2+h\nu(4710 \text{ A})\rightarrow CH_2+N_2.$$

[23] Brewer, Gilles, and Jenkins, J. Chem. Phys. **16**, 797 (1948).
[24] Marshall and Norton, J. Am. Chem. Soc. **72**, 2166 (1950).
[25] Long, Proc. Roy. Soc. (London) **198**, 62 (1949).
[26] Kirkbridge and Norrish, J. Chem. Soc. 119 (1933).

The two determinations of the ionization potential of the methyl radical have given 10.0_7 and 9.8_5 ev. The best value is then $9.9_6\pm0.1$ and the energy of CH_3^++H with respect to methane is $14.3_8\pm0.1$. The three appearance potentials of CH_2^+, $A_1(CH_2^+)$, $A_2(CH_2^+)$, and $A_3(CH_2^+)$, when recalculated according to the relations of Table III, give for the level of CH_2^++2H with respect to CH_4, the values, 19.9_8, 19.7_2 and 20.07, respectively, or $19.9_2\pm0.14$ as the best value. This corresponds to the best value for the ionization potential of methylene equal to 11.7_5. The three appearance potentials of CH^+, $A_1(CH^+)$, $A_2(CH^+)$, and $A_3(CH^+)$, according to the assignments of Table III, give for CH^++3H with respect to CH_4, 23.4 ± 0.2, 22.1 ± 0.2, and 22.3 ± 0.2, or 22.6 ± 0.5 that is to be compared with the best value that may be presumed to be the sum of the spectroscopic value of the ionization potential of CH, $I^z(CH)=11.13$ and the level of $CH+3H$ with respect to methane given above, $12.1_6\pm0.3$, or CH^++3H at $23.2_9\pm0.3$. It is of interest to note that the level of CH^++3H deduced from $A_2(CH^+)$ and $A_3(CH^+)$ and the assignments of Table III is in agreement with the appearance potential of CH^+ in the methane mass spectrum found by McDowell and Warren,[10(f)] and Geerk and Neuert,[10(e)] 22.4 and 22.5, respectively, rather than the higher value, 23.4 found by Smith[10(a)] and ourselves.

The best value for the level of C^++4H with respect to CH_4 is the sum of the heat of atomization of methane, $A_t(CH_4)=15.6_3$ plus the spectroscopic value of the ionization potential of the carbon atom, 11.26,[14] or 26.8_9. The three appearance potentials of C^+, $A_1(C^+)$, $A_2(C^+)$ and $A_3(C^+)$ corrected according to the assignments of Table III give for this level 27.0, 26.7, and 26.2, respectively, or 26.6 ± 0.3. It may be noted that whereas the value for this level deduced from the appearance potential of C^+ in the methyl mass spectrum, 26.7 is in agreement with the energy of this level according to both Smith's[10(a)] and our determination of the appearance potential of C^+ in the methane mass spectrum, the value from the appearance potential in the methylene mass spectrum 26.2 agrees with the energy from the McDowell and Warren[10(f)] determination of the appearance potential of C^+ in the methane mass spectrum.

There are summarized in Table IV the successive dissociation energies of CH_j and CH_j^+ according to the best values of the energy levels of $CH_j+(4-j)H$ and $CH_j^++(4-j)H$ with respect to CH_4 given above. In

TABLE IV. Dissociation energies of CH_j and CH_j^+ ev/molecule.

	CH_4 Electron impact	Voge[a]	CH_4^+ Electron impact
$D(CH_3-H)$	$4.4_2\pm0.03$	4.54	$1.3_4\pm0.1$
$D(CH_2-H)$	$3.7_5\pm0.3$	4.14	$5.5_4\pm0.2$
$D(CH-H)$	$3.9_9\pm0.3$	3.46	$3.3_7\pm0.2$
$D(C-H)$	(3.47)[b]		(3.60)[b]

[a] Reference 2 calculated under assumption that $A_t(CH_4)=15.6$ ev and $D(C-H)=3.47$.
[b] Spectroscopic value, reference 7.

this Table IV there are also given for comparison the dissociation energies of CH_j calculated by Voge.[2] Contrary to an opinion expressed elsewhere by one of authors,[27] the electron impact data do not support Voge's calculations other than in the case of $D(CH_3-H)$, except when the extreme range of uncertainty of $D(CH_2-H)$ and $D(CH-H)$ are taken, i.e., $D(CH_2-H)=3.7_5+0.3=4.0_5$ and $D(CH-H)=3.9_9-0.3=3.6_9$. Professor E. B. Wilson has remarked[28] that the more or less monotonic variation of $D(CH_j-H)$ with j, causes the comparison of the experimental values with those of Voge's calculations to be an insignificant test of the quality of the calculations since the latter are essentially interpolations. Thus a comparison of calculations of the dissociation energies of CH_j^+ with the experimental values given in Table IV would be of considerable interest in view of the marked alternation of their magnitude.

APPENDIX

In addition to lead tetramethyl two other substances, mercury dimethyl and dimethyl disulfide, were found to be potentially useful sources of methyl radicals by pyrolysis in our furnace, while a number of others, azomethane, methyl sulfide, methyl iodide, trimethylamine, ethane, methylether, and silicon tetramethyl gave no evidence of pyrolysis to methyl at temperatures less than 1000°C. In Figs. 3 and 4 there are shown the intensity of methyl ion in the mass spectrometer for constant flow rate of mercury dimethyl and dimethyl disulfide, respectively, as a function of furnace temperature. Like lead tetramethyl, the yield of methyl from mercury dimethyl has a maximum value between 700 and 800°C and then decreases rapidly, presumably due to a different mode of decomposition. The rate of decrease with temperature above the maximum yield temperature is too rapid to be accounted for by 100 percent decomposition of the metal alkyl and the normal decrease of mass spectrometer sensitivity with increasing gas temperature.[29]

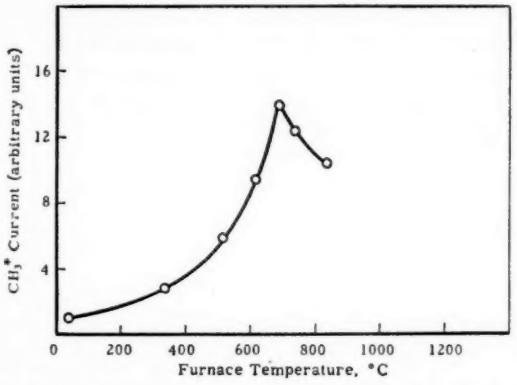

FIG. 3. CH_2^+ current as a function of temperature for constant flow of $Hg(CH_3)_2$—electron energy ~11.0 volts (corrected).

[27] D. P. Stevenson, Phys. Rev. **87**, 195 (1952).
[28] Private communication to D. P. S.
[29] D. P. Stevenson, J. Chem. Phys. **17**, 101 (1949).

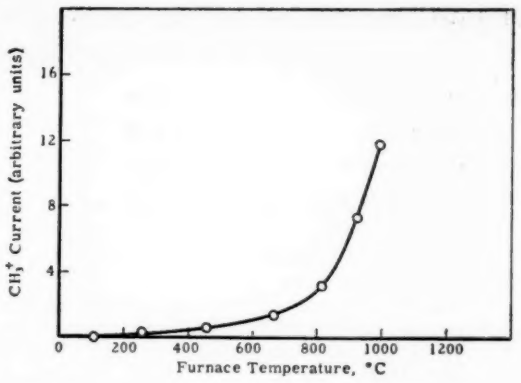

FIG. 4. CH_3^+ current as a function of temperature for constant CH_3SSCH_3 flow—electron energy ~11 volts (corrected).

In contrast to the behaviour of the metal alkyls, it will be seen in Fig. 4 that the yield of methyl radicals by pyrolysis of dimethyl disulfide is still increasing rapidly at 1000°C, the nominal maximum attainable temperature of the inlet furnace.

OTHER DATA ON CH_2^+

In addition to the four substances discussed previously the appearance potential of the ion CH_2^+ has been measured in the mass spectra of ethylene, ethane, methyl cyanide, methanol, and ethanol. It is of interest to examine the compatability of these data with the conclusion based on the measurements on methylene, methyl, and methane. The four substances, ethane, methyl cyanide, methanol, and ethanol can be written as

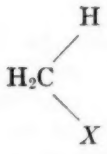

with X equal to methyl, cyanide, hydroxyl, and CH_2OH respectively. Thus the lowest energy process for the formation of CH_2^+ from these four substances will be

$$H_2CHX+\epsilon^-\rightarrow CH_2^++HX+2\epsilon^-,$$

and this type of process seems very probable in view of the fact that CH_2^+ formation from methane (at the first appearance potential) proceeds by the process

$$H_2CH_2+\epsilon^-\rightarrow CH_2^++H_2+2\epsilon^-.$$

The heats of formation from the elements in their standard state of H_2CHX (gas) and HX are (ev/molecule)

	$\Delta H_f^0(H_2CHX)$	$\Delta H_f^0(HX)$
H_2CHCH_3	−0.88	−0.78
H_2CHCN	+0.91	+1.36
H_2CHOH	−2.09	−2.51
H_2CHCH_2OH	−2.44	−2.09.

If the heat of the reaction

$$CH_4=CH_2+H_2$$

is called ΔH_x, then the heats of the four reactions of formation of CH_2^+ are

			$\Delta H_f(HX)+\Delta H_f(CH_4)-\Delta H_f(H_2CHX)+\Delta H_x+I^z(CH_2)$	
H_2CHCH_3	-0.78	-0.78	$+0.88$	$+\Delta H_x+I^z(CH_2)$
H_2CHCN	$+1.36$	-0.78	-0.91	$+\Delta H_x+I^z(CH_2)$
H_2CHOH	-2.51	-0.78	$+2.09$	$+\Delta H_x+I^z(CH_2)$
H_2CHCH_2OH	-2.09	-0.78	$+2.44$	$+\Delta H_x+I^z(CH_2)$,

or

	$A_{min}(CH_2^+)$	$A_{min}(CH_2^+)$	$A_{obs}(CH_2^+)$
H_2CHCH_3	$-0.68+\Delta H_x+I^z(CH_2)$	14.7_6	16.3 ± 1
H_2CHCN	$-0.33+\Delta H_x+I^z(CH_2)$	15.1_1	$15.6_2\pm0.04$
H_2CHOH	$-1.20+\Delta H_x+I^z(CH_2)$	14.2_4	15.4 ± 0.5
H_2CHCH_2OH	$-0.43+\Delta H_x+I^z(CH_2)$	15.0_1	16.5 ± 0.5.

The $A_{min}(CH_2^+)$ given in the third column are calculated from the second column taking for $\Delta H_x+I^z(CH_2)$ the "best value" found above, 15.44 ev.

The observed appearance potentials, given in the fourth column, range from 0.5 to 1.5 ev greater than the calculated values, $A_{min}(CH_2^+)$. In the first three cases any fragmentation of the neutral particle HX would require in excess of 3.5 ev, thus the process as written must be the correct one. The difference between the calculated and assumed values suggest that extra energy, either as kinetic energy or electronic excitation of the fragment is required for the formation of CH_2^+, or that the value assigned to $\Delta H_x+I^z(CH_2)$ is *low*. This latter possibility seems unlikely in view of the excellent agreement between the various measurements of the first appearance potential of CH_2^+ in the methane mass spectrum.

In the case of ethanol the difference between the calculated and observed energy of formation of CH_2^+ can again signify an extra energy requirement in the form of kinetic energy or electronic energy of the fragments or that the process is more disruptive of the molecule than the assumed process. It requires $+0.89$ ev to dissociate methanol into hydrogen plus formaldehyde or 0.95 ev to dissociate methanol into two hydrogen molecules plus carbon monoxide. Thus the minimum energies for the reactions

$$C_2H_5OH+\epsilon^-\rightarrow CH_2^++H_2+H_2CO+2\epsilon^-,$$
$$C_2H_5OH+\epsilon^-\rightarrow CH_2^++2H_2+CO+2\epsilon^-,$$

are 15.9_0 and 15.9_6 ev, respectively, both significantly less than the observed appearance potential of CH_2^+ in the ethanol mass spectrum, 16.5 ± 0.5 ev. No final assignment of process can thus be made for CH_2^+ formation from ethanol.

In the case of ethylene we may write

$$C_2H_4+2H_2=2CH_4, \qquad \Delta H=-2.10,$$
$$\epsilon^-+CH_4=CH_2^++H_2+2\epsilon^-, \qquad \Delta H=\Delta H_x+I^z(CH_2),$$
$$CH_4=CH_2+H_2, \qquad \Delta H=\Delta H_x,$$

or

$$C_2H_4+\epsilon^-=CH_2^++CH_2+2\epsilon^-,$$
$$A_{min}(CH_2^+)=2\Delta H_x+I^z(CH_2)-2.10,$$

or since

$$\Delta H_x+I^z(CH_2)=15.44,$$
$$C_2H_4; \quad A_{min}(CH_2^+)=\Delta H_x+13.3_4 \text{ ev}.$$

The best value assigned to ΔH_x is 3.69 ev thus, C_2H_4; $A_{min}(CH_2^+)=17.0_3$ ev, that is to be compared with the observed

$$C_2H_4; \quad A(CH_2^+)=19.3\pm0.3 \text{ ev}.$$

Since further disruption of CH_2 to CH+H or C+H_2 would require 3.9_9 or 2.9_8 ev we may conclude that neutral CH_2 accompanies CH_2^+ formation from ethylene and that the fragments share the order of 2 ev kinetic energy or one or both of the fragments is (are) electronically excited.

Frequency Assignments for Normal Aliphatic Compounds: I. The Normal Paraffins in the Range 1450 cm^{-1} to 650 cm^{-1}*

HUBERT TSCHAMLER†
First Chemical Institute, University of Vienna
(Received February 15, 1954)

It is assumed that the normal aliphatic hydrocarbons in their crystalline forms belong to the symmetry groups C_{2v} (odd number of carbon atoms) or C_{2h} (even number of carbon atoms), and that the selection rules for these symmetry groups hold exactly. It is then possible to work out a "theoretical distribution pattern" for the carbon-stretching modes, and for most types of the hydrogen deformation modes. Comparison of these patterns with available experimental data leads to a complete assignment of frequencies of these types in all the normal hydrocarbons for which data are available, and accounts satisfactorily for all spectral features for these materials in the solid and liquid state. The results might evidently be extended to other aliphatic series.

NUMEROUS authors have discussed the assignment of molecular vibration frequencies for individual hydrocarbons but, to the writer's knowledge, there have been no attempts to do this systematically for a number of members of the series except for a paper by Brown, Sheppard and Simpson[1] which discusses some compounds with an *even* number of carbon atoms. In the present work, full use is made of the spectra of the normal paraffins in the *solid* state where differences between members of the series with even and with odd numbers of carbon atoms first make themselves felt and, proceeding from the interpretation of these data, a complete assignment is proposed for the hydrogen-deformation and carbon-stretching frequencies which is shown to apply to all available spectra, and can undoubtedly be extended to normal paraffins of arbitrary length.

GENERAL FEATURES OF THE PARAFFIN SPECTRA

In Fig. 1(a) are shown, schematically, the positions of infrared absorption maxima for the normal paraffins in the *solid* state together with an indication of estimated intensities (line lengths). These were taken from the work of Axford and Rank[2] for the C_4 to C_7 compounds, and from that of Brown *et al.*[1] for the C_8 to C_{10} materials. The infrared spectra of the n-Paraffins C_6 to C_{10} in the liquid state, and some individual members in the solid state, were also measured in the writer's laboratory using a Perkin-Elmer-Model-12C-Spectrometer. However, since the results agreed completely with those of the above references they will not be further discussed here. Similarly, the Raman spectra for the liquids with their corresponding intensities are shown in Fig. 1(b). These were taken from the compilation in "Landolt-Börnstein" augmented by the more recent measurements of Sheppard and Szasz,[3] Simanouti and Mizushima,[4] and Cleveland and Porcelli.[5]

When arranged in this way [Fig. 1(a)], the array of infrared frequencies for the series is seen to possess the following easily recognized characteristics:

(a) *A band (sometimes a doublet) of constant frequency at ca 1460 cm^{-1}.* This band is known to be associated with the H—C—H scissor frequencies of CH_2 and CH_3 (antisymmetric) groups.

(b) *A constant frequency band at 1380 cm^{-1}.* This band is undoubtedly to be associated with the *symmetric* H—C—H scissor frequency of the CH_3 end groups as is further established by a study of other organic com-

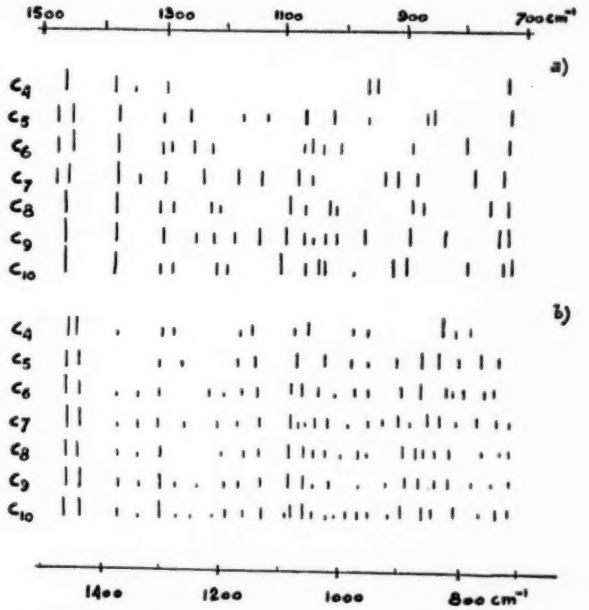

FIG. 1. (a) The infrared spectra of *solid* n-paraffins (n-butane to n-decane). [The positions of the lines indicate the band maxima, the lengths of them the estimated intensities]. (b) The Raman spectra of the same *liquid* n-paraffins.

* This material was presented in abridged form in the course of a meeting of the "Verein Oesterreichischer Chemiker" in the fall of 1952 in Graz.

† Present address: European Research Associates, S. A., Brussels, Belgium.

[1] Brown, Sheppard, and Simpson, Discussions Faraday Soc. **9**, 26 (1950).

[2] D. W. E. Axford and D. H. Rank, J. Chem. Phys. **17**, 430 (1949) and **18**, 51 (1950).

[3] N. Sheppard and G. J. Szasz, J. Chem. Phys. **17**, 86 (1949).

[4] T. Simanouti and S. Mizushima, J. Chem. Phys. **17**, 1102 and 1321 (1949).

[5] F. F. Cleveland and P. Porcelli, J. Chem. Phys. **18**, 1459 (1950).

TABLE I. Symmetry classes and number of vibrations in each class for the odd and even n-paraffins from C_4-C_{10}.

	CH_2 wagging		CH_2 twisting		C–C stretching		CH_2 rocking		CH_3 wagging		CH_3 rocking	
n-Propane	B_1		A_2		A_1	B_1	B_2		A_1	B_1	A_2	B_2
n-Pentane	A_1	$2B_1$	$2A_2$	B_2	$2A_1$	$2B_1$	A_2	$2B_2$	A_1	B_1	A_2	B_2
n-Heptane	$2A_1$	$3B_1$	$3A_2$	$2B_2$	$3A_1$	$3B_1$	$2A_2$	$3B_2$	A_1	B_1	A_2	B_2
n-Nonane	$3A_1$	$4B_1$	$4A_2$	$3B_2$	$4A_1$	$4B_1$	$3A_2$	$4B_2$	A_1	B_1	A_2	B_2
n-Butane	Ag	Bu	Au	Bg	2Ag	Bu	Au	Bg	Ag	Bu	Au	Bg
n-Hexane	2Ag	2Bu	2Au	2Bg	3Ag	2Bu	2Au	2Bg	Ag	Bu	Au	Bg
n-Octane	3Ag	3Bu	3Au	3Bg	4Ag	3Bu	3Au	3Bg	Ag	Bu	Au	Bg
n-Decane	4Ag	4Bu	4Au	4Bg	5Ag	4Bu	4Au	4Bg	Ag	Bu	Au	Bg

pounds containing methyl groups. It is very noticeable, however, that in spite of the decreasing contribution of methyl groups as the chain length increases, the intensity of the band remains substantially constant.

(c) *A zone of bands between 1300 cm^{-1} and 1200 cm^{-1}.* Here, at the 1300 cm^{-1} zone boundary, there is a constant-frequency, infrared active band which becomes a doublet in the higher members of the series with an even number of carbon atoms. Beginning with C_4, there is also an infrared active branch, decreasing in frequency with increasing chain length, which appears only in the members with an even number of carbons (this series is represented in Fig. 1(a) by the seventh band for C_6, and by the sixth bands for C_8 and C_{10} counting from the left).

(d) *A zone between 1200 cm^{-1} and 1100 cm^{-1}.* Two constant frequency bands, which occur only in the *odd* paraffins, are observed in this region.

(e) *A zone from 1100 cm^{-1} to 880 cm^{-1}.* Here is found a bell-shaped pattern of bands with its apex near 960 cm^{-1} in n-butane and spreading out toward the zone boundaries with increasing chain length. These infrared active bands are especially numerous between 1100 cm^{-1} and 1000 cm^{-1}.

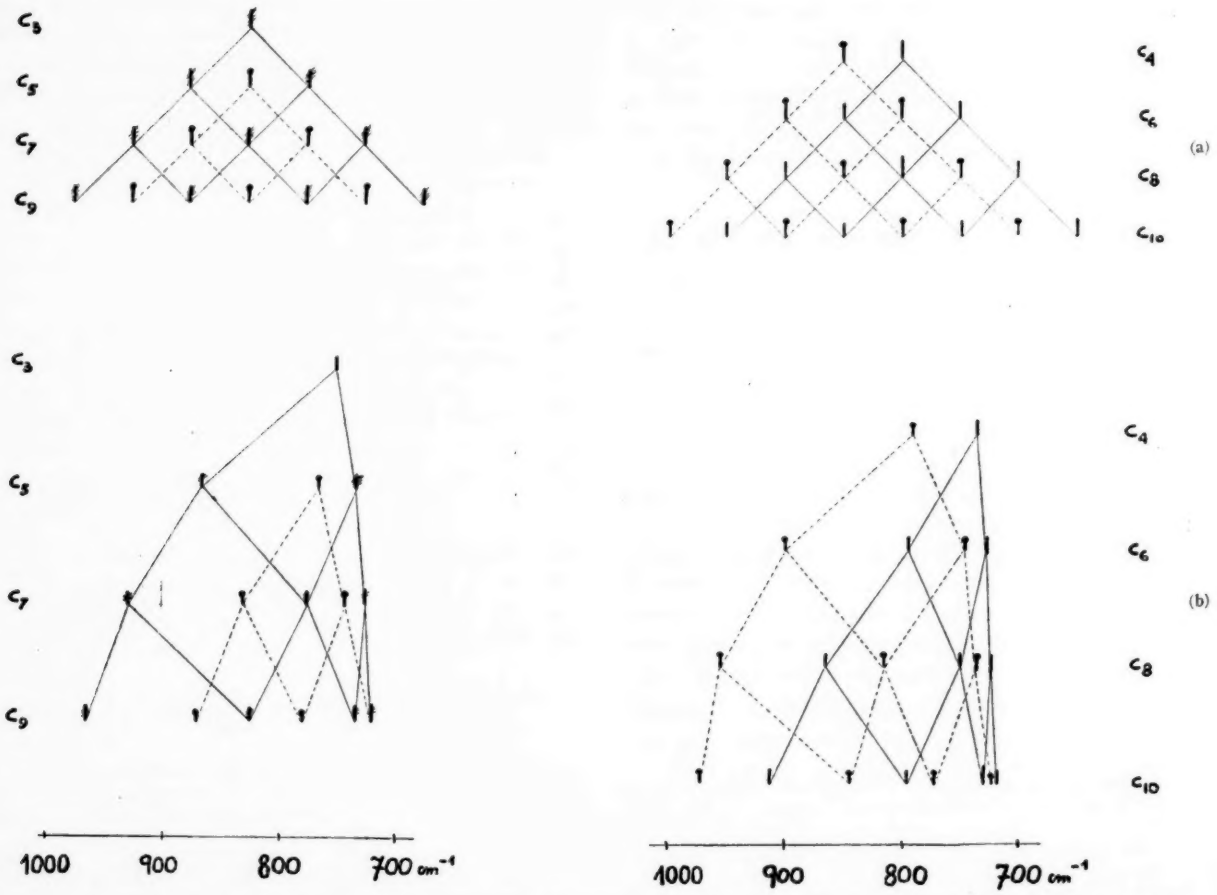

FIG. 2. (a) The theoretical distribution pattern for the CH_2 rocking frequencies of the n-paraffins with an odd (left side) and even (right side) number of C atoms. (A single line indicates an infrared active frequency, a line with a head a Raman active one and a cross-hatched line a frequency active in both.) (b) The actual spectral positions for the CH_2 rocking modes.

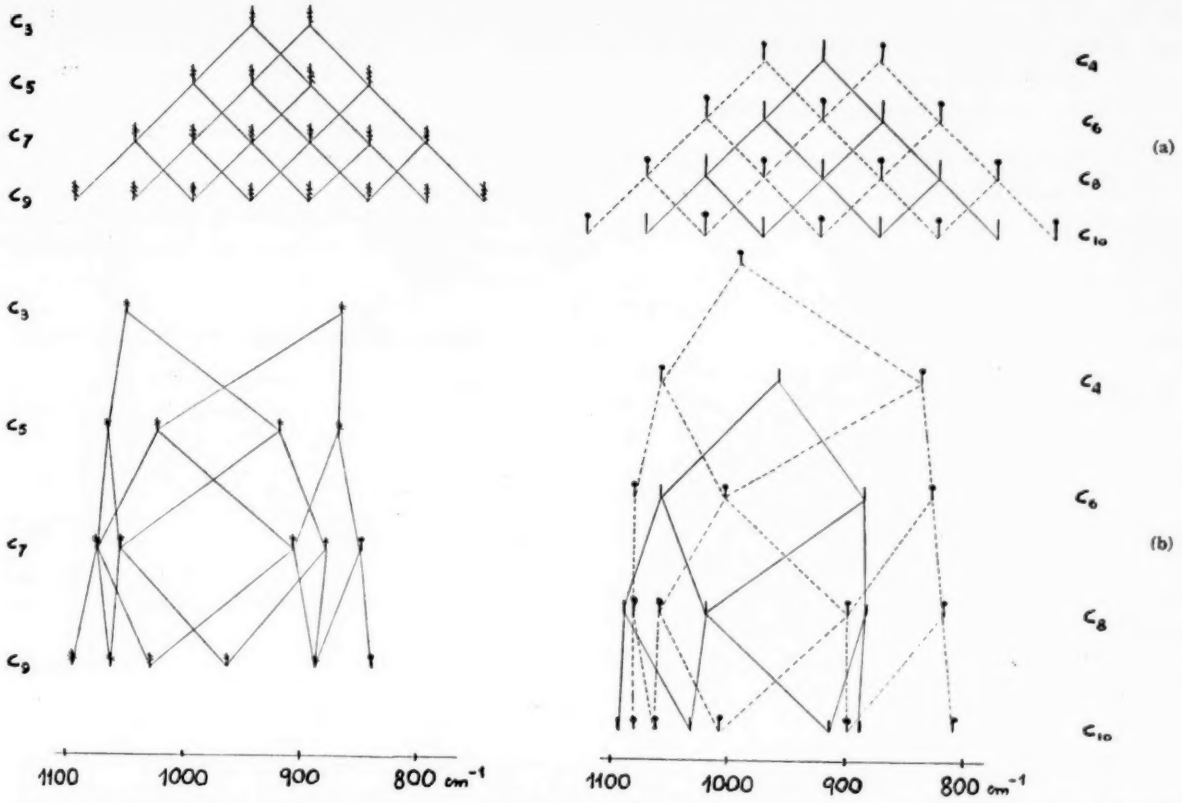

FIG. 3. (a) The theoretical distribution pattern for the C—C stretching frequencies of the n-paraffins with an odd (left side) and even (right side) number of C atoms. (A single line indicates an infrared active frequency, a line with a head a Raman active one and a cross-hatched line a frequency active in both.) (b) The actual spectral positions for the C—C stretching modes.

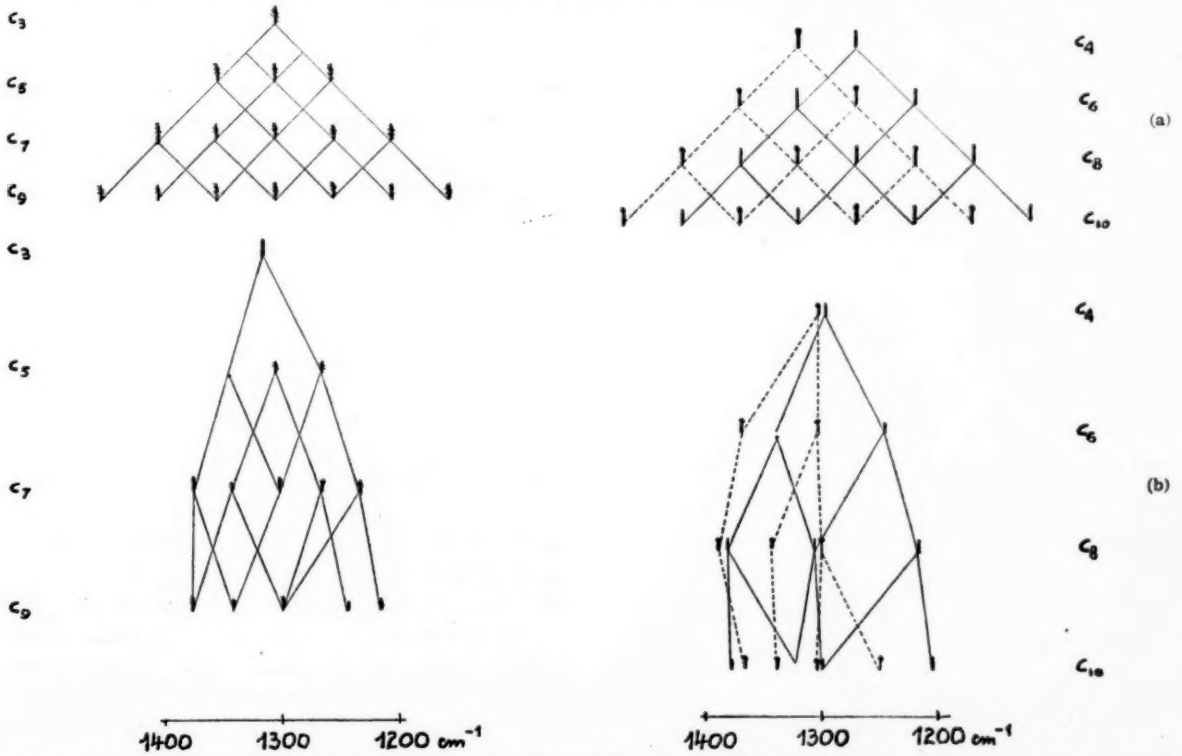

FIG. 4. (a) The theoretical distribution pattern for the CH_2 wagging frequencies of the n-paraffins with an odd (left side) and even (right side) number of C atoms. (A single line indicates an infrared active frequency, a line with a head a Raman active one and a cross-hatched line a frequency active in both.) (b) The actual spectral positions for the CH_2 wagging modes.

(f) *A zone between 880 cm^{-1} and 725 cm^{-1}.* In this region is found an intense, nearly constant, frequency band at the low-frequency zone boundary and two clearly visible branches running toward this frequency.

An examination of Fig. 1(b) reveals the following structural characteristics of the array of Raman frequencies of the normal paraffins:

(a) *A constant-frequency doublet near 1450 cm^{-1}.* This undoubtedly has the same origin as the corresponding infrared bands.

(b) *A weak, constant frequency line at 1375 cm^{-1}.* Although, again, the origin is the same as that of the infrared bands, it is noticeable that the intensity regularly increases with increasing chain length.

(c) *A zone of lines between 1300 cm^{-1} and 1190 cm^{-1}.* A constant-frequency, Raman-active line occurs at the upper-zone boundary and increases regularly in intensity down the series. A further Raman-active branch begins at C_4 and occurs in all members.

(d) *A zone between 1180 cm^{-1} and 1120 cm^{-1}.* In this region occur two almost constant-frequency, Raman-active lines in all members of the series, and in all cases the line at lower frequency is the more intense.

(e) *A zone between 1100 cm^{-1} and 820 cm^{-1}.* This region is fairly uniformly populated with lines but there is a very noticeable tendency for those near the two zone boundaries to be more intense.

(f) *A zone between 820 cm^{-1} and 720 cm^{-1}.* Here at least three easily recognizable Raman-active branches move toward the lower-zone boundary with increasing chain length.

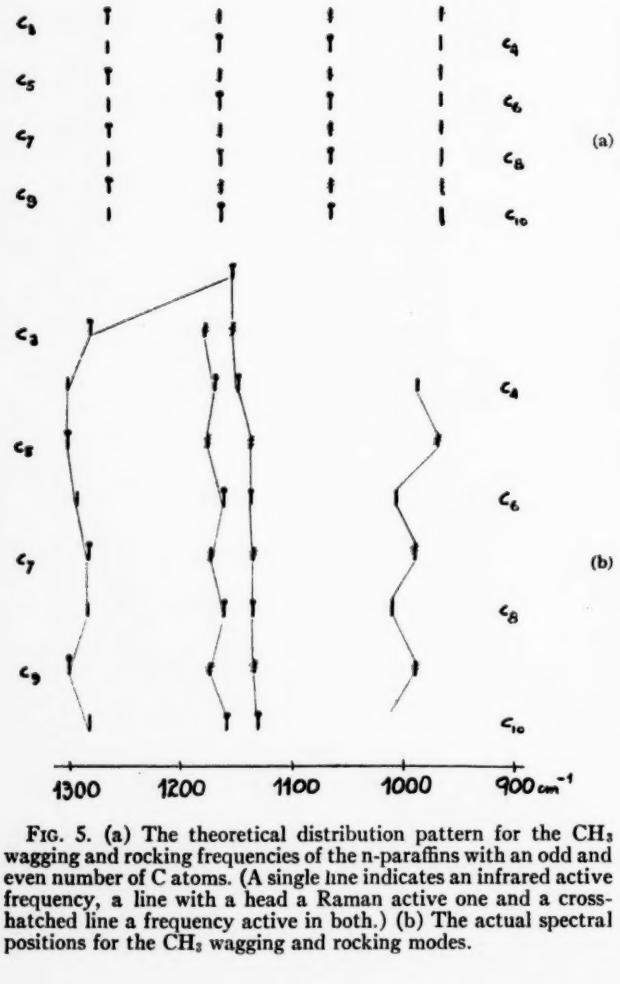

FIG. 5. (a) The theoretical distribution pattern for the CH_3 wagging and rocking frequencies of the n-paraffins with an odd and even number of C atoms. (A single line indicates an infrared active frequency, a line with a head a Raman active one and a cross-hatched line a frequency active in both.) (b) The actual spectral positions for the CH_2 wagging and rocking modes.

NORMAL FREQUENCIES TO BE ASSIGNED

It is now necessary to enumerate the types of normal vibrations which occur in the frequency range which is the subject of this paper. These are

1. The H−C−H scissor frequencies of the CH_2 groups. These were mentioned above and will not be further treated.
2. The antisymmetric H−C−H scissor frequencies of the CH_3 end groups (same comment as under 1 above).
3. The symmetric H−C−H frequencies of the CH_3 end groups (same comment).
4. The H−C−C wagging frequencies of the CH_2 groups. The possible number of frequencies of this type is the same as the number of CH_2 groups or n−2 for an n-carbon paraffin.
5. The H−C−C wagging frequencies of the two CH_3 groups. Two frequencies of this type occur in each member of the series independently of n.
6. The H−C−C twisting frequencies of the CH_2 groups. Again n−2 such frequencies should occur.
7. The C−C stretching frequencies. These should occur to the number n−1 in an n-carbon paraffin.
8. The H−C−C rocking frequencies of the CH_3 groups, which occur to the number of two per molecule independently of n.
9. The H−C−C rocking frequencies of the CH_2 groups which occur to the number n−2.

ASSIGNMENT OF FREQUENCIES

If it is assumed that the *solid* normal paraffins with an uneven number of carbons have the symmetry C_{2v}, while those with an even number of carbons have the symmetry C_{2h}, then the vibrations listed under points 4 to 9 of the last section will be divided among the symmetry classes of these groups as shown in Table I. We now wish to use the selection rules inherent in these symmetry classes together with a minimal number of well-established experimental data to arrange the frequencies available for assignment into such a form that comparison with the pattern discussed in the first section leads to a straightforward and complete assignment. The supplementary experimental data selected to

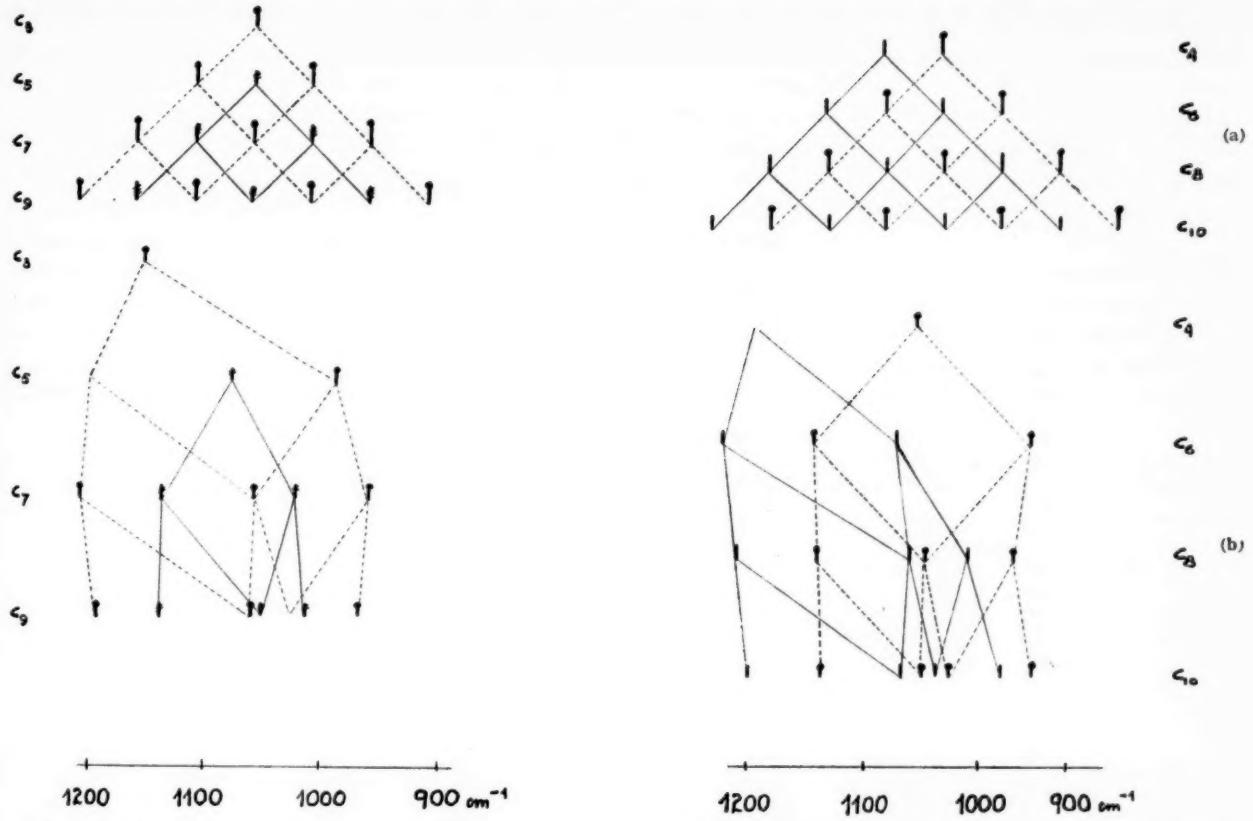

FIG. 6. (a) The theoretical distribution pattern for the CH_2 twisting frequencies of the n-paraffins with an odd (left side) and even (right side) number of C atoms. (A single line indicates an infrared active frequency, a line with a head a Raman active one and a cross-hatched line a frequency active in both.) (b) The actual spectral positions for the CH_2 twisting modes.

assist in locating the characteristic patterns of frequencies for the different oscillation types within the whole spectrum are the following:

(a) The infrared-active frequency at 720 cm^{-1} in gaseous propane can, on the basis of the band shape as well as the comparison of the spectra of $CH_3-CH_2-CH_3/CH_3-CD_2-CH_3$ and $CD_3CH_2CD_3$,[6] be unequivocally assigned to the CH_2 rocking frequency.

(b) The completely symmetric C—C stretching frequency, which is always strongly Raman-active and polarized but only weakly infrared-active, invariably occurs at the lowest frequency of all the expected C—C stretching modes.

(c) As in (a) above the gaseous propane frequency at 1300 cm^{-1} can be unequivocally assigned to the CH_2 wagging mode.

(d) In any homologous series, the frequencies associated with end groups are generally of quite constant frequency.

It has already been pointed out that the experimental data on the solid hydrocarbons show regularities which are most naturally interpreted as the operation of selection rules. If both infrared and Raman spectra were available on the solids, it should be possible to pick out patterns of lines in each spectral region which satisfy the selection rules and thus arrive at an assignment. Unfortunately, the Raman spectra of the solids are, due to experimental difficulties, extremely fragmentary; only a fraction of the expected lines is actually observed. This complicates the assignment since in the liquid state, as will be seen below, all evidence indicates that at least a considerable fraction of the molecules

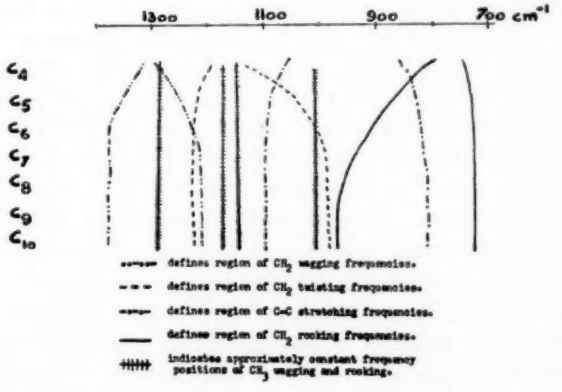

FIG. 7. The zone boundaries for the different vibration types.

[6] H. L. McMurry and V. Thornton, J. Chem. Phys. **19**, 1015 (1951).

TABLE II. Assignment of the infrared frequencies in the solid and liquid, and of the Raman lines in liquid state and such as occur in the solid state to the CH_2 rocking modes of the n-paraffins C_4-C_{10}.

	Infrared				Raman			
	Liquid		Solid		Liquid		Solid	
n-Paraffin:	*gauche*	planar	*cis*	*trans*	*gauche*	planar	*cis*	*trans*
n-Butane				732(A_u)				
					809	789(B_g)		
			728(B_2)		734	734(B_2)		
n-Pentane					764	764(A_2)		
			861(B_2)		864	864(B_2)	869(B_2)	
	725	725(A_u)		726(A_u)	729			
	758				760	746(B_g)		
n-Hexane	795	795(A_u)		794(A_u)	794			
	903				900	900(B_g)		898(B_g)
	723	723(B_2)	724(B_2)		721	721(B_2)		
	741				742	742(A_2)		
n-Heptane	773	773(B_2)	773(B_2)		775	775(B_2)		
	831				829	829(A_2)		
	928	928(B_2)	930(B_2)		930	930(B_2)		
	722	722(A_u)		722(A_u)	723			
	735				735	735(B_g)		
	763	763(A_u)		748(A_u)	765			
n-Octane	793				815	815(B_g)		
	877	877(A_u)		864(A_u)	861			
	966				953	953(B_g)		
	723	723(B_2)	721(B_2)		721	721(B_2)		
	723				721	721(A_2)		
	753	753(B_2)	736(B_2)		751	751(B_2)		
n-Nonane	771				781	781(A_2)		
	829	829(B_2)	826(B_2)		820	820(B_2)		
	872				871	871(A_2)		
	972	973(B_2)	962(B_2)		970	970(B_2)		
	722	722(A_u)		720(A_u)	723			
	722				723	723(B_g)		
	740	740(A_u)		730(A_u)	744			
	768				772	772(B_g)		
n-Decane				795(A_u)	810			
					844	844(B_g)		
	918	918(A_u)		912(A_u)	921			
					971	971(B_g)		

rotate into configurations of lower symmetry (probably C_2) in which all frequencies are permitted in both infrared and Raman spectra. Nevertheless, it turns out that the clue given by the infrared spectra of the solids compared with the Raman spectra of the liquids is sufficient to permit the selection of a pattern of bands and lines for each type of motion which satisfies the selection rules insofar as they are applicable, which is confirmed in all cases by those Raman lines which occur in the solids, and which lays a thoroughly reasonable groundwork from which the remaining features of all the spectra can be successfully accounted for. What has been said in this paragraph is tantamount to the additional reasonable assumption that the observed regularities in the experimental patterns is the result of the tendency of the frequencies of a given type to appear in their own spectral region (although the regions for different types may overlap), and that the regularities are strictly governed by the selection rules which are applicable. From this assumption, it follows that a theoretical distribution pattern can be prepared for each type of motion using the data above together with the breakdown into symmetry classes shown in Table I. It is the comparison of this theoretical distribution pattern with experiment which leads to the assignment proposed.

As a detailed example of the procedure followed we take the *CH_2 rocking frequencies*. From (a) above we can locate the single frequency of this type for propane: it belongs to B_2 and hence is infrared and Raman-active. In butane, according to Table I, there occur two such frequencies, A_u (infrared-active) and B_g (Raman-active). Referring to Fig. 1, we find the A_u mode immediately at a slightly lower frequency than the propane band and further note in the Raman spectrum a line at a somewhat higher frequency having no infrared analogue. In pentane there are two B_2 (infrared and Raman-active) frequencies one of which evidently continues

the low frequency branch, while the second starts a new branch at a higher frequency. Between the two occurs the Raman line belonging to A_2 and having no infrared analogue. Continuing in this way, the theoretical distribution pattern shown schematically in Fig. 2(a) is established (for greater clarity, the even and odd numbers have been separated). In this figure, a single line means only infrared active, a line with a head only Raman-active, while a cross-hatched line should appear both in the Raman and infrared spectra. The actual spectral positions for the CH_2 rocking modes taken from Fig. 1 are redrawn on a larger scale in Fig. 2(b) and the different branches connected.

Removing the CH_2 rocking frequencies which have now been assigned, we proceed to the assignment of the *C—C stretching modes* for which the theoretical distribution pattern shown in Fig. 3(a) can be obtained as above, making use of the information from (b) to locate the pattern in the spectrum and taking full account of the polarization of the Raman lines. The assignment is given in Fig. 3(b).

Proceeding in exactly the same manner, the *CH_2 wagging modes* may now be assigned since, by reference to (c), and comparison with Fig. 1, we note that they are well separated from other modes. The theoretical distribution pattern is shown in Fig. 4(a), and the actual

TABLE III. Assignment of the infrared frequencies in the solid and liquid, and of the Raman lines in liquid state and such as occur in the solid state to the C—C stretching modes of the n-paraffins C_4—C_{10}.

	Infrared				Raman			
	Liquid		Solid		Liquid		Solid	
n-Paraffin:	*gauche*	planar	*cis*	*trans*	*gauche*	planar	*cis*	*trans*
n-Butane				958(B_u)	837 955 1057	837(A_g) 1057(A_g)		837(A_g) 1059(A_g)
n-Pentane			868(A_1) 919(B_1) 1025(A_1) 1067(B_1)		838 904 1025 1072	864(A_1) 904(B_1) 1035(A_1) 1072(B_1)	869(A_1) 1031(A_1) 1069(B_1)	
n-Hexane	868 888 1004 1040	 882(B_u) 1058(B_u)		884(B_u) 1057(B_u)	868 890 1005 1040 1080	826(A_g) 1005(A_g) 1080(A_g)		1005(A_g) 1064(A_g)
n-Heptane	864 873 900 1070 1080	864(A_1) 885(B_1) 900(A_1) 1070(A_1) 1080(B_1)	··· (A_1) 875(B_1) 908(A_1) 1055(B_1) 1075(A_1) 1075(B_1)		838 888 901 1057 1044 1086	851(A_1) 888(B_1) 909(A_1) 1057(B_1) 1071(A_1) 1086(B_1)	 905(A_1) 1056(B_1) 1072(A_1)	
n-Octane	842 891 898 1078 1078	 877(B_u) 1078(B_u) 		881(B_u) 1020(B_u) 1088(B_u) 	843 878 896 1026 1060 1083 1083	815(A_g) 896(A_g) 1060(A_g) 1083(A_g)		899(A_g) 1062(A_g)
n-Nonane	843 889 889 953 1030 1062 1087 1087	843(A_1) 889(B_1) 889(A_1) 973(B_1) 1030(A_1) 1062(B_1) 1087(A_1) 1087(B_1)	··· (A_1) 889(B_1) 889(A_1) 962(B_1) 1029(A_1) 1063(B_1) 1094(A_1) 1094(B_1)		820 892 892 970 1019 1062 1082 1082	843(A_1) 892(B_1) 892(A_1) 970(B_1) 1019(A_1) 1062(B_1) 1082(A_1) 1082(B_1)	 888(B_1) 888(A_1) 1060(B_1) 	
n-Decane	894 918 1015 1090 1078	894(B_u) 918(B_u) 1090(B_u) 		890(B_u) 912(B_u) 1034(B_u) 1103(B_u)	844 886 898 921 1008 1023 1062 1092 1080	810(A_g) 898(A_g) 1008(A_g) 1062(A_g) 1080(A_g)		886(A_g) 1060(A_g)

assignment in Fig. 4(b). Furthermore, making use of (d) we can immediately assign two of the four possible *CH_3 modes* to the bands between 1100 cm^{-1} and 1200 cm^{-1}, again in accord with the selection rules and the polarization of the Raman lines (see Fig. 5). Having proceeded this far and removed the assigned bands and lines from Fig. 1 we are left with those which are to be assigned to the *CH_2 twisting modes* and to the remaining two *CH_3 frequencies*. Taking into account some overlapping in especially congested regions, the given assignments which are believed to be the best possible at present are shown in Figs. 5 and 6(b), in full agreement with the selection rules and the theoretical distribution pattern of the *CH_2 twisting modes* in Fig. 6(a). It should be remarked here that the end-group assignments, although reasonable, are not entirely unequivocal.

Finally, in Fig. 7, the zone boundaries for each of the vibration types are assembled on a diagram similar to Fig. 1. From this, it is immediately seen that there is substantially no overlapping of the different regions below C_5. This shows that for the lowest members of the series the representation by models corresponds, in large measure, to actuality. These models begin to lose their value as the overlapping of the zones with increasing chain length shows that the localization of the different modes in a characteristic frequency range becomes a progressively poorer approximation even though, as seen from above, it is still possible to arrive at reasonable assignments for the members above pentane by extrapolation of the frequencies for the lower members.

In a work to be published, the methods herein described will be extended to the series $CH_3-(CH_2)_nX$ (X = Cl, Br) and the series $Y-(CH_2)_nY$ (Y = COOH, Br).

TABLE IV. Assignment of the infrared frequencies in the solid and liquid, and of the Raman lines in liquid state and such as occur in the solid state to the CH_2 wagging modes of the n-paraffins C_4-C_{10}.

	Infrared				Raman			
	Liquid		Solid		Liquid		Solid	
n-Paraffin:	*gauche*	planar	*cis*	*trans*	*gauche*	planar	*cis*	*trans*
n-Butane				1299(B_u)				
					1301	1301(A_g)		1300(A_g)
n-Pentane			1265(B_1)		1264	1264(B_1)		
			1308(A_1)		1302	1302(A_1)	1303(A_1)	
			··· (B_1)		···	··· (B_1)		
n-Hexane	1250	1250(B_u)		1246(B_u)	1250			
	1304				1302	1302(A_g)		1300(A_g)
	1343	1343(B_u)		··· (B_u)	1343			
					1366	1366(A_g)		
n-Heptane	1237	1237(B_1)	1232(B_1)		1237	1237(B_1)		
			··· (A_1)		1264	1264(A_1)		
	1307	1307(B_1)	1300(B_1)		1298	1298(B_1)	1296(B_1)	
	1343	1343(A_1)	1342(A_1)		1342	1342(A_1)		
	1380	1380(B_1)	1377(B_1)		1364	1364(B_1)		
n-Octane	1227	1227(B_u)		1218(B_u)	1226			
	1301				1299	1299(A_g)		1297(A_g)
	1301	1301(B_u)		1303(B_u)	1299			
	1343				1342	1342(A_g)		
	1380	1380(B_u)		1378(B_u)	1386			
	1380				1386	1386(A_g)		1384(A_g)
n-Nonane	1220	1220(B_1)	1215(B_1)		1217	1217(B_1)		
	1265	1265(A_1)	1243(A_1)		···	··· (A_1)		
	1292	1292(B_1)	1298(B_1)		1299	1299(B_1)	1297(B_1)	
	1307	1307(A_1)	1298(A_1)		1299	1299(A_1)	1297(A_1)	
	1343	1343(B_1)	··· (B_1)		1340	1340(B_1)		
	1380	1380(A_1)	1376(A_1)		1365	1365(A_1)		
	1380	1380(B_1)	1376(B_1)		1365	1365(B_1)		
n-Decane	1215	1215(B_u)		1208(B_u)	1211			
	1250				1250	1250(A_g)		
	1307	1307(B_u)		1303(B_u)	1301			
	1307				1301	1301(A_g)		1295(A_g)
				··· (B_u)				
	1343				1340	1340(A_g)		
	1380	1380(B_u)		1378(B_u)				
					1366	1366(A_g)		

TABLE V. Assignment of the infrared frequencies in the solid and liquid, and of the Raman lines in liquid state and such as occur in the solid state to the CH_3 wagging and rocking modes of the n-paraffins C_4-C_{10}.

	Infrared				Raman			
	Liquid		Solid		Liquid		Solid	
n-Paraffin:	*gauche*	planar	*cis*	*trans*	*gauche*	planar	*cis*	*trans*
				984(B_u)	980			
					1150	1150(A_g)		1151(A_g)
n-Butane					1163	1168(B_g)		
				1300(A_u)	1281			
			965(B_1)		953	953(B_1)		
			1138(A_1)		1142	1142(A_1)	1145(A_1)	
n-Pentane			1176(B_2)		1165	1165(B_2)		
					1302	1302(A_2)		
	1004	1004(B_u)		1005(B_u)	1005			
	1138				1140	1140(A_g)		1143(A_g)
n-Hexane					1165	1165(B_g)		
	1298	1298(A_u)		1293(A_u)	1302			
	987	987(B_1)	··· (B_1)		988	988(B_1)		
	1138	1138(A_1)	1137(A_1)		1139	1139(A_1)	1139(A_1)	
n-Heptane			1176(B_2)		1163	1163(B_2)		
	1282				1281	1281(A_2)		
	1005	1005(B_u)		1108(B_u)	999			
	1134				1137	1137(A_g)		1138(A_g)
n-Octane					1162	1162(B_g)		
	1283	1283(A_u)		1286(A_u)				
	987	987(B_1)	··· (B_1)		970	970(B_1)		
	1134	1134(A_1)	1138(A_1)		1134	1134(A_1)	1136(A_1)	
n-Nonane			1178(B_2)		1159	1159(B_2)		
	1292				1299	1299(A_2)	1297(A_2)	
				··· (B_u)				
	1134				1133	1133(A_g)		1136(A_g)
n-Decane					1161	1161(B_g)		
	1280	1280(A_u)		1283(A_u)	1271			

CONCLUSIONS

Starting from the above assignment of the infrared spectra of the *solid* hydrocarbons together with systematically selected lines from the liquid Raman spectra, it should be possible to account for all the infrared and Raman frequencies in this region observed in the various states of aggregation. A number of investigators[7] have shown that it is very probable that the planar form of highest symmetry (C_{2v} or C_{2h}), which exists exclusively in the crystalline solid, partially reverts to forms of lower symmetry in the liquid by rotation about the carbon-carbon bonds. In all probability the structures thus achieved are "gauche" forms of symmetry C_2. If this is the case, the selection rules permit all modes of vibration to occur both in the infrared and Raman spectra. Evidently, it is also to be expected that the frequencies for the "gauche" forms might be slightly shifted with respect to those for the planar form, due to changed group interactions, although this is expected to be a small effect. Proceeding from the above assumption, the assignments listed in Tables II to VI have been made. These account for all the Raman and infrared frequencies reported in the literature for the region in question, and it is particularly gratifying that so many frequencies can be explained in such a completely straightforward way on the basis of so reasonable an assumption. It is notable that a few lines appear to be missing and it was not possible to obtain complete agreement with the work of Szasz and Sheppard[3] and Szasz, Sheppard, and Rank[8] who sorted the Raman frequencies for the symmetric and less symmetric (low energy and high energy) forms on the basis of measurements at two temperatures. On the other hand, the spectra of these workers did not contain the number of frequencies in this region to be expected from the selection rules.

[7] Mizushima, Morino, and Nakamura, Sci. Papers Inst. Chem. Research (Tokyo) **37**, 208 (1940); H. J. Bernstein, J. Chem. Phys. **17**, 256 (1949); Mizushima, Morino, Watanabe, Simanouti and Yamaguchi, J. Chem. Phys. **17**, 591 (1949); Mizushima, Shimanouchi, Nakagawa, and Miyake, J. Chem. Phys. **21**, 215 (1953).

[8] Szasz, Sheppard, and Rank, J. Chem. Phys. **16**, 704 (1948).

TABLE VI. Assignment of the infrared frequencies in the solid and liquid, and of the Raman lines in liquid state and such as occur in the solid state to the CH_2 twisting modes of the n-paraffins C_4-C_{10}.

	Infrared				Raman			
	Liquid		Solid		Liquid		Solid	
n-Paraffin:	*gauche*	planar	*cis*	*trans*	*gauche*	planar	*cis*	*trans*
n-Butane				··· (A_u)	1077	1077(B_g)		
					990	990(A_2)		
n-Pentane			1080(B_2)		1072	1072(B_2)	1072(B_2)	
					···	··· (A_2)		
	973				976	952(B_g)		
	1068	1068(A_u)		1066(A_u)	1065			
n-Hexane	1138				1140	1140(B_g)		1143(B_g)
	1225	1225(A_u)		1219(A_u)	1220			
	962				960	960(A_2)		
	1020	1020(B_2)	··· (B_2)		1023	1023(B_2)	1028(B_2)	
n-Heptane					1057	1057(A_2)	1056(A_2)	
	1138	1138(B_2)	1137(B_2)		1139	1139(B_2)	1139(B_2)	
	1211				1206	1206(A_2)		
	966				970	970(B_g)		
	1005	1005(A_u)		1008(A_u)	999			
					1045	1045(B_g)		1045(B_g)
n-Octane				1058(A_u)	1060			
	1134				1137	1137(B_g)		1138(B_g)
	1200	1200(A_u)		1205(A_u)	1199			
	973				970	970(A_2)		
	1012	1012(B_2)	1012(B_2)		1019	1019(B_2)		
					···	··· (A_2)		
n-Nonane	1043	1043(B_2)	1049(B_2)		1046	1046(B_2)		
	1062				1062	1062(A_2)	1060(A_2)	
	1134	1134(B_2)	1138(B_2)		1134	1134(B_2)	1136(B_2)	
					1192	1192(A_2)		
					952	952(B_g)		
				980(A_u)	991			
	1015				1023	1023(B_g)		
n-Decane				1034(A_u)				
					1047	1047(B_g)		
				1062(A_u)	1062			
	1134				1133	1133(B_g)		1136(B_g)
	1186	1186(A_u)		1195(A_u)	1189			

It is a pleasure to acknowledge indebtedness to Mr. H. Voetter of the Technische Hochschule in Vienna, for his valuable assistance in assembling and organizing the considerable mass of material, to N. Sheppard, Cambridge, England, for a short discussion, and to Dr. R. H. Gillette of European Research Associates, Brussels, for many helpful discussions, and for translating the manuscript.

THE JOURNAL OF CHEMICAL PHYSICS VOLUME 22, NUMBER 11 NOVEMBER, 1954

Potassium Bromide Disk Method for the Infrared Studies of Coördination Compounds*

THOMAS J. LANE, D. N. SEN, AND J. V. QUAGLIANO†
Department of Chemistry, University of Notre Dame, Notre Dame, Indiana
(Received April 19, 1954)

The infrared absorption of tetrakis(ethylenethiocarbamide)copper(I) nitrate, ethylenethiocarbamide, and potassium nitrate have been measured by the potassium bromide disk method. The assignment of the frequencies of ethylenethiocarbamide explains that part of the spectrum (the wavelength region between 7 and 13 microns) in which various CH_2 deformation frequencies are expected to appear. Generally speaking the infrared spectrum of tetrakis(ethylenethiocarbamide)copper(I) nitrate can be regarded as the superposition of the spectra of ethylenethiocarbamide and potassium nitrate, except for the absorption peaks at 9.6 and 14 microns, which do not appear in the infrared spectra of ethylenethiocarbamide and potassium nitrate. It is interesting to note that these wavelengths correspond to the Raman frequencies (1050 cm^{-1} and 720 cm^{-1}) of potassium nitrate, which should be infrared-inactive. The appearance of these frequencies in the absorption spectrum is explained by the distortion of the nitrate ion in tetrakis(ethylenethiocarbamide)-copper(I) nitrate.

INTRODUCTION

INTERESTING and important studies of absorption spectra of inorganic compounds in solvents have provided much information regarding the structures of molecules. In addition, spectral studies of substances in the gaseous, liquid and solid states permit a useful comparison of the entities present. It is of great advantage to work with solutions, and for the study of association of molecules, it is necessary. However, the absorption spectra of many substances in solution are affected by the nature and role of the solvent. In cases where fundamental changes take place upon solution or when solids are insoluble in suitable solvents, the absorption spectra of compounds are best studied in the solid state.

An examination of the literature reveals few spectral investigations of solid inorganic coördination compounds. It seems desirable, both from theoretical and practical considerations, to investigate the spectroscopic properties of solid inorganic compounds, since this method should prove valuable in studies of the structural properties of ligands coördinated about a central atom. Recently an extremely interesting and important technique for obtaining absorption spectra of compounds in the solid state employing potassium bromide disks was introduced by Stimson and O'Donnell.[1]

The potassium bromide disk method is most useful in the study of the spectra of inorganic coördination compounds, since generally these are insoluble in suitable solvents, or are chemically reactive with the solvents or, due to the unstable oxidation state of the central metal of the complex, undergo auto oxidation reduction in solvents. Other general advantages of the disk method are the absence of objectionable absorption peaks of the dispersing medium, the ease of preparation and the control of concentration of samples for analyses. Furthermore, a greater resolution is obtained in many cases than by conventional methods. An infrared study of tetrakis (ethylenethiocarbamide) copper (I) nitrate, a complex containing a central metal ion in an unstable oxidation state, was carried out by means of the potassium bromide disk method.

EXPERIMENTAL

Absorption Spectra

Measurements of the inorganic complex were made in the solid state using the potassium bromide disk method, introduced by Stimson and O'Donnell[1] for the infrared and ultraviolet studies of solid organic compounds. The potassium bromide used in the preparation of the disks was reagent grade, spectrophotometrically pure, ground to 200 mesh or better and dried in an oven at 110° for several days. Samples of 2 mg of the complex were mixed and ground with 298 mg of potassium bromide powder in an agate mortar with successive mixing and grinding for five minutes. A disk of pure potassium bromide of the same weight present in the sample disks was used as the comparison plate. A Perkin-Elmer model 21 double beam recording infrared spectrophotometer was used to obtain the infrared spectra in the wavelength region from 2 to 15 microns.

Preparation of Compound

Matheson reagent grade ethylenethiocarbamide was twice recrystallized from water. Tetrakis(ethylenethiocarbamide)copper(I) nitrate was prepared essentially according to the directions of Morgan and Burstall[2] by mixing warm aqueous solutions of ethylenethiocarbamide and copper(II) nitrate (Baker's analyzed reagent). After the green color faded and sulfur separated, the solution was boiled gently while stirring. A small amount of "Norite" charcoal was added to remove

* Presented in part before the Physical and Inorganic Division of the 124th National Meeting of the American Chemical Society, Chicago, Illinois, September 1953.

† Member, Radiation Project operated by the University of Notre Dame and supported in part under U. S. Atomic Energy Commission Contract AT(11-1)-38.

[1] M. M. Stimson and M. J. O'Donnell, J. Am. Chem. Soc. **74**, 1805 (1952).

[2] G. T. Morgan and F. H. Burstall, J. Chem. Soc. **131**, 147 (1928).

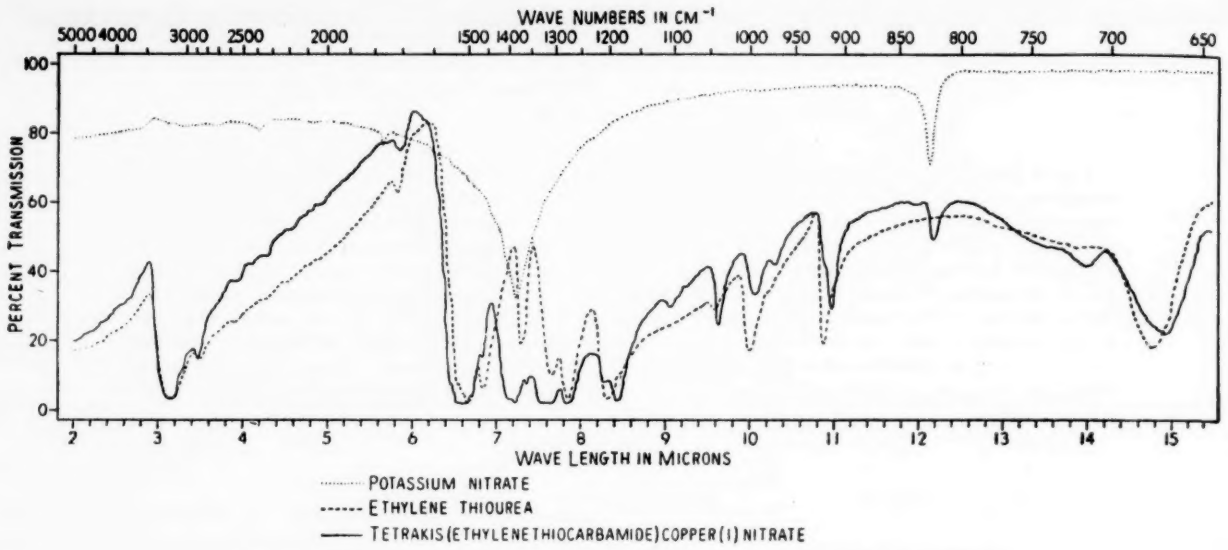
WAVE NUMBERS IN CM⁻¹
5000 4000 3000 2500 2000 1500 1400 1300 1200 1100 1000 950 900 850 800 750 700 650
PERCENT TRANSMISSION
100 80 60 40 20 0
2 3 4 5 6 7 8 9 10 11 12 13 14 15
WAVE LENGTH IN MICRONS
POTASSIUM NITRATE
ETHYLENE THIOUREA
TETRAKIS(ETHYLENETHIOCARBAMIDE)COPPER(I) NITRATE

FIG. 1. Infrared absorption spectra. The spectra were determined in the KBr disks.

the slight yellow coloration and to adsorb the colloidal sulfur. On cooling, the clear filtrate deposited shining, colorless crystals which were purified by recrystallizing twice from warm water.

Anal. Calcd. for $[Cu\{SC(NHCH_2)_2\}_4]NO_3$: C, 26.93; H, 4.50; S, 23.96; N, 23.56. Found C, 27.27; H, 4.46; S, 23.71; N, 23.66.

RESULTS AND DISCUSSION

The infrared absorption spectra of ethylenethiocarbamide, tetrakis(ethylenethiocarbamide)copper(I) nitrate and potassium nitrate in potassium bromide disks are given in Fig. 1.

The peaks at 3.08μ and 3.48μ observed for both the complex and the ligand can be assigned, respectively, to the NH and CH_2 stretching frequencies. The corresponding deformation frequencies are observed in the longer wavelength region (longer than 6μ). Thus, the band at 6.6μ of tetrakis(ethylenethiocarbamide)copper-(I) nitrate and ethylenethiocarbamide can be assigned to NH deformation and that at 7.2μ of the complex to the overlapping of the CH_2 deformation vibrations and one of the NO_3^- vibrations and possibly to C=S vibration.

We may consider the vibrations of the $-CH_2-CH_2-$ grouping of the ligand to be similar to those of the normal vibrations of the gauche form of 1,2-dichloroethane for which Nakagawa and Mizushima[3] have made calculations. According to these calculations the bands observed at 7.65μ and 7.84μ may tentatively be ascribed largely to CH_2 wagging vibration; those at 8.3μ and 8.43μ to CH_2 twisting vibration; that at 10μ to C—C stretching vibration; and that at 11μ to CH_2 rocking vibration. Undoubtedly, some of the frequencies of the ring

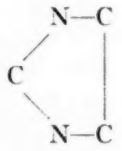

should also appear in these frequency ranges, and therefore some of the observed bands should be ascribed to these motions, possibly mixed with the CH_2 vibrations.

The spectrum of the copper(I) complex can be explained satisfactorily as the superposition of the spectra of ethylenethiocarbamide and the nitrate ion. Thus the peak at 12.16μ observed for the complex is explained as due to the nitrate ion contained in the complex. In this connection it is very interesting to find a peak at 14.0μ for the coördination compound, while no corresponding peak appears for the ligand nor for the potassium nitrate. This wavelength corresponds to an inactive frequency for the nitrate ion which can be observed as the Raman frequency. Therefore, this peak may be assigned to this vibration which is considered to become infrared active because of the distortion of the symmetrical structure in the formation of the solid complex compound. The band at 9.6μ observed for the complex may be explained quite similarly. This wavelength is close to the frequency of a strong Raman line, 1050 cm^{-1}, which is inactive in the infrared absorption. A very weak absorption seems to exist at 9.6μ for ethylenethiocarbamide; therefore, the fairly strong absorption at this wavelength may be explained as the overlapping of the two bands.

[3] I. Nakagawa and S. Mizushima, J. Chem. Phys. **21**, 2195 (1953). We are indebted to Professor San-ichiro Mizushima, University of Tokyo, for a discussion which brought to light these relationships.

Theory of the Differential Capacitance of the Double Layer in Unadsorbed Electrolytes

JAMES ROSS MACDONALD
Texas Instruments Incorporated, 6000 Lemmon Avenue, Dallas 9, Texas
(Received March 4, 1954)

A partly phenomenological, one-dimensional theory is presented of the double layer formed at an ideal polarized electrode in uni-univalent aqueous electrolytes showing no specific adsorption. The system analyzed consists of the metallic electrode with its surface charge density, a charge-free layer next to the electrode, and a diffuse layer containing positive and negative charges in unequal concentration extending into the body of the electrolyte. The theory includes the effect of dielectric saturation in both layers due to the field produced by an applied negative bias potential, and compression of the charge-free layer by this field is also taken into account.

The theory is compared with experimental data of D. C. Grahame on 0.916 N to 0.001 N NaF, which shows little or no adsorption on negative polarization. Good agreement is found both for the dependence of the differential capacitance of the entire system on negative polarizing potential (measured from the electrocapillary maximum) and on concentration. Such agreement allows several constants of the charge-free layer to be obtained relatively accurately. In particular, values for its initial thickness, modulus of linear compressibility, initial dielectric constant, and dielectric saturation constant are obtained. Comparison of these results with corresponding results for bulk water affords strong evidence that the charge-free layer consists of a single molecule of water and thus that cations nearest the polarized electrode are hydrated.

INTRODUCTION

THE study of the electrical double layer in electrolytes has been recognized for a long time as a fruitful avenue of investigation of the microscopic properties of solute and solvent. The experimental and theoretical work of Grahame[1–3] over the past ten years has done much to clarify the physical situation in an electrolyte adjacent to an ideal, polarized metallic electrode. Since such an electrode is blocking and will not allow conduction current to flow in either direction at the junction with the electrolyte, a final static distribution of charge in the electrolyte will eventually be reached after a potential difference is established between the electrode and the bulk of the electrolyte. It is, of course, necessary in practice that the applied potential difference be sufficiently small that there is negligible hydrogen evolution at the electrode in order that the electrode approximate ideal polarized behavior; we shall assume that this condition is always satisfied.

The double layer which is established near the metallic electrode is generally considered[3] to consist of four regions, and so is really not a double layer at all. These regions comprise the metallic electrode, on whose surface there may be an excess or deficit of electrons, an inner region next to the electrode into which the electrical centers of ions cannot move because of their physical size, a further region accessible to the electrical centers of anions but not of cations, and a final region of the diffuse type containing both anions and cations in differing concentrations. If there is a layer of anions in the third region at their distance of closest approach to the electrode, this layer is termed the adsorbed layer because the anions are held not by simple Coulomb forces but by specific short-range forces.

The presence of specific adsorption considerably complicates an analytical treatment of the double layer problem. In the present work, we shall therefore consider only those situations where such adsorption is absent. The double layer then consists of surface charge on the electrode, a charge-free region next to the electrode, and a diffuse region extending on into the bulk of the electrolyte. This situation is found experimentally on negative polarization of such solutes as NaF whose anions are not specifically adsorbed at a mercury electrode.[1]

The diffuse layer has been fully treated theoretically by Müller,[4] Grahame,[1,2] and the present author together with M. K. Brachman.[5] A theoretical analysis of the entire system without adsorption has not as yet been given. Grahame has, however, treated the problem by combining theoretical results for the diffuse layer with experimental results for the initial charge-free layer.[1] A theoretical treatment of the charge-free layer as well as the diffuse layer should allow some of the properties of the initial layer to be deduced by comparison of theory and experiment. The present work is designed to allow such information to be obtained and treats the entire system in a theoretical, although partly phenomenological, fashion.

The simplest measurements that can be carried out on the entire electrode-electrolyte system are determinations of the dependence of the differential capacitance of the whole system $C_T{}^d$ on static bias potential and on electrolyte concentration. It is found that the resulting curves are quite complex even in the absence of adsorption. Present qualitative explanations of their

[1] D. C. Grahame, Chem. Revs. **41**, 441 (1947).
[2] D. C. Grahame, J. Chem. Phys. **18**, 903 (1950).
[3] D. C. Grahame, Comptes Rendus de la III[e] Réunion, Comite International de Thermodynamique et de Cinetique Electrochimiques, Berne, 8–12 August, 1951. References to further work of Grahame and others will be found in these first three references.
[4] H. Müller, Cold Spring Harbor Symposia Quant. Biol. **1**, 1 (1933).
[5] J. R. Macdonald and M. K. Brachman, J. Chem. Phys. **22**, 1314 (1954).

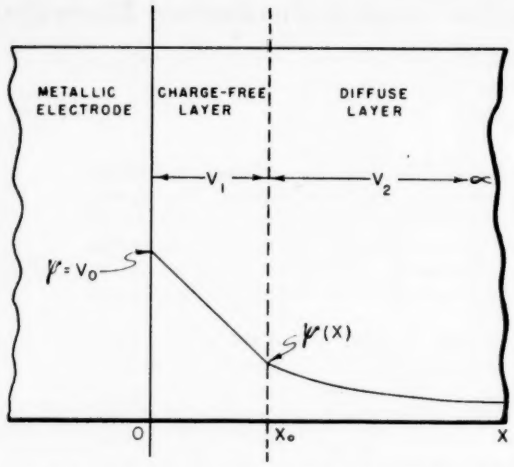

FIG. 1. Schematic representation of the electrical double layer without specific absorption. The dependence of the potential ψ on position is shown for positive polarization ($V_0>0$).

complicated dependence by Grahame[3] and others include the effects of high-field dielectric saturation and of high-field compression of the charge-free layer, increasing as the polarizing potential is increased. Both of these phenomena are included in the present theory, and it is found that they can indeed explain many of the experimental results.

The matter of potentials between different phases in the system is fairly complicated and is dealt with at length by Grahame.[1] For our purposes, it is only necessary to know that when the applied potential between the polarized electrode and the body of the electrolyte is equal to the electrocapillary maximum potential, there is no surface charge on the polarized electrode.[1] We shall therefore choose to measure applied potential V_0 from this point and specify that the surface charge is zero at $V_0=0$.

The one-dimensional system which we shall analyze is shown in Fig. 1. An ideal polarized metallic electrode is placed at $x=0$. This electrode is blocking for both positive and negative charge carriers. Next to this electrode there is a charge-free layer extending to $x=x_0$. Finally, polar material containing univalent positive and negative charge carriers extends from $x=x_0$ to $x=\infty$. The dielectric constants in the two layers may be different and may depend on electric field strength and position. Also, the thickness x_0 of the charge-free layer may be a function of electric field strength. We are interested in the dependence of the differential capacitance $C_T{}^d$ of this whole system on the applied dc bias potential V_0 and on the bulk concentration of the charge carriers. As shown in the figure, the zero of potential is taken at $x=\infty$, and the potential drop across the charge-free layer designated as V_1, that across the diffuse layer by V_2. The mean local potential inside the material ψ will thus be zero at $x=\infty$ and equal to V_0 at $x=0$.

In order to simplify the succeeding work, we shall introduce the following normalized quantities: $\psi^*=\psi/(kT/e)$; $V^*=V/(kT/e)$; $\mathcal{E}^*=\mathcal{E}/(kT/eL_D{}^0)$; $\rho^*=\rho/2c_0e$; $\sigma^*=\sigma/(kT/e)$; $z=x/L_D{}^0$. In these expressions $\mathcal{E}$ is the mean local field strength within the material, ρ the volume charge density, and σ a surface charge density. The normal concentration of positive or negative ions in the bulk of the material far from the electrode is c_0, and the Debye length $L_D{}^0$ in the diffuse layer is given by $[\epsilon_2{}^0kT/8\pi c_0e^2]^{\frac{1}{2}}$ for zero applied voltage. In this expression, $\epsilon_2{}^0$ is the static dielectric constant in the diffuse layer for $V_0=0$. In general, we shall use a superscript zero to designate the value of a quantity at zero potential and the subscripts one and two to identify quantities defined in the charge-free and diffuse layers, respectively.

CONDITIONS IN THE DIFFUSE LAYER

In order to obtain the differential capacitance of the complete system, it is necessary to determine the charge and potential distributions within the system when an external bias potential is applied. It will be most convenient to consider first conditions within the diffuse layer. The dependence of charge density on potential in this layer may be obtained either from the Debye-Hückel equations[5] or by potential energy considerations.[1,4] The result obtained is

$$\rho^*(z)=-sinh\psi^*(z). \tag{1}$$

This result holds for either anodic or cathodic polarization. If a positive potential is applied to the electrode at $x=0$, $V_2{}^*$, ψ^*, and $\mathcal{E}^*$ will all be positive quantities.

Next, we need to know the dependence of $\mathcal{E}_2{}^*$, the normalized field strength in the diffuse layer at $z=z_0$ on $V_2{}^*$. To obtain this result we shall require expressions for the dependence on field strength of the static dielectric constant and the differential dielectric coefficient. These quantities are defined by $\epsilon=D^*/\mathcal{E}^*$ and $\kappa=dD^*/d\mathcal{E}^*$, respectively, where D^* is the normalized electric displacement. They therefore satisfy the relation

$$\mathcal{E}^*\frac{d\epsilon}{d\mathcal{E}^*}=(\kappa-\epsilon). \tag{2}$$

Grahame[2] has given a rather complete discussion of dielectric saturation effects in the diffuse layer, and we shall draw heavily on his work for the results of the present section. In particular, since there is no adequate fundamental theory of dielectric saturation in a polar material, we shall use Grahame's heuristic formula for field-strength dependence

$$\kappa=c_2+a_2[1+2b_2\mathcal{E}^2]^{-\frac{1}{2}}=c^2+a_2[1+2b_2{}^*\mathcal{E}^{*2}]^{-\frac{1}{2}}, \tag{3}$$

where c_2, a_2, and b_2 are constants. Grahame actually considers a family of equations similar to (3) and decides that the form (3) is one of a number of reasonable choices which will fit experimental data on electrolytes. We choose the specific form (3) because it lends

itself to algebraic and numerical calculations. Note that if b_2 is independent of concentration, $b_2^* \equiv (kT/eL_D^0)^2 b_2$ will depend thereon because of the presence of L_D^0.

The effective static dielectric constant may be derived from (3) by integration. We find, using Eq. (2),

$$\epsilon = \frac{1}{\mathcal{E}^*}\int_0^{D^*} dD^* = \frac{1}{\mathcal{E}^*}\int_0^{\mathcal{E}^*} \kappa d\mathcal{E}^*$$

$$= c_2 + a_2[(2b_2^*)^{\frac{1}{2}}\mathcal{E}^*]^{-1} \sinh^{-1}[(2b_2^*)^{\frac{1}{2}}\mathcal{E}^*]. \quad (4)$$

It follows that when $\mathcal{E}^*=0$, $\epsilon=\epsilon^0=\kappa=\kappa^0=a_2+c_2$. Also, when $\mathcal{E}^*=\infty$, $\epsilon=\epsilon^\infty=\kappa=\kappa^\infty=c_2$. Thus, c_2 is the nonpolar contribution to the dielectric constant remaining after the polar contribution has been completely saturated. It is perhaps worth mentioning that the mean local field $\mathcal{E}^*$ appearing in these expressions is that computed from the charge distribution at equilibrium after a dc potential has been applied so long that the initial charging current has died out.

The dependence of $\mathcal{E}_2^*$ on V_2^* may now be obtained from Poisson's equation written in terms of normalized variables as

$$-\frac{dD^*}{dz} = -\left\{\mathcal{E}^*\frac{d\epsilon}{d\mathcal{E}^*} + \epsilon\right\}\frac{d\mathcal{E}^*}{dz} = -\kappa\frac{d\mathcal{E}^*}{dz}$$

$$= \kappa\frac{d^2\psi^*}{dz^2} = \frac{\kappa}{2}\frac{d}{d\psi^*}(\mathcal{E}^*)^2 = -\epsilon_2^0\rho^*(z). \quad (5)$$

Equation (2) was used in simplifying this equation. We now introduce Eq. (1) in (5) and integrate

$$\int_0^{\mathcal{E}_2^*} \kappa d(\mathcal{E}^*)^2 = -2\epsilon_2^0\int_0^{V_2^*}\rho^* d\psi^* = 2\epsilon_2^0\int_0^{V_2^*}\sinh\psi^* d\psi^*.$$

Using Eq. (3) for κ, we find

$$c_2\mathcal{E}_2^{*2} - a_2/b_2^* + (a_2/b_2^*)(1+2b_2^*\mathcal{E}_2^{*2})^{\frac{1}{2}} = 4\epsilon_2^0\sinh^2(V_2^*/2). \quad (6)$$

Equations formally identical to (4) and (6) have been given by Grahame.[2] Now let

$$u \equiv (2b_2^*)^{\frac{1}{2}}\mathcal{E}_2^*, \qquad B \equiv (1+u^2)^{\frac{1}{2}}, \quad (7)$$

and

$$\eta = 2b_2^*\sinh^2(V_2^*/2).$$

We find from (6) that

$$B = -a_2/c_2 + [(\epsilon_2^0/c_2)^2 + (4\epsilon_2^0/c_2)\eta]^{\frac{1}{2}}, \quad (8)$$

and since from (7)

$$u = (B^2-1)^{\frac{1}{2}}, \quad (9)$$

we have succeeded in expressing $\mathcal{E}_2^*$ in terms of V_2^*. If $\mathcal{E}_2^*$ is known, we can compute u; and from a curve of u *versus* η, then compute η. Finally V_2^* can be obtained most simply from the relation

$$\cosh V_2^* = 1 + \eta/b_2^*. \quad (10)$$

Of couse, if V_2^* is known, the equations can be used directly to calculate $\mathcal{E}_2^*$. It is worth pointing out that, although $\mathcal{E}^*$ will vary with position in the diffuse layer, thereby causing κ and ϵ to vary also, the calculation of the differential capacity of either the diffuse layer[2] of or the whole system requires only a knowledge of the functional dependence of $\mathcal{E}_2^*$ on V_2^*.

CONDITIONS IN THE CHARGE-FREE LAYER

Since by definition there is no charge in the charge-free layer, we may solve Laplace's equation directly for this region with the boundary conditions $\psi^*=V_0^*$ at $z=0$ and $\psi^*=V_2^*$ at $z=z_0$. We assume that there is no discontinuity in potential at the plane $z=z_0$. Since $V_1^*=V_0^*-V_2^*$ is the potential difference across the layer, we obtain from Laplace's equation

$$\mathcal{E}_1^* = V_1^*/z_0, \quad (11)$$

and

$$\psi^* = V_0^* - (z/z_0)V_1^*. \quad (12)$$

The field strength $\mathcal{E}_1^*$ is constant in the region $0 \leqslant z \leqslant z_0$.

Next, we must consider the effects of dielectric saturation in the charge-free layer. We shall choose equations for the dependence of ϵ_1 and κ_1 on $\mathcal{E}_1^*$ of the same form as those used for these quantities in the diffuse layer. However, since the charge-free layer may have properties different from those of the solvent, the constants which enter the saturation equations must be taken different from those of the diffuse layer for generality. Even when the charge-free layer does consist of solvent material (perhaps only one or two molecules thick), one would not necessarily expect that the saturation and other constants of the material on such a microscopic scale should be equal to the corresponding constants of the bulk material. The equations therefore are

$$\kappa_1 = c_1 + a_1[1+2b_1^*\mathcal{E}_1^{*2}]^{-\frac{1}{2}}, \quad (13)$$

and

$$\epsilon_1 = c_1 + a_1[(2b_1^*)^{\frac{1}{2}}\mathcal{E}_1^*]^{-1}\sinh^{-1}[(2b_1^*)^{\frac{1}{2}}\mathcal{E}_1^*]. \quad (14)$$

Thus,

$$\kappa_1^0 = \epsilon_1^0 = c_1 + a_1.$$

Finally, we must consider the possibility that a high electric field strength in the charge-free layer can cause compression of this layer. In an aqueous electrolyte, one might expect the thickness of the charge-free layer to be the sum of the ionic radius of the ion attracted to the electrode plus the diameter of one or more water molecules if the ion is hydrated. If the force between ion and electrode is made sufficiently great, any water molecules present between the two will be flattened, and the shape of the ion itself may be somewhat distorted. Such compression might be expected to be linear for relatively small pressures with a gradual transition to a much smaller dependence on pressure for higher pressures.

We shall choose the following heuristic expression to represent the dependence of the thickness of the

charge-free layer on pressure applied to it:

$$z_0/z_0^0=[1+\beta p]^{-1}, \tag{15}$$

where β is a constant and z_0^0 is the value of z_0 for $V_0^*=0$. Note that in the present one-dimensional treatment no distinction need be made between force and pressure. The above expression is linear for $\beta p \ll 1$, yet an infinite pressure is required to reduce z_0 to zero. Equation (15) should be a good approximation for small pressures, but it certainly cannot be expected to represent the behavior of real materials very accurately at high pressures such as those present in the charge-free layer when a relatively large negative polarizing potential is applied. Greater accuracy might be obtained by using a more sophisticated equation of state applicable to the actual material of the charge-free layer. Nevertheless, we shall see later that the above simple expression actually seems to describe the behavior of the charge-free layer quite accurately for aqueous electrolytes. The use of a more complicated expression is therefore not justified at present.

The electrostrictive pressure in the material is, from electrostatic theory,[6]

$$p=\epsilon_1\mathcal{E}_1^2/8\pi. \tag{16}$$

We may now rewrite Eq. (15) as

$$z_0/z_0^0=[1+(\beta/8\pi)\epsilon_1\mathcal{E}_1^2]^{-1}=[1+\alpha\epsilon_1\mathcal{E}_1^2]^{-1} =[1+\alpha^*\epsilon_1\mathcal{E}_1^{*2}]^{-1}, \tag{17}$$

where $\alpha=\beta/8\pi$ is another constant. This equation is more formidable than it appears, since ϵ_1 is also a function of $\mathcal{E}_1$ as shown by (14). We shall neglect any direct dependence of ϵ_1 and κ_1 on pressure since this effect can be at least partly included together with their dependence on the field $\mathcal{E}_1$ which produces the pressure.

Finally, it will be useful to derive the initial isothermal modulus of linear compressibility δ^0 from (15). Since $\delta^0=-(z_0^0)^{-1}(\partial z_0/\partial p)_T$ evaluated at $p=0$, we find

$$\delta^0=\beta=8\pi\alpha. \tag{18}$$

Since α can be obtained by fitting experimental results with the theory, δ^0 may also be obtained.

JOINING CONDITIONS AT $z=z_0$

Since we have specified that there be no discontinuity in potential across the plane $z=z_0$, the principal additional condition which must be satisfied there is that the normal component of the electric displacement be continuous. In this one-dimensional treatment, this is the only component present and we obtain

$$D_1^*=D_2^*, \tag{19}$$

or

$$w\equiv(2b_1^*)^{\frac{1}{2}}\mathcal{E}_1^*\epsilon_1=(2b_1^*)^{\frac{1}{2}}\mathcal{E}_2^*\epsilon_2=(b_1^*/b_2^*)^{\frac{1}{2}}\epsilon_2 u.$$

This may be written as

$$w=(b_1^*/b_2^*)^{\frac{1}{2}}[c_2u+a_2\sinh^{-1}u], \tag{20}$$

using Eqs. (4) and (7). We thus see that if $\mathcal{E}_1^*$ is specified, w may be computed using (14) and u determined from a graph of w *versus* u. We can then calculate V_2^*, as discussed previously, and can obtain V_1^* from (11) if z_0 is known. From $V_0^*=V_1^*+V_2^*$, we can finally obtain the applied potential which would result in the value of $\mathcal{E}_1^*$ originally assumed. This appears to be a complicated procedure but, since most of the quantities in which we are interested are implicit functions of each other, it seems to be the simplest possible method.

THE DIFFERENTIAL CAPACITANCE FORMULA

The introduction of dielectric saturation in both layers and compression of the first layer complicates the calculation of the total differential capacitance. It may be obtained from any of the following equivalent equations

$$C_T{}^d=\frac{d\sigma_m^*}{dV_0^*}=\frac{d\sigma_m^*}{d\mathcal{E}_2^*}\frac{d\mathcal{E}_2^*}{dV_2^*}\frac{dV_2^*}{dV_0^*}=\frac{d\sigma_m^*}{d\mathcal{E}_1^*}\frac{d\mathcal{E}_1^*}{dV_0^*}. \tag{21}$$

Here, σ_m^* is the normalized charge density on the metal electrode. We shall use the last of these expressions since it turns out to be the simplest to apply. We shall now calculate the factors in this expression separately. The first is readily obtained from Gauss' law, $D^*=4\pi\times L_D{}^0\sigma_m^*$, written in terms of normalized variables. On differentiating this equation with respect to $\mathcal{E}_1^*$ and using the definition of κ_1 we find

$$\frac{d\sigma_m^*}{d\mathcal{E}_1^*}=\frac{\kappa_1}{4\pi L_D{}^0}. \tag{22}$$

The calculation of $(d\mathcal{E}_1^*/dV_0^*)$ is considerably more difficult. If we take $z=z_0$ in (12) and differentiate with respect to $\mathcal{E}_1^*$, using $V_0^*=V_1^*+V_2^*$ and (11), we obtain

$$\left(\frac{d\mathcal{E}_1^*}{dV_0^*}\right)^{-1}=\frac{d\psi^*}{d\mathcal{E}_1^*}+z_0+\mathcal{E}_1^*\frac{dz_0}{d\mathcal{E}_1^*}. \tag{23}$$

The last term may be calculated from (17) using (2). We obtain

$$\mathcal{E}_1^*\frac{dz_0}{d\mathcal{E}_1^*}=\left(1+\frac{\kappa_1}{\epsilon_1}\right)(z_0-z_0^0)(z_0/z_0^0). \tag{24}$$

Further, we find from (19) that at $z=z_0$

$$\frac{d\psi^*}{d\mathcal{E}_1^*}=\frac{\kappa_1}{\kappa_2}\frac{d\psi^*}{d\mathcal{E}_2^*}. \tag{25}$$

Equation (5) may be rewritten as

$$\frac{d^2\psi^*}{dz^2}=-\mathcal{E}^*\frac{d\mathcal{E}^*}{d\psi^*}=-\epsilon_2{}^0\rho^*/\kappa. \tag{26}$$

[6] L. Page and N. I. Adams, *Principles of Electricity* (D. Van Nostrand Company, Inc., New York, 1949), second edition, p. 50.

If we now substitute (1) in (26) and evaluate the result in the diffuse layer at $z=z_0$, we finally obtain

$$\frac{d\psi^*}{d\mathcal{E}_2^*}=\frac{\kappa_2}{\epsilon_2^0}\frac{\mathcal{E}_2^*}{\sinh V_2^*}. \tag{27}$$

These results may now be substituted in Eq. (21) to yield the following formula for C_T^d

$$C_T^d=C_1^0\left[\left(\frac{\kappa_1^0}{\kappa_1}+\frac{\epsilon_1^0}{\epsilon_1}\right)\left(\frac{z_0}{z_0^0}\right)^2 -\frac{\epsilon_1^0}{\epsilon_1}\left(\frac{z_0}{z_0^0}\right)+\gamma\mathcal{E}_2^*(\sinh V_2^*)^{-1}\right]^{-1}, \tag{28}$$

where

$$\gamma\equiv\kappa_1^0/(\kappa_2^0 z_0^0)=(\kappa_1^0 L_D^0)/(\kappa_2^0 x_0^0) \tag{29}$$

and

$$C_1^0\equiv\kappa_1^0/(4\pi x_0^0). \tag{30}$$

The quantity C_1^0 is the differential (and static) capacitance of the first layer alone with $V_0^*=0$. Similarly, the corresponding capacitance of the diffuse layer for $V_0^*=0$, C_2^0, may be obtained from

$$C_2^0=(d\sigma_m^*/dV_2^*)_{V_0^*=0}$$

and Eqs. (19), (22), and (27), together with the limiting result that $\mathcal{E}_2^*/\sinh V_2^*=1$ at $V_0^*=0$. This result itself follows directly from Eq. (6). We finally obtain

$$C_2^0\equiv\kappa_2^0/(4\pi L_D^0). \tag{31}$$

We thus note that $\gamma=C_1^0/C_2^0$ and that Eq. (28) yields the usual expression for these two capacitances in series at $V_0^*=0$. In the opposite limit of very high applied potentials, Eq. (6) shows that $\mathcal{E}_2^*/\sinh V_2^*$ approaches zero, so that C_T^d approaches

$$C_1^0\left[\left(\frac{\kappa_1^0}{\kappa_1^\infty}+\frac{\epsilon_1^0}{\epsilon_1^\infty}\right)\left(\frac{z_0^\infty}{z_0^0}\right)^2-\left(\frac{\epsilon_1^0}{\epsilon_1^\infty}\right)\left(\frac{z_0^\infty}{z_0^0}\right)\right]^{-1},$$

which may considerably exceed C_1^0 if $z_0^\infty\ll z_0^0$. Equation (28) is independent of the sign of V_0^* since $\mathcal{E}_2^*$ and V_2^* will always have the same sign. Although the method of obtaining Eq. (28) is completely general, the equation itself applies only to the case where z_0/z_0^0 is given by (17).

The use of Eq. (28) to calculate C_T^d for a given value of V_0^* is not completely straightforward even when all the constants are known because of the implicit relations between the various variables. In practice such calculation can be carried out most simply by first calculating the values of κ_1, ϵ_1, and w corresponding to an initially selected value of $\mathcal{E}_1^*$. The quantity u is then determined from a graph of w *versus* u and this value of u entered in a graph of η *versus* u to yield the corresponding value of η. Then, V_2^* can be calculated from Eq. (10). Next, after calculating z_0 from (17), V_1^* can be obtained using (11). The normalized applied potential $V_0^*=V_1^*+V_2^*$ corresponding to the selected value of $\mathcal{E}_1^*$ is thus finally obtained and the value of C_T^d corresponding to this potential obtained from (28), all of whose factors are now known.

There are, unfortunately, a number of constants entering the theory which will not be known independently of measurements of C_T^d *versus* V_0. Thus, in order to fit the theoretical curves to such data, the constants will have to be derived from the data. Luckily, most of the constants are independent of each other. First, $\kappa_2^0=\epsilon_2^0$ is just the normal dielectric constant of the solution; for aqueous solutions, it will be that of water at the given temperature with possibly a small correction for solute concentration at high concentrations. The quantity $c_2=\kappa_2^\infty$ is the nonpolar part of the dielectric constant of the diffuse layer remaining after the polar contribution is saturated by a high electric field. It may be approximately inferred from the optical index of refraction. Since the frequency at which differential capacitance measurements are commonly carried out is less than 10^5 cps, the use of n^2 for c_2 represents a hazardous extrapolation. Hasted and El Sabeh[7] quote a figure of 4 for the far infrared dielectric constant of water. From their measurements on water at wavelengths between 1 and 10 cm, however, they find a high-frequency limiting dielectric constant ϵ_∞ of 5.2 ± 0.5 at 20° and 30°C. This latter figure should at least approximately represent the dielectric constant of water after the polar contribution is entirely relaxed. We shall therefore choose the value $c_2=5$ for the diffuse layer. In addition, since evidence to be presented later derived from the experimental data on NaF indicates that the charge-free layer itself consists of water molecules, we shall take the same value for c_1 and let $c_1=c_2\equiv c=5$. The lack of a more precise value for c will not affect most of our conclusions appreciably.

Luckily, it is possible to obtain the ratio κ_1^0/x_0^0 in an unambiguous way from measurements of C_T^d at $V_0^*=0$ for various concentrations.[8] This is the case because the constants α and b which control compression and saturation arising from the applied field have no effect on the value of C_T^d at $V_0^*=0$. Further, κ_1^0/x_0^0 is essentially independent of concentration in NaF and other electrolytes which show no specific absorption. After the determination of κ_1^0/x_0^0, κ_1^0 can be determined either from an independently known value of x_0^0, or can be found from detailed curve fitting. In the latter case, x_0^0 is itself determined. Finally, the constants a_1, b_1, b_2, and α must be found from a fit of the experimental curve of C_T^d *versus* V_0 for a given concentration. A check of the resulting values can then be made by using the same values to compute the theoretical dependence of C_T^d on V_0 for another concentration for comparison with experimental results. The agreement between theory and experiment should be good for

[7] J. B. Hasted and S. H. M. El Sabeh, Trans. Faraday Soc. **49**, 1003 (1953).

[8] J. R. Macdonald, J. Chem. Phys. **22**, 763 (1954).

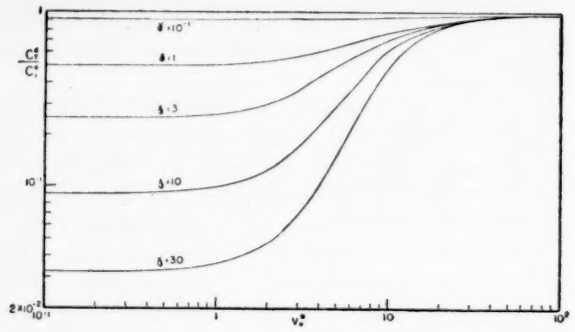

FIG. 2. Dependence of normalized differential capacitance on normalized potential for different values of $\gamma = C_1^0/C_2^0$ with no dielectric saturation and no compression.

the new concentration for a correct initial choice of the constants.

When $\alpha = b_1 = b_2 = 0$, the formula for $C_T{}^d$ and its calculation for various values of $V_0{}^*$ is greatly simplified. The capacitance of the initial charge-free layer is then $C_1{}^0$ and is independent of applied potential. This capacitance is in series with the normal differential capacitance of the diffuse layer without dielectric saturation, $C_2{}^d$. This capacitance is nonlinear and depends strongly on $V_0{}^*$. Curves showing the dependence of the total capacitance $C_T{}^d$ on $V_0{}^*$ for this situation are presented in Fig. 2, with γ as a parameter. The shape of these curves is readily explained. When γ is large, $C_1{}^0$ is much larger than $C_2{}^0$. Thus, $C_2{}^0$ determines the value of $C_T{}^d$ for $V_0{}^* < 1$. However, as $V_0{}^*$ increases, $C_2{}^d$ increases until it is much larger than $C_1{}^0$, which itself then determines $C_T{}^d$. On the other hand, when $\gamma \ll 1$, $C_2{}^d$ is much larger than $C_1{}^0$ for all values of $V_0{}^*$, so that $C_T{}^d$ is essentially independent of $V_0{}^*$. Note that at 25°C, a value of 10 for $V_0{}^*$ corresponds to an applied potential of about 0.26 volt; thus, saturation of these curves occurs at low potentials.

COMPARISON WITH EXPERIMENT

In this section, we shall compare the predictions of the theory with experimental data on NaF for various concentrations at 25°C. These data were obtained by D. C. Grahame,[9] who has found that NaF shows little or no specific adsorption on negative polarization. Although the theory indicates that the shape of the $C_T{}^d$ *versus* V_0 curves should be symmetric about $V_0 = 0$, the experimental curve shape for $V_0 > 0$ differs from that for $V_0 < 0$ even for NaF. The lower the concentration, the larger the range of $|V_0|$ about zero over which the symmetry is preserved, but even at 0.001N deviations between the two halves begin to appear for $|V_0| \gtrsim 0.2$ volt. It is probable that the large increase in $C_T{}^d$ observed with strong positive polarization arises from specific adsorption of the highly polarizable anions. Since we present theory does not include adsorption effects, we shall restrict attention to data for which $V_0 < 0$.

The first step in the curve-fitting is the calculation of $\kappa_1{}^0/x_0{}^0$. We take $\kappa_2{}^0$ and $\epsilon_2{}^0$ as 78.5, the value for water at 25°C.[10] We shall neglect the small concentration dependence of these quantities. After calculating $L_D{}^0$ for the various concentrations, $C_2{}^0$ can be computed from theory. Finally, $C_1{}^0$ can be obtained from the experimental values of $C_T{}^d$ at $V_0 = 0$ and the values of $C_2{}^0$. Then γ can be calculated for each concentration. The resulting values of $\kappa_1{}^0/x_0{}^0$ are shown in Table I. Since $\kappa_1{}^0/x_0{}^0$ is determined from the difference of two large numbers for low concentrations, the resulting values are inaccurate. The value of $\kappa_1{}^0/x_0{}^0$ is essentially constant for concentrations of 0.1N and higher; thus, we have averaged the last three values in the table to obtain the value $\kappa_1{}^0/x_0{}^0 = 3.257 \times 10^8$ cm^{-1}, which may be presumed to be independent of concentration. The corresponding value of $C_1{}^0$ is 28.9 μf/cm^2. We have used this average value of $\kappa_1{}^0/x_0{}^0$ in the computation of the γ's which also appear in Table I.

We now have sufficient information to compare the theoretical curves for the various γ's with the experimental results, provided that we take $\alpha = b_1 = b_2 = 0$. Such comparison is presented in Fig. 3. The curve for 0.660N is omitted since it is similar to that for 0.916N and lies too close to it for clarity of presentation. Two conclusions may be drawn from this graph; first, that agreement between theory and experiment is satisfying for very low potentials near $V_0 = 0$; and second, that the deviations between theory and experiment begin to occur at lower and lower potentials the higher the concentration. It is worth noting that the agreement indicated in Fig. 3 is based on the use of only a single constant, $\kappa_1{}^0/x_0{}^0$, derived from the experimental results.

In the preceding theoretical development, we have introduced the saturation constants b_1 and b_2, which are, in general, unequal. For the present comparison with experiment, however, it turns out that although there is appreciable saturation in the diffuse layer with a large polarizing potential applied, such saturation has only a very small effect on $C_T{}^d$.[2,9] The reason for this behavior is that when the potential across the diffuse layer is sufficiently large to produce saturation, it is also large enough to increase the capacitance of this layer to the point where it no longer has much effect on the total capacitance $C_T{}^d$. Thus, the value of b_2 chosen will have little effect on the shape of the

TABLE I. Dependence of $\kappa_1{}^0/x_0{}^0$ and $\gamma (= C_1{}^0/C_2{}^0)$ on concentration for NaF at 25°C.

Normality:	10^{-3}	10^{-2}	10^{-1}	0.660	0.916
$\kappa_1{}^0/x_0{}^0$(cm^{-1}):	$3.79 \cdot 10^8$	$3.39 \cdot 10^8$	$3.268 \cdot 10^8$	$3.241 \cdot 10^8$	$3.293 \cdot 10^8$
γ:	3.97	1.26	0.397	0.155	0.131

[9] D. C. Grahame (private communication). To be published in J. Am. Chem. Soc. Also available from D. C. Grahame, Amherst College, as O.N.R. Report No. 14, 18 February, 1954.

[10] Dorsey, *Properties of Ordinary Water-Substance* (Reinhold Publishing Corporation, New York, 1940), p. 367.

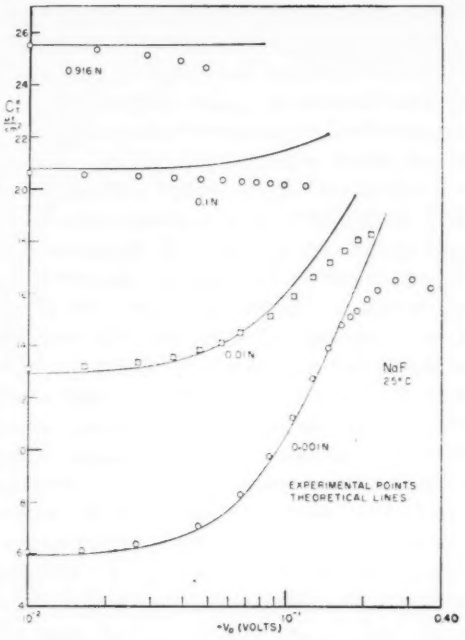

FIG. 3. Comparison of theory without dielectric saturation and compression with experimental data on NaF at 25°C.

$C_T{}^d$ curves, and b_2 cannot therefore be obtained even as to order of magnitude from $C_T{}^d$ data. Since there is evidence that the charge-free layer consists of water, one might expect that b_1 would equal b_2 unless local conditions near the boundary should preferentially affect b_1. We shall therefore choose $b_1=b_2\equiv b$. The value of b derived from the data will thus apply to the charge-free layer and will be only slightly affected by any difference between b_1 and b_2. While it would be possible to take $b_2=0$ with less than a percent change in the theoretical curves, it seems preferable to include its small effect as above, especially since it is possible to obtain agreement between theory and experiment to better than two percent when the assumption that b_1 is equal to b_2 is made.

Next, we shall discuss the determination of the constants $\kappa_1{}^0$, α, and b, and the fitting of complete $C_T{}^d$ curves for negative polarization. It is possible to obtain an approximate value of $\kappa_1{}^0$ from the expected value of $x_0{}^0$ based on the assumption that only a single water molecule lies between the metallic electrode and each of the nearest positive ions. This assumption yields a value of $x_0{}^0$ of 4.4 A, made up of about 1.0 A, the radius of a Na^+ ion,[11] and 3.4 A, the approximate diameter of a water molecule.[12] These figures and the result for $x_0{}^0$ are quite approximate because of the difficulty of attaching a precise meaning to the diameters of contiguous ions and molecules in solution. In spite of possible inaccuracy, the figure 4.4 A furnishes a starting point for our calculations and leads to a value of about 14 for $\kappa_1{}^0$.

Initially, however, a value of $\kappa_1{}^0$ of 78.5 was used in fitting the experimental curve for 0.01N in order to see if a good fit could be achieved for this value and to see to what consequences such a value would lead. It was found that the experimental curve could indeed be fairly well fitted over its entire range provided that c was taken about 30. This large a value of the nonpolar contribution to the dielectric constant is exceedingly unlikely. Furthermore, the above value of $\kappa_1{}^0$ leads to $x_0{}^0=24$ A, a value which would require many water molecules between electrode and the nearest positive ions. Since both of these results are very unlikely, it is obviously necessary to choose a smaller value of $\kappa_1{}^0$, such as the value 14 considered above.

When the value $\kappa_1{}^0=14$ was employed together with $c=5$, values of b and α could be found which would give a fair fit of the 0.01N $C_T{}^d$ curve. However, slightly better agreement was found with $\kappa_1{}^0=15$, which still allows us to conceive of the charge-free layer as involving only a single water molecule since it yields a thickness of 4.6 A for this layer. Figure 4 shows the results of such a curve fit. Theory and experiment agree to better than two percent over the full range of V_0. Such agreement is, however, not very surprising when one remembers that we have used three or four adjustable constants in making the fit. Also shown on this graph are the curves for $\alpha=b=0$ and for $\alpha=0$ which show the individual effects of these constants. Since the best value of α has little effect on the curve near its maximum at about -0.26 volt, the initial determination of b can be carried out largely independent of knowledge of α. Then, after a good value of b has been obtained with the neglect of α, points near the high end of the curve may be used to obtain a good value of α. The

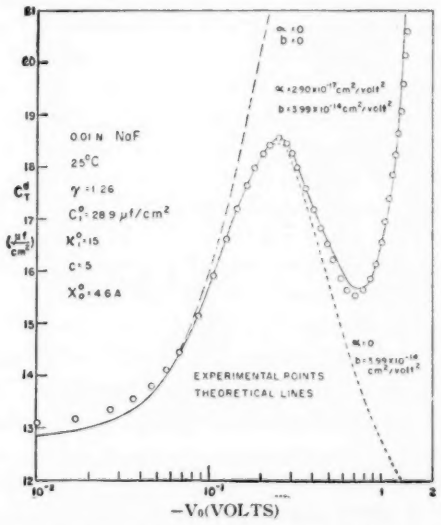

FIG. 4. Comparison of experimental data on 0.01N NaF at 25°C with theory for (a) no dielectric saturation, no compression ($\alpha=b=0$), (b) no compression ($\alpha=0$), and (c) both saturation and compression effects included.

[11] C. Kittel, *Introduction to Solid State Physics* (John Wiley and Sons, Inc., New York, 1953), p. 40.

[12] N. K. Adam, *The Physics and Chemistry of Surfaces* (Oxford University Press, London, 1941), third edition, p. 125.

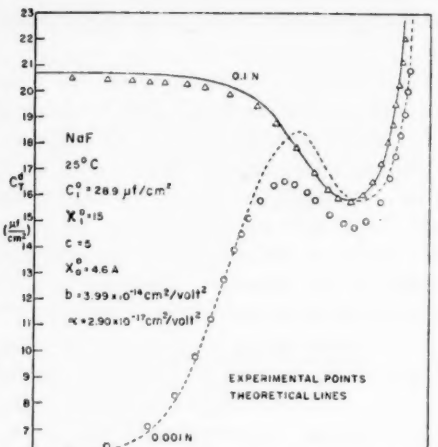

FIG. 5. Comparison of experimental data on 0.1 N and 0.001 N NaF at 25°C with theory using constants derived from 0.01 N data.

approximate independence between the effects of the two constants simplifies curve fitting greatly. It might also be mentioned that the choice of κ_1^0 has only a small effect on the value of b which allows the best fit between theory and experiment to be obtained.

The above results show that it is possible to obtain good agreement between theory and experiment for a single concentration by properly selecting several parameters. A much more stringent test of the theory is to use the parameters determined for one concentration to compute theoretical curves for comparison with experimental results for different concentrations. In Fig. 5, we show such results for 0.1N and 0.001N NaF at 25°C. The agreement between the theoretical line and the experimental points for 0.1N NaF is better than one percent over most of the range. At very small potentials, the difference is of the order of 1.5 percent. This small discrepancy (and the corresponding one for the 0.01N curve of Fig. 4) could have been reduced even further by different choices of γ. The value of γ used for each curve is that shown in Table I and is therefore that which is most consistent with the $V_0^*=0$ data for all the other concentrations. The small discrepancy between the theoretical and experimental 0.1N curves at the highest negative polarizing potentials will be discussed later in connection with the value of α. When the constants derived from the 0.01N data are used to calculate curves for the higher concentrations above 0.1N, substantially as good agreement between theory and experiment is found as that shown for the 0.1N curve.

The discrepancy between theory and experiment for the 0.001N curve also shown in Fig. 5 requires special comment, however. The evidence of good agreement between theory and experiment for all other concentrations strongly suggests that the present discrepancy arises from experimental error in the 0.001N data. Grahame[9] has analyzed these same data by a method which involves the use of an experimentally determined curve of the dependence of the differential capacitance of the charge-free layer on polarizing potential, and has likewise obtained excellent agreement between his data and calculated curves except for the present case of 0.001N. In addition, his calculated curve for 0.001N is in good agreement with that of the present work in spite of a considerable difference in the methods of calculation. Grahame himself feels that the discrepancy arises from experimental error, which is most likely to occur at this lowest concentration. The consistent agreement between theory and experiment suggests that we can have considerable confidence in the applicability of the theory to the experimental situation found with negative polarization and no adsorption. Thus the saturation and other constants derived from curve fitting should be quite accurate and should describe some of the properties of the charge-free layer well. Next, we shall compare some of these constants with corresponding values for bulk water obtained from very different experiments. The resulting agreement or disagreement should allow a decision to be reached as to the nature of the charge-free layer.

First, we have found that good agreement between theory and experiment can be obtained with $c=5$, a reasonable value for water. Even though such agreement is not strongly dependent on the value of c chosen, the above result is at least consistent with the supposition that the charge-free layer involves only a single molecule of water. The next result, $\kappa_1^0=15$, leads to a thickness for the layer again consistent with the single-molecule hypothesis. However, the value of 15 is about five times smaller than the value of the initial dielectric constant of bulk water. If this reduction were ascribed to an initial partial saturation of the layer dielectric constant by the inhomogeneous image-charge field of the nearest ion even in the absence of an applied potential, one would expect to find κ_1^0 considerably less than ϵ_1^0. On the contrary, however, the degree of agreement between the data and theory shown in Fig. 3 for potentials sufficiently small that the effect of b is still negligible can only be obtained if κ_1^0 and ϵ_1^0 are taken substantially equal. We are thus left with the possibilities that the principal material of the charge-free layer is either not water or that some of its properties are different from those of ordinary bulk water. If the charge-free layer consists of a single water molecule and half of a sodium ion, as the thickness result suggests, the initial dielectric constant of the layer could perhaps be less than that of ordinary water either because the water molecule was not surrounded by the usual number of neighboring water molecules and/or possibly because the effective dielectric constant of the layer was some kind of complicated average of the dielectric constant of a single water molecule and that of the part of the sodium ion between its center of

charge and the water molecule. In view of the conceptual difficulty in attaching a precise meaning to the dielectric constants of these microscopic entities, the discrepancy between the effective value of 15 and that of bulk water should not be weighted heavily in deciding whether the ion nearest the polarized electrode is indeed hydrated.

Next, we may compare the value of b of 3.99×10^{-14} cm^2/volt^2 obtained from the curve-fitting with that obtained for water by other methods. Malsch[2,13] found $b=1.2\times10^{-13}$ cm^2/volt^2 by direct measurement of the differential dielectric constant of water up to applied fields of the order of 2.5×10^5 volts/cm. At these fields κ would be reduced from its initial value by less than one percent by using Malsch's own value of b. Thus his result cannot be expected to be very accurate, and it is possible that our value, which is three times smaller, is the more accurate if it indeed applies to water. Since the present work shows that the field $\mathcal{E}_1$ in the charge-free layer can reach values as large as 3×10^7 volts/cm, one would expect very strong saturation effects to occur in this layer. The order of magnitude of these effects can be seen by comparing the various curves in Fig. 4. Thus the present method of obtaining b does not suffer from the disadvantage of deriving it from data for which it effect is very small, and the resulting value of b is hence probably quite accurate. Since the value of b obtained applies to a very small amount of material, however, it may be unreasonable to expect this value to be the same as that of the material in bulk. If b is the saturation constant of a single water molecule, either this constant is approximately the same as that of bulk water, in which case Malsch's result is somewhat in error, or else both values are approximately correct and the saturation constant for a single molecule of water is less than that for bulk water. Further direct measurements of κ to higher field strengths than Malsch employed will be required to decide between these possibilities. Nevertheless, the arrangement to order of magnitude between Malsch's result and that of the present work again affords strong evidence that the ion nearest the electrode is hydrated.*

Finally we shall investigate what information may be obtained from the experimentally derived value of α of 2.90×10^{-17} cm^2/volt^2. Now if the units of α are converted to those of an inverse pressure, α becomes 2.61×10^{-12} cm^2/dyne. Next we may use Eq. (18) to obtain the effective linear compression modulus of the charge-free layer. The result is $\delta^0=6.56\times10^{-11}$ cm^2/dyne. There are no results available for the linear compressibility of bulk water since water is a liquid. We can make a rough comparison, however, between the above value and the volume compressibility of bulk water. First, it will be of interest to inquire how well bulk water volume follows a law of the form (15) with z_0/z_0^0 replaced by v/v_0. We calculate $(v_0/v-1)$ by using Bridgman's data for water[14] and plot this quantity *versus* pressure on a log-log graph. If an equation of the form (15) is well satisfied, we should obtain a straight line of slope unity. It is actually found that such a procedure yields a straight line of unity slope only for pressures up to about 10^3 atmospheres and that thereafter there is a transition to a slope of about 0.7 up to 10^4 atmospheres. From the low pressure region, we can obtain a value for the initial compressibility modulus k^0. Interpolating Bridgman's data for 20° and 30°C, we find

$$k^0\cong4.2\times10^{-11}\text{ cm}^2\text{/dyne at 25°C.}$$

In an isotropic solid, k^0 should be three times larger than δ^0. Our value for δ^0 is, however, almost five times larger than $k^0/3$ for bulk water. Since it is patently impossible to consider a single water molecule as an isotropic solid, the above difference is not surprising, and the degre of agreement between the value of k^0 for bulk water and the present value of δ^0 is strong evidence that a water molecule is being compressed in the charge-free layer. The result that δ^0 is slightly larger than k^0 may be evidence that the water molecule can belly out to the sides rather freely under linear compression as one might expect. If we consider the charge-free layer to consist of a single water molecule plus that part of a sodium ion between its center of charge and the water molecule, compression of the water molecule must be accompanied by some compression of the sodium ion as well. Since the bulk compressibility of sodium is about five times smaller than our value for the linear compressibility of the entire charge-free layer, we shall probably make only a small error by neglecting any compression of the sodium.

If the linear compression of a water molecule has a dependence on pressure of roughly the same form as does the volume compression for bulk water, then Bridgman's data indicates that Eq. (15) can only be expected to apply well for relatively low pressures and that for high pressures compression should occur less rapidly with increasing pressure than predicted by (15). Now a pressure of 10^3 atmospheres is reached in the charge-free layer at a bias potential of about -0.7 volt for a concentration of 0.01N; and at -1.4 volts the

[13] F. Malsch, Physik Z. **29**, 770 (1928); **30**, 837 (1929).

* *Note added in proof.*—I wish to thank Professor D. C. Grahame for pointing out that since any direct pressure dependence of the dielectric constant is included herein with its dependence on electric field strength, the value of b determined from electrolyte data may not be directly comparable with that from Malsch's experiment. Since the dielectric saturation in both kinds of experiment arises from an electric field which produces an electrostrictive pressure in the material, this pressure will be the same in either experiment for a given field strength. Thus, Malsch's determination of b must also tacitly include a pressure effect in the resulting value of b. However, since the pressure may act differently on a single water molecule in the charge-free layer than on bulk water, the direct pressure contribution to b may differ in the two cases and perhaps accounts for some or all of the discrepancy between the b values.

[14] *International Critical Tables* (McGraw-Hill Book Company, Inc., New York, 1928), Vol. 3, p. 40.

pressure is of the order of 4×10^3 atmospheres or greater. Therefore, we may expect (15) to be a poorer and poorer approximation for polarizing potentials more negative than about -0.7 volt. The theory would thus predict a more rapid compression and consequent rise in $C_T{}^d$ than would be observed experimentally for numerically larger polarizing potentials than -0.7 volt. Some such tendency is actually observed for all the curves, since near the largest negative polarizing potentials the theoretical lines rise slightly faster than the experimental points for all concentrations. It might be noted that the maximum compression of the charge-free layer leads to only about a 20-percent decrease in the thickness of the layer. It is certainly not unreasonable to imagine that a water molecule could be compressed by this amount by the very high pressure present in the layer.

The effect of temperature on the theoretical curves is rather complex. Since there are no data available showing temperature dependence for a constant concentration in electrolytes with no adsorption, we shall only discuss this matter qualitatively. If we assume that $x_0{}^0$ and the dielectric parameters are relatively independent of temperature in the range considered, an increase in temperature will increase $L_D{}^0$ and γ in the same fashion as would a decrease in concentration. At the same time, $z_0{}^0$ will decrease while b^* and α^* will increase if b and α remain constant. Finally, for fixed $V_0{}^*$, a temperature increase will increase V_0, stretching the potential scale. These various changes partly cancel out of the curve of $C_T{}^d$ *versus* V_0. Thus an increase from 25°C to 75°C is found to decrease the theoretical value of $C_T{}^d$ at $V_0=-0.4$ volt by only about three percent for 0.001N concentration.

CONCLUSIONS

In spite of the approximate character of those assumptions of the theory involving dielectric saturation and compression and the use of a one-dimensional approximation to represent a truly two-dimensional problem, good agreement has been found between the predictions of the theory and experiment in respect to the dependence of the differential capacitance on negative polarizing potential and on concentration. The agreement between theory and experiment is especially satisfying since it is obtained using the same values of the constants c, $\kappa_1{}^0$, $x_0{}^0$, b, and α for all concentrations. Since these quantities describe properties of the charge-free layer, one would not expect them to depend on electrolyte concentration in the bulk of the system.

The following results are consistent with the assumption that the charge-free layer involves a single molecule of water so that positive ions nearest the negative electrode are hydrated: (*a*) The nonpolar part of the dielectric constant of the charge-free layer is 5. (*b*) The initial thickness of the charge-free layer is 4.6 A, made up of about 1 A, the radius of a Na^+ ion, and 3.6 A, the diameter of a water molecule. (*c*) The dielectric saturation constant of 3.99×10^{-4} cm²/volt² is three times smaller than the approximate value obtained by Malsch for bulk water using direct methods but relatively low field strengths. (*d*) The initial linear isothermal compressibility modulus of the charge-free layer is 50 percent larger than the initial volume compressibility of bulk water. The maximum pressure in the charge-free layer of 4×10^4 atmospheres or greater results in a reduction in thickness of the layer of about 20 percent.

The complete theory applies not only to aqueous electrolytes, but also to any solid or liquid polar materials containing mobile positive and negative univalent ions blocked at an electrode. It may be readily generalized to include the case of ions of higher valency. Without the refinements of dielectric saturation and compression of the charge-free layer, the theory describes the behavior for reverse bias of nonpolar rectifiers with intrinsic conduction which contain an insulating film between the metallic electrode and the bulk of the material.

ACKNOWLEDGMENTS

The author is greatly indebted to Professor D. C. Grahame for permission to use his recent data on NaF prior to publication and for much helpful correspondence. It is a pleasure to acknowledge the many helpful suggestions of Dr. M. K. Brachman throughout this investigation.

THE JOURNAL OF CHEMICAL PHYSICS VOLUME 22, NUMBER 11 NOVEMBER, 1954

A Thermodynamic and Spectroscopic Study of Gaseous Magnesium Oxide

LEO BREWER AND RICHARD F. PORTER*†
Chemistry and Chemical Engineering Department and Radiation Laboratory, University of California, Berkeley, California‡
(Received February 1, 1954)

Vapor pressure measurements on solid magnesium oxide show that the solid vaporizes mainly into molecular species. Spectroscopic experiments have been conducted and have shown that the known gaseous $^1\Sigma$ electronic state of MgO is not the principal vaporizing species. A study of the ultraviolet bands, produced originally by magnesium burning in air, proves the lower electronic level of the molecule involved in this transition is more important than the $^1\Sigma$ state of MgO. Within experimental uncertainty the heat of sublimation obtained from vapor pressure measurements agrees with a spectroscopically determined heat of sublimation of the molecule involved in the ultraviolet transition. The ultraviolet bands are shown to originate from a gaseous monomer of MgO. The vapor pressure of MgO at 2200°K is 3.8×10^{-4} atmos, and the vapor pressure over MgO reaches 1 atmos at 3040±60°K. The D_0 value for MgO gas is 4.7 ev.

INTRODUCTION

RECENT reviews[1–3] of the thermochemical and spectroscopic data of the gaseous alkaline earth oxides have revealed several discrepancies in the dissociation energies of these molecules. In general, heats of dissociation obtained from vapor pressure measurements do not agree with spectroscopically obtained values. These reviewers point out that where thermochemical data are available, with the exception of BaO, the spectroscopic value is much lower than the thermochemical value. The spectroscopic values obtained from Birge-Sponer extrapolations of the vibrational levels of the lowest known $^1\Sigma$ states are in some cases as much as three electron volts lower than the thermochemical values. Vapor pressure measurements will give erroneous heats when the principal vaporizing species is unknown and an incorrect one is assumed. On the other hand, spectroscopic values may be for an excited state of the molecule and since thermochemical data refer to ground states, agreement would not be expected.

With a flame technique Huldt and Lagerqvist[1] obtained independent values which in most cases agreed with values based on vapor pressure measurements. If one accepts the high values for the thermochemical dissociation energy and the low value for the spectroscopic dissociation energy of the $^1\Sigma$ states, then some molecule other than the $^1\Sigma$ must be the principal gaseous species. Since vapor pressure data do not eliminate the possibility of a complex molecule, the principal vaporizing species must be another electronic state of the monomer or a polyatomic molecule. In their flame work Huldt and Lagerqvist considered only the monomer to be important and do not indicate whether or not their results were sufficient to eliminate the possibility of other molecules.

If a monomer were suspected of being the main species the problem of establishing the true ground state would still remain. A further study of the spectra in a hope of finding transitions involving the ground state would be necessary. Other systems such as the unanalyzed bands obtained in absorption in flames by Barrow and Crawford[4] may involve a lower state of MgO. Brewer[3] has pointed out that the ground states of these molecules may be triplet instead of singlet states. Correlation rules allow only triplet states to be produced from the ground states of the free atoms.

Evidence for the existence of polymers has been shown by Aldrich.[5] He was able to produce ions such as $Ba_2O_2^+$ in a mass spectrograph, and hence the existence of oxide dimers cannot arbitrarily be discounted. Brewer and Mastick[6] have shown from theoretical bonding considerations, however, that such molecules as Mg_2O should have no chemical importance.

In a hope of explaining the nature of the gaseous state of these oxides, a specific investigation of MgO was initiated. The following equations show the various possible modes of vaporization:

$$MgO(s)=Mg(g)+xO_2(g)+(1-2x)O(g) \quad (1)$$

$$MgO(s)=MgO(g,{}^1\Sigma) \quad (2)$$

$$MgO(s)=MgO(g,X) \quad (3)$$

$$MgO(s)=1/x(MgO)_x. \quad (4)$$

X and $(MgO)_x$ represent possible gaseous electronic states of MgO and polymers, respectively, $MgO(g,{}^1\Sigma)$ refers to the gaseous $^1\Sigma$ state of MgO, and $MgO(s)$ refers to the solid standard state. The basic problem is to determine which of these is the principal vaporization process. The essential phases to be considered then are:

* Abstracted in part from the thesis by Richard F. Porter in partial satisfaction of the requirements for the degree of Doctor of Philosophy in Chemistry at the University of California.

† Present address: Department of Physics, University of Chicago, Chicago 37, Illinois.

‡ This document is based in part on work performed under Contract No. W-7405-eng-48B for the U. S. Atomic Energy Commission.

[1] L. Huldt and A. Lagerqvist, Arkiv Fysik **2**, 333 (1950).

[2] G. Drummond and R. F. Barrow, Trans. Faraday Soc. **47**, 1275 (1951).

[3] L. Brewer, Chem. Revs. **52**, 48 (1953).

[4] R. F. Barrow and D. V. Crawford, Proc. Phys. Soc. (London) **57**, 12 (1945).

[5] L. T. Aldrich, J. Appl. Phys. **22**, 1168 (1951).

[6] L. Brewer and D. F. Mastick, J. Am. Chem. Soc. **73**, 2045 (1951).

(1) Does MgO(s) vaporize mainly to the elements or to molecules?

(2) If MgO(s) does vaporize into molecules, is MgO(g,$^1\Sigma$) the most important species?

(3) If MgO(g,$^1\Sigma$) is not the principal species, is there another electronic state of MgO which is important or does the solid vaporize into polyatomic molecules?

I. VAPOR PRESSURE DETERMINATIONS

Little direct vapor pressure data for MgO have been reported and the significant thermochemical data for the vapor is that reported by Huldt and Lagerqvist.[1] The vapor pressure of MgO was therefore measured by the Knudsen effusion technique. The observed rate of effusion is the sum of the rates of the individual atoms and molecules, and hence the weight loss per unit time is an integral quantity. For MgO, however, it is possible from known thermodynamic data to calculate the equilibrium concentrations of Mg(g), O(g), and O_2(g). Furthermore, if these are the only important species, the observed pressure should be in agreement with the calculated pressure.

Experimental

In the initial runs the Knudsen cells consisted of tungsten crucibles with tungsten covers. In every case the empty crucibles and the MgO were weighed separately before and after heating. The crucibles were heated inductively in a vacuum, the same technique as that used by Brewer and Searcy.[7] Pressures within the vacuum system varied from 0.1 to 0.05 micron, increasing slightly at the beginning of a run and then rapidly decreasing. In later experiments the same procedure was used when BeO and ZrO_2 crucibles were used as containers, except that tungsten shields were used as heating elements. Crucibles containing the MgO were placed inside slightly larger ones to prevent them from being attacked by contact with tungsten radiation shields. The MgO used was the Reagent Special grade of Baker and Adamson.

Results of Vapor Pressure Measurements

The tungsten crucibles were not completely satisfactory as containers for MgO as there was some reaction forming Mg gas and a tungsten oxide which vaporized to some extent. The total volatility observed with tungsten crucibles was higher than that observed with BeO and ZrO_2 crucibles, and the results with the tungsten crucible were too inaccurate to be of value.

More satisfactory results were obtained when BeO and ZrO_2 crucibles were used as MgO containers. Table I shows the results of the vapor pressure measurements.

Runs 1, 2, and 3 were with BeO crucibles while Run 4 was with a ZrO_2 crucible. In all four runs BeO covers were used. The holes in the covers were ground as close as possible to knife edges. In Runs 1 and 2 the MgO charge was removed from the crucible and weighed separately. The reported values are the weight losses of the MgO itself. The total weight losses of the cells were found to be slightly less than those of the MgO itself. In Runs 3 and 4 the total loss of the crucible plus MgO is reported since the MgO melted at the points of surface contact with the crucibles and could not be removed upon cooling.

The initial assumption is that only Mg(g), O(g), and O_2(g) are important, and the rate of effusion of Mg(g) is simply the gram atoms of magnesium vaporized per second. The partial pressures of Mg(g) were calculated from the rate equation

$$R=\frac{P(44.383)a}{(MT)^{\frac{1}{2}}}$$

where R is the number of gram atoms or moles effusing per second, a is the area of effusion hole in cm^2, T the absolute temperature, M the atomic or molecular weight of the effusing species, and P its partial pressure in atmos. Pressures calculated on this assumption are shown in Column 6.

TABLE I. Experimental and calculated vapor pressure data.

Run	Temp. °K	Time in sec	Area of hole in cm²	Weight loss in g	P_{Mg} (from rate Eq.) in atmos	P_{Mg} (calculated theoretically) in atmos
1	2040	3900	0.0177	0.025	4.5×10^{-5}	6.6×10^{-6}
2	2040	3900	0.0177	0.018	3.3×10^{-5}	6.6×10^{-6}
3	2140	9300	0.0177	0.184	1.4×10^{-4}	2.4×10^{-5}
4	2200	3600	0.0177	0.145	3.0×10^{-4}	5.6×10^{-5}

[7] L. Brewer and A. W. Searcy, J. Am. Chem. Soc. **73**, 5308 (1951).

Comparison of Experimental and Theoretical Values

From known values of $-(\Delta F_T-\Delta H_{298})/T$ and ΔH_{298}, it is possible to calculate the equilibrium constants for the following reactions:

$$\mathrm{MgO}(s)=\mathrm{Mg}(g)+\mathrm{O}(g), \quad K_1=P_{Mg}P_O,$$

$$\Delta H_{298}=238.8\pm0.5 \text{ kcal},$$

$$-\left(\frac{\Delta F_{2000}-\Delta H_{298}}{2000}\right)=66.66\pm0.4 \text{ cal/deg}, \quad (1)$$

$$\tfrac{1}{2}O_2=0, \quad K_2=P_O/(P_{O_2})^{\frac{1}{2}},$$

$$\Delta H_{298}=59.55\pm0.02 \text{ kcal},$$

$$-\left(\frac{\Delta F_{2000}-\Delta H_{298}}{2000}\right)=15.24\pm0.1 \text{ cal/deg}. \quad (2)$$

Knowing K_1 and K_2 together with the auxiliary condition that the rate of effusion of magnesium must equal

the total rate of effusion of oxygen (as O_2 and O), we can calculate the true theoretical pressures of magnesium inside the Knudsen cell.

The value of $-(F_{2000}-H_{298})/2000$ for MgO(s) was calculated from Kelley's tables[8,9] and the values for Mg(g), O(g), and O_2(g) were obtained from tabulated values.[10] The best accepted value of -143.7 ± 0.1 kcal[11] for the heat of formation of MgO, and the most recent value[12] for the heat of dissociation of O_2 were used in the calculations. For the heat of sublimation of magnesium several sources of vapor pressure data were treated. Using Kelley's free energy functions[13] together with the vapor pressure data we obtained $\Delta H_{298}=35.3\pm0.2$ kcal from the measurements of Coleman and Egerton,[14] and $\Delta H_{298}=35.4\pm0.5$ kcal from the measurements of Baur and Brunner.[15] Combining these results with the value of $\Delta H_{298}=35.9$ kcal, calculated by Kelley[13] from measurements of Hartmann and Schneider,[16] we take a value of $\Delta H_{298}=35.6\pm0.3$ kcal. Since $-(\Delta F_T-\Delta H_{298})/T$ is not strongly dependent on temperature, the values at $T=2000°$K were considered constant over a 200° range.

The three necessary relationships are:

$$P_{Mg}P_O=K_1 \tag{1}$$

$$P_O/(P_{O_2})^{\frac{1}{2}}=K_2 \tag{2}$$

and $R_{Mg}=2R_{O_2}+R_O$, which expressed in terms of pressures is

$$\frac{P_{Mg}}{(M_{Mg})^{\frac{1}{2}}}=\frac{2P_{O_2}}{(M_{O_2})^{\frac{1}{2}}}+\frac{P_O}{(M_O)^{\frac{1}{2}}}. \tag{3}$$

Partial pressures of Mg, O, and O_2 were calculated by successive approximations until two place accuracy was achieved. The values for Mg are shown in Column 7 of Table I.

Comparison of Columns 6 and 7 shows the observed pressures are consistently a factor of five or six times higher than the theoretical pressures. With the widest limits of uncertainty in the thermochemical data the error in ΔF for reaction 1 at 2000°K is 1.3 kcal. This corresponds to an error in K_1 of about 40 percent and an error of 20 percent in the calculated pressures in Column 7. On the other hand, the vapor pressure measurements are reproducible to better than a factor of two. The discrepancy therefore between the observed and calculated pressures is not just experimental error. The initial assumption is consequently false and we are not permitted to assume that only Mg(g), O(g), and O_2(g) are the important vapor species. Molecular species must contribute appreciably to the vapor and the solid does not vaporize simply to the elements.

[8] K. K. Kelley, U. S. Bur. Mines Bull. 476 (1949).
[9] K. K. Kelley, U. S. Bur. Mines Bull. 477 (1950).
[10] L. Brewer, Paper 3, National Nuclear Energy Series, Vol. 19B, Edited by L. L. Quill (McGraw-Hill Book Company, Inc., New York, 1950).
[11] C. Shomate and E. Huffman, J. Am. Chem. Soc. **65**, 1625 (1943).
[12] G. Herzberg, Can. J. Phys. **30**, 185–210 (1952).
[13] K. K. Kelley, U. S. Bur. Mines Bull. 383 (1935).
[14] F. F. Coleman and A. Egerton, Phil. Trans. Roy. Soc. **A234**, 177 (1935).
[15] E. Baur and R. Brunner, Helv. Chim. Acta. **17**, 958 (1934).
[16] H. Hartmann and R. Schneider, Z. Anorg. u. allgem. Chem. **180**, 275 (1929).

II. THE HEAT OF SUBLIMATION OF MgO (g,$^1\Sigma$)

Having shown from the vapor pressure measurements that MgO(s) vaporizes principally into molecular species, the next problem is to consider the importance of the lowest known $^1\Sigma$ state of MgO(g). The method to be used is similar to that used by Brewer, Gilles, and Jenkins.[17] If an electronic state of the gaseous molecule in equilibrium with the solid emits a measurable amount of radiation, the heat of sublimation of that particular state can be determined from the variation of intensity with temperature. The transition to be treated is the well-known $^1\Sigma^*\rightarrow{}^1\Sigma$ transition of MgO lying in the green region of the spectrum. The desired heat is the heat of sublimation of MgO(g,$^1\Sigma^*$) minus the excitation energy of the $^1\Sigma^*$ as shown by the following equations:

$$\text{MgO}(s)=\text{MgO}(g,{}^1\Sigma^*), \qquad \Delta H_1 \tag{1}$$

$$\text{MgO}(g,{}^1\Sigma^*)=\text{MgO}(g,{}^1\Sigma), \qquad \Delta H_2=-h\nu \tag{2}$$

$$\text{MgO}(s)=\text{MgO}(g,{}^1\Sigma), \qquad \Delta H_3=\Delta H_1+\Delta H_2. \tag{3}$$

ΔH_1 is to be obtained graphically, and this value together with the known excitation energy gives us ΔH_3.

Experimental

To obtain a heat of sublimation by variation of intensity with temperature the two following conditions are necessary:

(1) The gas must be in equilibrium with the solid.
(2) The temperature must be high enough to populate the upper electronic level sufficiently to produce an observable amount of emission.

The King type resistance furnace as described by Brewer, Gilles, and Jenkins was used as the heating unit for MgO. The same type of graphite tubes was used except that the MgO could not be placed directly into the tubes as it is reduced rapidly by the graphite at higher temperatures. Instead the graphite tubes were lined with a 0.002-in. sheet of tantalum and a 0.002-in. sheet of tungsten was placed inside this tantalum lining. The MgO was therefore only in contact with the tungsten. Graphite reacting with the tantalum formed a TaC layer and the carbon could not readily penetrate the tungsten. Consequently, except for some attack by the tungsten, rapid reduction of the MgO was prevented. After evacuating the furnace, argon was passed in to decrease diffusion of MgO vapor out the ends of the tube. An argon pressure of 0.1 to 0.2 atmos was suffi-

[17] Brewer, Gilles, and Jenkins, J. Chem. Phys. **16**, 797–807 (1948).

cient. A 22-kva power source, producing 800 amp or more in the graphite tubes, was required to produce the desired temperatures. All temperatures were read with a calibrated optical pyrometer. Twenty grams of pressed MgO placed inside the tungsten lining would last for about an hour at temperatures around 2500°K.

Emitted light from the MgO vapor was passed on to the slit of a 3-meter concave grating spectrograph and reflected directly on to an RCA 1P21 photomultiplier tube. Stray light emitted from the sides of the furnace tube was cut out of the beam to prevent high backgrounds. The photo tube, amplifying unit, and recording device was that described by Phillips.[18] The phototube was part of the scanning device and could be set immediately at the desired wavelength. Several tracings of each spectral feature were made at each temperature until it was sure that equilibrium within the furnace had been attained. A characteristic tracing of the 0,0 sequence of the $^1\Sigma^* \rightarrow {}^1\Sigma$ system is shown in Fig. 1. The actual dispersion of the grating is about 4 A/mm in the first order, whereas the scanner was set to a slow enough speed to produce a spread of 10.6 A/inch on the tracing. The slit width of the spectrograph was 0.1 mm.

Calculations and Results

Tracings of the 0,0 sequence of the $^1\Sigma^* \rightarrow {}^1\Sigma$ transition of MgO in equilibrium with the solid were made at various temperatures. The heights of the 0,0 band head at 5007.3 A, as seen in Fig. 1, were measured from the lowest dotted line representing the lowest extrapolated background. The heights multiplied by the proper amplification factor are proportional to the intensity of emitted radiation. The intensities presented in Table II are the heights in centimeters. The upper dotted line in Fig. 1 is an extrapolation of MgH rotational structure, the MgH appearing as an impurity in the furnace. The variation in heights measured from the upper dotted line is about 10 percent of the reported values. The true background lies somewhere between the two dotted lines. At temperatures above 2650°K the intensities diminish rapidly since the solid disappears at a rapid rate and equilibrium is not maintained.

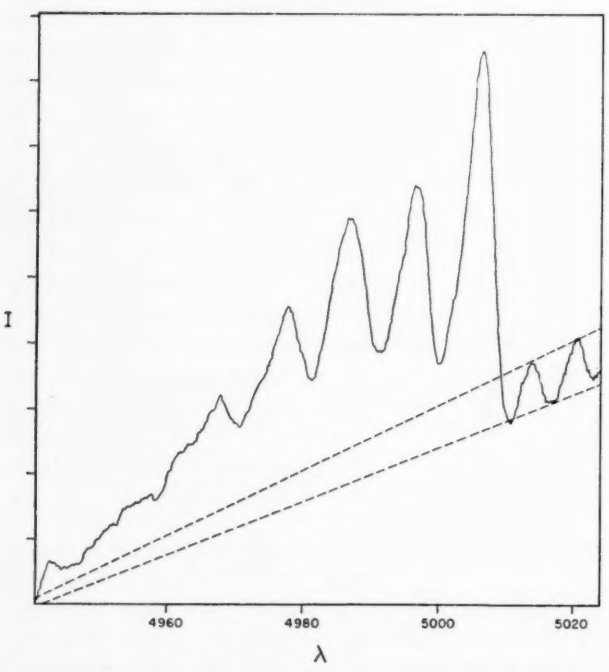

FIG. 1. Emission tracing of the 0,0 sequence of the green bands of MgO produced from MgO vapor in equilibrium with MgO solid at $T = 2550$°K. Dotted lines represent limits of the true background.

[18] J. G. Phillips, ONR Contract No. Nonr.—160(00) (1953).

TABLE II. Experimental intensity data.

T°K	Relative intensity of 0,0 band
2498	13.6
2488	11.3
2488	10.2
2533	23.0
2533	21.2
2528	21.8
2598	74.0
2598	66.0
2593	70.0
2648	128.0
2653	104.0

Determination of ΔH_1 for Reaction (1) $\mathbf{MgO}(s) = \mathbf{MgO}(g, {}^1\Sigma^*)$

To obtain the heat of sublimation of the $^1\Sigma^*$ state, a Σ plot, which includes the variation in heat capacity with temperature, was made instead of a simple $\Delta F/T$ *vs* $1/T$ plot.

Since the intensity of emitted radiation is proportional to the concentration of $^1\Sigma^*$, we have the relationship: $\Delta F = -RT \ln P_{^1\Sigma^*} = -RT \ln kIT$, k being the proportionality constant. From the relationship:

$$\Delta H - \Delta H_{298} = \int_{298}^{T} \Delta Cp \, dT,$$

and from known heat capacities of the solid and gas we obtain for reaction (1)

$$\Delta H = \Delta H_{298} - 5.21T - 0.87 \times 10^{-3}T^2 - (1.48/T) \times 10^5 + 2100.$$

The heat capacity for MgO(s) was extrapolated from Kelley's table.[8] For the gas we are considering a single vibrational level of a particular electronic state, and hence vibrational and electronic terms do not contribute to the total heat capacity. A rotational contribution should be included but, since only a few rotational levels are involved in forming the head of the band, this is

TABLE III. Data for Σ plot.

T°K	Σ
2488	63.08
2533	64.67
2598	67.20
2648	68.58

small as compared to the translational term. Therefore a Cp of $5/2R$ was taken for the gas.

Substituting ΔH into the van't Hoff equation and integrating we obtain:

$$\Delta F/T=(\Delta H_{298}+2100)/T+5.21\ \ln T+0.87\times 10^{-3}T-\frac{0.74\times 10^{5}}{T^{2}}+\text{const.}$$

Setting ΔF equal to $-RT\ \ln kIT$ and letting $-(\Delta H_{298}+2100)/T+\text{const}$ be Σ, we obtain:

$$\Sigma=-\left(\frac{\Delta H_{298}+2100}{T}\right)+\text{const}$$
$$=4.575\ \log I+16.55\ \log T+0.87\times 10^{-3}T-\frac{0.74\times 10^{5}}{T^{2}}.$$

The slope of a Σ *vs* $1/T$ plot gives us ΔH_{298}. The values of Σ calculated from the averaged sets of data presented in Table II are shown in Table III. The Σ *vs* $1/T$ plot is given in Fig. 2 in which the same weight is given to each point. From the slope of the line we obtain $\Delta H_{298}=230$ kcal.

In general, with a limited number of points it is difficult to obtain accurate heats. A small uncertainty in the slope of the line will produce a large uncertainty in the heat. In this case there is an uncertainty of 10 kcal alone in establishing the best position of the curve.

Errors may also be due to temperature gradients along the graphite tube. In order to minimize this uncertainty the MgO was placed in the central uniformly heated portion of the tube. In making the temperature measurements the optical pyrometer was focused directly onto the hot surface of the MgO and the temperature was observed to be constant over the total surface area. Temperatures read on an exposed central portion of the graphite tube agreed with readings on the surface of the MgO; and since the hot graphite approaches a black body radiator, it was presumed that the MgO was also radiating as a black body.

Reduction of the MgO by tungsten produces a solid oxide of tungsten and eventually the MgO layer will be completely reduced. As long as pure solid MgO is still present in the interior of the tube, the true equilibrium pressure of MgO vapor will be maintained. This is shown by the constancy of the MgO spectrum intensity for long periods of time until reaction has become appreciable. Only above 2700°K does the tungsten reaction interfere seriously with the spectral measurements.

The temperature range which can be studied is limited since at lower temperatures the amount of emission is too small to observe while at higher temperatures the gas will not reach its true equilibrium pressure and the observed intensities will be too small. A plot of this type will therefore tend to give low results if the points at high temperatures are treated equally with points at lower temperatures. To obtain ΔH_3 for reaction (3), $MgO(s)=MgO(g,{}^1\Sigma)$, we subtract from the graphical value the sum of the electronic and rotational energies of the ${}^1\Sigma^*$. The electronic energy calculated from the band origin is 57 kcal. The band head forms approximately at the rotational level $J=40$ giving a rotational contribution of 2.7 kcal. We therefore obtain for the heat of sublimation of $MgO(g,{}^1\Sigma)$ a lower limit of 170 kcal. In order to include uncertainties in both directions we shall take a ΔH_{298} of 185 ± 15 kcal.

From Kelley's tables[8,9] we obtain for the reaction

$$MgO(s)=MgO(g,{}^1\Sigma),\quad -\left(\frac{\Delta F_{2000}-\Delta H_{298}}{2000}\right)=41.7.$$

Using a ΔH_{298} of 170 kcal as a lower limit and setting ΔF equal to $-RT\ \ln P_{1\Sigma}$ we calculate $P_{1\Sigma}\lesssim 10^{-10}$ atmos at 2000°K. Comparing this value with the pressure of

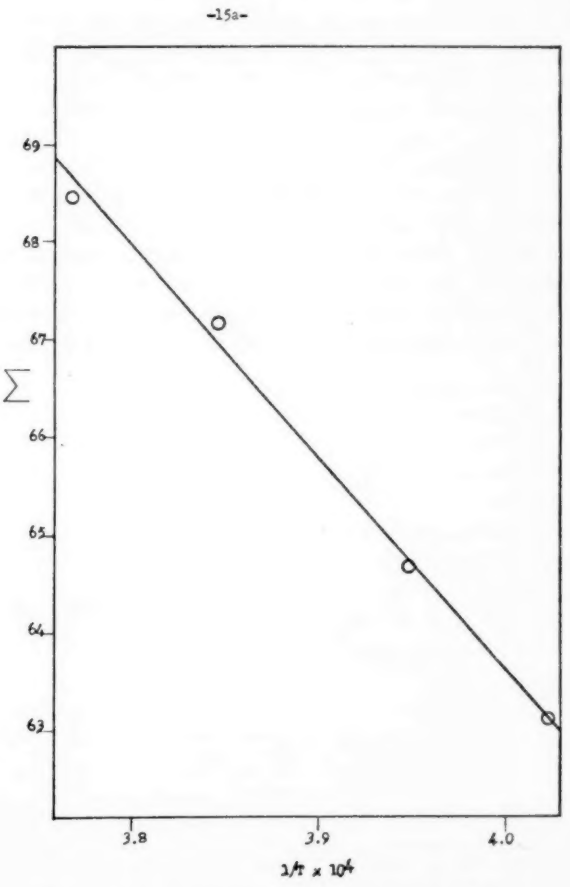

FIG. 2. Σ plot for the reaction $MgO(s)=MgO(g,{}^1\Sigma^*)$.

Mg(g) in Column 7 of Table I, we see that MgO(g,$^1\Sigma$) is even less important than Mg(g) and also cannot be the principal vaporizing species.

III. THE ULTRAVIOLET BAND SYSTEM

The 3700 A band system appearing in emission from magnesium burning in air and also in absorption in flames containing magnesium[4] will now be considered. Although the bands are complex and have not been analyzed, there are good reasons to suspect from the various ways they have been produced that they either involve electronic states of MgO or states of a more complex molecule containing magnesium and oxygen. If this transition occurs with equal or greater intensity than the $^1\Sigma^* \rightarrow {}^1\Sigma$ transition, we ought to observe it in the King furnace as we did the green bands and further ought to be able to study the states involved in the transition. Experiments were therefore undertaken to obtain the 3700 A bands both in emission and absorption under equilibrium vapor conditions and to study the importance of the lowest electronic state of the transition relative to MgO(g,$^1\Sigma$).

Experimental

The technique used to produce the $^1\Sigma^* \rightarrow {}^1\Sigma$ bands was also successful in studying the ultraviolet system. Light from the MgO vapor in equilibrium with the solid was passed on to the slit of the 3 meter grating and reflected onto a 1P28 photomultiplier tube. Slit widths of 0.1 mm were required to give a reasonable response by the phototube. A quartz optical system was used throughout the ultraviolet experiments. Several tracings at temperatures about 2600°K between wavelengths of 3800 and 3600 angstroms were made in order to locate the bands. Several molecular and atomic features appeared on the emission tracings; and after identifying the important atomic lines, the bands were definitely shown to be the ones observed by Barrow and Crawford.[4]

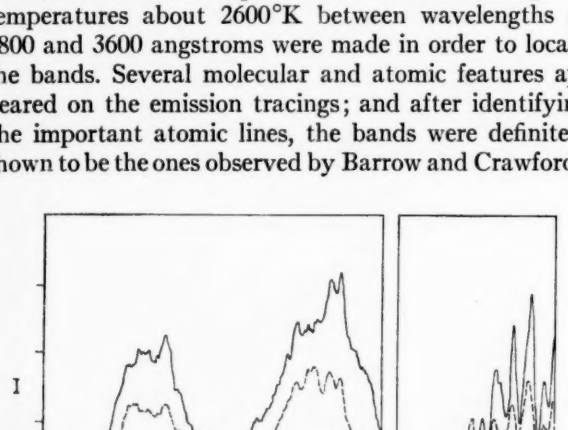

FIG. 3. (a) Thermal emission tracings of the ultraviolet bands. (b) Thermal emission tracings of the green bands. Solid lines represent tracings made at $T=2600$°K, while dotted lines represent tracings made at $T=2550$°K. Extrapolated backgrounds are also indicated.

Figure 3a is a reproduction of tracings made at two different temperatures. The recording device was set to produce a dispersion of 42.3 A/inch on the tracing paper.

For absorption experiments a xenon lamp with a high effective arc temperature in this wavelength region was used as a source. Parallel light from the source was passed through the calcium fluoride windows of the furnace and on to the slit of the spectrograph. Figure 4 shows tracings of the transmitted light from the xenon lamp with absorption by the MgO vapor at two different furnace temperatures. The absorption features in Fig. 4 are seen to be just the reverse of the emission features in Fig. 3a. On this low dispersion the tracings show only an integrated shape of absorption features, and small fluctuations in the lamp intensity are also present.

Intensity Comparison of the Two Band Systems

From a comparison of rates of rise in intensities with temperature for the two band systems we can qualitatively establish which of the lower states involved in the transitions has the smaller heat of sublimation.

TABLE IV. Determination of ΔH_{298} for reaction MgO(s) = MgO(g).

T°K	P_{MgO} in atmos (calculated from rate Eq.)	$-\left(\frac{\Delta F_T - \Delta H_{298}}{T}\right)$ MgO(s) = MgO(g)	ΔH_{298} in kcal MgO(s) = MgO(g)
2040	5.84×10^{-5}	43.84	128.0
2040	4.20×10^{-5}	43.84	129.2
2140	1.84×10^{-4}	43.51	129.8
2200	3.81×10^{-4}	43.31	129.9

Simultaneous tracings were made for both the green and ultraviolet systems. The furnace was first brought to the desired temperature and held constant to allow the MgO vapor to equilibrate with the solid. The spectrograph was adjusted to permit study of both regions with one setting. The scanner was first set at approximately λ5000 and a tracing of the green system was made. The scanner was then set at approximately λ3700 and a tracing of the ultraviolet region was taken. Several tracings of each system were made at a particular temperature until equilibrium was established and tracings of each system were reproduced with the same shape and magnitude. The furnace temperature was then changed and another series of tracings were made. Figure 3a is a reproduction of two tracings of the ultraviolet region, and Fig. 3b shows two tracings of the green system. The solid lines are tracings made at $T=2600$°K while the tracings shown by dotted lines were made at $T=2550$°K. The backgrounds are extrapolations of the observed backgrounds.

First we consider the excited states and the reactions:

$$\text{MgO}(s) = X^*(g) \qquad \Delta H_1^* \qquad (1)$$

$$\text{MgO}(s) = \text{MgO}(g,{}^1\Sigma^*) \qquad \Delta H_2^*. \qquad (2)$$

$X(g)^*$ represents an excited state of the unknown molecular species.

For comparison purposes in the ultraviolet system we will consider the strong molecular features in the region of λ3720 as seen in Fig. 3a. The features appearing at approximately λ3840 contain the strong $^3D \rightarrow {}^3P^0$ transition of magnesium and cannot be used. For the green system we will treat the sequence of bands beginning at λ5007.3. Using the areas enclosed by the solid and dotted lines as measures of integrated intensities for both systems, we find

$$\frac{I_{1,\,T=2600°K}}{I_{1,\,T=2550°K}}=1.6\pm0.1, \qquad \frac{I_{2,\,T=2600°K}}{I_{2,\,T=2550°K}}=2.0\pm0.1.$$

We see that the green system is rising more rapidly with temperature than the ultraviolet system. Assuming the ultraviolet bands involve a monomer of MgO, we can plot $\log I_1/I_2$ *vs.* $1/T$ and obtain from the slope the difference in heats of sublimation of the two excited electronic states. A plot of this type was made using the integrated intensities from the tracings shown in Fig. 3a, and a difference of roughly 50 kcal was obtained. With an estimated uncertainty of 20 kcal we have:

$$\Delta H_1^*=\Delta H_2^*-50 \text{ kcal.}$$

To obtain a relation between the heats of sublimation of the lower levels we subtract from ΔH_1^* and ΔH_2^* the electronic energies. The reactions are:

$$\text{MgO}(s)=\text{MgO}X(g) \quad \Delta H_1 \qquad (3)$$

$$\text{MgO}(s)=\text{MgO}(g,{}^1\Sigma) \quad \Delta H_2. \qquad (4)$$

$X(g)$ represents the lower state of the unknown molecular species. The energy for the $^1\Sigma^*$ is 57 kcal. For X^* we shall take the origin of the system at λ3700 giving an electronic energy of 77 kcal.

We have then the following relations:

$$\Delta H_1=\Delta H_1^*-77 \text{ kcal}$$
$$\Delta H_2=\Delta H_2^*-57 \text{ kcal.}$$

Since $\Delta H_1^*=\Delta H_2^*-50\pm20$ kcal, we obtain the relation

$$\Delta H_1=\Delta H_2-70\pm20 \text{ kcal,}$$

showing the lower level of ultraviolet system lies significantly lower than the lower level of the green system.

On the tentative assumption that a monomer is the principal vaporizing species, we can calculate a heat of sublimation from the vapor pressure data shown in Table I, taking the weight loss due mainly to $\text{MgO}(g)$. Table IV gives results of such calculations. It has been assumed that the ground state is a $^3\Sigma$ state, and an electronic contribution of R ln3 has been included in the free energy functions in Table IV. The vibrational and rotational contributions to the free energy functions were assumed the same as for the $^1\Sigma$ state.

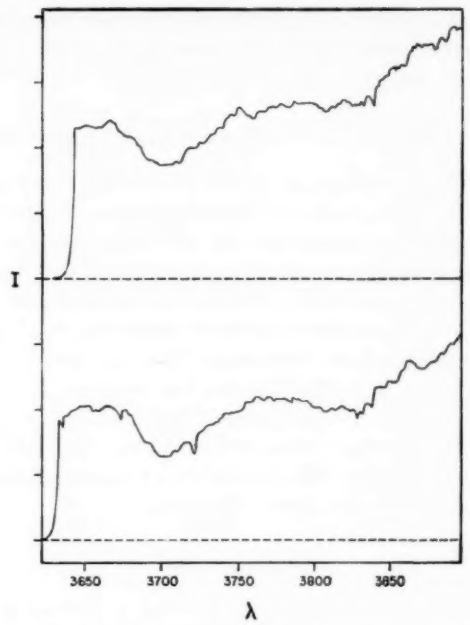

FIG. 4. Intensity tracings of light transmitted from a xenon lamp through MgO vapor showing absorption of radiation by the vapor. The upper tracing was made at $T=2320°K$ and the lower at $T=2420°K$. Dotted lines are zero light reference lines.

As the ΔH_{298}^0 values in Table IV were calculated assuming that the vapor consisted entirely of MgO, these heats are lower limits. One can correct these values for the amount of Mg vapor due to dissociation of MgO to the elements. The presence of oil or other reducing agents in the vacuum system could increase the concentration of magnesium vapor somewhat. Taking these corrections into account and averaging the results of Table IV yields $\Delta H_{298}=130\pm1$ kcal for the heat of sublimation of MgO solid to MgO gas. Comparison of this value with the experimentally obtained value of 185 ± 15 kcal for the heat of sublimation of the $^1\Sigma$ state of MgO gas shows that the principal vaporizing species must be 55 ± 15 kcal lower than the $^1\Sigma$ state. This is in agreement with the value of 70 ± 20 kcal obtained for the difference between the $^1\Sigma$ state and the lower state of the ultraviolet system. As no species can have a lower heat of sublimation than that given by the total pressure, one can state that the spectroscopic results indicate the lower state of the ultraviolet system cannot be lower than 70 kcal below the $^1\Sigma$ state but may be as close as 50 kcal below the $^1\Sigma$ state. On the other hand the Knudsen experiments fix the main species in MgO vapor between 70 and 40 kcal below the $^1\Sigma$ state. Thus it is quite reasonable to conclude that the lower state of the ultraviolet system is the main species in MgO vapor. These same conclusions can be drawn whether the ultraviolet system is due to diatomic MgO or to a polyatomic molecule.

Huldt and Lagerqvist[4] obtained a thermochemical value of 5.0 ev for the dissociation energy of MgO gas calculated on the basis of a $^3\Sigma$ state. With the same

heats of reaction used previously we calculate a heat of sublimation of 123 kcal from their data, which is within 7 kcal of the value obtained here.

The Ultraviolet Bands on High Dispersion

Further investigation of the ultraviolet band system is necessary in order to identify the molecular states involved in the transition. On low dispersion the bands are too complex to permit a vibrational or rotational analysis. Barrow and Crawford[4] measured many band heads but did not have sufficient resolution to attempt a vibrational analysis. Verhaeghe[19] has classified the bands into distinct sets of sequences, but over all, little work has been done on the ultraviolet system. In a hope of obtaining further information about the electronic states involved in this transition we have obtained the bands again under higher dispersion.

Experimental

All spectrograms were made with a 21-foot grating, ruled with 30 000 lines/inch, giving a linear dispersion of 0.67 A/mm at λ3700 in the second order. An eighteen-inch photographic plate was placed on the Rowland circle with the center of plate at approximately λ3750 so as to include a range between λ3600 and λ3900. Eastman Kodak IIa-0 plates were used and found to give sharp contrast. The three following methods of excitation were used.

(1) *Burning Magnesium*

Light from the burning end of a thin piece of magnesium ribbon fed through a quartz tube was focused directly onto the slit. The height of the quartz tube could be adjusted to allow only selective portions of the flame to focus on the slit, but the erratic burning of the ribbon would not allow complete exclusion of continuous radiation from the glowing mass. Slit widths of 0.05 mm with an exposure time of ten minutes were required to give observable spectral features. In some cases burning pellets of magnesium, which give a brighter instantaneous source, were used; but in all cases backgrounds were too high. On the best plates several sequences of bands appeared with partially resolved rotational structure, but overlapping of many vibrational bands forbid a vibrational analysis.

(2) *Magnesium Arc*

Magnesium electrodes of one-half inch diameter and approximately 3 in. long were fastened to the clamps of a conventional iron arc. The arc was powered by a 220-volt dc source. The green portion of the arc was focused onto the slit, and the position of the arc could be adjusted to allow only a certain portion to be exposed to the slit. The arc could be run for only 30 seconds at a time as the electrodes became overheated. In some cases the arc went out by itself after a few seconds because of MgO formation at the surface of the electrodes. Slit widths were 0.05 mm and the total exposure times were about 10 minutes. Backgrounds on the plates were considerably reduced and rotational structure was more obvious than on the exposures with burning magnesium. Many impurity lines and bands also appeared. Bands of CN were particularly strong, and presence of these impurities would not permit an analysis.

(3) *Thermal Excitation*

The bands were obtained in emission and absorption in the manner previously described.

(a) For emission the MgO was brought to temperatures of about 2550°K, and light from the vapor was focused onto the slit. With a slit width of 0.03 mm an exposure time of 35 minutes was required.

(b) For absorption a xenon lamp was used as a source of continuum. An MgO temperature of 2550°K was found to be the most ideal for reversal of the bands. This temperature is lower than the effective lamp temperature and still high enough to produce a large concentration of vapor. The slit width was again 0.03 mm. At this temperature the solid MgO lasted about 40 minutes which was a sufficient exposure time.

Description of the Ultraviolet Bands

Spectrograms of the bands obtained under high excitation as in the case of burning magnesium and magnesium arcs are too complex to permit a vibrational analysis by themselves. The spectrograms obtained under equilibrium vapor conditions, however, are considerably less complex since only lower vibrational levels are populated and only a few of the principal bands appear. In our analysis of the bands we will treat them as we would a simple diatomic spectrum, assuming a monomer of MgO is involved in the transition. From the vibration frequencies of the singlet state of MgO we would expect this molecule to have a vibration frequency between 800 and 900 cm^{-1}. The spacing between the 0,0 band and the 0,1 band would therefore be of the order of 100 angstroms. Close examination of all the plates shows, not one, but several sets of sequences separated by approximately this distance. If the molecule is a simple monomer, the only conclusion is that more than two electronic states are involved in the transition. The splittings are too great to be simply multiplet splittings. Three measured sets of sequences are shown in Table V.

All of the band heads presented in Table V were observed in thermal absorption. If the bands were distinguishable on other plates, the other methods of excitation are also listed. The measurements in general agree with those of Barrow and Crawford.[4]

The most outstanding sequence begins at λ3721. On the absorption spectrograms several members of the

[19] J. Verhaeghe, Wis-en Natuurk. Tijdschr. **7**, 224 (1935).

TABLE V. Principal ultraviolet band heads, produced with a dispersion of 0.67 A/mm.

	1st sequence Q heads λ(A)	ν(K)	Methods of excitation	Direction of degradation	2nd sequence Q heads λ(A)	ν(K)	Methods of excitation	Direction of degradation
	3721.41	26863.9	1, 2, 3*a*, 3*b*	*V*	3626.73	27565.2	3*b*	*V*
	3731.75	26789.5	1, 2, 3*a*, 3*b*	*V*	3659.95	27315.0	3*b*	*R*
	3742.27	26714.2	3*a*, 3*b*	*V*				
	3751.33	26649.7	3*a*, 3*b*	*V*	3rd sequence Q heads			
	3759.38	26592.6	3*a*, 3*b*	*V*	λ	ν		
System I	3766.50	26542.3	1, 2, 3*a*, 3*b*	*R*	3846.84	25988.0	3*a*, 3*b*	?
	3772.86	26497.6	1, 2, 3*a*, 3*b*	*R*	3854.81	25934.3	3*a*, 3*b*	?
	3778.3	26459	1, 2, 3*a*, 3*b*	*R*				
	P head							
	3725.7	26833	1, 2, 3*a*, 3*b*	*V*				
	1st sequence Q heads				2nd sequence Q heads			
	λ	ν			λ	ν		
System II	3704.2	26988.7	3*b*	*V*	3802.4	26291	3*a*, 3*b*	*V*
	3695.2	27053.7	3*b*	*V*	3792.8	26358	3*a*, 3*b*	*V*
	3686.5?	27118.3	3*b*	*V*	3784.5	26416	3*a*, 3*b*	*V*
	1st sequence heads undesignated				2nd sequence heads undesignated			
	λ	ν			λ	ν		
	3798.3	26319	1, 2, 3*a*, 3*b*	*R*	3684	27137	3*b*	*R*
	3804.4	26278	1, 2	*R*	3691.2?	27084	3*b*	?
System III	3805.4	26271	1, 2, 3*a*, 3*b*	*R*				
	3810.2	26237	1, 2, 3*a*	*R*				
	3815.7	26200	1	*R*?				
	3816.3	26192	1	*R*?				

Methods of excitation are: (1) burning magnesium, (2) magnesium arc, (3*a*) thermal emission, (3*b*) thermal absorption.

sequence appear. The members converge off toward the red while the first members are obviously shaded toward the violet. The third and fourth members of the sequence are barely visible on the emission spectrograms obtained by burning magnesium. We see, therefore, a sequence of bands initially shaded to the violet, becoming headless, and finally shading toward the red. The sixth member of the sequence appears quite intense on the emission spectrograms and indeed is shaded to the red. From this we can conclude nearly equal rotational constants for the two states, $B_1' \simeq B_1''$. From the direction in which the bands are progressing we can also conclude: $\omega_1' < \omega_1''$. Another interesting feature is that the band heads at λ3721.49, λ3725.7, and λ3731.75 each have multiple components, an indication of multiplet states with Hund's case (b) coupling.

The second system has two sequences of comparable intensity both degrading and progressing toward the violet, $B_2' > B_2''$, $\omega_2' > \omega_2''$.

A third system has one intense sequence of bands at λ3798 shaded and progressing toward the red and a second weaker sequence at λ3684 also shading and progressing to the red. This shows us: $B_3' < B_3''$ and $\omega_3' < \omega_3''$.

Other weaker bands also appear in thermal absorption but were not measured. Some of these may be members of the systems already mentioned or may be part of another system. In order to explain the presence of so many band systems as part of a simple diatomic spectrum we are forced to recognize the existence of several electronic states. One explanation is that there are two upper electronic states lying close together and two lower states lying close together. Correlation rules allow a $^3\Sigma$ and $^3\pi$ state to form from the ground-state magnesium and oxygen atoms. An alternate explanation is that the molecule is polyatomic and we are observing more than one mode of vibration. Considering all aspects of the spectrum, however, the former solution appears to be the more likely. Verhaeghe[19] is also of the opinion that several states are involved.

A provisional vibrational scheme is given for System I in Table VI. We have taken the intense band at λ3721 as the beginning of the 0,0 sequence. This scheme must be taken tentatively until the numbering of the bands is definitely established.

IV. IDENTIFICATION OF THE "ULTRAVIOLET SPECIES"

A rotational analysis of the ultraviolet spectrum would give us a moment of inertia which would be more conclusive in identifying the unknown molecule. Even on the high dispersion obtained here, however, the rotational structure was only partially resolved and a rotational analysis proved to be too difficult. A study of the isotope shift would also give us additional information about the molecule. A third method to distinguish a monomer from a polymer is to study the intensities of the ultraviolet and green bands together under equi-

TABLE VI. Vibrational analysis of one principal ultraviolet system (in kaysers).

V' \ V''	0	1	2	3	4	5	6	7
0	26863.9 (875.9)	25988.0						
		(801.5)						
1		26789.5 (855.2)	25934.3					
		(775.7)	(779.9)					
2		27565.2 (851)	26714.2					
3				26649.7				
4					26592.6			
					(722.4)			
5					27315.0 (772.7)	26542.3		
6							26497.6	
7								26459
	$\omega_e''\simeq 902$, $X_e''\omega_e''\simeq 13$							
	$\omega_e'\simeq 817$, $X_e'\omega_e'\simeq 9.5$							

librium vapor conditions, at constant temperature, but varying the thermodynamic activity of the solid MgO. The chemical equilibria are:

$$\text{MgO } (s, \text{activity } 1) = \text{MgO}(g, {}^1\Sigma) = 1/x(\text{MgO})_x(g) \quad (1)$$

$$\text{MgO } (s, \text{activity } 2) = \text{MgO}(g, {}^1\Sigma) = 1/x(\text{MgO})_x(g). \quad (2)$$

The thermodynamic relationship is:

$$\left(\frac{P_{1\Sigma(\text{activity } 1)}}{P_{1\Sigma(\text{activity } 2)}}\right)^x_T = \left(\frac{P_{(\text{MgO})x(\text{activity } 1)}}{P_{(\text{MgO})x(\text{activity } 2)}}\right)_T$$

or, expressed in terms of intensities:

$$\left(\frac{I_{1\Sigma(\text{activity } 1)}}{I_{1\Sigma(\text{activity } 2)}}\right)^x_T = \left(\frac{I_{(\text{MgO})x(\text{activity } 1)}}{I_{(\text{MgO})x(\text{activity } 2)}}\right)_T$$

where $I_{1\Sigma}$ and $I_{(\text{MgO})_x}$ refer to intensities of the green and ultraviolet bands, respectively.

Comparing the intensities of the two band systems at different activities of the solid will give a value for x.

Experimental

Solid MgO was heated in the King furnace as described earlier. The graphite heating element was lined with tantalum and tungsten, respectively, and the MgO was in contact with the tungsten only. When the furnace had reached the desired temperature, several emission tracings of both systems were made. The intensities and corresponding temperatures are shown in the first three columns of Table VII. The furnace temperature was then increased to 2750°K at which temperature the MgO reacted rapidly with the tungsten lining. The furnace was then lowered to approximately its original temperature and several tracings of each system were made. These results are shown in Columns 4, 5, and 6 of Table VII. In the initial runs solid MgO existed in the furnace and hence the intensities pertain to the solid at unit activity. Tungsten reacting with the solid eventually removes the MgO phase and produces a second phase at reduced MgO activity. This reduction in activity causes a corresponding reduction in intensity.

For both systems integrated intensities were measured. The reported values are proportional to the areas inclosed by the bands and extrapolated background, as shown in Fig. 3, and all intensities are adjusted to the same amplification gain. For the ultraviolet system the region between λ3700 and λ3830 was used, and the 0,0 sequence at λ5007 was treated for the green system.

Discussion of Data

The comparison of the two sets of data is shown in the last two columns in Table VII. The values of each set at reduced solid activity are compared with the average value of each set at unit solid activity. The ratios of each set of values at most deviate 20 percent from the average values, and within this experimental uncertainty the two sets of values are equal. We conclude, therefore, $x=1$ and a monomer of MgO is involved in the ultraviolet transition.

If the molecule were a dimer, that is if $x=2$, the ultraviolet bands should decrease as $(0.32)^2$ or to approximately one tenth of their original value. If this were the case, the ultraviolet intensities would be off by a factor of three which is far from the limit of uncertainty.

If the gaseous molecules were not in equilibrium within the furnace, we would expect an anomalous trend in the two sets of figures. Equilibrium is fairly certain since all runs were made under 0.2 atmos of argon to cut down diffusion of the vapor out the ends of the tube. In case a dimer had been formed in the gas phase, the total pressure of MgO vapor would still be high enough to insure a sufficient number of collisions between vapor species themselves.

It was also possible to reduce the solid activity by heating MgO and ZrO_2 mixtures. A mixture of 20 mole percent MgO was heated to 2600°K, and tracings of both systems were made. The two systems appeared with comparable intensity, and both were decreased to approximately one-fifth the intensity observed with pure MgO at the same temperature. Accurate integrated intensities could not be compared, however, since chloride impurities in the ZrO_2 produced MgCl(g) which

has many strong bands in the same ultraviolet region as MgO.

Term Diagram

Treating the "ultraviolet species" as the principal vaporizing monomer, using the thermochemical heat of sublimation and the spectroscopically determined heat of sublimation of the $^1\Sigma$ state, employing the correlation rules and using the frequency measurements in Table V, we set up the following energy level diagram for the gaseous molecules.

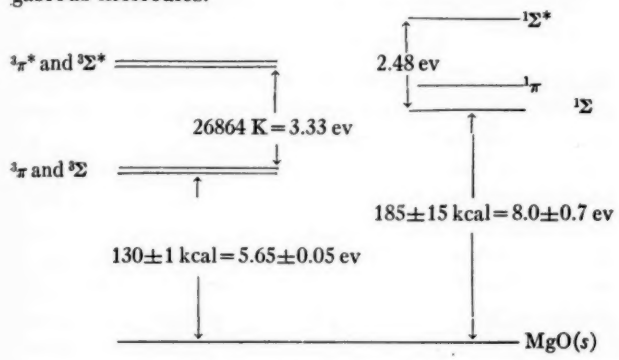

Sublimation Point of MgO

Since solid MgO vaporizes mainly to MgO gas, the calculation of the boiling point or sublimation point will depend strongly on the heat of sublimation for the reaction $MgO(s)=MgO(g)$. The partial pressures of $Mg(g)$, $O(g)$, and $O_2(g)$ contribute only slightly to the total vapor pressure. With known thermochemical data we calculate the temperature at which the sum of the partial pressures of all gaseous species is one atmosphere. The important equilibria and thermochemical data are as follows:

$$MgO(s)=Mg(g)+O(g);$$

$$-\left(\frac{\Delta F_{3000}-\Delta H_{298}}{3000}\right)=65.57\pm0.9 \text{ cal/deg},$$

$$\Delta H_{298}=238.8\pm0.5, \quad K_1=P_{Mg}P_O, \quad (1)$$

$$\tfrac{1}{2}O_2(g)=O(g); \quad -\left(\frac{\Delta F_{3000}-\Delta H_{298}}{3000}\right)=15.50\pm0.1,$$

$$\Delta H_{298}=59.55\pm0.02, \quad K_2=\frac{P_O}{P_{O_2}^{\frac{1}{2}}}, \quad (2)$$

$$MgO(s)=MgO(g,{}^3\Sigma),$$

$$-\left(\frac{\Delta F_{3000}-\Delta H_{298}}{3000}\right)=42.4\pm0.9,$$

$$\Delta H_{298}=130\pm1, \quad K_3=P_{MgO(g)}. \quad (3)$$

TABLE VII. Experimental data showing relative intensities of green and ultraviolet systems at different activities of solid MgO and proving a monomer of MgO is involved in the ultraviolet transition.

T°K	$I_{^1\Sigma}$ (unit solid activity)	$I_{(MgO)_x}$ (unit solid activity)	T°K	$I_{^1\Sigma}$ (reduced solid activity)	$I_{(MgO)_x}$ (reduced solid activity)
2605	12.4	28.6	2595	3.5	11.3
2600	13.5	25.8	2595	4.75	8.25
2600	12.3	23.4	2595	4.0	7.8

$\left(\frac{I_{^1\Sigma\ \text{(reduced solid activity)}}}{I_{^1\Sigma\ \text{(unit solid activity)}}}\right)_{T=2595-2600}$	$\left(\frac{I_{(MgO)_x\text{(reduced solid activity)}}}{I_{^1\Sigma\ \text{(unit solid activity)}}}\right)_{T=2595-2600}$
0.27	0.43
0.36	0.32
0.31	0.30
Average 0.32	0.35

Considering the free energy functions to be constant over a 100° range, and using the relation $P_{Mg}=2P_{O_2}+P_O$, successive temperature approximations were made until the calculated sum of all partial pressures was one atmosphere. At $T=3040$°K we find: $P_{Mg}+P_{O_2}+P_O\simeq0.1$ atmos and $P_{MgO(g)}\simeq0.9$ atmos.

The free energy functions for solid MgO were calculated to 2100°K from Kelley's tables,[8,9] and an estimated heat capacity of 14 cal/deg was used to extend the calculations to 3000°K. The principal uncertainty in the calculation of the sublimation temperature is the uncertainty in the free energy functions of solid MgO. This corresponds to an uncertainty of ±60°K in the calculated sublimation point. We therefore take the sublimation temperature as 3040±60°K.

It is well to note that this calculated sublimation point lies very close to the reported melting point of MgO.[20] The most accepted value of 3075°K for the melting point was obtained from heating curve experiments from which it appears the solid could have either melted or vaporized. The results of our calculation show the solid oxide should sublime before it melts or if the solid does melt at 3075°K, liquid MgO must boil very close to the melting point.

ACKNOWLEDGMENT

We would like to thank Professor John G. Phillips for use of the intensity recorder and for his assistance with the intensity measurements. We would also like to thank Professor Francis A. Jenkins and Professor Karl Wieland for help on several spectroscopic phases of this work.

[20] C. W. Kanolt, J. Wash. Acad. Sci. 3, 315 (1913).

Free-Electron Network Model for Conjugated Systems. V. Energies and Electron Distributions in the FE MO Model and in the LCAO MO Model*†

KLAUS RUEDENBERG
Laboratory of Molecular Structure and Spectra, Department of Physics, The University of Chicago, Chicago 37, Illinois

(Received August 14, 1953)

A comparative study is made of the LCAO MO model (including overlap) and the FE MO model. Energies and electronic distributions are examined and the concepts "atom population" and "bond population" are analyzed. A close correspondence is found to exist between the two theories.

IN the preceding articles of the present series, the free-electron model was defined, its mathematics were developed for the case of hydrocarbons with the neglect of electronic interaction, and the results of a number of calculations were reported.[1a,b] These investigations had shown certain similarities with the *LCAO MO model*, whereby we wish to understand the LCAO MO theory, simplified by the neglect of electronic interaction operators and integrals between non-neighboring atomic orbitals, *but including the overlap effects between neighbors*.[1c] In the present paper this relation will be examined more closely, and a remarkable kinship will be uncovered between these two MO theories which superficially appear to be so different.

It was already pointed out in (I) that the free-electron model is not so strictly a one-dimensional theory as is commonly believed and that, on the other hand, the LCAO model is not so completely a three-dimensional theory as is usually assumed. Indeed, *both* theories yield molecular orbitals of a "tubular" form, and the fourth section of the present paper will discuss this matter in more detail.

Furthermore, it will be shown that in both theories the mathematical apparatus of the quantum-mechanical problem is clearly divided into three steps, namely:

Step 1: Solution of the eigenvalue problem of a certain auxiliary matrix;

Step 2: Calculation of the energies from the eigenvalues of Step 1;

Step 3: Construction of the wavefunctions from the eigenvalues and eigenvectors of Step 1.

This formal analogy permits a step-by-step comparison and thereby leads to a comparative study of the energies and the distribution of electrons.

The auxiliary matrix of Step 1 in the conventional LCAO model will be called $\mathbf{M}$; the corresponding matrix in the conventional FE model, i.e., the model considered in our previous papers, is called $\mathbf{F}$.[2] Since one has in general $\mathbf{F} \neq \mathbf{M}$, the two models seem to differ with respect to Step 1. We shall however see that it is reasonable to construct a *modified LCAO model* which has the matrix $\mathbf{F}$ for Step 1, and a *modified FE model* which has the matrix $\mathbf{M}$ for Step 1. Thus Step 1 actually presents no real difference between the FE model and the LCAO model: each has a "M variant" and a "F variant." On the other hand, the relations which form Step 2 and Step 3 are formally quite different in the two models. Hence, we shall actually deal with *four* different theories, namely two variants (determined by Step 1) of both models (determined by Steps 2 and 3).

The principal result of the present investigation will be that, in spite of the formal differences, Steps 2 and 3 are really quite similar in nature in the two models and that therefore, for a given variant of Step 1, the FE and the LCAO models yield nearly identical numerical results for the energies and the electron distributions. The quantitative differences are certainly smaller than the errors introduced by the approximations involved in either model, and the differences between the M and F variant of one model may exceed the differences between the FE and the LCAO model for one variant.

For the purpose of studying the electronic distributions, the concepts of electronic populations around atoms and in bonds will be developed. Their analysis will lead incidentally to a precise physical interpretation of the quantities a and b defined in (I) and of the quantity q defined in the LCAO model.

1. THE LCAO MO MODEL

We start with a short description of the LCAO model with constant resonance and overlap integrals,

* Presented at the Symposium for Molecular Structure and Spectroscopy, held June 15–19, 1953 at The Ohio State University, Columbus, Ohio.

† This work was assisted by the Office of Naval Research under Task Order IX of Contract N6ori-20 with The University of Chicago.

[1] (a) K. Ruedenberg and C. W. Scherr, J. Chem. Phys. **21**, 1565 (1953), hereafter quoted as (I); C. W. Scherr, J. Chem. Phys. **21**, 1582 (1953); J. R. Platt, J. Chem. Phys. **21**, 1597 (1953); C. W. Scherr, J. Chem. Phys. **21**, 1413 (1953); K. Ruedenberg and C. W. Scherr, J. Chem. Phys. **22**, 151 (1954). (b) Recently J. S. Griffith has independently derived part of the results presented in the papers mentioned in reference 1(a). See J. Chem. Phys. **21**, 174 (1953) and Trans. Faraday Soc. **49**, 345 (1953). (c) Hence the "LCAO model" may be defined as "Tight-binding approximation with neglect of electronic interaction operators."

[2] The present paper introduces a slight modification in notation: by $\mathbf{F}$ we now denote the matrix which was called $\mathfrak{F}$ in paper (I); its eigenvalues [called F_n in paper (I)] are now denoted by f_n. No use is made of the matrix denoted in (I) by $\mathbf{F}$, which now would be written as $(\mathbf{T}^{-1}\mathbf{F}\mathbf{T}^{-1}-f\mathbf{I})$.

including overlap effects, in a form suitable for the intended comparison.[3]

Conventional LCAO MO Model

In this theory a π electronic one-electron wave function $\Phi_n(x,y,z)$ of a conjugated system is expressed as

$$\Phi_n(x,y,z)=\sum_{P=1}^{N} c_{Pn}'\chi_P(x,y,z), \tag{1.1}$$

where the summation extends over all atoms P, and

$$\chi_P=(2p\pi)_P \tag{1.2}$$

is a normalized $2p\pi$ orbital on atom P, having the molecular plane as nodal plane and its positive part above the plane. We collect the coefficients $c_{1n}'\cdots c_{Nn}'$ in the column matrix

$$\mathbf{c}_n'=\begin{pmatrix} c_{1n}' \\ \cdot \\ \cdot \\ \cdot \\ c_{Nn}' \end{pmatrix}; \tag{1.3}$$

and the matrix elements

$$\int dV\chi_P\mathcal{G}\chi_Q=G_{PQ}' \tag{1.4}$$

of an operator $\mathcal{G}$ in the square matrix

$$\mathbf{G}'=\{G_{PQ}'\}. \tag{1.5}$$

$\mathcal{G}=1$ and $\mathcal{G}=\mathcal{H}$ yield the matrices

$$S_{PQ}=\int dV\chi_P\chi_Q \tag{1.6}$$

$$H_{PQ}'=\int dV\chi_P\mathcal{H}\chi_Q. \tag{1.7}$$

The precise nature of the Hamiltonian $\mathcal{H}$ need not be specified. The variation principle leads to the eigenvalue equation

$$(\mathbf{H}'-\mathbf{S}\epsilon_n)\mathbf{c}_n'=0, \tag{1.8}$$

with the normalization

$$\int dV\Phi_m\Phi_n=(\mathbf{c}_n')^*\mathbf{S}\mathbf{c}_m'=\delta_{mn}. \tag{1.9}$$

Equations (1.8) and (1.9) can be rewritten as

$$(\mathbf{H}-\epsilon_n\mathbf{I})\mathbf{c}_n=0, \tag{1.10}$$

$$\mathbf{c}_n^*\mathbf{c}_m=\delta_{mn}, \tag{1.11}$$

where $\mathbf{I}$ is the unit matrix and

$$\mathbf{H}=\mathbf{S}^{-\frac{1}{2}}\mathbf{H}'\mathbf{S}^{-\frac{1}{2}}, \tag{1.12}$$

$$\mathbf{c}_n=\mathbf{S}^{\frac{1}{2}}\mathbf{c}_n'. \tag{1.13}$$

[3] The inclusion of overlap effects in the LCAO theory is described by B. H. Chirgwin and C. A. Coulson, Proc. Roy. Soc. (London) **A201**, 196 (1950), and by P. O. Löwdin, J. Chem. Phys. **18**, 365 (1950); **21**, 496 (1953). These papers also contain references to earlier work. The present approach resembles Löwdin's.

The reason for this *algebraic* orthogonality of the column matrices $\mathbf{c}_n$, $\mathbf{c}_m$ is that the $c_{1n}\cdots c_{Nn}$ defined by (1.13) are the coefficients in the expansion

$$\Phi_n=\sum_{P=1}^{N} c_{Pn}\chi_P^0, \tag{1.14}$$

where the Löwdin orbitals $\chi_1^0\cdots\chi_N^0$ form an orthonormal set of functions defined by[4]

$$\chi_Q^0=\sum_{P=1}^{N}(S^{-\frac{1}{2}})_{PQ}\chi_P. \tag{1.15}$$

Similarly, $\mathbf{H}$ is the matrix of $\mathcal{H}$ in this basis:

$$H_{PQ}=\int dV\chi_P^0\mathcal{H}\chi_Q^0. \tag{1.16}$$

The matrices $\mathbf{S}^{\frac{1}{2}}$ and $\mathbf{S}^{-\frac{1}{2}}$ are defined as those matrices which have the same eigenvectors as $\mathbf{S}$ and which have the eigenvalues $(+\sqrt{s_n})$ and $(+1/\sqrt{s_n})$, respectively, where s_n are the eigenvalues of $\mathbf{S}$. A definition by series expansion has been given by Löwdin.[3]

The following two assumptions are now made: (1) Only integrals between neighbors do not vanish. (2) Analogous integrals have the same value for all neighbor pairs in the molecule. As a consequence, the matrices $\mathbf{S}$ and $\mathbf{H}'$ of (1.6,7) have the form

$$\mathbf{S}=\mathbf{I}+S\mathbf{M}, \tag{1.17}$$

$$\mathbf{H}'=\alpha\mathbf{I}+\beta\mathbf{M}, \tag{1.18}$$

where

$$S=\int dV\chi_P\chi_Q, \tag{1.19}$$

$$\beta=\int dV\chi_P\mathcal{H}\chi_Q, \tag{1.20}$$

P and Q being neighbor atoms,

$$\alpha=\int dV\chi_P\mathcal{H}\chi_P, \tag{1.21}$$

and $\mathbf{M}$ is *a matrix characteristic of the molecule*, having the elements:

$$M_{PQ}=\begin{cases} 1 & \text{if } P \text{ and } Q \text{ are neighbor atoms,} \\ 0 & \text{otherwise, also if } P=Q. \end{cases} \tag{1.22}$$

Since $\mathbf{H}'$ and $\mathbf{S}$ both are functions of $\mathbf{M}$ they commute, and the matrix $\mathbf{H}$ (1.12) becomes

$$\mathbf{H}=(\alpha\mathbf{I}+\beta\mathbf{M})(\mathbf{I}+S\mathbf{M})^{-1}, \tag{1.23}$$

$$\mathbf{H}=\alpha\mathbf{I}+\gamma\mathbf{M}(\mathbf{I}+S\mathbf{M})^{-1}, \tag{1.24}$$

with

$$\gamma=\beta-\alpha S. \tag{1.25}$$

Let $\mathbf{c}_n$ be an eigenvector and m_n an eigenvalue of $\mathbf{M}$:

$$(\mathbf{M}-m_n\mathbf{I})\mathbf{c}_n=0. \tag{1.26}$$

[4] In Eq. (1.15), $(S^{-\frac{1}{2}})_{PQ}$ denotes an element of the matrix $\mathbf{S}^{-\frac{1}{2}}$.

$\mathbf{M}$ is symmetric, and has N orthonormalized eigenvectors $\mathbf{c}_1 \cdots \mathbf{c}_N$. Since $\mathbf{H}$ and $\mathbf{S}$ are functions of $\mathbf{M}$, these eigenvectors of $\mathbf{M}$ are simultaneously eigenvectors of $\mathbf{H}$ and $\mathbf{S}$, i.e., solutions of Eq. (1.10) and of

$$(\mathbf{S}-s_n\mathbf{I})\mathbf{c}_n=0, \tag{1.27}$$

$$(\mathbf{S}^{\frac{1}{2}}-s_n^{\frac{1}{2}}\mathbf{I})\mathbf{c}_n=0, \tag{1.28'}$$

$$(\mathbf{S}^{-\frac{1}{2}}-s_n^{-\frac{1}{2}}\mathbf{I})\mathbf{c}_n=0. \tag{1.28''}$$

By virtue of (1.17,24) the eigenvalues of $\mathbf{H}$ and $\mathbf{S}$ are

$$\epsilon_n=\alpha+\gamma m_n/(1+Sm_n), \tag{1.29}$$

$$s_n=1+Sm_n. \tag{1.30}$$

The column vector $\mathbf{c}_n'$ (1.3), corresponding to the eigenvector $\mathbf{c}_n$, follows from (1.13), which, by virtue of Eqs. (1.27,28',28''), simplifies to

$$\mathbf{c}_n'=\mathbf{S}^{-\frac{1}{2}}\mathbf{c}_n=s_n^{-\frac{1}{2}}\mathbf{c}_n=(1+Sm_n)^{-\frac{1}{2}}\mathbf{c}_n, \tag{1.31}$$

so that the wave functions (1.1) become

$$\Phi_n=(1+Sm_n)^{-\frac{1}{2}}\sum_P c_{Pn}\chi_P. \tag{1.32}$$

Hence the subscript P in c_{Pn}, *if* $\mathbf{c}_n$ *is an eigenvector of* $\mathbf{M}$, still indicates a meaningful relationship to the *atom* P—a relationship which does *not* exist for the subscript denoting the different components of a *general* $\mathbf{c}_n$ given by (1.13).

It is customary[3] to define the π-electronic "charge density" q_P at an atom P and the π-electronic "bond order" (mobile bond order) p_{PQ} of a bond PQ by the following equations:

$$q_P=\sum_n g_n c_{Pn}^2, \tag{1.33}$$

$$p_{PQ}=\sum_n g_n c_{Pn}c_{Qn}, \tag{1.34}$$

where $g_n=0, 1, 2$ is the number of electrons in the nth orbital [See (I), Eq. (2.68')]. The definitions (1.33,34) contain the quantities c_{Pn} and *not* the quantities c_{Pn}'.

It can now be seen that the quantum-mechanical problem can indeed be decomposed into three steps: Step 1 is the solution of the eigenvalue equation (1.26) of the auxiliary matrix $\mathbf{M}$; Step 2 is the calculation of the energies ϵ_n from the eigenvalues m_n by means of Eq. (1.29); Step 3 is the construction of the wave functions ϕ_n from the eigenvalues m_n and the eigenvectors $\mathbf{c}_n$ by means of Eq. (1.32).

Modified LCAO MO Model

Although the motive for the construction of the modified LCAO model is the intended comparison with the FE model, an argument can be given to show that the modification is not unreasonable.

Since the joint atoms are in a particular physical surrounding, a better approximation can be expected if, in the expansion of Eq. (1.1), the orbitals χ_P corresponding to joint atoms are chosen so as to be slightly different from the orbitals on the other atoms. Since it is furthermore recognized that bonds between joint atoms and their neighbors are longer and therefore less populated than other bonds, the orbitals on the joints, if assumed to be different, should be chosen in such a manner as to yield smaller numerical values for the resonance and overlap integrals in which they are involved. *Let us therefore assume the joint-atom orbitals to be such* that

$$\left.\begin{aligned} S_{PQ}&=T_PT_QS,\\ \beta_{PQ}&=T_PT_Q\beta,\end{aligned}\right\} \tag{1.35}$$

where T_P (and T_Q) is the quantity defined in (I), Eq. (2.50), namely

$$T_P=\begin{cases} 1, & \text{if } P \text{ is not a joint,}\\ (\frac{2}{3})^{\frac{1}{2}}, & \text{if } P \text{ is a joint,}\end{cases} \tag{1.36}$$

although the reduction of the integrals by the factors $(\frac{2}{3})^{\frac{1}{2}}=0.82$ and $(\frac{2}{3})=0.67$ may seem somewhat drastic. Let us furthermore assume that, similar to the normalization integral, the Coulomb integral α of Eq. (1.21) is the same for joints and nonjoints.[5] As a consequence, Eqs. (1.17), (1.18) of the preceding section have to be replaced by

$$\mathbf{S}=\mathbf{I}+S\mathbf{F}, \tag{1.37}$$

$$\mathbf{H}'=\alpha\mathbf{I}+\beta\mathbf{F}, \tag{1.38}$$

where $\mathbf{F}$ is the matrix defined in (I), (2.53), namely[2]

$$F_{PQ}=\begin{cases} T_PT_Q, & \text{if } P \text{ and } Q \text{ are neighbors,}\\ 0, & \text{otherwise, also if } P=Q.\end{cases} \tag{1.39}$$

If we introduce the matrix

$$\mathbf{T}=\{T_{PQ}\},\quad T_{PQ}=T_P\delta_{PQ}, \tag{1.40}$$

which was already defined in (I), Eq. (2.50), we may also write

$$\mathbf{F}=\mathbf{TMT}, \tag{1.41}$$

where $\mathbf{M}$ is the matrix defined in (1.22).

The effect of the substitution of Eqs. (1.37), (1.38) for Eqs. (1.17,18) is the following one: Substitute $\mathbf{F}$ for $\mathbf{M}$ in Eqs. (1.23)–(1.25); replace Eq. (1.26) by[2]

$$(\mathbf{F}-f_n\mathbf{I})c_n=0; \tag{1.42}$$

substitute $\mathbf{F}$ for $\mathbf{M}$ and f_n for m_n in all equations following Eq. (1.26). In other words: Step 1 of the quantum-mechanical problem has been changed from (1.26) into (1.42), but Steps 2 and 3 have remained unchanged.

In the case of polyenes we have $\mathbf{T}=\mathbf{I}$, hence

$$\mathbf{F}=\mathbf{M}, \tag{1.43}$$

[5] This assumption of lowering the absolute value of S and β for joints and of keeping α the same is actually similar to the more frequently proposed improvement, i.e., of increasing the absolute value of α and of keeping S and β the same.

since the molecule contains no joints; and consequently, the modified LCAO model becomes identical with the conventional LCAO model.

2. THE FE MO MODEL

Conventional FE MO Model

The FE model has been described in (I); some further developments are contained in the appendix of the the present paper. We adopt here the model as defined in Eqs. (A.1) ff. of this appendix. The electrons are then assumed to move under the influence of the potential $V(x,y,z)$ which, according to Eq. (A.1), is

$$V(x,y,z)=\begin{cases}\infty & \text{outside the path tube,}\\ E^t=\text{const} & \text{inside the tube,}\end{cases} \tag{2.1}$$

and we find the following three steps for the solution of the FE problem.

Step 1: Solve the auxiliary eigenvalue equation (2.52) of (I):

$$(\mathbf{F}-f_n\mathbf{I})\,\hat{\boldsymbol{\varphi}}_n=0, \tag{2.2}$$

where $\mathbf{F}$ is the matrix[2] of Eqs. (1.39,41) and

$$\hat{\boldsymbol{\varphi}}_n=\begin{pmatrix}\varphi_{1n}\\ \cdot\\ \cdot\\ \varphi_{Pn}\\ \cdot\\ \cdot\\ \varphi_{Nn}\end{pmatrix}. \tag{2.2a}$$

Step 2: Calculate the energy by means of (I), Eq. (2.49), and Eq. (A.3,4) of the appendix, which we rewrite in the form[2]

$$E_n=E_D[\arccos^2(\tfrac{1}{2}f_n)-\tfrac{1}{4}\pi^2]+E^0, \tag{2.3}$$

with

$$E^0=\tfrac{1}{4}\pi^2E_D+E^{tr}+E^t, \tag{2.3'}$$

where

$$f_n=2\cos\kappa_n, \tag{2.3''}$$

$$E_D=E_H(a/D)^2, \tag{2.3'''}$$

(E_H = ionization potential of hydrogen, a = Bohr radius, D = internuclear distance) and E^{tr} is discussed in the appendix. Since

$$E_n-E^0\gtreqless 0 \quad \text{for} \quad f_n\lesseqgtr 0,$$

the groundstate orbitals have their energies ≤ 0, if E^0 is chosen as the zero point of energy.

Step 3: Construct the FE wave functions $\phi_n(x)$ from the eigenvectors $\hat{\boldsymbol{\varphi}}_n$: Eqs. (2.32) and (2.50) of (I) yield

$$\left.\begin{aligned}D^{\frac{1}{2}}\boldsymbol{\phi}_n&=\mathbf{T}\hat{\boldsymbol{\varphi}}_n,\\ \text{i.e.,}\quad D^{\frac{1}{2}}\phi_n(P)&=T_P\varphi_{Pn},\end{aligned}\right\} \tag{2.4}$$

where T_P is given by (1.40), and where $\phi_n(P)$ is the value of $\phi_n(x)$ at the atom P. The vector $\hat{\boldsymbol{\phi}}_n$ is defined in (I), Eq. (2.17). One then finds the total function $\phi_n(x)$ by means of (I), Eqs. (2.21)–(2.30), and of Eqs. (A.8)–(A.15). The three-dimensional FE MO's $\Phi_n(x,y,z)$ are then constructed in the manner outlined in Sec. 1 of (I).

Step 1 of this model is identical with Step 1 of the modified LCAO model, in particular one has the identity

$$\hat{\boldsymbol{\varphi}}_n=\mathbf{c}_n. \tag{2.5}$$

Furthermore, the FE problem can be converted into a form similar to Eq. (1.10) of the LCAO model. For this purpose we define the "FE energy matrix"

$$\mathbf{E}=E_D[\arccos^2(\tfrac{1}{2}\mathbf{F})-\tfrac{1}{4}\pi^2\mathbf{I}]+E^0\mathbf{I} \tag{2.6}$$

by the usual stipulation that $\mathbf{E}$ has the same eigenvectors as $\mathbf{F}$ and that the corresponding eigenvalues of $\mathbf{E}$ are given by Eq. (2.3). Since, for the present purpose, $\kappa_n=\arccos\frac{1}{2}f_n$ is restricted to the interval $0\leq\kappa_n\leq\pi$ [see (I), Sec. 2, subsection "Discussion"], $\arccos\frac{1}{2}f_n$ represents a monotonic function, and the matrix $\arccos(\frac{1}{2}\mathbf{F})$ can also be defined by the series

$$\arccos(\tfrac{1}{2}\mathbf{F})=\tfrac{1}{2}\pi\mathbf{I}-(\tfrac{1}{2}\mathbf{F})-\tfrac{1}{6}(\tfrac{1}{2}\mathbf{F})^3-(3/40)(\tfrac{1}{2}\mathbf{F})^5-\cdots, \tag{2.7}$$

whence

$$\mathbf{E}-E^0\mathbf{I}=E_D\pi[-(\tfrac{1}{2}\mathbf{F})+(\tfrac{1}{2}\mathbf{F})^2/\pi-(\tfrac{1}{2}\mathbf{F})^3/6+(\tfrac{1}{2}\mathbf{F})^4/3\pi\cdots]. \tag{2.8}$$

By means of this matrix Steps 1 and 2 of the FE problem can then be combined in the equation

$$(\mathbf{E}-E_n\mathbf{I})\,\hat{\boldsymbol{\varphi}}_n=0, \tag{2.9}$$

which is entirely analogous to Eq. (1.10). We shall see that this analogy is not only formal: The LCAO matrix $\mathbf{H}$ of Eq. (1.23), if modified by the substitution $\mathbf{M}\rightarrow\mathbf{F}$ [see the sentence before Eq. (1.42)], can be considered as an approximation of the FE matrix $\mathbf{E}$.

Step 3, namely to find the wave functions, is formally of course a quite different procedure in the two models.

Modified FE MO Model

The modified FE model differs from the previous FE model inasmuch as the free-electron path is defined differently; the equations of motion on the path remain unchanged. The difference in the electron path is illustrated by Fig. 1 for the case of styrene: Fig. 1a shows the path for the conventional FE model; Fig. 1b

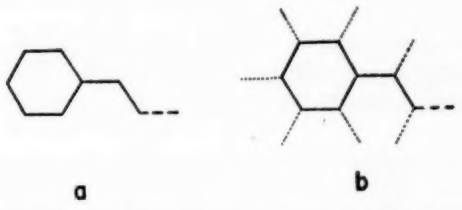

FIG. 1. Electron path in styrene: (a) conventional FE model, (b) modified FE model.

shows the path for the modified FE model. Thus, the modified model is obtained by adding a tail of one bond length to each nonjoint atom so that every atom is now a joint where three branches meet at angles of 120°.[6] In this case, it is useful to be able to distinguish between the "genuine" joints which already existed in the conventional model and the "fictitious" joints created by the modification at those atoms which were previously nonjoints. The former will be called "true joints"; the latter will be called "false joints."

Carrying through the theory of this FE problem in the manner described in (I), Sec. 2, and in the appendix of this paper, one realizes that, for this particular bond path, where all atoms are joints, the rôle of the matrix **F** of (I), (2.53) is taken over by the matrix $\frac{2}{3}\mathbf{M}$, where **M** is the matrix defined in Eq. (1.22). As a consequence, the modified FE problem can be formulated in the following fashion:

Step 1: Solve the auxiliary eigenvalue equation

$$(\mathbf{M}-m_n\mathbf{I})\,\mathfrak{k}_n=0 \tag{2.10}$$

instead of Eq. (2.2). Accordingly, Eq. (2.3″) is replaced by

$$m_n=3\cos\kappa_n. \tag{2.11}$$

Step 2: Calculated the energy which, according to Eqs. (A.3), (A.4) and (2.11), is now given by

$$E_n=E_D[\arccos^2(\tfrac{1}{3}m_n)-\tfrac{1}{4}\pi^2]+E^0 \tag{2.12}$$

rather than by Eq. (2.3). The constant E^0 is still defined by Eq. (2.3′).

Step 3: Construct the wave functions $\phi_n(x)$ from the vectors $\mathfrak{k}_n$: Since all atoms are joints, one has now

$$\left.\begin{aligned} D^{\frac{1}{2}}\boldsymbol{\phi}_n&=(\tfrac{2}{3})^{\frac{1}{2}}\mathfrak{k}_n,\\ D^{\frac{1}{2}}\phi_n(P)&=(\tfrac{2}{3})^{\frac{1}{2}}\varphi_{Pn},\end{aligned}\right\} \tag{2.13}$$

i.e.,

instead of Eq. (2.4). From the values $\phi_n(P)$ at the atoms one finds $\phi_n(x)$ again according to (I), Eqs. (2.21)—(2.30) and of Eqs. (A.8)–(A.15); and hence $\Phi_n(x,y,z)$. The normalization integral,

$$\int_L dx\phi_n^2(x)=1 \tag{2.14}$$

extends now over a larger one-dimensional space L than in the unmodified FE model. However, the eigenvectors $\mathfrak{k}_n$ are still normalized by

$$\mathfrak{k}_n^*\mathfrak{k}_n=1; \tag{2.15}$$

and the dimension (=number of components) of the eigenvector $\mathfrak{k}_n$ is unaffected by the addition of free end points and therefore the same as in the unmodified FE model.

In constructing the wave function $\phi_n(x)$, *every* bond, and furthermore *every* one-bond tail at a false joint, must now be treated as a *branch by itself*. Since an amplitude a_B and a phase δ_B is associated with each branch, it follows that the wave function $\phi_n(x)$ contains $2N_B$ constants, if N_B is the number of bonds; i.e., more than twice as many parameters than the eigenvector $\mathfrak{k}_n$. It is therefore in practice advisable to avoid explicit calculation of the wave function and to express all desired quantities in terms of the elements of $\mathfrak{k}_n$.

In the preceding formulation of the modified FE model we have purposely avoided the use of a matrix **F**, because we wish to adopt the convention that for *one molecule* there exists only *one* matrix **F**, namely the one defined in Eq. (1.39), and *one* matrix **M**, namely the one defined in Eq. (1.22). The same convention shall hold concerning the matrix **T** of (1.36,40). This is to say, that in the language of the modified FE model **T** is defined by

$$\mathbf{T}=\{T_{PQ}\},\quad T_{PQ}=T_P\delta_{PQ}, \tag{2.16}$$

$$T_P=\begin{cases}1, & \text{if } P \text{ is a false joint,}\\ (\frac{2}{3})^{\frac{1}{2}}, & \text{if } P \text{ is a true joint,}\end{cases} \tag{2.16′}$$

so that for *a particular molecule* the definition (1.36,40) and the definition (2.16,16′) lead to the same matrix. The matrix **F** is then defined by Eq. (1.39), and it is obvious that the problem of the modified FE model cannot be formulated in terms of *this* **F**.

One recognizes that Step 1, Eq. (2.10), is indeed identical with Step 1, Eq. (1.26), of the conventional LCAO model and, in particular, that Eq. (2.5) is again valid. Also Eq. (2.11) furnishes the result that the eigenvalues m_n of the matrix **M** lie in the range

$$-3\leq m_n\leq 3. \tag{2.17}$$

Finally, let us define the "energy matrix" for the modified FE model:

$$\mathbf{E}=E_D[\arccos^2(\tfrac{1}{3}\mathbf{M})-\tfrac{1}{4}\pi^2\mathbf{I}]+E^0\mathbf{I}, \tag{2.18}$$

$$\mathbf{E}-E^0\mathbf{I}=E_D\pi[-(\tfrac{1}{3}\mathbf{M})+(\tfrac{1}{3}\mathbf{M})^2/\pi - (\tfrac{1}{3}\mathbf{M})^3/6+(\tfrac{1}{3}\mathbf{M})^4/3\pi\cdots], \tag{2.19}$$

which is analogous to the matrix (2.6) of the unmodified FE model. Steps 1 and 2 of the modified FE problem can then be condensed into Eq. (2.9), if the matrix **E** in that equation is now understood to be defined by (2.18).

In the case of polyenes, Eq. (1.43) holds, and hence Step 1 yields identical eigenvalues $m_n=f_n$ and eigenvectors $\mathfrak{k}_n$ for the two FE variants [see Eqs. (2.2) and (2.10)]. [According to (2.3″), the relation (2.17) can be replaced by $-2\leq m_n\leq 2$ in this case.] Steps 2 and 3 however do not become identical: (1) The wave functions $\phi_n(x)$ are obviously quite differently defined; (2) the **F** variant uses the energy formula (2.3), whereas the **M** variant uses the energy formula (2.12). Since the modified model provides a larger path for the motion of

[6] The suggestion of adding these one-bond tails was first made by Dr. M. J. S. Dewar (personal communication through Dr. J. R. Platt).

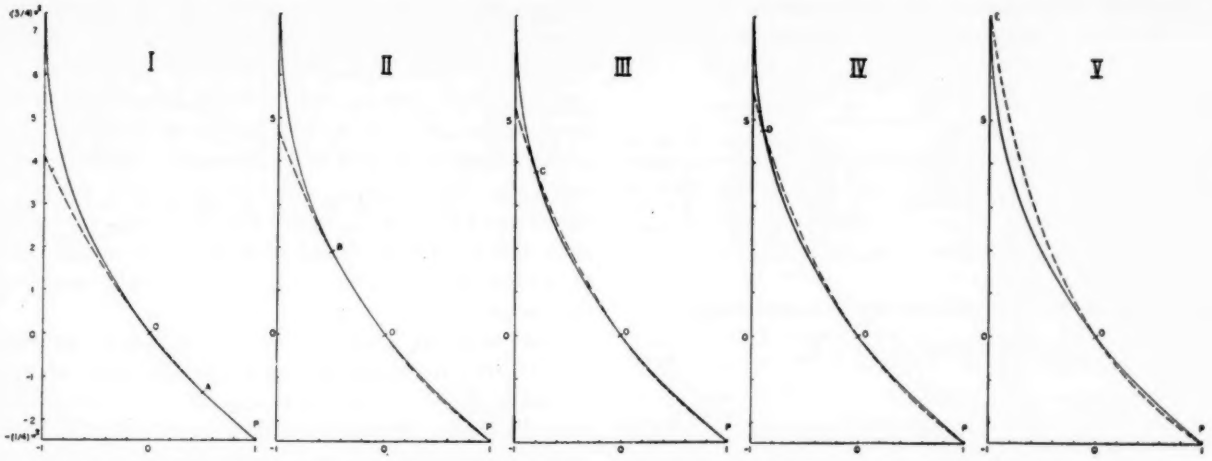

FIG. 2. Energy curves. Heavy lines: $\arccos^2 x-\frac{1}{4}\pi^2$; dashed lines: hyperbolas of the form of Eq. (3.7). See Table I.

the electrons, it is to be expected that it leads to narrower energy spacings than the unmodified model. This expectation is easily verified by means of Eqs. (2.3), (2.12), and the curve of $(\arccos^2 x-\frac{1}{4}\pi^2)$ in Fig. 2.I. However, since physical considerations suggest that the electron path of polyenes may be even shorter than in the conventional FE model, it is not very plausible to apply the modified FE model here.

3. ENERGIES

We have examined in detail the three steps which constitute the quantum-mechanical problem in each of the four theories. It was established that each model has a **M** variant and a F variant and that for the same variant the two models coincide with respect to Step 1. Step 2, i.e., the calculation of the energy, will now be considered.

In the **M** variant, we have to compare the energy function [see Eq. (1.29)]

$$\epsilon(m)=\alpha+\gamma m(1+Sm)^{-1} \tag{3.1}$$

of the conventional LCAO model with the energy function [see Eq. (2.12)]

$$E(m)=E_D[\arccos^2(\tfrac{1}{3}m)-\tfrac{1}{4}\pi^2]+E^0 \tag{3.2}$$

of the modified FE model.

In the **F** variant, we have to compare the energy function [see Eq. (1.29) and the remarks after Eq. (1.42)]

$$\epsilon(f)=\alpha+\gamma(1+Sf)^{-1} \tag{3.3}$$

of the modified LCAO model with the energy function [see Eq. (2.3)]

$$E(f)=E_D[\arccos^2(\tfrac{1}{2}f)-\tfrac{1}{4}\pi^2]+E^0 \tag{3.4}$$

of the conventional FE model.

In each of the Figs. 2.I, 2.II, 2.III, 2.IV, 2.V, the heavy line represents the function

$$y=\arccos^2 x-\tfrac{1}{4}\pi^2, \tag{3.5}$$

and the dotted lines represent five different hyperbolas

$$y=(a-bx)/(1+cx). \tag{3.6}$$

In each case, the three points in which the hyperbola intersects the function (3.5) determine the three parameters a, b, c. Since, in all five cases, the two points $0(0;0)$ and $P(1;-\frac{1}{4}\pi^2)$ are common to both curves, Eq. (3.6) simplifies to

$$y=-bx/(1+cx), \quad b=\tfrac{1}{4}\pi^2(1+c). \tag{3.7}$$

The values of the parameters b and c are listed in Table I for all five cases. We may say that the Figs. 2.I–2.V, show five different ways of approximating the curve (3.5) by an hyperbola.

These graphs show that, for a given variant, the LCAO energy function and the FE energy function are extremely similar to each other:

$$\epsilon(m)\approx E(m); \quad \epsilon(f)\approx E(f), \tag{3.8}$$

provided that the parameters α, γ, S in the LCAO

TABLE I. Specifications of the five hyperbolas in Fig. 2.

Figure	Points of intersection (x,y)			c	$\frac{1}{4}b$
2.I	$P(1;-\frac{1}{4}\pi^2)$,	$A(\frac{1}{3};-5\pi^2/36)$,	$0(0,0)$	0.25	1.0281
2.II	$P(1;-\frac{1}{4}\pi^2)$,	$0(0,0)$,	$B(-\frac{1}{2};7\pi^2/36)$	$0.3125=(5/16)$	1.0795
2.III	$P(1;-\frac{1}{4}\pi^2)$,	$0(0,0)$,	$C(-0.8;0.38229\pi^2)$	0.36038	1.1189
2.IV	$P(1;-\frac{1}{4}\pi^2)$,	$0(0,0)$,	$D(-0.9;0.48348\pi^2)$	0.39156	1.1445
2.V	$P(1;-\frac{1}{4}\pi^2)$,	$0(0,0)$,	$E(-1;\frac{3}{4}\pi^2)$	0.5	1.2337

TABLE II. Values of γ and S for the five cases of Table I.

	F-variant			M-variant		
	$-\gamma$			$-\gamma$		
Case	cm^{-1}	kcal/mole	S	cm^{-1}	kcal/mole	S
2.I	24 176	69.128	0.125	16 117	46.084	0.08333
2.II	25 385	72.586	0.15625	16 923	48.389	0.10417
2.III	26 311	75.234	0.18019	17 541	50.155	0.12013
2.IV	26 914	76.957	0.19578	17 942	51.303	0.13052
2.V	29 011	82.954	0.25	19 341	55.301	0.16667

energy function are appropriately chosen, namely,

$$\alpha = E^0 = \tfrac{1}{4}\pi^2 E_D + E^{tr} + E^t, \tag{3.9}$$

$$\left.\begin{aligned}\gamma &= -\tfrac{1}{2}bE_D \\ S &= \tfrac{1}{2}c\end{aligned}\right\} \quad \text{for the F variant,} \tag{3.10}$$

$$\left.\begin{aligned}\gamma &= -\tfrac{1}{3}bE_D \\ S &= \tfrac{1}{3}c\end{aligned}\right\} \quad \text{for the M variant,} \tag{3.11}$$

where b and c have the values of Table I. The first equation of (3.8) states that the eigenvalues of **H**, (1.23), are very close to the eigenvalues of **E**, (2.18); hence, the matrix **H** represents an approximation to the matrix **E**. The second equation of (3.8) states that the eigenvalues of **H**, (1.23), if modified by the substitution **M**→**F**, are close to the eigenvalues of **E**, (2.6); hence the matrix **H** represents an approximation of the matrix **E** also in this case.

It should be noted that the very high energies are practically unimportant, so that the hyperbolas in Figs. 2.I–2.IV, approximate Eq. (3.5) in the useful region. Within this region the fit is seen to be close. It is moreover satisfying that, for a given modification, the *order* of the energy levels is the same in the two models, regardless of the choice of the parameters α, γ, S.

On the other hand, the order of the eigenvalues f_n of **F** is *not* always the same as the order of the corresponding eigenvalues m_n of **M**. Consequently, the order of the energy levels in the F variant differs sometimes from the order of the corresponding energy levels in the M variant. This fact was already mentioned in (I) between Eq. (2.67) and Eq. (2.68), where it was also explained that symmetry characteristics establish a one-to-one correspondence between the eigenvalues of **F** and **M**.

It may also be noted that the neglect of overlap in the LCAO model ($S=0$) amounts to replacing the hyperbola (3.6) by a straight line; this approximation is therefore comparable to Simpson's approximation for the FE model [see Eqs. (A.5)–(A.7) of the appendix].

The Eqs. (3.10), (3.11) show that the comparison of the FE model with the LCAO model leads to numerical values for the overlap integral S of Eq. (1.19) and for the parameter γ, which is related to the resonance integral β of Eq. (1.20). Equation (3.9) establishes a relation between those quantities in the two theories which determine the zero point of the binding energy. If the value of (I), Eq. (2.66), is used for E_D in Eqs. (3.10), (3.11), then the five cases of Table I yield the values of γ and S given in Table II. It is extremely gratifying to note that these "theoretical values" lie in the same range as the semiempirical values of γ and S. According to (2.3‴) we furthermore find the correct result that $|\gamma|$ decreases with increasing D in the region where the FE model is valid. Also one finds, in accordance with the LCAO model, that all γ's are of the order of magnitude of $\frac{1}{2}$ the π-electronic binding energy of ethylene.

The principal result of our discussion is however that the resonance parameter γ is of the order of magnitude of the energy constant E_D defined in Eq. (2.3‴) and in (I), Eq. (2.62). According to (I), Eq. (2.61) ff, the latter determines also the order of magnitude of the lowest excitation energies. It follows that $E_D=(a/D)^2E_H \approx 1.9$ ev *is the natural energy unit for those processes in conjugated systems which have their origin in the* π *electrons.* It can be interpreted by the following atomic picture: In order that the lowest orbit of an (hypothetical) atom have the radius of the benzene ring ($\approx D$), a central charge of $Z=(a/D)\approx 0.38$ proton unit is required; the energy of an electron in such an orbit would be E_D. Also E_D is the lowest kinetic energy permitted by the uncertainty principle to an electron cloud of linear dimension D.

The usual procedure in the conventional LCAO model is to assume for S the value 0.25 and then to determine γ empirically from spectroscopic data or from resonance energies. One finds the spectroscopic γ's to be different from the resonance γ's. Table III lists the empirical values of γ for polyenes and for ring systems in the first and third columns. Since these values are obtained from the conventional LCAO model, we have to compare them with our figures for the M variant in the case of ring systems. In the case of polyenes, the values of either variant would be comparable; but in view of the arguments presented at the end of Sec. 2, we choose here the F variant. Furthermore, we can try to account for the difference between the two types of γ values by arguing: the resonance energy is a property of the ground state and should therefore yield the γ of the hyperbolas in Fig. 2.I; the spectroscopic γ, on the other hand, involves excitations and should rather belong to the hyperbola in Fig. 2.IV. In this fashion, one obtains the four different theoretical γ values which are given in the second and

TABLE III. "Theoretical" and empirical values of γ.

	Resonance γ[a]		Spectroscopic γ[a]	
	Emp[b]	Theor[d]	Emp[c]	Theor[d]
Ring systems	14 000	16 100	23 000	17 900
Polyenes	7500	24 200	32 000	26 900

[a] The table lists $(-\gamma)$ in units of cm^{-1}.
[b] G. W. Wheland, J. Am. Chem. Soc. **63**, 2025 (1941).
[c] J. R. Platt, J. Chem. Phys. **18**, 1168 (1950).
[d] From Table III.

fourth columns of Table III. Except for the resonance γ of polyenes, the empirical differences are qualitatively reflected by the theoretical values. A more exact comparison would be obtained, of course, if the semi-empirical γ's were determined under the assumption that S has the corresponding values given in Table II.

4. ELECTRON DISTRIBUTIONS

Populations

Concept

We now focus our attention upon the result of Step 3 in the quantum-mechanical problem, i.e., upon the wave functions. Although the results of Step 1 are identical in the two models (for a given variant), it is obvious that the FE wave functions will look rather different from the LCAO wave functions. Nevertheless, it will turn out that the distribution of electrons is remarkably similar in the two theories.

There are two basic quantities which can be defined in a conjugated system to give *useful information* about the distribution of π electrons *without going into too much detail:* the atom populations and the bond populations.[7] The definition of these quantities is based upon the fact that the electronic wavefunctions have, in the FE *and* in the LCAO model, a "tubular" shape as has been discussed in (I), Sec. 1. [See Fig. 3 of (I) and also Fig. 5.I of the present paper.] Let us decompose the total tube volume into sections in such a fashion that each section is centered around one atom and all sections together exhaust the entire tube; let $V(P)$ be the volume of the section belonging to the atom P. Then we define the population at atom P by[8]

$$\mathrm{pop}'V(P)=\int_{V(P)} dV\rho(x,y,z), \tag{4.1}$$

where $\rho(x,y,z)$ is the total electron density,

$$\rho(x,y,z)=\sum_n g_n\Phi_n{}^2(x,y,z). \tag{4.2}$$

[$g_n=0,1,2$ denotes the number of electrons in the orbital Φ_n.] Similarly, if one decomposes the total tube volume into sections in such a fashion that each section contains one bond and all sections together exhaust the total tube volume, and if furthermore $V(M)$ denotes the section containing the bond with the midpoint M, then

$$\mathrm{pop}'V(M)=\int_{V(M)} dV\rho(x,y,z) \tag{4.3}$$

defines the population of this bond. The normalization of the wave functions, in conjunction with the "exhaustive property" of the population definitions, guarantees the conservation relations

$$\sum_P \mathrm{pop}'V(P)=\sum_M \mathrm{pop}'(M)=N, \tag{4.4}$$

where the summation extends over all atoms P or over all bond midpoints M, respectively; and where N is the total number of electrons.

It should be noted that these definitions cannot be interpreted to mean that a certain percentage of all electrons belongs to atoms and the rest form the bonds. Such a picture would be quite contrary to the concept of the π-electronic mobility. The two population definitions are mutually exclusive; they represent *two different* ways of building up the *total* π-electronic population: *either* from atomic contributions *or* from bond contributions. The populations will be the topic of this section; relatively simple expressions will be obtained for them, and one result of the theory will be the demonstration of the near-identity of FE and LCAO populations.

FE Populations

Consider a section of the FE tube [see (I), Sec. 1]; let L be its "longitudinal extension," Q its "transversal cross section," and V its volume. In view of (I), Eq. (1.18), the FE population of this section can be written as

$$\mathrm{pop}'V=\int_L dx\omega(x)=\mathrm{pop}'L, \tag{4.5}$$

where

$$\omega(x)=\lim_{Q\to 0}\int_Q dQ\rho(x,y,z)=\sum_n g_n\phi_n{}^2(x) \tag{4.6}$$

is the *linear* FE density. The FE atom populations will be denoted by

$$a'(P)=\mathrm{pop}'L_P; \tag{4.7}$$

the FE bond populations will be denoted by

$$b'(M)=\mathrm{pop}'L_M. \tag{4.8}$$

The integration paths L_P and L_M which enter these definitions in the case of the conventional FE model are shown as heavy lines in Fig. 3. Minor particularities arise at the free end points:

(1) L_P for the last atom contains the entire "tail," which exceeds the atom by one bondlength [see (I), after Eq. (1.34)];

(2) There exists a "bond population" for the "tail" which is formed by the FE path L_M which exceeds the last atom. Although this "tail" is not a bond in the original sense of the word, we shall define a separate population for it. These particularities are necessary in order to insure the validity of Eq. (4.4); they are a consequence of the "exhaustive property" of the population definitions. Equations (4.7), (4.8) are in agreement with Eqs. (2.68)–(2.68″) and (2.70) of (I).

[7] The distinction between electron densities and electron populations was first suggested by J. R. Platt.

[8] The term "atom population" has been chosen for simplicity. A more correct name would be: "population in the neighborhood of an atom."

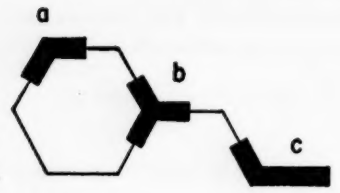

FIG. 3. Integration paths for populations in the conventional FE model. (a) Population for nonjoint atom; (b) Population for joint atoms; (c) Population for end atom; (d) Population for bond between nonjoint atoms; (e) Population for bond between joint and nonjoint atom; (f) Population for tail.

The integration paths L_P, L_M for the modified FE model which are shown in Fig. 4 need explanation. Let us call the "tail" which originates from a "false joint" [see Sec. 2, beginning of the second subsection] a "false tail."[9] Observe:

(1) The atom population of a false joint comprises integration over the *total* false tail. In the case of a genuine end atom, the integration therefore includes *two* tails, a "true" and a "false" one.

(2) It would be unreasonable to treat the false tails and their populations separately; it is more sensible to consider them as being involved in the adjoining bonds. Therefore, we do *not* define separate populations for the false tails, and at the same time we *redefine*, for the modified FE model, the population of the bond between two atoms P and Q in the following manner:

population of bond $PQ=b'(M)$
$=$ (population of electron path between P and Q)
$+\frac{1}{2}$ (population of false tail at P)
$+\frac{1}{2}$ (population of false tail at Q).

If P or Q is a true joint and therefore has no false tail, then the corresponding term vanishes in the preceding definition. *Genuine* tails do have separate tail populations in the modified as well as in the conventional FE model; since they always originate from false joints, their population comprises $\frac{1}{2}$ of the population of the false tail originating from the end atom. The conservation relation (4.4) still holds for the populations thus defined.

LCAO Populations

A fundamental assumption of the LCAO model is the neglect of all integrals between orbitals on non-neighboring atoms. Since this hypothesis determines the character of the entire theory, there is no reason why one should not frankly express the physical meaning of this assumption, namely that only orbitals with a finite extension are admitted. Indeed, if the orbital χ_P is used in a molecule which contains rings, then χ_P must vanish outside a radius of $\frac{1}{2}\sqrt{3}=0.87$ bondlength in the molecular plane. It is true that the neglect of non-neighbor interaction may be considered as a first-order approximation in an expansion according to overlap integrals or other parameters of a theory involving atomic orbitals with *infinite* range; but the physical picture which represents this first approximation is that of orbitals with a *finite* range. The heavy circles in Figs. 5.I and 5.II show a possible picture of the orbitals χ_P which are used in the styrene molecule. Since any molecular orbital is a superposition of these χ_P's, it can indeed be said to have a tubular shape.

The χ_P's are, of course, supposed to be antisymmetric with respect to the plane of the paper. The actual size and shape of the orbitals is irrelevant; only the following information will be needed:

$$\left.\begin{aligned} &\chi_P \text{ is cylindrically symmetric,}\\ &\chi_P \equiv 0 \quad \text{outside its finite limits,}\\ &\int dV \chi_P^2 = 1,\\ &\int dV \chi_P \chi_Q = \begin{cases} S & \text{for neighbors in the conventional LCAO model,}\\ T_P T_Q S & \text{for neighbors in the modified LCAO model.}\end{cases}\end{aligned}\right\} \quad (4.9)$$

In the conventional LCAO model, the orbital wave function χ_P is the same for all atoms. In the modified

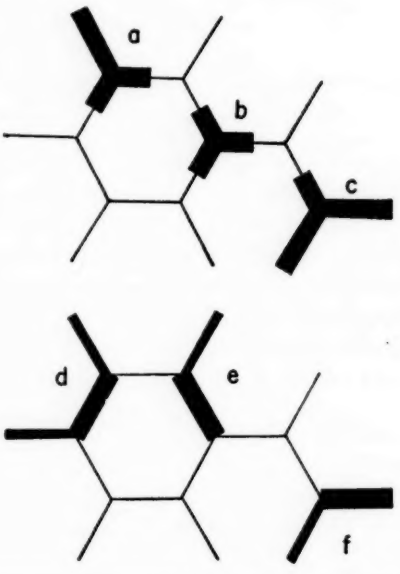

FIG. 4. Integration paths for populations in the modified FE model. Cases (a) to (f): as in Fig. 3. On the false tails, the heavy line is only half as broad if only $\frac{1}{2}$ of the population of the false tail is to be taken.

[9] This name shall *not* however imply that the "false tail" is definitely a mathematical fiction. The π electrons may have some tendency to move toward the hydrogen atoms.

LCAO model, the atomic orbitals at the joints have a different internal structure: *We still assume them to have the same finite range as the orbitals at nonjoint atoms; but in that region of a joint orbital χ_P which overlaps its neighbor orbital, its wave function is (essentially) smaller by a factor $(\frac{2}{3})^{\frac{1}{3}}$ than the wave function of a nonjoint atomic orbital would be.*

The LCAO atom populations will be denoted by [see (4.1)]

$$q'(P)=\mathrm{pop}'V(P); \tag{4.10}$$

the LCAO bond populations will be denoted by [see (4.3)]

$$r'(M)=\mathrm{pop}'V(M). \tag{4.11}$$

There can be little question how the volumes of integration, $V(P)$ and $V(M)$, have to be chosen in these definitions. They are shown as shaded areas in Fig. 5 for all possible cases which may arise. Again we find particularities at the end points:

(1) The atom population of the last atom is differently defined (Case c in Fig. 5).

(2) There exist a bond population for the "tail" beyond the last atom (Case *f* of Fig. 5). Again these special definitions guarantee the validity of the conservation relation (4.4).

Approximate Populations

The conservation relation (4.4) furnishes population average values. If the number of electrons equals the number of atoms, one finds for the atom populations

$$[\mathrm{pop}'V(P)]_{\mathrm{Av}}=1, \tag{4.12}$$

and for the bond populations (including tails)

$$[\mathrm{pop}'V(M)]_{\mathrm{Av}}=[1+\tfrac{1}{2}(J+E)/N]^{-1}, \tag{4.13}$$

where J is the number of joints and E the number of endpoints in the molecule [the number of branches is $\frac{1}{2}(E+3J)$]. These average values give the order of magnitude for the respective populations, since the latter, being superpositions of many orbital populations, do not vary excessively.

It is however useful to have approximate populations which, while being easier to calculate than the exact populations, are more differentiating than the estimates (4.12), (4.13). In the following it will be shown that, for the theories considered here, all atom and bond populations can be written in the form

$$\mathrm{pop}'V=\mathrm{pop}V+\delta\,\mathrm{pop}V, \tag{4.14}$$

i.e.,

$$a'(P)=a(P)+\delta a(P), \tag{4.15}$$

$$b'(M)=b(M)+\delta b(M), \tag{4.16}$$

$$q'(P)=q(P)+\delta q(P), \tag{4.17}$$

$$r'(M)=r(M)+\delta r(M), \tag{4.18}$$

where $\delta\,\mathrm{pop}V$ is a small correction term and $\mathrm{pop}V$ has a simpler mathematical expression than $\mathrm{pop}'V$. The

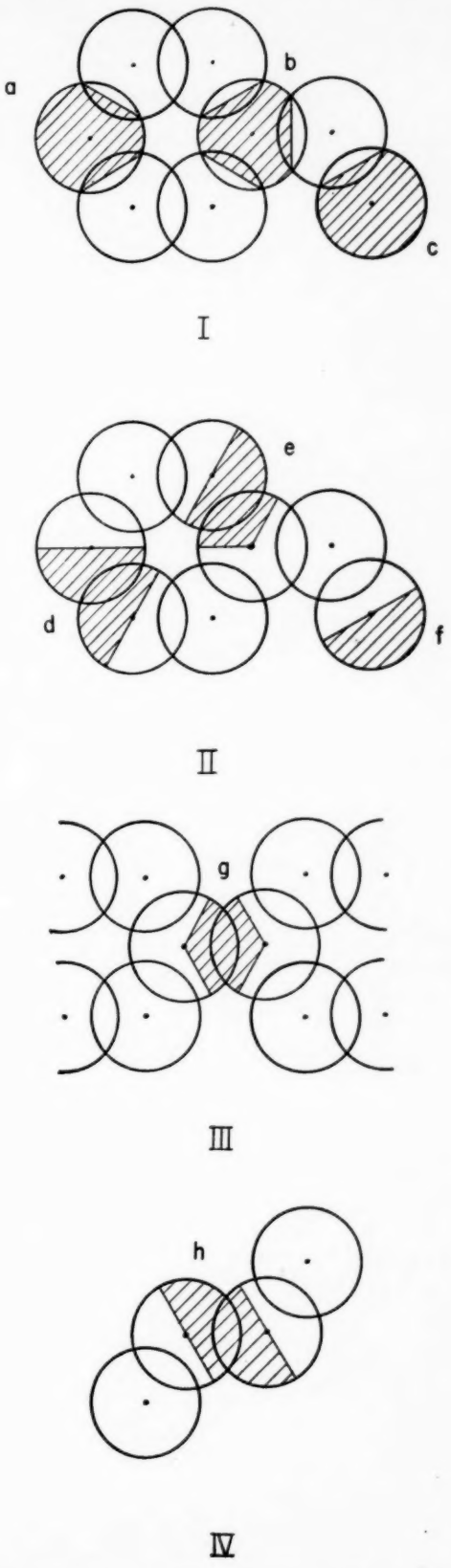

FIG. 5. Integration volumes for populations in the LCAO model. Cases (a) to (f): as in Fig. 3. (g) Population of bond between two joints; (h) Bond population in polyene chain.

pop$'V$'s are called exact or integrated population; the pop$V$'s are called approximate populations.

Conventional FE Model

The population (4.5) in the interval $(x_0-\frac{1}{2}L, x_0+\frac{1}{2}L)$ is given by

$$\text{pop}'V=\sum_n g_n\int_{x_0-\frac{1}{2}L}^{x_0+\frac{1}{2}L} dx a_n^2\cos^2(k_nx+\delta_n),$$
$$=\sum_n g_n\tfrac{1}{2}a_n^2\{L+k^{-1}\sin kL[2\cos^2(kx_0+\delta)-1]\}_n, \quad (4.19)$$

whence

$$\text{pop}'L=\text{pop}L+\delta\,\text{pop}L, \quad (4.20)$$

with

$$\text{pop}L=L\sum_n g_n\phi_n^2(x_0), \quad (4.20')$$

$$\delta\,\text{pop}L=L\sum_n g_n[1-(k_nL)^{-1}\sin k_nL][\tfrac{1}{2}a_n^2-\phi_n^2(x_0)]. \quad (4.20'')$$

Bond Populations

Let M be the bond midpoint between the atoms P and Q. Putting $x_0=M$ and $L=D$ in Eqs. (4.20), (4.20′), (4.20″) and taking into account the definition (4.6), we find for the two terms on the right-hand side of Eq. (4.16)

$$b(M)=D\omega(M), \quad (4.21)$$

$$\delta b(M)=D\sum_n g_n(1-\kappa_n^{-1}\sin\kappa_n)[\tfrac{1}{2}a_n^2-\phi_n^2(M)], \quad (4.22)$$

where $\kappa_n=Dk_n$ [see (I), Eq. (2.14)]. The amplitudes a_n can be eliminated by means of Eqs. (A.13), (A.14) of the appendix, whence

$$\delta b(M)=D\sum_n g_n(1-\kappa_n^{-1}\sin\kappa_n)(2\sin^2\kappa_n)^{-1}(1+\cos\kappa_n)$$
$$\times[\phi_n^2(P)+\phi_n^2(Q)-2\phi_n^2(M)], \quad (4.23)$$

and

$$\delta b(M)=D\sum_n g_n(1-\kappa_n^{-1}\sin\kappa_n)(2\sin^2\kappa_n)^{-1}(1+\cos\kappa_n)$$
$$\times[\cos\kappa_n\phi_n^2(M)-\phi_n(P)\phi_n(Q)]. \quad (4.24)$$

Substitution of Eqs. (A.8), (A.12) of the appendix in Eqs. (4.21), (4.22) yields

$$b(M)=D\sum_n g_n(1+\cos\kappa_n)^{-1}$$
$$\times\{\tfrac{1}{2}[\phi_n^2(P)+\phi_n^2(Q)]+\phi_n(P)\phi_n(Q)\}, \quad (4.25)$$

$$\delta b(M)=D\sum_n g_n(1-\kappa_n^{-1}\sin\kappa_n)(2\sin^2\kappa_n)^{-1}\cos\kappa_n$$
$$\times[\phi_n^2(P)+\phi_n^2(Q)-(2\phi_n(P)\phi_n(Q)/\cos\kappa_n)]. \quad (4.26)$$

Thus, $b(M)$, $\delta b(M)$, and hence also the exact population $b'(M)$ can be found from the eigenvectors $\boldsymbol{\phi}_n$ without calculating the wave functions $\phi_n(x)$ themselves. Equations (4.21-4.26) also hold for the bond population of a "tail"; in that case P is the last atom and Q is the end point where $\phi_n(Q)=0$.

Atom Populations

The population of a nonjoint atom is obtained in similar manner. Equations (4.20′), (4.20″) and (A.9) yield the form (4.15) with

$$a(P)=D\omega(P), \quad (4.27)$$

$$\delta a(P)=D\sum_n g_n(1-\kappa_n^{-1}\sin\kappa_n)[\tfrac{1}{2}a_n^2-\phi_n^2(P)], \quad (4.28)$$

$$\delta a(P)=D\sum_n g_n(1-\kappa_n^{-1}\sin\kappa_n)(2\sin\kappa_n)^{-2}$$
$$\times[\phi_n^2(Q)+\phi_n^2(R)-2\phi_n^2(P)], \quad (4.29)$$

where Q and R are the two neighbors of P.

For an end atom, Eq. (4.28), (4.29) has to be replaced by

$$\delta a(P)=\delta_0a(P)+\delta_ea(P), \quad (4.30)$$

where $\delta_0a(P)$ is again the expression in Eqs. (4.28), (4.29), and

$$\delta_ea(P)=\sum_n g_n\int_{x_0}^{x_0+\frac{1}{2}D} dx a_n^2\cos^2(k_nx+\delta_n), \quad (4.31)$$

x_0 being the free end point of the free-electron path, where the wave function vanishes. One finds

$$\delta_ea(P)=D\sum_n g_n(1-\kappa_n^{-1}\sin\kappa_n)\tfrac{1}{4}a^2, \quad (4.32)$$

or, by virtue of Eq. (A.8),

$$\delta_ea(P)=D\sum_n g_n(1-\kappa_n^{-1}\sin\kappa_n)(2\sin\kappa_n)^{-2}\phi_n^2(P). \quad (4.32')$$

In Eq. (4.30) we now substitute Eq. (4.29) [for $\delta_0a(P)$] and Eq. (4.32′), whence

$$\delta a(P)=D\sum_n g_n(1-\kappa_n^{-1}\sin\kappa_n)(2\sin\kappa_n)^{-2}[\phi_n^2(Q)-\phi_n^2(P)] \quad (4.33)$$

for end atoms, Q being the neighbor of P.

The population of a joint atom is given by

$$a'(P)=\sum_n g_n\sum_{B=1}^{3}\int_{x_{JB}}^{x_{JB}+\frac{1}{2}D} dx_B a_{Bn}^2\cos^2(k_nx_B+\delta_{Bn}), \quad (4.34)$$

where x_{JB} is the coordinate of the joint P on branch B. After a few transformations several terms cancel by virtue of the joint conditions (I), Eq. (1.28), and the amplitudes can be eliminated by means of Eq. (A.10). Hence the form (4.15) is obtained with

$$a(P)=\tfrac{3}{2}D\omega(P), \quad (4.35)$$

$$\delta a(P)=D\sum_n g_n(1-\kappa_n^{-1}\sin\kappa_n)[\tfrac{1}{2}\sum_{B=1}^{3}\tfrac{1}{4}a_{Bn}^2-\tfrac{3}{2}\phi_n^2(P)], \quad (4.36)$$

$$\delta a(P)=D\sum_n g_n(1-\kappa_n^{-1}\sin\kappa_n)(2\sin\kappa_n)^{-2}$$
$$\times[\sum_B\phi_n^2(Q_B)-3\phi_n^2(P)], \quad (4.37)$$

where Q_1, Q_2, Q_3 are the three neighbors of the joint P.

Modified FE Model

Bond Populations

According to our earlier discussion and by virtue of Eq. (2.16′) the bond populations in the modified FE model may be written as

$$b'(M)=(\text{population of electron path between } P \text{ and } Q)$$
$$+(\tfrac{3}{2}T_P^2-1)(\text{population of false tail at } P)$$
$$+(\tfrac{3}{2}T_Q^2-1)(\text{population of false tail at } Q). \quad (4.38)$$

In this equation the bond population formulas of the conventional FE model can directly be substituted. If Eqs. (4.25), (4.26) are used for the latter, and if the elements φ_{Pn} of the normalized FE eigenvectors $\boldsymbol{\varphi}_n$ are introduced by means of Eq. (2.13), when Eq. (4.38) yields

$$b(M)=\sum_n g_n(1+\cos\kappa_n)^{-1}$$
$$\times[\tfrac{1}{2}(T_P^2\varphi_{Pn}^2+T_Q^2\varphi_{Qn}^2)+\tfrac{2}{3}\varphi_{Pn}\varphi_{Qn}], \quad (4.39)$$

$$\delta b(M)=\sum_n g_n(1-\kappa_n^{-1}\sin\kappa_n)(2\sin^2\kappa_n)^{-1}\cos\kappa_n$$
$$\times[T_P^2\varphi_{Pn}^2+T_Q^2\varphi_{Qn}^2-(4\varphi_{Pn}\varphi_{Qn}/3\cos\kappa_n)]. \quad (4.40)$$

From the remarks following Eq. (2.15) it is clear that the expressions (4.39), (4.40), involving the eigenvector elements, are more convenient, in the modified FE model, than the expressions obtained by substituting Eqs. (4.21), (4.22) in Eq. (4.38). For a "true tail" Eqs. (4.39), (4.40) still hold, if Q is assumed to be the endpoint where $\varphi_{Qn}=0$.

Atom Populations

Consider first a true joint P. Here, Eqs. (4.35, 37) from the conventional FE model can be directly applied. Introduction of

the φ_{Pn}'s by means of Eq. (4.6) and (2.13) yields

$$a(P)=\sum_n g_n\varphi_{Pn}^2, \tag{4.41}$$

$$\delta a(P)=\sum_n g_n(1-\kappa_n^{-1}\sin\kappa_n)(6\sin^2\kappa_n)^{-1}[\sum_B \varphi_{Bn}^2-3\varphi_{Pn}^2], \tag{4.42}$$

where Q_1, Q_2, Q_3 are the three neighbors of P, and φ_{Bn} refers to the atom Q_B.

In the case of a false joint P, one has to observe that the entire false tail contributes to the population so that

$$\delta a(P)=\delta_0 a(P)+\delta_e a(P), \tag{4.43}$$

where $\delta_0 a(P)$ is again the expression in Eq. (4.42) and $\delta_e a(P)$ is the term of Eq. (4.32′). Let $P_1=Q$, $P_2=R$ be the two neighbors of P; then, Eq. (4.43) yields

$$\delta a(P)=\sum_n g_n(1-\kappa_n^{-1}\sin\kappa_n)(6\sin^2\kappa_n)^{-1}[\varphi_{Qn}^2+\varphi_{Rn}^2-2\varphi_{Pn}^2] \tag{4.44}$$

for false joints.

At a genuine end atom P, finally, two tails (the true and a false tail) contribute so that

$$\delta a(P)=\delta_0 a(P)+2\delta_e a(P), \tag{4.45}$$

where $\delta_0 a(P)$ and $\delta_e a(P)$ are again given by Eqs. (4.42) and (4.32′), respectively. Let $P_1=Q$ be the neighbor of P; then Eq. (4.45) yields

$$\delta a(P)=\sum_n g_n(1-\kappa_n^{-1}\sin\kappa_n)(6\sin^2\kappa_n)^{-1}[\varphi_{Qn}^2-\varphi_{Pn}^2] \tag{4.46}$$

for genuine end atoms. The expression of Eq. (4.41) is of course valid for *all* atoms.

Conventional LCAO Model

Atom Populations

The definitions (4.1), (4.2), (4.10), in conjunction with the expression (1.32) for the MO's, yield for the LCAO population at an atom P the result

$$q'(P)=\sum_n g_n(1+Sm_n)^{-1}\sum_Q\sum_R c_{Qn}c_{Rn}\int_{V(P)} dV\chi_P\chi_Q, \tag{4.47}$$

where Q and R are summed over all atoms.

Consider first the case of a nonjoint atom whose integration volume $V(P)$ is given in Fig. 5a. The integrations in (4.47) can be carried out if one employs the relations (4.9) and moreover introduces the integral

$$\mathfrak{S}=\int_{\tau_P} dV\chi_P^2, \tag{4.48}$$

where τ_P is the volume of integration indicated in Fig. 6. The result is

$$q'(P)=\sum_n g_n(1+Sm_n)^{-1}[c_{Pn}^2+\mathfrak{S}(c_{Qn}^2+c_{Rn}^2-2c_{Pn}^2)+S c_{Pn}(c_{Qn}+c_{Rn})], \tag{4.49}$$

where Q and R are the two neighbors of P. Now it is easily seen from Fig. 6 that $2\mathfrak{S}$ is smaller than the overlap integral S, but of the same order of magnitude:[10]

$$\mathfrak{S}=\tfrac{1}{2}\theta S \quad \text{with} \quad \theta\lesssim 1; \tag{4.50}$$

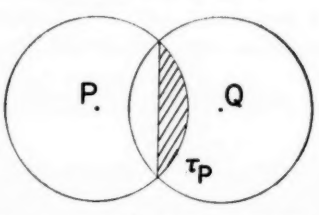

FIG. 6. Integration volume for Eqs. (4.48) and (4.69).

[10] It is assumed that χ_P decreases monotonicly to zero while approaching the limiting surface in a plane parallel to the nodal plane.

and, furthermore, Eq. (1.26) yields

$$c_{Qn}+c_{Rn}=m_n c_{Pn}. \tag{4.51}$$

By substituting Eqs. (4.50) and (4.51) in Eq. (4.49), we may therefore write $q'(P)$ in the form (4.17) with

$$q(P)=\sum_n g_n c_{Pn}^2, \tag{4.52}$$

$$\delta q(P)=\tfrac{1}{2}\theta\sum_n g_n(S^{-1}+m_n)^{-1}[c_{Qn}^2+c_{Rn}^2-2c_{Pn}^2]. \tag{4.53}$$

If P is an end atom, then the integration volume $V(P)$ is given by Fig. 5c. It is easily seen that in this case one finds

$$q(P)=\sum_n g_n c_{Pn}^2, \tag{4.54}$$

$$\delta q(P)=\tfrac{1}{2}\theta\sum_n g_n(S^{-1}+m_n)^{-1}[c_{Qn}^2-c_{Pn}^2], \tag{4.55}$$

where Q is the only neighbor of P.

Finally, if P is a joint atom, the volume of integration $V(P)$ is the one shown in Fig. 5b. In analogy to Eq. (4.49) we now obtain

$$q'(P)=\sum_n g_n(1+Sm_n)^{-1}[c_{Pn}^2+\mathfrak{S}(\sum_{B=1}^{3} c_{Bn}^2-3c_{Pn}^2)+S c_{Pn}\sum_{B=1}^{3} c_{Bn}]; \tag{4.56}$$

and Eq. (4.51) is replaced by

$$\sum_{B=1}^{3} c_{Bn}=m_n c_{Pn}, \tag{4.57}$$

where c_{Bn} refers to the atom Q_B; Q_1, Q_2, Q_3 being the three neighbors of P. Hence,

$$q(P)=\sum_n g_n c_{Pn}^2, \tag{4.58}$$

$$\delta q(P)=\tfrac{1}{2}\theta\sum_n g_n(S^{-1}+m_n)^{-1}[\sum_{B=1}^{3} c_{Bn}^2-3c_{Pn}^2]. \tag{4.59}$$

Bond Populations

In analogy to Eq. (4.47), a bond with the midpoint M has the population [see the definition (4.11)]

$$r'(M)=\sum_n g_n(1+Sm_n)^{-1}\sum_P\sum_Q c_{Pn}c_{Qn}\int_{V(M)} dV\chi_P\chi_Q, \tag{4.60}$$

where P and Q are summed over all atoms. Figures 5d, e, g, h show the volume of integration $V(M)$ for the cases that none, one or both of the bond atoms are joints. By virtue of the Eqs. (4.9), the result can, in all three cases, be written as

$$r'(M)=\sum_n g_n(1+Sm_n)^{-1}[\tfrac{1}{2}(T_P^2c_{Pn}^2+T_Q^2c_{Qn}^2)+2Sc_{Pn}c_{Qn}], \tag{4.61}$$

where T_P and T_Q are defined in (1.36). For an end tail, one has the volume $V(M)$ given by Fig. 5f, which leads to the population

$$r'(M)=\sum_n g_n(1+Sm_n)^{-1}\tfrac{1}{2}c_{Pn}^2. \tag{4.62}$$

Hence Eq. (4.61) still applies if one puts $c_{Qn}=0$ in it.

Let us indicate the dependence of $r'(M)$ on S by writing $r(M,S)$. Actually $r'(M,S)$ does not depend very strongly upon S, as may be seen by investigating the difference

$$r'(M,S)-r'(M,S_0)=\sum_n g_n[m_n(S_0-S)/(1+S_0m_n)(1+Sm_n)]\times[\tfrac{1}{2}(T_P^2c_{Pn}^2+T_Q^2c_{Qn}^2)-(2c_{Pn}c_{Qn}/m_n)]. \tag{4.63}$$

We shall show later that this expression as well as the remarkably similar expression for $\delta b(M)$ in Eq. (4.40) is small compared to the bond population itself.

In view of the intended comparison with the modified FE model,[11] we define the quantity $r(M)$ of Eq. (4.18) as

$$r(M)=r'(M, S=\tfrac{1}{3}), \tag{4.64}$$

i.e.,

$$r(M)=\sum_n g_n(1+\tfrac{1}{3}m_n)^{-1}[\tfrac{1}{2}(T_P^2c_{Pn}^2+T_Q^2c_{Qn}^2)+\tfrac{2}{3}c_{Pn}c_{Qn}]; \tag{4.65}$$

and accordingly

$$\delta r(M)=\delta r(M,S)=r'(M,S)-r'(M, S=\tfrac{1}{3}), \tag{4.66}$$

i.e.,

$$\delta r(M,S)=\sum_n g_n[\tfrac{1}{2}m_n(\tfrac{1}{3}-S)/(1+\tfrac{1}{3}m_n)(1+Sm_n)]$$
$$\times[T_P^2c_{Pn}^2+T_Q^2c_{Qn}^2-(4c_{Pn}c_{Qn}/m_n)], \tag{4.67}$$

so that[11]

$$r'(M,S)=r(M)+\delta r(M,S). \tag{4.68}$$

The formulas (4.65), (4.67) apply also to tailes if one puts $c_{Qn}=0$ in them [see Eq. (4.62)].

Modified LCAO Model

The construction of the populations in the modified LCAO model follows the same pattern as the derivations in Eqs. (4.47)–(4.68). There are only three basic changes which have to be made:

(1) The factors $(1+Sm_n)^{-1}$ in Eqs. (4.47) and (4.60) have to be replaced by the expressions $(1+Sf_n)^{-1}$, where the f_n's are the eigenvalues of the matrix **F** [see Eq. (1.42)];

(2) The integration over two neighbor orbitals, $\chi_P\chi_Q$, yields now T_PT_QS instead of S [see Eq. (4.9)];

(3) For the integral of Eq. (4.48) one obtains no longer the estimate of Eq. (4.50) in all cases, but in view of the discussion of the joint orbitals given after Eq. (4.9), one has now [see also Fig. 6]

$$\int_{\tau_P} dV\chi_P^2=S_P=\tfrac{1}{2}\theta T_P^2S, \quad \theta\lesssim 1. \tag{4.69}$$

These changes have then to be carried through for all derivations.

Atom Populations

Instead of Eq. (4.49), we now find

$$q'(P)=\sum_n g_n(1+Sf_n)^{-1}[c_{Pn}^2+(S_Qc_{Qn}^2+S_Rc_{Rn}^2-2S_Pc_{Pn}^2)$$
$$+ST_Pc_{Pn}(T_Qc_{Qn}+T_Rc_{Rn})] \tag{4.70}$$

for the atom population of a nonjoint atom. At the same time, Eq. (4.51) is replaced by

$$T_PT_Qc_{Qn}+T_PT_Rc_{Rn}=f_nc_{Pn}, \tag{4.71}$$

which follows from Eq. (1.42). Substitution of Eqs. (4.69) and (4.71) in Eq. (4.70) yields

$$q(P)=\sum_n g_nc_{Pn}^2, \tag{4.72}$$

$$\delta q(P)=\tfrac{1}{2}\theta\sum_n g_n(S^{-1}+f_n)^{-1}[T_Q^2c_{Qn}^2+T_R^2c_{Rn}^2-2c_{Pn}^2]. \tag{4.73}$$

For end atoms and joint atoms, the derivation proceeds analogously. For $q(P)$ one obtains again Eq. (4.72), whereas $\delta q(P)$ is found to be

$$\delta q(P)=\tfrac{1}{2}\theta\sum_n g_n(S^{-1}+f_n)^{-1}[\sum_B T_B^2c_{Bn}^2-2c_{Pn}^2] \tag{4.74}$$

for joint atoms, and

$$\delta q(P)=\tfrac{1}{2}\theta\sum_n g_n(S^{-1}+f_n)^{-1}[T_Q^2c_{Qn}^2-c_{Pn}^2] \tag{4.75}$$

for tails.

[11] From the point of view of the LCAO model alone, the decomposition (4.68) is rather a complication than a simplification, since Eq. (4.64,65) is only a special case of Eq. (4.61). The same is true for the decomposition (4.82) based upon the definition (4.78,79).

Bond Populations

The bond populations of the modified LCAO model are constructed by the same method which was employed in Eqs. (4.60–68) for the conventional LCAO model. Introducing the changes mentioned in the beginning of this subsection, we therefore obtain [see (4.61), (4.62)]

$$r'(M,S)=\sum_n g_n(1+Sf_n)^{-1}[\tfrac{1}{2}(T_P^2c_{Pn}^2+T_Q^2c_{Qn}^2)$$
$$+2ST_PT_Qc_{Pn}c_{Qn}], \tag{4.76}$$

which applies for all types of bonds (put $c_{Qn}=0$ in end bonds). Hence [see (4.63)]

$$r'(M,S)-r'(M,S_0)$$
$$=\sum_n g_n[f_n(S_0-S)/(1+Sf_n)(1+S_0f_n)]$$
$$\times[\tfrac{1}{2}(T_P^2c_{Pn}^2+T_Q^2c_{Qn}^2)-(2T_PT_Qc_{Pn}c_{Qn}/f_n)]. \tag{4.77}$$

In view of the intended comparison with the conventional FE model,[11] we now define the quantity $r(M)$ of Eq. (4.18) as [note the difference from the definition (4.64)!]:

$$r(M)=r'(M, S=\tfrac{1}{2}), \tag{4.78}$$

$$r(M)=\sum_n g_n(1+\tfrac{1}{2}f_n)^{-1}[\tfrac{1}{2}(T_P^2c_{Pn}^2+T_Q^2c_{Qn}^2)+T_PT_Qc_{Pn}c_{Qn}], \tag{4.79}$$

$$r(M)=\sum_n g_n(2+f_n)^{-1}(T_Pc_{Pn}+T_Qc_{Qn})^2. \tag{4.79'}$$

Accordingly, we put

$$\delta r(M)=\delta r(M,S)=r'(M,S)-r'(M, S=\tfrac{1}{2}), \tag{4.80}$$

$$\delta r(M,S)=\sum_n g_n[\tfrac{1}{2}f_n(\tfrac{1}{2}-S)/(1+\tfrac{1}{2}f_n)(1+Sf_n)]$$
$$\times[T_P^2c_{Pn}^2+T_Q^2c_{Qn}^2-(4T_PT_Qc_{Pn}c_{Qn}/f_n)], \tag{4.81}$$

so that we have[11]

$$r'(M,S)=r(M)+\delta r(M,S) \tag{4.82}$$

in accordance with Eq. (4.18). For tails one has to put $c_{Qn}=0$, if P is the last atom.

Similarity between FE and LCAO Model

Table IV collects all population results in a systematic arrangement. Since the relations (2.5), (2.13) exist between the conventional LCAO model and the modified FE model, populations in *both* models are expressed in terms of the quantities c_{Pn}; similarly in view of the relations (2.4), (2.5) populations in the conventional FE model *and* in the modified LCAO model are expressed in terms of the quantities $\phi_n(P)$. The following conclusions can now be established:

(1) For a given variant the approximate (atom or bond) populations are identical in the FE and LCAO models.

(2) The correction terms in the two models are of the same order of magnitude and have the same sign.

(3) The correction terms vanish on the average:

$$\sum_P \delta\ \mathrm{pop}V(P)=\sum_M \delta\ \mathrm{pop}V(M)=0. \tag{4.83}$$

(The summation extends over all atoms or bonds of a molecule, respectively.)

(4) The correction terms are small compared with the approximate populations:

$$\delta\ \mathrm{pop}V\ll\mathrm{pop}V. \tag{4.84}$$

TABLE IV. Formulas for atom and bond populations.

	F variant	M variant
	Conventional FE model	Modified FE model
$a(P)$	$T_P^{-2}D\sum_n g_n\phi_n^2(P)=\sum_n g_n\varphi_{Pn}^2$	$\sum_n g_n c_{Pn}^2$
$\delta a(J)$[a]	$D\sum_n \mathfrak{A}_n^F[\sum_B \phi_n^2(Q_B)-3\phi_n^2(J)]$	$\sum_n \mathfrak{A}_n^M[\sum_B c_{Bn}^2-3c_{Jn}^2]$
$\delta a(P)$[a]	$D\sum_n \mathfrak{A}_n^F[\phi_n^2(Q)+\phi_n^2(R)-2\phi_n^2(P)]$	$\sum_n \mathfrak{A}_n^M[c_{Qn}^2+c_{Rn}^2-2c_{Pn}^2]$
$\delta a(E)$[a]	$D\sum_n \mathfrak{A}_n^F[\phi_n^2(Q)-\phi_n^2(E)]$	$\sum_n \mathfrak{A}_n^M[c_{Qn}^2-c_{En}^2]$
coeff.	$\mathfrak{A}_n^F=\frac{1}{4}g_n(1-\kappa_n^{-1}\sin\kappa_n)\sin^{-2}\kappa_n$	$\mathfrak{A}_n^M=\frac{1}{6}g_n(1-\kappa_n^{-1}\sin\kappa_n)\sin^{-2}\kappa_n$
$b(M)$[b]	$D\sum_n g_n(1+\cos\kappa_n)^{-1}\{\frac{1}{2}[\phi_n^2(P)+\phi_n^2(Q)]+\phi_n(P)\phi_n(Q)\}$ $=D\sum_n g_n(1+\cos\kappa_n)^{-1}\frac{1}{2}[\phi_n(P)+\phi_n(Q)]^2$	$\sum_n g_n(1+\cos\kappa_n)^{-1}[\frac{1}{2}(T_P^2c_{Pn}^2+T_Q^2c_{Qn}^2)+\frac{2}{3}c_{Pn}c_{Qn}]$
$\delta b(M)$[b]	$D\sum_n \mathfrak{B}_n^F\{\phi_n^2(P)+\phi_n^2(Q)-[4\phi_n(P)\phi_n(Q)/F_n]\}$	$\sum_n \mathfrak{B}_n^M[T_P^2c_{Pn}^2+T_Q^2c_{Qn}^2-(4c_{Pn}c_{Qn}/m_n)]$
coeff.	$\mathfrak{B}_n^F=\frac{1}{2}g_n(1-\kappa_n^{-1}\sin\kappa_n)\sin^{-2}\kappa_n\cos\kappa_n$	$\mathfrak{B}_n^M=\frac{1}{2}g_n(1-\kappa_n^{-1}\sin\kappa_n)\sin^{-2}\kappa_n\cos\kappa_n$
	Modified LCAO model	Conventional LCAO model
$q(P)$	$T_P^{-2}D\sum_n g_n\phi_n^2(P)=\sum_n g_n c_{Pn}^2$	$\sum_n g_n c_{Pn}^2$
$\delta q(J)$[a]	$\theta D\sum_n \mathfrak{Q}_n^F[\sum_B \phi_n^2(Q_B)-3\phi_n^2(J)]$	$\theta\sum_n \mathfrak{Q}_n^M[\sum_B c_{Bn}^2-3c_{Jn}^2]$
$\delta q(P)$[a]	$\theta D\sum_n \mathfrak{Q}_n^F[\phi_n^2(Q)+\phi_n^2(R)-2\phi_n^2(P)]$	$\theta\sum_n \mathfrak{Q}_n^M[c_{Qn}^2+c_{Rn}^2-2c_{Pn}^2]$
$\delta q(E)$[a]	$\theta D\sum_n \mathfrak{Q}_n^F[\phi_n^2(Q)-\phi_n^2(E)]$	$\theta\sum_n \mathfrak{Q}_n^M[c_{Qn}^2-c_{En}^2]$
coeff.	$\mathfrak{Q}_n^F=\frac{1}{2}g_n(S^{-1}+f_n)^{-1}$	$\mathfrak{Q}_n^M=\frac{1}{2}g_n(S^{-1}+m_n)^{-1}$
$r(M)$	$D\sum_n g_n(1+\cos\kappa_n)^{-1}\{\frac{1}{2}[\phi_n^2(P)+\phi_n^2(Q)]+\phi_n(P)\phi_n(Q)\}$ $=D\sum_n g_n(1+\cos\kappa_n)^{-1}\frac{1}{2}[\phi_n(P)+\phi_n(Q)]^2$	$\sum_n g_n(1+\cos\kappa_n)^{-1}[\frac{1}{2}(T_P^2c_{Pn}^2+T_Q^2c_{Qn}^2)+\frac{2}{3}c_{Pn}c_{Qn}]$
$\delta r(M)$	$D\sum_n \mathfrak{R}_n^F\{\phi_n^2(P)+\phi_n^2(Q)-[4\phi_n(P)\phi_n(Q)/f_n]\}$	$\sum_n \mathfrak{R}_n^M[T_P^2c_{Pn}^2+T_Q^2c_{Qn}^2-(4c_{Pn}c_{Qn}/m_n)]$
coeff.	$\mathfrak{R}_n^F=\frac{1}{2}g_n f_n(S^{-1}-2)/(f_n+2)(f_n+S^{-1})$	$\mathfrak{R}_n^M=\frac{1}{2}g_n m_n(S^{-1}-3)/(m_n+3)(m_n+S^{-1})$
Auxiliary	$c_{Pn}=\varphi_{Pn}=D^{\frac{1}{2}}T_P^{-1}\phi_n(P)$	$c_{Pn}=\varphi_{Pn}=(\frac{3}{2}D)^{\frac{1}{2}}\phi_n(P)$
Relations	$f_n=2\cos\kappa_n$	$m_n=3\cos\kappa_n$
	$\theta\lesssim 1$	$\theta\lesssim 1$

[a] J = joint atom, P = nonjoint or false-joint atom, E = end atom.
[b] In the table the bond populations are expressed in terms of quantities referring to the adjoining atoms. For formulations in terms of quantities referring to bond midpoints in the conventional FE model (F variant), see Eqs. (4.21), (4.22).

Conclusion (1) is evident. In order to evince Conclusion (2), we note that the correction terms differ only in the coefficients $\mathfrak{A}$, $\mathfrak{Q}$, $\mathfrak{B}$, $\mathfrak{R}$. Comparative graphs of corresponding coefficients as functions of κ are given in Fig. 7 for the region covered by the κ_n's in the ground state. The LCAO coefficients $\mathfrak{Q}$ and $\mathfrak{R}$ are given for three values of the overlap integral S.

Concerning Conclusion (3) we note that the approximate populations $a(P)$ and $b(M)$ are identical with those defined in (I), Eq. (2.69), (2.69′) and that the relations

$$\sum_P a(P)=\sum_M b(M)=N \tag{4.85}$$

were shown in (I), Eq. (2.71). The approximate populations $q(P)$ are identical with the q_P's defined in (1.33), and one has

$$\sum_P q(P)=\sum_M r(M)=N. \tag{4.86}$$

The first of these equations follows from Eq. (1.11), the second from Eqs. (4.4), (4.64), (4.78). Hence *the approximate populations satisfy the same conservation conditions as the exact populations, viz.* Eq. (4.4), and Eq. (4.83) follows.

Conclusion (4) is obtained by estimating the correction terms. Numerical calculations[12] indicate that the average of the eigenvalues κ_n lies near $\frac{1}{3}\pi$ for any molecule. Replacing all coefficients $\mathfrak{A}$, $\mathfrak{Q}$, $\mathfrak{B}$, $\mathfrak{R}$ by the values which they assume for $\kappa=\bar{\kappa}=\frac{1}{3}\pi$, one finds the following estimates:

M variant:

$$\left.\begin{aligned}\delta a(E)\approx\delta q(E)\ &\approx 0.1\{q(Q)-q(E)\},\\ \delta a(P)\approx\delta q(P)\ &\approx 0.2\{\tfrac{1}{2}[q(Q)+q(R)]-q(P)\},\\ \delta a(J)\approx\delta q(J)\ &\approx 0.3\{\tfrac{1}{3}\sum_B q(Q_B)-q(J)\},\end{aligned}\right\} \tag{4.87}$$

$$\delta b(M)\approx\delta r(M)\approx 0.2\{\bar{r}(M)-s(M)\}, \tag{4.87′}$$

[12] See N. S. Ham and K. Ruedenberg (to be published).

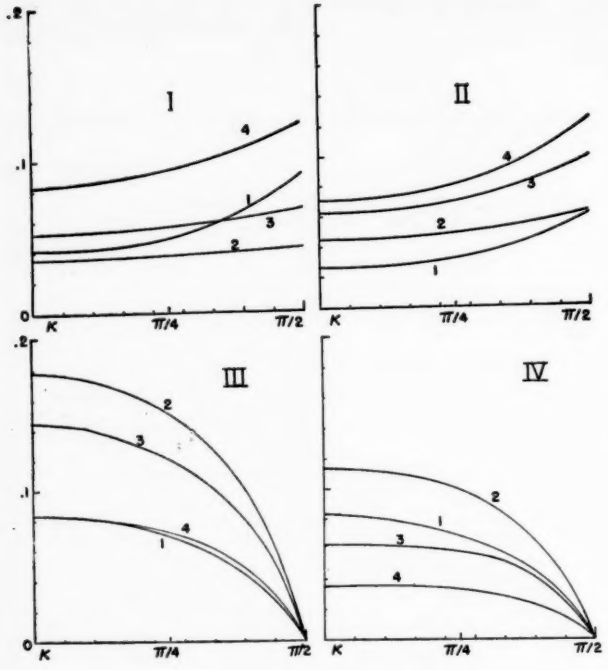

FIG. 7. Coefficients of Table IV as functions of κ.

I.1 $\mathfrak{A}^F$
I.2, I.3, I.4 $\}\mathfrak{Q}^F\{$ $(S=1/12)$, $(S=2/15)$, $(S=1/4)$,

II.1 $\mathfrak{A}^M$
II.2, II.3, II.4 $\}\mathfrak{Q}^M\{$ $(S=1/8)$, $(S=1/5)$, $(S=1/4)$,

III.1 $\mathfrak{B}^F$
III.2, III.3, III.4 $\}\mathfrak{R}^F\{$ $(S=1/12)$, $(S=2/15)$, $(S=1/4)$,

IV.1 $\mathfrak{B}^M$
IV.2, IV.3, IV.4 $\}\mathfrak{R}^M\{$ $(S=1/8)$, $(S=1/5)$, $(S=1/4)$.

with

$$\bar{r}(M)=\tfrac{1}{2}[T_P{}^2q(P)+T_Q{}^2q(Q)], \tag{4.88}$$

$$s(M)=\sum_n g_n(2c_{Pn}c_{Qn}/m_n). \tag{4.89}$$

F variant:

$$\left.\begin{aligned}\delta a(E)\approx\delta q(E)\ &\approx 0.1\{q(Q)-q(E)\},\\ \delta a(P)\approx\delta q(P)\ &\approx 0.2\{\tfrac{1}{2}[T_Q{}^2q(Q)\\ &\qquad +T_R{}^2q(R)]-q(P)\},\\ \delta a(J)\approx\delta q(J)\ &\approx 0.2\{\tfrac{1}{2}\sum_B T_B{}^2q(Q_B)-q(J)\},\end{aligned}\right\} \tag{4.90}$$

$$\delta b(M)\approx\delta r(M)\approx 0.2\{\bar{r}(M)-s(M)\}, \tag{4.90'}$$

where now

$$\bar{r}(M)=\tfrac{1}{2}[T_P{}^2q(P)+T_Q{}^2q(Q)], \tag{4.91}$$

$$s(M)=T_PT_Q\sum_n g_n(2c_{Pn}c_{Qn}/f_n). \tag{4.92}$$

(E denotes an end atom, P denotes a nonjoint atom, J denotes a joint atom.) The quantities defined in Eqs. (4.88), (4.89), (4.91), (4.92) satisfy the conservation relation (4.4):

$$\sum_M \bar{r}(M)=\sum_M s(M)=N. \tag{4.93}$$

The first of these equations follows from Eq. (4.86); the second follows from Eqs. (1.26), (1.42), which yield for the M and F variant, respectively:

$$2\sum_M c_{Pn}c_{Qn}=\mathbf{c}_n{}^*\mathbf{M}\mathbf{c}_n=m_n, \tag{4.93}$$

$$2\sum_M T_PT_Qc_{Pn}c_{Qn}=\mathbf{c}_n{}^*\mathbf{F}\mathbf{c}_n=f_n. \tag{4.94}$$

By arguments analogous to those advanced in connection with Eqs. (4.12, (4.13) one concludes that the quantities occurring in Eqs. (4.86), (4.93) are in general all of the same order of magnitude as the exact populations, and hence the inequality (4.84) results from Eqs. (4.87), (4.87′), (4.90), (4.90′). Other estimates are possible.

The population definitions are also applicable to excited states. It is likely that the similarities found for the ground state still exist for the lower excited states.

Similarity between M and F Variant

In alternant hydrocarbons one has the well-known result

$$a(P)=q(P)=1 \tag{4.94}$$

for all approximate atom populations in both variants. The quantities $\bar{r}(M)$ defined in Eqs. (4.88), (4.91), which represent approximations to the approximate bond populations, therefore assume in both variants the values

$$\bar{r}(M)=\begin{cases}(2/3) & \text{for } JJ \text{ bonds},\\ (5/6) & \text{for } JN \text{ bonds},\\ 1 & \text{for } NN \text{ bonds},\end{cases} \tag{4.95}$$

i.e., the populations group the bonds into the three classes: JJ = joint-joint, JN = joint-nonjoint, NN = nonjoint-nonjoint. Since Eqs. (4.94), (4.95) hold for both variants, their respective electron distributions cannot be too different in alternant hydrocarbons. The wire models of the two variants as well as the arguments which introduced the modified LCAO model [see text before Eq. (1.35)] indicate that the F variant will tend to stress the variation between densely and sparsely populated bonds more than the M variant. This is found to be true, but the differences between the two variants are only slight.[12]

Relation to the Quantities q and p

The present investigation has revealed the precise meaning of the quantities q of Eq. (1.33) in terms of *observable physical quantities:* they are approximate atom populations. Since they involve an integration over the electron density, the name "electron densities," sometimes employed for them, is dimensionally incorrect.[7]

An analogous correlation between bond populations and the bond orders p_{PQ} defined in Eq. (1.34) has not come to light in the previous discussions. Since the

bond orders (1.34) do not even satisfy the population conservation relations (4.4), the question arises whether such a correlation exists at all. This problem will be considered in a separate investigation.[12] In this connection it is of interest that the quantities $s(M)$ defined in Eqs. (4.89), (4.92) while bearing a great similarity to the bond orders p_{PQ} do satisfy the conservation relation (4.93).

CONCLUSION

The present investigation establishes the equivalence between the FE MO model and the LCAO MO model (=tight binding approximation of the LCAO MO theory with neglect of electronic interaction operators) in the case that the LCAO MO's contain only one AO per atom. It has to be concluded that the simultaneous neglect of all non-neighbor interactions simplifies the LCAO theory (containing only one AO per atom) to the extent that it reflects the same broad outlines of the molecule as the FE model. It is futile to argue whether the success of the FE model is due to its resemblance to the LCAO model, or whether the inverse is correct. Since the simplifications introduced in the LCAO theory are no less drastic than the assumptions of the FE theory, neither can be taken litterally. Both are *models* based on the same essential idea: While being three-dimensional, they are trimmed to neglect "transverse excitations" of the electron cloud and to describe only "longitudinal excitations" along the geometric bond path. To achieve this purpose, they moreover employ very similar mathematical tools, and consequently their results agree closely. In view of the identity in *basic concept* and the near-identity in *mathematical formulation*, it is a matter of taste which *picture* is given preference.[13] Although the equivalence has been demonstrated only for the case that analogous LCAO integrals have identical values (corresponding to a constant FE potential), it can be expected to hold equally well if different values are used for the integrals of different bonds and atoms, an assumption which corresponds to a varying FE potential. The influence of such a potential, required for heteroatoms, and of electronic interaction will be studied in subsequent papers.

APPENDIX[14]

Energy of an FE MO

The derivations in (I), Sec. 2, are based on the assumption that the potential in which the electrons move is infinitely high everywhere except within a thin tube of diameter ϵ, *and that it is zero inside this tube.* Let us generalize this assumption by adopting the potential

$$\begin{aligned} V(x,y,z)&=\infty && \text{outside the tube,}\\ V(x,y,z)&=E^t=\text{const} && \text{inside the tube.}\end{aligned} \tag{A.1}$$

Then the wave functions are [see (I), Eq. (1.17)]

$$\Phi_n(x,y,z)=\phi_n(x)(2/\epsilon)\sin(\pi y/\epsilon)\sin(2\pi z/\epsilon)+O(\epsilon), \tag{A.2}$$

where

$$\lim O(\epsilon)=0 \quad \text{for} \quad \epsilon\to 0,$$

and the energy levels are given by [see (I), Eqs. (1.4), (1.5)]

$$E_n=E_n{}^{\text{long}}+E^{tr}+E^t+O'(\epsilon), \tag{A.3}$$

where we have used the symbol $E_n{}^{\text{long}}$ to denote the energy of the longitudinal part of the wave function (A.2):

$$E_n{}^{\text{long}}=E_D\kappa_n{}^2, \tag{A.4}$$

which was called[2] E_n in (I) [see (I), Eqs. (1.14′), (1.62)]. The term E^{tr} is the ground-state energy of the transversal part of the wave function (A.2); since the transversal excitation energies become infinite for $\epsilon\to 0$, they are large compared to the longitudinal excitations, and hence E^{tr} is considered to be a constant. The term $O'(\epsilon)$ finally is again a function which vanishes for $\epsilon\to 0$.

Simpson's Approximation (Finite Difference Method)

For small values of κ the expansion [see (I), Eqs. (2.14′), (2.62)]

$$\cos\kappa=1-\tfrac{1}{2}\kappa^2+\cdots=1-\tfrac{1}{2}(E^{\text{long}}/E_D)+\cdots \tag{A.5}$$

can be broken off after the quadratic term. The relation (I), (2.44), thereby becomes

$$\phi(P_+)+\phi(P_-)=[2-(E^{\text{long}}/E_D)]\phi(P_0), \tag{A.6}$$

where P_-, P_0, P_+, are three consecutive atoms. Equation (A.6) is identical with the equation obtained by W. T. Simpson[15] who considered the atoms on a bond path as a lattice for numerical differentiation in formulating the Schrödinger equation:

$$(-\hbar^2/2m)[\phi(P_+)-2\phi(P_0)+\phi(P_-)]/D^2 = E^{\text{long}}\phi(P_0) \tag{A.7}$$

[see Eq. (2.62) of (I)]. This lattice is indeed satisfactory for numerical approximation of the trigonometric function if $\lambda_\phi \gg 2\pi D$, i.e., $\kappa \ll 1$. The eigenvalues of physical interest (*viz.*, the highest filled and the lowest unfilled levels) do not fulfill this condition however, and any conclusion conceiving the FE model based on the approximation *alone* is therefore inconclusive.

[13] It should be noted that it is adequate to base the discussion on the "finite difference approximation" of the FE model [see Appendix, after Eq. (A.7)]. The inclusion of overlap in the LCAO model is therefore essential for the comparison.

[14] The appendix contains some developments which supplement the first article of this series (See reference 1a) and which, in part are used in the present paper.

[15] W. T. Simpson, J. Chem. Phys. **17**, 1218 (1949). See also: C. A. Coulson, Proc. Phys. Soc. **66**, 652 (1953).

Amplitudes of an FE MO

The following identities express the amplitudes of a FE wave functions in terms of its values at atoms and bond midpoints. They are similar to those given in (I), Eq. (2.21)–(2.30).

Between the amplitude a_B on branch B and the values $\phi_B(P)$, $\phi_B(Q)$, which the wave function

$$\phi(x)=\sum_B a_B \cos(kx_B+\delta_B)$$

assumes at the neighboring atoms P, Q, on branch B, one has

$$a_B^2 \sin^2\kappa=\phi_B^2(P)+\phi_B^2(Q)-2\cos\kappa\phi_B(P)\phi_B(Q). \quad (A.8)$$

It is obtained by squaring the identity

$$\phi_B(Q)-\cos\kappa\phi_B(P)=-\sin\kappa[a^2-\phi_B^2(P)]^{\frac{1}{2}},$$

which follows immediately from (I), Eq. (2.18), by putting $x_B=P$, $x_B+\xi=Q$, $\xi=D$.

Furthermore, consider three consecutive atoms P_-, P_0, P_+, on branch B, and add the two corresponding equations of the type (A.8). The result can be transformed by means of (I), Eq. (2.44), whence

$$2a_B^2 \sin^2\kappa=\phi_B^2(P_+)+\phi_B^2(P_-)+2(1-2\cos^2\kappa)\phi_B^2(P_0). \quad (A.9)$$

Similarly, for a joint atom P_J and its three neighbors Q_B ($B=1,2,3$), one obtains, by adding the *three* relations of the type (A.8) and subsequently applying (I), Eq. (2.46):

$$\sin^2\kappa \sum_{B=1}^{3} a_B^2=\sum_{B=1}^{3}\phi_B^2(Q_B)+3(1-2\cos^2\kappa)\phi^2(P_J). \quad (A.10)$$

Let M be the bond midpoint between the neighbors P and Q. The relation

$$\phi_B(P)+\phi_B(Q)=(2\cos\tfrac{1}{2}\kappa)\phi_B(M) \quad (A.11)$$

can be derived in the same way as Eq. (2.44) of (I) was obtained. Squaring Eq. (A.11) yields

$$2(1+\cos\kappa)\phi_B^2(M)=\phi_B^2(P)+\phi_B^2(Q)+2\phi_B(P)\phi_B(Q), \quad (A.12)$$

and elimination between Eqs. (A.8) and (A.12) furnishes

$$a_B^2 \sin^2\kappa(1+\cos\kappa)^{-1}=\phi_B^2(P)+\phi_B^2(Q)-2\cos\kappa\phi_B^2(M), \quad (A.13)$$

and

$$a_B^2 \sin^2\kappa(1+\cos\kappa)^{-1}=2\phi_B^2(M)-2\phi_B(P)\phi_B(Q). \quad (A.14)$$

If the amplitudes a_B are obtained by one of the previous relations, then the phases δ_B are given by

$$\delta_B=\arccos[a_B^{-1}\phi_B(P)]-kx_P. \quad (A.15)$$

Equation (A.15) depends on the choice of the origin of x_B; the relations (A.8), (A.9), (A.10), (A.13), (A.14) are independent of it.

Alternant System with an Odd Number of Atoms

From the derivations in (I), Eqs. (2.72)–(2.98′) it follows that the FE model furnishes the same characteristics for odd-numbered alternant systems as the LCAO model. The atoms are divided into the starred and the unstarred class, the former being the majority class with $\frac{1}{2}(N+1)$ atoms, the latter being the minority class with $\frac{1}{2}(N-1)$ atoms. At least one "zero-energy orbital" exists; it has $\kappa=\frac{1}{2}\pi$, i.e., $\lambda=4D$, and its wave function vanishes for the atoms of the minority class. A general analysis of these systems has been given by H. C. Longuet-Higgins.[16]

Wire Plot of the Electron Distribution

In his wire plot of the total electron density $\omega(x)$, Platt has replaced the analytical joint conditions (I), Eq. (1.33), by a geometrical joint condition.[1a] The equivalence of both formulations is a peculiar property of those joints which occur in organic molecules. At *any* joint Eq. (1.27) of (I) yields

$$\sum_{B=1}^{3}(d\omega_B/dx_B)=0. \quad (A.16)$$

Let

$$\mathbf{v}_B=\{X_B,Y_B,Z_B\},$$

be the vector tangential to $\omega_B(x_B)$ at the joint (the coordinate system X, Y, Z has its origin in the joint, the $X-Y$ plane being parallel to the molecular plane, the Z axis being perpendicular to it; the density ω is plotted as Z-coordinate). Equation (A.16) may be written as

$$\sum_{B=1}^{3} Z_B C_B=0 \quad (A.17)$$

with

$$C_B=(X_B^2+Y_B^2)^{-\frac{1}{2}}.$$

Now, since the projections of $\mathbf{v}_1$, $\mathbf{v}_2$, $\mathbf{v}_3$, on the $X-Y$ plane form angles of 120° with each other, the equations

$$\sum_{B=1}^{3} X_B C_B=\sum_{B=1}^{3} Y_B C_B=0$$

hold, whence

$$\sum_B C_B\mathbf{v}_B=\{0,0,\sum_B Z_B C_B\}.$$

It follows that Eq. (A.17), and hence Eq. (A.16), is equivalent to

$$\sum_{B=1}^{3} C_B\mathbf{v}_B=0. \quad (A.19)$$

In the case of three branches in one plane meeting at 120°, the joint condition (A.16) is therefore equivalent to the condition that the tangential vectors $\mathbf{v}_1$, $\mathbf{v}_2$, $\mathbf{v}_3$, are linearly dependent, i.e. that they lie in one plane. Hence at all atoms the wire model gives the correct values for $\omega(x)$ and the correct behavior for $(d\omega/dx)$. It can therefore be expected that $\omega(x)$ is reasonably well approximated between the atoms. (The unit of density is D^{-1}.) it should be noted that the analytical joint condition (I), Eq. (1.33), is valid for any number of branches meeting at arbitrary angles in three-dimensional space.

The wire plot can be generalized to nonalternant systems. In this case, the values of the atomic populations are not known beforehand. But when the FE problem has been solved mathematically and when the atom populations are calculated for a particular molecule, then its wire plot can be constructed, if one has dowels available whose height can be easily and precisely adjusted to the theoretical values of $\omega(x)$. The model may also be applicable to individual orbitals.

[16] H. C. Longuet-Higgins, J. Chem. Phys. **18**, 265 (1950).

Electron Impact Studies of Some Aromatic Hydrocarbons. Implications Regarding Certain Aromatic Reactions

F. H. FIELD AND J. L. FRANKLIN
Humble Oil and Refining Company, Baytown, Texas
(Received September 15, 1953)

The ionization potential of several alkyl-substituted aromatics have been measured by an electron impact method, and the results are found to agree with values predicted by equivalent orbital calculations. The appearance potential of several alkyl-substituted benzyl ions have been measured, and the results show that the energies of these ions are independent of ring substitution. The appearance potential of several alkyl-substituted phenyl ions were measured, and the results appear to be anomalous. The results can be understood if it is assumed that the ions rearrange during decomposition to the isomeric benzyl ions. The implications of these results in terms of several chemical reactions are discussed. The heat of formation of the phenyl and ethyl phenyl radicals were found to be approximately 66 and 49 kcal/mole, respectively.

THE literature contains extensive studies of the energies of ions from paraffinic and olefinic hydrocarbons and from a few other classes of compounds, but surprisingly little information is available on the energies of ions from aromatics. To date, one study of the energies of ions from benzene[1] and a few measurements of ionization potentials[2] have been made. Since aromatics are an interesting and important class of compounds, and a large number of their reactions seem to occur through ionic intermediates, it is pertinent to determine the energies of characteristic aromatic ions. The present investigation was undertaken with this end in view and consists of the measurement of the ionization and appearance potentials of a number of such ions by electron impact. In particular, the ionization potentials of several aromatic hydrocarbons and the appearance potentials of certain benzyl and phenyl ions have been measured. In addition the implications of the resulting energies for certain chemical reactions are discussed. The compounds studied and the results obtained are listed in Table I.

IONIZATION POTENTIALS OF ALKYL AROMATICS

In a previous study Franklin[3] applied the group orbital method of Hall[4] to the calculation of the ionization potentials of alkyl aromatics. The calculations agreed well with the limited number of measured values available. Several additional ionization potentials were determined in the present investigation, and in Table II these measured values are compared with the calculated ionization potentials. Here also the calculated and measured values of ionization potentials agree within 0.1 volt, which is undoubtedly within the limits of experimental error. The agreement re-enforces our conclusion that the method of calculation is sound. In these calculations, following Franklin,[3] the potential parameters employed are the ionization potential of benzene (9.52 ev) and the adjusted ionization potential of methane (13.31 ev). Alkyl-alkyl interactions (1.55 ev) were calculated from the ionization potentials in the paraffin series and alkyl-ring interactions (1.09 ev) from the ionization potential of toluene (9.23 ev).

It will be observed from Table II that the ionization potential drops fairly rapidly as additional groups are substituted around the benzene nucleus. Additional length of the substituent chain, however, has a relatively minor effect. Of particular interest is the fact that orientation plays but a small part in the ionization potential of a given group of isomers. If one is optimistic, one might conclude tentatively that *meta*-orientation tends to give slightly higher ionization potentials than does *ortho*- or *para*-orientation. The difference however, is small and probably represents about the limit of accuracy of the work. We are inclined to think that the difference may be real; but this, of course, may represent a slight bias based upon the experience of organic chemists.

BENZYL IONS

The energies of benzyl-type ions are of interest for several reasons. From the standpoint of the mechanisms of chemical reactions, the benzyl halides are thought to undergo S_{N1} solvolysis, for which the heterolytic cleavage of the C−X bond is rate determining; i.e., the rate should be dependent upon the energy of the benzyl ion. From the standpoint of molecular theory, the energies of benzyl type ions are theoretically subject to the effects of resonance involving the ring π electrons and hyperconjugation with ring substituents.

Hughes, Ingold, and Taher[5] have determined the rates of the unimolecular solvolysis of alkyl substituted benzhydryl halides ($R-\bigcirc-CH\phi-Cl$) in 80 percent aqueous acetone. They find the rates to be strongly affected by substitution, i.e., activation energies of 21.0, 18.9, 19.4, 19.8, and 20.05 kcal/mole for R=H, CH_3, C_2H_5, i-C_3H_7, and t-C_4H_9, respectively. These energy differences are attributed to differing

[1] Hustrulid, Kusch, and Tate, Phys. Rev. **54**, 1037 (1938).
[2] See especially J. D. Morrison and A. J. C. Nicholson, J. Chem. Phys. **20**, 1021 (1952).
[3] J. L. Franklin, J. Chem. Phys. (to be published).
[4] G. G. Hall, Trans. Faraday Soc. **49**, 113 (1953).
[5] Hughes, Ingold, and Taher, J. Chem. Soc. **1940**, 950.

amounts of hyperconjugation stabilization in the carbonium ions formed in the course of the solvolysis. The energy differences actually observed by them (*ca* 2 kcal/mole) are too small to be detected in our measurements, but it must be remembered that their measurements are in solution, and it might be expected that any changes in the inherent energy of the ions engendered by changes of substituents would be magnified in the gas phase. For example, the difference in the activation energies for the $S_{N}1$ hydrolyses of i-C_3H_7Cl and t-C_4H_9Cl is 4 kcal/mole,[6] but the difference in the gas phase appearance potentials of the i-$C_3H_7^+$ and $C_4H_{t\text{-}9}^+$ ions from their chlorides is 14 kcal/mole.[6] The difference between the values of 14 kcal/mole and 4 kcal/mole is doubtless due to different amounts of solvation of the i-$C_3H_7^+$ and t-$C_4H_9^+$ ions, and so with the benzyl ions we might reasonably hope to see a similar relation between the reported solution energies and gas phase energies. Consequently we have measured the appearance potentials of several primary benzyl ions with various alkyl groups substituted on the benzene ring. In Table III, we compare the appearance potentials of these ions as formed by a common process; i.e., that of removing a methyl group from suitable parent molecules. Under these circumstances, the appearance potentials will reflect unambiguously the presence in the ions of interactions between the substituent group and the charge.

The values given in Table III show very little, if any, influence of a substituent upon the energy of a benzyl ion. The values shown do indicate a small reduction in energy for para-methyl substitution and a small elevation for *meta*-ethyl substitution, but we are inclined to doubt that these differences are significant. The averages of the appearance potentials for the methyl- and ethyl-substituted isomers are 11.13 and 11.32 ev, respectively, and a comparison of these with the value of 11.21 ev for unsubstituted benzyl makes it clear that

TABLE I. Measured appearance potentials of aromatic ions.

	AP, volts	Number of measurements	ΔH_f(ion) (kcal/mole)
$C_6H_6 \rightarrow C_6H_6^+$	$9.5_2 \pm 0.10$	3	240
$C_6H_6 \rightarrow C_6H_5^+ + H$	$14.3_0 \pm 0.18$	5	298
$C_6H_5CH_3 \rightarrow CH_3^+ + \cdots$	15.6	1	···
$C_6H_5C_2H_5 \rightarrow C_6H_5^+ + C_2H_5$	$16.3_3 \pm 0.25$	4	359
$+C_2H_4+H$			320
$+C_2H_3+H_2$			302
$\rightarrow C_6H_6^+ + C_2H_4$	$11.4_1 \pm 0.15$	4	257
$-CH_2^+ + CH_3$	$11.2_1 \pm 0.15$	4	234
$\rightarrow C_8H_8^+$(styrene)$+H_2$	$10.1_8 \pm 0.35$	3	242
$\rightarrow C_2H_3^+ + C_6H_5 + H_2$	14.8 ± 0.8	5	66 phenyl (radical)
$\rightarrow CH_3^+ + \cdots$	14.3 ± 0.7	3	···
1.2—$C_6H_4(CH_3)_2 \rightarrow C_6H_4^+(CH_3)_2$	$8.9_7 \pm 0.10$	4	211
$\rightarrow$ 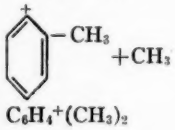 $+CH_3$	$11.7_3 \pm 0.15$	5	243
1.3—$C_6H_4(CH_3)_2 \rightarrow C_6H_4^+(CH_3)_2$	$9.0_2 \pm 0.15$	4	212
$\rightarrow$ 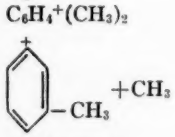 $+CH_3$	$11.7_8 \pm 0.06$	4	244
1.4—$C_6H_4(CH_3)_2 \rightarrow C_6H_4^+(CH_3)_2$	$8.8_8 \pm 0.05$	3	209
$\rightarrow CH_3-C_6H_4^+ + CH_3$	$11.5_7 \pm 0.10$	3	239
1.2—$C_6H_4(C_2H_5)_2 \rightarrow C_6H_4^+(C_2H_5)_2$	$8.9_1 \pm 0.15$	3	201
$\rightarrow$ 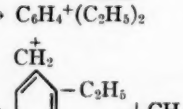 $+CH_3$	$11.2_4 \pm 0.15$	4	222
$\rightarrow$ 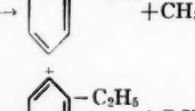 $+C_2H_5$	$11.0_1 \pm 0.07$	3	224

[6] (a) A. G. Evans, Trans. Faraday Soc. **42**, 719 (1946). (b) J. L. Franklin, Trans. Faraday Soc. **48**, 443 (1952).

TABLE I.—*Continued.*

	AP, volts	Number of measurements	ΔH_f (ion) (kcal/mole)
1,3—$C_6H_4(C_2H_5)_2 \rightarrow C_6H_4^+(C_2H_5)_2$	$8.9_9 \pm 0.07$	4	202
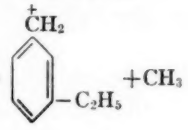	$11.4_4 \pm 0.20$	5	226
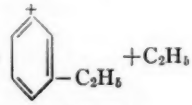	$11.0_3 \pm 0.04$	3	224
1,4—$C_6H_4(C_2H_5)_2 \rightarrow C_6H_4^+(C_2H_5)_2$	$8.9_3 \pm 0.17$	4	200
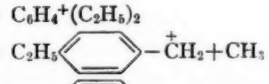	$11.2_7 \pm 0.20$	5	222
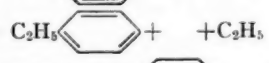	$10.9_4 \pm 0.10$	3	221
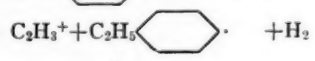	14.6 ± 0.4	7	49 (ethyl phenyl radical)
1,2,3$(CH_3)_3C_6H_3 \rightarrow$ 1,2,3$(CH_3)_3\overset{+}{C}_6H_3$	$8.7_5 \pm 0.02$	2	200
1,3,5$(CH_3)_3C_6H_3 \rightarrow$ 1,3,5$(CH_3)_3C_6H_3$	$8.7_9 \pm 0.25$	3	199
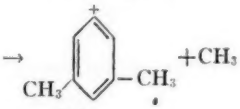	$11.7_8 \pm 0.10$	3	236
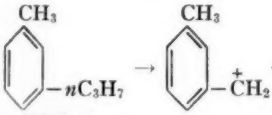	$11.1_6 \pm 0.10$	3	226
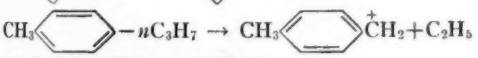	$10.9_7 \pm 0.10$	3	222
1,2 $C_6H_4(iC_3H_7)_2 \rightarrow C_3H_7^+ + \cdots$	13.9	1	...
1,3 $C_6H_4(iC_3H_7)_2 \rightarrow C_3H_7^+ + \cdots$	13.7	1	...
1,4 $C_6H_4(iC_3H_7)_2 \rightarrow C_3H_7^+ + \cdots$	13.8	1	...

the trend of the ionic energies in the gas phase do not at all parallel that in solution.

The solution phenomena are generally explained in terms of hyperconjugation of the alkyl substituent with the charge, and thus our failure to detect any appreciable stabilization attributable to alkyl substitution means that one of two conclusions must be drawn. Either we are incorrect in our expectations with regard to the enhancement of interaction energies in the gas phase as compared with those in solution, i.e., the magnitude of the hyperconjugation stabilization is too small for us to detect; or hyperconjugation in benzyl ions does not exist, and the solution phenomena must be attributed to some other effect such as differing amounts of solvation.

This problem of the existence of hyperconjugation in substituted benzyl ions is but part of a larger problem concerning the existence of any kind of resonance involving the charge in carbonium ions. We have discussed at considerable length elsewhere[7] the question of whether even first-order conjugation of the charge with the ring π electrons occurs in benzyl ions, and while the question must be considered as remaining open, it is true that the most straightforward interpretation of the observed facts leads to the conclusion that such conjugation does not occur (or at least that no stabilization energy is to be observed). Since this is the case, it is not surprising that no effects of second-order conjugation can be found.

We are of the opinion that our results with substituted benzyl ions are of interest with regard to the energies of aliphatic carbonium ions. It is well-known that the energies of these ions lie in the order Me>Et >*i*-Pr>*t*-Bu (heat of formation values of 265, 225, 190, and 167 kcal/mole, respectively). A possible explanation for the large energy lowering effected by progressive methyl substitution involves increasing hyperconjugation in going from Me to *t*-Bu. Such hyperconjugation has been represented from the point of view of the valence bond and molecular orbital theories. In the former, for instance, three resonance structures such as $CH_2=\overset{H^+}{C}H_2$ can be written for ethyl

[7] J. L. Franklin and F. H. Field, J. Chem. Phys. (to be published).

TABLE II. Ionization potentials (volts) of aromatic hydrocarbons.

	Calc.	Meas. this res.	Meas. others
Benzene	...	9.52	9.52,[a] 9.43[b]
Toluene	...	...	0.23,[a] 9.23[a]
o-xylene	8.98	8.97	
m-xylene	8.98	9.02	
p-xylene	8.98	8.88	
1,2 diethyl benzene	8.91	8.91	
1,3 diethyl benzene	8.91	8.99	
1,4 diethyl benzene	8.91	8.93	
1,2,3 trimethyl benzene	8.74	8.75	
1,3,5 trimethyl benzene	8.74	8.79	

[a] J. D. Morrison and A. J. C. Nicholson, J. Chem. Phys. **20**, 1021 (1952).
[b] R. E. Honig, J. Chem. Phys. **16**, 105 (1948).

H^+

ion and nine such as $CH_2=C(CH_3)_2$ can be written for *t*-butyl ion; hence *t*-butyl is less energetic than ethyl.

H^+

However, we think that structures such as $CH_2=CH_2$ are of very high energy ($\Delta H_f(H^+)=367$ kcal/mole), and we find it hard to believe that such structures will interact strongly enough with the ground state structure to produce the 40 kcal/mole lowering observed in going from CH_3^+ to $C_2H_5^+$.

Be this as it may, if in truth hyperconjugation is the explanation for the aliphatic ion phenomena, we might expect a lowering in going from benzyl to methyl benzyl somewhat similar in size to that involved in going from methyl to ethyl. The greater distance in the alkyl benzyl ions separating the atom to which the charge is formally assigned from the interacting alkyl group should be of no consequence if the interaction is completely the result of a resonance effect. The absence of the appreciable benzyl ion stabilization predicted on the basis of this argument in our opinion throws doubt on the role of hyperconjugation in the aliphatic ions. The very least to be said is that the benzyl ion and aliphatic ion results are not adequately correlated by the theory of hyperconjugation.

PHENYL IONS

Wheland[8] showed from quantum-mechanical considerations that the charge on the various carbons in substituted benzenes differed with the nature of the substituent and its orientation. On the basis of his calculations he obtained good qualitative agreement with the chemical evidence from substitution reactions. We undertook to measure the appearance potentials of various substituted phenyl ions in the hope that in this way we might obtain a direct measure of the energy required to produce a charge at various points on a substituted benzene ring and thus to determine the effect of substitution and orientation on electron availability. In Table IV we compare the energy required to form a phenyl ion and various methyl- and ethyl-substituted ions by the common process of removing a methyl group from the proper parent compound. It is of interest that the heat of formation of the phenyl ion obtained in this study (298 kcal/mole) agrees fairly well with the value of 305 kcal/mole obtained by Hustrulid, Kusch, and Tate[1] in their study of benzene.

Examination of the data in Table IV shows two rather surprising anomalies. First, the energies of the tolyl ions are much lower (about 55 kcal/mole) than those of phenyl ion. This in itself is not without its analogue in the aliphatic ion series (see discussion in the previous section), but by contrast with the aliphatic ion behavior, the substitution of a second methyl to form the xylyl ion does not result in any stabilization beyond that observed with the tolyl ions. Second, single ethyl substitution results in an appreciably greater lowering than single methyl substitution. A similar phenomenon is observed with the *n*-alkyl ions, but this further stabilization has been attributed by Stevenson[9] and by Franklin and Field[7] to rearrangement to the more stable secondary ion in the course of fragmentation of the parent ion.

In order to test more quantitatively whether the observed phenyl type ion phenomena are mutually self-consistent, group orbital calculations of the energies of the various substituted phenyl ions were made. The

TABLE III. Appearance potentials and energies of benzyl ions.

	AP (volts)	ΔH_f (ion) (kcal/mole)
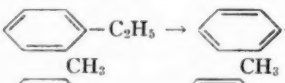	11.21	234
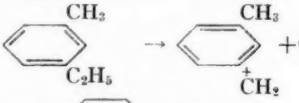	11.21[a]	226
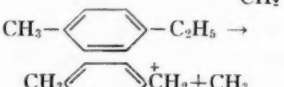	11.05[a]	222
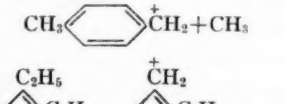	11.24	222
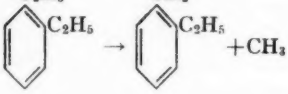	11.44	226
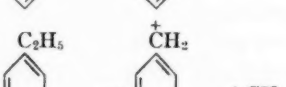	11.27	222

[a] Calculated from $Ap(CH_3C_6H_4\overset{+}{C}H_2)$ from the *o* and *p*—$CH_3C_6H_4$-($N-C_2H_7$), respectively. The *ortho*-isomer was not available to us.

[8] G. W. Wheland, J. Am. Chem. Soc. **64**, 900 (1942).

[9] D. P. Stevenson, Trans. Faraday Soc. **49**, 867 (1953).

calculations show that indeed the phenomena are not consistent, for on the basis of the observed lowering in going from phenyl ion to tolyl ion, a further lowering of more than a volt should be observed in going to the xylyl ion, but no significant further lowering should be observed in going to the ethyl phenyl ion.

Finally, it should be recalled that ring substitution effected no significant stabilization of the benzyl ions, and there does not appear to be a straightforward reason why methyl substitution should strongly stabilize phenyl ion but benzyl ion not at all.

These difficulties are removed if we postulate that except for the ion from benzene ($\Delta H_f = 298$ kcal/mole), phenyl ions are not formed at all, but rather the ions rearrange to the benzyl structure. Specifically, the observed energy relationships are accounted for as follows. The $C_6H_5^+$ ion from benzene is, of course, a true phenyl ion, but the great energy-lowering attendent on methyl substitution is the result of the actual formation of benzyl ions. In Table V the heats of formation of the ions in question are compared with the heats of formation of the isomeric benzyl ions taken from Table III.

TABLE IV. Appearance potentials and energies of phenyl ions.

	AP (volts)	ΔH_f (ion) (kcal/mole)
	13.80[a]	298
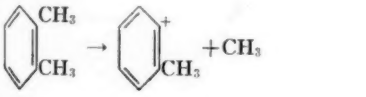	11.73	243
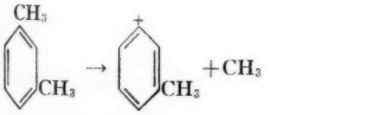	11.78	244
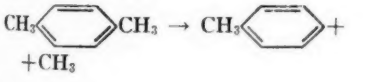	11.57	239
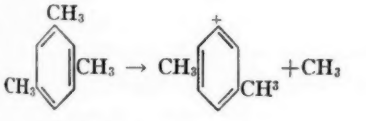	11.78	236
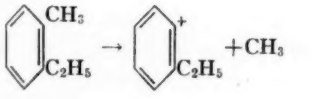	11.10[b]	224
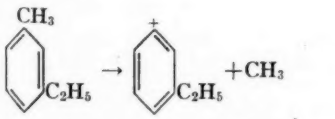	11.12[b]	224
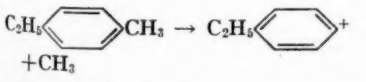	11.01[b]	221

[a] Calculated from AP($C_6H_5^+$) from benzene.
[b] Calculated from AP($C_6H_4{}^+C_2H_5$) from the *o*-, *m*-, and *p*-, diethyl benzenes, respectively.

TABLE V. Comparison of the heats of formation of substituted phenyl and benzyl ions.

Ion nominally formed	Observed ΔH_f, kcal/mole	Isomeric benzyl ion	Observed ΔH_f, kcal/mole
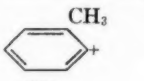	243		
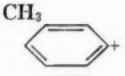	244	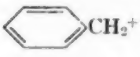	234
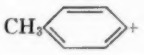	239		
		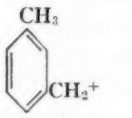	226
	236		
			222
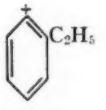	224		
	224	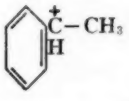	219[a]
	221		

[a] J. L. Franklin and F. H. Field, J. Chem. Phys. (to be published).

The average of the heats of formation of the three $C_7H_7^+$ ions is seen to be only about 6 kcal/mole greater than the benzyl ion heat of formation, and this difference is of the correct magnitude to be the activation energy for the rearrangement. Similarly, the $C_8H_9^+$ (nominally dimethyl phenyl) ion energy approaches that of the methyl benzyl, again with some activation energy required, and finally the $C_8H_9^+$ (nominally ethyl phenyl) energy approaches that of *s*-methyl benzyl, which is somewhat lower than that of the normal benzyl ions and thus accounts for the low nominal ethyl phenyl ion appearance potentials listed in Table IV.

The following considerations are also pertinent. From a comparison of the heats of formation of the unsubstituted benzyl and phenyl ions one might reasonably predict that the phenyl → benzyl rearrangement is strongly exothermic, and in the somewhat similar situation involving *n*-propyl and *i*-propyl ions there is at least a strong suspicion that the *n*-propyl ion when formed by electron impact tends to rearrange to the less energetic *i*-propyl ion. Thus there is a precedent for postulating the phenyl → benzyl rearrangement, and in addition it is characteristic that the atoms in ions

formed by electron impact show in many cases a very great degree of lability.

On the other hand, a possible argument against the postulate of the rearrangement to benzyl ions lies in the fact that the relationship that one might reasonably expect between the magnitude of the rearrangement activation energy and the relative orientation of charge and substituent does not exist. For example, in the case of the tolyl → benzyl rearrangements one might think that the order of the activation energies would parallel the distances between charge and methyl group, i.e., *para*>*meta*>*ortho*. Table V shows that some variation in the heats of formation of the tolyl ions does occur, which variation conceivably might be a manifestation of differing amounts of activation energies, but clearly the order is not that expected. Because of the possibility of high lability of atoms in ions, we do not think that the postulate of rearrangement must be rejected, but its acceptance must be subject to some reservation.

SOLVOLYSIS OF DIAZONIUM SALTS

In water solution benzene diazonium salts are highly ionized and at slightly elevated temperatures hydrolyze to give phenol and other products. The rates of the reaction of various diazonium salts have been investigated by Crossley, Kienle, and Benbrook[10] and by Moelwyn-Hughes and Johnson.[11] The subject has been reviewed briefly, and the conclusions to be drawn have been summarized by Ingold[12] and by Bunnett and Zahler.[13] The consensus is that the hydrolysis is of the first order, S_{N1} type, which suggests that the mechanism involves the formation of a phenyl ion as a slow step, followed by a rapid reaction with the nucleophilic species present in the solution.

It is of interest to consider this reaction in the light of the energies of phenyl and benzyl ions discussed above. In so doing we find that the chemical evidence and electron impact evidence are quite contradictory. We have tentatively concluded that in the gas phase the substituted phenyl ions rearrange to benzyl-type ions. Assuming that the rearrangement will also occur in solution (the assumption will be discussed more fully below), we would expect to find benzyl-type alcohols to be produced in the solvolysis. However, to our knowledge no such products have ever been reported, and consequently doubt is cast upon (a) our conclusions concerning the rearrangement in the gas phase, (b) the validity of applying gas phase, electron impact data to reactions in solutions, or (c) the ionic nature of the solvolysis reaction.

Let us first assume that we are incorrect regarding rearrangement, that is, the energy values measured by electron impact actually refer to phenyl-type ions. Then for an ionic solvolysis mechanism the much lower energy (about 55 kcal/mole) of tolyl ion as compared with phenyl ion would require that the rate of solvolysis of tolyl diazonium ion be very much greater than that of phenyl diazonium ion. In actuality, while the rate of reaction of the tolyl ion is somewhat larger (4–5 times)[10] than that of the phenyl ion, the difference is trivial as compared with that to be expected from ths observed difference in the gas phase energies of the iont. Thus the assumption of no gas-phase rearrangement does not reconcile the chemical and electron impact evidence.

With regard to the problem of the applicability of electron-impact data to solution phenomena, it is certainly true that the mechanism by which ions are formed in solution is entirely different from that by which they are formed under electron impact in the gas phase, and thus the behavior of the ions in the two phases might be quite different. If the $C_7H_7^+$ ion formed under electron impact from xylene indeed has the benzyl ion structure the rearrangement must occur during the decomposition of the xylene molecule-ion initially formed by the bombarding electron. However, any $C_7H_7^+$ ion formed in solution from tolyl diazonium ion is obviously not formed through a molecule-ion intermediate, and the activation energy for its rearrangement to benzyl ion could be quite different from that involved in the gas phase reaction. Furthermore, in solution the ion is not isolated as it is in the mass spectrometer, and it is quite conceivable that reaction with the solvent would take place more rapidly than rearrangement even in the presence of a small activation energy for rearrangement.

These are powerful arguments which cannot be directly refuted. We can point out, however, that in other cases parallels between electron impact chemistry and solution chemistry do exist. Thus the electron-impact energies of the alkyl carbonium ions correlate nicely with the occurrence of S_{N1} or S_{N2} types of solvolysis for the corresponding alkyl halides.[6a] Further, in solution chemistry the carbonium ion rearrangements that one observes are those which are known from electron impact energies to be exothermic. Somewhat more specifically, there is a strong possibility that the gaseous n-$C_3H_7^+$ ion is appreciably more energetic than the i-$C_3H_7^+$ ion[14] and, furthermore, that the i-$C_3H_7^+$ ion is sometimes formed by electron impact from n-propyl derivatives.[14] Thus it is of interest to note that in the treatment of n-$C_3H_7NH_2$ with nitrous acid much i-C_3H_7OH is formed.[15] Similarly, the evidence indicates that the $C_3H_5^+$ ion formed from cyclopropane

[10] Crossley, Kienle, and Benbrook, J. Am. Chem. Soc. **62**, 1400 (1940).

[11] E. A. Moelwyn-Hughes and M. Johnson, Trans. Faraday Soc. **36**, 948 (1940).

[12] (a) C. K. Ingold, *Structure and Mechanism in Organic Chemistry* (Cornell University Press, Ithaca, 1953), pp. 799 *ff*; (b) pp. 246, 257–259.

[13] J. F. Bunnett and R. E. Zahler, Chem. Revs. **49**, 273 (1951).

[14] D. P. Stevenson, Trans. Faraday Soc. **49**, 867 (1953); J. L. Franklin and F. H. Field (to be published).

[15] See, for instance, L. F. Fieser and M. Fieser, *Organic Chemistry* (D. C. Heath and Company, Boston, 1944), p. 237.

by electron impact does not have a cyclic structure,[16] and chemically it is found that cyclopropyl amine and nitrous acid yield chiefly allyl alcohol.[17]

In assessing the possibility of the rearrangement of substituted phenyl ions in solution we are hindered somewhat by the fact that because of the postulated rearrangement under electron impact we do not know the values of the ionic energies in the gas phase. However, in view of the small effect of alkyl substitution on the energy of benzyl-type ions, it seems unreasonable to think that the effect on the energies of phenyl-type ions will be much different. Thus we can at least conclude from our electron impact results that the energetics for rearrangement in solution are favorable, a situation which with other compounds leads to the observance of rearranged products.

Although our considerations concerning the electron impact data involve some doubtful points, on the surface, at least, the data are not in accord with the postulate of an S_{N1} solvolysis of diazonium salts. It is consequently of interest to note that Bunnett and Zahler observe that the kinetic evidence for this mechanism is not conclusive. We are also of this opinion, and this uncertainty coupled with these electron impact results indicate that a new study of the kinetics of the reaction might be warranted.

AROMATIC SUBSTITUTION

Electrophilic substitution on the benzene nucleus is generally considered to involve attack by an ion upon the ring in the following manner:

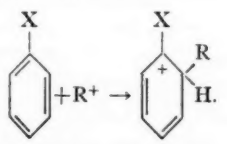

Most such reactions probably are limited in rate by the attack on the benzene nucleus (there are apparently a few exceptions to this, as for example the rate of nitration of benzene). Consequently, we might anticipate that information concerning the energies of ions might be of value in understanding this type of reaction.

It is well known that the effect of ring substituents on the rates of substitution reactions depends upon the electrical nature of the substituent; that is, rates are increased by substituents tending to increase the ring electron density, and conversely. Similarly, the ionization potentials of substituted benzenes are low for electron releasing substituents and high for electron attracting substituents, and we should expect, then, the rate of reaction to be approximately inversely related to the ionization potential of the aromatic.

Unfortunately, there are few sets of kinetic data in which the rates of a common reaction with various substituted aromatics are measured at comparable conditions. In Table VI we compare the rates of chloromethylation and the rates of sulfonation of several aromatic compounds with their ionization potentials. It is readily apparent that, broadly speaking, the expected relation is found; although, as is oftentimes the case, chlorobenzene and bromobenzene do not fit the pattern exactly.

TABLE VI. Rates of aromatic substitution reactions.

	Chloromethylation[a] (relative rate)	Sulfonation[b] in nitrobenzene at 40°C using SO_3 (k)	H_2SO_4 ($k \times 10^6$)	IP (volts)
Nitrobenzene	Too slow to measure	7.8×10^{-6}	0.24	...
Benzonitrile	...	...	...	9.95
Benzene	1	48	15.5	9.52
Chlorobenzene	...	2.4	10.6	9.42
Bromobenzene	...	2.1	9.5	9.41
Toluene	3	...	79	9.23
m-xylene	24	...	...	9.02
Mesitylene	600	...	...	8.79
Anisole	1300	...	...	8.9[c]
3,5 dimethylanisole	100 000	...	...	8.7[c]

[a] Relative rates from ORI, 66.
[b] E. A. Braude, Ann. Repts. **46**, 131 (1949).
[c] Estimated by equivalent orbital calculations.

However, while large changes in rates of substitution seem to follow ionization potential, it must be emphasized that the small effects usually attributed to hyperconjugation do not. Thus, we compare de la Mare and Robertson's[18] data on relative rates of chlorination and bromination of substituted benzenes in 15 percent aqueous acetic acid at 24°C with the ionization potentials of C_6H_5R.

R	H	Me	Et	*i*Pr	*t*-Bu
Chlorination	0.29	100	84	51	32
Bromination	...	100	76	44	23
IP (volts)	9.52	9.23	9.12	9.13	9.35

Obviously the correlation is poor. However, the comparatively small reaction rates of the higher alkyl benzenes may be attributed, at least in part, to steric interference with attack at the *ortho* positions. Ingold[12b] has discussed this problem with regard to relative rates and orientation in the nitration reaction and has shown that the higher alkyl substituents such as *t*-butyl increase the sensitivity of the *para* position, although the total rate of mono-nitration is decreased with respect to toluene. Unfortunately the situation is further complicated by the fact that the quoted ionization potential of *t*-butyl benzene is suspiciously high. If the ionization potential is calculated by the equivalent orbital method a value of 9.06 v is obtained. This is more nearly concordant with the other values given. Thus we do not think that these data invalidate the relationship of rate of electrophylic substitution to ionization potential.

[16] F. H. Field, J. Chem. Phys. **20**, 1734 (1952).
[17] R. C. Fuson, *Advanced Organic Chemistry* (John Wiley and Sons, Inc., New York, 1950), p. 523.
[18] P. B. D. de la Mare and P. W. Robertson, J. Chem. Soc. **1943**, 279.

Although one can only speculate, it is perhaps still of value to postulate somewhat more detailed reasons for the occurrence of this relationship. For purposes of illustration the reaction may be considered as hypothetically occurring through the following series of steps:

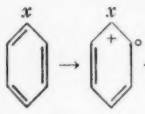

$$+e+I_A-Es_1,$$

$$R^+ + e \rightarrow \overset{\circ}{R} - I_R^\circ + Es_{R^+},$$

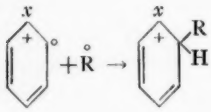

$$-D+Es_1-Es_2,$$

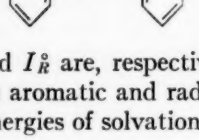

$$+I_A-I_R^\circ-D+Es_{R^+}-Es_2.$$

I_A and I_R° are, respectively, the ionization potentials of the aromatic and radical R; Es_1, Es_{R^+} and Es_2 are the energies of solvation of

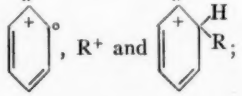

and D is the C−R bond strength. But $I_A-I_R^\circ-D+Es_{R^+}-Es_2=\Delta H_R$, the heat of the reaction written above. It will be assumed that this endothermic heat of reaction is approximately equal to the energy of activation. While this would be difficult to prove, similar assumptions have been successfully employed in interpreting the mechanisms of other ionic reactions. Thus, based upon this assumption, Evans[6a] and Franklin[6b] have calculated the activation energies of SN_1 solvolysis of several alkyl halides and Franklin[6b] has calculated the activation energy for the acid catalyzed hydration of isobutylene. The calculated results agreed quite well with experiment in all cases. When the attacking ion R^+ and the solvent are kept constant, I_R° and Es_{R^+} will remain constant. D and Es_2 will vary somewhat with the original substituent X, whereas I_A varies considerably. It is our opinion that the variations in D and Es_2 are small, and to the extent that this is true the activation energies for electrophilic substitution reactions should depend primarily on the difference in ionization potentials of the aromatic molecule and the attacking group. However, variations in D and Es_2 might well be large enough to prevent the manifestation of the dependency of rate on ionization potential for aromatics with very similar ionization potentials, and indeed this might be the explanation for the fact that the order for benzene, chlorobenzene, and bromobenzene is scrambled.

TABLE VII. Effect of substituents upon energies of carbonium ions.

	AP, volts	Reference
$CH_3CN \rightarrow \overset{+}{C}H_2-CN+H$	14.5	a
$CH_4 \rightarrow \overset{+}{C}H_2-H+H$	14.4	b
$CH_3CH_3 \rightarrow \overset{+}{C}H_2-CH_3+H$	12.9	c
$CH_3OH \rightarrow \overset{+}{C}H_2-OH+H$	11.8	d
$C_3H_8 \rightarrow \overset{+}{C}(CH_3)_2-H+H$	11.6	e
$iC_3H_7Cl \rightarrow \overset{+}{C}(CH_3)_2-Cl+H$	11.2	f
$iC_4H_{10} \rightarrow \overset{+}{C}(CH_3)_2-CH_3+H$	10.8	g

[a] C. A. McDowell and J. W. Warren, Trans. Faraday Soc. **48**, 1084 (1952).
[b] C. A. McDowell and J. W. Warren, Discussions Faraday Soc. **10**, 53 (1951).
[c] D. P. Stevenson and J. A. Hipple, J. Am. Chem. Soc. **64**, 1588 (1942).
[d] Calculated from the appearance potential of the CH_3O^+ ion from ethanol, C. S. Cummings and W. Bleakney, Phys. Rev. **58**, 787 (1940).
[e] Calculated from the appearance potential of the $C_3H_7^+$ ion from iC_4H_{10} (see reference c above).
[f] Calculated from the appearance potential of the $C_3H_6Cl^+$ ion from t-C_4H_9Cl, D. P. Stevenson and J. A. Hipple, J. Am. Chem. Soc. **64**, 2766 (1942).
[g] Calculated from the appearance potential of the $C_4H_9^+$ ion from neopentane, D. P. Stevenson, Discussions Faraday Soc. **10**, 35 (1951).

Perhaps the most fruitful application of ionic energies to the problem of aromatic substitution is in connection with the orienting influences of substituents. Electrophilic attack on aromatic molecules is thought to occur through an intermediate such as the benzenium ion 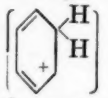 formed in the protonation of benzene. Now the energy required to produce a carbonium ion is greatly influenced by the groups attached to the carbon bearing the charge. This is illustrated in Table VII, where we compare the appearance potentials of several RCH_2^+ ions formed by the common process of removing a hydrogen atom. Since this is true the ionic attack on substituted benzenes will be such as to place the charge in the benzenium ion analogue at the position of least energy. In the case of electron releasing substitutents such as methyl this is the 1-position, and as a consequence *ortho-para* attack occurs, i.e.,

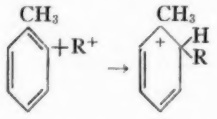

Under meta attack the charge cannot be referred to the 1-position by simple bond rearrangement. On the other hand, with an electron attracting group such as −CN the charge will tend to avoid residing on the high energy 1-position and meta attack occurs, i.e.,

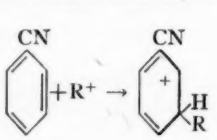

MISCELLANEOUS

In Table I, the appearance potential of the $C_6H_6^+$ ion from ethylbenzene is reported. The reaction by which this is formed is probably $C_6H_5C_2H_5+e \rightarrow C_6H_6^+ + C_2H_4 + 2e$. It is of interest that the heat of formation of the benzene ion calculated from these results is 257 kcal/mole. The heat of formation of $C_6H_6^+$ ion as calculated from the ionization potential of benzene is 239 kcal/mole, so the activation energy for the reaction $C_6H_6^+ + C_2H_4 \rightarrow C_6H_5C_2H_5^+$ is about 18 kcal/mole. The activation energy of 18 kcal/mole, while somewhat larger than that commonly found, is still surprisingly small for the type of process encountered here.

As is shown in Table I the appearance potential of the $C_8H_8^+$ ion from ethylbenzene was determined. This ion is almost surely the styrene ion, and the reaction involved is as follows:

$$C_6H_5C_2H_5+e \rightarrow C_6H_5C_2H_3^+ + H_2 + 2e.$$

It is of interest that the heat of formation for the ion calculated from this measured value is 242 kcal/mole, whereas that obtained from the ionization potential of styrene as measured by Morrison and Nicholson[2] is 238 kcal/mole. This difference is probably within the accuracy of the experimental work, but even if taken at face value it shows an activation energy for the four-center reaction of only 4 kcal/mole. This, of course, is in agreement with the small activation energy found for a large number of other four-center ionic reactions.

As a matter of interest, the appearance potential of the mass 77 ion from ethylbenzene was measured. In Table I the appearance potential is seen to be 16.33 volts. If it is assumed that the reaction involves the formation of an ethyl radical, we calculate a heat of formation for the phenyl ion of 359 kcal/mole. This would represent an excess energy of nearly three volts. Other alternatives are possible, however; thus ethylene and a hydrogen atom, or H_2 and a vinyl radical are possible products of reaction. Of these, the latter, which gives a heat of formation for the phenyl ion of 302 kcal/mole, seems to be the more reasonable, or at least to agree most nearly with the value determined from benzene.

In addition to the study of the aromatic ions, an attempt has been made to measure the heat of formation of the phenyl and ethyl phenyl radicals. One would expect the appearance potential of the ethyl ion from ethylbenzene to give a direct measure of the heat of formation of the phenyl radical since the heat of formation of the ethyl ion is well known. Unfortunately, in the case of ethylbenzene, the mass 29 peak is so small as to be unsuited to appearance potential measurements. However the mass 27 peak, while not large, is sufficiently great for this purpose, and accordingly we measured the appearance potential of the vinyl ion from ethylbenzene. Similar considerations apply in the case of the 1,4-diethylbenzene, and the vinyl ion was also measured from this compound. Unfortunately, because of the small slope of the ionization efficiency curves near the vanishing current, the precision of these measurements is poor. We assume the reaction in the case of ethylbenzene to be $C_6H_5C_2H_5+e \rightarrow C_6H_5 + C_2H_3^+ + H_2 + 2e$. A similar reaction would be expected with the diethyl benzenes. We find the heat of formation of the phenyl radical to be 66 kcal/mole, which is in good agreement with Szwarc and Williams[19] value of 70 kcal/mole. Similarly in the case of the ethyl phenyl radical, we calculate a heat of formation of 49 kcal/mole. If the Szwarc and Williams value for the phenyl radical is correct, and if, as seems reasonable, the ring-hydrogen bond strength is not influenced by substituent, we would find a heat of formation for the ethyl phenyl radical of 57 kcal/mole. The agreement, while not good, is within the precision of our measurement of the appearance potentials for the vinyl ion by this process.

It should be mentioned that these values are made somewhat questionable by the fact that one can write for the formation of the vinyl ions alternative mechanisms which are almost compatible with the observed appearance potentials, namely,

$$C_6H_5C_2H_5+e \rightarrow C_2H_3^+ + C_6H_6 + H + 2e$$

(and analogously for diethyl benzene). However, if these reactions actually do occur, our appearance potentials are erroneously low by as much as perhaps a volt, and we are inclined to think that the mechanisms producing the phenyl and ethyl phenyl radicals are correct.

The appearance potentials of the methyl ions from toluene and ethyl benzene and the *i*-propyl ions from the isomeric di-isopropyl benzenes were measured, but the values obtained do not correspond to any recognizable ionization mechanisms. The energies to be associated with the neutral fragments formed in conjunction with the above ions are 108, 72, and 110 kcal/mole, respectively. The only conclusion to be drawn is that extensive excitation and/or decomposition occurs in the reactions.

Finally, from the energies of the phenyl and benzyl ions obtained in this work and the published energies of the corresponding radicals, the ionization potentials of the radicals can be calculated. For phenyl radical $I = 298 - 70 = 228$ kcal/mole $= 9.89$ ev, and for benzyl $I = 234 - 37.5 = 196.5$ kcal/mole $= 8.52$ ev or $234 - 49.5 = 184.5$ kcal/mole $= 8.0_0$ ev, the two values resulting from the divergent literature values for $\Delta H_f(C_6H_5CH_2^\circ)$.[20-22]

[19] M. Szwarc and D. Williams, J. Chem. Phys. **20**, 1171 (1952).
[20] M. Szwarc, Chem. Revs. **47**, 75 (1950).
[21] Anderson, Scheraga, and Van Artsdalen, J. Chem. Phys. **21**, 1258 (1953).
[22] Since this paper was submitted for publication, D. O. Schissler and D. P. Stevenson (J. Chem. Phys. **22**, 151 (1954)) have reported values for the appearance potentials of the benzyl ions formed from toluene, ethylbenzene, and bibenzyl, namely, 11.80, 11.25, and 10.53 volts, respectively. The benzyl ion heats of formation

EXPERIMENTAL

The appearance potential measurements were made by the vanishing current method using a modified Westinghouse Type LV mass spectrometer. The modifications consisted of the replacement of mass spectrometer tube originally supplied with the instrument with one manufactured by Dr. J. A. Hipple and the use of a Brown recording electrometer to measure the ion currents. The minimum ion current which could be detected was on the order of 1×10^{-15} amp. The electron accelerating voltage was varied continuously by means of a motor driven potentiometer, and thus a plot of the ionization efficiency curve in the neighborhood of the threshold voltage could be obtained in ten minutes and with a minimum of effort. The remainder of the technique used was similar to that previously described.[23]

The apparatus and method were checked by measuring ionization and appearance potentials of various compounds for which these quantities are known. Quite satisfactory agreement with published values was obtained.

All the compounds used in this study were NBS Standard Samples.

corresponding to the toluene and ethylbenzene appearance potentials are 232 and 234 kcal/mole, in excellent agreement with the value found by us. When this value is combined with the bibenzyl appearance potential, the heat of formation of the benzyl radical is found to be 37 kcal/mole, in excellent agreement with Szwarc's value. The corresponding value for the ionization potential of the benzyl radical is 8.50 volts.

ACKNOWLEDGMENT

We wish to express our thanks to Mr. B. L. Clark for assistance in making the experimental measurements.

[23] F. H. Field, J. Chem. Phys. **21**, 1506 (1953).

THE JOURNAL OF CHEMICAL PHYSICS VOLUME 22, NUMBER 11 NOVEMBER, 1954

Mechanism of Formation of the Quinonoid Hydrocarbon $CH_2:C_6H_4:CH_2$*

M. Levy, M. Szwarc, and J. Throssell
State University of New York, College of Forestry, Syracuse 10, New York

(Received March 17, 1954)

Para-xylyl radicals were generated by pyrolysing *para*-xylyl bromide in the presence of toluene or of *para*-xylene. Investigation of their behavior led to the conclusion that the quinonoid hydrocarbon $CH_2:C_6H_4:CH_2$ is formed by the disproportionation process. Further information about this reaction was secured by studying the pyrolysis of ω,ω' dibromo *para*-xylene ($Br\cdot CH_2\cdot C_6H_4\cdot CH_2\cdot Br$). Semiquantitative treatment of the data indicates that the activation energy of the dissociation process

$$CH_2\cdot C_6H_4\cdot CH_3 \rightarrow CH_2:C_6H_6:CH_2+H$$

is of the order 70 kcal/mole. Consequently, the dissociation process is too slow to account for the formation of the quinonoid hydrocarbon, at temperatures below 1100°K. We therefore attribute the formation of the quinonoid hydrocarbon to the disproportionation reaction.

Reinvestigation of the pyrolysis of benzyl bromide confirmed the past results and particularly the value for $D(C_6H_5\cdot CH_2-Br)$. It was shown that the rate constant for the decomposition of *para*-xylyl bromide is essentially equal to the rate constant for the decomposition of benzyl bromide, and it appears that the rate constant for the decomposition of ω,ω' dibromo *para*-xylene is higher by statistical factor of 2 from the rate constant of the decomposition of *para*-xylyl bromide.

IT was found by one of us[1] that the low-pressure pyrolysis of *para*-xylene yields a quinonoid hydrocarbon of the following structure:

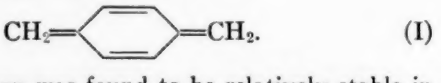

(I)

This hydrocarbon was found to be relatively stable in gaseous phase, but on cooling and subsequent condensation it polymerizes rapidly, forming a tough, transparent or white film which is deposited on the walls of a condenser. The polymeric material thus produced is insoluble in organic solvents when heated to temperatures lower than 200°C, and it is infusible below 400°C. Its constitution which was deduced from analytical data, infrared investigations, and oxidative degradation seems to be described adequately by formulas II

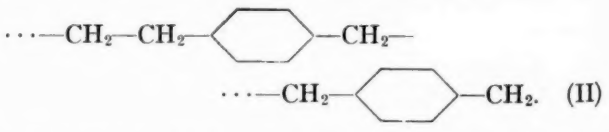

(II)

The past work[1-4] proved conclusively that the pyrolysis of *para*-xylene is initiated by reaction (1)

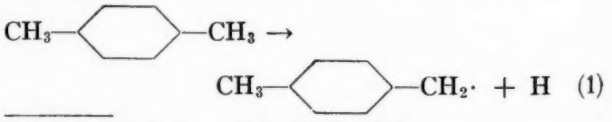

(1)

* This investigation has been supported by grants from National Science Foundation and Research Corporation.

[1] M. Szwarc, Discussions Faraday Soc. **2**, 46 (1947); J. Polymer Sci. **6**, 319 (1951).

[2] M. Szwarc, J. Chem. Phys. **16**, 128 (1948).

[3] Kaufman, Mark, and Mesrobian, J. Polymer Sci. **13**, 3 (1954).

[4] Corley, Haas, Kane, and Livingston, J. Polymer. Sci. **13**, 137 (1954).

and that the quinonoid hydrocarbon I is formed subsequently from *para*-xylyl radicals. The assumption that *para*-xylyl radicals are indeed the primary products of pyrolysis of *para*-xylene seems to be sound and it is based primarily on the following observations: (a) Dibenzyl is the main product of the pyrolysis of toluene[2] while the substituted dibenzyls are the main products of pyrolyses of toluene derivatives (see, e.g., reference 5); (b) Small quantities of 4,4′ dimethyl dibenzyl are present among the products of pyrolysis of *para*-xylene; (c) The pyrolyses of toluene and of toluene derivatives seem to be essentially first-order reactions which have the characteristics of unimolecular decompositions. On the other hand, the nature of the reaction which yields the quinonoid hydrocarbon I has not been established conclusively, and two alternative reactions need consideration: the disproportionation of *para*-xylyl radicals (reaction 2) and the decomposition of *para*-xylyl radicals (reaction 3)

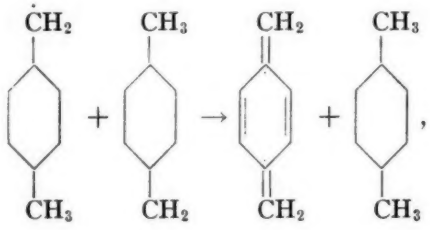

(2)

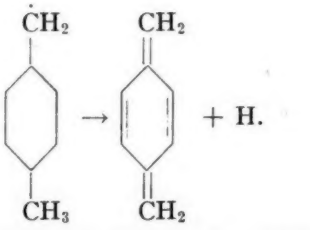

(3)

In the complete mechanism of pyrolysis of *para*-xylene, reaction (2) would represent a termination step, while reaction (3) would be a chain propagation step. Participation of either reaction in the over-all decomposition would lead to the same products and the same stoichiometry of the over-all reaction. Hence, any discrimination between these two alternatives must be based either on kinetics grounds, or on the results of entirely new experiments.

Let us consider first of all the effect of reaction (2) or (3) on the kinetics of the over-all decomposition of *para*-xylene. Reaction (2) leads to the formation of hydrocarbon I and to the regeneration of a molecule of *para*-xylene. No hydrogen is produced by this process. On the other hand, reaction (3) demands the formation of a hydrogen atom for each monoradical $CH_3\cdot C_6H_4\cdot CH_2\cdot$ which disappears. Now, it has been shown[2] that hydrogen atoms react rapidly with toluene, the xylenes, and other toluene derivatives according to the equations exemplified by (4).†

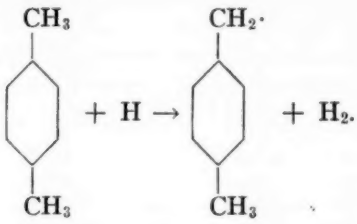

(4)

It follows, therefore, that as a result of reactions (3) and (4) each disappearing monoradical $CH_3\cdot C_6H_4\cdot CH_2\cdot$ would regenerate another radical of the same type. Hence, the occurrence of reaction (3) should initiate a chain decomposition of *para*-xylene, and one would expect that under such circumstances the rate of decomposition of *para*-xylene might be much higher than the rate of decomposition of toluene or of *meta*-xylene (the decompositions of the latter compounds were shown to proceed by a simple unimolecular mechanism). Actually, the rate of decomposition of *para*-xylene exceeds only by a factor of three the rate of decomposition of *meta*-xylene, and thus this observation was considered as an evidence against reaction (3).

Studies of pyrolyses of organic bromides, carried out in our laboratories, suggested a new approach to the problem. It was shown[6] that the pyrolysis of benzyl bromide in the presence of an excess of toluene proceeds, according to Eqs. (5)–(7),

$$C_6H_5\cdot CH_2\cdot Br \rightarrow C_6H_5\cdot CH_2\cdot + Br, \quad (5)$$

$$C_6H_5\cdot CH_3 + Br \rightarrow C_6H_5\cdot CH_2\cdot + H\cdot Br, \quad (6)$$

$$2C_6H_5\cdot CH_2\cdot \rightarrow \text{dibenzyl}. \quad (7)$$

Moreover, it appears that the pyrolyses of benzyl bromide derivatives (including *para*-xylyl-bromide) proceeds essentially in the same manner.[7] In view of these observations we reinvestigated the pyrolyses of benzyl bromide and *para*-xylyl-bromide and extended

TABLE I. Pyrolysis of benzyl bromide.

Expt. No.	T°K	Pcompd. mm Hg	% decomp	t; sec	$k\cdot10^2$ sec^{-1}
25	747	0.276	3.78	0.795	4.82
26	751	0.278	4.34	0.806	5.48
27	755	0.282	5.2	0.830	6.45
16	763	0.572	6.4	0.822	8.05
21	776	0.224	14.0	0.788	19.1
22	778	0.219	14.8	0.784	20.0
17	790	0.515	20.7	0.778	29.8
28	799	0.279	27.5	0.700	45.8
18	821	0.23	54.5	0.754	104
19	824	0.22	56.5	0.684	121
20	825	0.25	60.8	0.755	124

[5] M. Szwarc and J. S. Roberts, J. Am. Chem. Soc. **70**, 2831 (1948).

† The reaction between hydrogen atoms and toluene or the xylenes takes slightly more complex course (see reference 2 for the details). However, these complications are irrelevant for our argument.

[6] Szwarc, Ghosh, and Sehon, J. Chem. Phys. **18**, 1142 (1950).

[7] Leigh, Sehon, and Szwarc, Proc. Roy. Soc. (London) **A209**, 97 (1951).

these studies to the investigation of the pyrolysis of dibromo *para*-xylene. Furthermore, we carried out ouf experiments using both toluene and *para*-xylene as carrier gases.‡ The decomposition of these bromides takes place in the temperature region of 500°–600°C, while the decomposition of *para*-xylene is negligible below 800°C. Hence, we secured the means of producing *para*-xylyl radicals by reactions (8) and (9) and of studying their behavior under conditions which are not complicated by the thermal decomposition of *para*-xylene.

PYROLYSIS OF BENZYL BROMIDE AND *PARA*-XYLYL BROMIDE

The reinvestigation of the pyrolysis of benzyl bromide confirmed fully the previous results obtained by Leigh,

TABLE II. Pyrolysis of *para*-xylyl bromide.

Expt. No.	T°K	Pcompd. mm Hg	% decomp	tsec	$k \times 10^2$ sec^{-1}
57	748	0.70	4.74	0.850	5.67
68	749	1.02	5.25	0.840	6.47
56	752	0.63	5.17	0.820	6.42
10	757	0.38	6.25	0.820	7.80
79	760	0.41	7.40	0.820	9.03
112	761	0.052	6.86	0.805	8.30
111	764	0.051	6.06	0.795	7.83
69	766	0.40	9.40	0.790	12.60
110	768	0.053	9.60	0.826	12.20
108	769	0.062	8.95	0.846	11.05
73	770	0.43	12.20	0.810	16.10
109	781	0.050	17.20	0.830	22.90
71	781	0.360	19.10	0.790	26.80
34[a]	783	0.071	27.00	1.152	27.20
101	787	0.054	20.80	0.790	29.40
81	788	0.370	25.90	0.790	37.80
91	788	0.290	25.00	0.780	36.90
102	789	0.054	22.70	0.795	32.40
74	792	0.400	29.80	0.790	45.00
65	793	0.540	31.30	0.750	50.30
63	795	0.680	34.30	0.730	57.20
33[a]	799	0.072	48.00	1.200	54.50
106	811	0.058	48.40	0.795	82.90
86	813	0.290	56.00	0.790	107.00
107	814	0.047	53.50	0.807	96.50

[a] Using *para*-xylene as carrier gas.

Sehon, and Szwarc[7] and by Szwarc, Ghosh, and Sehon.[6] Our present data are summarized in Table I and presented in Fig. 1. To stress the agreement between this set of data and those reported in reference 7, we plotted also the results of the latter investigation on Fig. 1. Using the present data, we computed the activation energy of the dissociation process (5) at 51.0 kcal/mole, while the value reported in reference 6 is 50.5 kcal/mole, the difference being well within the experimental uncertainty.§

‡ See references 6 and 7 for details of experimental technique.

§ It has been stressed in previous publication that the absolute value of the rate constants might be a subject of an error due to the uncertainties resulting from the nonideal temperature distribution in the reaction vessel and from other calibration errors. Hence, whenever a comparison of the rates of various pyrolyses is desired, the relevant data are redetermined on the same apparatus (see, e.g., footnote on p. 98, in reference 7).

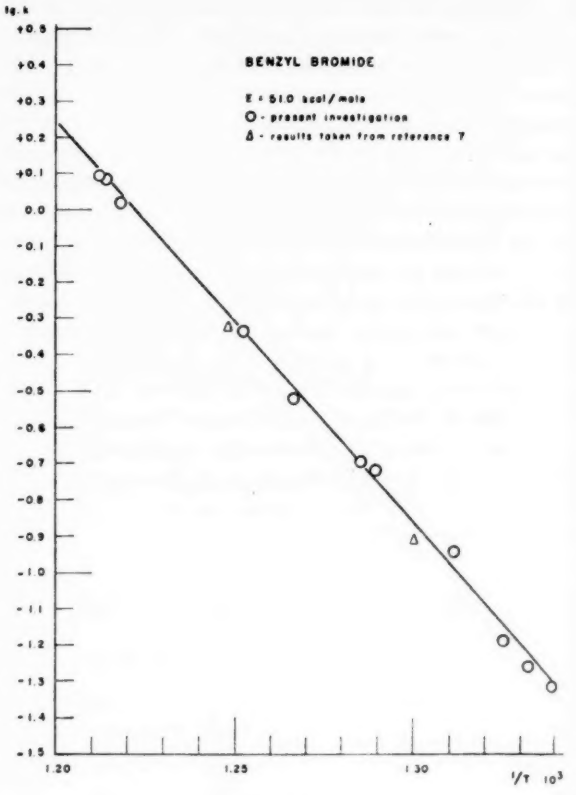

FIG. 1.

On the other hand, the reinvestigation of the pyrolysis of *para*-xylyl bromide led to results which are not entirely in accord with those reported in reference 7. It is probable that a slight decomposition of the melted xylyl bromide occurred in previous experiments. We found, indeed, that some compounds belonging to this class of organic bromides decompose easily on melting, particularly if they are slightly impure. Such decomposition would account for the observed discrepancy.

We summarized in Table II and in Fig. 2 our present data on the pyrolysis of *para*-xylyl bromide. It is striking that at lower-temperature range the unimolecular rate constants (which are based on the rate of formation of HBr) are essentially the same for benzyl bromide and for *para*-xylyl bromide. This observation suggests that the rate of rupture of C–Br bond is not affected by substituting a methyl group for a hydrogen atom (i.e., by converting a molecule of benzyl bromide into *para*-xylyl-bromide).||

Furthermore, we have found that the rate of formation of HBr is not altered when *para*-xylene is introduced instead of toluene as a carrier-gas (see runs 33 and 34 in Table II). These observations assure us that

|| This statement differs from the conclusion arrived at in reference 2. Further discussion of this point will be offered in the latter part of this communication.

reaction (8)

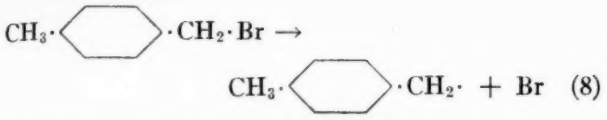

is indeed the rate determining step in the pyrolysis of *para*-xylyl bromide, and that this reaction is followed by a rapid reaction (6) if toluene in an excess is present in the system, or by a rapid reaction (9)

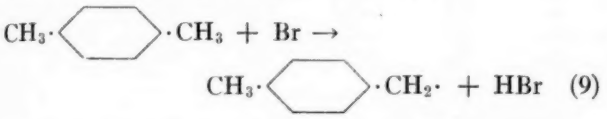

if *para*-xylene in an excess is present in the system.

DISTINCTION BETWEEN THE DECOMPOSITION AND THE DISPROPORTIONATION OF *PARA*-XYLYL RADICALS

The results reported in the preceding section suggest the following experiments. Let us decompose *para*-xylyl bromide in the presence of an excess of *para*-xylene and thus to produce *para*-xylyl radicals [according to Eq. (8) and (9)]. Now, if these radicals disproportionate—the quinonoid hydrocarbon I produced would yield eventually the polymer II, and the only gaseous product of the pyrolysis should be hydrogen bromide. On the other hand, if the *para*-xylyl radicals decompose [according to Eq. (3)], hydrogen atoms formed would initiate a chain decomposition of *para*-xylene, and consequently hydrogen as well as hydrogen bromide would be present in the gaseous products of pyrolysis. Moreover, in the latter case the molar ratio of H_2/HBr would measure the length of the kinetic chain of the decomposition.

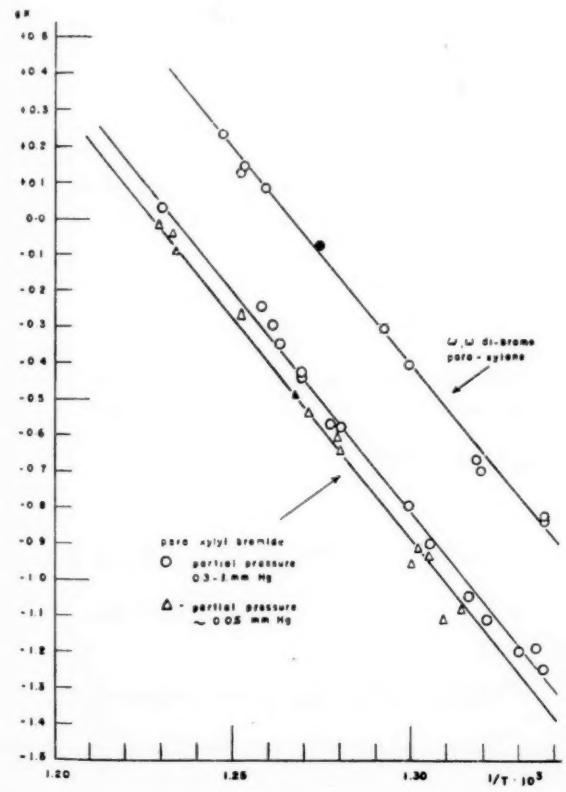

FIG. 2.

We performed these experiments and found that the hydrogen bromide formed contains only traces of hydrogen, but we found at the same time that *no* polymer was produced. Examination of the solid products of the pyrolysis revealed that they contain an impure 4,4′ dimethyl dibenzyl. When the temperature of the pyrolysis was raised by about 50° up to about 600°C, we found an appreciable amount of hydrogen in the products of pyrolysis. At the same time we found that the solid products of the decomposition contain 4,4′ dimethyl stilbene, and still no detectable amounts of the polymer.¶ To obtain detectable amounts of polymer we had to raise the temperature of the pyrolysis to about 800°C, i.e., to the temperature at which *para*-xylene begins to decompose slightly.

Our results show clearly that *para*-xylyl radicals are formed, but they neither decompose nor disproportionate in the temperature range 500°–600°C. They disappear simply by dimerisation.

PYROLYSIS OF ω, ω′ DIBROMO *PARA*-XYLENE

To gain further information relevant to our problems, we studied the pyrolysis of ω, ω′ dibromo *para*-xylene. The primary step in the decomposition of this compound is undoubtedly represented by Eq. (10)

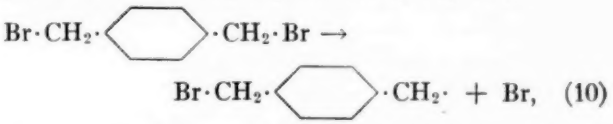

and one would expect that the rate constant of this reaction would be twice as high as that for reaction (8).** At temperatures at which the dibromo compound decomposes one might expect a decomposition of the bromo radical ($Br\cdot CH_2\cdot C_6H_4\cdot CH_2\cdot$) which is formed in reaction (10).

Now, if this decomposition, which is represented by Eq. (11)

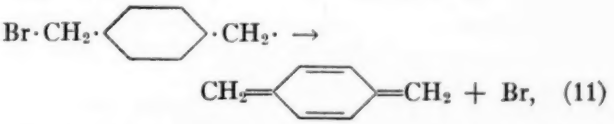

proceeds more rapidly than decomposition (10) one would expect formation of *two* bromine atoms, and consequently *two* HBr molecules, for each molecule of dibromo compound decomposed. Thus, the unimolecu-

¶ Hence the hydrogen produced under these conditions results from dehydrogenation of dimethyl-dibenzyl into dimethyl stilbene.

** The factor 2 is purely statistical factor. See in this connection M. Szwarc and D. Williams, Proc. Roy. Soc. (London) **A219**, 355 (1953).

lar rate constant of reaction (10) should be computed from the formula

$$k^1=\frac{1}{t}\cdot\ln\cdot\frac{1}{(1-f/2)},$$

where

$$f=\frac{\text{amount of HBr formed in the decomposition}}{\text{amount of dibromo compound pyrolysed}},$$

and the amount of HBr produced at lower fraction of decomposition should be by a factor of 4 higher than the amount of HBr formed by the pyrolysis of *para*-xylyl bromide. The rate constants computed in such a way are presented in Table III and on Fig. 2. A closer inspection of these data shows that the amounts of HBr produced at lower temperature range is higher only by about a factor of 3 than that produced by the pyrolysis of *para*-xylyl bromide carried out at the corresponding temperature and time of contact. However, a relatively greater amount of HBr is produced at higher temperatures. These facts suggest that the rate of decomposition of $Br\cdot CH_2\cdot C_6H_4\cdot CH_2\cdot$ radical is comparable to the rate of decomposition of *para*-xylyl bromide, and that the mechanism of decomposition of the dibromo compound is given essentially by the following system of equations:

$$Br\cdot CH_2\cdot C_6H_4\cdot CH_2\cdot Br \xrightarrow{k_2} Br\cdot CH_2\cdot C_6H_4\cdot CH_2\cdot + Br, \quad (10)$$

$$\left\{\begin{array}{l} \cdot CH_2\cdot C_6H_4\cdot CH_2\cdot Br \xrightarrow{k_d} CH_2{=}C_6H_4{=}CH_2 + Br, \quad (11) \\ \text{or} \\ \cdot CH_2\cdot C_6H_4\cdot CH_2Br + C_6H_5\cdot CH_3 \xrightarrow{k_e} CH_3\cdot C_6H_4\cdot CH_2\cdot Br + C_6H_5\cdot CH_2\cdot \quad (12) \end{array}\right.$$

Reaction (12) is followed by reaction (8)

$$CH_3\cdot C_6H_4\cdot CH_2\cdot Br \xrightarrow{k_1} CH_3\cdot C_6H_4\cdot CH_2\cdot + Br, \quad (8)$$

and finally Br atoms react according to Eq. (6)

$$C_6H_5\cdot CH_3 + Br \rightarrow C_6H_5\cdot CH_2\cdot + HBr. \quad (6)$$

Reactions (11) and (12) represent two alternative ways for the disappearance of radicals

$$\cdot CH_2\cdot C_6H_4\cdot CH_2\cdot Br.\dagger\dagger$$

†† Mr. Rembaum, working in our laboratories, succeeded in isolating *para*-xylyl bromide from the products of pyrolysis of dibromo xylene. This result proves the occurrence of reaction (12) in the pyrolysis of dibromo *para*-xylene.

TABLE III. Pyrolysis of ω, ω' dibromo *para*-xylene.[a]

Expt. No.	T°K	Pcompd. mm Hg	"% decomp" $=f$	tsec	$k'\cdot 10^2$ sec^{-1}
258	748	0.068	11.2	0.82	7.25
267	748	0.038	13.2	0.90	7.55
278	758	0.035	16.8	0.87	10.05
277	759	0.028	18.4	0.90	10.7
272	770	0.029	31.7	0.88	19.6
262	774	0.049	39.2	0.88	24.9
280	785	0.034	60.1	0.87	42.0
235[b]	787	0.066	75	1.132	41.7
275	794	0.036	81.7	0.86	60.7
284	798	0.034	88.5	0.84	69.5
285	799	0.033	85.0	0.84	66.0
266	802	0.030	99.7	0.85	81.5

[a] $k'=(1/t)\ln\cdot 1/(1-f/2)$.
[b] Using *para*-xylene as carrier gas.

The foregoing scheme corresponds to the following kinetic equations:

$$\frac{d[HBr]}{dt}=k_2\cdot[Br\cdot CH_2\cdot C_6H_4\cdot CH_2\cdot Br]+k_1\cdot[CH_3\cdot C_6H_4\cdot CH_2\cdot Br]+y,$$

where y represents the rate of formation of HBr resulting from the decomposition of the radical

$$\cdot CH_2\cdot C_6H_4\cdot CH_2\cdot Br.$$

It is easy to see that y has the form

$$y=k_2\cdot[Br\cdot CH_2\cdot C_6H_4\cdot CH_2\cdot Br]\cdot x,$$

where x denotes *the fraction* of radicals

$$\cdot CH_2\cdot C_6H_4\cdot CH_2\cdot Br$$

decomposed, while $1-x$ denotes *the fraction* of radicals which react according to Eq. (12). It follows that

$$\frac{x}{1-x}=\frac{k_d}{k_e\cdot[C_6H_5\cdot CH_3]},$$

and thus one can integrate the differential equation which gives $d[HBr]/dt$, keeping in mind that

$$\frac{d[CH_3\cdot C_6H_4\cdot CH_2Br]}{dt}=k_2\times(1-x)\cdot[CH_2Br\cdot C_6H_4\cdot CH_2\cdot Br]-k_1\cdot[CH_3\cdot C_6H_4\cdot CH_2Br],$$

and that

$$[CH_2Br\cdot C_6H_4\cdot CH_2\cdot Br]=C_0\cdot\exp(-k_2\cdot t),$$

where C_0 denotes the initial concentration of dibromo compound.

Assuming that $k_2=2k_1=2k$ one derives the following

integrated result:

"The total HBr formed in the pyrolysis"

$$=2C_0\cdot\{1-\exp(-kl)\}\cdot\{1+x\cdot\exp(-kl)\}.$$

Since we defined f as "The total HBr formed"$/C_0$, we can rewrite the above equation in the following way

$$x=\left[\frac{f}{2\cdot\{1-\exp(-kl)\}}-1\right]\cdot\exp(kl).$$

The last result can be utilized for calculating x from experimentally determined f, using values k as determined from the pyrolysis of benzyl bromide.‡‡ Table IV contains the relevant data needed for the computation of x and of $x/(1-x)$, the latter values being equal to

$$(k_d/k_e)\cdot[\text{toluene}]^{-1}.$$

In our experiments the concentration of toluene was kept constant. Hence, we can obtain the difference in the activation energy of the decomposition process (11) and the activation energy of the bimolecular reaction (12) by plotting $\ln\{x/(1-x)\}$ *versus* the reciprocal of temperature. Figure 3 shows the results, and the straight line drawn gives a rough estimate for the value of E_d-E_e.

Before we proceed further with our discussion let us remark that the formula by which we calculated the values of x amplifies enormously any experimental errors. These errors are squared again when we compute $x/(1-x)$. Consequently, one should not be surprised by the scatter of points as seen in Fig. 3. To demonstrate the difficulties let us compare the results of runs 258 and 257. The corresponding f's are very close, namely, 0.112 and 0.132, and in view of the fact that the latter run corresponds to a longer time of contact than the former (see Table IV) these results lead to a very close value for k', namely, 7.25 and 7.55. However, this small discrepancy leads to a very large difference in the value of $x/(1-x)$ which are 0.478 and 0.725, respectively.

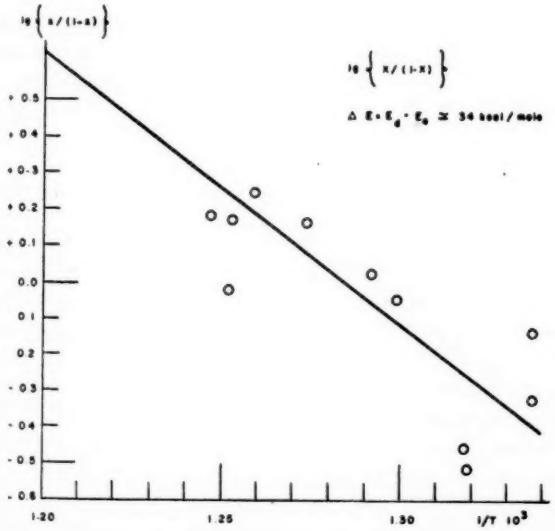

FIG. 3.

‡‡ The discussion given in a later section will make it clear why we prefer to use the values of k as determined from the pyrolysis of benzyl bromide and not from the pyrolysis of *para*-xylyl bromide.

The value for E_d-E_e as derived from Fig. 3, seems to be about 34 kcal/mole. On the other hand, we can compute E_d-E_e in an entirely different way. Let us start from the premises that k_d as a unimolecular rate constant is given by the expression

$$k_d\simeq 10^{13}\cdot\exp(-E_d/RT),$$

and k_e as a bimolecular rate constant is given by the expression

$$k_e\simeq 10^{11}\cdot\exp(-E_e/RT).$$

The frequency factor of 10^{11} is reasonable for a hydrogen transfer reaction involving an interaction between large radicals and molecules (see references 8 and 9). Since the concentration of toluene is of the magnitude 3.10^{-7} mole/cc, we conclude that

$$E_d-E_e\simeq[8.5-\log\{x/(1-x)\}]\cdot 4.6\cdot T$$

at $T=800°\text{K}$, $\log\{x/(1-x)\}$ is about 0.2. Hence

$$E_d-E_e\simeq 30 \text{ kcal/mole.}$$

Admittedly, these calculations are very approximate, nevertheless they show that the proposed value of E_d-E_e is self-consistent and probably correct within ± 5 kcal/mole. It is probable that E_e is of the order of 10 kcal/mole,§§ and hence E_d would be of the order of 40 kcal/mole.

FURTHER DISCUSSION OF THE PYROLYSIS OF *PARA*-XYLYL BROMIDE

We are now in a position to explain some peculiar features of the pyrolysis of *para*-xylyl bromide. A closer inspection of the data collected in Table II as well as an examination of Fig. 2 reveals that the calculated first-order rate constants are slightly pressure dependent. Changing the partial pressure of *para*-xylyl bromide by a factor of 10 from a few hundredths of a mm Hg to a few tenths of a mm Hg increases the rate constant by about 10 percent. Furthermore, the apparent activation energy seems to be of the order of 55 kcal/mole, i.e., it is higher than the activation energy obtained for the pyrolysis of benzyl bromide.

[8] E. W. R. Steacie and M. Szwarc; J. Phys. Chem. **19**, 1309 (1951).

[9] Dobres and P. W. Selwood, J. Am. Chem. Soc. **72**, 5731 (1950).

§§ We arrive at this value by considering the published data on activation energies of similar hydrogen transfer reactions. See A. D. Trotman-Dickenson and E. W. R. Steacie, J. Am. Chem. Soc. **72**, 2310 (1950).

Both these phenomena may be explained by assuming that the following reaction

$$Ph\cdot CH_2\cdot + CH_3\cdot C_6H_4\cdot CH_2Br \rightarrow Ph\cdot CH_3 + \cdot CH_2\cdot C_6H_4\cdot CH_2Br \quad (13)$$

takes place in the pyrolysis of *para*-xylyl bromide. It is natural to introduce reaction (13) which is the reverse of reaction (12), and one may expect that the rate constant for those two reactions should be approximately equal. It follows from the calculations, which are given below, that the rate of reaction (13) is negligible when the partial pressure of *para*-xylyl bromide is of the order of a few hundredths of a mm Hg and the fraction of decomposition not too high. Since all our experiments with ω, ω' dibromo *para*-xylene were carried out with a very low partial pressure of the compound, it is superfluous to include reaction (13) in the scheme representing the mechanism of pyrolysis of this compound.

Let us examine now in a semiquantitative way the consequences of the occurrence of reaction (13). We assumed previously that the bimolecular rate constant for reaction (12) is given by the expression

$$k_e = 10^{11}\cdot\exp(-10\,000/RT).$$

Taking the same expression for the bimolecular rate constant of (13) we derive a value of about $1.6\cdot10^8$ for k_{13} at 770°K. At this temperature about 10 percent of *para*-xylyl bromide decomposes in about 0.8 sec. Hence, the average concentration of benzyl radicals present in the system should be of the order of 10^{-9} mole/cc if the concentration of *para*-xylyl bromide is of the order 10^{-8} mole/cc (the partial pressure of the order of a few tenths of a mm Hg), and it would be of the order 10^{-10} mole/cc if the concentration of *para*-xylyl bromide is of the order of 10^{-9} mole/cc (the partial pressure of the order of a few hundredths of a mm Hg). It follows that the relative amount of $\cdot CH_2\cdot C_6H_4\cdot CH_2Br$ radicals produced by reaction 13, i.e.,

$$\frac{[\cdot CH_2\cdot C_6H_4\cdot CH_2\cdot Br]}{[CH_3\cdot C_6H_4\cdot CH_2\cdot Br]}$$

would be about 0.13 for $P_{CH_3\cdot C_6H_4\cdot CH_2\cdot Br}\simeq 0.3$ mm Hg, and about 0.013 for $P_{CH_3\cdot C_6H_4\cdot CH_2Br}\simeq 0.03$ mm Hg. Since about $\frac{1}{2}$ of these radicals are decomposed under these conditions we expect an increase of about 6 percent in the amount of HBr collected at higher partial pressure of *para*-xylyl bromide, and of about 0.6 percent at lower range of partial pressures. The increase in the amount of HBr formed would produce a similar increase in the apparent rate constant. Hence by introducing reaction (13) into the mechanism of the pyrolysis of *para*-xylyl bromide, we can account not only for the observed change in the apparent rate constant, but also for the magnitude of this change.

Similarly we can account for the apparent high activation energy of the pyrolysis. At higher temperatures the fraction of decomposition is higher, and hence the concentration of benzyl radicals increases. Furthermore, the fraction of $\cdot CH_2\cdot C_6H_4\cdot CH_2\cdot Br$ decomposed increases also. Both these factors make the apparent activation energy of the pyrolysis higher, and semiquantitative calculations show again that the increase is of the proper order of magnitude.

TABLE IV. Calculation of x and of $x/(1-x)$.

Run	$1/T\cdot10^3$	$\ln\cdot k$	$\exp(kt)$	f	x	$x/(1-x)$
258	1.337	−1.27	1.0449	0.112	0.324	0.478
267	1.337	−1.27	1.0495	0.132	0.420	0.725
278	1.319	−1.08	1.0750	0.168	0.215	0.305
277	1.318	−1.07	1.0795	0.184	0.259	0.349
272	1.299	−0.86	1.1275	0.317	0.473	0.896
262	1.292	−0.78	1.157	0.392	0.515	1.06
280	1.274	−0.58	1.257	0.601	0.592	1.45
275	1.259	−0.42	1.387	0.817	0.638	1.76
284	1.253	−0.35	1.456	0.885	0.597	1.48
285	1.252	−0.34	1.468	0.850	0.485	0.942
266	1.247	−0.28	1.562	0.997	0.600	1.50

DISCUSSION OF THE PYROLYSIS OF *PARA*-XYLENE

Our present data enables us to deduce an approximate value for the activation energy of the dissociation process (3)

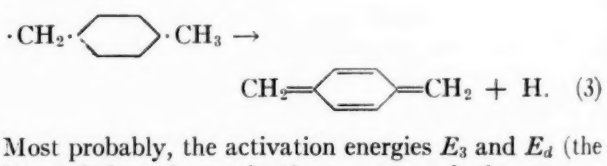

$$\cdot CH_2\cdot C_6H_4\cdot CH_3 \rightarrow CH_2{=}C_6H_4{=}CH_2 + H. \quad (3)$$

Most probably, the activation energies E_3 and E_d (the latter being the activation energy of the process $\cdot CH_2\cdot C_6H_4\cdot CH_2Br \rightarrow CH_2{:}C_6H_4{:}CH_2 + Br$) are only slightly higher than the respective bond dissociation energies, i.e., $D(\cdot CH_2\cdot C_6H_4\cdot CH_2 - H)$ and $D(\cdot CH_2\cdot C_6H_4\cdot CH_2 - Br)$. This conclusion is based on the assumption that the respective reverse reactions should not require more than a few kcal/mole of activation energy, if any. Hence,

$$E_3 - E_d \simeq D(\cdot CH_2\cdot C_6H_4\cdot CH_2 - H) - D(\cdot CH_2\cdot C_6H_4\cdot CH_2 - Br).$$

Now, the available data seems to indicate that the differences between the various R−H bond dissociation energies and the corresponding R−Br bond dissociation energies are approximately constant. For example, the difference $D(C_6H_5\cdot CH_2-H)-D(C_6H_5\cdot CH_2-Br)$ has been obtained directly from the determined values of the dissociation energies and indirectly from the thermochemical data.[10] The first method leads to $\Delta D=27$ kcal/mole while the second yields $\Delta D=29$ kcal/mole. The inspection of other thermochemical data[11] gives for various $D(R-H)-D(R-Br)$ values ranging from 30 kcal/mole to 33 kcal/mole. Thus, if we choose 30

[10] O. H. Gellner and H. A. Skinner, J. Chem. Soc. **1949**, 1145.
[11] M. Szwarc, Chem. Revs. **47**, 75 (1950); J. S. Roberts and H. A. Skinner, Trans. Faraday Soc. **45**, 339 (1949).

kcal/mole as an average value for ΔD, and accept the previously deduced value of ~40 kcal/mole for E_d, we conclude that E_3 is approximately 70 kcal/mole.

On the whole, a dissociation energy of a bond in a radical is very low if the radical is converted by the dissociation process into a stable molecule. For example $D(\cdot CH_2 \cdot CH_2 - H)$ is 41 kcal/mole only, i.e., about 50 kcal/mole less than the C—H bond dissociation in the parent molecule. On the other hand, the bond dissociation energy in a radical which is stabilized by a resonance might be not much lower than the dissociation energy of a bond in the parent molecule. For example, $D(CH_2:CH \cdot CH_2 - H)$ is 78 kcal/mole while

$$D\left(\begin{matrix}CH_2: \\ \\ CH_2\cdot\end{matrix}\!\!\!

THE JOURNAL OF CHEMICAL PHYSICS VOLUME 22, NUMBER 11 NOVEMBER, 1954

Derivations of Onsager's Reciprocal Relations

EUGENE P. WIGNER
Palmer Physical Laboratory, Princeton University, Princeton, New Jersey
(Received May 24, 1954)

Two derivations of Onsager's reciprocal relations are presented in simplified form, and the range of their validity is discussed.

1. GENERAL STATEMENTS

THERE appear to be two groups of derivations of Onsager's reciprocal relations.[1] In the first of these, it is assumed that the macroscopic laws of motion hold for the averages of the macroscopic coordinates (such as temperature gradient, concentration gradient, etc.) even if their values are microscopic, i.e., in the usual range of fluctuations.[2] The second group assumes a definite statistical law for the path representing the system in phase space.[3] Both types of derivations will be reviewed briefly below.

Common to both derivations is the concept of macroscopic coordinates $Q_1, \cdots, Q_n$ which are functions of the microscopic coordinates $q_1, \cdots, q_N, p_1, \cdots, p_N$. The latter are the coordinates of the phase space Γ; the space of the former will be called γ. A typical set of macroscopic coordinates are the components of the temperature gradient. This can be defined as

$$(2/3k)\sum \mathbf{q}_i(p_i^2/2m_i - 3kT/2),$$

and similar definitions apply to other macroscopic variables.

There corresponds to every domain in γ a domain in phase space but the ratio of the volume of the latter domain to that of the former is not constant. The integral of $e^{-H/kT}$ over the domain in Γ space gives the unnormalized probability of the domain in γ space to which it corresponds. This probability has a sharp maximum at the "equilibrium values" of the Q which will be assumed to be 0. Second, it will be assumed that, for small but macroscopic values of the Q, the entropy of the system can be expanded into a quadratic function of the Q:

$$S(\mathbf{Q})-S(\mathbf{O}) = -k\sum s^{ik}Q_iQ_k = -k(\mathbf{Q},s\mathbf{Q}), \quad (1)$$

in which $s=(s^{ik})$ is a symmetric positive definite matrix and $\mathbf{Q}$ stands for $Q_1, \cdots, Q_n$. The normalized probability of a unit volume element at $\mathbf{Q}$ is then given by

$$P(\mathbf{Q}) = Z^{-1}\exp(\mathbf{Q}, -s\mathbf{Q}). \quad (1a)$$

This is, by the connection between entropy and extension in Γ space adopted here, the integral of $e^{-H/kT}$ over that part of Γ space which corresponds to the unit volume element at $\mathbf{Q}$ in γ space, divided by the integral $Z=\int e^{-H/kT}dpdq$ over the whole Γ space. Z can be defined also by the condition that

$$\int P(\mathbf{Q})d\mathbf{Q}=1; \quad Z=\pi^{-n/2}|\det s|^{\frac{1}{2}}. \quad (1b)$$

One can easily verify, furthermore, that

$$2\int Q_iQ_kP(\mathbf{Q})d\mathbf{Q}=\sigma_{ik} \quad (1c)$$

forms the reciprocal matrix to s

$$\sigma = s^{-1}. \quad (1d)$$

Only σ will occur in subsequent work so that (1c) can be taken as the definition of σ. The relation to the entropy is given, however, by (1) and (1d).

It will be assumed, finally, that the Q contain the time variable only in even order, i.e., that they are invariant with respect to time inversion and that the same holds also for the whole system, i.e., its Hamiltonian. Let us denote then by Γ_Q the domain in Γ space which corresponds to a unit volume element at $\mathbf{Q}$ in γ. Similarly, $\Gamma_{Q'}$ corresponds to a unit volume element at $\mathbf{Q}'$. In proper units, the volumes of Γ_Q and $\Gamma_{Q'}$ are equal to $P(\mathbf{Q})$ and $P(\mathbf{Q}')$. As time flows, the systems

[1] L. Onsager, Phys. Rev. **37**, 405 (1931); **38**, 2265 (1931). These articles contain also extensive references to earlier literature. See also I. Prigogine, *Etude Thermodynamique des Phenomenes Irreversibles* (Editions Desoer, Liege, 1947) and S. de Groot, *Thermodynamics of Irreversible Processes* (North Holland Publishing Company, Amsterdam, 1951). For a review of the recent work on the subject see E. M. Montroll and M. S. Green, "Statistical Mechanics of Transport and Nonequilibrium Processes" (to be published in Annual Reviews of Physical Chemistry).

[2] For the first type of derivation, see in addition to Onsager's articles, particularly R. T. Cox, Revs. Modern Phys. **22**, 238 (1950); **24**, 312 (1952). This article uses quantum concepts, in particular the notion of the transition probability. It is assumed that the system changes its state by means of spontaneous quantum jumps. This assumption eliminates the induction period discussed in the text [after Eq. (14a)] and entails the validity of differential equations of the form (4a) for the macroscopic variables. It is, therefore, not entirely clear that the reasoning contained in these articles would remain valid in all details if quantum mechanical concepts were used. In quantum mechanics, the probability of a state decreases, initially, as $1-ct^2$ rather than $1-ct$ and the latter, linear, law takes over only after an induction period. Ideas similar to those of Cox have been put forward also by H. B. Callen and R. Greene, [Phys. Rev. **86**, 702 (1952); **99**, 1387 (1952)], based on work by H. B. Callen and T. A. Welton [Phys. Rev. **83**, 34 (1951)] and by J. Jackson [Phys. Rev. **87**, 471 (1952)]. These papers also assume the "law of transition probabilities."

[3] The basis of the second type of consideration seems to have been provided by J. G. Kirkwood [J. Chem. Phys. **14**, 180 (1946)]. For the actual derivation see M. S. Green [Princeton dissertation (1951) and J. Chem. Phys. **20**, 1281 (1952)] and N. Hashitzume [Progr. Theoret. Phys. **8**, 461 (1952)]. It was developed with particular elegance by L. Onsager and S. Machlup [Phys. Rev. **91**, 1505, 1512 (1953)].

represented by the points in Γ_Q will change. Let us denote by $\Gamma_{Q\to Q'}$ the part of the domain of Γ_Q the points of which move, in the time interval t, into the domain $\Gamma_{Q'}$. Then

$$T_t(\mathbf{Q}\to\mathbf{Q}') = \text{volume of } \Gamma_{Q\to Q'}/\text{volume of } \Gamma_Q = \text{volume of } \Gamma_{Q\to Q'}/P(\mathbf{Q}) \tag{2}$$

is the transition probability from $\mathbf{Q}$ to $\mathbf{Q}'$. Since every point in Γ_Q will arrive, after time t, in some $\Gamma_{Q'}$,

$$\int T_t(\mathbf{Q}\to\mathbf{Q}')d\mathbf{Q}' = 1. \tag{2a}$$

Let us consider now the domain $\Gamma_{Q\to Q'}{}^*$ which can be obtained from $\Gamma_{Q\to Q'}$ by replacing all points $q_1, \cdots, q_N$, $p_1, \cdots, p_N$ of $\Gamma_{Q\to Q'}$ by $q_1, \cdots, q_N, -p_1, \cdots, -p_N$, or, more generally, by applying the operation of time inversion to $\Gamma_{Q\to Q'}$. Clearly, the volume of $\Gamma_{Q\to Q'}$ is equal to the volume of $\Gamma_{Q\to Q'}{}^*$

$$\text{volume of } \Gamma_{Q\to Q'} = \text{volume of } \Gamma_{Q\to Q'}{}^*. \tag{3}$$

Furthermore, because of the invariance of the Q with respect to time inversion, $\Gamma_{Q\to Q'}{}^*$ is also contained in Γ_Q. We note, finally, that the points which are at time 0 in $\Gamma_{Q\to Q'}{}^*$ were, at time $-t$, in $\Gamma_{Q'}$ just as the points which are at time 0 in $\Gamma_{Q\to Q'}$ will be, at the time t, in $\Gamma_{Q'}$. In fact, the points which are, at time 0, in $\Gamma_{Q\to Q'}{}^*$ formed, at time $-t$, the domain $\Gamma_{Q'\to Q}$. Hence, because of Liouville's theorem,

$$\text{volume of } \Gamma_{Q'\to Q} = \text{volume of } \Gamma_{Q\to Q'}{}^*. \tag{3a}$$

It follows (see Fig. 1) that the volumes of $\Gamma_{Q\to Q'}$ and of $\Gamma_{Q'\to Q}$ are equal, or because of (2)

$$P(\mathbf{Q})T_t(\mathbf{Q}\to\mathbf{Q}') = P(\mathbf{Q}')T_t(\mathbf{Q}'\to\mathbf{Q}), \tag{3b}$$

i.e., that *the principle of detailed balance holds in γ space.* This conclusion is based solely on the postulate of the invariance of the Q and of H with respect to time inversion and, of course, on Liouville's theorem and on the independence of H from time.

2. ASSUMPTION OF THE MICROSCOPIC VALIDITY, ON THE AVERAGE, OF THE MACROSCOPIC EQUATIONS

It is in conformity with the idea of a relaxation phenomenon to demand, at least for macroscopic values of the Q, that the average values of the Q, at time t, be linear functions of the initial values

$$\int T_t(\mathbf{Q}\to\mathbf{Q}')Q_i'd\mathbf{Q}' = \sum \epsilon(t)_i{}^k Q_k. \tag{4}$$

In fact, from a purely macroscopic point of view, one would expect (4) to hold even for infinitely short times, i.e., one would expect equations of the form

$$(d/dt)\bar{Q}_i(t) = -\sum l_{ik}\bar{Q}_k \tag{4a}$$

to be valid. This would not be consistent, however,

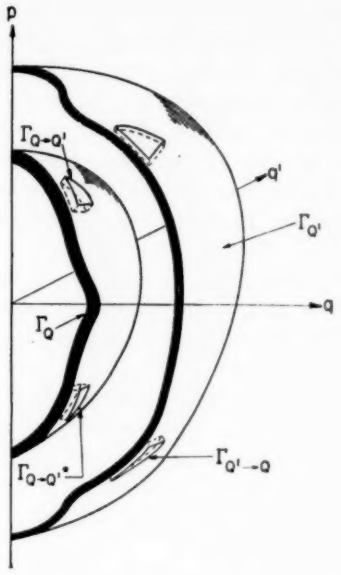

FIG. 1.

with the microscopic point of view; in fact, because of the invariance of the Q with respect to time inversion, the average of each dQ/dt over Γ_Q vanishes. However, the integrated form (4) of (4a) can be expected to be valid after a certain induction period. This induction period t is so long that dQ/dt already undergoes substantial changes during this period, i.e., $|d^2Q/dt^2|t$ is, for most points of Γ_Q, much larger than $|dQ/dt|$. We shall use, below, only the integrated form (4).

However, the integrated form will be assumed to be valid for all, even microscopically small Q. The reciprocal relations then follow at once: multiplication of (4) with $P(\mathbf{Q})Q_l$ and integration yields, because of (1c),

$$\int\int P(\mathbf{Q})T_t(\mathbf{Q}\to\mathbf{Q}')Q_lQ_i'd\mathbf{Q}d\mathbf{Q}' = \tfrac{1}{2}\sum \epsilon(t)_i{}^k\sigma_{kl}. \tag{5}$$

One sees by means of (3b) that the left side is symmetric in l and i,

$$\int\int P(\mathbf{Q})T_t(\mathbf{Q}\to\mathbf{Q}')Q_lQ_i'd\mathbf{Q}d\mathbf{Q}' = \int\int P(\mathbf{Q}')T_t(\mathbf{Q}'\to\mathbf{Q})Q_lQ_i'd\mathbf{Q}d\mathbf{Q}' = \int\int P(\mathbf{Q})T_t(\mathbf{Q}\to\mathbf{Q}')Q_iQ_l'd\mathbf{Q}'d\mathbf{Q}.$$

The last part follows by interchanging the variables Q and Q'. It follows that the matrix $\epsilon\sigma$ is symmetric

$$\epsilon\sigma = (\epsilon\sigma)' = \sigma\epsilon' \quad \text{or} \quad \sigma^{-1}\epsilon\sigma = \epsilon'. \tag{5a}$$

The last form shows that (5a) holds also if any function of ϵ is substituted for ϵ; (5a) embodies the reciprocal relations. Because of $\sigma = s^{-1}$, one can write it also in the form

$$s\epsilon = \epsilon' s = (s\epsilon)'. \tag{5b}$$

It was first noted by Casimir[4] that the validity of the assumption, that (4) holds even for very small Q, is very difficult to assess. In fact, the significance of (4) for such values of Q as are assumed in the course of ordinary fluctuations, is quite different from the macroscopic case. In the latter case, the $T_t(\mathbf{Q}\rightarrow\mathbf{Q}')$, as function of $\mathbf{Q}'$, has a rather sharp maximum, the width of which is much smaller than its distance from the point $\mathbf{Q}'=0$. If the Q are microscopic to begin with, most of the systems represented by Γ_Q will have gone through all the planes $Q_i'=0$ several times during the time interval t; after the time t the system will have only a rather faint memory of its initial state Q. It is not at all clear that this memory should be subject to the same macroscopic laws which govern the values of the Q in the macroscopic case. In the macroscopic case the value of the macroscopic variables at time t is given by the right side of (4) for practically all systems represented by the points of Γ_Q.

The above point can be illustrated on the example of the stopping of a macroscopic particle by the viscosity of the medium in which it is moving. If the velocity of the particle is many times in excess of the equilibrium average value, a Stokes' flow will establish itself around it. The energy loss will be determined by the properties of this flow. On the other hand, if the energy is of the order kT, it is very likely that the atoms around it will not assume any ordered motion. One must recall that, in thermal equilibrium, there are no correlations between the velocities of any particles: $e^{-H/kT}$ is, as far as the velocities are concerned, a product of functions, each depending on one velocity only. Hence, on the average, there is no Stokes' flow; an ordered motion of the gas is contingent on the macroscopic body having moved, some time before the observation, with an even higher than its velocity at the time of observation.

The reader interested in mathematical implications may note that, according to (3b),

$$K(\mathbf{Q},\mathbf{Q}')=P(\mathbf{Q})^{\frac{1}{2}}T_t(\mathbf{Q}\rightarrow\mathbf{Q}')P(\mathbf{Q}')^{-\frac{1}{2}} \tag{5c}$$

is the kernel of a symmetric operator in the real Hilbert space of square integrable functions of the $Q_1, \cdots, Q_n$. The normalization property (2a) (which was not used in the above derivation) then expresses the fact that $P(\mathbf{Q})^{\frac{1}{2}}$ is a characteristic function of K with characteristic value 1. The macroscopic equations (4) show that the subspace of the functions $Q_iP(\mathbf{Q})^{\frac{1}{2}}$ is invariant under K.

3. MOTION OF THE SYSTEM CAN BE REPRESENTED AS A BROWNIAN MOTION IN THE SPACE OF THE MACROSCOPIC VARIABLES

A rather different and very suggestive derivation of the reciprocal relations[3] is based on the explicit assumption that the point representing the state of the system in γ space performs a Brownian motion. More specifically, it is assumed that

$$T_t(\mathbf{Q}\rightarrow\mathbf{Q}')=C\exp-\{(\mathbf{Q},\alpha\mathbf{Q})+2(\mathbf{Q}',\beta\mathbf{Q})+(\mathbf{Q}',\gamma\mathbf{Q}')\}. \tag{6}$$

The matrices α and γ are symmetric. They, as well as β, depend on t. The normalization condition (2a) can be satisfied only if $\alpha=\beta'\gamma^{-1}\beta$. Hence, writing $\epsilon=-\gamma^{-1}\beta$, one obtains

$$T_t(\mathbf{Q}\rightarrow\mathbf{Q}')=C\exp-(\mathbf{Q}'-\epsilon\mathbf{Q},\gamma(\mathbf{Q}'-\epsilon\mathbf{Q})). \tag{6a}$$

This shows that γ must be positive definite. One sees that the most probable value of the Q' after the time t, as well as their average value, is given by $\mathbf{Q}'=\epsilon\mathbf{Q}$. Hence, ϵ plays the same role in the present derivation as it did in the preceding section.

Clearly, (6a) constitutes a particularly simple assumption for T_t which entails, furthermore, the validity of (4). Hence, the reciprocal relations will surely follow from (6a) and (3b), if (6a) is assumed to be valid for all $\mathbf{Q}$. However, and this is the point of the present consideration (in addition to the suggestive nature of the picture which it presents), it will be necessary to assume (6a) only for macroscopic $\mathbf{Q}$. Instead, the form (1a) will be explicitly assumed for $P(\mathbf{Q})$. One may recall, however, that (1a), as well as (3b), followed from the general principles of statistical mechanics.

Inserting therefore (1a) and (6a) into (3b), one obtains

$$\exp-\{(\mathbf{Q},s\mathbf{Q})+(\mathbf{Q}'-\epsilon\mathbf{Q},\gamma(\mathbf{Q}'-\epsilon\mathbf{Q}))\}$$
$$=\exp-\{(\mathbf{Q}',s\mathbf{Q}')+(\mathbf{Q}-\epsilon\mathbf{Q}',\gamma(\mathbf{Q}-\epsilon\mathbf{Q}'))\}. \tag{6b}$$

One has to assume the validity of this equation only for a few different values $\mathbf{Q}$, $\mathbf{Q}'$, to conclude that

$$s+\epsilon'\gamma\epsilon=\gamma \quad \epsilon'\gamma=\gamma\epsilon. \tag{7}$$

Inserting the second equation into the first one gives $s+\gamma\epsilon^2=\gamma$ or

$$\gamma=s(1-\epsilon^2)^{-1}, \tag{7a}$$

and substitution of this into the second one

$$\epsilon's(1-\epsilon^2)^{-1}=s(1-\epsilon^2)^{-1}\epsilon. \tag{7b}$$

Since $1-\epsilon^2$ and ϵ commute, this is equivalent to (5b), i.e., the reciprocal relations.

It might appear from the above that the assumption (6) is used only in a very mild form. This is indeed true as far as the necessity is concerned to use (6) for $\mathbf{Q}$ which are close to equilibrium: It is not necessary to use (6) for such $\mathbf{Q}$. However, at least one of the pairs $\mathbf{Q}\rightarrow\mathbf{Q}'$ or $\mathbf{Q}'\rightarrow\mathbf{Q}$ in (7) is such that the corresponding transition probability is extremely small. The assumption that (6) can be used in such a case is a rather stringent one.

Again, the reader may be interested to note the consequences of the Markoffian nature of the process, i.e., the consequences of the condition that $T_{t+t'}(\mathbf{Q}\rightarrow\mathbf{Q}'')$ is the integral, over $d\mathbf{Q}'$, of $T_t(\mathbf{Q}\rightarrow\mathbf{Q}')T_{t'}(\mathbf{Q}'\rightarrow\mathbf{Q}'')$. This condition gives two equations for the matrices $\epsilon(t)$ and $\gamma(t)$ which occur in (6a). The first of these is obtained

[4] H. B. G. Casimir, Revs. Modern Phys. **17**, 343 (1945).

most easily by means of (4) which is valid also in this case

$$\epsilon(t+t')=\epsilon(t')\epsilon(t). \tag{8}$$

It follows from this that

$$\epsilon(t)=e^{-lt}, \tag{8a}$$

where l is a positive definite matrix. The condition for γ reads

$$\gamma(t+t')^{-1}=\gamma(t')^{-1}+\epsilon(t')\gamma(t)^{-1}\epsilon'(t'). \tag{9}$$

This is satisfied by the γ given by (7a)

$$\gamma(t)^{-1}=(1-e^{-2lt})\sigma, \tag{9a}$$

if the reciprocal relations (5a) are assumed to hold. Both l and σ are independent of t. However, (9a) is not a consequence of (9) but follows from it only if (3b), (1a) and (1d) are also assumed to be valid. Actually, as was explained after (4a), none of the equations (8) or (9) holds for very small t.

It might appear from the above discussion that both derivations of Onsager's relations assume additional conditions which are hard to justify rigorously. Actually, as was pointed out by Casimir[4] (and in a particular case already by Onsager)[1], there are cases in which the deviation from the equilibrium decays exponentially even after it has become so small that it is in the normal range of fluctuations. According to Casimir, this will always be the case for processes which can be described by means of Boltzmann's distribution function $f(x,y,z,p_x,p_y,p_z;t)$ in the space of the variables of single atoms and if the deviation of f from the equilibrium f is sufficiently small at every point of this space to justify the usual linear approximation. In such a case, the first derivation[1,2] is fully justified. No similar argument can be made on the basis of considerations in Γ space, because the deviation from the equilibrium distribution in Γ space is large for all nonequilibrium systems.

THE JOURNAL OF CHEMICAL PHYSICS VOLUME 22, NUMBER 11 NOVEMBER, 1954

Structure of a Steady-State Plane Detonation Wave with Finite Reaction Rate

JOHN G. KIRKWOOD, *Sterling Chemical Laboratory, Yale University, New Haven, Connecticut*

AND

WILLIAM W. WOOD, *Los Alamos Scientific Laboratory, University of California, Los Alamos, New Mexico*

(Received April 30, 1954)

An analytical elaboration of von Neumann's model of the detonation wave is presented. A hydrodynamic argument for the well-known Chapman-Jouguet condition is advanced, and the sound speed to be used therein is identified as that obtained with frozen chemical equilibrium, in agreement with a recent result of Brinkley and Richardson. Possible situations in which the classical Chapman-Jouguet hypothesis might be incorrect are very briefly discussed.

I

THE propagation of a plane detonation wave through a semi-infinite explosive medium has been discussed theoretically by a number of investigators,[1–12] beginning with Chapman[1] and Jouguet.[2] The central problem is the selection of a unique detonation process from a one-dimensional continuum of processes all of which satisfy the usual conservation laws for mass, momentum, and energy. The rule by which this selection is made is known as the Chapman-Jouguet (denoted in the following by C-J) hypothesis, after these early investigators. The chemical reaction responsible for the detonation process has been treated as an instantaneous transformation in many of these discussions.[1–5,9,11] In particular, Brinkley and Kirkwood have studied the stability of the C-J detonation under this assumption.

Chemical reaction rates are of course finite, and as a consequence the region in which the chemical transformation takes place must be of nonvanishing dimen-

[1] D. L. Chapman, Phil. Mag. **47**, 90 (1889).
[2] E. Jouguet, Compt. rend. **132**, 573 (190); **144**, 415 (1907).
[3] R. Becker, Z. Elektrochem. **23**, 40, 304 (1917); Z. Physik **8**, 321 (1922).
[4] W. Jost, Z. Elektrochem. **41**, 183 (1935); Z. physik. Chem. **42**, 136 (1939).
[5] R. L. Scorah, J. Chem. Phys. **3**, 425 (1935).
[6] Y. B. Zeldovitch, J. Exptl. Theoret. Phys. (USSR) **10**, 542 (1940).
[7] J. von Neumann, OSRD 549 (1942); see also W. Doering, Ann. Physik **43**, 421 (1943).
[8] Eyring, Powell, Duffy, and Parlin, Chem. Revs. **45**, 69 (1949).
[9] S. R. Brinkley, Jr. and J. G. Kirkwood, *Third Symposium on Combustion, Flame, and Explosion Phenomena* (Williams and Wilkins Company, Baltimore, 1949), p. 586.
[10] S. R. Brinkley, Jr. and J. M. Richardson, *Fourth Symposium (International) on Combustion* (Williams and Wilkins Company, Baltimore, 1953), p. 450.
[11] R. Courant and K. O. Friedrichs, *Supersonic Flow and Shock Waves* (Interscience Publishers, Inc., New York), p. 204.
[12] Curtiss, Hirschfelder, and Campbell, *The Theory of Flame Propagation and Detonation*, CM-690, University of Wisconsin (1952).

sions. Certain well-known properties of detonation waves in finite geometry afford experimental verification of this, and in fact considerable interest is attached to the determination of such parameters as the reaction time, etc. The classical paper in the discussion of the influence of finite reaction rates on the detonation process is that of von Neumann.[7] The present work is essentially an analytical elaboration of his geometrical discussion, which we hope will clarify several points. Brinkley and Richardson[10] have also recently considered this question, and our Sec. IV is similar in certain respects to their work.

II

Our model is that of a fluid undergoing one-dimensional, compressible, nondissipative, adiabatic, reactive flow.* Shocks are treated as mathematical jump discontinuities in certain of the hydrodynamic-thermodynamic variables. Among the variables specifying the state of the system are certain composition variables λ^j, $j=1,2,\cdots r$, corresponding to certain independent chemical reactions, r in number, involving the n components of the fluid, which reactions are denoted by

$$\sum_{\alpha=1}^{n} \nu_\alpha{}^j X_\alpha = 0, \quad j=1,2,\cdots r. \tag{1}$$

The $\nu_\alpha{}^j$ are stoichiometric coefficients, positive for products, negative for reactants, and so chosen that (1) expresses the transformation of unit mass of reactants to products; X_α denotes unit mass of component α. The λ^j are progress variables, specifying the increase in mass of the various components within a fluid element of total mass m due to the r chemical reactions:

$$dm_\alpha = m \sum_{j=1}^{r} \nu_\alpha{}^j d\lambda^j, \quad \alpha=1,2,\cdots n. \tag{2}$$

We assume throughout this discussion the existence of local thermodynamic quasi-equilibrium, such as to permit the definition of local temperature, etc., and to permit the assumption that the various thermodynamic quantities may be regarded as functions of a suitable set of independent thermodynamic variables. We also suppose the Lagrangian time derivatives of the progress variables to be given by

$$d\lambda^j/dt = r_j, \tag{3a}$$

$$r^j = r_f{}^j - r_b{}^j, \quad j=1,2,\cdots r, \tag{3b}$$

where $r_f{}^j$ and $r_b{}^j$ are chemical rate functions for the forward and back directions of reaction j, given as functions of the local thermodynamic state.

In the regions of space-time in which shocks are absent the flow is governed under our assumptions by the usual hydrodynamic equations

$$\frac{d\rho}{dt} + \rho \frac{\partial u}{\partial x} = 0, \tag{4a}$$

$$\frac{du}{dt} + v \frac{\partial p}{\partial x} = 0, \tag{4b}$$

$$\frac{dE}{dt} + p \frac{dv}{dt} = 0, \tag{4c}$$

$$\frac{d}{dt} = \frac{\partial}{\partial t} + u \frac{\partial}{\partial x}, \tag{4d}$$

$$\frac{\partial}{\partial t} = \left(\frac{\partial}{\partial t}\right)_x, \quad \frac{\partial}{\partial x} = \left(\frac{\partial}{\partial x}\right)_t.$$

We use ρ to denote matter density; u the mass velocity in a coordinate system with x as space variable, t as time variable; p the fluid pressure; v the specific volume equal to $1/\rho$; E the specific internal energy, assumed to be a known function of the local thermodynamic state, say the variables λ, ρ, S, where λ denotes the set of variables λ^j; S the specific entropy. The equation of state is also assumed, giving p as a function of λ, ρ, and S.

From the alternative form of the first law

$$\frac{dE}{dt} = T\frac{dS}{dt} - p\frac{dv}{dt} + \frac{1}{m}\sum_\alpha \mu_\alpha \frac{dm_\alpha}{dt}, \tag{5}$$

in which μ_α denotes the specific chemical potential, we obtain the entropy transport due to chemical reaction:

$$\frac{dS}{dt} = -\sum_j \frac{\Delta^j F}{T}\frac{d\lambda^j}{dt}, \tag{6a}$$

$$\Delta^j F = \sum_\alpha \nu_\alpha{}^j \mu_\alpha. \tag{6b}$$

Corresponding to the classical Riemann analysis of the hydrodynamic equations in the nonreactive case, we now utilize the equation of state, and the entropy transport equation as well, to establish the relation between the substantive derivatives of p, ρ, and λ. The usual rule for differentiation gives

$$\frac{dp}{dt} = \left(\frac{\partial p}{\partial \rho}\right)_{S,\lambda}\frac{d\rho}{dt} + \left(\frac{\partial p}{\partial S}\right)_{\rho,\lambda}\frac{dS}{dt} + \sum_j \left(\frac{\partial p}{\partial \lambda^j}\right)_{S,\rho}\frac{d\lambda^j}{dt}. \tag{7}$$

With the definitions

$$c_0{}^2 = (\partial p/\partial \rho)_{S,\lambda}, \tag{8a}$$

$$\beta_0 = (\partial v/\partial T)_{p,\lambda}, \tag{8b}$$

$$c_p{}^0 = (\partial H/\partial T)_{p,\lambda}. \tag{8c}$$

* See reference 12 for a discussion in which dissipative and diffusion processes are considered.

we obtain after some manipulation the relation

$$\frac{d\rho}{dt}=\frac{1}{c_0^2}\frac{dp}{dt}-\rho\sum_j \sigma^j\frac{d\lambda^j}{dt}, \tag{9}$$

where

$$\sigma^j=\frac{\rho\beta_0}{c_p^0}\left(\frac{c_p^0}{\beta_0}\Delta^j v-\Delta H\right)=\frac{1}{\rho c_0^2}\left(\frac{\partial p}{\partial\lambda^j}\right)_{E,\rho}$$

$$=-\frac{\rho\beta_0}{c_p^0}\left(\frac{\partial E}{\partial\lambda^j}\right)_{p,v}, \tag{10a}$$

$$\Delta^j H=\sum_\alpha \nu_\alpha{}^j\bar{H}_\alpha=\left(\frac{\partial mH}{\partial\lambda^j}\right)_{T,p}, \tag{10b}$$

$$\Delta^j v=\sum_\alpha \nu_\alpha{}^j\bar{v}_\alpha=\left(\frac{\partial mv}{\partial\lambda^j}\right)_{T,p}. \tag{10c}$$

Here H denotes the specific enthalpy, $\bar{H}_\alpha$ and $\bar{V}_\alpha$, respectively, the usual thermodynamic partial specific enthalpy and volume of component α. It will be noted that the quantities c_0, β_0, and $c_p{}^0$ are the sound speed, volume expansion coefficient, and constant pressure heat capacity evaluated with the composition frozen at its instantaneous value. The parameters σ^j are thermodynamic variables which, as we shall see, determine in conjunction with the rate functions r^j the explosive behavior of the medium.

Use of (9) permits the elimination of the derivatives of the density from the hydrodynamic equations:

$$\rho\frac{\partial u}{\partial x}+\frac{1}{c_0^2}\frac{dp}{dt}=\rho\sum_j \sigma^j r^j, \tag{11a}$$

$$\rho\frac{du}{dt}+\frac{\partial p}{\partial x}=0, \tag{11b}$$

$$\frac{d\lambda^j}{dt}=r^j,\quad j=1\cdots r. \tag{11c}$$

We note that these equations are similar to the well-known equations for nonreactive flow, the frozen sound speed appearing in the expected place, but with a non-vanishing right-hand side in the first equation. We also note that when our reactive system is at chemical equilibrium, the right-hand side vanishes, since r^j becomes zero when the forward and backward rates become equal. The appearance of the frozen sound speed is of some interest.

The differential Eqs. (11) hold in regions of the flow which are free from shocks. Treating the latter as mathematical discontinuities, they are governed by the well-known Rankine-Hugoniot conditions,

$$\rho_2(U-u_2)=\rho_1(U-u_1), \tag{12a}$$

$$p_2-p_1=\rho_1(U-u_1)(u_2-u_1), \tag{12b}$$

$$E_2-E_1=\tfrac{1}{2}(p_2+p_1)(v_2-v_1), \tag{12c}$$

in which U denotes the shock velocity, and the other symbols have their usual meaning with the subscripts distinguishing the values on the two sides of the shock. These relations across discontinuities, and the differential equations in regions free from them, supplemented by suitable boundary conditions, determine the flow of our one-dimensional, reactive fluid.

We now apply them to the propagation of a steady-state plane detonation wave through a semi-infinite explosive medium in a direction perpendicular to the plane surface. We suppose the detonation to have been initiated at this surface at zero time, and suppose the boundary condition at this rear surface to be imposed by a prescribed motion of an infinite piston (see, e.g., references 7 and 11). We will consider only the steady-state detonation assumed to be approached eventually, at least for some modes of initiation. Here we adopt the model of the detonation wave used by von Neumann, in which the reaction is initiated by a shock wave in the unreacted medium preceding the reaction zone. (The reaction rates r^j are assumed to vanish in the medium in front of the shock wave.) We denote by D the velocity at which this shock propagates along the x axis (taken as perpendicular to the rear surface and pointing into the explosive), the unreacted, unshocked medium being stationary in this coordinate system. During the approach to steady state, D may depend on t, but is assumed to approach a constant value as t increases. In addition to this assumption, the notion of a steady state also includes the supposition that there exists immediately following the shock a region of constant length in which the various hydrodynamic variables are independent of time when viewed from a coordinate system moving with the velocity D. This steady zone is followed by a flow region whose character is determined by the rear boundary condition. In certain simplified cases it may have approximately the form of a centered-rarefaction wave, reducing the pressure and mass velocity from their values at the boundary between this region and the steady zone to their values at the rear surface. We now proceed to discuss these two flow regions separately, beginning with the steady zone.

III

We introduce the moving coordinate system mentioned above. For convenience we take as space variable the distance measured *backwards* from the shock front. The transformation is

$$\xi=\int_0^t D(t')dt'-x,$$
$$t=t. \tag{13}$$

With this change of independent variable the differen-

tial Eqs. (11) become

$$-\rho c_0^2 u_\xi + (D-u)p_\xi + p_t = \rho c_0^2 \sum_j \sigma^j r^j, \quad (14a)$$

$$\rho(D-u)u_\xi - p_\xi + \rho u_t = 0, \quad (14b)$$

$$(D-u)\lambda_\xi{}^j + \lambda_t{}^j = r^j, \quad j=1,2\cdots r, \quad (14c)$$

$$u_\xi = \left(\frac{\partial u}{\partial \xi}\right)_t, \text{ etc.}; \quad u_t = \left(\frac{\partial u}{\partial t}\right)_\xi, \text{ etc.}$$

Solving the first two equations for u_ξ and p_ξ, we obtain

$$u_\xi = -\frac{1}{\eta}\left[\sum_j \sigma^j r^j - \frac{1}{\rho c_0^2} p_t - \frac{D-u}{c_0^2} u_t\right], \quad (15a)$$

$$p_\xi = -\frac{1}{\eta}\left[\rho(D-u)\left(\sum_j \sigma^j r^j - \frac{1}{\rho c_0^2} p_t\right) - \rho u_t\right], \quad (15b)$$

$$\eta = 1 - \frac{(D-u)^2}{c_0^2}. \quad (15c)$$

If we assume a region of steady-state behavior, the time derivatives vanish, and the equations reduce to

$$u_\xi = -\frac{1}{\eta}\sum_j \sigma^j r^j, \quad (16a)$$

$$p_\xi = -\frac{\rho(D-u)}{\eta}\sum_j \sigma^j r^j, \quad (16b)$$

$$\lambda_\xi{}^j = \frac{1}{D-u} r^j, \quad j=1\cdots r. \quad (16c)$$

It is easily seen from these equations that the state variables in the steady zone satisfy the Rankine-Hugoniot relations (12), with states 1 and 2 being any points in the steady zone. Since the steady zone point just to the rear of the shock is connected to the medium ahead by these same relations it is clear that we may write

$$\rho(D-u) = \rho_0 D, \quad (17a)$$

$$p - p_0 = \rho_0 D u, \quad (17b)$$

$$E - E_0 = \tfrac{1}{2}(p+p_0)(v_0 - v); \quad (17c)$$

the zero subscripts denote values of the quantities in the medium ahead; unsubscripted quantities are at any point in the steady zone. Equations (17), coupled with any one of the differential Eqs. (16), determine the state variables as functions of the distance behind the leading shock, for any assumed value of D. The latter is not yet determined.

We note that we will encounter difficulty in integrating (16a) or (16b) if η becomes zero. Since the flow back of a plane shock relative to the shock front is always subsonic, η will be positive at $\xi=0$.

IV

Corresponding to the classical Riemann analysis for the case of nonreactive flow, we anticipate that, for piston motions opposite in direction to that of the motion of the detonation wave, there will be a rarefaction wave of nonsteady character reducing the pressure from its value at the end of the steady zone to a lower value, possibly zero, at the piston surface. Consequently we devote this section to a brief discussion of the characteristic curves of the set of differential Eqs. (11). Without reproducing all the steps, we state the results as follows. The set of Eqs. (11) is always hyperbolic. The characteristics in the $x-t$ plane, $r+2$ in number, are given by the following equations:

$$(dx/dt)_{r+1,\,r+2} = u \pm c_0, \quad (18a)$$

$$(dx/dt)_j = u, \quad j=1,2\cdots r. \quad (18b)$$

The first two characteristics may be thought of as giving the paths of "sound waves" through a given point in the $x-t$ plane. The other characteristics are degenerate, all coinciding with the streamline through the point.

These results are similar to the well-known results for nonreactive flow, c_0 appearing in the place of the ordinary nonreactive sound speed. There is, however, an important difference; Eqs. (11) are not homogeneous, and therefore not *reducible*, contrary to the case with the nonreactive equations. Thus part of the usual theory of hyperbolic flow fails to carry over into the reactive case. However, certain general properties of hyperbolic equations remain, among them the following: *the boundary between two space-time regions in which the flows are of different type (for example, a region in which the flow is steady adjacent to a region in which the flow is nonsteady) must be a characteristic.* In the next section we make an important application of this principle.

V

We now proceed to draw certain conclusions concerning the detonation process from the analyses of the preceding two sections. As noted at the end of the last section, the boundary between our steady region and the succeeding flow must be a characteristic curve, assuming that the differential equations remain valid across the boundary—i.e., assuming the boundary is not a shock. It then follows that the flow variables are continuous (not necessarily their derivatives); hence the flow variables are constant along the boundary, and it follows from 18) that the boundary characteristic is straight. Since it is clear that it cannot be a streamline, and since in our coordinate system the wave is forward facing, it must be a $u+c_0$ characteristic. Still further, in order for the x dimension of the steady zone to be constant in time, it is necessary that the slope of this characteristic in the $x-t$ plane be the same as

that of the leading shock locus. We obtain as a necessary condition at the end of the steady zone

$$D=u+c_0, \tag{19}$$

a result which has also been obtained by Brinkley and Richardson.[10]

Returning to relations (16) for the steady zone, we note that the preceding result makes η, the denominator of the expressions for μ_ξ and p_ξ, vanish. In order to avoid singularities in these space derivatives the numerators must also vanish, which requires as an additional condition at the end of the steady zone

$$\sum_j \sigma^j r^j=0. \tag{20}$$

These two equations, (19) and (20) may be taken as a generalized statement of the C-J condition. That the indeterminacy of (16) is as it should be is readily appreciated from the fact that (16) holds for the space derivatives in *both* directions at the end of the steady zone. The indeterminacy thus permits these derivatives to be discontinuous at the end of the steady zone, and in particular allows the derivatives on the nonsteady side to be time dependent.

Clearly (20) is satisfied if all the rate functions vanish,

$$r^j=0, \quad j=1,\cdots r, \tag{21}$$

corresponding to instantaneous chemical equilibrium. This, coupled with (19) corresponds to von Neumann's normal C-J condition. It is the one in common use; see, e.g., Lewis and Friauf,[13] papers by Kistiakowsky and co-workers.[14]† We note that (17), (19), and (21), with the equation of state taken as $E=E(\lambda,p,v)$, constitute $r+4$ equations for the $r+4$ unknowns D, p, v, u, and λ. Thus we may expect to be able to solve them for D and the state variables at the end of the steady zone. Of course, in actual practice, rather than (21) one uses the ordinary relations for chemical equilibrium

$$\sum_\alpha \nu_\alpha{}^j \mu_\alpha=0, \quad j=1,2\cdots r. \tag{22}$$

It is also possible for $\sum_j \sigma^j r^j$ to vanish with some or all r^j nonvanishing, due to some of the σ^j becoming negative (or conceivably some of the r^j); this corresponds to von Neumann's pathological case. In this case we obtain a sufficient number of equations to determine D and the C-J values of the state variables by eliminating ξ from (16c), obtaining $r-1$ equations

$$d\lambda^j/d\lambda^1=r^j/r^1, \quad j=2,3\cdots r. \tag{23}$$

These may be integrated by use of the initial conditions at the shock front; with (17), (23), (19), and (20) we then obtain $r+4$ equations. In general, such a calculation requires explicit knowledge of the rate functions r^j, in addition to the usual thermodynamic data; this is to be contrasted with the normal case, where the latter information suffices. There might even be multiple zeros of $\sum\sigma^j r^j$, in which case the C-J condition is ambiguous.

For the special case of a single reaction the analysis can be carried a little further: the particular case in which σ might become negative while η is positive, σ thereafter remaining negative, so that the C-J point would have to correspond to $r=0$, can be eliminated. It is possible to show under reasonable assumptions concerning the finiteness of certain thermodynamic variables, that it is impossible for η to vanish under these conditions.

Also, for the case of a single reaction, the relation of our treatment to von Neumann's discussion of the pathological case, in terms of the envelope to the family of partial Hugoniot curves with parameter λ, is readily seen from the third of the equivalent expressions for σ given in (10a). In this case also, the calculation of detonation velocity can be performed in the pathological case in the absence of detailed knowledge of the rate function, since (20) reduces to $\sigma=0$, which is a purely thermodynamic relation. It is, of course, necessary to know what reaction is involved.

No example of a pathological detonation is definitely known. From (10a) it is clear that a negative σ requires either a volume decrement or an endothermic reaction under the local conditions. Thus the possibility of pathological behavior may arise, for instance, in gaseous detonations not too strongly exothermic involving an over-all mole decrement, or in detonations in which an exothermic reaction is succeeded by an endothermic one, possibly involving a mole decrement. In condensed explosives the situation is considerably obscured by uncertainties in our present knowledge of equations of state, not to mention kinetics. A possible example might occur in the case of aluminized explosives.

[13] B. Lewis and J. B. Friauf, J. Am. Chem. Soc. **52**, 3905 (1930).
[14] Kistiakowsky, Knight, and Malin, J. Chem. Phys. **20**, 884 (1952); other papers by Kistiakowsky and co-workers.

† It may be noted that the C-J condition used by these investigators actually implies the use of c_0, although it has apparently been regarded as an approximation to a sound speed defined by $(\partial p/\partial\rho)_S$, $\Sigma\nu_\alpha\mu_\alpha=0$.

THE JOURNAL OF CHEMICAL PHYSICS VOLUME 22, NUMBER 11 NOVEMBER, 1954

Diameter Effect in Condensed Explosives. The Relation between Velocity and Radius of Curvature of the Detonation Wave

WILLIAM W. WOOD, *Los Alamos Scientific Laboratory, University of California, Los Alamos, New Mexico*

AND

JOHN G. KIRKWOOD, *Sterling Chemical Laboratory, Yale University, New Haven, Connecticut*

(Received April 30, 1954)

The limiting slope of the detonation velocity-wave front curvature locus for small velocity deficits is obtained under an assumption concerning the "reaction zone length" as related to the charge diameter and the radius of curvature of the wave front. The model is an extension to two dimensions of von Neumann's classical theory of the plane wave detonation.

I

THE relationship between the velocity with which a detonation wave propagates axially along a cylindrical charge and the finite radius of the charge has been studied theoretically by Eyring, Powell, Duffey, and Parlin[1] and by Jones.[2] Our objective in the present work is somewhat different, namely, to give an account of the relation between velocity and radius of curvature of the wave front, rather than the charge radius. It happens that it is possible to derive such a relation under considerably more straightforward assumptions than have been needed by the investigators mentioned. The theory of Eyring *et al.* is commonly called the curved front theory; the present work is closely related to it in many of its details, although the basic model, as well as the objective, is considerably different. In the following we will use certain results from the preceding paper on the structure of the steady-state plane detonation wave, which we shall abbreviate as SSPD.

II

Our model is once again a compressible, nondissipative, adiabatic, reactive medium into which a detonation wave is propagating in steady state. Here, however, the medium is a cylinder of indefinite length but finite radius. We introduce a system of cylindrical coordinates with z-axis along the charge axis in the direction of propagation, and with r denoting the radial distance from this axis. The origin of z is conveniently taken as the position of the intersection of the wave front and z axis at time $t=0$. We assume cylindrical symmetry throughout, so that none of the variables depend on azimuthal angle, and all velocities lie in planes containing the z-axis. Under these conditions the equations of hydrodynamics, including the first law and the reaction rate law, become

$$\frac{d\rho}{dt}+\rho\left(\frac{\partial u}{\partial z}+\frac{\partial \omega}{\partial r}\right)+\rho\frac{\omega}{r}=0, \tag{1a}$$

$$\rho\frac{du}{dt}+\frac{\partial p}{\partial z}=0, \tag{1b}$$

$$\rho\frac{d\omega}{dt}+\frac{\partial p}{\partial r}=0, \tag{1c}$$

$$\frac{dE}{dt}+p\frac{dv}{dt}=0, \tag{1d}$$

$$\frac{d\lambda}{dt}=R, \tag{1e}$$

and

$$\frac{d}{dt}=\frac{\partial}{\partial t}+u\frac{\partial}{\partial z}+\omega\frac{\partial}{\partial r}. \tag{1f}$$

The notation is the same as in SSPD, except that u now denotes the axial component of mass velocity, ω the radial component, and R the rate function. For simplicity in notation we consider here the case of a single reaction; there is no difficulty in extending the argument to the case of several reactions.

As in SSPD we suppose the reaction zone to be preceded by a (curved) shock, across which we apply the (vector) Rankine-Hugoniot conditions. We assume the medium ahead of the detonation front to be at rest. With **D** denoting the detonation velocity along the z-axis, **U** the vector mass velocity at any point on the back side of the shock, **n** the unit normal to the shock at the same point drawn in the forward direction, **l** any unit vector perpendicular to **n**, variables behind the shock by unsubscripted symbols, and zero subscripts for values in the medium ahead of the shock, the

[1] Eyring, Powell, Duffey, and Parlin, Chem. Revs. **45**, 69 (1949); see also Parlin, Thorne, and Robinson, Tech. Report No. 1, Institute for the Study of Rate Processes, University of Utah, Salt Lake City, Utah.

[2] H. Jones, Proc. Roy. Soc. (London) **A189**, 415 (1947).

Rankine-Hugoniot conditions are

$$\rho(\mathbf{D}-\mathbf{U})\cdot\mathbf{n}=\rho_0\mathbf{D}\cdot\mathbf{n}, \tag{2a}$$

$$(p-p_0)/(v_0-v)=\rho_0^2D^2, \tag{2b}$$

$$E-E_0=\tfrac{1}{2}(p+p_0)(v_0-v), \tag{2c}$$

$$\mathbf{U}\cdot\mathbf{l}=0, \tag{2d}$$

and

$$\lambda=0. \tag{2e}$$

For any assumed initial shape and velocity for the leading shock, the preceding equations determine the state immediately behind the shock. Thereafter the differential equations (1), coupled with the jump conditions determine the flow, which would not be steady in general. Our next step is to ascertain what shock front shapes and detonation velocities are compatible with the steady-state assumption. According to the latter, the flow region immediately behind the shock should be steady when viewed from a coordinate system moving with velocity **D**. Introducing such a coordinate system by the transformation

$$\xi=Dt-z, \tag{3}$$

ξ being the axial distance measured *backwards* from the shock, and putting derivatives with respect to t at constant ξ and r equal to zero, we obtain

$$(D-u)\rho_\xi-\rho u_\xi+\omega\rho_r+\rho(\omega_r+\omega/r)=0, \tag{4a}$$

$$\rho(D-u)u_\xi-p_\xi+\rho\omega u_r=0, \tag{4b}$$

$$\rho(D-u)\omega_\xi+p_r+\rho\omega\omega_\xi=0, \tag{4c}$$

$$\frac{dE}{dt}+p\frac{dv}{dt}=0, \tag{4d}$$

$$\frac{d\lambda}{dt}=R, \tag{4e}$$

and

$$\frac{d}{dt}=(D-u)\frac{\partial}{\partial\xi}+\omega\frac{\partial}{\partial r}, \tag{4f}$$

$$u_\xi=\left(\frac{\partial u}{\partial\xi}\right)_r,\quad u_r=\left(\frac{\partial u}{\partial r}\right)_\xi, \text{ etc.}$$

To eliminate the derivatives of ρ from these equations we use Eq. (9) from SSPD,

$$\frac{d\rho}{dt}=\frac{1}{c_0^2}\frac{dp}{dt}-\sigma\rho R, \tag{5}$$

where the thermodynamic parameter σ is defined in SSPD, Eqs. (10a). Use of (5) in (4) then gives

$$-\rho c_0^2u_\xi+(D-u)p_\xi=\rho c_0^2\varphi, \tag{6a}$$

$$\varphi=\sigma R-\omega_r-\frac{\omega}{\rho c_0^2}p_r-\omega/r, \tag{6b}$$

$$\rho(D-u)u_\xi-p_\xi=-\rho\omega u_r, \tag{6c}$$

$$(D-u)\omega_\xi+\omega\omega_r=-(1/\rho)p_r, \tag{6d}$$

$$(D-u)\lambda_\xi+\omega\lambda_r=R, \tag{6e}$$

and

$$(D-u)(E_\xi+pv_\xi)+\omega(E_r+pv_r)=0. \tag{6f}$$

III

The explicit solution of the set of partial differential equations (6) would be an extremely difficult task. Here we follow a different procedure, and begin by specializing them to the axis.* From obvious conditions of symmetry the radial component of velocity ω vanishes on the axis:

$$\omega(\xi, r=0)=0, \tag{7a}*$$

$$u(\xi,0)=U(\xi,0). \tag{7b}*$$

Equations (6) specialized to the axis give

$$-\rho c_0^2U_\xi+(D-U)p_\xi=\rho c_0^2(\sigma R-2\omega_r), \tag{8a}*$$

$$\rho(D-U)U_\xi-p_\xi=0, \tag{8b}*$$

$$p_r=0, \tag{8c}*$$

$$(D-U)\lambda_\xi=R, \tag{8d}*$$

and

$$E_\xi+pv_\xi=0, \tag{8e}*$$

where all variables are to be evaluated at any ξ with $r=0$. Solving (8a) and (8b) as linear equations for u_ξ and p_ξ we obtain

$$u_\xi=-\frac{1}{\eta}(\sigma R-2\omega_r), \tag{9a}*$$

$$p_\xi=-\frac{\rho(D-U)}{\eta}(\sigma R-2\omega_r), \tag{9b}*$$

and

$$\eta=1-(D-U)^2/c_0^2. \tag{9c}$$

Since the flow behind a shock propagating in the direction normal to itself is subsonic (the curved shock in question clearly satisfying this condition because of symmetry), it is clear that $\eta(\xi=0, r=0)>0$. Furthermore, it is clear that in steady state the flow behind the shock must be similar to that of Prandtl-Meyer steady state expansion, in which the flow becomes supersonic (see reference 2). Consequently we expect η to vanish at some point in the steady zone, and therefore the

* In the following we designate equations valid only on the axis with an asterisk.

numerators in (9a) and (9b) must vanish at the same point. Thus we obtain a generalized "Chapman-Jouguet condition" for detonation in a finite stick:

$$D=U+c_0, \tag{10a}*$$

$$\sigma R-2\omega_r=0. \tag{10b}*$$

This result is similar to that of Eyring *et al.*, Eq. B-12, which is attributed by them to Devonshire.[3] Equation (10b) may be interpreted as relating the degree of reaction at the sonic point to the radial flow divergence at this point.

In the plane wave theory, the Rankine-Hugoniot relations are integrals of the differential equations of steady-state motion. We now proceed to derive an analogous relations for the steady zone of the present theory, where, however, the flow divergence introduces certain correction terms.

For this purpose we return to Eq. (4a), and, specializing it to the axis, we obtain

$$(D-U)\rho_\xi-\rho U_\xi=-2\rho\omega_r. \tag{11}*$$

This may be integrated immediately with use of the Rankine-Hugoniot condition (2a) at $\xi=0$ to give

$$\frac{\rho}{\rho_0}\left(1-\frac{U}{D}\right)=1-2L(\xi), \tag{12a}*$$

$$L(\xi)=\int_0^\xi \frac{\rho(\xi')}{\rho_0}\frac{\omega_r(\xi')}{D}d\xi'. \tag{12b}*$$

It will be noted immediately that this is the usual plane wave relation for mass conservation with the divergence perturbation given by (12b) added.

In a similar way (8b) may be integrated with use of (12a) and (2b) to give†

$$p=\rho_0 DU\left\{1-2\int_0^\xi\left(1-\frac{U(\xi')}{U(\xi)}\right)\frac{\rho(\xi')}{\rho_0}\frac{\omega_r(\xi')}{D}d\xi'\right\}. \tag{13}*$$

With neglect of terms in ω_r^2, this may be reduced to

$$p=\rho_0 D^2(1-v/v_0)\times\left\{1+2\frac{v/v_0}{1-v/v_0}\left(2L(\xi)-\frac{\rho}{\rho_0}\Omega(\xi)\right)\right\}, \tag{14a}*$$

$$\Omega(\xi)=\int_0^\xi \frac{\omega_r(\xi')}{D}d\xi'. \tag{14b}$$

We again obtain a plane wave relation with added perturbation. In similar fashion, Eq. (4d), specialized to steady-state flow on the axis, may be integrated to

$$E-E_0-\tfrac{1}{2}p(v_0-v)=D^2\left\{(1+v/v_0)\Omega(\xi)-2\frac{v}{v_0}L(\xi)\right\}, \tag{15}*$$

again with neglect of terms in ω_r^2. With the equation of state, (10a), (10b), (12a), (14a), and (15) constitute a sufficient number of equations to determine D and also the axial values of p, U, ρ, and λ throughout the steady zone, providing we are able to determine $\omega_r(\xi)$. In the following we designate the C-J point by $\xi=\xi^*$, which is determined by

$$\xi=\int_0^\lambda \frac{D-U(\lambda')}{R(\lambda')}d\lambda' \tag{16}*$$

obtained from (8d).

IV

In order to determine $\omega_r(\xi)$ we first return to (6d), differentiate it with respect to r, and then specialize to the axis, obtaining

$$(D-U)\frac{\partial\omega_r}{\partial\xi}+\omega_r^2=-vp_{rr}. \tag{17}*$$

With neglect of ω_r^2 and use of (12a), this may be integrated to give

$$\omega_r(\xi)=\omega_r(0)-\frac{1}{\rho_0 D}\int_0^\xi p_{rr}(\xi')d\xi'. \tag{18}*$$

The value of ω_r at $\xi=0$ can be obtained from the Rankine-Hugoniot conditions in terms of the radius of curvature S of the shock front at its intersection with the axis:

$$\omega_r(0)=U(0)/S. \tag{19}*$$

It remains to estimate $p_{rr}(\xi)$. For this purpose we introduce an assumption concerning the geometry of the reaction zone. We assume the plane $\xi=\xi^*$ intersects the shock front in the explosive, and that the portion of the shock front for $\xi<\xi^*$ can be adequately represented by a sphere of radius S; i.e., we neglect the variation of radius of curvature over this part of the shock wave; see Fig. 1. Our procedure is to use the shock relations to obtain the pressure at any point on the shock front for $\xi<\xi^*$. Then expanding the pressure into a power series in r for fixed ξ, and retaining only the quadratic term [the linear term vanishes because of (8c)] we obtain an approximation to the second radial derivative of p,

$$p_{rr}(\xi)=(p_s(\xi)-p(\xi))/S_\xi, \tag{20}*$$

where $p_s(\xi)$ denotes the pressure at the point ξ on the shock front. In (20) we have approximated the equation of the spherical front as

$$r^2=2S\xi. \tag{21}$$

Furthermore, with neglect of terms of order $1/S$, $p_s(\xi)$ is equal to $p(0)$, the axial shock pressure. Thus we finally obtain an expression for $p_{rr}(\xi)$, correct to terms

[3] A. F. Devonshire, Theoretical Research Report No. 3/43.

† We have neglected p_0 in the customary fashion.

of order $1/S$,

$$p_{rr}(\xi)=\frac{p(0)}{S\xi}\left(1-\frac{p(\xi)}{p(0)}\right). \tag{22}*$$

Substitution of (22) and (19) into (18) with use of (12a) yields

$$\frac{\omega_r(\xi)}{D}=\frac{U(0)}{D}\frac{1}{S}b(\xi), \tag{23a}*$$

$$b(\xi)=1-\int_0^\xi\left(1-\frac{p(\xi')}{p(0)}\right)\frac{d\xi'}{\xi'}. \tag{23b}*$$

With the preceding expression for ω_r we may summarize the important equations as follows:

$$\frac{\rho}{\rho_0}\left(1-\frac{U}{D}\right)=1-\alpha(\xi)/S, \tag{24a}*$$

$$\alpha(\xi)=2\frac{U(0)}{D}\int_0^\xi\frac{\rho(\xi')}{\rho_0}b(\xi')d\xi', \tag{24b}*$$

$$p=\rho_0D^2(1-v/v_0)(1+\beta(\xi)/S), \tag{25a}*$$

$$\beta(\xi)=2\frac{v/v_0}{1-v/v_0}\frac{U(0)}{D}\times\left\{2\int_0^\xi\frac{\rho(\xi')}{\rho_0}b(\xi')d\xi'-\frac{\rho}{\rho_0}\int_0^\xi b(\xi')d\xi'\right\}, \tag{25b}*$$

$$E-E_0-\tfrac{1}{2}p(v_0-v)=D^2\delta(\xi)/S, \tag{26a}*$$

$$\delta(\xi)=(1+v/v_0)\int_0^\xi b(\xi')d\xi'-2\frac{v}{v_0}\int_0^\xi\frac{\rho(\xi')}{\rho_0}b(\xi')d\xi', \tag{26b}*$$

$$\sigma(\xi^*)R(\xi^*)=2U(0)b(\xi^*)/S, \tag{27a}*$$

$$[D-U(\xi^*)]^2=G(\xi^*), \tag{27b}*$$

$$G\equiv c_0^2, \tag{27c}*$$

and

$$\lambda=\int_0^\xi\frac{R(\xi')}{D-U(\xi')}d\xi'. \tag{28}$$

Equations (24), (25), (26), and (28) hold throughout the steady zone; Eqs. (27) hold only at the C-J point. Equations (24a), (25a), and (27b) may be manipulated to obtain

$$\frac{pv^2}{v_0-v}\left(1-\frac{2\alpha+\beta}{S}\right)=G^*, \tag{29a}*$$

$$D^2=\frac{v_0^2p}{v_0-v}(1-\beta/S). \tag{29b}*$$

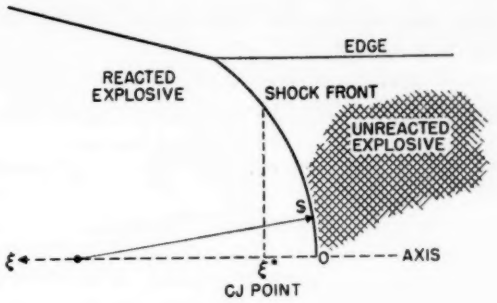

FIG. 1.

We may conveniently regard (26a), (27a), (28), and (29a) as determining the C-J values of p, v, and λ, with (29b) then determining D.

V

The theory at this point is formally complete, since the solution of the above equations will yield the desired relation between D and S, correct to order $1/S$. To actually proceed further we require explicit information concerning (a) the equation of state in the reaction zone and (b) the rate function R. Here we shall limit ourselves to a very brief and preliminary discussion which *may* be appropriate to the detonation of liquid explosives.

With respect to the chemical kinetics problem, a model often used is that of a homogeneous, self-heating reaction with a rate

$$R\sim f(\lambda)e^{-\Delta E/RT}, \tag{30}$$

where $f(\lambda)\sim(1-\lambda)^n$ with n a number of order of magnitude one or two; ΔE is a molar activation energy. The appearance of the temperature in the exponential results in a rate of reaction which is initially small behind the shock front (assuming the temperature at this point to be appreciably lower than that near complete reaction, as is almost surely the case), at first increases very slowly, rises to a sharp maximum very close to complete reaction, then falls to zero (asymptotically, for most $f(\lambda)$). If this be true, it is plausible to expect the von Neumann pressure spike to be quite flat-topped during the induction period, then fall rather rapidly to its C-J value. In the following we idealize this pressure spike into a square wave:

$$p(\xi)=\begin{cases}p(0), & \xi<\xi^*,\\ p(\xi^*), & \xi=\xi^*.\end{cases} \tag{31}$$

Furthermore, the above discussion suggests that the rate R will be very large for some λ close to complete reaction, then will decrease as λ increases. This suggests that for large radii of curvature the value of λ obtained from (27a) will be very close to its plane wave C-J value. In the following we assume this to be true.

The same assumption has been made in other discussions of diameter effect.[1,2]

We now perform a simple perturbation calculation on Eqs. (26a) and (29a) to obtain the increments

$$\Delta v = v(\xi^*) - v^{(0)} \tag{32a}$$

and

$$\Delta p = p(\xi^*) - p^{(0)}, \tag{32b}$$

where $v^{(0)}$ and $p^{(0)}$ denote the plane wave C-J values. The result is two linear equations for the determination of Δp and Δv:

$$\left\{\frac{pE_p}{D^2} - \frac{1}{2}\left(1-\frac{v}{v_0}\right)^2\right\}\frac{\Delta p}{p} + \left\{\frac{vEv}{D^2} + \frac{1}{2}\frac{v}{v_0}\left(1-\frac{v}{v_0}\right)\right\}\frac{\Delta v}{v} = \frac{\delta}{S} \tag{33a}$$

and

$$\left(1-\frac{pG_p}{G}\right)\frac{\Delta p}{p} + \left(\frac{2-(v/v_0)}{1-(v/v_0)} - \frac{vG_v}{G}\right)\frac{\Delta v}{v} = \frac{2\alpha+\beta}{S}, \tag{33b}$$

where $E_p = (\partial E/\partial p)_v$, $E_v = (\partial E/\partial v)_p$, etc. From (29b) we obtain the detonation velocity deficit

$$\frac{D^{(0)}-D}{D^{(0)}} = \frac{1}{2}\left[\frac{\beta}{S} - \frac{\Delta p}{p} - \frac{1}{(v_0/v)-1}\frac{\Delta v}{v}\right]. \tag{34}$$

We have used (31) to estimate the plane wave values of the quantities α, β, and δ, and a free volume equation of state‡ to estimate the values of the various thermodynamic variables under conditions which may be representative for the C-J point of liquid explosives. We assumed $v/v_0 = 0.7$ at the C-J point, $v/v_0 = 0.55$ at the shock. The result for velocity deficit is

$$(D^{(0)} - D)/D^{(0)} = 3.5\xi^*/S. \tag{35}$$

The exact value of the coefficient is quite sensitive to the C-J and spike compressions, especially the former, as well as being dependent on the equation of state. The above value should be regarded as only approximate. We hope in the near future to apply the present theory to specific explosives.

‡ The equation of state is based on an intermolecular potential energy of the Buckingham type.

THE JOURNAL OF CHEMICAL PHYSICS VOLUME 22, NUMBER 11 NOVEMBER, 1954

Magnetic Behavior of the System CoO − MgO at Elevated Temperatures*

NORMAN ELLIOTT
Chemistry Department, Brookhaven National Laboratory, Upton, Long Island, New York

(Received June 11, 1954)

The magnetic susceptibilities of solid solutions of CoO and MgO have been measured at elevated temperatures. The data fit a Curie-Weiss law $\chi = C/(T+\theta)$ with $C = 3.23 \pm 0.04$. θ varies linearly with the mole fraction of CoO. The magnetic measurements indicate that CoO has an antiferromagnetic ordering of spins of the first kind below the Curie point.

THE x-ray and magnetic measurements on CoO[1,2] are in agreement in that they show CoO to have an antiferromagnetic ordering of magnetic moments of the first kind below the Curie temperature. The neutron diffraction results, however, indicate that the antiferromagnetic coupling is between second nearest neighbors and that ordering is of the second kind.[3]

An investigation of the magnetic susceptibilities of solid solutions of CoO and MgO was undertaken to establish whether or not the interaction constant θ of the Curie-Weiss law for CoO was entirely due to antiferromagnetic exchange.[4]

CoO and solid solutions of CoO and MgO were prepared by precipitating the carbonates from solutions of the chlorides.[5] The source materials were Baker's C. P. Analyzed $CoCl_2 \cdot 6H_2O$, and Baker and Adamson Reagent $MgCl_2 \cdot 6H_2O$ and $NaHCO_3$. The oxides were made by heating the carbonates to 500°C in vacuum. X-ray powder photographs, using CuKα radiation, showed that homogeneous solid solutions were obtained, by clear resolution of the α doublet.

Magnetic measurements were made on a Gouy balance. Temperatures were obtained with an electric furnace through which ran a heavy walled copper tube. The samples were suspended inside the tube, and temperatures were recorded with thermocouples at the middle and each end of the sample. Magnetic fields of 7500–10 000 gauss were used. The susceptibilities were not found to be field dependent. Several samples of each solid solution and of pure CoO were measured. Results

* Research performed under the auspices of the U. S. Atomic Energy Commission.

[1] H. P. Rooksby and N. C. Tombs, Nature **167**, 364 (1951).
[2] J. Samuel Smart, Phys. Rev. **86**, 968 (1952).
[3] Shull, Strauser, and Wollan, Phys. Rev. **83**, 333 (1951).
[4] Corliss, Delabarre, and Elliott, J. Chem. Phys. **18**, 1256 (1950).
[5] Bacon, Street, and Tredgold, Proc. Roy. Soc. (London) **A217**, 252 (1953).

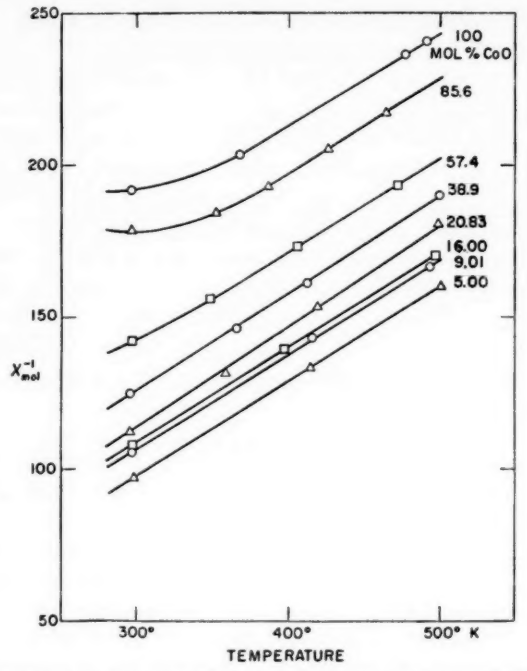

FIG. 1. Magnetic susceptibilities as a function of temperature.

were consistent to ±2 percent, and are given in Table I, and Fig. 1.

The susceptibilities found for CoO in this investigation are in good agreement with the measurements of Bhatnagar, Prakash, and Qayyum,[6] considering the difficulty of preparing pure oxides, and also with the results reported by Trombe.[7]

At elevated temperatures, CoO and its solid solutions with MgO follow a Curie-Weiss law,

$$\chi_{mol}=C/(T+\theta).$$

Dilution of the CoO with MgO has no effect on the Curie constant C which has an average value 3.23±0.04. This leads to a magnetic moment of 5.1 Bohr magnetons

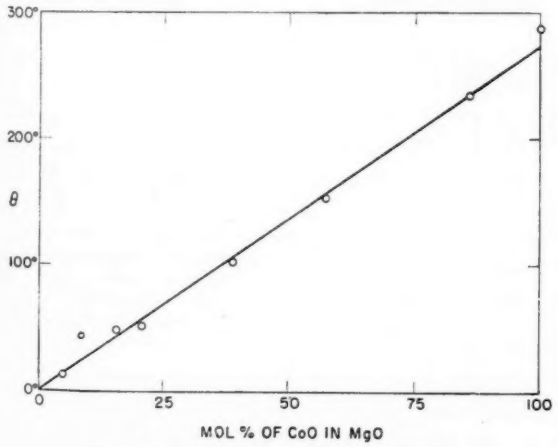

FIG. 2. Paramagnetic Curie temperature as a function of composition.

[6] Bhatnagar, Prakash, and Qayyum, J. Indian Chem. Soc. **18**, 540 (1941).

[7] M. F. Trombe, J. phys. radium **12**, 170 (1951).

TABLE I.

Magnetic susceptibility of CoO					
Temp. °K	297°	368°	477°	492°	
$\chi_{mol}\times10^6$	5235	4915	4240	4150	
Magnetic susceptibility of 85.6 Mol % CoO					
Temp. °K	296°	352°	386°	426°	464°
$\chi_{mol}\times10^6$	5890	5440	5180	4875	4620
Magnetic susceptibility of 57.4 Mol % CoO					
Temp. °K	296°	348°	406°	472°	
$\chi_{mol}\times10^6$	7050	6420	5775	5180	
Magnetic susceptibility of 38.9 Mol % CoO					
Temp. °K	296°	366°	412°	500°	
$\chi_{mol}\times10^6$	8000	6840	6225	5250	
Magnetic susceptibility of 21.09 Mol % CoO					
Temp. °K	296°	352°	411°	486°	
$\chi_{mol}\times10^6$	8880	7625	6625	5650	
Magnetic susceptibility of 20.83 Mol % CoO					
Temp. °K	296°	358°	419°	498°	
$\chi_{mol}\times10^6$	8820	7560	6450	5465	
Magnetic susceptibility of 16.00 Mol % CoO					
Temp. °K	296°	397°	496°		
$\chi_{mol}\times10^6$	9305	7200	5875		
Magnetic susceptibility of 9.01 Mol % CoO					
Temp. °K	298°	415°	493°		
$\chi_{mol}\times10^6$	9500	7020	6010		
Magnetic susceptibility of 5.00 Mol % CoO					
Temp. °K	297°	414°	500°		
$\chi_{mol}\times10^6$	10300	7520	6260		

for the Co^{++} ion, in agreement with other values found in more dilute salts.

The paramagnetic Curie temperature θ decreases with dilution, and is a linear function of the mole fraction of CoO, approaching zero at infinite dilution. This is shown graphically in Fig. 2. The behavior is similar to that of the system MnF_2-ZnF_2.[4] However, uncertainties in the preparation of these oxides do not allow one to rule out a small residual crystalline field term of perhaps ±10° which might be expected on theoretical grounds.[8]

Below room temperature the susceptibility of CoO passes through a rather flat maximum at 290°K. The ratio θ/T_c, therefore, has the value 1.0, which may be compared with the value 0.96 given in Smart's paper.[2] The ratio of the molecular field coefficients γ_2/γ_1 is equal to 1, where the subscripts 1 and 2 refer to coupling between nearest and second near neighbors, respectively. This result is only in accord with the Neel model if CoO has the first kind of ordering below the Curie temperature with antiferromagnetic coupling between nearest neighbors and ferromagnetic coupling between second near neighbors.

ACKNOWLEDGMENT

I wish to thank Dr. R. W. Stoenner and his staff for their analyses of the materials used in this research, and Dr. Max Wolfsberg for the opportunity of discussing this problem with him.

[8] J. H. Van Vleck, Phys. Rev. **41**, 208 (1932).

Vibrational Spectra of Molecules and Complex Ions in Crystals VII. The Raman Spectrum of Crystalline Ammonia and 3-Deutero-Ammonia*†

F. P. REDING‡ AND D. F. HORNIG
Metcalf Chemical Laboratories, Brown University, Providence 12, Rhode Island

(Received May 17, 1954)

The Raman spectra of crystalline NH_3 and ND_3 were measured at −82°C, using Hg 2536.5A exciting radiation. The fundamentals ν_1, ν_2, and ν_3 were observed, but ν_4 was not. ν_2 was split into two components by intermolecular coupling. Lattice frequencies of both translational and rotational origin were observed, and there was evidence of very little coupling between them.

INTRODUCTION

THE Raman spectrum of crystalline ammonia and 3-deutero-ammonia has been observed in conjunction with the previously reported infrared study of these crystals.[1]

In that paper it was pointed out that on the basis of the present theory of crystalline spectra[2,3] the motions of the four molecules in the unit cell of the cubic ammonia crystal (symmetry T^4) may be expected to couple so that the symmetrical vibrations of NH_3 or ND_3, ν_1 and ν_2, each yield one component of species A and one of species F. Similarly, the doubly degenerate vibrations, ν_3 and ν_4, should each yield one component of species E and two of species F in the crystals. Only the species F components may be active in the infrared spectrum whereas all three (A,E,F) may be active in the Raman spectrum. Actually, although all four fundamentals were observed in the infrared spectrum, only one component arising from each degenerate vibration was observed. In addition, evidence was produced that the second, Raman active, component of ν_2 was displaced by 10 cm^{-1} from the infrared active component.

Since all ten components arising from the four internal vibrations may be Raman active, it was hoped that the frequency separation between components originating in the different phases of coupling of the four molecules could be determined. This splitting would give a quantitative measure of the intermolecular interaction. In addition, it was hoped that the limiting lattice vibrations, five of which originate in molecular rotation and four in molecular translation, might be observed at low frequencies.

In previous work on the Raman spectrum of crystalline NH_3 Sutherland[4] reported lines at 3369, 3303, and 1585 cm^{-1} with relative intensities of 4, 1, and 0, respectively. The Raman spectrum of ND_3 was not found in the literature.

EXPERIMENTAL

The ultraviolet absorption spectrum of crystalline NH_3 begins at 2345A.[5]

Consequently the Hg 2536.5 A proved most satisfactory as an exciting line. The mercury arc used was an eight-turn quartz helix. The vapor pressure of the mercury in the lamp was kept low by using amalgamated gold foil electrodes. No evidence of resonance absorption by the cool mercury vapor along the wall of the tube was noted. The exciting line was filtered from the Raman radiation by filling the spectrograph with mercury vapor.

A diagram of the sample tube and cooling jacket is shown in Fig. 1. Nitrogen which had been cooled by bubbling through liquid nitrogen was used to cool the Raman tube. In preparation for an investigation, the system was evacuated and the sample condensed from a storage flask into the Raman tube. The liquid was slowly crystallized and a highly cracked semitransparent crystal was obtained. Since this proved to be satisfactory, no attempt was made to form a flawless single crystal. The NH_3 used§ was stated to be 99.97 per-

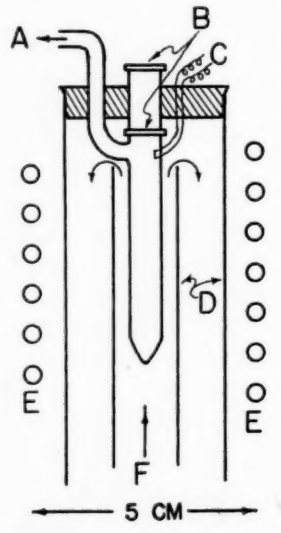

FIG. 1. Low-temperature Raman cell. Principal parts are: (A) inlet from NH_3 reservoir, (B) double quartz window to avoid frosting, (C) thermocouple, (D) quartz baffle, (E) helical quartz lamp, and (F) inlet for cold nitrogen.

* Based on a thesis presented by F. P. Reding in partial fulfillment of the requirements for the Ph.D. degree, Brown University, 1951.

† This work was supported in part by the Office of Naval Research.

‡ Present address: Carbide and Carbon Chemicals Company, South Charleston 3, West Virginia.

[1] F. P. Reding and D. F. Hornig, J. Chem. Phys. **19**, 594 (1951).
[2] D. F. Hornig, J. Chem. Phys. **16**, 1063 (1948).
[3] H. Winston and R. S. Halford, J. Chem. Phys. **17**, 607 (1949).
[4] G. B. B. M. Sutherland, Proc. Roy. Soc. (London) **141A**, 546 (1933).
[5] A. Prikhotko, Acta Physicochim. U.S.S.R. **12**, 559 (1940).

§ Mathieson Alkali Works.

cent pure. The ND_3 was prepared by the procedure described in the previous paper.

A medium Hilger E-3 303 Spectrograph with quartz optics was used to record the spectra. Depending upon the intensity desired, exposure times varied from 20 minutes to two hours, using a slit of 0.01 mm. The resolution of the spectrometer was approximately three cm^{-1} in the region employed. For wavelength determinations, an iron arc spectrum was recorded using a Hartman diaphragm. The error in the measurement of the Raman line displacement was approximately ± 5 cm^{-1}.

RESULTS

The Raman spectra obtained from crystalline NH_3 and ND_3 at $-82°C$, reproduced from the microphotometer tracings, are shown in Figs. 2 and 3, respectively. The mercury lines included are marked, and the 2536.5 A exciting line is indicated by A. The frequencies of the band centers and approximate intensities are shown in Table I. For comparison the fundamental bands observed in the infrared spectrum are also listed.

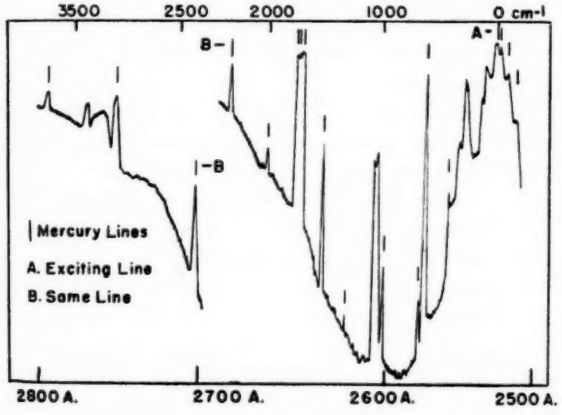

FIG. 2. Raman spectrum of crystalline NH_3.

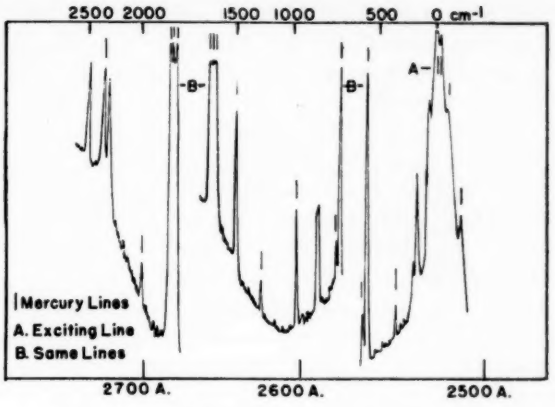

FIG. 3. Raman spectrum of crystalline ND_3.

Two components of the symmetrical bending vibration ν_2 at 1048 and 1058 cm^{-1} were clearly resolved in the NH_3 spectrum. A corresponding doublet was indicated in the ND_3 spectrum by the shoulder at 817 cm^{-1} on the high-frequency side of the peak at 810 cm^{-1}. From the very near coincidence of the bands at 1058 and 817 cm^{-1} with the corresponding bands for ν_2 in the infrared spectrum, it is safe to conclude that these Raman components arise from the species F vibration. The other two components at 1048 and 810 cm^{-1} in NH_3 and ND_3 must therefore be the species A components.

The symmetric stretching frequency ν_1 could not be determined for NH_3 because it lies in the broad intense band which extends from 3160 cm^{-1} to 3330 cm^{-1} and has a maximum at approximately 3210 cm^{-1}. This difficulty did not arise for the corresponding line in the ND_3 spectrum at 2330 cm^{-1} which is sharp. It is seen in Table I that ν_1 in the infrared spectrum of crystalline ND_3, which must be of species F, has its center at 2318 cm^{-1}. The 12 cm^{-1} frequency separation between the infrared and Raman components of this fundamental in ND_3 is outside of the experimental error in this region. Consequently these Raman lines probably arise from the species A rather than the species F vibration.

The Teller-Redlich product ratio for the F components of the symmetric vibrations was found to be 1.808 (harmonic value = 1.842). If the product ratio is the same for the A components, ν_1 of NH_3 would occur at 3240 cm^{-1}. The broad band in which it is located is apparently the first overtone region corresponding to the intense infrared absorption running from 1575 cm^{-1} to the fundamental ν_4 at 1648 cm^{-1}. A similar band in ND_3 would be expected in the region 2350–2400 cm^{-1} which underlies the Hg line adjacent to ν_1.

A component of the antisymmetrical stretching vibration ν_3 was observed at 3375 cm^{-1} in NH_3 and 2507 cm^{-1} in ND_3. This vibration gives rise to a species E and two species F phases of coupling. Since the ob-

TABLE I. Observed vibrational frequencies in crystalline ammonia and 3-deutero-ammonia.

Assignment[a]	NH_3 Raman (cm^{-1})		Infrared (cm^{-1})	ND_3 Raman (cm^{-1})		Infrared (cm^{-1})
lattice vibrations	...		53[b]	...		41[b]
	99	s	...	91.5	s	...
	129	m	...	121	m	...
	284	vs	250[b]	142–161	vw	...
	325–375	w	362[b]	213	vs	200[b]
	~386	vw	...	245–270	w	<300
	430–462	vw	...	280–312	w	...
	...		527	330–380	w	...
				...		406
				505–540	vw	...
ν_2'	1048	s	...	810	s	...
ν_2	1058	m	1060	817	m	815
ν_4	...		1646	...		1196
ν_1', (plus $2\nu_4$ in NH_3)	3160–3330	s	...	2330	s	...
ν_1	...		3223	...		2318
ν_3, ν_3', or ν_3''	3375	s	3378(ν_3)	2507	vs	2500(ν_3)

[a] ν_1, ν_2, ν_3, ν_4 refer to the internal modes of NH_3, species F if unprimed, species A if single primed, and species E if double primed.
[b] From combination bands in the infrared spectrum.

served lines occur so near the corresponding infrared active vibrations at 3378 and 2500 cm^{-1}, they may arise from the same F component observed in the infrared spectrum. However, since in all cases the observed splitting between components was very small, it may be that the bands arise from either of the other components or from a superposition of the three. The frequency found for ν_3 in the crystal in this and the previous paper are in accord with that recently found in the gas from its Raman spectrum.[6]

The lines at 3303 and 3369 cm^{-1} reported by Sutherland[2] certainly correspond to those at 3160–3330 cm^{-1} and 3375 cm^{-1} in the work reported here. Sutherland assigned the line he observed at 1585 cm^{-1} to ν_4, which like ν_3 may have three active Raman components in the crystal. No line was observed in this region in the present work. Since Sutherland did not observe the lines at 1058 and 1048 cm^{-1} at all, any comparable Raman scattering in the present study in the vicinity of 1585 cm^{-1} would be expected to be more intense than the lines around 1050 cm^{-1}. Sutherland observed the spectrum at $-185°C$, whereas the present study was performed at $-82°C$; therefore, the possibility remains that the relative intensities of the lines around 1050 cm^{-1} and 1585 cm^{-1} change enough with temperature to account for the apparent discrepancy, although this seems highly improbable.

In addition to the well-defined features, the microphotometer trace shows a broad band with a maximum at about 2700 cm^{-1} (2730 A) which can be ascribed to $\nu_2+\nu_4$. There may also be other diffuse bands running from 2630 A to 2670 A and from 2670 A to 2700 A, (1300–1900 cm^{-1}, 1900–2300 cm^{-1}).

Lattice Vibrations

As pointed out before, there are five fundamental lattice vibrations originating in molecular torsion, three of symmetry species F and one each of species A and E, and four fundamental lattice vibrations originating in molecular translation, two of species F and one each of species A and E. (There are actually three species F translational vibrations but one of them is the zero frequency motion corresponding to translation of the crystal as a whole.) Because of the small moments of inertia, one expects the translational motions in these molecules to be of lower frequency than the torsional motions, although the two types of motion of a given symmetry species may be coupled. These motions may also be coupled to the internal vibrations of the molecules of the same symmetry species, but because of the large frequency separation it is doubtful if such coupling is of any consequence.

As seen in Table I, a number of lattice vibrations were observed. A complete assignment of the observed bands is not possible but several features should be noted. From the low frequency and the small frequency separation between NH_3 and ND_3 the bands at 99 and 129 cm^{-1} in NH_3 and 91 and 121 cm^{-1} in ND_3 are certainly translational modes. The Teller-Redlich ratios of the species A and E translations are both 1.084, and the ratio for the two species F translations is 1.177. The observed ratios of the above two bands are both 1.08. Although the symmetry of the bands cannot be determined, the observed ratios indicate that there is very little coupling between the translational and torsional lattice modes.

From the high intensity, relatively high frequency and large frequency shift in going from NH_3 to ND_3, the bands at 284 cm^{-1} in NH_3 and 213 cm^{-1} in ND_3 are almost certainly fundamental torsional modes. The observed frequency ratio of these bands is 1.33. The Teller-Redlich product ratio for the species A torsion is 1.41 for the species E torsion is 1.39 and for the three species F torsions is 2.736. Although again it is not possible to determine the symmetry of the motion, the observed ratio indicates that it is a nearly uncoupled torsion.

The band between 325 and 375 cm^{-1} in NH_3 almost certainly arises in part from the species F torsion observed at 362 cm^{-1} in the infrared spectrum.[1] The high-frequency shoulder of the corresponding band in ND_3 was observed in the infrared spectrum, but the position of the band center could not be determined because the low-frequency limit of the spectrometer used was 300 cm^{-1}. The band between 245 and 270 cm^{-1} in the Raman spectrum of ND_3 corresponds to the band between 325 and 375 cm^{-1} in NH_3. This indicates that the band center of the species F torsion in ND_3 is approximately 260 cm^{-1}.

There was no evidence of Raman scattering corresponding to the bands observed at 527 and 406 cm^{-1} in the infrared spectrum of NH_3 and ND_3, respectively. These bands must be of species F, but it is doubtful if they are fundamental vibrations. The remaining low-frequency bands in the Raman spectrum of NH_3 and ND_3 are probably combinations and overtones of lattice fundamentals.

In conclusion, the interaction between the molecules in the NH_3 and ND_3 crystals must be small. Not only is the separation between the different phases of coupling of the internal vibrations small but also it appears that the low-frequency translational and torsional modes are only slightly coupled.

ACKNOWLEDGMENT

We should like to acknowledge the assistance of Mr. John W. Schultz who remeasured all the plates and helped to establish the lattice frequencies.

[6] C. Cumming and H. L. Welsh, J. Chem. Phys. **21**, 1119 (1953).

Photolysis of Methyl Bromide in the Presence of Mercury*

CHARLES F. BOYNTON, JR., AND H. AUSTIN TAYLOR
Chemistry Department, New York University, New York 53, N. Y.

(Received June 7, 1954)

A study has been made of the photolysis of methyl bromide in the presence of liquid mercury over a pressure range of the bromide from 25 to 100 mm and at temperatures from 35° to 200°C. The removal of the bromine atoms formed in the initial split as mercurous bromide reduces the back reaction. Unlike the corresponding reaction with silver, ethane is formed in considerable amounts. The rate of methane formation decreases while that of ethane formation increases with duration of photolysis. The rate of methane formation increases and that of ethane decreases with increase in pressure of methyl bromide. The energy of activation of methane production in the absence of mercury is 2.1 kcal. In the presence of mercury the energy of activation for methane is approximately zero while that for ethane is less than 2 kcal. The results are interpreted as indicating the formation of mercury methyl radicals or mercury dimethyl.

THE absence of ethane as a major product in the photolysis of the methyl halides has usually been attributed to the low concentration of methyl radicals. Ethane has not been observed as a product of photolysis of methyl bromide[1] and has been found in only small amounts from methyl iodide.[2] In the mercury sensitized decomposition of methyl chloride[3] very small amounts of ethane were found. The quantum yield of the primary split has been shown to be unity in each case. For methyl bromide[1] and methyl iodide[2,4] this was accomplished by introducing silver to remove the halogen as formed and thus prohibit the back reaction. For methyl iodide, the presence of silver increased the rate of formation of ethane such that it became the predominant product. No ethane, however, was observed from methyl bromide in presence of silver.

In the photodecomposition of mercury dimethyl the observed results have, for the most part, been accounted for, while disregarding the back reaction of mercury with methyl radicals, though it is well known that in reactions involving methyl radicals in presence of mercury, mercury dimethyl can always be smelled. Saunders and Taylor[5] showed that the presence of mercury in the photolysis of acetone led to results similar to those found in the photolysis of mixtures of acetone and mercury dimethyl. Since ethane has not previously been observed as a product from methyl bromide and since mercury should be very effective in fixing bromine and at least partially effective in fixing methyls, the products of photolysis of methyl bromide in presence of mercury should resemble those of mercury dimethyl, ethane becoming a major product.

EXPERIMENTAL

Two reaction systems were used during the course of the work. The first, patterned after that of Gordon and Taylor, consisted of a quartz cylinder 2.5 cm in diameter, 10 cm long, having a volume of 51 cc. One end was flat while the other end of the cylinder was constricted for a quartz to pyrex graded seal carrying a ground glass joint to the system. A low pressure helical quartz mercury arc closely surrounding the reaction cylinder was energized by a 720 VA luminous tube transformer. The second system was a quartz cylinder 9 cm in diameter, 4.7 cm long, having a volume of 320 cc with both ends flat. A tube from the side of the cylinder was connected as before to the rest of the system. A low pressure quartz mercury arc, coiled in a flat spiral and energized with the transformer previously used, illuminated one end of the reaction vessel. The current in the primary of the transformer was maintained constant at 5.5 amp by manual adjustment during a run.

In the early work with the first vessel, provision was made for gently shaking the reaction vessel by means of a vibrator in order to present as large and renewed a mercury surface as possible. In the second vessel a pyrex encased iron rod was floated on the mercury surface and rotated by means of a magnetic stirrer, thus cleaning the surface as reaction occurred. The stirrer, reaction vessel, and the flat spiral of the lamp were enclosed in an air oven, which was thermostatted to ±0.5°C, the temperature being measured using a mercury thermometer. The electrodes of the lamp passed through the top of the oven and were thus approximately at room temperature.

The methyl bromide used was distilled through phosphorus pentoxide into a reservoir while open to the pump system. It was frozen in liquid nitrogen, degassed, and stored over mercury at dry ice temperature. The mercury dimethyl, prepared in the laboratory, boiled at 62–64°C at 340 mm. It was distilled from freshly fused calcium chloride and then twice purified by bulb to bulb distillation, the middle fraction being retained.

Since mercury was used to pick up bromine, pressures

* Abstract from a thesis presented in partial fulfillment of the requirements for the degree of Doctor of Philosophy at New York University, June, 1952.

[1] A. Gordon and H. A. Taylor, J. Am. Chem. Soc. **63**, 3435 (1941).

[2] W. West and L. Schlessinger, J. Am. Chem. Soc. **60**, 961 (1938).

[3] C. R. Masson and E. W. R. Steacie, J. Chem. Phys. **19**, 183 (1951).

[4] R. D. Schultz and H. A. Taylor, J. Chem. Phys. **18**, 194 (1950).

[5] K. W. Saunders and H. A. Taylor, J. Chem. Phys. **9**, 616 (1941).

before and after a run were measured with a mercury manometer. Even for the runs in which no liquid mercury was present in the reaction cell, no protection was taken to avoid mercury vapor getting to the cell, since it was the effect of the presence or absence of the liquid mercury that was thought to be significant and not that of mercury sensitization.

The mercurous bromide, which always formed during runs, covered the mercury surface and after a short time reduced the pick-up of bromine atoms. It was to reduce this covering that the second reaction vessel was designed in which the mercury surface was continually swept clean by the rotating glass tube. Although this system proved more efficient than the first, the results reflect the lack of reproducibility of the mercury surface. After each run the cell was removed from the system, the mercury poured out, and the cell cleaned with dilute nitric acid and rinsed thoroughly. Although mercurous bromide is insoluble in water and in dilute acids, it was apparently mixed with enough mercury or possibly mercuric bromide so that it was loosened by the dilute nitric acid and could be washed out. The property of mercurous bromide of becoming yellow on heating and returning to a white color on cooling was observed throughout the work.

Prior to each run a sample of methyl bromide was drawn from the storage tube, frozen in liquid nitrogen, and degassed. The reaction vessel was evacuated to less than 10^{-5} mm, using a conventional two stage mercury diffusion pump backed by an oil pump, and filled with methyl bromide to the desired pressure. The second cell held a layer of mercury of about 90 cc volume. The oven was adjusted to the required temperature and the lamp allowed to warm up for fifteen minutes with an aluminum sheet shielding the reaction vessel from the radiation. The shield was removed to initiate the run. After the desired exposure time, the lamp was turned off and the residual pressure in the cell measured. Product gases were drawn by a Toepler pump first through a trap cooled to -196°C and transferred to the analyzer. A second fraction was obtained by warming the trap to -131°C using melting secondary butyl chloride. The pressure of each fraction was measured when occupying the standard volume of 2.97 cc of the analyzer. The efficiency of fractionation was tested with known mixtures and found to be adequate if allowance was made for a small amount of methyl bromide which could be pumped through at -131°C.

When two gases were used, the reaction vessel was filled with one gas to the desired pressure, the connecting lines pumped out, and then the other gas was admitted under a pressure head sufficient to preclude back diffusion. Mixing of the gases was assured during the warm-up period of the lamp.

Since the amount of gaseous products was of the order of 1 cc NTP, the micro-analytical method of Saunders and Taylor[6] was used. Several absorption tubes were attached to the analyzer so that the gas could be passed into any one tube as desired. To avoid nonreproducible absorption due to adsorption on the absorbents and walls, these tubes were not evacuated by the diffusion pump but by the Toepler pump only. This was accomplished with one or two pulls before each analysis.

The fraction of the products not condensible in liquid nitrogen was passed over copper oxide at 300°C for two minutes and then over Anhydrone in a cool part of the same tube. The gas passed thence over Ascarite in a tube also containing Anhydrone. Hydrogen if present would have been detected in the first tube. Carbon monoxide oxidized in the first tube to carbon dioxide was absorbed in the second tube. The residual gas, methane, was confirmed by a spark combustion in excess oxygen. After several such confirmations, the methane was measured simply by difference.

The second fraction could contain C_2 gases. Hydrogenation over a nickel catalyst at 100°C resulted in a consistent contraction of less than 5 percent of the sample. This was shown to be attributable to traces of methyl bromide drawn over by prolonged pumping rather than to ethylene. The remaining gas was shown by combustion to be ethane.

Especially in the runs in which mercury dimethyl was present initially, though also in the higher temperature runs of longer duration, a second solid deposit, in addition to the mercurous bromide, was observed. This brown deposit was insoluble in dilute nitric acid and was not readily soluble in organic solvents. A warm mixture of concentrated nitric and sulfuric acids was required to remove it. This deposit may have been a polymethylene.

When liquid mercury was not present in the reaction cell, the photolysis of methyl bromide alone showed a small pressure increase amounting to less than 2 percent of the initial pressure. In the presence of mercury a small pressure decrease approximately proportional to the duration of the run was always observed. This is to be expected from the formation of ethane which was always found.

RESULTS AND DISCUSSION

It is already well established that the primary step in the photolysis of the alkyl halides involves a breaking of the carbon-halogen bond. Thus for methyl bromide:

$$CH_3Br \rightarrow CH_3 + Br. \quad (1)$$

Secondary reactions include the following:

$$CH_3 + Br \rightarrow CH_3Br, \quad (2)$$

$$2\,Br + M \rightarrow Br_2 + M, \quad (3)$$

and

$$CH_3 + CH_3Br \rightarrow CH_4 + CH_2Br. \quad (4)$$

These have been shown to be satisfactory to account for the observed low quantum yields.

In the presence of mercury the following additional

TABLE I. Small reaction vessel.

Runs	Time (min)	Temp. °C	Press. (mm) CH_3Br	$Hg(CH_3)_2$	Conditions	Rate (ml/min) CO	CH_4	C_2H_6
1–6	5	25	100	0	No Hg	0.01	0.04	0
9, 10	5	25	100	0	Hg, no shaking	0.01	0.05	trace
12–15	1–5	70	100	0	Hg, shaking	0.02	0.23	0.11
16, 17	2, 5	70	50	0	Hg, shaking	0.01	0.23	0.09
18–27	1–10	70	25	0	Hg, shaking	trace	0.21	0.04
29, 33	2	70	0	40	No Hg	0	0.22	0.85
30	2	70	25	35	No Hg	0	0.14	1.31
31	2	70	25	30	No Hg	0	0.12	1.15
32	2	70	25	20	No Hg	0	0.08	0.84

reactions may be considered:

$$Hg+Br\rightarrow HgBr, \tag{5}$$

$$2\,HgBr\rightarrow Hg_2Br_2, \tag{6}$$

$$2\,CH_3\rightarrow C_2H_6, \tag{7}$$

$$CH_3+Hg\rightarrow HgCH_3 \tag{8}$$

$$CH_3+HgCH_3\rightarrow CH_4+HgCH_2, \tag{9}$$

and

$$CH_3+HgCH_3\rightarrow Hg(CH_3)_2. \tag{10}$$

In Table I are summarized the results of the exploratory runs carried out in the first, small reaction vessel. It seemed apparent that when the bromine atom pick-up was made more efficient, that is, when the mercury surface was cleaned by shaking the cell, although the rate of methane production increased slightly with increasing concentration of methyl bromide, ethane production appeared to increase more rapidly. The significance, however, of the duration of a run was only realized from the results obtained with the second reaction cell, wherein it was observed that the rate of methane formation decreased while the rate of ethane formation increased during a run. To see the specific effect of the methyl bromide pressure rate comparisons had therefore to be made at the same stage of the reaction.

Since mercury dimethyl, as evidenced by its smell, was always formed when mercury was present in the photolyzing methyl bromide, the effect of added mercury dimethyl was investigated. Although no liquid mercury was added in these runs the decomposition of the mercury alkyl frees mercury atoms which can pick up bromine. It can be seen from Table I that as the partial pressure of the mercury dimethyl increases the rates of formation of both methane and ethane increase, maintaining a constant ratio of $R_{C_2H_6}/R_{CH_4}$ of about 10. The ratio with mercury dimethyl alone is only 4.

Table II presents the effect of the pressure of methyl bromide as also of the duration of a run when mercury is present. These are data obtained using the larger reaction vessel with the mercury surface constantly swept during the exposure, the better to maintain the equilibrium vapor pressure. All the runs quoted were at 100°C. It can be seen that the rate of methane production decreases while that of ethane tends to increase with duration of a run at each pressure of methyl bromide. This may be attributed to an initial build-up of $HgCH_3$ or $Hg(CH_3)_2$ which, maintaining a lower methyl radical concentration, favors methane production. Further, comparison of rates after a given time at the three methyl bromide pressures used shows that methane formation increases while ethane formation decreases as the initial pressure increases. Finally, if the rate of decomposition of methyl bromide is taken as $2R_{C_2H_6}+R_{CH_4}$, it can be seen that the rate is higher initially and decreases with duration. While this might be attributable to a normal decrease in rate with progress of reaction, it cannot be the whole explanation, since even after the longest time the amount decomposed is less than twenty percent. Undoubtedly it is due to a decrease in the efficiency of bromine pick-up. This would permit the back reaction (2) to occur, decreasing the methyl radical concentration and thus decreasing ethane production. Paralleling this, there would also be a less efficient pick-up of methyl radicals according to reactions (5) and (10), leading to mercury dimethyl, which thus appears to be the principal source of ethane.

If the only function of mercury was to pick up bromine and reduce the rate of the back reaction, silver should serve the same purpose. Gordon and Taylor found no ethane when methyl bromide was photolyzed in the presence of silver. Two experiments were performed in the present work with silver in the cell instead

TABLE II. Effect of pressure of CH_3Br in presence of mercury. Temperature 100°C.

Run	Press. CH_3Br (mm)	Time (min)	Rate (ml/min) CO	CH_4	C_2H_6
65	100	2.5	0.10	0.52	0.15
61	100	5	0.08	0.42	0.13
64	100	7.5	0.05	0.35	0.18
57	100	10	0.05	0.35	0.19
67	50	2.5	0.06	0.34	0.21
63	50	5	0.04	0.28	0.19
68	50	7.5	0.02	0.19	0.22
60	50	10	0.02	0.21	0.23
108	25	2	0.02	0.12	0.23
109	25	3	0.01	0.07	0.24

TABLE III. Effect of temperature in absence of mercury $P_{CH_3Br} = 100$ min.

Runs	Temp. °C	Conditions	Time (min)	Rate (ml/min) CO	Rate (ml/min) CH_4
59–66	100	No Hg added	0	0.11	0.31
69–72	65	No Hg added	0	0.07	0.23
73–75	35	No Hg added	0	0.06	0.17
103	35	No Hg added	5	0.01	0.05
104	35	50 mm CO_2 added	5	0.01	0.05
101	35	100 mm CO_2 added	5	0.01	0.06
102	35	200 mm CO_2 added	5	0.01	0.06

of mercury which in both cases confirmed the absence of ethane. Obviously mercury, unlike silver, is capable of reacting with methyl radicals, effectively prolonging their life. As the mercury vapor concentration is increased, the over-all decomposition of methyl bromide increasingly resembles that of mercury dimethyl with respect to the high percentage of ethane in the products.

The effect of temperature on the rate of methane production in the absence of liquid mercury is shown in Table III. No ethane is found under these conditions. Rates quoted at zero time are initial rates extrapolated from the average rates for four runs over intervals up to ten minutes at each temperature. The energy of activation of methane production is 2.1 kcal. This may be compared with the value 0.8 kcal obtained by Masson and Steacie[4] using methyl chloride and with the zero value found by Schultz and Taylor[4] in the photolysis of methyl iodide. In both of these latter studies the addition of carbon dioxide was found to decrease methane production. No effect of added CO_2 is observed here. If the effect of CO_2 in the methyl chloride study is due, as attributed by Masson and Steacie, to quenching of the resonance radiation, it can only be concluded that the photolysis yielding the results in Table III is not effectively mercury sensitized. This is not inconceivable since no attempt was made to equilibrate the system with mercury vapor from the manometer which was the only source of mercury vapor in the system and the system was cut off by a stopcock from the manometer during the course of the run. An alternative explanation of the low energy of activation was suggested by Schultz and Taylor that methane is produced from hot methyl radicals. If this explanation is applicable here, the absence of retardation by CO_2 must indicate that at the pressures of methyl bromide used deactivation is already extensive and added inert gas has little effect. A similar result was found by Williams and Ogg[6] in the photolysis of methyl iodide-hydrogen halide mixtures.

To determine the effect of temperature on the photolysis in the presence of mercury a series of runs of one minute duration was made over the temperature range 35° to 200°C. A summary of the results is given in Table IV. From the discussion of the results in Table II concerning the dependence of methane and ethane formation on the duration of the exposure, it follows that the data in Table IV cannot be used directly to determine energies of activation, since the extent to which the rate of methane production has fallen off and that of ethane increased in the one minute interval may differ at each temperature. It may nevertheless be concluded that the energy of activation of methane production must be close to zero while that of ethane production must be less than 2 kcal, which is the apparent value derived directly from the data found. This apparent energy of activation of ethane production is in excellent agreement with the value 1.8 ± 0.5 kcal found by Trotman-Dickenson and Steacie[7] as a measure of the increase with temperature in methyl radicals from five different sources.

That the efficiency of bromine pick-up is never perfect is shown by the presence of carbon monoxide. The rate of formation of carbon monoxide increases with increase in temperature when mercury is absent but is approximately independent of temperature with mercury present. At the higher temperatures where the mercury vapor concentration is high and hence bromine pick-up more efficient only traces of carbon monoxide were found. The inverse relation shown in Table II between the dependence of the rate of formation of carbon monoxide and of ethane on the pressure of methyl bromide indicates that both processes depend on mercury concentration, one directly, the other inversely. When bromine pick-up is efficient, little carbon monoxide is found and ethane production is high. When no mercury is present or when the efficiency of pick-up is low, more carbon monoxide and less ethane are found. It seems probable that the formation of carbon monoxide originates in an attack by bromine atoms on the silica walls of the reaction vessel, a reaction which is aided by the presence of a reducing agent such as the carbonaceous deposit observed. The latter in turn probably originates from methylenes either from the methylene bromide or mercury methylene radicals the production of which accompanies methane formation.

TABLE IV. Effect of temperature in presence of mercury. $P_{CH_3Br} = 100$ mm.

Temp. °C	Rate (ml/min) CO	Rate (ml/min) CH_4	Rate (ml/min) C_2H_6
200	trace	0.08	0.49
150	trace	0.09	0.42
100	trace	0.14	0.34
80	0.02	0.18	0.26
65	0.03	0.20	0.18
35	0.02	0.15	0.18

[6] R. R. Williams Jr. and R. A. Ogg, Jr., J. Chem. Phys. **15**, 696 (1947).

[7] A. F. Trotman-Dickenson and E. W. R. Steacie, J. Phys. & Colloid Chem. **55**, 908 (1951).

In view of the results reported here a reconsideration of all the studies involving methyl radicals produced by mercury sensitization would appear to be called for. Obviously, however, no blanket opinion can be expressed since the procedure of introducing or of maintaining mercury vapor in such reaction systems has differed widely. The effects observed in this work with large amounts of liquid mercury present in the reaction vessel could be expected to be greater than those in typical mercury sensitization procedures, but estimates of methyl radical concentration should not ignore the presence of mercury.

THE JOURNAL OF CHEMICAL PHYSICS VOLUME 22, NUMBER 11 NOVEMBER, 1954

Nuclear Magnetic Resonance Spectra and Structure of Borohydride Ion and Diborane

RICHARD A. OGG, JR.
Department of Chemistry, Stanford University, Stanford, California
(Received August 2, 1954)

High resolution proton magnetic resonance spectra are presented for aqueous $NaBH_4$ and liquid B_2H_6 at 30 and 40 megacycles. B^{11} magnetic resonance spectra at 6 megacycles are presented for these same substances. The details of the spectra constitute powerful confirmation of a tetrahedral model for BH_4^- and a bridge proton model for B_2H_6. The bridge protons in the latter display resonance at higher applied magnetic field than do the terminal protons, suggesting a more hydride-ion like character for the former. Quantitative spin-spin multiplet separations and chemical shifts are recorded.

HIGH resolution proton magnetic resonance spectra have been studied with the 30 megacycle spectrometer used previously,[1] and with the 40-megacycle spectrometer of the Shell Development Laboratories, Emeryville, California. High resolution B^{11} magnetic resonance spectra have been studied with the 6-megacycle spectrometer of the latter laboratories.

In Fig. 1 are presented the proton magnetic resonance spectra of solutions of $NaBH_4$ in H_2O or D_2O (chosen to avoid interference by protons of ordinary water). It is seen that except for absolute position on the magnetic scale (and somewhat inferior adjustment of the resolution at 30 megacycles) the spectra at the two frequencies are identical. This constitutes the simplest proof of the chemical identity of the protons in BH_4^- ion, the structure of the spectrum resulting from the field invariant spin-spin interaction of protons and boron nuclei. The isotope B^{11}, with a natural abundance of some 80 percent, has nuclear spin quantum number $\frac{3}{2}$, giving rise to the four intense lines in the spectrum. The less abundant B^{10} has nuclear spin quantum number 3. The corresponding seven weaker lines are

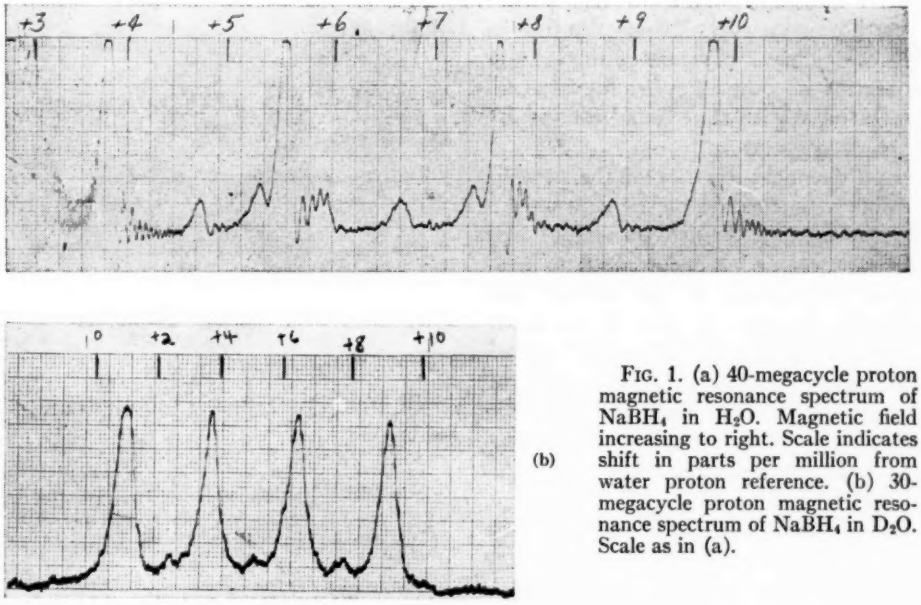

FIG. 1. (a) 40-megacycle proton magnetic resonance spectrum of $NaBH_4$ in H_2O. Magnetic field increasing to right. Scale indicates shift in parts per million from water proton reference. (b) 30-megacycle proton magnetic resonance spectrum of $NaBH_4$ in D_2O. Scale as in (a).

[1] Richard A. Ogg, Jr., J. Chem. Phys. **22**, 560 (1954).

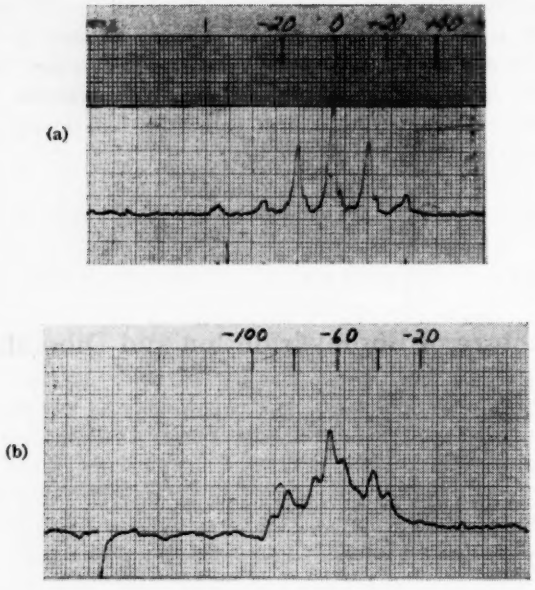

FIG. 2. (a) 6-megacycle B^{11} magnetic resonance spectrum of $NaBH_4$ in H_2O. Magnetic field increasing to right. Scale indicates separation in parts per million. Center peak chosen as reference. (b) 6-megacycle B^{11} magnetic resonance spectrum of liquid B_2H_6. Scale as in (a), with reference to arbitrary zero given there.

completely resolved in the 40-megacycle spectrum. The relative separations of the quadruplet and the seven fold multiplet are in satisfactory agreement with the known relative gyromagnetic ratios of the two boron isotopes.

In Fig. 2(a) is presented the B^{11} magnetic resonance of aqueous $NaBH_4$. The B^{11} resonance in BH_4^- is split by spin-spin interaction with four protons into sixteen lines. The experimental observation of five groups, of relative intensities 1, 4, 6, 4, 1, is independent proof of the identity of the boron-hydrogen bonds, leading to the corresponding coincidences of some of these lines. The observed separation of some 82 cycles for adjacent lines agrees quantitatively with that found for the B^{11} quadruplet in the proton spectrum.

The above proven chemical identity of the protons in BH_4^- is compatible with three geometrical structures —respectively square planar, square pyramidal and tetrahedral. The first two models would lead to relatively large angular dependence of the electric field gradients at the boron nucleus. In view of the fairly large electric quadrupole moments of B^{11} and B^{10} nuclei, corresponding electrically induced relaxation of the Zeeman levels should lead to broad magnetic resonance lines. The experimentally observed narrow lines provide an objective basis for assignment of the tetrahedral structure to BH_4^- ion.

The sample of diborane, provided through the courtesy of Professor Anton B. Burg of the University of Southern California, was normally gaseous at a pressure of about one atmosphere, contained in a sealed Pyrex glass cylinder some 100 cm^3 in volume, terminating in a tip of glass tubing of 5-mm diameter. Immersion of this tip in liquid nitrogen resulted in condensation of the sample. The tip was inserted into the spectrometer probe, and the spectrum was traced while the sample was still in liquid state.

In Fig. 3 are presented the proton magnetic resonance spectra of B_2H_6. These automatically exclude the now discredited ethane like structure, but are in excellent agreement with the currently accepted bridge model. The four identical terminal protons would be expected to have an electronic environment differing from that of the two identical "bridge" protons—i.e., there should be a "chemical shift" between the respective resonances. The terminal proton resonance should display the same type of spin-spin multiplet structure as that in BH_4^-. It will be observed that the dominant feature of the spectra embodies four intense lines. The bridge protons, symmetrically placed with respect to two chemically identical boron nuclei, are expected to display a more complex resonance. With the natural abundances of boron isotopes, the relative probabilities of configurations $B^{11}-H-B^{11}$, $B^{11}-H-B^{10}$ and $B^{10}-H-B^{10}$ are 16, 8 and 1. In the first of these, the proton resonance is split into sixteen lines, falling into seven groups of relative intensities 1, 2, 3, 4, 3, 2, 1. For the second, there are twenty-eight lines, with only accidental coincidences. Since each is only one-half as intense as the least intense line of the sevenfold group, the configuration $B^{11}-H-B^{10}$ should contribute an almost unobservable background to the bridge proton resonance. Finally, the third configuration should contribute forty-nine lines, grouped 1, 2, 3, 4, 5, 6, 7, 6, 5, 4, 3, 2, 1—for intensity reasons indistinguishable from background.

In Fig. 3(a) the peak at 6.3 is interpreted as the center of the sevenfold group, and those at 2.0 and 11.4,

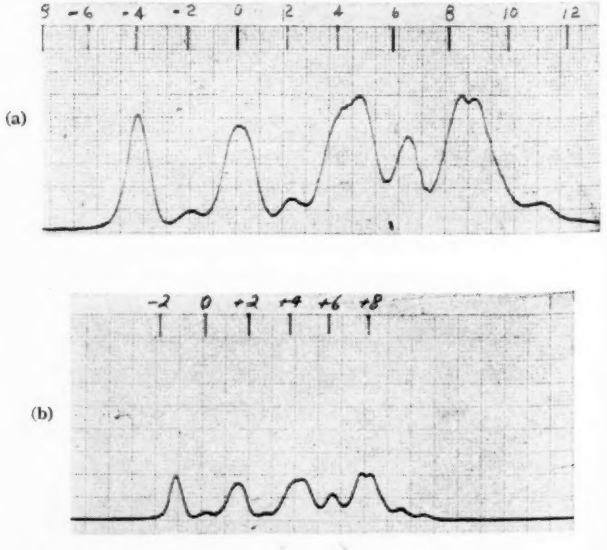

FIG. 3. (a) 30-megacycle proton magnetic resonance spectrum of liquid B_2H_6. Scale as in Fig. 1. (b) 40-megacycle proton magnetic resonance spectrum of liquid B_2H_6. Scale as in Fig. 1.

respectively, as the two outermost members. The remaining four members of the group overlap symmetrically the two right members of the quadruplet due to terminal protons. In Fig. 3(b) the higher frequency has caused a greater relative chemical shift of the bridge proton resonance, exposing two members of the sevenfold group on the high field side. The peak now appearing between the two intense ones corresponds to the third member of the group (intensity 3). The remainder overlap the quadruplet peaks, leading to an unsymmetrical intensity distribution. From the spectra in Fig. 3, the respective separations of the terminal proton quadruplet and the sevenfold group caused by $B^{11}-H-B^{11}$ bridge protons are 125 cycles and 43 cycles.

The B^{11} resonance in Fig. 2(b) further substantiates the structural features indicated by proton resonance. The more strongly interacting terminal protons split the B^{11} resonance into a triplet of relative intensities 1, 2, 1 and separation 125 cycles. Each of the members of this large triplet is split by the pair of bridge protons into a small triplet of relative intensities 1, 2, 1 and separation 43 cycles. Qualitatively and quantitatively the B^{11} spectrum found experimentally shows these expected details. The fairly narrow lines observed in both proton and boron spectra support the assignment of approximately tetrahedral arrangement of the four protons bonded to a given boron atom in B_2H_6, excluding such structures as, say, completely planar arrangement of all nuclei.

It will be observed that the sense of chemical shift between terminal and bridge protons in B_2H_6 is that the resonance of the latter is found at higher magnetic fields. In the currently accepted interpretation, this indicates a greater diamagnetic shielding of the bridge protons. That is, the latter are more hydride-ion like than are the terminal protons. The bond coupling constants for spin-spin interaction of protons and boron nuclei are greater for the terminal protons. Such details are of value in appraising any valence theory of diborane. Attention may also be called to the experimental differences in chemical shift and bond coupling constants between protons in BH_4^- and B_2H_6. A more hydride-ion like character for the former is suggested. The theory of chemical shift of higher atomic number nuclei is not yet sufficiently advanced to justify discussion of the marked chemical shift for B^{11} resonance between B_2H_6 and BH_4^-, the latter displaying resonance at higher field.

The author wishes to acknowledge the generosity of personnel of the Shell Development Company, notably Dr. Charles Reilly, in making available the indicated nuclear resonance spectrometers. Likewise invaluable has been the assistance of Dr. James Shoolery, of Varian Associates, in studies at 30 megacycles.

Letters to the Editor

THIS section will accept reports of new work, provided these are terse and contain few figures, and especially few half-tone cuts. The Editorial Board will not hold itself responsible for opinions expressed by the correspondents. Contributions to this section should not exceed 600 words in length and must reach the office of the Editor not later than the 15th of the second month preceding that of the issue in which the Letter is to appear. No proof will be sent to the authors. A publication charge of $10.00 per Letter is made which, when honored, will entitle the Institution to 100 free reprints.

Extrapolations of Electron Affinities

H. O. PRITCHARD AND H. A. SKINNER
Chemistry Department, University of Manchester, Manchester, England
(Received June 22, 1954)

MARGRAVE[1] has recently applied an extrapolation of the type suggested by Hellmann and Mamotenko[2] (through ascending ionization potentials) to derive a value for the electron affinity of the fluorine atom of 83.2±0.3 kcal/mole, in close agreement with the experimentally observed value (82.2±4) of Metlay and Kimball.[3] As Bates[4] and Pritchard[5] have already pointed out, the well-known extrapolation method of Glockler[6] (through ionization potentials in isoelectronic series) gives values for the electron affinities of F, Cl, and O which are decidedly low by comparison with experimental determinations, and the apparent success of Margrave's extrapolation has caused us to enquire if there is special merit in it.

Margrave assumes that the mean ionization potential ϵ/n of an atom or ion with n outer p-electrons may be expressed by a cubic equation in $(n-1)$,

$$\epsilon/n=a+b(n-1)+c(n-1)^2+d(n-1)^3, \quad (1)$$

where a, b, c, d are constants for a given nuclear charge Z. It is by the inclusion of the term in $(n-1)^3$ that (1) differs from the formula used by Hellmann.

We have applied (1) to the systems $Z=9$, $Z=17$, $n=1, 2, 3, 4, 5$, and obtained the unknown constants a, b, c, d by making a least-squares fit of the experimental data (taken from the compilation by Moore)[7] to the equation. Results are summarized below:

$$Z=9;\quad \epsilon/n=920965.7-118078.6(n-1)+3444.8(n-1)^2+107.6(n-1)^3 \quad (2)$$

	ϵ/n (expt.)	ϵ/n (calc.)	Δ
F V	920 952.7	920 965.7	+13.0 cm^{-1}
F IV	806 491.8	806 439.5	−52.3 cm^{-1}
F III	699 369.9	699 448.5	+78.6 cm^{-1}
F II	600 690.8	600 638.3	−52.5 cm^{-1}
F I	510 641.3	510 654.5	+13.2 cm^{-1}
F$^-$		(430 142.7)	

$$Z=17;\quad \epsilon/n=545\,982.3-61\,291.6(n-1)+764.7(n-1)^2+98.4(n-1)^3 \quad (3)$$

	ϵ/n (expt.)	ϵ/n (calc.)	Δ
Cl V	546 005.3	545 982.3	−23.0
Cl IV	485 461.0	485 553.8	+92.8
Cl III	427 384.3	427 245.1	−139.2
Cl II	371 554.0	371 646.6	+92.6
Cl I	319 371.9	319 348.7	−23.2
Cl$^-$		(270 941.8)	

Equation (2) differs significantly from the corresponding equation given by Margrave, and leads to a value for the electron affinity of F of 27 515 cm^{-1}≡78.6 kcal/mole. In part, the difference from Margrave arises from a revision in the ionization potential of F from 140 553.5 to 140 524.5 cm^{-1}, (now accepted by Moore following new spectroscopic studies by Liden[8]) but the main reason for divergence arises from a difference in his method of "least-squares fitting" of the experimental data. We have employed the standard procedure described by Fisher and Yates.[9] The root mean square deviation from Eq. (2) is 49.0 cm^{-1}, compared with 60.5 cm^{-1} in Margrave's paper.

Equation (3) leads to a value for the electron affinity of Cl of 28 498 cm^{-1}≡81.5 kcal/mole. The root mean square deviation from (3) is 87 cm^{-1}. The best experimental value[5] for the electron affinity of Cl is 88 kcal/mole. Thus, Eq. (1) gives values both for F and Cl that are low by some 5–6 kcal/mole. On the other hand, Glockler's extrapolation gives values some 16 kcal/mole too low.

We have observed that it is possible to fit the *total* energies* of ionization in the series FI–FV to the cubic equation.

$$\epsilon=920\,955.2+804\,235.3(n-1)-116\,607.8(n-1)^2+4391.2(n-1)^3 \quad (4)$$

(where $\epsilon=n.\ \epsilon/n$) with quite remarkable fidelity, *viz.*,

n	ϵ (expt.)	ϵ (calc.)	Δ
1	920 952.7	920 955.2	+2.5
2	1 612 983.6	1 612 973.9	−9.7
3	2 098 109.7	2 098 124.2	+14.5
4	2 402 763.2	2 402 753.3	−9.9
5	2 553 206.5	2 553 208.4	+1.9
6		(2 575 836.7)	

The root mean square deviation (9.0 cm^{-1}) represents a *fivefold* improvement on the fit given by (2) to the same data—*but*, extrapolation to $n=6$ now gives for the electron affinity 22 496 cm^{-1}≡64.3 kcal/mole. This failure emphasizes the sensitivity of this type of extrapolation.

Equation (1) has the advantage of partial theoretical justification (see Hellmann),[2] although it cannot claim to possess the finality, e.g., of Hylleraas'[10] equation for the ionization energies of 2-electron atoms. In addition to the test of (1) on the electron affinities of F and Cl (where it achieves an accuracy>90 percent), we find the equation can be applied with accuracy>99 percent to the extrapolation of ionization potentials in Na II (through the series Na III→Na VII) and in Mg III (series Mg IV→Mg VIII). But (1) fails dismally when the attempt to extrapolate the second electron affinity in O (i.e., $O^-+e\rightarrow O^=$) is made [see Eq. (5)].

$$Z=8;\quad \epsilon/n=624\,110.0-98\,497.4(n-1)+3189.1(n-1)^2+227.5(n-1)^3 \quad (5)$$

	ϵ/n (expt.)	ϵ/n (calc.)	Δ
O IV	624 138.8	624 110	−29
O III	528 914.6	529 029	+115
O II	441 864.1	441 692	−172
O I	363 347.2	363 462	+115
O$^-$	295 735†	295 706	−29
O$^=$		239 788	

The calculated ϵ/n for $O^=$ corresponds to a negative value for the second electron affinity, $O^-\rightarrow O^=$ −39 997 cm^{-1}≡−114 kcal/mole. The experimental value [see reference (5)] is −210 kcal/mole.

[1] J. L. Margrave, J. Chem. Phys. **22**, 636 (1954).
[2] H. Hellmann and M. Mamotenko, Acta Physicochim. U.R.S.S. **7**, 127 (1937).
[3] M. Metlay and G. E. Kimball, J. Chem. Phys. **16**, 779 (1948); R. B. Bernstein and M. Metlay, J. Chem. Phys. **19**, 1612 (1951).
[4] D. R. Bates, Proc. Roy. Irish Acad. **A51**, 151 (1947).
[5] H. O. Pritchard, Chem. Revs. **52**, 529 (1953).
[6] G. Glockler, Phys. Rev. **46**, 111 (1934).
[7] Charlotte E. Moore, *Atomic Energy Levels*, Vols. I, II, Circular 467, Natl. Bur. Standards, Washington.
[8] K. Liden, Arkiv Fysik. **1**, No. 9, 229 (1949).
[9] R. A. Fisher and F. Yates, *Statistical Tables* (Oliver and Boyd, Edinburgh, 1949), p. 23.
* Measured from the centers of gravity of each configuration s^2p^n, to the limit F VI ($^1S_0$).
[10] E. A. Hylleraas, Z. Physik. **65**, 209 (1930).
† Assuming 2.2 ev for the electron affinity of O (see Pritchard, reference 5).

Extrapolation Methods for Electron Affinities

JOHN L. MARGRAVE
Department of Chemistry, University of Wisconsin, Madison, Wisconsin
(Received July 8, 1954)

EXTRAPOLATION methods for determining ionization potentials and electron affinities have been widely applied and used. For example, the extrapolation of the average removal energy per p electron to the atom or ion of one more p electrons has been used for several of the first row elements.[1] Pritchard and Skinner[2] have pointed out that this extrapolation is greater than 99 percent accurate for the series of positive ions leading to Na II and Mg III. By fitting a cubic equation by least squares to the p electron removal energies for the Ne ions (Ne II through Ne VII), one can also predict the ionization potential of Ne I (electron affinity of Ne II) with less than one percent error. It is of considerable interest obviously to inquire into the validity of this extrapolation for atoms which form negative ions by addition of electrons.

The electron affinities of fluorine and chlorine have been obtained in this manner[2] and it has been shown that the extrapolated values are about 10 percent lower than the experimental values.[3] Although the extrapolations are less reliable because fewer points are available for curve fitting, it is interesting to look at the extrapolated data for oxygen. From the spectroscopic data of Moore[4] for O I through O IV, one finds the average removal energy per p electron is given by

$$\epsilon/n = 624\,138.8 - 99\,189.8(n-1) + 3905.6(n-1)^2 + 60.3(n-1)^3,$$

where n is the number of p electrons in the atom or ion. Extrapolation to $n=5$ (O^-) indicates an electron affinity for the oxygen atom of 22 kcal/mole in comparison with the experimental value of 54 kcal/mole.

Pritchard and Skinner[2] have fitted their least squares equation to five experimental points for p electrons in oxygen atoms by using the experimental electron affinity of O, and then extended the extrapolation to $n=6$ ($O^=$). The cubic equation which they obtained has definitely different coefficients than that given above which fits the removal energies for the first four p electrons exactly. The main difference is in the magnitude of the term in $(n-1)^2$ and the term in $(n-1)^3$. The electron affinity for O^- computed from the equation of Pritchard and Skinner is in very poor agreement with that computed through termochemical cycles involving ionic oxides.

Some of the reasons for the apparent failure of this extrapolation when extended to negative ions seem clear. When one extrapolates for the series Mg IV to Mg VIII or Na III to Na VII, all the extrapolations merely involve extension to a positive ion of one less charge. For the Ne series, only the last step involves the neutral Ne atom. For the other cases, however, the extrapolations are extended to include electronic arrangements for negative ions and new effects, not completely predictable on the basis of positive ion and neutral atom energy levels, are important. For the extrapolation from O^- to $O^=$, where electrostatic repulsion must play an important role, it does not seem at all surprising that this simple extrapolation fails completely.

Spectral extrapolations of this type are not very useful for nitrogen or carbon because there are so few experimental points. For N atoms, however, this sort of data is all that is available, and recalculation after Hellmann and Mamotenko[1] (fitting the experimental removal energies with a parabola) with the data of Moore[4] indicates that an electron would be added to a nitrogen atom in a slightly endothermic process. Formation of a cubic equation for the average removal energies by using coefficients extrapolated from those found to fit Ne, F, and O, however, leads one to predict a value of 15–25 kcal/mole for the electron affinity of nitrogen. Similar extrapolation indicates a positive electron affinity for carbon.

Another extrapolation method which may be applied to N and C is that of Finkelnberg and Stern.[5] ΔS (the difference in effective atomic number between the ion or atom being considered and the ion or atom having atomic number one less) is found by extrapolation to be 0.75 for $(S_{O^-} - S_{N^-})$ and 1.12 for $(S_{N^-} - S_{C^-})$. These values indicate an electron affinity for the nitrogen atom of 26 kcal/mole and an electron affinity for the carbon atom of 38 kcal/mole.

[1] (a) H. Hellmann and M. Mamotenko, Acta Physicochim. U.R.S.S. **7**, 127 (1937); (b) J. Margrave, J. Chem. Phys. **22**, 636 (1954).
[2] H. O. Pritchard and H. A. Skinner, J. Chem. Phys. **22**, 1936 (1954).
[3] The constants in the least squares equation in reference 1(b) for the fluorine extrapolation are in error and the equation should read

$$\epsilon/n = 920\,965.9 - 118\,076.1(n-1) + 3442.1(n-1)^2 + 108.2(n-1)^3.$$

The extrapolated electron affinity of fluorine is then 78.6 kcal/mole as indicated in reference 2.
[4] C. Moore, "Atomic Energy Levels," National Bureau of Standards, Circular 467, Vols. I and II.
[5] W. Frinkelnberg and F. Stern, Phys. Rev. **77**, 303 (1950).

Vibration Force Constants of $SiO_4(CH_3)_4$

KAORU IGUCHI
Electrical Communication Laboratory, Nippon Telegraph and Telephone Public Corporation, Tokyo, Japan
(Received August 27, 1954)

SEVERAL authors have investigated the molecular vibration of some silicates,[1–4] but the vibration force constants seem to be not yet determined satisfactorily.

Here we have tried to determine them by evaluating the normal vibration frequencies of $SiO_4(CH_3)_4$, comparing with experimental data.

The form of the molecule is shown in Fig. 1, and we have treated

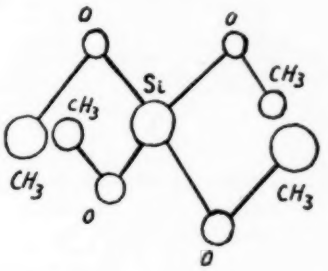

FIG. 1. $SiO_4(CH_3)_4$ molecule.

the CH_3 radical as if an atom, because we know well about the proper frequencies and force constants of the radical.[5] The rotation of CH_3 radical about Si–O axis may be neglected at low temperature.

The symmetry of the molecule is V_a, and the number of irreducible representations contained in the vibration is A_1..four, A_2..one, B_1..two, B_2..four, E..five; here the rigid rotations and translations are excluded.

As the potential energy V, we have taken the following form:

$$2V = k_1 \sum_{i=1}^{4} l_i^2 + k_2 \sum_{i=1}^{4} l_i'^2 + g \cdot_a b \sum_{i=1}^{4} \alpha_i^2 + f \cdot_a \sum_{1=i<j}^{4} \beta_{ij}^2 + h \sum_{1=i<j}^{4} q_{ij}^2,$$

here

l_i..$Si-O_{No.i}$	bond elongation,
l_i'..$O_{No.i}-CH_3$	bond elongation,
α_i..$Si-O_{No.i}-CH_3$	angle variation,
β_{ij}..$O_{No.i}-Si-O_{No.j}$	angle variation,
q_{ij}..$O_{No.i}-O_{No.j}$	distance variation,
a..$Si-O$	distance=1.65A,
b..$O-CH_3$	distance=1.43A.

Using group theoretical method, we can factorize the secular equation and the normal frequencies can be evaluated by inserting appropriate values for the force constants. We have taken these values,

$k_1=3.7$, $k_2=5.7$, $g=0.30$, $f=0.22$, $h=0.06$, in 10^5 dyne/cm.

For simplicity we have assumed the SiO_4 to be tetragonal.

TABLE I. Calculated and observed wave numbers in cm^{-1}.

Symmetry	A_1	A_2	B_1	B_2	E
Calculated values	279	···	303	292	400
	665			899	825
	1145			1142	1146
Activity	Raman	none	Raman	Raman	Raman and infra.
Observed Values	642[a] 4*s*		302[b] 0*d*		422[b] 0*d*
					840[a] 2
					1100[a] 1*d* and
					1200 0*d*

[a] See reference 6.
[b] See reference 7.

TABLE II. Values of force constants (in 10^5 dyne/cm).

	k_1	k_2	g	f	h
Author	3.7	5.7	0.30	0.22	0.06
Barriol[a]	4.5	···	···	0.7	···
Matossi[b]	4.0	···	···	0.38	···

[a] See reference 3.
[b] See reference 4.

The result is shown in Table I and Table II, compared with experimental data,[6,7] and the calculated values of smaller wave number are omitted. Our values are a little smaller than others, but, in spite of the simple form of potential function and some simplifying approximations, the result shows rather good coincidence with experimental values.

Details will be later published in the *Journal of the Physical Society of Japan*.

[1] D. M. Dennison, Astrophys. J. **62**, 84 (1925).
[2] C. Schafer, Z. Physik. **60**, 584 (1930).
[3] J. Barriol, J. phys. radium **7**, 209 (1946).
[4] F. Matossi, J. Chem. Phys. **17**, 679 (1949).
[5] G. Hertzberg, *Infrared and Raman Spectra of Polyatomic Molecules* (D. Van Nostrand Company, Inc., New York, 1945).
[6] J. Weiler, Z. Physik. **80**, 617 (1933).
[7] R. Signer and J. Weiler, Helv. Chim. Acta **16**, 115 (1933).

Some Remarks to Golden's Rate Theory

IWAO YASUMORI AND SHIN SATO
Laboratory of Physical Chemistry, Tokyo Institute of Technology, Ookayama, Meguro-ku, Tokyo
(Received June 4, 1954)

THE nature of Golden's rate theory, with the rate calculation of the reaction $H_2+Br\rightarrow H+HBr$, has been discussed recently by Golden, Bauer, and Wu.[1]

In the discussion Golden stated briefly that his first approximation theory using the plane wave function for the translational motion is not adequate for the reaction $H_2+H\rightarrow H+H_2$, in which the zero-point energies of reactants and products are identical. We, independently from his work, have calculated the rates of the same reaction to examine the validity of his theory and found the obtained results to be quite unsatisfactory;[2] this calculation gives a negative apparent activation energy and too large rates in comparison with the observed value and with the estimated one by the other theory (Table I).

The above disagreement seems to originate in the fact: the perturbation potential defined in his theory cannot be sufficiently small, whereas his first approximation just corresponds to Born's zero-order approximation in collision theory,[3] because the wave functions in actual calculation express only the nuclear motion in a potential field given by the electronic energy of the system.

Nevertheless, his results obtained for the reaction $H_2+Br\rightarrow H+HBr$ are reasonable.[4] But this seems to depend on the following fortuitous reason: the experimental value of the activation energy of the above reaction is nearly equal to the zero-point energy difference between reactants and products, 17.7 and 16.6 kcal/moles, respectively. Then, by only considering energy conservation, the exponential factor in the rate constant $k=A\exp(-E/RT)$ can be obtained approximately.

TABLE I. Rates calculated for the reaction $H_2+H\rightarrow H+H_2$.

Temp. °K	300	500	1000
$k(\rho^a=0.12)^b$	2.1×10^{15}	1.6×10^{15}	8.9×10^{14}
$k(\rho=0.20)$	1.7×10^{14}	1.2×10^{14}	6.6×10^{13}
$k_a{}^c(\rho=0.14)$	7.8×10^{2}	1.8×10^{7}	4.5×10^{10}
$k_a(\rho=0.20)$	4.8×10^{7}	1.3×10^{10}	1.2×10^{12}
k_{obs}	9.0×10^{7}	···	2.2×10^{12}

[a] Coulombic energy fraction in the H−H bond.
[b] cc $mole^{-1}$ sec^{-1}.
[c] Calculated by the absolute reaction rate theory on the same approximate interaction potential.

On the other hand, from Eq. (42) (in his paper Part I) under the restriction

$$x=(E_j^{(\alpha)}+E_\nu^{(\alpha)})-(E_0^{(\beta)}-E_0^{(\alpha)})\geqq 0, \tag{1}$$

one obtains as the activation energy E^*

$$E^*=(E_0^{(\beta)}-E_0^{(\alpha)}) + \left(\frac{\Sigma_{j'}\Sigma_{k'}\int\cdots\int x\exp(-x/kT)\,|I|^2 d\Omega_\beta(\mu)dp_1{}^\alpha\cdots dp_{3S}{}^\alpha}{\Sigma_{j'}\Sigma_{k'}\int\cdots\int\exp(-x/kT)\,|I|^2 d\Omega_\beta(\mu)dp_1{}^\alpha\cdots dp_{3S}{}^\alpha} - E^{(\alpha)}\right). \tag{2}$$

Then, one can easily find that E^* for the reaction $H_2+Br\rightarrow H+HBr$ depends on the first term in Eq. (2) and for the reaction $H_2+H\rightarrow H+H_2$ on the second term. Since the results for the latter reaction on the same approximation are quite unsatisfactory, it may be unacceptable that the calculation of second term in Eq. (2) is valid for the former one. His value 17.0 kcal/mole by no means shows that the approximation is suitable.

For the frequency factor, the matter is rather complicated. But the perturbation potential including κ as a parameter, can be adjusted, so that the calculation may agree with the observed rates, since the variation of κ does not affect the exponential factor so much but the frequency factor markedly.

Consequently, it seems clear that not only in the case where the zero-point energy difference between reactants and products is small, but in general, his approximation is not suitable.

The use of wave function including the repulsion between molecules in reactants would suggest some way to improve the matter, but it causes considerable change in his formula and will be a very complicated work. By the way, Golden's theory has a great advantage to the other phenomenological theory in giving some detailed knowledge of a chemical reaction.

We are grateful to Dr. S. Shida for his helpful encouragement. Also we wish to thank Professor S. Golden for his kindness in letting us see his reply before publication.

[1] S. Golden, J. Chem. Phys. **21**, 2071 (1953); E. Bauer and T. Y. Wu, *ibid.* **21**, 2072 (1953). For Golden's theory, see J. Chem. Phys. **17**, 620 (1949).
[2] I. Yasumori and S. Sato, Busseiron Kenkyu **69**, 37 (1953).
[3] N. F. Mott and H. S. W. Massey, *Theory of Atomic Collisions* (Clarendon Press, Oxford, 1949), second edition, Chap. VIII, p. 136; Chap. XII, p. 270; Chap. XIV, p. 352.
[4] S. Golden and A. M. Peiser, J. Chem. Phys. **17**, 630 (1949); **17**, 842 (1949).

Adequacy of the Born Approximation in the Calculation of Chemical Reaction Rates: A Reply to Yasumori and Sato

SIDNEY GOLDEN
Brandeis University, Waltham, Massachusetts
(Received June 28, 1954)

THE preceding note, which the authors kindly let me see prior to publication, contains a criticism of the use of Born's approximation in calculating chemical reaction rates. The present note supports that criticism.

Calculation of the thermal *ortho-para* conversion rate of hydrogen in terms of the formulation employed for the reaction of hydrogen molecules and bromine atoms led to negative activation energies.[1,2] The results noted in reference (1) were obtained for temperatures in the vicinity of 1000°K. They could be summarized by the rate constant expression.[3]

$$k(para \rightarrow ortho) = \frac{1.6\times10^{20}}{T^{\frac{1}{2}}} \exp(-1100/RT) \text{ cc mole}^{-1} \text{ sec}^{-1},$$

where the symbols have their usual meaning. This expression yields results which differ from the values reported by Yasumori and Sato[4] by a more or less fixed factor (of about three), indicating substantial agreement particularly as to temperature coefficients.

Further concordance with the results of reference (2) is found in the relative importance of excited vibrational states: for molecules in the ground vibrational state leading to transitions (*para→ortho*) resulting in molecules in the first excited vibrational state the rate at 1000°K relative to that leading to vibrationally unexcited molecules was 1.1×10^{-4}; for molecules initially in the first excited vibrational state leading finally to molecules similarly excited the value was 1.6×10^{-4}. The value reported by Yasumori and Sato[2] for a representative pair of rotational states, with a singly excited vibrational final state only, is 0.3×10^{-4}. While Yasumori and Sato report the rate of all interchanges: $H_2+H\rightarrow H_2+H$, and the results alluded to in reference (1) (and elaborated here) pertain to the *para→ortho* transitions, it seems clear that both investigations lead to substantially the same results—and the same conclusions.

To assess further the applicability of the Born approximation, a "second-order" treatment was carried out in which the essential departure from the conventional Born approximation was to take into account the physical scattering of the hydrogen molecule and atom. For two typical pairs of rotational states ($K=2$, $L=1$; $K=6$, $L=3$), with reactants and products in the ground vibrational state, the second-order result was a factor of (6×10^4; 2×10^4) the first-order result. These results unquestionably rule out the applicability of the Born approximation in this case.

As to criticism of the results obtained for the reaction $H_2+Br\rightarrow H+HBr$,[5] the remarks of Yasumori and Sato are well made. Those which relate to the frequency factor have already been emphasized in reference (5). Those which relate to the activation energy are, in my opinion, completely valid. However, the results of the investigation by Bauer and Wu[6] pertaining to the translational wave functions in this case suggest that the Born approximation is perhaps not as inadequate here as might have been imagined. In any case, considerations of this sort should not detract from the general conclusions reached by Yasumori and Sato.

[1] S. Golden, J. Chem. Phys. **21**, 2071 (1953).
[2] I. Yasumori and S. Sato, Busseiron Kenkyu **69**, 37 (1953).
[3] These unpublished results, as well as others referred to herein, were obtained in collaboration with Dr. A. M. Peiser and Dr. S. Katz under ONR contract N9onr-86101 with Hydrocarbon Research, Inc.
[4] I. Yasumori and S. Sato, preceding note, Table I, with $\rho=0.12$.
[5] S. Golden and A. M. Peiser, J. Chem. Phys. **17**, 630 (1949).
[6] E. Bauer and T. Y. Wu, J. Chem. Phys. **21**, 726 (1953); **21**, 2072 (1953).

Infrared Spectral Studies of BrF_3 and BrF_5†

H. M. HAENDLER, S. W. BUKATA, AND B. MILLARD, *Department of Chemistry, University of New Hampshire, Durham, New Hampshire*

AND

E. I. GOODMAN AND J. LITTMAN, *Chemical Engineering Division, Brookhaven National Laboratory, Upton, New York*

(Received August 30, 1954)

THE extreme chemical reactivity of bromine trifluoride and pentafluoride hinders satisfactory measurement of their infrared spectra. Resistant window materials are not sufficiently transparent, and transparent window materials lack stability. Consequently, the region available for study is limited.

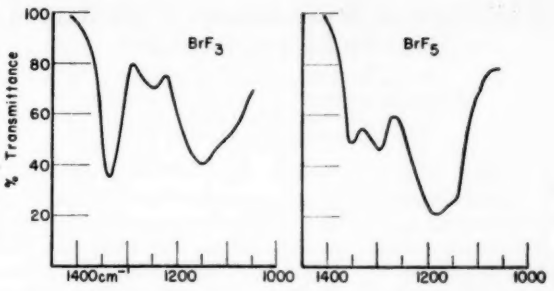

FIG. Infrared spectra of liquid BrF_3 and BrF_5 in the CaF_2 range.

Sodium chloride, potassium bromide, barium fluoride, and silver chloride are attacked by these interhalogens. It had been hoped that the recently developed barium fluoride could be used, but the windows became etched immediately, possibly with resultant formation of $Ba(BrF_4)_2$. Calcium fluoride, however, retains 90 percent or more of its transmittance even after repeated exposure and was used for windows to measure the spectra of liquid bromine trifluoride and bromine pentafluoride from 2.5–9.5 μ. The solubility of calcium fluoride in bromine trifluoride is considerably less than that of barium fluoride.[1]

The results are given in Table I and Fig. 1. Raman and infrared data have been given by Stephenson and Jones[2] for the bromine pentafluoride fundamentals, and the bands reported here fall well into the overtone and summation region. Although silver chloride is attacked readily by bromine trifluoride, it was possible to obtain an indication of strong absorption in the range 600–670 cm^{-1}, where the fundamentals would be expected, by using low vapor concentration.

The bromine fluorides, obtained from the Harshaw Chemical Company, were purified by distillation in a nickel column, packed with nickel "Heli-pak" (Podbielniak). The proper fraction was distilled directly into the cell which had been pretreated with chlorine trifluoride. The cells were of Monel, patterned on a Perkin-Elmer sealed liquid cell, with Monel valves. Three and ten mil Teflon spacers were used with the calcium fluoride windows. A Perkin-Elmer 12-C spectrometer was used, and some runs were checked on a model 21 spectrometer by Perkin-Elmer.

A band of variable intensity occurred at about 3450 cm^{-1} (2.9 μ) in the bromine trifluoride runs. Absorbance measurements were made at several wavelengths, using the Perkin-Elmer densitometer attachment and cells of different path length. Calculated absorptivities agreed at all frequencies except 3450 cm^{-1}. Kel-F (chlorotrifluoroethylene polymer) is sufficiently transparent in this latter region to permit its use as a window. In that test, the band was still present; thus, window attack is not involved. When BrF_3 was exposed by surface contact to HF vapor, the resultant liquid gave a greatly enhanced 3450 cm^{-1} band, varying in intensity with different exposures to HF. It thus seems possible that traces of HF form a complex with BrF_3 similar to that reported for HF and ClF_3.[3]

TABLE I. Infrared bands of BrF_3 and BrF_5.

Bromine trifluoride cm^{-1}	Bromine pentafluoride cm^{-1}
1337	1355
1250	1298
1154	1187

† Research carried out under the auspices of the U. S. Atomic Energy Commission.
[1] Sheft, Hyman and Katz, J. Am. Chem. Soc. **75**, 5221 (1953).
[2] C. V. Stephenson and E. A. Jones, J. Chem. Phys. **20**, 1830 (1952).
[3] J. P. Pemsler and D. F. Smith, Report K-1096, K-25 Plant, Oak Ridge, Tennessee, January 29, 1954.

Radiochemical Measurements of the Natural Fission Rate of Uranium*

P. K. KURODA AND R. R. EDWARDS
Department of Chemistry, University of Arkansas, Fayetteville, Arkansas
(Received August 27, 1954)

RECENT mass spectrometric analyses of the stable fission product gases in uranium minerals[1–3] have indicated that neutron-induced fission makes a significant contribution to the total fission occurrence in pitchblendes. However, uncertainty concerning possible loss of gaseous products over the lifetime of the mineral has prohibited a reliable estimation of the total fission rate from these data.

In an attempt to obtain the current total (spontaneous plus neutron-induced) fission rate in a common uranium mineral, we have isolated about 40 mg of strontium (as the carbonate) without added carrier from 2.5 kg of Great Bear Lake pitchblende (41.70 percent U_3O_8). The sample was decontaminated from radium and barium activities by repeated additions of barium carrier, followed by barium chromate precipitations, until the barium chromate activity became negligible. Similar operations were performed with bismuth carrier (precipitated as the sulfide), and lanthanum carrier (precipitated as the hydroxide) until all activity following these carriers was removed. The strontium was then precipitated as the carbonate and mounted on aluminum for measurement with an end-window Geiger tube. Recovery of the strontium was about 65 percent.

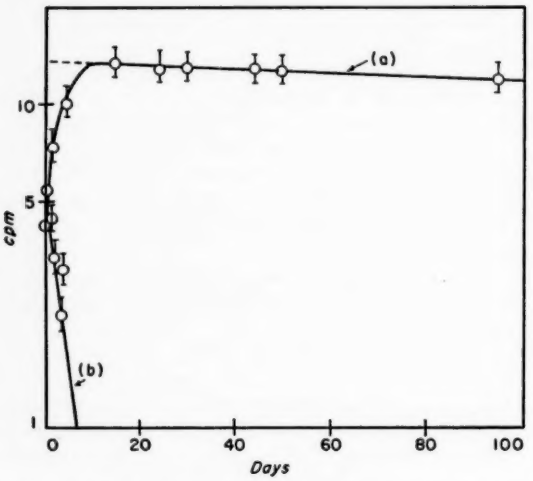

FIG. 1. Growth and decay of Sr fraction. (a) Growth of Y^{90}, decay of Sr^{89}; (b) decay of Y^{90}.

Results of the radioactivity measurements are shown in Fig. 1. The initial rise is presumably due to the growth of the 61-*h* Y^{90}, and the final decay appears to be that of the 55-*d* Sr^{89}. The sample was redissolved, and a lanthanum hydroxide precipitation was performed, yielding a sample showing, within experimental error, the decay of Y^{90}.

Assuming a fission yield of 5 percent for Sr^{90}, the data indicate $(1.3\pm0.1)\times10^{-14}$ curie Sr^{90}/g. U^{238}, corresponding to an over-all fission half-life of $(5.9\pm0.6)\times10^{15}$ years. A value of $(6.1\pm1.5)\times10^{15}$ years was obtained from the Sr^{89}/U^{238} ratio, assuming a fission yield of 4.5 percent for Sr^{89}. Taking the value of Segrè,[4] $(8.04\pm0.3)\times10^{15}$ years, for the spontaneous fission half-life of U^{238}, the contribution of neutron-induced fission is estimated to be about 25 percent. This compares with the value of 35 percent reported by Wetherill[3] for Belgian Congo pitchblende. However, considerable discrepancy exists in the reports of the spontaneous fission half-life, values between 10^{16} and 10^{17} years having been reported.[5]

It is worthy of note that the Sr^{89}/Sr^{90} activity ratio in the experiment reported here is near unity, as would be expected for fission products in equilibrium with the fission process. Sr^{89} should predominate over Sr^{90} by factors up to 135 in nuclear detonation fission products of recent vintage.

Measurements of the Sr^{89}/U^{238} ratio in samples of uranium metal and uranium acetate have indicated a fission half-life of about 2×10^{15} years for each. In these samples Sr^{90} was barely detectable, presumably because the samples were young relative to its half-life of about 20 years. Because of the uncertain history of these samples it is difficult to attribute any significance to the lower apparent value of the fission half-life. We propose to attempt a radiochemical determination of the spontaneous fission half-life under conditions minimizing the contribution of neutron-induced fission.

* This work was supported in part by the U. S. Atomic Energy Commission.
[1] J. Macnamara and H. G. Thode, Phys. Rev. **80**, 471 (1950).
[2] W. H. Fleming and H. G. Thode, Phys. Rev. **90**, 857 (1953).
[3] G. W. Wetherill, Phys. Rev. **92**, 907 (1953).
[4] E. Segrè, Phys. Rev. **86**, 21 (1952).
[5] G. N. Flerov and K. A. Petrzhak, J. Phys. (U.S.S.R.) **3**, 275 (1940); Phys. Rev. **58**, 89 (1940).

The Reaction Zone in Gaseous Detonations

G. B. KISTIAKOWSKY AND PAUL H. KYDD
Gibbs Chemical Laboratory, Harvard University, Cambridge, Massachusetts
(Received August 2, 1954)

DIRECT evidence in support of the Zeldovitch–van Neumann theory of the reaction zone in detonation waves has been obtained in the form of density *vs* time records by the x-ray absorption method.[1] The theory states that the detonation wave consists of a shock moving at the detonation velocity and leaving heated and compressed gas behind it. The chemical reaction then starts and as it progresses the temperature rises and the density falls, till they reach the Chapman-Jouguet values and the reaction attains equilibrium. A rarefaction wave then sets in, whose steepness depends on the distance traveled by the wave.[2,3] The density *vs* time relation, observed as a wave moves by a fixed plane normal to the tube axis, should show a virtually discontinuous[4] rise from the initial density to the value characteristic of the initial shock and then a decrease to the Chapman-Jouguet value, the form of the decrease depending on the kinetics of the reactions occurring.

With an improved apparatus similar to that described in reference 1, using mixtures of 70 percent H_2 and 30 percent O_2 with sufficient Xe (10–15 mm) to give adequate x-ray absorption, the reaction zone has been consistently observed at sufficiently low reactant pressures. The waves in these mixtures were produced by detonating equimolar acetylene-oxygen mixtures, introduced at slightly higher pressures and separated from the Knallgas by thin diaphragms. Ionization gauges[5] placed along the tube demonstrated that the resultant waves were plane and normal to the tube axis and had attained a steady velocity. Below 20 mm the gauges performed less satisfactorily and only the velocity could be determined. The resolving power of the x-ray equipment was limited by the width of the beam (1.5 mm$\cong$0.7 μsec) and the residual nonplanarity of the wave front (3 mm$\cong$1.5 μsec).

The duration of the reaction zone is found to be related to the pressure of the reactant gases. At pressures above 1/5 atmos, no evidence of the spike has been obtained with the present resolving power. At 115 mm it begins to be visible as an abnormally sharp rise in the wave front and at 75 mm the spike is fully developed. Its appearance at 65 mm and at 20 mm is shown in Fig. 1 of the CRO record. The rarefaction wave following the Chapman-Jouguet state is not obvious in these tracings because of the length of the explosion tube used and the short duration of the CRO sweep. Rough estimate indicates that the duration of the reaction zone is inversely proportional to the *square* of the reactant pressure over the range 115–15 mm.

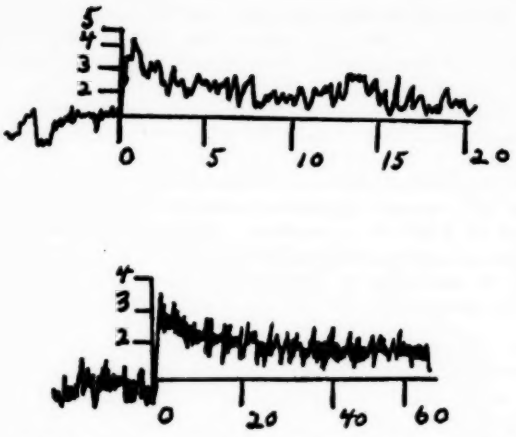

FIG. 1. Density *vs* time records at 65 mm reaction pressure (upper tracing) and 20 mm (lower tracing). Ordinates are density in multiples of initial density, abscissas are time in microseconds.

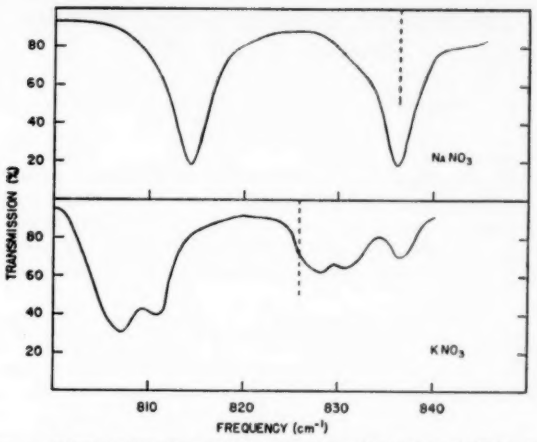

FIG. 1. Infrared absorption of Nujol mulls of $NaNO_3$ and KNO_3 in the 12-μ region; N^{15}:N^{14}=1:1. The dotted lines indicate positions of N^{14} peak in natural $NaNO_3$ and KNO_3.

Experiments with 71 mm $2H_2-O_2$ and 309 mm A rather than 12 mm Xe give no evidence of the reaction zone, implying that added rare gas increases the reaction rate even though it lowers the shock temperature.

The spikes show no evidence of induction periods, the density decreasing as soon as the highest value is attained. The density scale in the tracings is in multiples of the initial density. A simplified hydrodynamic treatment assuming constant specific heat and no dissociation yields the following results for the two mixtures shown:

Mixture			
Reactants	Xe	Shock density	Chapman-Jouguet density
65 mm	10 mm	5.4 d_0	1.7 d_0
20 mm	15 mm	4.8 d_0	1.7 d_0

where d_0 is the initial density. In no case yet studied does the peak density attain the expected shock value, due, presumably, to the finite resolving power of the equipment, coupled with a high initial rate of reaction.

This work is being continued. It has been supported by the Office of Naval Research (Contract N5ori-76, T.O. XIX, NR-053-094). Thanks are also due Mr. Roger Humberger who constructed much of the equipment used, to the General Electric x-ray Corporation for the gift of an x-ray tube, and to the Linde Air Products Company for the gift of xenon.

[1] G. B. Kistiakowsky, J. Chem. Phys. **19**, 1611 (1951).
[2] G. I. Taylor, Proc. Roy. Soc. (London) **A2 0**, 235 (1950).
[3] G. B. Kistiakowsky and Paul H. Kydd (to be published).
[4] E. F. Greene and D. F. Hornig, J. Chem. Phys. **21**, 617 (1953).
[5] H. T. Knight and R. E. Duff, Rev. Sci. Instr. (to be published).

N^{15} Isotope Shift of the Perpendicular Bending Frequency in KNO_3 and $NaNO_3$†

J. C. DECIUS
Department of Chemistry, Oregon State College, Corvallis, Oregon
(Received August 30, 1954)

IN the course of studies of the N^{15} isotope effect in several crystalline nitrates we have observed some striking dissimilarities between the infrared absorption of KNO_3 and $NaNO_3$ as Nujol mulls in the 12-μ region. As shown in Fig. 1, at 50–50 $N^{14}-N^{15}$ composition, $NaNO_3$ yields two simple, sharp peaks whose frequencies (836.1 and 814.4 cm^{-1}) almost exactly satisfy the Teller-Redlich ratio: experimental ratio=0.9740, theoretical ratio=0.9739. Moreover, the relative intensities of absorption are certainly qualitatively, and probably quantitatively, in the expected ratio.

KNO_3 behaves quite differently. The N^{15} region is split into two partly resolved peaks, while three distinct maxima occur in the N^{14} region. Moreover, with gradual increase in the N^{15} concentration, the center of gravity of the N^{14} region moves towards higher frequencies, while that of the N^{15} region moves towards lower frequencies. An even more striking difference in the spectra of the two salts is the much greater apparent intensity of the absorption in the N^{15} region in the case of KNO_3.

The N^{15} peak is definitely observable in natural KNO_3 at 811 cm^{-1}. If one calculates this frequency with the aid of the product rule, the result is 804.2 cm^{-1}, in significant disagreement with the observed value.

X-ray diffraction studies[1] have shown that the closest pairs of NO_3^- ions occur at distances of 3.225 A in KNO_3 and at 5.064 A in $NaNO_3$; in the former case the planes of the ions are perpendicular to their mutual threefold axis,[2] while in $NaNO_3$ the nearest neighbors are coplanar. We believe that the phenomena described above can be explained in terms of the interaction energy between the dipoles of the nearest neighbor ions, produced during the vibration in the ν_2 mode. The inverse cube dependence upon the distance accounts primarily for the existence of observable effects in KNO_3, where the NO_3^- ions are relatively close together. The introduction of N^{15} atoms perturbs the lattice symmetry and breaks down the selection rule which otherwise permits absorption only in that mode in which all out-of-plane bending vibrations occur with identical phase. Since such a totally symmetric mode necessarily has the lowest frequency in the ν_2 branch for the dipole-dipole coupling considered here, it is evident that introduction of N^{15} will shift the absorption in the N^{14} region to somewhat higher values, as observed.

We have estimated the magnitude of the dipole derivative from these effects and find $(\partial\mu/\partial\delta)_0 \approx 0.9$ debye/A, where δ measures the displacement of nitrogen perpendicular to the plane of the oxygens. This may be compared with a value of 0.985 debye/A for the bending mode of CO_2,[3] expressed in similar units. A more detailed development of the theory yields a qualitative explanation of the observed inequality of intensities.

Studies on other nitrates and carbonates ($BaCO_3$ exhibits effects very similar to those observed in KNO_3) are in progress, and a more detailed report on the theory and KNO_3 measurements is being prepared. Needless to say, these effects are of considerable significance in connection with the use of infrared absorption in measurements of the N^{15}/N^{14} isotope ratio.

The author wishes to thank E. I. du Pont de Nemours and Company for a Summer Research Grant which has permitted continuation of these studies.

† Presented in part at the June, 1954, Symposium on Molecular Spectroscopy and Molecular Structure, Ohio State University, Columbus, Ohio.

[1] R. W. G. Wyckoff, *Crystal Structures* (Interscience Publishers, Inc., New York, 1948).

[2] Here we neglect the slight perturbation which reduces the "free molecule" symmetry in the aragonite-type lattice, since we are concerned with an out-of-plane mode.

[3] D. F. Eggers, Jr., and B. L. Crawford, Jr., J. Chem. Phys. **19**, 1554 (1951).

The Microwave Spectrum and Molecular Structure of $(CH_3)_3SiF$†

R. C. GUNTON, J. F. OLLOM, AND H. N. REXROAD
Department of Physics, West Virginia University, Morgantown, West Virginia
(Received August 8, 1954)

THE rotational lines of trimethylfluorosilane were observed with a Stark-modulation microwave spectrograph employing a 3-meter x-band absorption cell. An oscilloscope presentation was used. The frequencies of the observed transitions are given in Table I. The lines lie very nearly in a harmonic series characteristic of a symmetric-top rotor and similar to that of $(CH_3)_3SiCl$.[1] In each transition a number of lines were observed which appear to originate from molecules in different vibrational states. The most intense line in each transition is assumed to be due to the ground vibrational state. The separation of the lines in a given transition appears in this molecule to be too great to be explained as a resolution of the K components. The ground vibrational states are nearly equally spaced indicating negligible centrifugal distortion constants. No quadrupole hyperfine structure is possible. A change in isotopic species of the silicon atom has a negligible effect since the latter is very close to the center of mass of the molecule.

TABLE I.

Transition	Frequency in mc/sec
$J=3\rightarrow4$	27 287.8 ±0.3[a]
$J=4\rightarrow5$	34 088.6 ±0.5
	34 094.9 ±0.5
	34 109.8 ±0.3[a]
	34 133.4 ±0.3
	34 148[b]
	34 171[b]
	34 219.0 ±0.5
$J=5\rightarrow6$	40 906.3 ±0.3
	40 913.0 ±0.5
	40 931.6 ±0.3[a]
	40 959.4 ±0.5
	40 977[b]
	41 008[b]
	41 062.5 ±0.5

[a] Ground vibrational state.
[b] Groups of unresolved lines several megacycles wide.

TABLE II. Rotational Constants and structure.

B_0(mc/sec)	I_B($\times10^{40}$ gcm^2)	d_{SiF}
3411.00 ±0.03	245.943	1.55 A

(Assumption in calculating d_{SiF}: $d_{CH}=1.093$ A, $d_{SiC}=1.87$ A and all angles tetrahedral).

The ground state line in each transition is of the order of 2 mc wide, whereas the other lines are at least twice as wide. There appear, as indicated in Table I, groups of several unresolved lines which are about 8 mc wide. Some of this vibrational structure is very likely due to the possible torsional modes of oscillation of the three methyl groups. An attempt will be made to elucidate this structure.

Values of the rotational constants are given in Table II.

† Supported by the Office of Ordnance Research, U. S. Army.
[1] Mockler, Bailey, and Gordy, J. Chem. Phys. **21**, 1710 (1953).

Sodium and Potassium Cation Dependence of the Infrared Absorption of COO^- †

MIRIAM MICHAEL STIMSON
Department of Chemistry, Siena Heights College, Adrian, Michigan
(Received September 10, 1954)

THE examination in solid KBr[1] of a number of benzoic acids and their ammonium, sodium, and potassium salts shows considerable difference in the spectral response to salt formation between the ammonium compounds and the alkali salts. In the former there is only partial loss of the COOH bands although there is also characteristic COO^- absorption, as determined by a comparison with the absorption spectrum of the free acid under the same methods of sample preparation. The data for the ammonium salts will be reported elsewhere.

Sodium benzoate has been reported by Davies and Jones,[2] who have assigned the band at 1411 cm^{-1} (7.09 μ) to the symmetrical COO^- vibration and the band at 1554 cm^{-1} (6.43 μ) to the asymmetric vibration. We have studied the corresponding bands in a number of substituted benzoic acids, and the deformability of the anion by the sodium or potassium cation[3] seems to be indicated by the displacement of these bands as shown in Table I. This deformability is expressed by the separation of the asymmetric and symmetric vibrations and is more pronounced for the potassium salts.

TABLE I.

Compound	COO^- Band Asym. (microns)	COO^- Band Sym. (microns)	Sep'n.	Δ	COO^- Band Asym. (cm^{-1})	COO^- Band Sym. (cm^{-1})	Sep'n.	Δ
Sodium benzoate	6.44	7.08	+0.54	0	1554	1413	−141	+15
Potassium benzoate	6.44	7.16	+0.72	+0.08	1554	1398	−156	
Sodium *m*-aminobenzoate	6.40	7.10	+0.70	−0.02	1563	1410	−153	+3
Potassium *m*-aminobenzoate	6.38	7.14	+0.76	+0.04	1566	1400	−166	−10
Sodium *o*-aminobenzoate	6.55	7.16	+0.51	−0.03	1518	1398	−120	+17
Potassium *o*-aminobenzoate	6.52	7.20	+0.68	+0.04	1535	1390	−145	−8
Sodium *p*-aminobenzoate	6.50	7.12	+0.62	−0.06	1540	1410	−130	+15
Potassium *p*-aminobenzoate	6.44	7.14	+0.70	+0.02	1555	1400	−155	−10

The second regularity is the direction of the displacement of the asymmetric and the symmetric vibration bands. The former is shifted toward shorter wavelengths under the influence of the potassium ion, whereas the symmetric vibration shows a displacement toward longer wavelengths.

Changing the position of the second substituent on the ring shows that the *ortho-* and the *para*-positions are more effective than the *meta*-position in shifting the entire COO^- absorption, and of the two the *ortho*-position is more influential, when the substituent is the NH_2 group. These investigations are being extended to the salts of other organic acids to determine the contribution of adjacent areas of high-electron density on the deformation of anions.

† This work has been supported in part by the Research Corporation and the American Cancer Society upon recommendation of the Committee on Growth of the National Research Council.
[1] M. M. Stimson and M. J. O'Donnell, J. Am. Chem. Soc. **74**, 1805 (1952); U. Scheidt and H. Reinwein, Z. Naturforsch. **76**, 270 (1952).
[2] M. Davies and R. L. Jones, J. Chem. Soc. **1954**, 120.
[3] K. Fajans, *Radioelements and Isotopes: Chemical Forces and Optical Properties* (McGraw-Hill Book Company, Inc., New York, 1931), Chap. IV.

Concerning the Coexistant Phases in the System $NaCl-H_2O$ above 374°C

JAMES FOGO, SIDNEY W. BENSON, AND CHARLES S. COPELAND
Chemistry Department, University of Southern California, Los Angeles 7, California
(Received September 3, 1954)

IN a recent note to the editor of this journal, Corwin and Owen[1] have suggested that the conductivities in the supercritical system $NaCl-H_2O$, recently reported from this laboratory,[2]

represented average values for a two-phase system rather than for a one-phase system as originally proposed by us.

These conclusions of Corwin and Owen seem to be based entirely on impedance measurements made earlier by themselves and Swinnerton.[3] In restricting themselves in this way they seem to have ignored the rather large body of quantitative data on the phase behavior of this two component system[4–7] which in our opinion are quite conclusive in establishing the coexistence region for the two phases. These data, to the extent that they overlap are consistant with each other, represent independent methods of measurement (including direct visual observation on sealed tubes) and show that all of the solutions used in our own conductivity measurements[2] were one-phase systems. (This was stated explicitly in the paper.)

Corwin and Owen have inferred that after agitation of the contents of our cell the conductivities varied in a manner consistant with the separation of two phases. This is a rather surprising inference since we had stated quite explicitly[8] that the maximum variation in conductance between the first and last measurement (at 1000 cps) was about 0.2 percent, hardly indicative of phase separation.

There is, however, a real need for agitation in these systems if one is to obtain reproducibility. Casual observations on our own cells have shown differences in conductance in the range 1–10 percent before and after agitation. That these differences do not arise from phase separation is shown by the fact that we have observed them with pure water above its critical temperature. In our opinion these differences arise from thermal gradients which can produce rather large density gradients near the critical temperature. In fact these effects are always most pronounced in the neighborhood of the critical temperature (and in the region of maximum compressibility above the critical) and decrease as the temperature rises. Finally we have always noted that the changes in conductance produced by agitation are invariably accompanied by a change in pressure, again indicative of the smoothing out of a thermal gradient rather than a phase separation.

[1] J. T. Corwin and G. E. Owen, J. Chem. Phys. **22**, 1257 (1954).
[2] Fogo, Benson, and Copeland, J. Chem. Phys. **22**, 212 (1954).
[3] Swinnerton, Owen, and Corwin, Discussions Faraday Soc. **5**, 172 (1949).
[4] Copeland, Silverman, and Benson, J. Chem. Phys. **21**, 12 (1953).
[5] A. Olander and H. Liander, Acta Chem. Scand. **4**, 1437 (1950).
[6] E. Schroer, Z. physik Chemie **129**, 79 (1927).
[7] F. G. Straub, University of Illinois, Bull. **43**, 59 (1946).
[8] Reference 2, Page 213, column 2.

Matrix Isolation Method for the Experimental Study of Unstable Species

ERIC WHITTLE,* DAVID A. DOWS,† AND GEORGE C. PIMENTEL
Department of Chemistry and Chemical Engineering, University of California, Berkeley, California
(Received September 7, 1954)

IN the study of free radicals and other unstable substances, an inherent difficulty is the maintenance of a suitable concentration. The matrix isolation method proposed here involves accumulation of a reactive substance under environmental conditions which prevent reaction. The intent of the method is to trap active molecules in a solid matrix of inert material, crystalline or glassy. If the temperature is sufficiently low, the matrix will inhibit diffusion of the trapped molecules, thus holding the active molecules effectively immobile in a nonreactive environment.

The active material can be produced in a variety of ways: by chemical reaction involving two reactants, by pyrolysis, by dissociation in a glow discharge or an arc, or by photolysis. Only the last permits forming the active molecules *after* the trapping process has been carried out.[1] Otherwise it is necessary to produce the active material and to trap it in the matrix shortly thereafter. This can be accomplished by spraying a gas mixture of the matrix and the active species onto a surface cold enough to condense the matrix immediately. If the mole ratio of matrix to active substance, hereafter called M/A is sufficiently large the matrix will isolate trapped molecules and prevent recombination reactions.

TABLE I. Tests of the matrix isolation method.

M Matrix	A Active species	Temperature	M/A	Success of isolation
Xe	NH_3	66°K	82	No
Xe	HN_3	66°K	100	No
CO_2	HN_3	85°K	70	Partial
CO_2	NH_4N_3	85°K	70	Partial
CCl_4	HN_3	85°K	100	Yes
		85°K	40	No
Methylcyclohexane	NO_2	115°K	100	Yes
		115°K	50	No

Several experimental tests of the method have been performed. One experiment indicated that the trapping process can occur even when the trapped material would not condense without the matrix. A mixture of carbon tetrachloride (the matrix) and methane was prepared with $M/A=50$. At a pressure below ten microns the mixture was condensed on a silver chloride window at 72°K. The infrared spectrum of the resulting solid film showed that a large fraction of the methane was trapped even though the vapor pressure of methane at this temperature is several millimeters.

Experiments testing the effectiveness of the matrix in preventing reactions were conducted using several matrix materials. The active materials were either NO_2 or one of the hydrogen bonding materials NH_3, HN_3, or NH_4N_3. The $2NO_2=N_2O_4$ equilibrium involves an easily accessible free radical, NO_2, and both NO_2 and N_2O_4 have well-known infrared spectra. Reaction of the other materials is detected by the spectral shift of bands accompanying hydrogen bond formation. Table I indicates the experiments performed and the success of isolation as indicated by the infrared spectra of the trapped materials. The isolation was considered to be successful if the spectrum showed the presence of NO_2 or, for NH_3, HN_3, and NH_4N_3, the absence of hydrogen bonding.

Xenon is not effective as an isolating matrix at 66°K. (Preliminary experiments using xenon as a matrix at 29°K indicate that it is effective at this temperature.) The experiments indicate that the ratio M/A should be 100 or greater.

The technique has been applied to the study of unstable products of the glow discharge decomposition of hydrazoic acid, and the low temperature spectral techniques and equipment will be described there.[2] It is apparent that conditions can be found for each of the matrices CO_2, CCl_4, and methylcyclohexane (and probably also for xenon) for which the method is successful. Hence the matrix isolation technique should be useful in spectral, magnetic or dielectric studies of free radicals, reaction intermediates and other unstable species.

* Present address: Chemistry Department, University College, Cardiff, Great Britain.
† Present address: Chemistry Department, Cornell University, Ithaca, New York.
[1] Lewis *et al.* utilized glassy matrices to study suspended materials produced by photolysis or photoexcitation. Lewis, Lipkin, and Magel proposed that the absorption of light by the suspended material may result in the production of radicals, but their interest lay with the products of photoexcitation [see J. Am. Chem. Soc. **63**, 3005 (1941)].
[2] Dows, Whittle, and Pimentel (to be published).

Polymorphism in Solution of *cis*- and *trans*-β-Methoxy-*p*-Nitrochalcone

YOSHIYUKI URUSHIBARA, FUJIRO IIMURA, AND KENRO IKEDA
Department of Chemistry, The University of Tokyo, Bunkyo-ku, Tokyo
(Received August 27, 1954)

SEVERAL studies[1,2] have been reported on the polymorphism of chalcone derivatives. However, only a few recent works[3,4] referred to their absorption spectra. By uv spectral study, Eistert and his co-workers[3] found that the stable β-methoxy-chalcone

melting at 65° was a *cis*-form* in solution, while other two labile polymorphs melting at 78° and 81°, respectively, were the same *trans*-form with no distinction in their spectra. A systematic study[5] of various nitrosubstituted chalcones showed that the uv spectra of these compounds were better interpreted by assuming the contribution of the following resonance forms:

trans-form

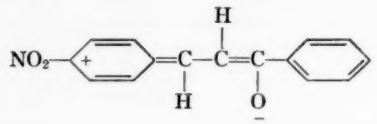

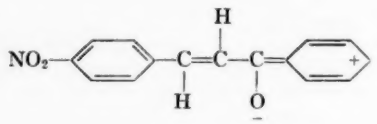

cis-form

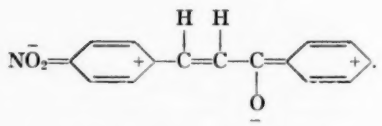

A β methoxy or a β-hydroxyl group has to do almost nothing with the absorption spectra of *trans*-form as shown by several researches.[6] Lutz *et al.*[7,8] discussed the configuration of *cis*-chalcone and related compounds from their uv spectra and steric inhibition of coplanarity of π-electron system in the *cis*-form.

In our studies on β-methoxy-*p*-nitrochalcone, the maxima of absorption of all polymorphs were found at the expected places, i.e., at 310–320 mμ in the *trans*-forms and at 260–270 mμ in the *cis*-forms.

By systematic precipitation and recrystallization from various solvents, ten crystalline varieties of *cis*-forms were obtained which gave five different uv absorption spectra in heptane showing the existence of five species in solution (see Table I). No other intense absorption than those with maxima at 250–270 mμ were observed in long wavelengths, and all these species are regarded as *cis*-forms. Five *trans*-forms could be prepared by irradiation of *cis*-forms in either solution followed by separation by making use of the differences in solubilities. They showed expected absorption in long wavelengths (see Table I). From the results of our spectral investigations, it followed that β-methoxy-*p*-nitrochalcone is able to exist in several quasi-stable constellations retained even in solution.

Furthermore, we have obtained several evidences indicating that these polymorphs exist as monomers in solution. Namely, (i) absorption spectra of each species in three different solvents generally show the same features including ordinary solvent effect; (ii) the similarity in solubilities is observed in all the species; and (iii) on irradiation, solutions of respective species undergo stepwise transition through two relatively stable states, finally turning to one and the same equilibrium mixture, and merely being left in a dark place for a long time in heptane solution or being dissolved in polar solvents such as chloroform or alcohol, some of the groups giving different spectra in heptane gave the same spectra as shown in the table. Groups giving the same spectra in chloroform are not the same as such in alcohol.

The possibility of existence of different constellations in polymorphic *cis*-cinnamic acid and chalcone was discussed by Guy,[9] who measured the ir and Raman spectra of these compounds in the solid state. However, the activation energy of transition between two eventual states being very low, most of the polymorphic species could not retain their original constellations in solution.

Our results, however, indicate that there is some particular region between chemical isomerism (*cis-trans* isomerism) and physical polymorphism (mode of crystal formation), where π-electron system combined with steric restriction produces some stable "Hindered-rotational isomers in solution." This, in turn, gives an evidence for the existence of rotational isomers in polymorphic crystals.

If resonance energy of π electron alone is insufficient to retain the configuration in solution, the suggestion by Eistert[10] of the possible configurations of polymorphic chalcone in the solid state may be extended to an assumption of specific affinities between two parts of a molecule in contact.

A comparison by x-ray analyses of the species giving the same spectra is now in progress.

TABLE I. Polymorphism and ultraviolet absorption spectra of β-methoxy-*p*-nitrochalcone.

	M.p. °C[a]	λmax (mμ) in *n*-heptane	Stability in heptane	λmax (mμ) in alcohol	λmax (mμ) in $CHCl_3$	Stability in $CHCl_3$
	57–60	245(1.45)[c]	rather stable	249(1.60)	252(1.60)	
	88					
	55–58	251(1.45)		260(1.70)		equilib. p.t. 263(1.60)
	67–69					
cis-form	76–79[b]				260(1.70)	
	78–81	255(1.65)	most stable (*ca* equilib. p.t.)	265(1.60)		
	89.5–90.5[b]					
	97[b]					
	117–120	260(1.80)				
	132–135	264(1.80)			266.5(1.60)	rather stable
	78–81	difficultly soluble		252(1.70)		
	125–128			325(1.00)		
	65.5–67	255(1.40)		262(1.40)		
		308(1.30)		313(1.30)		
trans-form	107–110	262(1.70)		267(1.40)		
		311(1.30)		316(1.20)		
	70–72	difficultly soluble		320(1.30)		

[a] Unsharp M.p. of some species may be ascribed to the increased velocity of transition at elevated temperatures.
[b] Confirmed to be a pure polymorph, and not a mixture by x-ray analyses.
[c] In brackets: molecular extinction coefficient $\times 10^{-4}$.

[1] C. Weygand, Lieb. Ann. **472**, 143 (1929).
[2] C. Weygand, Ber. deut. chem. Ges. **62**, 2603 (1929).
[3] Eistert, Weygand, and Csendes, Ber. deut. chem. Ges. **84**, 745 (1951); and private communications from Dr. B. Eistert.
[4] B. Eistert and E. Merkel, Ber. deut. chem. Ges. **86**, 895 (1953).

* We call 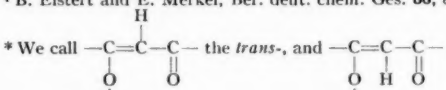 the *trans*-, and the *cis*-form.

[5] F. Iimura, (to be published).
[6] L. N. Ferguson and R. P. Barnes, J. Am. Chem. Soc. **70**, 3907 (1948).
[7] R. E. Lutz and R. H. Jordan, J. Am. Chem. Soc. **72**, 4090 (1950).
[8] Kuhn, Lutz, and Bauer, J. Am. Chem. Soc. **72**, 5063 (1950).
[9] J. Guy, Ann. Phys., (12) **4**, 704 (1949).
[10] Eistert, Weygand, and Csendes, Ber. deut. chem. Ges. **85**, 164 (1952).

Pure Quadrupole Spectra of Metal Bromates

KENJI SHIMOMURA, TOSHIMOTO KUSHIDA, AND NORIYOSHI INOUE,
Department of Physics, Hiroshima University, Hiroshima, Japan
AND
YOSHIRO IMAEDA, *Faculty of Technology, Tokushima University, Tokushima, Japan*

(Received July 9, 1954)

PURE quadrupole spectral lines of bromine in some alkali and alkaline earth metal bromates and silver bromate were reported in our previous papers.[1,2] The purpose of this note is to extend these previous data to other metal bromates and to suggest a general trend of the behavior of the spectra through this series of compounds. In our experiments a frequency-modulated superregenerative detector was used and the absorption lines were viewed on an oscilloscope. The observed resonance frequencies together with our previous data are summarized in Table I.

TABLE I. Pure quadrupole lines of Br^{79} in metal bromates.

Compound	Frequency mc/sec (room temp.)	Frequency mc/sec (dry ice temp.)
$LiBrO_3$	184.12[a,b] (20°C)	
$NaBrO_3$	178.95[a,b] (20°C)	180.01
$KBrO_3$	173.11[a,b] (20°C)	175.86
$Cu(BrO_3)_2 6H_2O$	175.70 (12°C)	177.48
$AgBrO_3$	168.19[a] (20°C)	169.51
$Mg(BrO_3)_2 nH_2O$	176.60[b] (12°C)	178.70
$Ca(BrO_3)_2 H_2O$	176.85[a,b] (20°C)	
$Zn(BrO_3)_2 6H_2O$	177.38 (12°C)	179.49
$Sr(BrO_3)_2 H_2O$	175.25[a,b] (20°C)	
$Cd(BrO_3)_2 H_2O$	174.71 (17°C)	176.25
$Ba(BrO_3)_2 H_2O$	173.69[a,b] (20°C)	174.92
$Hg(BrO_3)_2$	172.62 (12°C)	174.44
	170.78 (12°C)	
$HgBrO_3$	168.91 (12°C)	
$Pb(BrO_3)_2 H_2O$	174.30 (12°C)	
$Co(BrO_3)_2 6H_2O$	176.92 (17°C)	179.10
$Ni(BrO_3)_2 6H_2O$	177.62 (17°C)	179.51

[a] Reference 1.
[b] Reference 2.

The resonance frequencies are found to be distributed regularly with the kind of metal ions involved in a range from about 185 mc/sec to 165 mc/sec in spite of the possible variety of their crystal structures; the compounds that involve the metal ions belonging to the same group in the periodic table have resonance frequencies which vary regularly with the positions of the metals in the periodic table. This trend indicates that the electronic structure of bromine is affected by the metal ion involved. The bromine, after having given its two $4p$ electrons to the oxygens, forms pyramidal covalent bondings with the three oxygens which have accepted two electrons from the bromine and one electron from the metal. So its structure can be described as[3]

$$\begin{array}{c} O^- \\ | \\ Br^{++}-O^- \quad M^+. \\ | \\ O^- \end{array}$$

Now from the electronegativity values of $x_{Br}=2.8$ and $x_O=3.5$[3] we may conclude that the electronegativity difference of Br^{++} and O^- is very small, after the correction is made of the effect of the formal charge. And so the ionicity of the $Br^{++}-O^-$ bond may be neglected. Of course, some double-bond structure may resonate with this structure, and this double-bond-structure percentage may vary with the kind of metal ions.

The fact that the metal ion keeps away from the positive bromine ion and gets nearer to the negative oxygen ions (for example, in the case of $NaBrO_3$, $Na-Br \simeq 4.1$ A° and $Na-O \simeq 2.38$ A°)[4] is consistent with the electronic structure afore-mentioned. Since the single-covalent radii of Br and O are 1.14 A° and 0.66 A°,[3] respectively, the single-bond distance of Br—O is 1.78 A°, after the correction for the formal charges on the bromine and oxygen is made. In $KBrO_3$, and perhaps in the other bromates, the Br—O bond distance is smaller than 1.78 A°,[4] and the double-bond structure may be mixed in a small amount in these cases.

On the other hand, as the Br—O bond distance is 1.78 A° in $NaBrO_3$,[4] the bond is considered to be nearly pure single one and its electronic structure can be almost accurately described as the afore-mentioned form. The rather large observed coupling of Br reveals that the Br bonding orbitals are not pure p but have significant s character, since three pure p bonds would lead to a vanishing field gradient q.[5] Then the number of unbalanced p electrons U_p is:[6]

$$U_p=\frac{\text{molecular } eqQ}{2\times\text{atomic } eqQ}=-3\alpha,$$

where α represents the percent s character of this bonding orbital. With the value of the atomic eqQ obtained from the atomic-beam measurement and our data, one obtains $\alpha=0.15$ in $NaBrO_3$. The O—Br—O bond angle calculated from this value of α, 0.15, is 101°. This value is fairly smaller than the crystallographic value of 112°.[4]

In $KBrO_3$ and perhaps in the other bromates, the contribution of double-bond nature, namely, pd hybridization, may be significant, since it will decrease the coupling and reduce both the Br—O bond distance and the O—Br—O bond angle. But the possible contribution of the double-bond structure makes the estimate of α from the nuclear quadrupole coupling data considerably uncertain in the other bromates.

[1] Shimomura, Kushida, Inoue, and Imaeda, J. Chem. Phys. **22**, 350 (1954).
[2] K. Shimomura, J. Sci. Hiroshima Univ., Ser. A **17**, 383 (1954).
[3] L. Pauling, *The Nature of the Chemical Bond* (Cornell University Press, Ithaca, 1939).
[4] R. W. G. Wyckoff, *Crystal Structures* (Interscience Publishers, Inc., New York, 1948–1952), Vols. I and II.
[5] Robinson, Dehmelt, and Gordy, Phys. Rev. **89**, 1305 (1953).
[6] Gordy, Smith, and Trambarulo, *Microwave Spectroscopy* (John Wiley and Sons, Inc., New York, 1953), p. 281.

Raman Spectra of 2- and 3-Fluoropyridine

HAROLD P. STEPHENSON, *Department of Physics, Illinois Wesleyan University, Bloomington, Illinois*
AND
FRED L. VOELZ, *Spectroscopy Laboratory,* Department of Physics, Illinois Institute of Technology, Chicago 16, Illinois*
(Received September 13, 1954)

THE near-ultraviolet absorption spectra of 2- and 3-fluoropyridine (*ortho*- and *meta*-monofluoropyridine), in the vapor state were photographed some time ago by one of the authors.[1] Since a thorough analysis of these spectra has been hampered by the lack of infrared and Raman data in the literature, it was thought worthwhile to commence a program of research to obtain such data. The Raman spectra of these two substances in the liquid state have so far been obtained and are reported upon here.

The samples of 2- and 3-fluoropyridine were the same ones used in the earlier research,[1,2] and were believed to be of high purity. They were very kindly given to us by Dr. Arthur Roe of the Chemistry Department of the University of North Carolina. The physical properties of comparable samples made in the same laboratory have been described elsewhere.[3] For the past three years each of the samples has been kept in a vacuum-tight breakseal, and for the purposes of this research each compound was freshly distilled into a new breakseal attached to the sidearm of the Raman tube. Both samples appeared completely clear after this single distillation and have remained clear throughout this investigation.

The spectrograms were obtained on a Hilger E-612 spectrograph employing both the high dispersion camera (E-614) and the high-speed camera (E-613) by means of previously described techniques.[4] Excitation was by the Hg 4358 A line and the samples were at 30°C. Eastman type 103-J spectroscopic plates were used throughout with exposure times varying from 5 minutes up to 16 hours. A special small Raman tube of 0.4-ml capacity was used, with a plane mirror at the back end (outside the Raman tube) to increase the amount of scattered light. Of the two substances, the 3-fluoropyridine seemed to be somewhat the better scatterer.

The $\Delta\sigma$ and relative-intensity values for all the observed bands are tabulated in Table I. All of the $\Delta\sigma$ values were checked by using microphotometer (Leeds and Northrup) tracings of the plates. The intensity measurements were made with a calibrated Gaertner microdensitometer (visual reading). In each case the relative intensities have been given in relation to the strong frequency in the vicinity of 3070 K. In general the strong bands observed in high dispersion were rather sharp, whereas weak bands observed only with the high-speed camera were quite diffuse. For 2-fluoropyridine the bands at 556, 828, and 996 K were particularly sharp; correspondingly sharp bands for 3-fluoropyridine were those at 535, 818, and 1038 K, although nearly all the bands of 3-fluoropyridine appeared sharper than the 2-fluoropyridine bands.

TABLE I. Raman spectral data for liquid 2- and 3-fluoropyridine.

2-Fluoropyridine		3-Fluoropyridine	
$\Delta\sigma$,K	I	$\Delta\sigma$,K	I
230	4	244	6
556	1	(410)	vw
622	w	499	w
686	vw	535	2
(725)[a]	vw	616	1
(771)	vw	(702)	vw
828	2	(757)	vw
841	2	818	7
996	7	834	1
1045	3	(982)	vw
1099	1	1023	1
1146	vw	1038	33
1249	2	1095	w
1303	w	1187	1
1580	w	1225	2
1598	1	1247	1
(1881)	w	(1308)	vw
3074 (3094)[b]	10	(1425)	vw
		1480	w
		1584	1
		1594	1
		3003	w
		(3058)[c]	8
		(3069)	10

[a] Uncertain values are enclosed in parentheses.
[b] Observed as shoulder on microphotometer tracing.
[c] Not well defined due to mercury line at 3048 K.

This investigation was part of a research program which has been aided by a contract with the Office of Ordnance Research (Army) and by grants from the Research Corporation, the Socony-Vacuum Laboratories, and the American Academy of Arts and Sciences. The authors are grateful for this assistance. We would also like to thank Dr. Forrest F. Cleveland for his encouragement during the course of this research.

* Publication No. 111.
[1] Harold P. Stephenson, Phys. Rev. **87**, 213(A) (1952).
[2] Harold P. Stephenson, J. Chem. Phys. **22**, 1077 (1954).
[3] Miller, Knight, and Roe, J. Am. Chem. Soc. **72**, 1629 (1950).
[4] Forrest F. Cleveland, J. Chem. Phys. **11**, 1 (1943).

Intermolecular Coupling of the Out-of-Plane Bending Mode in Several Carbonates

J. C. DECIUS
Department of Chemistry, Oregon State College, Corvallis, Oregon
(Received September 7, 1954)

IN a recent communication[1] we have drawn attention to the fine structure of the out-of-plane bending mode of the nitrate ion in KNO_3 containing equal concentrations of the N^{14} and N^{15} isotopes. The present letter deals with similar phenomena in certain carbonates whose lattices are of the aragonite type.

Nujol mulls of $CaCO_3$, $SrCO_3$, and $BaCO_3$ were carefully ground between rocksalt windows whose inner faces had been left unpolished after grinding with 600 wet or dry paper. All visible traces of particles could thus be removed, yielding a transparent film with a yellow-orange cast, indicative of uniformly small particle size. With this technique it was possible to prepare samples with less than 10 percent transmission at the absorption peak and more than 90 percent transmission within about 6 cm^{-1} of the center of the band.

Table I presents the absorption peaks for C^{12} and C^{13} (the latter at the natural abundance of 1.1 percent). The final column gives the C^{13} frequency calculated from the observed C^{12} frequency neglecting any coupling with lattice modes. It will be noted that such a calculation is in excellent agreement with observation in the case of calcite, but that significant discrepancies occur for aragonite and the similar strontium and barium carbonates.

TABLE I. Out-of-plane bending mode in several carbonates (cm^{-1}).

	C^{12}(obs.)	C^{13}(obs.)	C^{13}(calc.)
Ca (aragonite)	861.0	845.2	834.0
Sr	858.1	842.1	831.2
Ba	857.3	840.5	830.4
Ca (calcite)	877.7	850.0	850.2

If a coupling constant is introduced into the potential energy for each pair of nearest neighbor carbonate ions, connecting their out-of-plane vibrations, the following expressions may be obtained for the extreme cases of a homogeneous C^{12} lattice and for the frequency of an isolated C^{13} carbonate ion, surrounded by C^{12}.

(i) Homogeneous C^{12} case:

$$\lambda = 4\pi^2 c^2 \omega^2 = (3\mu_{C12} + \mu_0)(F + 2F'), \tag{1}$$

(ii) Isolated C^{13} case:

$$\lambda = (3\mu_{C13} + \mu_0)(F + 2F'\rho), \tag{2}$$

where

$$\rho = \left(\frac{F'}{F}\right)\left[\frac{3\mu_{C12} + \mu_0}{3(\mu_{C13} - \mu_{C12})}\right].$$

In these equations the μ's are the reciprocals of the masses of the atoms, F is the principal force constant for bending of a single carbonate ion, and F' is the interaction or coupling constant. Unlike the case of deuterium substitution discussed by Hrostowski and Pimentel[2] and by Hiebert and Hornig,[3] the present case of isotopic substitution does not give rise to complete uncoupling of the isolated atom, since the percent mass change is small. Hence we have the term involving ρ in (2), which is the result of a second-order perturbation treatment.

TABLE II. Force constants for crystalline carbonates (md/A).

	F	F'
Ca (aragonite)	1.4513	−0.0270
Sr	1.4394	−0.0259
Ba	1.4305	−0.0226
Ca (calcite)	1.4513	+0.0003

Table II presents the values of the two potential energy parameters.

There is close agreement between the principal force constants for the two forms of $CaCO_3$, after allowing for the coupling constant which occurs in aragonite, but not in calcite (although the constants are reported to four places, they are probably only significant to the third). The negative sign, and increase in magnitude of the coupling constant for the sequence Ba, Sr, Ca is qualitatively in agreement with the hypothesis of a dipole-dipole coupling.

Finally, we remark that the parameters of Table II appear to be capable of accounting for the absorption band contours at enriched C^{13} concentrations, where we have apparently resolved the frequencies of pairs and triplets of carbon atoms of one mass, surrounded by those of the other.

The author is gratified to acknowledge the assistance rendered by E. I. du Pont de Nemours and Company in the form of a Summer Research Grant which made possible these studies.

[1] J. C. Decius, J. Chem. Phys. **22** (to be published).
[2] H. J. Hrostowski and G. C. Pimentel, J. Chem. Phys. **19**, 661 (1951).
[3] G. L. Hiebert and D. F. Hornig, J. Chem. Phys. **20**, 918 (1952).

The Activation Energy for Viscous Flow and Sutherland's Constant

C. J. G. RAW
Department of Chemistry and Chemical Technology, University of Natal, Pietermaritzburg, South Africa
(Received August 23, 1954)

IN two recent communications,[1,2] the author has proposed two approximate relations:

$$\epsilon/k \approx 0.88C,$$

and

$$\Delta E_{vis} \approx 4.5\epsilon/k \text{ cal mole}^{-1},$$

TABLE I. Experimental values of $\Delta E_{vis}/C$.

Gas:	A	N_2	O_2	CO	CH_4	C_2H_4
C:	142	104	125	101.2	164	241
ΔE_{vis}:	516	449	398	466	719	793
$\Delta E_{vis}/C$:	3.63	4.32	3.18	4.60	4.38	3.29

where C is Sutherland's constant (from the temperature dependence of the gas viscosity), ΔE_{vis} is the activation energy for viscous flow (from the temperature dependence of the liquid viscosity), ϵ is the maximum energy of attraction between two molecules each of which has an intermolecular force field described by the Lennard-Jones (12–6) potential, and k is Boltzmann's constant. These two approximations are useful for rough estimates, but are restricted to substances with simple, nonpolar, symmetrical molecules whose intermolecular potentials are well represented by the Lennard-Jones (12–6) model, and which condense to normal liquids. The following work is also restricted in application to such substances.

Eliminating ϵ/k between the two relations given above,

$$(\Delta E_{vis}/C) \approx 4. \quad (1)$$

Experimental values of the ratio of the activation energy to Sutherland's constant are given in Table I. The values of Sutherland's constants in degrees Absolute are from Partington,[3] and the values of the activation energy for viscous flow in cal mole^{-1} are those quoted by Ewell and Eyring.[4]

The ratio is seen to be approximately four for the type of molecule to which this theory is applicable. Equation (1) should prove useful for rough estimates.

Vogel[5] has shown that

$$C = 1.47 T_b,$$

where T_b is the normal boiling point. This relation in conjunction with Eq. (1) gives an expression for the activation energy for viscous flow in terms of the boiling point:

$$\Delta E_{vis} \approx 5.88 T_b. \quad (2)$$

The free energy of activation for viscous flow ($\Delta G\ddagger$) has been expressed[6] in terms of T_b as follows:

$$\Delta G\ddagger \approx 9.4 R T_b/2.45 \approx 7.6 T_b. \quad (3)$$

From (2) and (3),

$$\Delta G\ddagger/\Delta E_{vis} \approx 7.6/5.88.$$

Also:[7]

$$\Delta G\ddagger = \Delta U_{vap}/2.45 \quad \text{and} \quad \Delta E_{vis} = \Delta U_{vap}/n,$$

where ΔU_{vap} is the energy of vaporization and n is a constant which varies between 3 and 4 for most substances, and thus

$$\Delta G\ddagger/\Delta E_{vis} \approx n/2.45.$$

From these two expressions for the ratio of the free energy of activation to the activation energy for viscous flow, n is 3.17, which is certainly close to the value of n for the simple substances to which this work is applicable.

[1] C. J. G. Raw, J. S. African Chem. Inst. (to be published).
[2] C. J. G. Raw, J. Chem. Phys. (to be published).
[3] Partington, *An Advanced Treatise on Physical Chemistry*, (Longmans, Green and Company, New York, 1949), Vol. 1, pp. 858–861 (1949).
[4] R. H. Ewell and H. Eyring, J. Chem. Phys. **5**, 726 (1937).
[5] Vogel, Ann. Phys. **43**, 1235 (1914).
[6] Hirschfelder, Curtiss, and Bird, *Molecular Theory of Gases and Liquids* (John Wiley and Sons, Inc., New York, 1954), pp. 628–629.
[7] Glasstone, Laidler, and Eyring, *The Theory of Rate Processes* (McGraw-Hill Book Company, Inc., New York, 1941), pp. 492–493.

Decomposition in Liquid Scintillation Systems

C. REID
Department of Chemistry, The University of British Columbia, Vancouver, Canada
(Received July 22, 1954)

BURTON and Patrick[1] observe that the increased quantum yield of fluorescence above that of benzene alone, found when benzene containing anthracene or terphenyl is irradiated, is not accompanied by a decrease in the amount of chemical decomposition of the benzene. The authors speculate on two possible reasons for this state of affairs. The following considerations are relevant in this connection. For the state represented by A^*+B to make real transition to $A+B^*$, the two states must be degenerate. In the case under consideration the requirement for this is that the energy available as emission from A must be matched by an absorption process in B requiring the same energy. If we consider a highly excited benzene molecule such absorption process may occur equally well in benzene or in the added aromatic. Accordingly the latter will not be an especially good trap at such high energies and further, when a high-energy quantum does reach a polycyclic molecule the latter may equally well hand it back to benzene.

The situation is different when we reach the lowest excited state of benzene. Since there is little overlap between the absorption and emission spectra of this molecule the energy available in emission cannot appreciably be absorbed by other benzene molecules. The added polycyclic provides suitably matching absorption energies, however, and acts as a trap since the quantum is now too small for retransfer to benzene.

It follows that only after the energy of the benzene molecule has fallen well below the level likely to result in decomposition does the polycyclic trap become efficient. Consequently the fluorescence process in no way competes with chemical decomposition and Burton and Patrick's results are exactly what is to be expected.

[1] Burton, Milton, and Patrick, J. Chem. Phys. **22**, 1150 (1954).

Heat of Formation of NH(g) and the Bond Dissociation Energy D(NH−H)

AUBREY P. ALTSHULLER
2715 East 116th Street, Cleveland 20, Ohio
(Received September 7, 1954)

SUFFICIENT data are now available to complete the set of bond dissociation energies, $D(NH_2-H)$, $D(NH-H)$, $D(N-H)$, and the heats of formation of $NH_3(g)$, $NH_2(g)$, and $NH(g)$ by the evaluation of $\Delta H_f(NH,g)$ and $D(NH-H)$.

An activation energy of 60(±2) kcal/mole has been determined for the homogeneous decomposition of $N_2H_4(g)$ into NH_2 radicals.[1] By combining this value with a $\Delta H_f(N_2H_4,g)$ of 22.75 kcal/mole[2] one obtains $\Delta H_f(NH_2,g) = 41(\pm 2)$ kcal/mole, and consequently, $D(NH_2-H)$ equals 104(±2) kcal/mole.[3]

A bond dissociation energy for N−H of 3.8 ev or 88(±2–4) kcal/mole has been obtained spectroscopically.[4] From $D(N-H)$, $\Delta H_f(N,g)$ and $\Delta H_f(H,g)$, the heat of formation of NH(g) can be calculated. Unfortunately, the heat of dissociation of $N_2(g)$ has been a subject of considerable controversy for a number of years.[5] However, recent work on the near ultraviolet bands of N_2^+,[6,7] the spectra of C_2N_2 flames,[8] the detonation velocities of $C_2N_2+O_2$ mixtures,[9,10] and the dissociation of N_2 on hot W filaments,[11] all give support to the value of 9.764 ev or 225.1 kcal/mole. Certain earlier spectroscopic evidence also supports the above value.[5,12] Thus if a value for $\Delta H_f(N,g)$ of 112.6 kcal/mole is used along with $D(N-H)$ of 88(±2–4) kcal/mole and $\Delta H_f(H,g)$ of 52.1 kcal/mole,[13] then $\Delta H_f(NH,g)$ is equal to 77(±2–4) kcal/mole. Using $\Delta H_f(NH,g)$ of 41(±2) kcal/mole, $\Delta H_f(NH,g)$ of 77(±2–4) kcal/mole and $\Delta H_f(H,g)$ of 52.1 kcal/mole, one can calculate a value of 88(±4) kcal/mole for $D(NH-H)$. The value of the bond dissociation energies $D(NH_2-H)$, $D(NH-H)$, $D(N-H)$ and $\Delta H_f(NH_3,g)$, $\Delta H_f(NH_2,g)$ and $\Delta H_f(NH,g)$ are listed in Table I.

If the higher heat of dissociation of N_2 of 11.8 ev or 272 kcal/mole which has been suggested[14] is used, then $D(NH-H)$ would be 111 kcal/mole. Since the dissociation energies for methane[15] are $D(CH_3-H) = 102(\pm 1)$ kcal/mole,[3] $D(CH_2-H) = 85$–95 kcal/mole,[16–18] $D(CH-H) = 80$–90 kcal/mole,[16–18] $D(C-H) = 80$ kcal/mole;[5] for H_2O are $D(HO-H) = 118(\pm 1)$ kcal/mole and $D(O-H)$

TABLE I. Bond dissociation energies and heats of formation of some nitrogen hydrides.

Molecule	$D(NH_n-H)$, kcal/mole	$\Delta H_f(NH_n)$, kcal/mole
NH_2-H	$104(\pm 2)$[a]	-11.04[c]
$NH-H$	$88(\pm 4)$	$41(\pm 2)$[a]
$N-H$	$88(\pm 2-4)$[b]	$77(\pm 2-4)$

[a] See reference 3.
[b] See reference 4.
[c] See reference 13.

$=101(\pm 1)$ kcal/mole;[19] and for H_2S are $D(HS-H)\cong 91$ kcal/mole and $D(S-H)\cong 84$ kcal/mole,[20] it seems improbable that $D(NH-H)$ would be greater than $D(NH_2-H)$. If the lower value for $D(N_2)$ of 7.383 ev or 170.3 kcal/mole most frequently proposed in the past[5] were used, then $D(NH-H)$ would equal 60 kcal/mole. It seems unlikely that $D(NH-H) \ll D(NH_2-H)$ and $D(N-H)$, since $D(CH_3-H) > D(CH_2-H) \geq D(CH-H) \geq D(C-H)$. Furthermore, since $D(CH_3-H)-D(CH_2-H)=10$–15 kcal/mole,[15] $D(HO-H)-D(O-H)=17$ kcal/mole and $D(HS-H)-D(S-H) \cong 7$ kcal/mole, as large a difference as $D(NH_2-H)-D(NH-H) \cong 42$ kcal/mole seems unlikely also. Thus a $D(NH-H)$ of 88 kcal/mole seems the most probable value as does a $D(N_2)$ of 225 kcal/mole.

[1] M. Szwarc, Proc. Roy. Soc. (London) **A198**, 267 (1949).
[2] Scott, Oliver, Gross, Hubbard, and Huffman, J. Am. Chem. Soc. **71**, 2293 (1949).
[3] M. Szwarc, Chem. Rev. **47**, 75 (1950).
[4] G. Pannetier and A. G. Gaydon, J. chim. phys. **48**, 221 (1951).
[5] A. G. Gaydon, *Dissociation Energies and Spectra of Diatomic Molecules* (John Wiley and Sons, Inc., New York, 1947).
[6] A. E. Douglas, Can. J. Phys. **30**, 302 (1952).
[7] A. E. Douglas, Abstracts of New York Meeting of the American Chemical Society, (September, 1954).
[8] Thomas, Gaydon, and Brewer, J. Chem. Phys. **20**, 369 (1952).
[9] Kistiakowsky, Knight, and Malin, J. Am. Chem. Soc. **73**, 2972 (1951).
[10] Kistiakowsky, Knight, and Malin, J. Chem. Phys. **20**, 876 (1952).
[11] M. Farber and J. Darnell, J. Chem. Phys. **21**, 172 (1953).
[12] For other views as to the value of $D(N_2)$, see reference 5 and G. Glocker, "Bond Energies and Bond Distances," Annual Rev. Phys. Chem. Vol. 3, Annual Reviews, Inc., Stanford, California, (1952).
[13] F. D. Rossini, *et al.* "Selected Values of Chemical Thermodynamic Properties," Natl. Bur. Standards Circular 500 (1952).
[14] G. Glocker, J. Chem. Phys. **18**, 1518 (1950).
[15] For alternate sets of bond dissociation energies for CH_n-H see G. Glocker, Discussions Faraday Soc. **10**, 26 (1951).
[16] H. H. Voge, J. Chem. Phys. **4**, 581 (1936); **16**, 984 (1948).
[17] C. A. McDowell and J. W. Warren, Discussions Faraday Soc. **10**, 53 (1951).
[18] H. Branon and C. Smight, J. Am. Chem. Soc. **75**, 4133 (1953).
[19] R. J. Dwyer and O. Oldberg, J. Chem. Phys. **12**, 351 (1944).
[20] A. H. Schon, J. Am. Chem. Soc. **74**, 4722 (1952).

Benzyl-Hydrogen Bond Dissociation Energy*

J. B. FARMER,† I. H. S. HENDERSON,‡ C. A. MCDOWELL,‡ AND F. P. LOSSING

Division of Pure Chemistry, National Research Council, Ottawa, Canada

(Received July 7, 1954)

IN a recent publication, Schissler and Stevenson[1] have obtained a value for $D(C_6H_5CH_2-H)=77\pm 3$ kcal/mole from the appearance potentials of the $C_7H_7^+$ ion from toluene, ethylbenzene, and dibenzyl. This result is in good agreement with the dissociation energy obtained by Szwarc[2] from measurements of the rate of pyrolysis of toluene.

The data cited by Schissler and Stevenson also enable one to calculate the ionization potential of the benzyl radical. From the appearance potentials of $C_7H_7^+$ (presumably, $C_6H_5CH_2^+$), from toluene, $A_1(C_7H_7^+)=11.85\pm 0.1$ ev, and from dibenzyl, $A_2(C_7H_7^+)=10.53\pm 0.1$ ev, and from the heats of formation of toluene (+11.95 kcal/mole), of dibenzyl (+28.0 kcal/mole), and $D(H-H)=4.48$ ev/molecule, as quoted in reference (1), one can derive the equation

$$I(C_6H_5CH_2)=2A_1(C_7H_7^+)-A_2(C_7H_7^+)+2\Delta H_f(C_6H_5CH_3) -\Delta H_f(C_6H_5CH_2)_2-2\Delta H_f(H)=8.51 \text{ ev}. \quad (1)$$

This calculation does not depend on any bond dissociation energies in toluene or dibenzyl. However, the ionization potential of the benzyl radical, measured directly on radicals produced thermally from benzyl iodide, was found to be 7.73 ± 0.08 ev.[3] This value is reasonably consistent with the measured appearance potentials[4] of benzyl ion from the benzyl halides and recent estimates of the corresponding bond dissociation energies. A recent redetermination of the ionization potential of benzyl radicals produced by the pyrolysis of benzylamine gave $I(C_6H_5CH_2)=7.81\pm 0.08$ ev with an over-all average of 7.76 ± 0.08 ev. This ionization potential disagrees with the above indirectly calculated value to the extent of about 0.7 ev. If it is assumed that $I(C_6H_5CH_2)\sim 7.8$ ev and that the heats of formation of the compounds are correct, then it must be concluded that either $A_1(C_7H_7^+)$ or $A_2(C_7H_7^+)$ is in error. The ionization efficiency curves for $C_7H_7^+$ from toluene and dibenzyl have a large curvature at the foot which makes the exact determination of $A_1(C_7H_7^+)$ and $A_2(C_7H_7^+)$ difficult. An error could also arise if the values of $A_1(C_7H_7^+)$ and $A_2(C_7H_7^+)$ contain excess energy terms which do not cancel in the evaluation of $I(C_6H_5CH_2)$ from Eq. (1).

In an attempt to obtain a less ambiguous value for $A_1(C_7H_7^+)$, some experiments were carried out using trideuterotoluene, $C_6H_5CD_3$. These have shown that with electrons of 50 ev the processes

$$C_6H_5CD_3+e\rightarrow C_6H_5CD_2^++D+2e \quad (2)$$

and

$$C_6H_5CD_3+e\rightarrow C_6H_4CD_3^++H+2e \quad (3)$$

occur in the ratio to be expected on statistical grounds if all the hydrogens were equivalent in the dissociation process. The isotopic purity of the deutero-toluene (78 percent) was not sufficiently great to provide a clear separation of processes (2) and (3) at low electron energies, but further work is in progress.

The determination of $A_1(C_7H_7^+)$ from toluene depends on the measurement of the minimum energy which will bring about the process

$$C_7H_8+e\rightarrow C_7H_7^++H+2e. \quad (4)$$

Since the tolyl and benzyl ions are isomeric, it is important to be certain that the initial onset for the $C_7H_7^+$ ion in toluene occurs by process (2) and not by process (3). Although it may be expected on the basis of molecular orbital theory that $I(\text{tolyl}) > I(\text{benzyl})$ and consequently that $A_1(C_7H_7^+)$ should be associated with process (2), the fact remains that the dissociation process leading to the formation of the $C_7H_7^+$ ion from toluene is not a simple one.

Until the inconsistencies in $I(C_6H_5CH_2)$, $A_1(C_7H_7^+)$, and $A_2(C_7H_7^+)$ have been resolved, calculations of $D(C_6H_5CH_2-H)$ or $D(C_6H_5CH_2-CH_2C_6H_5)$ by the "direct" method cannot be made. Furthermore, it follows that the work of Schissler and Stevenson cannot be regarded as substantiating the Szwarc value for $D(C_6H_5CH_2-H)$, though the latter may indeed be correct.

* National Research Council Contribution No. 3349.
† National Research Council Postdoctorate Fellow 1953–1955.
‡ Guest worker.

[1] D. O. Schissler and D. P. Stevenson, J. Chem. Phys. **22**, 151 (1954).
[2] M. Szwarc, J. Chem. Phys. **16**, 128 (1948).
[3] Lossing, Ingold, and Henderson, J. Chem. Phys. **22**, 621 (1954).
[4] Lossing, Ingold, and Henderson, J. Chem. Phys. (to be published).

Effect of Compressive Stress on Self-Diffusion in Zinc

A. W. LAWSON

Institute for the Study of Metals, The University of Chicago, Chicago, Illinois

(Received August 19, 1954)

THE fractional changes $\Delta D_i/D_{0i}$ in the self-diffusion coefficient along the principal axes of a crystal when subjected to compressive stresses X_j are controlled by tensor relations, which may be written in Voigt's notation as

$$\Delta D_i/D_{0i}=\Sigma\gamma_{ij}X_j \quad j=1, 2, 3. \quad (1)$$

For a hexagonal crystal such as zinc we have $\gamma_{11}=\gamma_{22}$, $\gamma_{12}=\gamma_{21}$,

$\gamma_{13}=\gamma_{23}$, and $\gamma_{32}=\gamma_{31}$, and hence five independent constants, γ_{11}, γ_{12}, γ_{13}, γ_{31}, and γ_{33}, must be known in order to utilize Eq. (1), whose derivation is analogous to the corresponding equations for the piezo-optic[1] and piezoresistance[2] coefficients.

Recently Liu and Drickamer[3] have reported a series of measurements on self-diffusion in zinc, both parallel and perpendicular to the hexagonal axis, under hydrostatic pressure and under compressive stresses perpendicular and parallel to the direction of diffusion. In all cases the rate of self-diffusion is decreased by the application of compressive stresses.

The six independent experiments conducted by Liu and Drickamer permit the five independent piezodiffusion coefficients γ_{ij} (exclusive of the shear coefficient of self-diffusion γ_{44}) to be calculated and a test for self-consistency to be made. Unfortunately, the test for self-consistency fails by several orders of magnitude as we shall now proceed to demonstrate. For example, at atmospheric pressure and 326°C the self-diffusion constant D_c parallel to the hexagonal or c axis is 1.22×10^{-4} cm²/day. D_c at 326°C under a compressive stress of 475 psi parallel to the hexagonal axis is 6.1×10^{-5} cm²/day; D_c at 326°C under a compressive stress at 416 psi perpendicular to the hexagaonal axis is 7.7×10^{-5} cm²/day. From these data we find at this temperature $\gamma_{33}=-1.5\times10^{-2}$ cm²/kg and $\gamma_{31}=-1.26\times10^{-2}$ cm²/kg.

Since $\Delta D_c/D_{0c}\Delta P$ is $\gamma_{33}+2\gamma_{31}$ by Eq. (1), we calculate from the foregoing data that this quantity at 326°C should be -4.0×10^{-2} cm²/kg. From Liu and Drickamer's data we estimate that its value is -7.8×10^{-5} cm²/kg. The discrepancy of approximately a factor of five hundred between the calculated and observed pressure coefficient of D_c is too large to be accounted for by minor approximations involved in the calculation, e.g., neglecting the effect of dimensional changes on the γ_{ij}.

The origin of the discrepancy is unknown. It seems unlikely that plastic deformation is the source. It is noteworthy that the conditions of the experiment were such that the loading pistons could conduct a considerable amount of heat away from the sample and that the thermocouple used to measure the sample's temperature was off to one side, between the sample and the furnace wall. If we assume that the pistons were not in contact with samples measured under zero stress, a temperature difference of only 5° to 10°C between the samples under compression and the measuring thermocouple would be sufficient to explain the discrepancy between the observed and calculated values of the pressure coefficient of self-diffusion.

If a systematic error of this type were present in the experiments of Liu and Drickamer, their diffusion coefficients measured under stress should not extrapolate to the correct zero stress values. Unfortunately their data on diffusion coefficients is too sparse, and lacks sufficient precision to yield an unambiguous answer to this question.

[1] F. Pockels, *Lehrbuch der Kristalloptik* (Leipzig, 1906), p. 472.
[2] M. Allen, Phys. Rev. **49**, 648 (1936); J. W. Cookson, Phys. Rev. **47**, 194 (1935).
[3] T. Liu and H. G. Drickamer, J. Chem. Phys. **22**, 312 (1954).

Errata: Primary Photochemical Process in Bromine

[J. Chem. Phys. **21**, 2218 (1953)]

G. B. Kistiakowsky and James C. Sternberg*
Gibbs Chemical Laboratory, Harvard University, Cambridge, Massachusetts

Dr. A. L. G. Rees has privately brought to our attention the following points requiring correction. All are found on p. 2223 in our paper.

1. In Table IV, the statements at the feet of columns "Assignment I" and "Assignment II" should be interchanged.

2. In the first paragraph below Table IV, Dr. Rees has pointed out that his $^3\pi_0{}^+{}_u$ curve was actually constructed up to $v'=37$, instead of $v'=22$ as reported.

3. In the same paragraph, the last sentence should be changed to read, "The $^1\pi_u$ state is expected to be repulsive, according to Mulliken, and only a continuum associated with this state has been observed." We are grateful to Dr. Rees for his helpful comments.

* Present address: Department of Chemistry, Michigan State College, East Lansing, Michigan.

Intensity of the Bending Mode in Carbonyl Sulphide

Edward C. Wingfield and Joseph W. Straley
Department of Physics, University of North Carolina, Chapel Hill, North Carolina
(Received August 25, 1954)

The intensity of the ν_2 fundamental in OCS located at 19 microns has been measured in order to determine the CO and the CS bond moments. Although there is evidence that the intensity of the upperstage bands which overlay the fundamental are enhanced by Fermi resonance, an analysis of the absorption curves together with data secured at elevated temperatures has made possible the determination of the true intensity of the fundamental.

The sample was prepared by the addition of a concentrated water solution of KSCN to concentrated H_2SO_4 as described by Bartunek and Barker.[1] The evolved gas was purified by being sent successively through a cold trap, a KOH solution, and drying towers. The absolute band intensity was determined on a Perkin-Elmer 112 Spectrometer using the extrapolation method of Wilson and Wells.[2] Dry nitrogen to a total pressure of 30 psi was added to the OCS at partial pressures in the range 0 to 1.5 cm Hg in a 10-cm cell equipped with KBr windows.

In addition to the intense Q branch at 521 cm^{-1} two additional Q branches were clearly visible but contained under the same total envelope. The first of these at 516 cm^{-1} we have ascribed to the $2\nu_2-\nu_2(\Delta-\pi)$ transition; the second at 527 cm^{-1} we have ascribed to the $2\nu_2-\nu_2(\Sigma-\pi)$ transition. While this assignment does not agree with that frequently quoted in the literature[3] it is justified by the fact that, assuming the splitting in the $v_2=2$ levels to arise from Fermi resonance with $v_1=1$, the $\Sigma-\pi$ band should lie at the higher frequency and should experience the greater enhancement of its intensity.

The fact that the upper stage bands appear to be enhanced by Fermi resonance made necessary the correction of the observed integrated absorption areas. This was accomplished by assuming the ratio of the energies of the various subbands that make up the observed envelope to be equal to the ratio of the areas of the portion of the Q branches that protrude above the background. These ratios were then compared to those expected on the basis of the distribution law. Our confidence in the accuracy of the correction factor of 10 percent secured in this manner was increased by the fact that data was secured both at room temperature (25.8°C) and at 104°C. It should be noted that at the higher temperature there was evidence of considerable thermal decomposition of the gas. This negated the value of any measurement of the absolute intensity of the band at the higher temperature but did not affect the comparison of relative Q-branch intensities.

The corrected extrapolated integrated absorption A was found to be $(36.0\pm4.0)\times10^{10}$ cycles/sec cm at NTP. The dependence of the total dipole moment on the normal coordinate is related to the intensity through the equation

$$\partial\mu/\partial Q=\pm(3cA/2N\pi)^{\frac{1}{2}}, \tag{1}$$

where the factor of 2 has been introduced because we are here dealing with a doubly degenerate band. Letting θ represent the change in angle produced by vibration we may write

$$\frac{\partial\mu}{\partial\theta}=\frac{\partial\mu}{\partial Q}\frac{\partial Q}{\partial\theta}=-\mu_{oc}\frac{\partial\alpha}{\partial\theta}+\mu_{cs}\frac{\partial\beta}{\partial\theta}, \tag{2}$$

where α and β represent the angular departure of the CO and the CS bands from their equilibrium orientation. Making use of the

laws of conservation of momenta one finds that $\partial\alpha/\partial\theta=0.624$ and $\partial\beta/\partial\theta=0.376$.

The dependence of the normal coordinate Q on θ is given by

$$\partial Q/\partial\theta=(k_\theta)^{\frac{1}{2}}/2\pi\nu c. \tag{3}$$

Letting $k_\theta=6.7\times10^{-12}$ dyne cm/radiant[4] and $\nu=521$ cm^{-1} we find that $\partial Q/\partial\theta=2.64\times10^{-20}$ cgs. Equation (2) now becomes

$$0.376\mu_{cs}-0.624\mu_{oc}=\pm0.36. \tag{4}$$

The total dipole moment of the OCS molecule equals 0.72 debye. Treating the bond moments as vector quantities which combined yield the observed total dipole moment we may write,

$$\mu_{cs}+\mu_{oc}=0.72. \tag{5}$$

Solving Eqs. (4) and (5) simultaneously we may secure values of μ_{cs} and μ_{oc}. If one uses the positive sign in Eq. (4) he will secure an unreasonable answer. Using the negative sign, however, he finds

$$\mu_{cs}=0.09\pm0.02 \text{ debye},$$
$$\mu_{oc}=-\mu_{oc}=-0.63\pm0.02 \text{ debye}.$$

These values are in qualitative agreement with the known electronegative properties of oxygen and sulphur.

[1] P. F. Bartunek and E. F. Barker, Phys. Rev. **48**, 516 (1935).
[2] E. B. Wilson and A. J. Wells, J. Chem. Phys. **14**, 578 (1946).
[3] T. Y. Wu, *Vibrational Structure and Spectra of Polyatomic Molecules*, p. 150.
[4] G. Herzberg [*Infrared and Raman Spectra* (D. Van Nostrand Company Inc., New York, 1945), p. 174] quotes $k_\theta=0.66\times10^{-11}$ dyne cm/radian. He, however, has used $l_{cs}=1.54\times10^{-8}$ cm instead of the value 1.56×10^{-8} quoted by Cross and Brockway [J. Chem. Phys. **3**, 821 (1935)].

Covalent Boron-Boron Bonds in Crystals of Certain Metal Borides

INGA FISCHER-HJALMARS AND STIG FLODMARK
Institute of Theoretical Physics, University of Stockholm, Stockholm, Sweden
(Received September 10, 1954)

FROM experiments[1] it is shown that several metals, e.g., Ca, Sr, Ba, Y, form boron compounds, MeB_6, all of which have the same crystal structure. The metal atoms form a cubic lattice. Inside of every cube there is one octahedron of six B atoms. Every B atom has five nearest neighbors of B atoms, four in the same octahedron and one in the adjacent octahedron. The B–B distances vary between 1.7 and 1.8 A in the different MeB_6 lattices. This is about twice the covalent radius of B. As pure B does not form any simple lattice, our suggestion is that the stability of the B lattice in MeB_6 is due to oscillating covalent B–B bonds reinforced by the valence electrons of the Me atoms. This suggestion is supported by the fact that all the metals have low ionization potentials.

We have made a theoretical investigation of the possibility of forming covalent bonds in the five directions given by experiments. The ground state of B is $(1s)^2(2s)^2(2p)^2P$. To obtain orbitals in the five directions, we must construct linear combinations χ of the following atomic orbitals φ: $2s$, $2p_x$, $2p_y$, $2p_z$, $3d_{z^2}$, and $3d_{x^2-y^2}$. The Slater determinant[2] of three such χ's has extreme values when the electrons are located in three of the given five directions, if

$$\chi_1=2p_z, \quad \chi_2=3d_{x^2-y^2}, \quad \chi_3=c_1(2s)+c_2(3d_{z^2}), \tag{1}$$

where $c_1=0.24$ and $c_2=0.97$. Only the angular dependence is considered here.

According to our suggestion, the stability of the B lattice should be due to more than three electrons per atom participating in the B–B bonds. If every Me atom is ionized twice, the time average should be $3\frac{1}{3}$ electrons per B atom. To investigate the distribution of the valence electrons, we have studies the electronic density

$$\rho=\sum_i \chi_i^*\chi_i=\sum_{j,k=1}^{6} C_{jk}\varphi_j^*\varphi_k,$$

which should be normalized to $3\frac{1}{3}$. From symmetry considerations, it is found that

$$\rho=C_1(2s)^2+C_2\{(2p_x)^2+(2p_y)^2\}+C_3(2p_z)^2 +C_4(2s)(2p_z)+C_5(3d_{x^2-y^2})^2+C_6(2s)(3d_{z^2}) +C_7(2p_z)(3d_{z^2})+C_8(3d_{z^2})^2. \tag{2}$$

Generally, (2) corresponds to configurational interaction including 20 determinants. The parameters C_i have been determined from the condition that ρ shall have maxima in the five bond directions and minima between them. This gives 9 equations to determine the parameters C_1-C_8, r_{max}, and r_{min}. It is found that the contribution from $(3d_{x^2-y^2})^2$ forms the essential part of ρ. As the number of conditional equations is less than the number of parameters, the coefficients cannot be determined uniquely. We have chosen to assign certain values to C_8, whereby the other parameters are fixed. When $C_8\leq0.6$, it is possible to obtain maxima in the given directions. When $C_8=0.6$, we find $C_5=2.7$. If (1) and (2) were to correspond to each other, we should have $C_8=c_2^2=0.95$ and $C_5=1.0$. However, an assumption of slightly bent bonds reduces c_2^2 to 0.5. The extremely large value of $C_5=2.7$ in (2) is not consistent with the Pauli principle. This contradiction can depend on the simplifications introduced: orbitals of only one B atom in the charge density, r_{max} equal in the five directions, the same restriction on r_{min} which, furthermore, is supposed to lie symmetrically between the maxima. These approximations probably include an overestimation of the $3d$ orbitals. Moreover, introduction of slightly bent bonds in (2) would certainly reduce C_5-C_8. Still, it is our opinion that the contribution from the $3d$ orbitals is essential, because otherwise the charge density cannot attain the symmetry of the atomic lattice.

A few weeks ago, another theoretical investigation of MeB_6 has been published.[3] This study is most interesting, but both method and aim are rather different from ours.

We are indebted to P. Spiegelberg who drew our attention to this problem. Full details of the present investigation will be published by one of us (S.F.) in *Arkiv. Fysik*.

[1] R. Kiessling, Acta Chem. Scand. **4**, 209 (1950).
[2] See H. K. Zimmerman and P. van Rysselberghe, J. Chem. Phys. **17**, 598 (1949).
[3] H. C. Longuet-Higgins and M. de V. Roberts, Proc. Roy. Soc. (London) **A224**, 336 (1954).

Self-Consistent Field Method and the Benzene Molecule

C. R. MUELLER
Chemistry Department, Purdue University, Lafayette, Indiana
(Received June 8, 1953)

THE benzene molecule plays such an important role in valence theory that it has been the subject of many quantum-mechanical calculations. These calculations are either based on the primitive atomic or molecular orbital theories or on rather elaborate approximations involving configuration interaction. The primitive theories are unreliable, and the more elaborate theories are difficult to interpret. This note will describe an orbital procedure involving the use of the self-consistent field.

Let us first consider the case of a single Kekule structure. In analogy to the procedure used for ethylene,[1] we will use the Dirac vector method to obtain an expression for two bonding electrons, represented by eigenfunctions Φ_1 and Φ_2

$$E=\frac{Q+K_{12}-\frac{1}{2}K_{1k}-\frac{1}{2}K_{2q}}{I+S_{ij}^2-\frac{1}{2}S_{ik}^2-\frac{1}{2}S_{iq}^2}. \tag{1}$$

Q is the Coulomb integral, K_{12} the exchange integral, and K_{1k} and K_{2q} are exchange integrals of the bonding orbitals with orbitals centered on adjacent atoms.

The Hamiltonian is the usual two electron one with Coulombic repulsions, from electrons not involved in the exchange, included.

An expression similar to (1) for the two Kekule structure representation of benzene can be obtained by again applying

the Dirac vector model and will contain terms arising from the interaction of the two Kekule structures with one another.

In either case the results may be indicated by the general formula,

$$E=\{Q+\sum_{i>j} C_{ij}K_{(ij)}\}\div\{1+\sum_{i>j} C_{ij}S_{(ij)^2}\}. \quad (2)$$

We have not as yet considered the specific form of Φ_1 and Φ_2, the bonding orbitals.

Let

$$\Phi_1=\sum_{1=n}^{1=n} A_r\varphi_r. \quad (3)$$

We can obtain the value of the coefficients by substituting (3) into (2) and differentiating with respect to each coefficient. The condition that the resultant n-linear simultaneous equations have a nontrivial solution yields the secular equation

$$||Aqr||=0. \quad (4)$$

The matrix elements are

$$A_{qr}=(\varphi_q\varphi_r/H/\Phi_2^2)+\sum_{k\geq 2} C_{1k}(\varphi_q\Phi_k/H/\varphi_r\Phi_k) - E\{S_{qr}+\sum_{k\geq 2} C_{1k}S_{qk}S_{rk}\}. \quad (5)$$

Even though the study of benzene involves configuration interaction, if only the two Kekule structures are considered the total energy has the form of Eq. (2) after solution of a secular equation. A second secular equation (4), must be solved to find the orbital form.

The first solution of the secular equation and the symmetry conditions enable us to specify more accurately the other orbitals. Repeated solution in this manner finally leads to self-consistency. Using three centered orbitals (a linear combination of central A.O., φ_b, with adjacent atomic orbitals) we contain $\Phi_1=0.38\varphi_a+\varphi_b+0.66\varphi_c$. The adjacent bonding orbital (centered on atom a) is obtained by a 60° rotation of the molecule in the direction of atom A following by an exchange of the coefficients of φ_a and φ_c. The orbital in the second Kekule structure corresponding to Φ_1 is obtained by exchanging the coefficients of φ_a and φ_c.

A similar procedure was carried out for the single Kekule structure. The orbital $\Phi_1=0.38\varphi_a+\varphi_b+0.57\varphi_c$. The resonance energy can be computed by taking cognizance of those terms which are counted twice, and then calculating the total energy of the single and double Kekule structures. The difference is 63 kcal, leading to a resonance energy of roughly 27 kcal, after taking cognizance of the compressional energy.

We find a resonance energy roughly of the right order of magnitude. In addition it appears that the valence orbitals of benzene are largely localized on the original atoms.

[1] C. R. Mueller, J. Chem. Phys. **22**, 120 (1954).

Note on the Temperature Variation of the Configurational Energy of Regular Solutions

P. K. KATTI, *Department of Applied Science, Delhi Polytechnic, Delhi, India*

AND

S. M. BHAGAT, *Department of Physics, University of Delhi, Delhi, India*

(Received August 30, 1954)

IN the quasichemical treatment of the properties of regular binary mixtures Gugganheim[1] considers a crystalline lattice of N sites occupied by N_A molecules of one component A and N_B molecules of the other B such that $N_A+N_B=N$.

The configurational energy E_C is given by the relation

$$E_C=-N_Ax_A-N_Bx_B+X\omega, \quad (1)$$

where

$$-2x_A/Z=\varepsilon_{AA},\quad -2x_B/Z=\varepsilon_{BB}\quad\text{and}\quad(-x_A-x_B+\omega)/Z=\varepsilon_{AB}$$

TABLE I.

	$(d\omega/dt)$cal. cal/mole deg.	$(d\omega/dt)$ from V.P. data cal/mole deg.
Benzene and carbon tetrachloride	−0.185	−15
Carbontetrachloride and cyclohexane	−0.17	−0.23

are, respectively, the energies of each AA, BB, and AB pair, Z the coordination number of the lattice, and ZX the total number of AB pairs in the configuration. From the foregoing relations we have

$$\frac{2\omega}{Z}=2\varepsilon_{AB}-\varepsilon_{AA}-\varepsilon_{BB}. \quad (2)$$

From the Lennard-Jones and Devonshire model[2] the energy of a pair of molecules separated by a distance r can be expressed by the relation

$$\varepsilon_r=\varepsilon^*\left\{\left(\frac{r^*}{r}\right)^{12}-2\left(\frac{r^*}{r}\right)^{6}\right\}, \quad (3)$$

ε^* being the minimum potential energy of the pair and r^*, the corresponding distance between them.

If we now assume with Prigogine[3] that for regular solutions

$$r_{AA}^*\approx r_{BB}^*\approx r_{AB}^*,$$

then the energies of the AA, BB, and AB pairs are given by

$$\left.\begin{aligned}\varepsilon_{AA}&=\varepsilon_{AA}^*\{(r^*/r)^{12}-2(r^*/r)^6\};\\ \varepsilon_{BB}&=\varepsilon_{BB}^*\{(r^*/r)^{12}-2(r^*/r)^6\};\\ \varepsilon_{AB}&=\varepsilon_{AB}^*\{(r^*/r)^{12}-2(r^*/r)^6\};\end{aligned}\right\} \quad (4)$$

and

$$2\omega/Z=2\varepsilon_{AB}-\varepsilon_{AA}-\varepsilon_{BB} =(2\varepsilon_{AB}^*-\varepsilon_{AA}^*-\varepsilon_{BB}^*)\{(r^*/r)^{12}-2(r^*/r)^6\}, \quad (5)$$

where r is the distance between the lattice points on the crystal.

We may note that the distance between the lattice points is r^* in a crystal only at very low temperatures, where the thermal vibrations of the molecules about their mean positions are very small and the distances between their mean positions are governed only by the 6–12 power relation. At room temperatures, however, due to the thermal expansion of the crystal the distance between the lattice points r is much larger than r^*. The contribution of the 12 power term which falls off rapidly at distances greater than r^* can therefore be neglected in the first instance. We thus get at the room temperature

$$\omega=-2Z(2\varepsilon_{AB}^*-\varepsilon_{AA}^*-\varepsilon_{BB}^*)r\exp(*)^6\cdot r^{-6}=Kr^{-6}. \quad (6)$$

In order to calculate the temperature dependance of ω we can express it in the form

$$\omega=Kr_0^{-6}\{1+\tfrac{1}{3}\alpha t\}^{-6}=\omega_0(1+\tfrac{1}{3}\alpha t)^{-6}, \quad (7)$$

where r_0 is the distance between the lattice points at 0°C, α the thermal coefficient of cubical expansion of the mixture, and ω_0, the value of ω at 0°C.

In the first approximation

$$\omega=\omega_0\{1-2\alpha t\}\quad\text{and}\quad d\omega/dt=-2\alpha\omega_0. \quad (8)$$

Scatchard[4] has shown that the partial vapor pressures of benzene and carbon tetrachloride, and carbon tetrachloride and cyclohexane in binary mixtures can be explained only by assuming that ω varies with temperature. He[5] has developed a theory relating the temperature dependence of ω to the volume changes occurring on mixing the two components.

It may be noted that these two mixtures very nearly satisfy the conditions for regular solutions. Table I shows the values of $d\omega/dt$ calculated from relation (8) and the corresponding values of $d\omega/dt$ which fit in with Scatchard's vapor pressure data. Values of ω_0 used in these calculations were obtained by extrapolating Scatchard's results. For α, the mean for the pure constituents is used.

From Table I it is noticed that $d\omega/dt$ calculated from relation (8) are of the right order of magnitude. In any case it is obvious that most of the decrease in the value of ω with increase in the temperature of the mixture can be attributed to the thermal expansion of the crystal lattice.

Our grateful thanks are due Dr. D. S. Kothari, Professor of Physics, University of Delhi, for his interest in this investigation.

[1] E. A. Gugganheim, *Mixtures* (Oxford University Press, London, 1952).
[2] Lennard-Jones and Devonshire, Proc. Roy. Soc. (London) **A106**, 463 (1937).
[3] I. Prigogine and V. Methot, J. Chem. Phys. **20**, 49 (1952).
[4] Scatchard, Wood, and Mochel, J. Am. Chem. Soc. **62**, 712 (1940); **61**, 3206 (1939).
[5] Scatchard, Trans. Faraday Soc. **33**, 160 (1937).

Free Electron Treatment of the Orientation of Substituents in Aromatic Molecule

SADHAN BASU
Indian Association for the Cultivation of Science, Calcutta 32, India
(Received August 10, 1954)

IN treating the reactivity of organic compounds two methods have been applied by several authors: One may be called the π-electron density method[1] and the other the transition state method.[2] MO treatment has been applied to both these methods but, as far as the author is aware, the free electron treatment has been applied to the first method only.[3–5] The object of the present note is to show that the free electron treatment is applicable equally well to the second method.

It is now an accepted fact that any aromatic substitution reaction proceeds through the formation of an activated complex. In an electrophilic substitution, the part of the reagent R which is closest to the atomatic nucleus is considered not only to be positively charged, but also to have a gap into which a pair of electrons can be put. The problem is essentially to determine the amount of energy which must be supplied in order to provide at the point of attack, an unshared pair of electrons. This is equivalent to the problem of determining the difference in the π-electron energy of the activated complex and the parent molecule. Let us take the case of *o*-, *m*-, and *p*-substitution in aniline. The structures in the activated complex and in parent molecules are shown below.

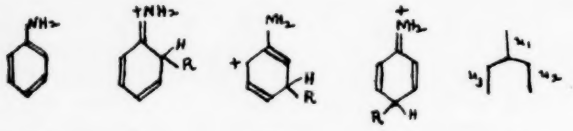

I II III IV V

Now the π-electron energies are calculated as follows:

For I, the π-electron energy levels are given by

$$E=(h^2/8ml^2)(4q/6^2),$$

where $q=0, \pm1, \pm2, \cdots$, and $l=$C–C bond distance (=1.41 A). Since there are only six electrons, they will occupy three lowest levels and the total π-electron energy is given by

$$2(h^2/8ml^2)(8/36)=0.44(h^2/8ml^2).$$

For II, the electron moves in a box of length $5l$ and the energy levels are given as

$$E=(h^2/8ml^2)(n^2/5^2)$$

where $n=1, 2, 3, \cdots$. There are 6 electrons which will occupy 3 lowest levels, so the total π-electron energy is $1.12(h^2/8ml^2)$.

For III, the electrons move in two boxes of the length l each, and each box contains two electrons. So the π-electron energy for this system is $4(h^2/8ml^2)$.

For IV, we use free electron network model, *i.e.*, we divide the conjugated system into the segments shown in V and express the wave function in each segment in the form $a\cos\omega\kappa+b\sin\omega\kappa$. We then apply continuity and conservation condition at the junction point and calculate the allowed values of ω.

The energy levels are given by $E=(h^2/8ml^2)\omega^2/\pi^2$, if x be expressed in unit of l and ω in terms of π. Six available electrons will occupy three lowest levels for which one has $\omega=0$ and two $=\pi/2$. So the total π-electron energy is $1.00(h^2/8ml^2)$. The difference in π-electron energy from parent structure is given below

	ΔE_π	
o-	0.68 K	
m-	3.56 K	$K=h^2/8ml^2$.
p-	0.56 K	

It is evident that the energy differences is least for *p*-, next is *o*-, and extremely high for *m*-substitution. So the compound will undergo *o*, *p*-substitution with *p*-predominating. Similar calculation with 2-naphthylanine shows that 1-substitution will predominate over 3. This treatment has also been shown to be valid for substitution in tropolone.[6]

[1] Wheland and Pauling, J. Am. Chem. Soc. **57**, 2086 (1935).
[2] Wheland, J. Am. Chem. Soc. **64**, 900 (1942).
[3] Bayliss, J. Chem. Phys. **16**, 287 (1948).
[4] H. Kuhn, Helv. Chim. Acta. **31**, 1441 (1948).
[5] Nakajima, Sci. Rep. Ritu. **5A**, 98 (1953).
[6] Basu, J. Chem. Phys. (to be published).

Erratum: The Surface Migration of Carbon on Tungsten

[J. Chem. Phys. **22**, 1406–1413 (1954)]

RALPH KLEIN
Explosives and Physical Sciences Division, Bureau of Mines, Pittsburgh, Pennsylvania

ON page 1408, second column, eight lines from the bottom, the word "decreased" should be changed to "increased."